

University of Alberta

**Petroleum Hydrogeology of the Great Hungarian Plain,
Eastern Pannonian Basin, Hungary**

by

István Almási



A thesis submitted to the Faculty of Graduate Studies and Research in partial fulfillment
of the requirements for the degree of Doctor of Philosophy

Department of Earth and Atmospheric Sciences

Edmonton, Alberta

Spring, 2001



**National Library
of Canada**

**Acquisitions and
Bibliographic Services**

**395 Wellington Street
Ottawa ON K1A 0N4
Canada**

**Bibliothèque nationale
du Canada**

**Acquisitions et
services bibliographiques**

**395, rue Wellington
Ottawa ON K1A 0N4
Canada**

Your file Votre référence

Our file Notre référence

The author has granted a non-exclusive licence allowing the National Library of Canada to reproduce, loan, distribute or sell copies of this thesis in microform, paper or electronic formats.

The author retains ownership of the copyright in this thesis. Neither the thesis nor substantial extracts from it may be printed or otherwise reproduced without the author's permission.

L'auteur a accordé une licence non exclusive permettant à la Bibliothèque nationale du Canada de reproduire, prêter, distribuer ou vendre des copies de cette thèse sous la forme de microfiche/film, de reproduction sur papier ou sur format électronique.

L'auteur conserve la propriété du droit d'auteur qui protège cette thèse. Ni la thèse ni des extraits substantiels de celle-ci ne doivent être imprimés ou autrement reproduits sans son autorisation.

0-612-60365-2

Canada

AJÁNLÁS
(Dedication)

Szüleimnek,
Dr. Erdélyi Mihálynak
és valamennyi magyar érdeklődő (hidro)geológusnak

[To my Parents, to Dr. Mihály Erdélyi,
as well as to all interested Hungarian (hydro)geologists]

ABSTRACT

The results of a regional scale hydrogeological investigation conducted in the Great Hungarian Plain, Eastern Pannonian Basin, for the purposes of petroleum exploration are presented. Two regional aquitards and three regional aquifers were determined in the poorly-to-well consolidated clastic basin fill of the Neogene-Quaternary age and the indurated basement of the Pre-Neogene age. The fluid-potential field was mapped using measured values of stabilised water level and pore-pressure. Two regional fluid flow regimes were recognised: an upper gravity-driven flow regime, and a lower overpressured regime, where super-hydrostatic pore pressures of 1 – 35 MPa are encountered. The transition between the two flow regimes does not correlate with any particular hydrostratigraphic boundary or elevation range. Apparently, its position and nature are controlled by the morphology of the rigid basement, and locally by the permeability contrasts within the overlying hydrostratigraphic units. Local hydrostratigraphic breaches and conduit faults facilitate hydraulic communication across the regional aquitards. The basin is hydraulically continuous. The mapped groundwater flow directions do not match the predictions of compactional flow models. At two gas-fields, up to 10 MPa overpressures are probably caused by buoyancy forces. Transient overpressures can not be maintained over geologic time in the basin, due to the rock's low hydraulic resistance. Regional tectonic compressive stress, probably with a Recent increase in intensity, offers a new and plausible explanation for the distribution pattern of overpressures in the Great Hungarian Plain. Gravity-driven groundwater flow plays a determinant role in petroleum migration and entrapment. Compactional flow models can explain the present-day position of several known petroleum accumulations within the

overpressured regime. However, most accumulations are also associated with particular fluid-potential anomaly-patterns of the actual flow field, which also suggest the possibility of petroleum remigration toward the graben centres and upward. The geothermal characteristics show that pure conduction is the dominant regional heat transfer mechanism within the entire basin. The encountered advective thermal anomalies correlate well with fluid potential anomalies observed in both fluid flow regimes, as well as with certain petroleum accumulations. Tóth's (1980) hydraulic theory of petroleum migration was found applicable in a deforming Neogene sedimentary basin, the Great Hungarian Plain.

ACKNOWLEDGEMENT

This study was funded through Research Grant No. A-8504 from the Natural Sciences and Engineering Research Council of Canada (NSERC) awarded to my principal supervisor, József Tóth, Professor Emeritus, and by the Domestic Exploration Division of the Hungarian Oil and Gas Co., Plc. (MOL, Plc.). From his NSERC grant, Dr. Tóth provided me with research assistantships, covered my tuition's differential fee, and made possible for me to participate at several memorable conferences and field trips, both in Canada and in Hungary. All these contributions are gratefully acknowledged. The teaching and research assistantships provided by the Department of Earth and Atmospheric Sciences, University of Alberta, are also greatly appreciated. During the last year of thesis preparation, I benefited from the generous support of Dr. Grant Sheng, York University, who provided work and excellent conditions to finish this thesis and care for my family – Thank You.

I wish to thank Dr. Tóth for introducing me into the fascinating world of petroleum hydrogeology and for shaping my thinking through many discussions. Thanks to the other members of the Supervisory Committee: Dr. Ben Rostron (Co-Supervisor), Dr. Carl Mendoza, and Dr. Hans Machel, for their suggestions and revisions of earlier drafts of this thesis. Also, thanks to my examiners, Dr. John Waldron, Dr. Walter Jones (Department of Physics), and Dr. John M. Sharp, Jr. (University of Texas, Austin) for reading the manuscript and providing insight into specific questions.

Dr. Dinu Pană, Dr. István Csató, and Dr. Irén Varsányi carefully read earlier versions of my manuscript; their advice and suggestions significantly improved the quality of the final product. Also, Thanks to my wife, Ms. Erika Almási-Klausz, and my colleague, Ms. Lisa Allen, for patiently proof-reading the last draft, and amending its English grammar and style.

The personal interest and support of Dr. István Bérczi, former Director of KUMMI, MOL, Plc., is very much appreciated. I also benefited from significant technical and scientific advice, logistical assistance, and friendship of Dr. István Révész, Sándor Pap (project manager), Dr. János Viszok, Jutka Török, Dr. Balázs Kiss, Györgyi Juhász, Imre Szilágyi, and István Horváth, all past and present employees of MOL, Plc.

Ms. Katalin Zimmermann, Secretary of the Hungarian Geological Society, provided invaluable help as relay person between organisations. This whole project would not have started without her tenacious assistance as a “midwife.”

I wish to thank my colleagues and good friends from Hungary, for their support, enlightening conversations about various aspects of my work, and warm friendship. Thank You: Andrea Mindszenty, Judit Mádlné Szőnyi, Ferenc Horváth, Péter Dövényi, László Fodor, László Csontos, Tamás Weiszbürg, Béla Angelus, Attila Arday, Réka Gaul, János Szanyi, Attila Juhász, Tivadar M. Tóth, Gábor Tari, Lilla Kónyi. I am grateful to Géza and Aji Gaul for their tremendous support, for providing a true home in Budapest, and, nevertheless, for putting up with me.

I am most grateful to my parents, István and Ildikó Almási, for their loving wisdom, unparalleled example, patience and trust with which they guided me.

My wife, Erika, and my daughter, Izabella, were great sources of motivation! Unfortunately, they had to suffer through the lengthy labour-pains of this thesis; I’m sure they are happy to see this done and us finally starting a decent life. Thanks for your patience! I have to catch up with many things I missed out over the past two years or so.

TABLE OF CONTENTS

1	INTRODUCTION.....	1
1.1	CONCEPTUAL FRAMEWORK.....	1
1.2	PROBLEMS	3
1.3	OBJECTIVES	6
1.4	WORKING HYPOTHESES	7
1.5	OUTLINE OF THESIS.....	8
1.6	PROJECT HISTORY	9
2	STUDY AREA: THE GREAT HUNGARIAN PLAIN, EASTERN PANNONIAN BASIN, HUNGARY.....	11
2.1	PHYSIOGRAPHIC SETTING.....	11
2.2	LIMITS OF THE STUDY AREA.....	13
2.3	HYDROGEOLOGIC ENVIRONMENT.....	15
2.3.1	<i>Climate</i>	15
2.3.2	<i>Topography</i>	15
2.3.3	<i>Geology</i>	17
2.4	REGIONAL TECTONIC HISTORY.....	18
2.5	SEDIMENTARY FILL OF THE BASIN.....	29
2.6	HYDROSTRATIGRAPHY.....	31
2.6.1	<i>Principles</i>	31
2.6.2	<i>Hydrostratigraphic units in the Great Hungarian Plain</i>	32
2.6.4	<i>A possible method for enhancing the resolution of regional hydrostratigraphic units</i>	43
2.7	PETROLEUM GEOLOGY	45
2.7.1	<i>Source rocks</i>	45
2.7.2	<i>Maturation</i>	46
2.7.3	<i>Carrier beds and reservoirs</i>	48
2.7.4	<i>Petroleum accumulations and migration</i>	50

2.7.5	<i>Hydrocarbon potential</i>	53
3	DATA	55
3.1	STRATIGRAPHY	55
3.2	FLUID PRESSURE AND WATER LEVEL DATA	56
3.2.1	<i>Data processing</i>	57
3.3	TOPOGRAPHY.....	60
3.4	SUBSURFACE TEMPERATURE.....	63
3.5	POROSITY AND PERMEABILITY	65
3.6	STRUCTURAL GEOLOGY.....	65
3.7	PETROLEUM OCCURRENCE	66
4	REGIONAL GROUNDWATER FLOW SYSTEMS	67
4.1	CHARACTERISATION OF GROUNDWATER FLOW SYSTEMS.....	67
4.1.1	<i>Hydrodynamic parameters</i>	67
4.1.2	<i>Characterisation of groundwater flow distribution</i>	70
4.2	GROUNDWATER FLOW SYSTEMS IN THE GREAT HUNGARIAN PLAIN	73
4.2.1	<i>Methods of characterisation</i>	73
4.2.1.1	<i>p(z) profiles</i>	73
4.2.1.2	<i>Fluid-potential maps, $h_{ij}(x,y)$</i>	73
4.2.1.3	<i>Hydraulic cross sections; $H_i(L,z)$</i>	77
4.2.2	<i>General observations and interpretations</i>	79
4.2.2.1	<i>p(z) profiles</i>	79
4.2.2.2	<i>Tomographic fluid-potential maps ($h_{ij}(x,y)$)</i>	98
4.2.2.3	<i>Hydraulic cross sections ($H_i(L,z)$)</i>	117
4.2.2.4	<i>Hydraulic role of faults:</i>	140
5	RELATIONS BETWEEN BASIN SCALE FLUID DYNAMICS AND PETROLEUM OCCURRENCES	143

5.1	SPATIAL CORRELATION BETWEEN FLUID-POTENTIAL ANOMALIES AND PETROLEUM ACCUMULATIONS	143
5.1.1	<i>Diagnostic p(z) anomalies</i>	145
5.1.2	<i>Diagnostic tomographic fluid-potential map anomalies</i>	154
5.1.3	<i>Diagnostic hydraulic cross section anomalies</i>	157
5.2	SUMMARY AND DISCUSSION.....	159
5.3	CONCLUSIONS.....	162
6	HYDRO-GEOTHERMAL CONDITIONS	165
6.1	INTRODUCTION	165
6.1.1	<i>Geothermal features of the Pannonian Basin</i>	166
6.1.2	<i>Objectives of present study</i>	168
6.2	THEORETICAL CONSIDERATIONS	168
6.2.1	<i>Definitions</i>	168
6.2.2	<i>Dimensionless parameters</i>	172
6.2.3	<i>Effects of sedimentation on heat flow</i>	178
6.2.4	<i>Regional scale heat transfer and groundwater flow</i>	179
6.2.5	<i>Geologic manifestations of advective heat transport</i>	180
6.3	METHODS OF CHARACTERISATION OF THE GEOTHERMAL FIELD.....	181
6.4	RESULTS AND DISCUSSION	184
6.4.1	<i>General observations and interpretations</i>	184
6.4.1.1	Temperature vs. depth profiles (T(d)):	184
6.4.1.2	Isotherm ($T_{ij}(x,y)$) and isogradient maps ($\mathbf{grad} T_{ij}(x,y)$):	195
6.4.1.3	Regional geothermal cross sections ($T_i(L,z)$):	213
6.4.2	<i>Heat transfer in the gravity flow region</i>	218
6.4.3	<i>Heat transfer in the overpressured regime</i>	220
6.4.3.1	Vertical seepage velocities estimated from the dimensionless Péclet number:.....	220
6.5	CONCLUSIONS.....	221

7	EVALUATION OF THE POSSIBLE MECHANISMS ABLE TO GENERATE AND MAINTAIN THE OVERPRESSURED REGIME IN THE PANNONIAN BASIN.....	223
7.1	INTRODUCTION.....	223
7.2	OVERPRESSURES AND RELATED HYDRODYNAMIC EQUATIONS.....	224
7.2.1	<i>Overpressuring mechanisms</i>	224
7.2.2	<i>Equation of fluid flow in deforming porous media</i>	225
7.2.3	<i>Lifetime of transient overpressures</i>	227
7.3	RESULTS AND DISCUSSION	228
7.3.1	<i>Compaction due to vertical loading</i>	229
7.3.1.1	Overview of the mechanism.....	229
7.3.3.2	The role of compaction in overpressure generation in the Great Hungarian Plain.....	231
7.3.2	<i>Aquathermal pressuring</i>	239
7.3.2.1	Overview of the mechanism.....	239
7.3.2.2	The possible role of aquathermal pressuring in the Great Hungarian Plain	240
7.3.3	<i>Osmosis</i>	241
7.3.3.1	Overview of the mechanism.....	241
7.3.3.2	The possible role of osmosis as an overpressuring mechanism in the Great Hungarian Plain.....	241
7.3.4	<i>Hydrocarbon generation</i>	242
7.3.4.1	Overview of the mechanism.....	242
7.3.3.1	The possible role of hydrocarbon generation as overpressuring mechanism in the Great Hungarian Plain	243
7.3.5	<i>Diagenesis</i>	244
7.3.6	<i>Buoyancy</i>	245
7.3.6.1	Overview of the mechanism.....	245
7.3.6.2	The role of buoyancy in overpressure generation in the Great Hungarian Plain.....	245
7.3.7	<i>Horizontal tectonic compression</i>	247
7.3.7.1	Overview of the mechanism.....	247
7.3.7.2	The role of compressive stress in overpressure generation in the Great Hungarian Plain.....	248

7.4 SUMMARY.....	256
8 SYNTHESIS.....	257
8.1 HYDROSTRATIGRAPHY.....	257
8.2 FLUID-POTENTIAL FIELD.....	257
8.2.1 Gravity-driven flow regime.....	258
8.2.2 Overpressured zone	260
8.2.3 Transition between the regional pressure regimes.....	261
8.3 ORIGIN OF OVERPRESSURES	262
8.4 PETROLEUM GEOLOGY	266
8.5 GEOTHERMICS	266
8.6 CROSS-FORMATIONAL FLOW	267
8.7 THESES	268
8.8 RECOMMENDATIONS.....	269
BIBLIOGRAPHY	273
APPENDIX 1: EXPLANATORY NOTES TO THE DATABASE CREATED AND USED FOR THIS STUDY INCLUDED ON THE ATTACHED CD-ROM.	303
APPENDIX 2: METHOD OF WELL-DATA SELECTION FOR CROSS SECTION CONSTRUCTION	305
APPENDIX 3: CALCULATION OF SPECIFIC STORAGE	309
APPENDIX 4: ESTIMATION OF THE HORIZONTAL TO VERTICAL STRESS RATIO.....	311

LIST OF TABLES

Table 2.1: Characteristic porosity (ϕ) and permeability (k) of petroleum reservoir rocks in the Pannonian Basin.-----	50
Table 4.1: Salient pressure data from the Kiskunhalas region. -----	83
Table 4.2: Codes of fluid-potential maps and corresponding figure numbers. -----	98
Table 4.3: Selected location of $h(z)$ profiles along hydraulic cross sections and associated basement morphology.-----	134
Table 6.1: Codes of geothermal maps with mean temperature and mean gradient values. -----	182
Table 6.2: Estimated vertical seepage velocity and Péclet number across the Algyő and Endrőd Aquitards from well Tázlár-6.-----	221

LIST OF FIGURES

Figure 1.1: Erdélyi's schematic diagram of the flow pattern in the Great Hungarian Plain (Erdélyi, 1976); trace of cross section shown on Figure 2.2. -----	4
Figure 2.1: Regional geographic context and physiographic setting of the study area. -----	12
Figure 2.2: Basemap of the study area with geographic and EOVS co-ordinates. -----	14
Figure 2.3: Topography of the study area and names of main physiographic features. -----	16
Figure 2.4: Schematic sedimentological and stratigraphic profile across the Great Hungarian Plain. -----	17
Figure 2.5: Neogene tectonic scheme of the Alpine – Mediterranean region -----	19
Figure 2.6: Major tectono-stratigraphic units in the Pannonian Basin: the Alpine-North Pannonian and the Tisza units. -----	20
Figure 2.7: Proposed relative position of the tectono-stratigraphic units at the end of the Eocene “flysch” stage. -----	21
Figure 2.8: Proposed relative position of the tectono-stratigraphic units at the beginning of the Miocene: the “molasse” stage. -----	22
Figure 2.9: Evolutionary diagram of the Pannonian Basin and the correlation between the Mediterranean and Central Paratethys time scales. -----	23
Figure 2.10: Diagram showing the three stages of thrust belt and basin evolution. -----	24
Figure 2.11: Neogene tectonic features and regional pattern of compressional stresses of the Alpine-Mediterranean region. -----	25
Figure 2.12: Tectonic lineaments and sub-basins in the Pre-Neogene basement of the Great Hungarian Plain. -----	27
Figure 2.13: Recent configuration of the Pannonian Basin and the associated Alpine Mountain belt, with the pattern of the Quaternary vertical movements. ----	28
Figure 2.14: Average porosity-depth trends of a) shales and b) sandstones in the Great Hungarian Plain. -----	33
Figure 2.15: Average permeability-depth trends of shales and sandstones in the Great Hungarian Plain based on core-permeability measurements.-----	34

Figure 2.16: Relative frequency distribution of core-permeability anisotropy from Neogene sandstone reservoirs. -----	35
Figure 2.17: Schematic hydrostratigraphic profile across the Great Hungarian Plain. ----	36
Figure 2.18: Hydrostratigraphic chart of the Great Hungarian Plain. -----	37
Figure 2.19: Structure contour map of the base of Szolnok Aquifer / top of Endrőd Aquitard. -----	38
Figure 2.20: Isopach contour map of the Endrőd Aquitard.-----	40
Figure 2.21: Structure contour map of the base of Nagyalföld Aquifer / top of Algyő Aquitard. -----	41
Figure 2.22: Isopach contour map of the Algyő Aquitard. -----	42
Figure 2.23: Integrated interpretation of a reflection seismic profile and an electric log. -----	44
Figure 2.24: Index map of hydrocarbon fields discussed in the text. -----	47
Figure 2.25: Depth to the oil birth line ($R_0 = 0.6\%$ iso-reflectance surface) in the ESE-Great Hungarian Plain. -----	48
Figure 2.26: Petroleum migration systems postulated by Szalay (1993). -----	49
Figure 2.27: Distribution of known petroleum accumulations and their spatial relation with the oil birth line in the Great Hungarian Plain. -----	51
Figure 3.1: Areal distribution of wells with acceptable fluid pressure and stabilised water level measurements in eastern Hungary. -----	61
Figure 3.2: Relative frequency vs. depth distribution of wells with accepted stabilised water level and DST pressure data from all sources. -----	61
Figure 3.3: Relative frequency vs. depth distribution of wells with accepted stabilised water level data from VITUKI, Plc. and MÁFI.-----	62
Figure 3.4: Relative frequency vs. depth distribution of wells with accepted drill-stem test (DST) pressure data from MOL, Plc. -----	62
Figure 3.5: Distribution of temperature data from Dövényi and Horváth (1988). -----	64
Figure 4.1a: Distribution of hydraulic head, flow systems, and hydraulic regimes, and the corresponding $p(d)$ profiles in a “unit basin.” -----	71

Figure 4.1b: Distribution of hydraulic head, flow systems, and hydraulic regimes, and the corresponding $p(d)$ in a “complex basin.”	72
Figure 4.2: Name, extent, and figure number of selected $p(z)$ profiles discussed in text, and Tari’s (1994) seismic profile.	74
Figure 4.3: Schematic block diagram of the tomographic maps.	76
Figure 4.4: Index map of regional hydraulic cross sections, and location of hydraulic head vs. elevation profiles.	78
Figure 4.5: $p(z)$ profile in the Debrecen region.	80
Figure 4.6: $p(z)$ profile in the Gödöllő region.	81
Figure 4.7: $p(z)$ profile in the Kecskemét region.	82
Figure 4.8: $p(z)$ profile in the Kiskunhalas region.	84
Figure 4.9: $p(z)$ profile in the Algyő region.	85
Figure 4.10: $p(z)$ profile in the Újkígyós region.	87
Figure 4.11: $p(z)$ profile in the Szentes - Csongrád region.	88
Figure 4.12: $p(z)$ profile in the Endrőd - Szarvas region.	90
Figure 4.13: $p(z)$ profile in the Dévaványa region.	92
Figure 4.14: $p(z)$ profile in the Földes region.	93
Figure 4.15: $p(z)$ profile in the Biharkeresztes region.	94
Figure 4.16: Interpreted reflection seismic profile across the Derecske Trough and the Komádi High in the Biharkeresztes region.	95
Figure 4.17: $p(z)$ profile in the Ruzsa - Üllés region.	96
Figure 4.18: Tomographic fluid-potential map based on data from wells shallower than 40 m: $h_{z0,04}$.	99
Figure 4.19: Tomographic fluid-potential map based on data from wells deeper than 40 m and elevation heads greater than sea level: $h_{04,0}$.	100
Figure 4.20: Tomographic fluid-potential map of the $z = 0$ (sea level) to -100 m elevation interval: $h_{0,1}$.	101
Figure 4.21: Tomographic fluid-potential map of the $z = -100$ m to -300 m elevation interval and hydrocarbon accumulations: $h_{1,3}$.	102
Figure 4.22: Distribution of regional groundwater regimes in eastern Hungary inferred from fluid-potential maps and $p(z)$ profiles.	103

Figure 4.23: Tomographic fluid-potential map of the $z = -300$ m to -600 m elevation interval and hydrocarbon accumulations: h_{3,6} .	----- 105
Figure 4.24: Tomographic fluid-potential map of the $z = -600$ m to -1000 m elevation interval and hydrocarbon accumulations: h_{6,10} .	----- 107
Figure 4.25: Tomographic fluid-potential map of the $z = -1000$ m to -1500 m elevation interval and hydrocarbon accumulations: h_{10,15} .	----- 108
Figure 4.26: Tomographic fluid-potential map of the $z = -1500$ m to -1900 m elevation interval and hydrocarbon accumulations: h_{15,19} .	----- 109
Figure 4.27: Tomographic fluid-potential map of the $z = -1900$ m to -2200 m elevation interval and hydrocarbon accumulations: h_{19,22} .	----- 110
Figure 4.28: Tomographic fluid-potential map of the $z = -2200$ m to -2500 m elevation interval and hydrocarbon accumulations: h_{22,25} .	----- 111
Figure 4.29: Tomographic fluid-potential map of the $z = -2500$ m to -2800 m elevation interval and hydrocarbon accumulations: h_{25,28} .	----- 112
Figure 4.30: Tomographic fluid-potential map of the $z = -2800$ m to -3100 m elevation interval and hydrocarbon accumulations: h_{28,31} .	----- 113
Figure 4.31: Tomographic fluid-potential map of the $z = -3100$ m to -3500 m elevation interval and hydrocarbon accumulations: h_{31,35} .	----- 114
Figure 4.32: Legend of symbols used on the hydraulic cross sections.	----- 119
Figure 4.33: Hydraulic cross section H1 and hydrocarbon accumulations (a 1:500 000 scale copy is included in the pocket).	----- 120
Figure 4.34: Hydraulic cross section H2 and hydrocarbon accumulations (a 1:500 000 scale copy is included in the pocket).	----- 121
Figure 4.35: Hydraulic cross section H3 and hydrocarbon accumulations (a 1:500 000 scale copy is included in the pocket).	----- 122
Figure 4.36: Hydraulic cross section H4 and hydrocarbon accumulations (a 1:500 000 scale copy is included in the pocket).	----- 123
Figure 4.37: Hydraulic cross section H5 .	----- 124
Figure 4.38: Hydraulic cross section H6 .	----- 125
Figure 4.39: Hydraulic cross section H7 and hydrocarbon accumulations (a 1:500 000 scale copy is included in the pocket).	----- 126

Figure 4.40: Hydraulic cross section H8 and hydrocarbon accumulations (a 1:500 000 scale copy is included in the pocket). -----	127
Figure 4.41: Hydraulic cross section H9 and hydrocarbon accumulations (a 1:500 000 scale copy is included in the pocket). -----	128
Figure 4.42: Hydraulic cross section H10 and hydrocarbon accumulations (a 1:500 000 scale copy is included in the pocket). -----	129
Figure 4.43: Schematic diagram of $h(z)$ profile preparation at a selected location (L) on a hydraulic cross section. -----	134
Figure 4.44: Hydraulic head vs. depth distribution associated with basement highs inferred from hydraulic cross sections. -----	136
Figure 4.45: Enlarged portion of figure 4.44. -----	137
Figure 4.46: Hydraulic head vs. depth distribution associated with basement depressions inferred from hydraulic cross sections. -----	138
Figure 4.47: Enlarged portion of figure 4.46. -----	139
Figure 4.48: Pressure and fluid flow distribution pattern in a sand/clay sequence containing a conduit fault. -----	142
Figure 5.1: Diagnostic $p(z)$ anomalies. -----	146
Figure 5.2: Kecskemét region: $p(z)$ profile and elevation of petroleum accumulations in a regional recharge area. -----	147
Figure 5.3: Biharkeresztes region: $p(z)$ profile and elevation of petroleum accumulations in a regional discharge area. -----	148
Figure 5.4: Dévaványa region: $p(z)$ profile and elevation of petroleum accumulations in a regional discharge area. -----	149
Figure 5.5: Endrőd region: $p(z)$ profile and elevation of petroleum accumulations in a regional discharge area. -----	150
Figure 5.6: Ruzsa - Úllés region: $p(z)$ profile and elevation of petroleum accumulations. -----	151
Figure 5.7: Kiskunhalas region: $p(z)$ profile and petroleum accumulations in a regional recharge area. -----	152
Figure 5.8: Ruzsa - Úllés region: $p(z)$ profile of initial gas and oil pool pressures. -----	153

Figure 5.9: Schematic illustration and classification of tomographic fluid-potential map anomalies ($h_{ij}(x,y) - DiPotAn-s$). -----	155
Figure 5.10: Schematic illustration and classification of hydraulic cross section anomalies, $H(L,z)-DiPotAn-s$.-----	158
Figure 6.1: Lateral distribution of average surface heat flow and the regional hydraulic regimes in Eastern Hungary.-----	167
Figure 6.2: Thermal conductivity of sandstones and shales. -----	170
Figure 6.3: Sketch of a leaky aquifer for the one-dimensional steady state heat transfer problem.-----	173
Figure 6.4: Type curves of Péclet numbers computed from equation (6.8).-----	174
Figure 6.5: Plot of hydraulic conductivity vs. total hydraulic head change for various Péclet numbers (equation 6.6).-----	176
Figure 6.6: Plot of hydraulic conductivity vs. total hydraulic head change for various values of the modified Péclet number at depth/length = 0.1.-----	177
Figure 6.7: Plot of hydraulic conductivity vs. total hydraulic head change for various values of the modified Péclet number at depth/length = 0.01. ----	178
Figure 6.8: Index map of temperature versus depth profiles and traces of geothermal cross sections. -----	183
Figure 6.9: Temperature vs. depth plot of all data from Eastern Hungary. -----	184
Figure 6.10: Temperature vs. depth plot in the Kecskemét region. -----	185
Figure 6.11: Temperature vs. depth plot in the Kiskunhalas - Tázlár region. -----	186
Figure 6.12: Temperature vs. depth plot in the Szeged-Algyő region. -----	188
Figure 6.13: Temperature vs. depth plot in the Szentes -Csongrád region. -----	189
Figure 6.14: Temperature vs. depth plot in the Endrőd-Szarvas region. -----	190
Figure 6.15: Temperature vs. depth plot in the Dévaványa. -----	191
Figure 6.16: Temperature vs. depth plot in the Biharkeresztes region.-----	193
Figure 6.17: Temperature vs. depth and thermal gradient vs. depth profiles of data from the Pusztaföldvár-1 well. -----	194
Figure 6.18: Distribution of subsurface temperature and hydrocarbon accumulations in the $z = -100$ to -300 m elevation range: $T_{1,3}$.-----	197

Figure 6.19: Distribution of subsurface temperature and hydrocarbon accumulations in the z = -300 to -600 m elevation range: $T_{3,6}$.	198
Figure 6.20: Distribution of subsurface temperature and hydrocarbon accumulations in the z = -600 to -1000 m elevation range: $T_{6,10}$.	199
Figure 6.21: Distribution of subsurface temperature and hydrocarbon accumulations in the z = -1000 to -1500 m elevation range: $T_{10,15}$.	200
Figure 6.22: Distribution of subsurface temperature and hydrocarbon accumulations in the z = -1500 to -1900 m elevation range: $T_{15,19}$.	201
Figure 6.23: Distribution of subsurface temperature and hydrocarbon accumulations in the z = -1900 to -2200 m elevation range: $T_{19,22}$.	202
Figure 6.24: Distribution of subsurface temperature and hydrocarbon accumulations in the z = -2200 to -2500 m elevation range: $T_{22,25}$.	203
Figure 6.25: Distribution of subsurface temperature and hydrocarbon accumulations in the z = -2500 to -2800 m elevation range: $T_{25,28}$.	204
Figure 6.26: Distribution of subsurface thermal gradient and hydrocarbon accumulations in the z = -100 to -300 m elevation range: $gradT_{1,3}$.	205
Figure 6.27: Distribution of subsurface thermal gradient and hydrocarbon accumulations in the z = -300 to -600 m elevation range: $gradT_{3,6}$.	206
Figure 6.28: Distribution of subsurface thermal gradient and hydrocarbon accumulations in the z = -600 to -1000 m elevation range: $gradT_{6,10}$.	207
Figure 6.29: Distribution of subsurface thermal gradient and hydrocarbon accumulations in the z = -1000 to -1500 m elevation range: $gradT_{10,15}$.	208
Figure 6.30: Distribution of subsurface thermal gradient and hydrocarbon accumulations in the z = -1500 to -1900 m elevation range: $gradT_{15,19}$.	209
Figure 6.31: Distribution of subsurface thermal gradient and hydrocarbon accumulations in the z = -1900 to -2200 m elevation range: $gradT_{19,22}$.	210
Figure 6.32: Distribution of subsurface thermal gradient and hydrocarbon accumulations in the z = -2200 to -2500 m elevation range: $gradT_{22,25}$.	211
Figure 6.33: Distribution of subsurface thermal gradient and hydrocarbon accumulations in the z = -2500 to -2800 m elevation range: $gradT_{25,28}$.	212
Figure 6.34: Geothermal cross section $T1-T1'-T1''$ and hydrocarbon accumulations (a 1:500 000 scale copy is included in the pocket).	214

Figure 6.35: Geothermal cross section T2-T2'-T2'' and hydrocarbon accumulations (a 1:500 000 scale copy is included in the pocket). -----	215
Figure 6.36: Geothermal cross section T3-T3'-T3'' and hydrocarbon accumulations (a 1:500 000 scale copy is included in the pocket). -----	216
Figure 6.37: Geothermal cross section T4-T4'-T4'' and hydrocarbon accumulations (a 1:500 000 scale copy is included in the pocket). -----	217
Figure 7.1: Graphic solution of the one-dimensional flow equation for vertical compaction by Bredehoeft and Hanshaw (1968). -----	230
Figure 7.2: p(d) profile of calculated compactional overpressures and observed anomalous pressures. -----	236
Figure 7.3: Schematic diagram of hydrostatic overpressuring due to buoyancy in a) gas accumulation and b) oil + gas accumulation. -----	246
Figure 7.4: Orientation of the Recent maximum horizontal compressive stress (σ_1) axis in and around the Pannonian Basin based on field observations-----	249
Figure 7.5: Structural features in the Derecske Trough interpreted from reflection seismic profile.-----	251
Figure 7.6: Structural features in the Földes region interpreted from reflection seismic profile.-----	252
Figure 7.7: Sources of recent compressive stress in the Pannonian region. -----	253
Figure A2.1: Schematic diagram of co-ordinate rotation and calculation of well location along and from a cross section (AB).-----	306

LIST OF PLATES INCLUDED IN THE POCKET

Figure 4.33: Hydraulic cross section **H1** and hydrocarbon accumulations at 1:500 000 horizontal scale.

Figure 4.34: Hydraulic cross section **H2** and hydrocarbon accumulations at 1:500 000 horizontal scale.

Figure 4.35: Hydraulic cross section **H3** and hydrocarbon accumulations at 1:500 000 horizontal scale.

Figure 4.36: Hydraulic cross section **H4** and hydrocarbon accumulations at 1:500 000 horizontal scale.

Figure 4.39: Hydraulic cross section **H7** and hydrocarbon accumulations at 1:500 000 horizontal scale.

Figure 4.40: Hydraulic cross section **H8** and hydrocarbon accumulations at 1:500 000 horizontal scale.

Figure 4.41: Hydraulic cross section **H9** and hydrocarbon accumulations at 1:500 000 horizontal scale.

Figure 4.42: Hydraulic cross section **H10** and hydrocarbon accumulations at 1:500 000 horizontal scale.

Figure 6.34: Geothermal cross section **T1-T1'-T1''** and hydrocarbon accumulations at 1:500 000 horizontal scale.

Figure 6.35: Geothermal cross section **T2-T2'-T2''** and hydrocarbon accumulations at 1:500 000 horizontal scale.

Figure 6.36: Geothermal cross section **T3-T3'-T3''** and hydrocarbon accumulations at 1:500 000 horizontal scale.

Figure 6.37: Geothermal cross section **T4-T4'-T4''** and hydrocarbon accumulations at 1:500 000 horizontal scale.

LIST OF SYMBOLS

SYMBOL	S.I. UNITS	DESCRIPTION
∇		Nabla operator, gradient
$[\varepsilon]$		Strain tensor
$[\sigma]$		Internal stress tensor
C	J/kg°C mg/l	In Chapter 6: heat capacity In Chapter 7: solute concentration
c	1/s	Hydraulic resistance ($= K/l_s$)
d	m or km	Depth (if not specified otherwise)
E	Pa	Young's modulus
$\frac{gradT}{\nabla T}$ or	°C/km or K/km	Thermal gradient
h	m	Hydraulic head relative to mean sea level
K	m/s	Hydraulic conductivity
k	m ²	Permeability
k_h	m ²	Horizontal permeability
k_v	m ²	Vertical permeability
L	km	Horizontal distance along cross sections
l_s	m	Sediment thickness
l_w	m	Water level relative to ground surface, positive above ground surface, negative below ground surface
N_p	-	Modified Péclet number
p	Pa (or MPa)	Pore pressure
P_e	-	Péclet number

SYMBOL	S.I. UNITS	DESCRIPTION
γ_{nom}	MPa/km	Nominal hydrostatic gradient for freshwater ($\rho_w=1000 \text{ kg/m}^3$)
γ_{st}	MPa/km	Hydrostatic fluid pressure gradient
κ	W/m K	Thermal conductivity
μ	kg/m s	Dynamic viscosity
ν		Poisson's ratio
θ	W/m ²	Heat flow
ρ_f	kg/m ³	Fluid density (in general)
ρ_{gas}	kg/m ³	Gas density
ρ_{oil}	kg/m ³	Oil density
ρ_s	kg/m ³	Bulk density of sediments
ρ_w	kg/m ³	Fresh water density
σ_h	Pa	Principal horizontal stress
σ_m	Pa	Mean principal stress
σ_T	Pa	Total stress
σ_v	Pa	Principal vertical stress
τ_L	m	Lithospheric thickness
ω	m ² /s	In Chapter 6: thermal diffusivity
	m/Myr	In Chapter 7: sedimentation rate
σ_l	Pa	Maximum principal compressive stress

Ma = "mega annum before present" = "million years ago"; it refers to age

Myr = "mega years" = million years, it refers to a time period or arbitrary duration of a process

SYMBOL	S.I. UNITS	DESCRIPTION
p_o	Pa (or MPa)	Overpressure, pressure in excess of hydrostatic
q	m/s	Specific discharge, flux
R_o	%	Vitrinite reflectance
R_a	-	Rayleigh number
S_s	-	Specific storage
T	°C or K	Temperature
t	s	Time
$Tr[]$		Trace of tensor = sum of members along principal diagonal
v	m/s	Fluid flow velocity
z	m	Elevation head relative to sea level, positive above sea level
z_o	m	Ground surface elevation relative to mean sea level
Φ	m ² /s ²	Fluid-potential
Γ	1/s	Geologic forcing
Γ_D		Dimensionless geologic forcing
α_c	L/mg	Density coefficient due to salinity changes
α_p	Pa ⁻¹	Compressibility of porous media
α_T	°C ⁻¹ or K ⁻¹	Coefficient of thermal expansion of porous media
δ_i^j		Kronecker-delta; $\delta_i^j = 1$ if $i = j$, and $\delta_i^j = 0$ if $i \neq j$
ϕ	%	Porosity
γ	MPa/km	Vertical fluid pressure gradient
γ_{dyn}	MPa/km	Vertical dynamic fluid pressure gradient

LIST OF ABBREVIATIONS

DST	= Drill-Stem Test
EOV	= Uniform National Projection System = Egységes Országos Vetületi Rendszer
Fm.	= Formation
HC	= hydrocarbon
HTPM	= Hydraulic Theory of Petroleum Migration
MÁFI	= Hungarian Geological Institute = Magyar Állami Földtani Intézet
MOL, Plc.	= Hungarian Oil and Gas Co., Plc. = Magyar Olaj és Gázipari, Rt.
TWT	= two-way travel time
VITUKI, Plc.	= Research Institute for Water Resources, Plc. = Vízgazdálkodási Tudományos Kutató Intézet, Rt.
VIFIR	= digital water well database of VITUKI, Plc.

Subscripts:

D	= discharge
dyn	= dynamic
f	= fluid
M	= Midline
m	= matrix
nom	= nominal
n	= nominal
obs	= observed (or measured) directly in the field
R	= recharge
ref	= reference
st	= static or hydrostatic (as defined where it occurs)
w	= water

1 INTRODUCTION

1.1 CONCEPTUAL FRAMEWORK

Moving groundwater is an active “geologic agent” for two fundamental reasons: first, it is able to interact with the environment through a host of physical, chemical, and kinetic processes; second, groundwater flow is distributed in space in nested systems of different hierarchical order (Tóth, 1984, 1999). Groundwater flow and its interaction with the environment occur simultaneously at every spatial and temporal scale, but with intensities and rates that are scale dependent. Therefore, the environmental effects of moving groundwater, which span over human and geologic time scales, can be detected/inferred everywhere in the porous subsurface. Due to the ability of groundwater flow to transport matter and energy, the effects of interaction with the environment are cumulative and systematically distributed. The environmental effects of groundwater flow are expressed by a large variety of natural phenomena that can be grouped as hydrologic, vegetal, pedologic, geomorphic, chemical-mineralogical, and also by transport and accumulation (Tóth, 1999). The system-nature of subsurface water flow in drainage basins was recognised and enunciated in the theory of gravity-drive flow by Tóth (1963). This theory provides a unifying conceptual framework for the analysis and interpretation of the various natural processes and phenomena related to the interaction of water with the rock framework. A fundamental assumption is that the rock framework has a finite permeability and it is hydraulically continuous (Tóth, 1967, 1995).

The ability of groundwater to mobilise, transport, and accumulate matter is of particular interest in the scope of mineral and petroleum exploration. Tóth’s (1980) Hydraulic Theory of Petroleum Migration (HTPM) postulates that in “geologically mature” (i.e., non-deforming) intermontane sedimentary basins, gravity-driven groundwater flow is an active transport agent of matter and energy, which controls the migration, accumulation, and entrapment of hydrocarbons. Hydrocarbon migration takes place along well-defined flow paths from source or carrier beds toward discharge areas or regions of convergent flow. *“The mechanism becomes operative after compaction of sediments and the concomitant primary migration cease, and subaerial relief develops”*

(Tóth, 1980, p. 121). Hydrocarbons may accumulate in locations where the hydraulic, hydrodynamic, sedimentologic, and structural factors are favourable. According to the HTPM, hydrocarbon pools are expected to be preferentially associated with stagnant zones, ascending limbs of flow systems or discharge areas, and artesian conditions. Such sites are characterised by relative potentiometric minima, reduced or zero lateral hydraulic gradients, high water salinity, and positive geothermal anomalies. The HTPM was successfully applied in basins with consolidated lithology, for instance in the Rhine Graben rift basin (Otto, 1992) and the Western Canada Sedimentary Basin (e.g., Garven, 1989; Barson, 1993; Rostron, 1995). Application of hydrogeological principles and techniques to petroleum exploration, i.e., petroleum hydrogeology, is a relatively new 'exploration tool,' which has gained acceptance among the traditional geological and geophysical methods. Nowadays, the techniques of petroleum hydrogeology are routinely used in Canada, the United States, Australia, and in the North Sea.

To date, there are no published accounts of the HTPM being applied and tested in sedimentary basins that are actively deforming and where sediment consolidation is in progress. In Neogene sedimentary basins, several ongoing geological processes act as energy sources for fluid flow (e.g., vertical and/or lateral compaction), which generate disequilibrium conditions (Neuzil, 1995). Thus, adjustment of pore pressures to the present-day water table relief and development of regional topography driven flow systems may be in progress; if equilibrium conditions were already achieved, then the gravity-driven flow systems may be altered by mechanisms of sub-recent activity. As a result, the gravity flow systems will have a spatial extent limited or modified by natural transient effects. Also, the role of gravity-driven flow systems in the migration and spatial (re)distribution of hydrocarbons can be subdued by transient flow (Tóth and Corbet, 1986; Neuzil, 1995). Whatever the flow driving forces may be, hydraulic transport mechanisms are believed to have a determinant effect on the distribution of matter and heat, even in deforming porous media. Several deforming Neogene sedimentary basins are prolific petroleum provinces, notably the Gulf of Mexico, Niger delta, Caspian basin, Orinoco delta, and Indus delta. Therefore, it is of paramount importance to understand the hydraulic conditions of such basins in order to facilitate prediction of potential migration paths and favourable locations for petroleum accumulation. One of the most extensively studied active basins where disequilibrium

conditions prevail is the Gulf of Mexico basin (e.g., Bredehoeft and Hanshaw, 1968; Bethke, 1989; Harrison and Summa, 1991).

1.2 PROBLEMS

Few tectonically active intermontane sedimentary basins have been explored in sufficient detail to allow comprehensive regional scale petroleum hydrogeological investigations. In this respect, the Pannonian Basin in Central-Eastern Europe is an exception. This is a well-explored Neogene intermontane sedimentary basin, which is currently undergoing tectonic deformation, and where consolidation of sediments is in progress. Over the past ~150 years extensive field and laboratory data were acquired by the petroleum and mining industry, the Hungarian Geological Institute (MÁFI), the Research Institute for Water Resources (VITUKI, Plc.), by subsidiaries of these companies/institutes, as well as by private companies. The nature of data and the explored depth ranges in the basin varied according to the profile of each company or institute. Thus, the potentially available data for the Pannonian Basin make it ideal for investigating certain manifestations of groundwater flow as an active geologic agent within the scope of hydrocarbon exploration in an actively deforming intermontane sedimentary basin. A practical problem related to the potentially available data in the basin was their accessibility, as the data acquired by the various companies and institutes were not shared, nor fully accessible for independent scientific research, because of proprietary and confidentiality reasons. This unfortunate situation hindered the development of a more thorough understanding of several aspects of the basin's evolution, relative to the potential knowledge that could be gained, if all the available information were accessible. On the positive side, the published results of several local scale investigations and theoretical research contributed to our current understanding of hydrogeologic features of the basin. Rónai (1961, 1978, and 1985) and Erdélyi (1976) made significant early attempts for regional hydrogeologic characterisation of the Great Hungarian Plain.

Ample evidence has been presented to indicate the existence of gravity-driven flow systems to a depth of about 500 to 1800 m in the basin (e.g., Rónai, 1961, 1985).

Erdélyi (1976) was the first to recognise the existence of gravity-driven flow systems within the Great Hungarian Plain (eastern Pannonian Basin) (Figure 1.1). He explained the observed hydrochemical and geothermal phenomena as the result of interaction between the moving groundwater and the rock framework. Prior to Erdélyi (1976), the system-nature of subsurface water flow (*sensu* Tóth, 1962, 1963) and gravity as a flow driving force was not recognised or accepted by the Hungarian hydrogeological community. For instance, the artesian conditions characteristic of the Great Hungarian Plain and the pore pressure distribution were correlated with the lithology of aquifers (Urbancsek, 1963, 1978), the high temperature, the overburden pressure, and the high dissolved gas content of groundwater (Rónai, 1978, 1985).

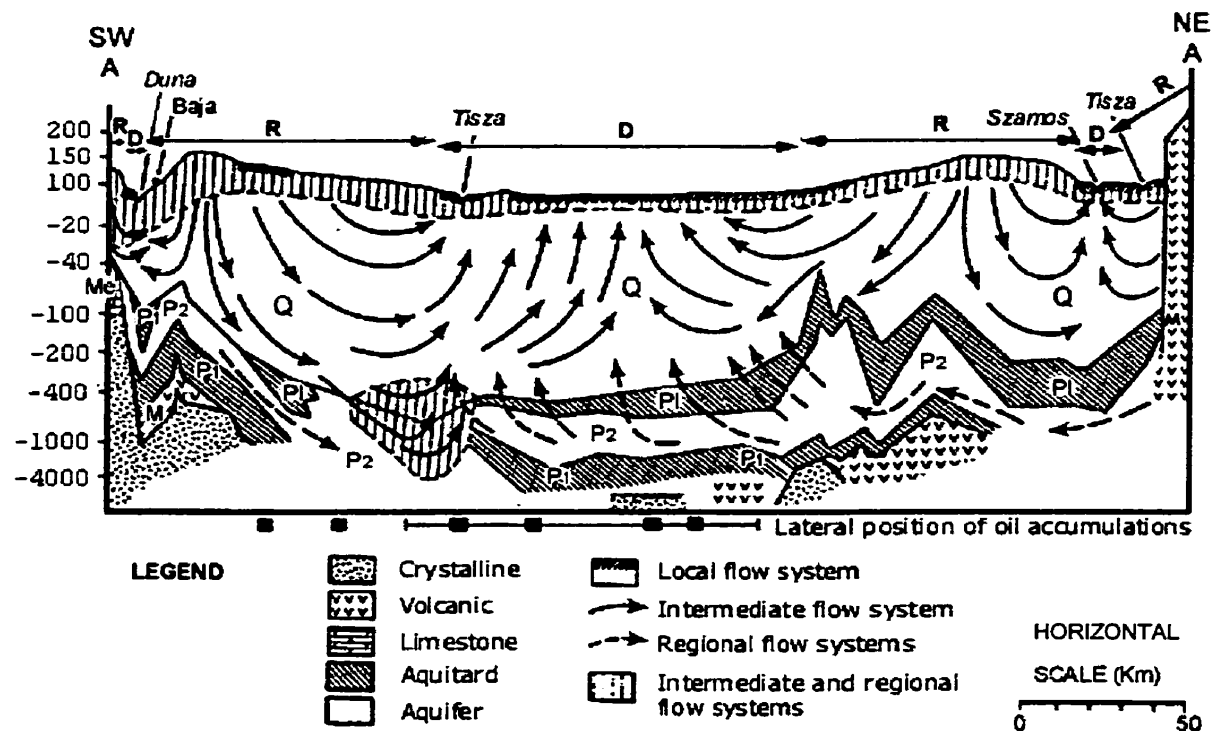


Figure 1.1: Erdélyi's schematic diagram of the flow pattern in the Great Hungarian Plain (after Erdélyi, 1976). The trace of the cross section is shown on Figures 2.2, p.14. Abbreviations: D = discharge, R = recharge, Q = Quaternary, P1 = Pliocene, P₁ = Lower Pannonian, P₂ = Upper Pannonian, M = Miocene, Me = Mesozoic

An overpressured regime exists in the Great Hungarian Plain below a depth of ~1800 m, with excess pressures of 1 to >30 MPa above hydrostatic (Somfai, 1970). This regime was believed to be the result of vertical compaction due to fast sedimentation

rates (up to ~7000 m thick clastic sedimentary pile deposited during the last 17 Ma) accompanied by aquathermal pressuring within sealed compartments (Somfai, 1976; Szalay, 1982, 1983, 1988) and kerogen transformation (Spencer et al., 1994). More recently, van Balen and Cloetingh (1994) suggested that the overpressures in the Pannonian Basin could be due to tectonic control on sedimentation. According to their concept, subsidence in the central parts of the basin and uplift and erosion on the marginal areas during the past ~2.5 Myr was enhanced by regional horizontal compressive stress. As a result, the increased sedimentation rates and subsequent vertical compaction have generated the overpressures, which persist to date. The problem with the current understanding of the actual cause(s) of overpressures in the Great Hungarian Plain is that a distributed analysis of pressure distribution within the basin has not yet been carried out to verify whether or not there is plausible field evidence to support the above mentioned causes. Additionally, there is uncertainty regarding the possible 'lifetime' (time span from initiation to 100% dissipation) of overpressures in the Pannonian Basins. Can these overpressures be the result of geologic processes that ended over one million years ago? Or rather, are they the result of ongoing processes?

Most petroleum accumulations in the Pannonian Basin were discovered below regional topographic depressions, and several accumulations are known to be associated with positive geothermal anomalies and relatively high water salinity (Boldizsár, 1959, 1966; Schmidt, 1962; Stegena, 1966; Bérczi and Kókai, 1978). These characteristics are in agreement with the predictions of the HTPM regarding the auxiliary phenomena expectably associated with petroleum accumulations. Based on the above observations, Erdélyi (1976) suggested that accumulation of petroleum in the Great Hungarian Plain is determined by fluid-potential configurations related to gravity-driven flow systems. In fact, the known petroleum accumulations are predominantly within the depth range of the overpressured regime (Somfai, 1994; Spencer et al., 1994). Szalay (1983, 1988) and Szalay and Koncz (1991, 1993) argued that petroleum migration was governed by compactional fluid flow from the deep grabens upwards and laterally toward the graben-flanks, and that "impervious" shales facilitated petroleum entrapment.

Anomalous pressures can be maintained over geologic time scales if the diffusion properties of the rock-fluid system permit it (Tóth and Millar, 1983; Neuzil and Pollock, 1983). Also, maintenance of overpressures depends on the lifetime, vigour, and spatial

distribution of the pressure-energy sources (Neuzil, 1995). By accepting Szalay's (1983, 1988) compactional migration model to explain the early stages of petroleum migration and accumulation, and viewing overpressures as transient phenomena over geologic time (Neuzil, 1995), a few fundamental questions arise. Namely, what is the relationship between the present day groundwater flow field and the distribution of HC's in the Great Hungarian Plain? In addition, is there, indeed, a direct cause-and-effect relationship between the present-day gravity-driven flow systems and the loci of known petroleum accumulation in the Great Hungarian Plain? From the petroleum exploration viewpoint the essential question is: -where are the locations favourable for petroleum accumulation in the basin under the present-day hydrodynamic conditions? To answer the above questions, a rigorous three-dimensional characterisation of the present-day flow field is required, based on direct field observations and measurements of pore pressure and permeability distribution.

Currently, there is no published comprehensive study presenting a systematic three-dimensional characterisation of the fluid flow field in the Great Hungarian Plain from the surface to the maximum explored depths based on all hydrogeological and petroleum industry data. Earlier hydrogeological studies were spatially limited to the upper 500 to ~1000 m depth of the Great Hungarian Plain because of constraints on data accessibility. Only conceptual and numerical models were prepared for the gravity-driven flow regime (Erdélyi, 1976; Galsa, 1998) and the overpressured regime (van Balen and Cloetingh, 1994; Lenkey, 1999); the latter focussed on the effects of vertical compaction.

1.3 OBJECTIVES

The present thesis attempts to address some of the problems and questions discussed in the previous section by:

- 1) Compiling a database of relevant hydrogeologic data (water level measurements, pore pressure data from drill-stem tests, geological formation limits, porosity, permeability, formation water temperature, hydrochemistry) from all possible sources (partially reported in Tóth and Almási, 1998).

- 2) Characterising the fluid-potential field in ‘three-dimensions’ based on measured values of pore pressure and water level, and updating Erdélyi’s (1976) model (partially reported in Tóth and Almási, 1998).
- 3) Identifying and explaining fluid-potential configuration patterns that are most likely associated with petroleum accumulations, i.e., finding fluid-potential configurations that are diagnostic for the prediction of prospective areas (partially reported in Tóth and Almási, 1998).
- 4) Evaluating the most likely mechanism(s) responsible for the creation and maintenance of the observed anomalous pressure regime, based on theoretical considerations and field observations.
- 5) Characterising the geothermal field using temperature measurements, and evaluating the possible coupled relations between the geothermal field and the fluid flow field, as well as evaluating the possibility of using geothermal information to petroleum exploration.
- 6) Synthesising the results with emphasis on aspects related to petroleum exploration.

1.4 WORKING HYPOTHESES

The initial principal working hypothesis was that cross-formational gravity-flow of formation waters has a determinant effect on the spatial positioning of petroleum accumulations in the Great Hungarian Plain. Additional hypotheses were formulated:

- The regional rock framework is hydraulically continuous;
- The Upper Pannonian and Quaternary sedimentary units act as an unconfined aquifer at regional scale, and as a layered aquifer system at local scale;
- Regional groundwater flow is driven primarily by gravity, secondarily by lateral lithospheric compression;
- Forced heat convection is an important heat transfer mechanisms in the Great Hungarian Plain.

1.5 OUTLINE OF THESIS

Chapter 2 provides a comprehensive overview of the Hydrogeologic Environment of the Great Hungarian Plain. It is a concise summary of the present knowledge and understanding of the basin's evolution, sedimentology, hydrostratigraphy, and petroleum geology, based on literature review. Details of the database compiled for this study are presented and discussed in Chapter 3. The database is included in digital format as ASCII text files and MS Excel 97 files on the attached CD-ROM, and instructions are provided in Appendix I.

In Chapter 4, the methodology applied for the characterisation of the fluid flow field is described. The essential observations from pressure-elevation profiles, fluid-potential maps, and hydraulic cross sections are discussed, and the interpretation of observed patterns is presented. The three-dimensional groundwater flow field presented here is the 'core' of the entire work. The spatial correlation between the present-day flow field and petroleum accumulation is examined in Chapter 5. Observed fluid-potential anomaly patterns are discussed, which are believed to be diagnostic for petroleum accumulations.

The possible coupled relations between the groundwater flow field and the geothermal field of the Great Hungarian Plain are investigated in Chapter 6. The possible role of groundwater flow in the regional heat transfer is investigated, and local indirect evidence is found for cross-formational flow across the regional aquitards. The probable causes of overpressures in the basin are evaluated in Chapter 7 by comparing theoretically expected manifestations of different mechanisms with the available field observations and patterns of the regional groundwater flow field. The Quaternary to Recent regional tectonic compression is found to be the most plausible mechanism to explain the cause of present-day overpressures in the basin. This conclusion is the central thesis of this work. Chapter 8 presents the synthesis of observations and interpretations discussed in the previous Chapters. Additional calculations and a method used for selection of wells for cross section construction is also presented in the appendices.

1.6 PROJECT HISTORY

In 1993, Dr. József Tóth submitted a research project proposal on the application of hydrogeological principles and methods for petroleum exploration in the Great Hungarian Plain to the Hungarian National Oil and Gas Co. (MOL, Plc.). MOL, Plc. embraced the idea of the project, and helped Dr. Tóth to recruit potential candidates to participate in this project as graduate students at the University of Alberta, Edmonton, working towards a doctoral degree. In September 1994, Dr. Tóth held an intensive course in Petroleum Hydrogeology in Budapest, Hungary, at MOL headquarters. On that occasion, the applicants – including the author of this work - were introduced to the principles of hydrogeology. Following a screening process, the Department of Earth and Atmospheric Sciences accepted the author's application, in March, 1995, and he started his work in July, 1995. Practically, the project started in April, 1995, during Dr. Tóth's visit to Hungary. The April, 1995 – January, 1998 period was dedicated to data acquisition and preliminary data analysis. Meanwhile, the MOL representatives and the "UofA-Group" held annual meetings and presented progress reports in Edmonton and at MOL headquarters in Hungary. The "productive stage" lasted from January to August, 1998. The first draft of the summary report was delivered to MOL in 1998 August 30 – on the due date. Following a review process and consultation with exploration specialists from MOL, the finalised version of the project report was delivered in 1998 November 15 (Tóth and Almási, 1998). The present thesis is an account of the author's individual work complemented with significant results of the above industrial project.

2 STUDY AREA: THE GREAT HUNGARIAN PLAIN, EASTERN PANNONIAN BASIN, HUNGARY

2.1 PHYSIOGRAPHIC SETTING

The Pannonian Basin is located in the eastern part of Central Europe. It is encircled by the Carpathian Mountains to the north and east, by the Dinarids to the south and by the Southern and Eastern Alps to the west (Figure 2.1). While the average elevation of the surrounding mountains is above 1000 m (Carpathians: ~1500 m a.s.l.; Dinarids: ~1000 m a.s.l.; Alps: ~2000 m a.s.l.), the average elevation of the Pannonian Basin is only about 150 m a.s.l. A few isolated mountains emerge from the plains with maximum elevations up to 1015 m, which divide the Pannonian Basin into smaller basins. The north-western part of the basin between the westernmost end of the Carpathians, the Eastern Alps, and the Transdanubian Central Range is called the Danube Basin, or Little Hungarian Plain (top of Figure 2.1). The Great Hungarian Plain occupies the largest area in the central part of the Pannonian Basin. The Transylvanian Basin lies between the Apuseni Mountains and the Eastern and Southern Carpathians; it belongs to the Pannonian Basin only in a wider sense.

Two major rivers flow across the intra-Carpathian region, the Danube and the Tisza (Figure 2.1). The Danube (in Hungarian “Duna”) is the largest river that enters the Pannonian Basin at its north-western end; it flows about 200 km eastward across the Danube Basin then it turns south. The source area of the Tisza is between the Western and Eastern Carpathians. It enters into the Pannonian Basin from the north-east, flows southward across the Great Hungarian Plain and discharges into the Danube. The other rivers that contribute to the drainage of the Great Hungarian Plain are the Zagyva, Berettyó, Körös, and Maros (Figure 2.1). These rivers are tributaries of the Tisza. Several lakes are scattered around the Pannonian Basin; Lake Balaton is the largest, and Lake Fertő is the second largest (Figure 2.1).

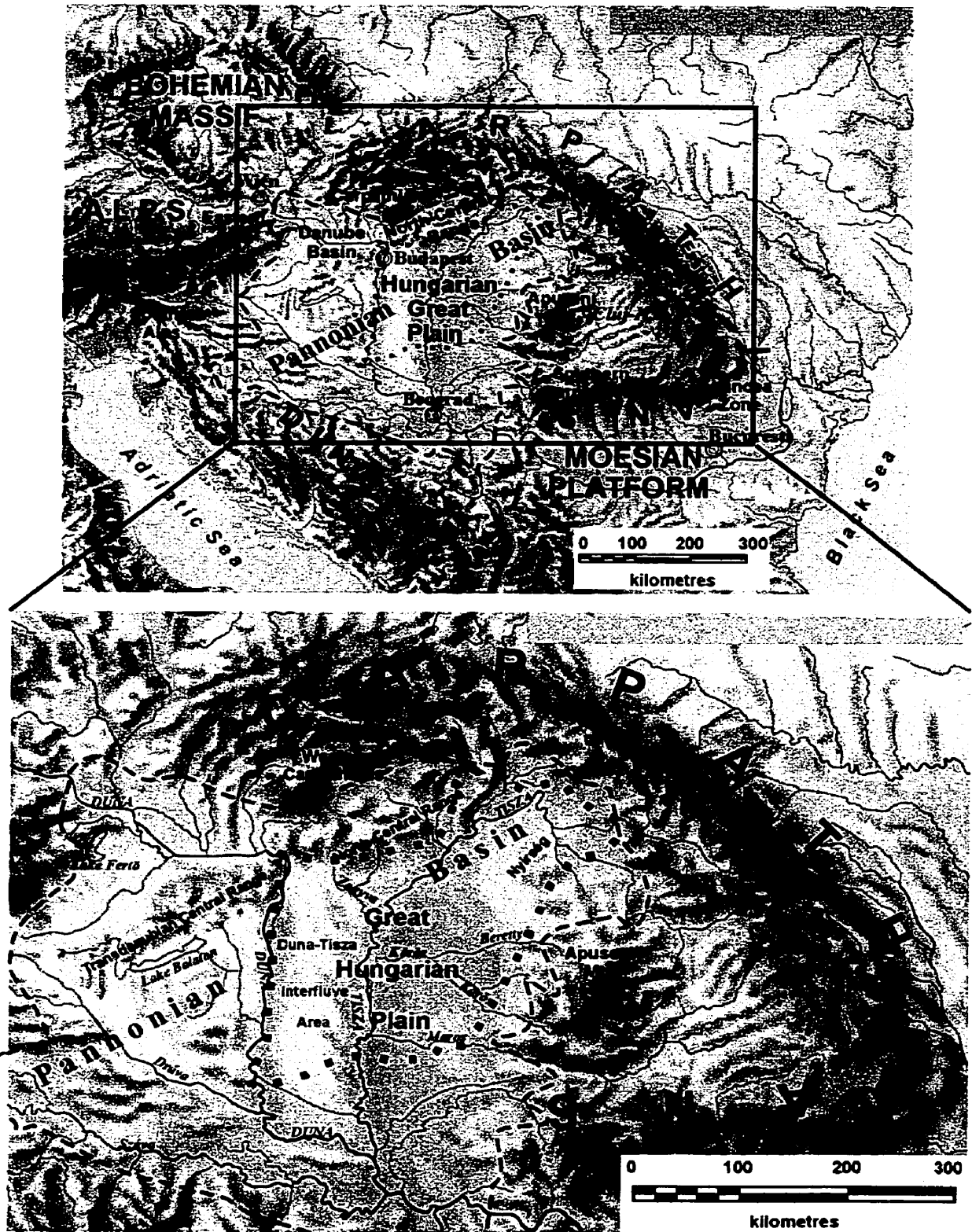


Figure 2.1: Regional geographic context and physiographic setting of the study area. The thick dashed line shows the boundary of the Pannonian Basin, and the study area is outlined by the thick dotted line (basemap modified after Zentay, 1996).

2.2 LIMITS OF THE STUDY AREA

The study area is approximately 45 000 km². It is delimited by the Danube to the west, the foothills of the North Central Range and by the actual state borders of Hungary, Slovakia, Ukraine, Romania, and Serbia to the north, north-east, east, and south, respectively (Figure 2.1 and 2.2). Throughout this work, all land surveying information, such as location and elevation of observation points, are expressed in EOV co-ordinates (EOV = Egységes Országos Vetületi rendszer = Uniform National Projection system). The EOV system has its origin to the south-west of the Hungarian border so that surveying can be expressed with positive co-ordinates. The co-ordinate axes (Y_{EOV} , X_{EOV} , z_0) are orthogonal along which distances are expressed in metres (or kilometres). Y_{EOV} is easting, X_{EOV} is northing, and the elevation (z_0) is measured with reference to the mean level of the Baltic Sea. The following EOV co-ordinates limit the base map of the study area:

SW corner: $Y_{EOV} = 620$ km, $X_{EOV} = 60$ km;

NE corner: $Y_{EOV} = 940$ km, $X_{EOV} = 360$ km.

The corresponding geographic co-ordinates expressed in decimal degrees are posted at each corner of the reference map (Figure 2.2). The perimeter of the study area shown by the “dash-dash-dot-dot” line in Figure 2.2 is the same as the thick dotted line on the lower map in Figure 2.1. Thus, a correspondence can be made between the basemap (Figure 2.2) and the larger geographic context of the study area (Figure 2.1).

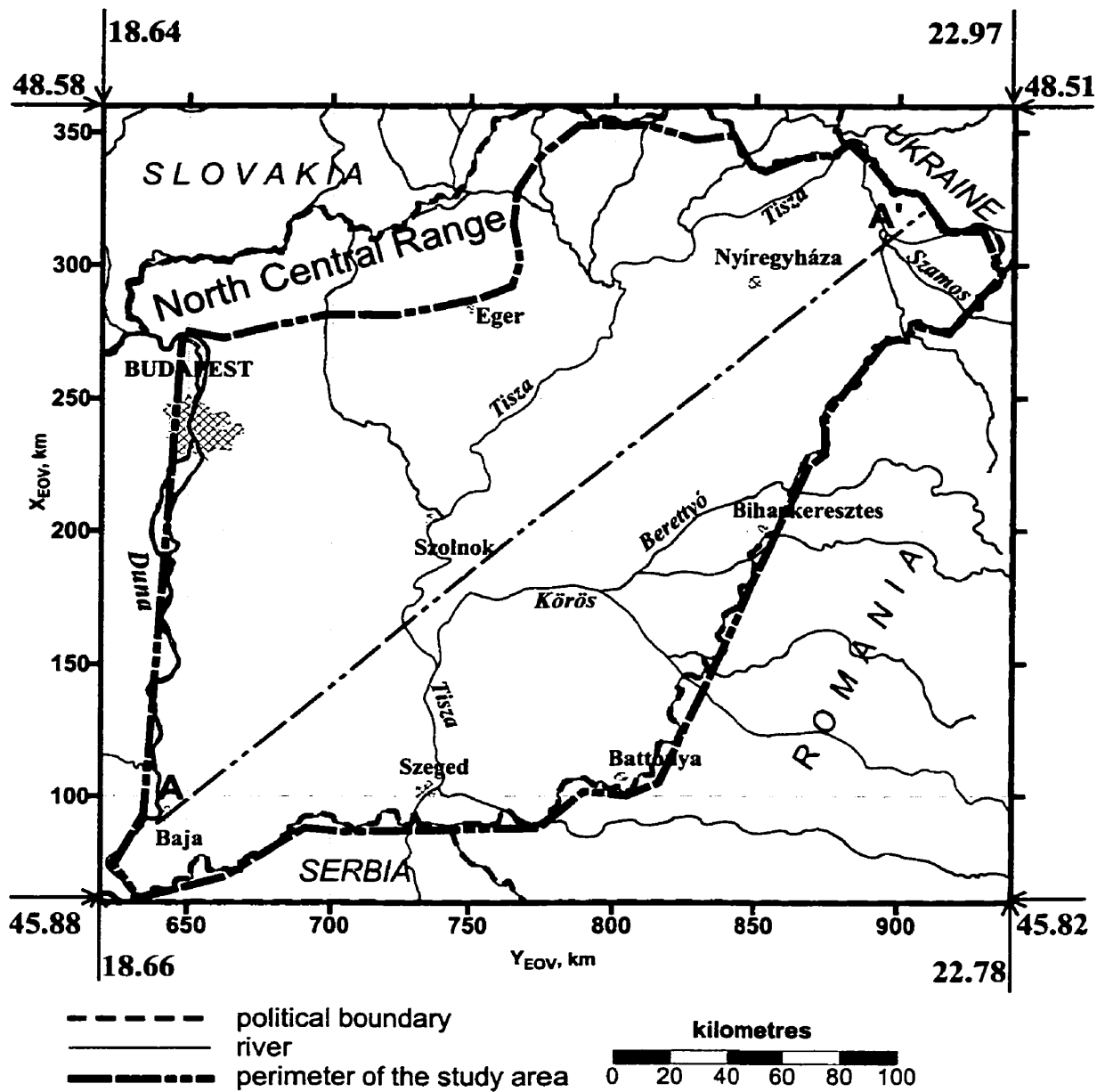


Figure 2.2: Basemap of the study area with geographic co-ordinates (decimal degrees) and EOV co-ordinates (Uniform National Projection system; map units in kilometres). The perimeter of the study area shown here is the same as the thick dotted line on the lower map in Figure 2.1, thus a correspondence can be made between this basemap and the larger geographic context of the study area (Figure 2.1). A-A' is the trace of the hydraulic cross section of Erdélyi (1976), Figure 1.1.

2.3 HYDROGEOLOGIC ENVIRONMENT

For the description, explanation, prediction, and control of hydrogeologic conditions, two systems of physical and chemical parameters are required that are in a cause-and-effect relationship: the “hydrogeologic environment” and the “groundwater regime” (Tóth, 1970). The hydrogeologic environment has three components: climate, topography, and geology each comprising several parameters. The groundwater regime has six parameters: amount of water, geometric distribution of water movement, velocity or volume of flow, chemical composition, temperature, and the changes in time of these five parameters.

2.3.1 Climate

The climate of the Pannonian Basin is continental-temperate, with mild winters (low of $-10\text{ }^{\circ}\text{C}$) and relatively hot summers (highs near $40\text{ }^{\circ}\text{C}$). Mean air temperature during the winter and summer ranges between 3 and $5\text{ }^{\circ}\text{C}$ and 17 and $18\text{ }^{\circ}\text{C}$, respectively. The mean annual air temperature is between 9.3 and $10.8\text{ }^{\circ}\text{C}$; the average annual precipitation ranges from 490 to 627 mm/a ($\sim 80\%$ is in the form of rain); the actual evapotranspiration ranges from 513 to 622 mm/a , while the potential evapotranspiration ranges between 750 to 900 mm/a (Pécsi, 1989). According to meteorological observations made between 1951 and 1993, the spatial distribution and temporal variation of precipitation and evapotranspiration in Hungary was not uniform (Liebe, 1994). The Great Hungarian Plain received the least precipitation and had the highest evapotranspiration relative to other parts of the country (Liebe, 1994).

2.3.2 Topography

The topography of the Great Hungarian Plain is characteristically flat, with a regional relief of about $0.1 - 3\text{ m/km}$ and a mean elevation of $\sim 110\text{ m a.s.l.}$ (Figure 2.3). The Duna Valley, between Budapest and Baja, and the area east from the Tisza (Alföld, or the Great Hungarian Plain in a strict sense) are the two main lowlands, with elevations

of 78 – 110 m a.s.l. (Figures 2.3). The Duna - Tisza Interfluve area is an elongated saddle-shaped topographic high with elevations of 110 to 170 m a.s.l., which continues northward in the Gödöllő Hills ($z_0 \sim 220$ m a.s.l.), then farther toward the north-east in the foothills of the North Central Range ($z_0 \sim 250$ m a.s.l.). In the Nyírség region (north-eastern part of Hungary), elevations do not exceed 160 m a.s.l. In the elevated hilly areas, the local relief may differ significantly from the regional one (10 m/km to 100 m/km).

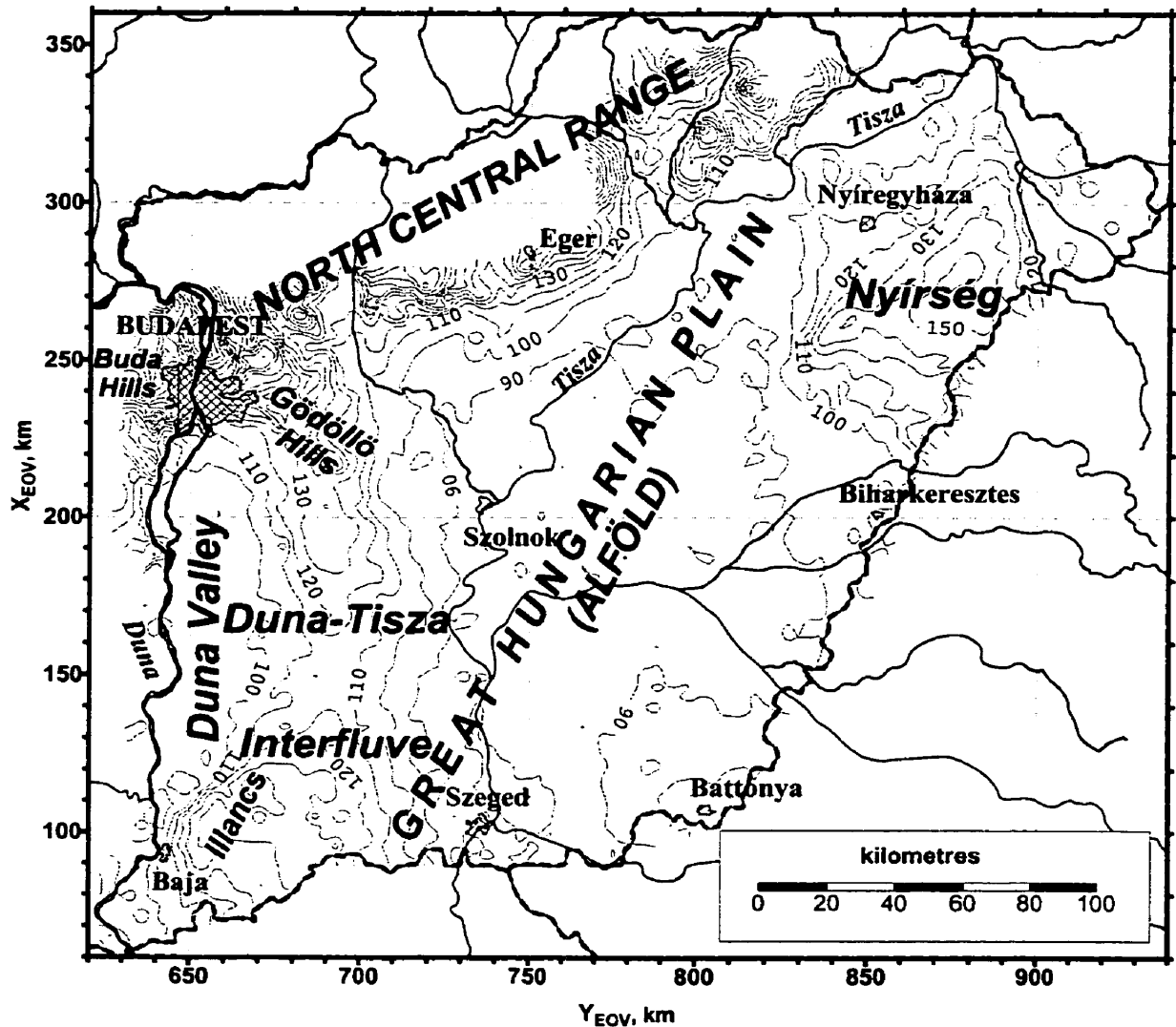


Figure 2.3: Topography of the study area and the names of main physiographic features. Topographic contour interval is 10 m.

2.3.3 Geology

The Great Hungarian Plain contains clastic sedimentary rocks reaching a thickness of up to 7 km, which were deposited during the Neogene and Quaternary, i.e., the past 17 Ma, on top of a heavily deformed Pre-Neogene basement. The Pre-Neogene basement rocks consist of indurated rocks of various origin, mainly crystalline and carbonate rocks. The Neogene - Quaternary sedimentary sequence consists of seven depositional units (Figure 2.4), which are from bottom to top: a basal unit, a deep basin unit, a prodelta turbidite unit, a delta slope unit, a delta front-delta plain unit, an alluvial plain unit, and a terrestrial unit (Bérczi, 1988; Juhász, 1992).

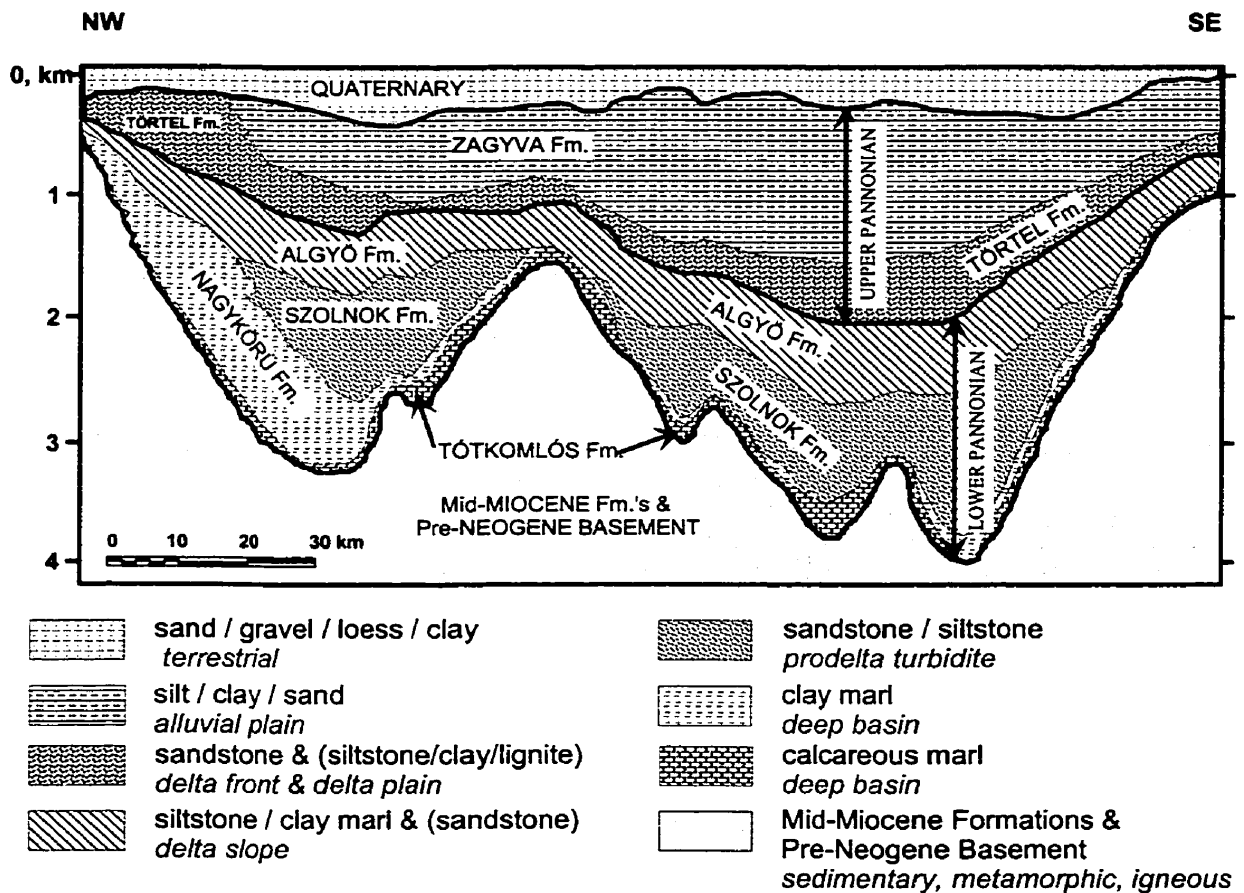


Figure 2.4: Schematic sedimentological and stratigraphic profile across the Great Hungarian Plain (modified after Juhász, 1992).

The lithology and degree of consolidation of the Neogene - Quaternary sedimentary units are as follows:

Basal unit: redeposited conglomerates alternating with marl beds at the base of sub-basins and abrasive coastal conglomerates at the top of basement highs; consolidated.

Deep basin unit: dark laminated silty marls without intercalation of coarse clastic sediments; consolidated.

Prodelta unit: turbidites; consolidated.

Delta slope unit: inclined siltstone and marl beds with interbedded sandstone; poorly to well consolidated from top to bottom.

Delta plain unit: horizontally bedded sandstones and marls with occasional lignite seams; degree of consolidation progressively changes from 'poor' at the top to 'good' at the bottom of the unit.

The *alluvial plain* and *terrestrial* units consist of poorly consolidated sand and clayey-sand.

2.4 REGIONAL TECTONIC HISTORY

An overview of the regional tectonic history of the Pannonian Basin is presented below based on the most recent data compilations and interpretations (e.g., Royden and Horváth, 1988; Csontos et al., 1991; Csontos et al., 1992; Horváth, 1993; Tari, 1994; Bada et al., 1998). This summary background information helped to determine regional hydrostratigraphic units, and to understand the relationship between basin evolution and regional groundwater flow. The schematic maps adapted from the literature are not adjusted to the scale of the maps prepared for this study, because their sole purpose is to illustrate an evolutionary history of the basin in a large regional context.

The Pannonian Basin is an intermontane sedimentary depression, which has evolved during the Neogene as an integral part of the Alpine, Carpathian, and Dinaride orogenic system (Figure 2.5). The Neogene sedimentary basin is superimposed on a Mid-Cretaceous thrust and fold belt, which consists of Mesozoic and Palaeozoic rocks genetically related to the surrounding mountains. The temporal evolution of this orogenic system is subdivided into four major stages (Trümpy, 1973): Pre-alpine (Permian to Early Cretaceous), Eo-alpine (Mid-Cretaceous to Paleocene), Meso-alpine (Eocene and Oligocene), and Neo-alpine (Miocene to Recent).

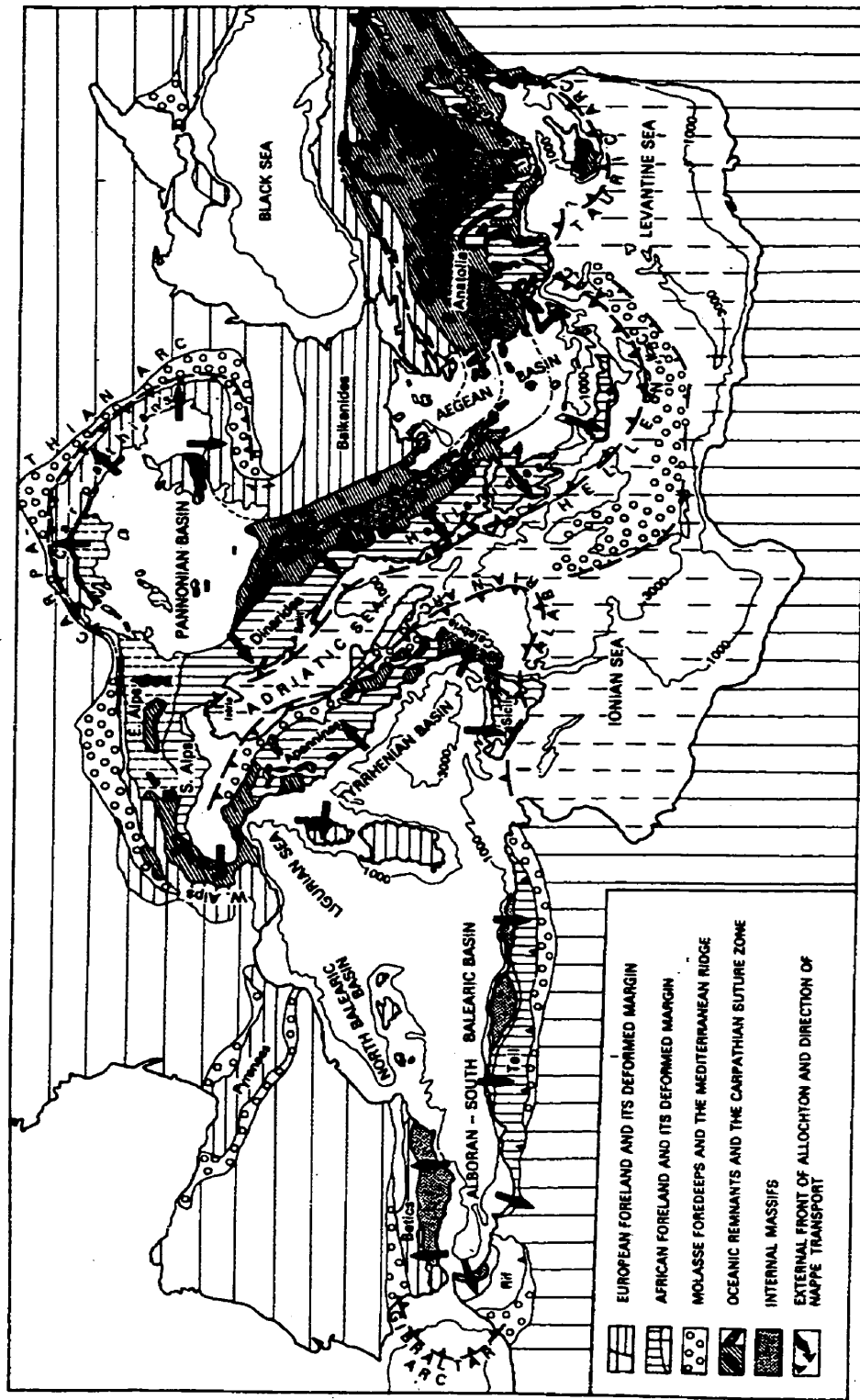


Figure 2.5: Tectonic scheme of the Alpine Mediterranean region (after Horváth, 1988)
 (contour values represent depth of seabed in metres below sea level)

The Pre-alpine evolution of the basement of the Pannonian Basin is not known because the available reflection seismic profiles did not reveal any Early Mesozoic structure (Tari, 1994). The Eo-alpine evolution is revealed by a number of field observations, core, and seismic data. For instance: a nappe complex in the Transdanubian Central Range, dextral strike-slip faults in the Bakony Mts., an Upper Cretaceous unconformity and breccias, and an imbricate stack of thrust sheets and fold belts in the Danube Basin. Horváth (1993) and Tari (1994) interpreted these observations as the result of a series of phases of compression that occurred during the Cretaceous. They have also suggested that an Upper Cretaceous flexural basin overlaps parts of the fold belt. Based on the different Mesozoic facies association observed within the nappe complex of the basement, Balla (1984) defined two tectono-stratigraphic units of the Pannonian Basin: the Alpine-North Pannonian Unit and the Tisza Unit (Figure 2.6). These two units are separated by the Mid-Hungarian Line, which is a poorly documented strike slip fault zone. The basement of the Great Hungarian Plain is dominantly part of the Tisza Unit, while in the northern part of the basin it belongs to the Alpine-North Pannonian Unit (Balla, 1984).

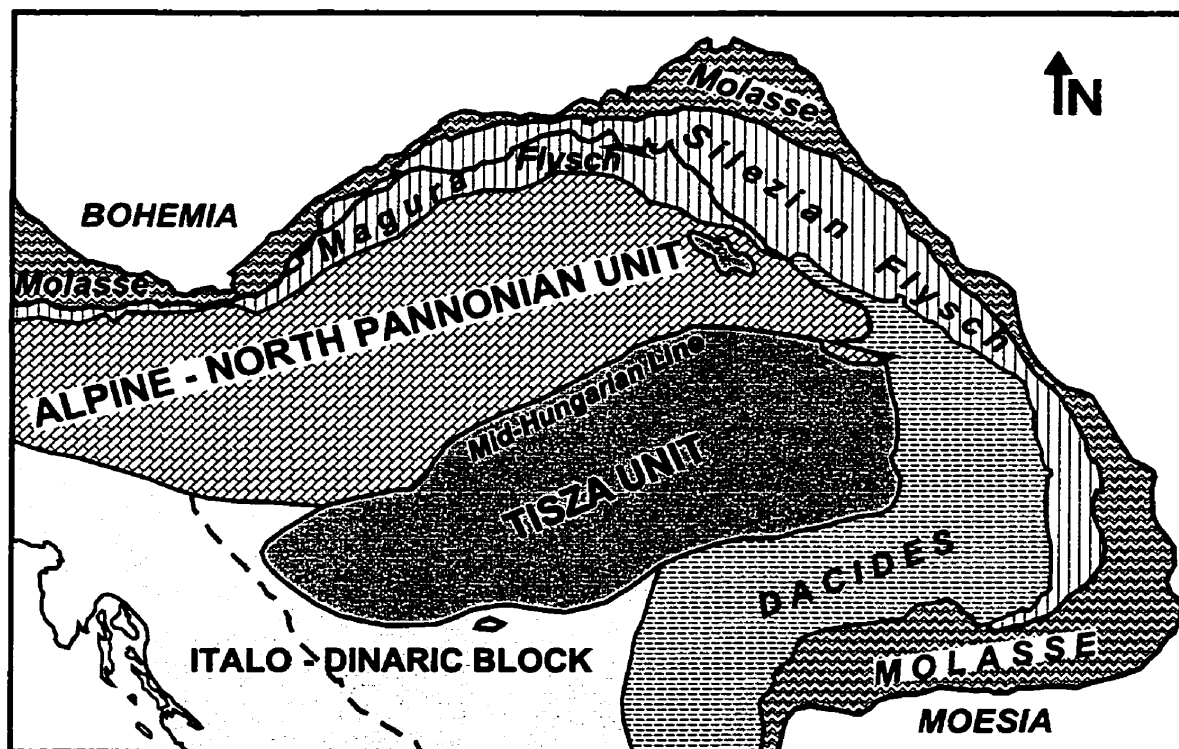


Figure 2.6: Sketch of major tectono-stratigraphic units in the Pannonian Basin: the Alpine-North Pannonian and the Tisza units (after Balla, 1984).

During the Meso-alpine evolution, the Alpine-North Pannonian Unit developed as a “retroarc flexural basin” (Hungarian Paleogene Basin) with respect to the Paleogene Carpathian thrust-and-fold belt (Tari et al., 1993). Basin subsidence was caused by flexural downwarp of the continental plate on the convex side of the continental collision zone, hence the term “retroarc flexural basin” (Bally and Snelson, 1980). By the Late Eocene, the collision of the African promontory with Europe and the oblique subduction of the outer Carpathian flysch trough beneath the Alpine-North Pannonian Unit initiated the collisional coupling of the Italo -Dinaric block and the eastward escape of the North Pannonian and Tisza Units along strike-slip faults (Csontos et al. 1992; Figure 2.7). The evolution of the Alpine-North Pannonian Unit shows the characteristics of the early “flysch” stage of a flexural basin during the Late Eocene (Figure 2.7), and it displays features of the “molasse” stage in the Early Miocene (Figure 2.8) (Csontos et al., 1992; Tari, 1994).

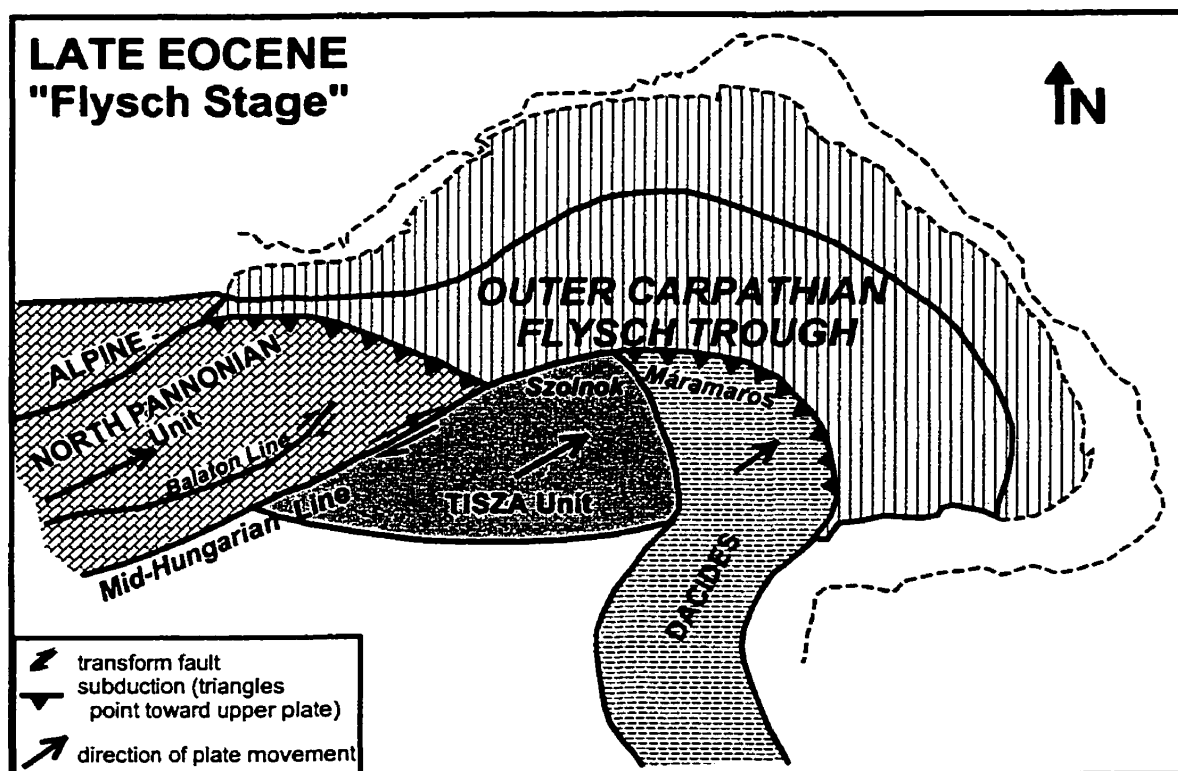


Figure 2.7: Sketch of the proposed relative position of the tectono-stratigraphic units in the Alpine-Pannonian-Carpathian region during the Late Eocene “flysch stage” (after Csontos et al., 1992).

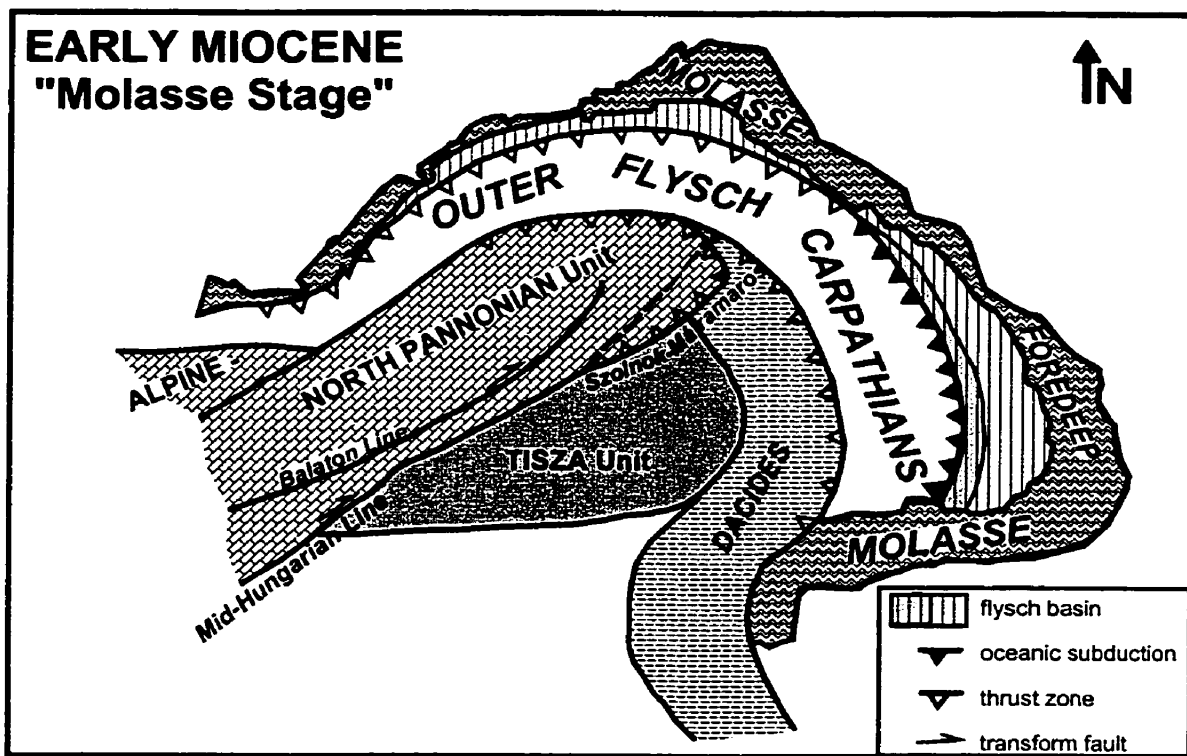


Figure 2.8: Sketch of the proposed relative position of the tectono-stratigraphic units in the Alpine-Pannonian-Carpathian region at the beginning of the Miocene: the “molasse” stage. Molasse was deposited in the foredeep (after Csontos et al., 1992).

Due to the uplift of the Dinarids and Southern Alps, the Intra-Carpathian region was temporarily isolated from the Mediterranean at the end of the Oligocene (~26 Ma), which resulted in the development of endemic faunal assemblages (Báldi, 1986). Later, during the Miocene, the Intra-Carpathian region was repeatedly isolated from the Mediterranean (Steininger et al., 1988). The different tectonic and faunal evolution of this region justified the need to define local biostratigraphic and chronostratigraphic units for the Intra-Carpathian region. This isolated bioprovince is called “Central Parathetys,” and it comprises the present territory of the Pannonian Basin and the Transylvanian Basin (Báldi, 1986; Steininger et al., 1988). Correlation of the local Central Parathetys chronostratigraphic nomenclature with the standard Mediterranean stages is illustrated in Figure 2.9, based on Tari (1994) and Horváth (1995). It is inevitable to use the Central Parathetys nomenclature in the discussion of the Neogene evolution of the Pannonian Basin.

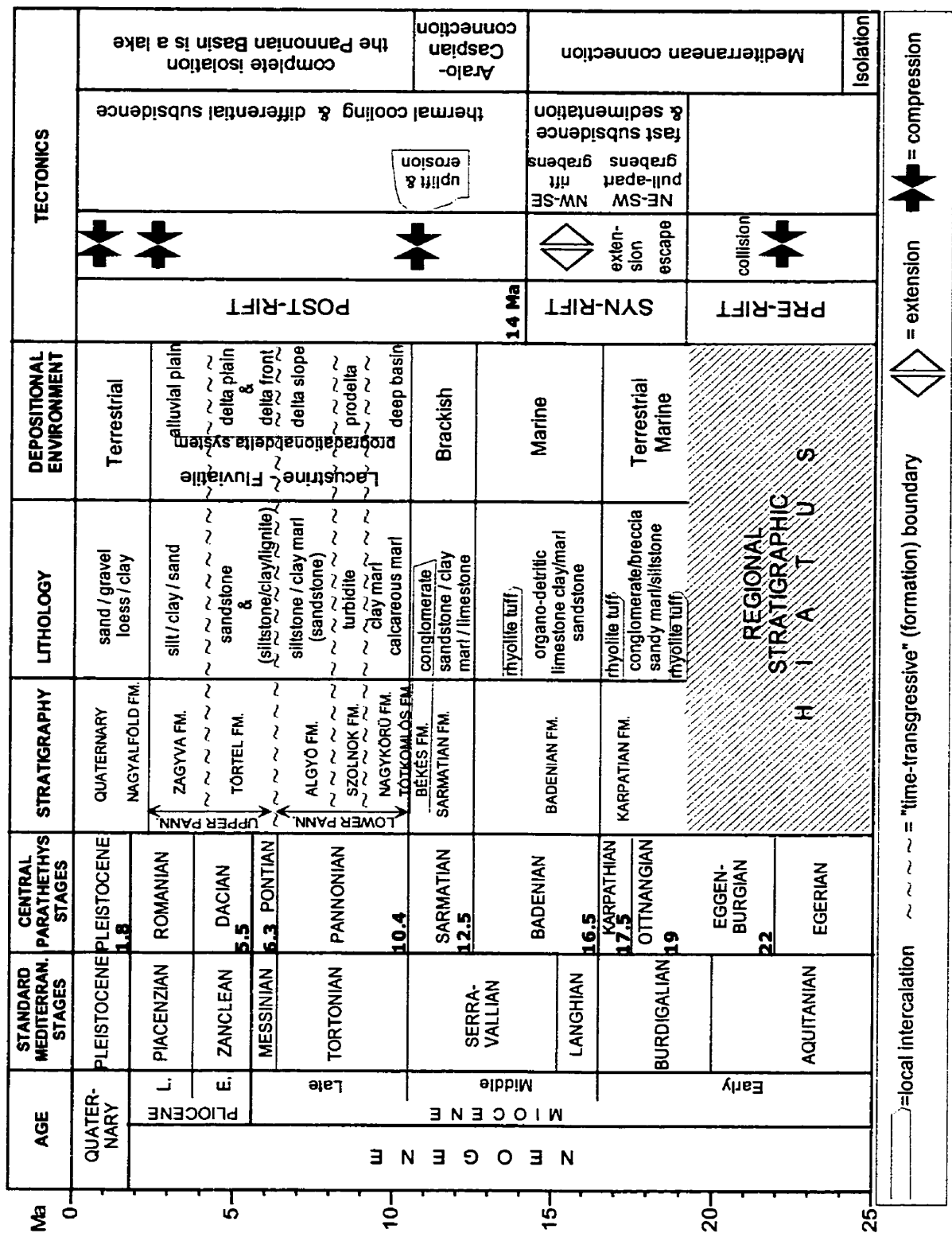


Figure 2.9: Generalised evolutionary diagram of the Pannonian Basin showing the correlation between the standard Mediterranean and Central Parathetys time scales, stratigraphy, lithology, depositional environment, and the main tectonic phases. Table compiled after Horváth and Pogácsás (1988), Tari (1994) and Horváth (1995). Abbreviations: "Ma = 10⁶ years; "E. = early; "L. = late; "Pann. = Pannonian; "FM" = formation.

The Neo-alpine evolution of the Pannonian Basin is a much-debated topic. Various tectonic models were proposed to explain this evolutionary stage of the basin. Some models are speculative and poorly supported by reliable data (see Tari, 1994 for a detailed review). The most popular tectonic and stratigraphic models proposed in the last two decades are summarised below.

It has been shown that the Neogene Pannonian Basin is the result of a complex basin formation mechanism that took place in a back-arc setting (Horváth and Berckhemer, 1982; Royden, 1988; Horváth, 1993). Back-arc basins develop as a result of continental collision on the concave side of an A-type subduction arc on the continental crust (Bally and Snelson, 1980). The total thickness of the predominantly clastic sediments deposited during the Neogene may exceed 7000 m. Extension and subsidence of the Pannonian Basin during the Miocene was coeval with compression and uplift of the surrounding Alps, Carpathians, and Dinarids (e.g., Royden et al., 1983).

By the end of the Early Miocene (19 – 17.5 Ma, Otnangian stage), the eastward escape of the North Pannonian and Tisza Units ceased (Horváth, 1988; Ratschbacher et al., 1991; Csontos et al., 1992;) and the regional stress regime had changed from compressional to extensional (Figures 2.8, 2.10, and 2.11). This event marked the onset of crustal stretching and extensional collapse of the Pre-Neogene structures (“rifting”), and the beginning of Neogene sedimentation (Horváth, 1988). During the initial stage of extension, variegated clays and conglomerates were deposited reaching a thickness of up to 300 m (Juhász, 1992). Extension was coeval with

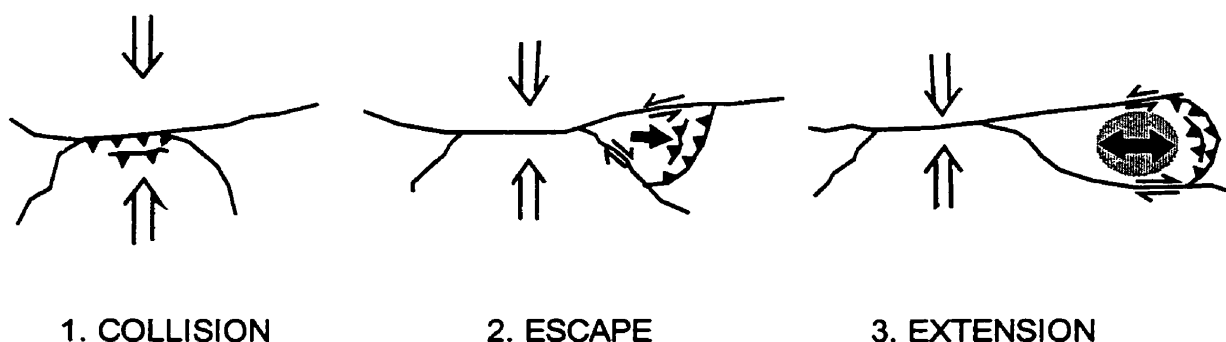


Figure 2.10: Diagram showing the three stages of thrust belt and basin evolution (after Horváth, 1988)

an intermediate to acidic volcanism in northern Hungary, which produced rhyolite tuff (Csató, 1993). Horváth (1995) proposed to define the beginning of extensional deformation (commonly referred to as “rifting”) by the general appearance of the first rhyolite tuff horizon of the Early Oligocene age (~19 Ma). This definition does not apply to the southern part of the Great Hungarian Plain because the rhyolite tuff does not exist there.

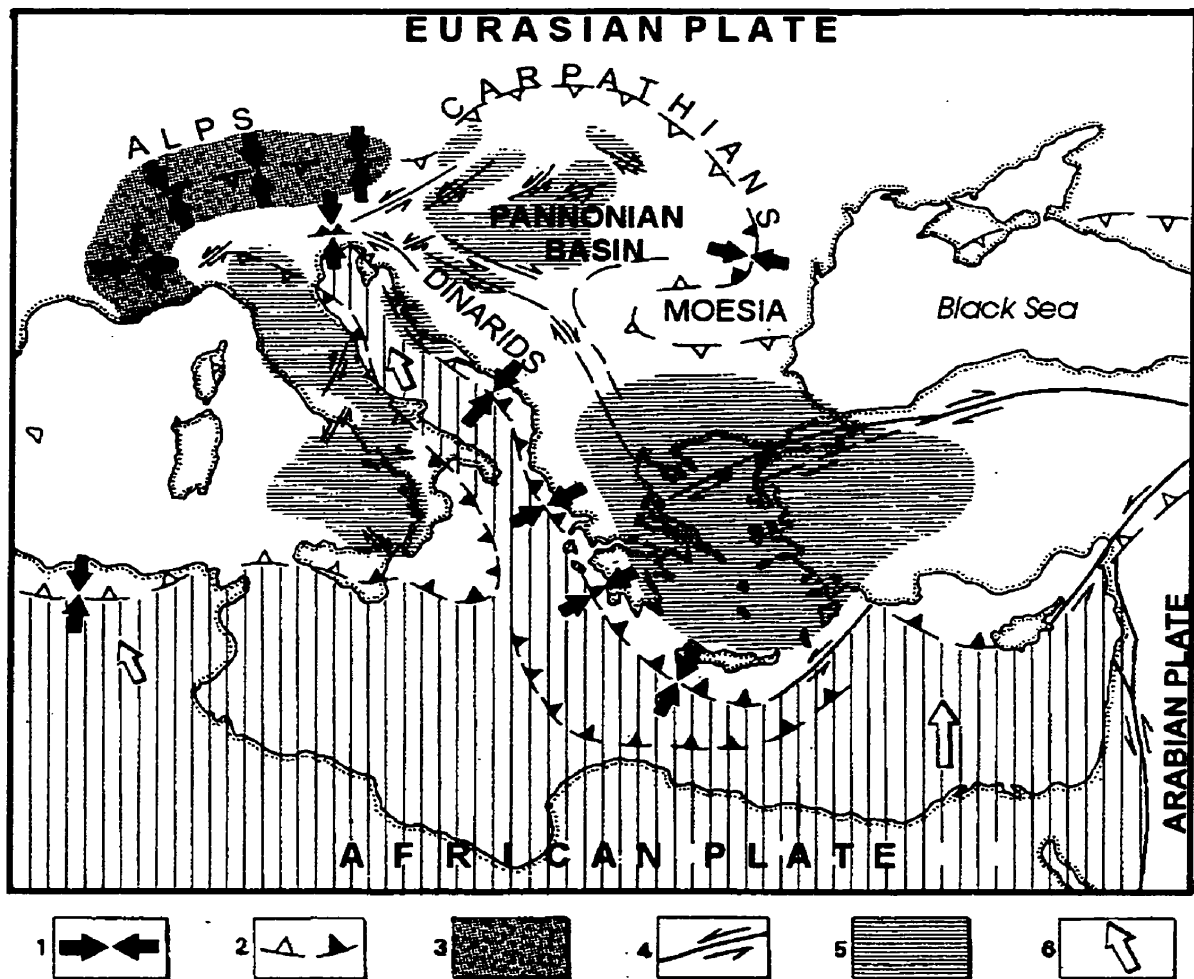


Figure 2.11: Neogene tectonic features and regional pattern of compressional stresses of the Alpine-Mediterranean region (after Horváth, 1988). Legend: 1 = average direction of predominant horizontal compression; 2 = external thrust front, active (closed barb) and inactive (open barb); 3 = compressional regime characterised by a complex system of transcurrent faults and folds; 4 = major transcurrent fault; 5 = areas of active extension and/or subsidence; 6 = motion vector of the African plate relative to Europe.

The Middle Miocene “syn-rift” extension (17.5 – 14 Ma; Tari, 1994) was enhanced by “subduction roll-back” of the European plate beneath the Carpathians

(Horváth and Berckhemer, 1982; Csontos et al., 1992) and the subsequent lithospheric thinning was followed by asthenospheric upwelling (Stegena et al., 1975). As a result, the average lithospheric and crustal thickness of the Pannonian Basin is ~60 km and ~25 km respectively, and the observed heat flow is anomalously high, i.e., 80 – 120 mW/m² (Horváth, 1993). The style and amount of extensional deformation throughout the Pannonian Basin is not uniform (Rumpler and Horváth, 1988; Tari et al., 1992). This resulted in the formation of several sub-basins separated by basement highs, displaying a Basin and Range-like topography (Figures 2.4 and 2.12).

The magnitude of extension of individual sub-basins was estimated from subsidence and thermal data (Royden and Dövényi, 1988). The estimated total amount of extension of the Pannonian Basin in an E-W direction exceeds 100 km and is approximately equal to the Miocene shortening of the outer Carpathian flysch belt (Csontos et al., 1992). Reactivation of Cretaceous thrust faults as low-angle normal faults and detachment faults as well as high-angle normal faults are thought to have contributed to the opening of rift basins in an E-W trending extensional regime (Horváth, 1993). The development of conjugate shear zones in a N-S compressional and an E-W extensional regime initiated pull-apart basins (Bergerat, 1989). In the basement of the Great Hungarian Plain, the Makó Trough and the Békés Depression have developed as rift-type basins and extension was accommodated by detachment faults. On the other hand, the Kiskunhalas, Csepel, and Derecske depressions (Figure 2.12) developed as pull-apart basins (Tari, 1994), and extension was accommodated by strike slip and normal faults.

Rifting ceased in the Middle Miocene (~14 Ma) and it was followed by a stage of compression, which terminated by the end of the Sarmatian (10.4 Ma). Apparently, the basin was in a tectonically relaxed state during the Late Miocene and Early Pliocene, and subsidence continued as a result of thermal cooling (Horváth, 1995). From the Late Pliocene, the regional stress regime became predominantly compressional (Horváth, 1995), which seems to persist to the Present (Gerner et al., 1995). Deformation patterns typically related to compressional stress regime (flower structures, folding, and uplift) are observed in Pliocene and Quaternary sediments (e.g., Tari, 1994, Pogácsás et al., 1994). Earthquake focal mechanism solutions, borehole-breakout analysis, and *in situ* stress measurements provide evidence for the compressional nature of the present day stress regime (Dövényi and Horváth, 1990; Gerner, 1992; Becker, 1993; Gerner et al., 1995;

Gerner et al., 1999). The orientation of the contemporary σ_1 principal stress axis is perpendicular to the Carpathian arc, except for the south-eastern part of the Great Hungarian Plain, where σ_1 is oriented roughly NE-SW (Bada et al., 1998) (Figure 2.13). Increased subsidence and sediment accumulation was observed from boreholes in the centre of the Pannonian Basin, while uplift and erosion was recorded in the marginal areas (van Balen and Cloetingh, 1994; Horváth, 1995) (Figure 2.13).

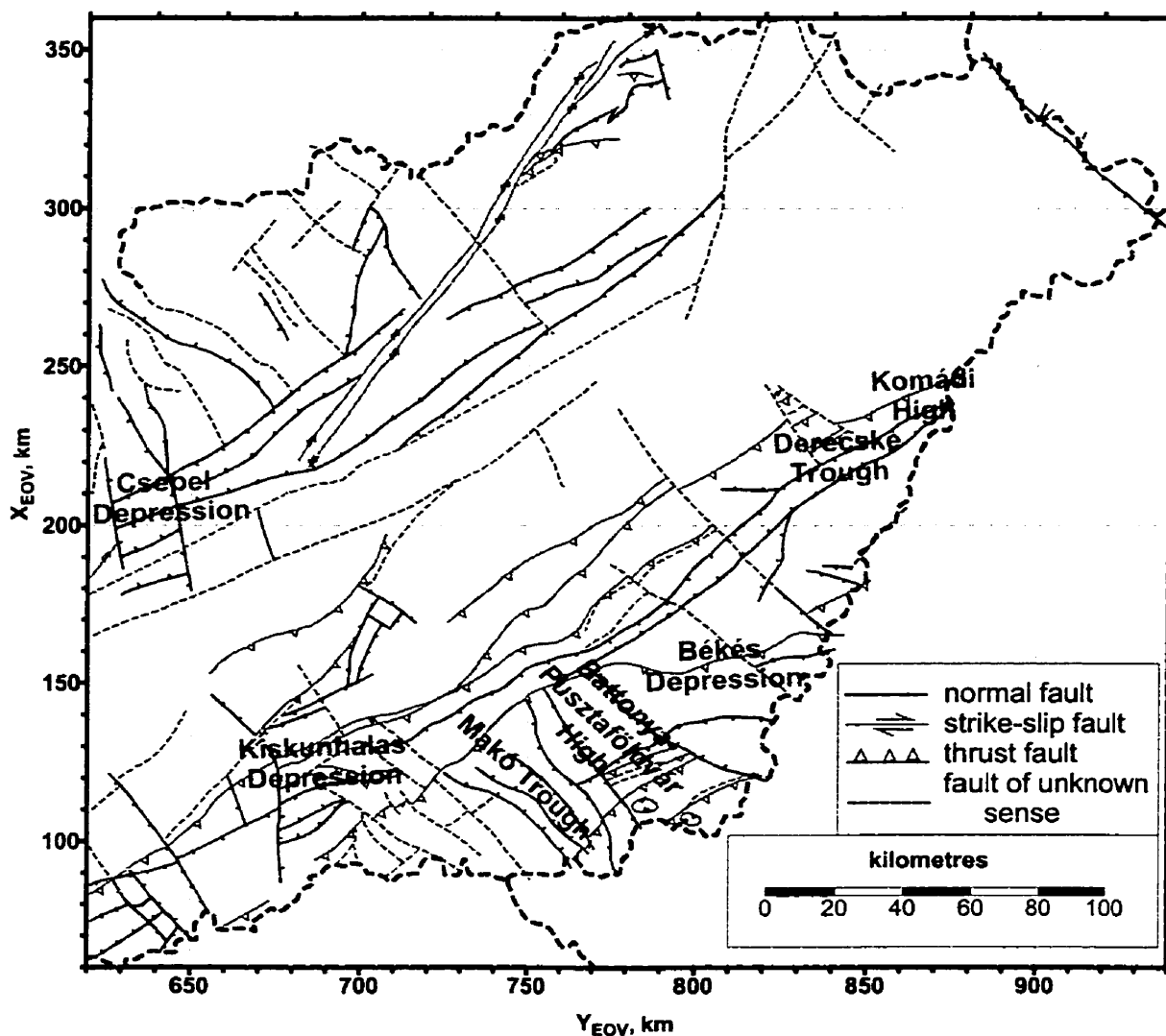


Figure 2.12. Tectonic lineaments and sub-basins in the Pre-Neogene basement of the Great Hungarian Plain (after Fülöp and Dank, 1987).

The rate of regional shortening of the Pannonian Basin caused by the late stage compression was recently constrained by geodetic measurements using high precision Geographical Positioning System (GPS) techniques (Grenerczy et al, 2000). Their results indicate that shortening rates are 10 – 12 ppb/a (ppb = parts per billion) along presently active strike-slip faults and less further away from the active faults.

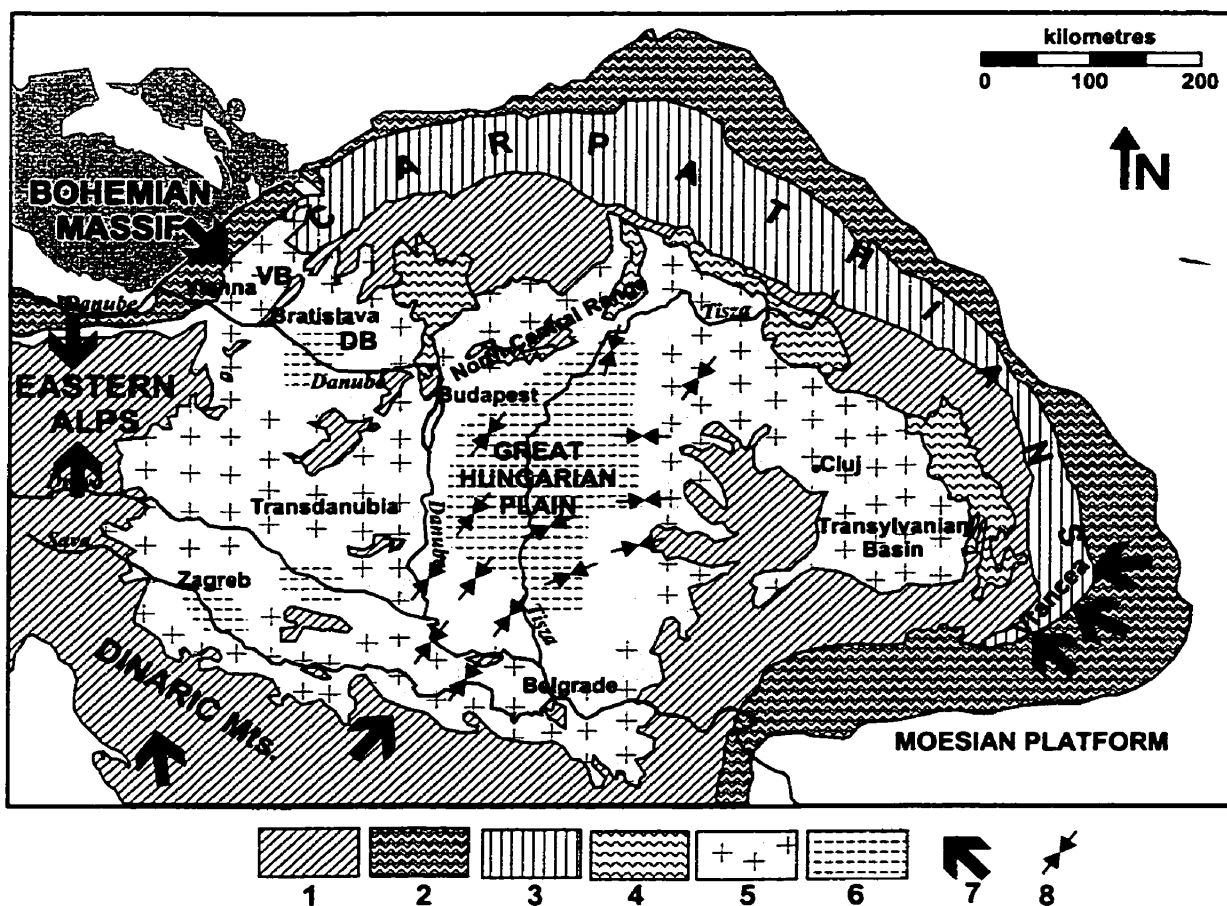


Figure 2.13: Recent configuration of the Pannonian Basin and the associated Alpine Mountain belt. The pattern of the Quaternary vertical movements is also shown. Symbols: 1 = inner Alpine, Carpathian, and Dinaric mountains; 2 = Alpine and Carpathian molasse foredeep; 3 = Alpine and Carpathian flysch belt; 4 = Neogene calc-alkaline volcanic rocks; 5 and 6 = areas of Quaternary uplift and subsidence, respectively; 7 = directions of present-day tectonic push; 8 = present-day direction of maximum horizontal compressive stress (modified after Horváth, 1995; directions of block motion and compressive stress are taken from Bada et al., 1998). Note that the Moesian platform acts as a rigid buttress, the Western and North-Eastern Carpathians are 'free'.

2.5 SEDIMENTARY FILL OF THE BASIN

The history of sedimentation and the evolution of depositional environments are discussed below in the framework of the tectonic evolution of the Pannonian Basin, i.e., sedimentation during the syn-rift and post-rift stages, respectively. The evolutionary diagram in Figure 2.9 summarises the details of the developmental stages of the Pannonian Basin during the Neogene.

During the Karpatian stage (17.5 – 16.5 Ma), the basin subsided rapidly and up to 3000 m of thick coarse clastic sediments were deposited in a terrestrial environment (Horváth, 1995). During the Badenian stage (16.5 – 14 Ma), “syn-rift” subsidence and sedimentation continued, and the sedimentary environment had gradually changed from terrestrial to marine. Organo-detritic limestone and marl layers with occasional turbiditic intercalations were deposited during this time, reaching an apparent thickness of ~3000 m in the western part of the Pannonian Basin. The great thickness of the Karpatian and Badenian sedimentary piles may have resulted from compressional deformation during the Late Miocene or Pliocene (Horváth, 1995). In contrast, the sub-basins in the central part of the Great Hungarian Plain were far away from the sources of clastic material. Therefore, they acted as “sediment starved basins” with a water depth of at least 1000 m (Mattick et al., 1988). With some exceptions (e.g., Kiskunhalas depression; Figure 2.12), the sediments of Early Miocene up to Middle Badenian age are thin (up to 300 m) or missing in the Great Hungarian Plain (Bérczi et al., 1988).

The cessation of rifting and the commencement of the “post-rift” phase is marked by a regional unconformity and by the last major rhyolite tuff volcanic event in the Middle Badenian, that is at ~14 Ma (Hámor et al., 1979; Tari, 1994). During the post-rift phase, clastic sediments were deposited in a changing sedimentary environment. The thickness of these sediments reaches ~6000 m, most of which accumulated during the Pannonian stage (Juhász, 1992). By the end of the Sarmatian stage (10.4 Ma), the regional stress field was compressional with σ_1 oriented E-W (Peresson and Decker, 1997), which resulted in uplift, subaerial exposure, and erosion of the syn-rift sediments. At this stage, the Intra-Carpathian region was again isolated from the Mediterranean and connected to the Aralo-Caspian region (Bérczi et al., 1988). During the Sarmatian, the

salinity of the isolated inland-sea had gradually decreased, and sediments reaching a thickness of ~100 m thick were deposited in brackish water (Bérczi et al., 1988).

In the Early Pannonian stage (~10.4 Ma), conditions of thermal subsidence were established and persisted until the Late Pliocene (~2.5 Ma) (Horváth, 1995). During this time, the entire Intra-Carpathian region was isolated from the world's seas, and clastic sediments originating in the elevated Carpathians were deposited in a lacustrine environment (Kázmér, 1990). The basin was filled by two delta systems prograding from the Carpathian arc toward the centre; one delta system moved in from the NW and another one from the NE (Csató, 1993). The north-western delta system became dominant after about 6 Ma (Csató, 1993). Additionally, smaller delta systems may have developed from other directions. The infilling process was punctuated by episodic effects of lake-level fluctuations, differential subsidence, and lateral dislocation of sediment sources in the hinterland (Csató, 1993). The stratigraphic subdivision of the sediments deposited by these delta systems is based on the various depositional facies of the system, i.e., prodelta, delta slope, delta front, delta plain (Gajdos et al., 1983; Bérczi et al., 1988; Juhász, 1991, 1992) (Figure 2.9). In a prograding delta system the facies boundaries are time-transgressive. Therefore, the lithostratigraphic units defined according to the various delta facies are also time-transgressive. The succession of lithostratigraphic units deposited during the past 10.4 Myr represents a general spatial relationship rather than a definite temporal relationship between the individual units (Figures 2.4 and 2.9).

Szalay and Szentgyörgyi (1988) suggested to group the predominantly pelitic deep basin marls (Tótkomlós Formation and Nagykörű Formation), prodelta turbidites (Szolnok Formation), and delta slope sediments (Algyő Formation) as "Lower Pannonian," and the predominantly psammitic delta plain - delta front (Törtel Formation) and alluvial plain (Zagyva Formation) sediments as "Upper Pannonian." The boundary between the Lower and Upper Pannonian units is the boundary between the delta slope and delta plain facies, which is time-transgressive. The Lower and Upper Pannonian sedimentary pile is commonly referred to as "Pannonian *sensu lato*" (Juhász, 1991). The Upper/Lower Pannonian subdivision may be confusing or misleading, because it arguably implies the division of a chronostratigraphic stage (Pannonian stage: 10.4 – 6.3 Ma), however, it refers to a time-transgressive facies boundary.

During the Late Pliocene and Quaternary, alluvial plain, terrestrial, and fluvial sediments were deposited, consisting of thin-bedded silts, clay, and sand. By the end of the Pliocene (~2.5 Ma), the depositional environment became predominantly terrestrial and over 1000 m of clastic sediments were accumulated. During the Quaternary, fluvial and eolian deposits were formed (Rónai, 1978, 1985). As a result, loess, sand, and gravel dominate the surficial geology of the lowlands in the Pannonian Basin.

2.6 HYDROSTRATIGRAPHY

2.6.1 Principles

Maxey (1964) defined hydrostratigraphic units as “*bodies of rock with considerable lateral extent that compose a geologic framework for a reasonably distinct hydrologic system.*” Based on their relative hydraulic properties, rock layers are classified as *aquifers*, *aquitards*, and *aquicludes*. Aquifers are saturated permeable rocks, which can transmit significant volumes of fluids with relative ease under ordinary hydraulic gradients. Aquitards can transmit fluids under ordinary hydraulic gradients with relatively less ease than aquifers. Aquicludes are incapable of transmitting fluids. The terms *aquifer* and *aquitard* are deliberately imprecise with respect to permeability (or hydraulic conductivity), so that they can be used in a relative sense (Freeze and Cherry, 1979). The term *aquiclude* implies zero permeability, which is never encountered in reality, therefore, this term should be reserved for theoretical no-flow boundaries.

Based on the relative permeability, regional distribution and continuity, and litho- and chronostratigraphy of strata, hydrostratigraphic units can be clustered into three hierarchical orders: 1st order: Formation; 2nd order: Group; 3rd order: System (Tóth, 1978). The basic unit is the Hydrostratigraphic Formation, bearing the lithostratigraphic name of the lithologic unit followed by the term aquifer or aquitard, e.g., Dakota Sandstone Aquifer, Ireton Shale Aquitard. A Hydrostratigraphic Group may contain two or more formations, and its name is derived from the name of the era that the formations belong to, followed by the term aquifer or aquitard, according to the property of the dominant formations, e.g., Pliocene Aquifer Group. A Hydrostratigraphic System comprises two or more Groups, and its name is derived from the name of the

chronostratigraphic period the groups belong to, e.g., Paleogene Aquifer System. Sometimes it is difficult to strictly adhere to the nomenclature of hydrostratigraphic hierarchical orders outlined above, particularly in cases where the formation boundaries are time transgressive and/or very large stratigraphic hiatuses are present.

Hydrostratigraphic units can be characterised qualitatively based on stratigraphic information and field experience. For quantitative characterisation of hydrostratigraphic units a large number of permeability and/or hydraulic conductivity data with a substantial lateral and vertical distribution are needed, which are rarely available.

2.6.2 Hydrostratigraphic units in the Great Hungarian Plain

Qualitative appraisal of the regional hydrostratigraphy of the Great Hungarian Plain was based on the regional lithologic and stratigraphic characteristics of the rock framework. It was complemented with empirical observations on the relative hydraulic conductivity of rock formations acquired during water and petroleum exploration and production (I. Révész and S. Pap, MOL, Plc., 1996, *personal communication*).

A common lithologic characteristic of the clastic basin fill is the spatial alternation of beds dominated by sand, silt, and clay. Frequently, these beds contain lithologic lenses of contrasting grain size, e.g., clay lenses in sand matrix, sand lenses in clay or silt matrix. The permeability of these lithologic units varies in function of grain size, packing, and sorting, which renders heterogeneous and anisotropic permeability to the individual strata. The bulk permeability of the beds is determined by the dominant lithology of the matrix. Halász (1975) demonstrated that the Quaternary terrestrial sediments form layered hydraulic systems at the local scale, and that the vertically confined aquifers may communicate laterally through lithologic continuity. Lateral and vertical hydraulic communication among the sandstone aquifers is permitted by interfingering of sandy layers, leakage across the confining shale layers of finite lateral extent, and locally through fracture zones.

Within the deltaic sediments, comprising most of the Neogene clastic deposits of the basin, the porosity and permeability distribution strongly varies in function of the sandstone/shale ratio and depth of each depositional facies. The hydraulic characteristics of stratigraphic formations (porosity, permeability, and anisotropy) in the study area can

not be adequately described by a unique permeability value due to the heterogeneous rock composition of strata and the structural discontinuities both within and across strata. The bulk permeability of deltaic sediments at discrete depth intervals can be estimated by applying statistical averages of sandstone/shale ratios, which serve as weighing factors of sand and shale permeability. The horizontal bulk permeability can be approximated with the weighted arithmetic mean of horizontal sand and shale permeability, respectively, whereas for the vertical bulk permeability a harmonic mean is considered the best approximator (Harrison and Summa, 1991).

In the Great Hungarian Plain, the average porosity depth trend of shale and sandstone was established from porosity measurements on core-plugs obtained from oil wells by Szalay (1982); the results are illustrated in Figure 2.14. The porosity of shales decreases exponentially from about 64% at the surface to ~5% at approximately 2400 m depth; at depths greater than 2400 m the shale porosity varies slightly around 5%. The porosity of sandstones also decreases exponentially with depth from about 46% at the surface to ~2% at 5000 m depth.

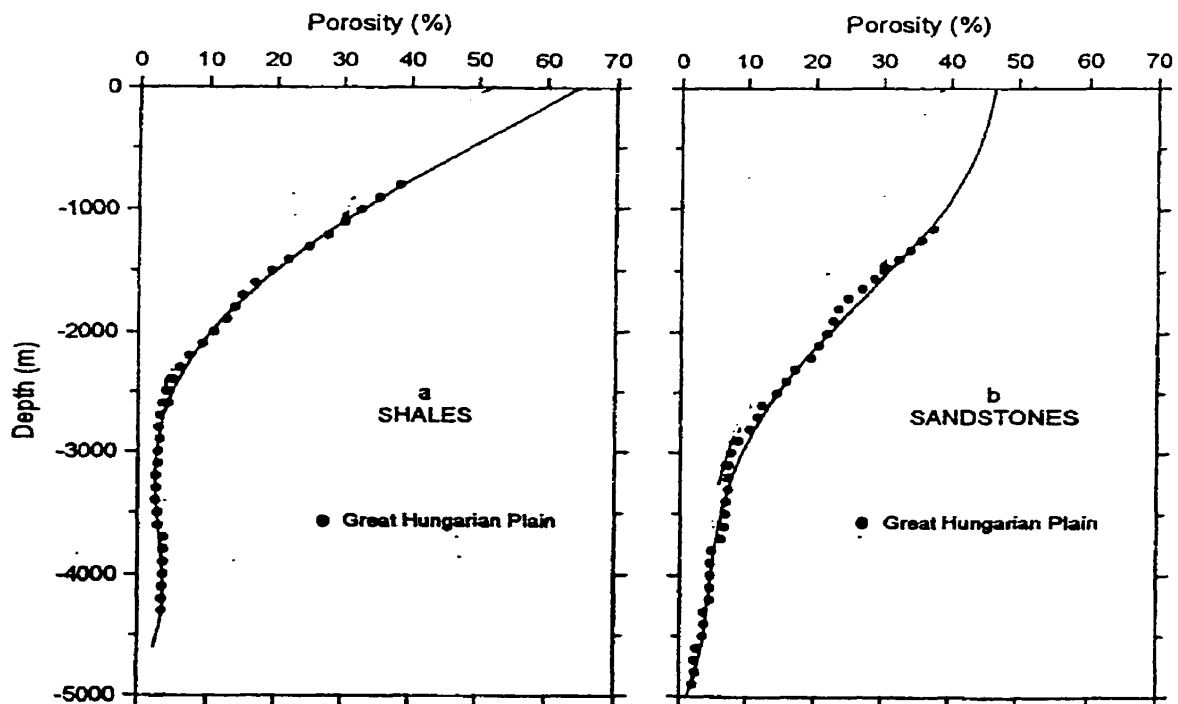


Figure 2.14: Average porosity-depth trends of a) shales and b) sandstones in the Great Hungarian Plain (after Szalay, 1982).

The vertical and horizontal core permeability values vary within five orders of magnitude at every depth ($10^{-12} - 10^{-16} \text{ m}^2$, with highs near 10^{-12} m^2 in the Quaternary sediments; corresponds to a hydraulic conductivity of $\sim 10^{-5} - 10^{-9} \text{ m/s}$), but their averages systematically decrease with depth (Figure 2.15). The permeability anisotropy (k_h/k_v) calculated from the sandstone core permeability values is ≤ 5 for over 90% of the measurements (Figures 2.15 and 2.16). The vertical anisotropy of shales increases with depth and it is approximately $k_h/k_v = 10$ below 1000 m depth. Probable formation permeability was estimated by the arithmetic and harmonic mean value of core permeability then “upscaled” intuitively to account for the role of faults and connectivity of aquifers and aquitards. These values are not recommended for accurate flux calculations at the local scale, as they are rough estimates for regional scale hydraulic properties of the rock framework and may not reflect the real local conditions.

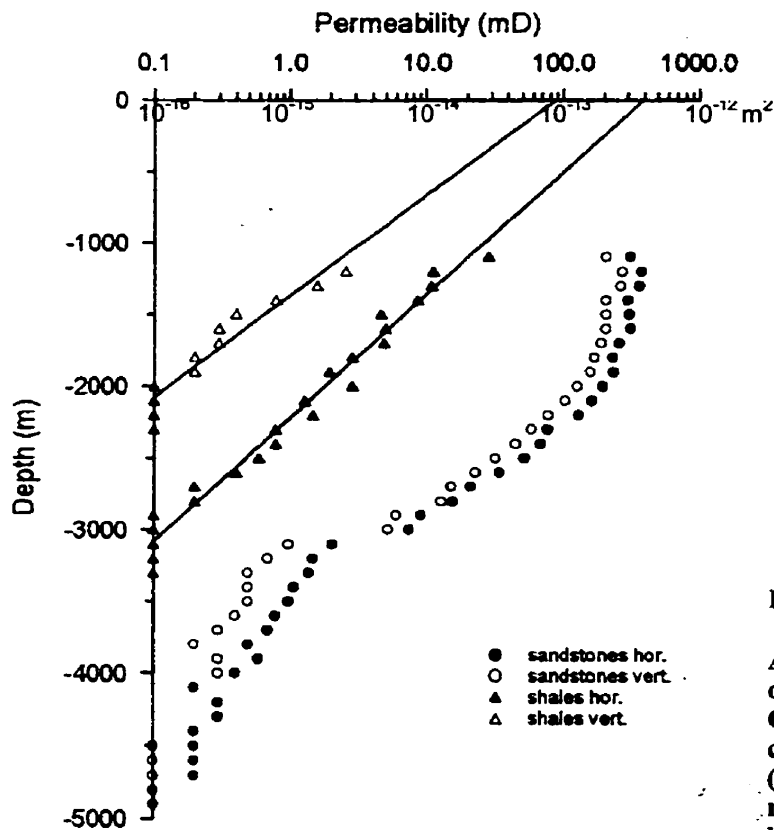


Figure 2.15:

Average permeability-depth trends of shales and sandstones in the Great Hungarian Plain based on core-permeability measurements (after Szalay, 1982). 1 mD $\approx 10^{-15} \text{ m}^2$, or 1 mD corresponds to a hydraulic conductivity of $\sim 10^{-8} \text{ m/s}$.

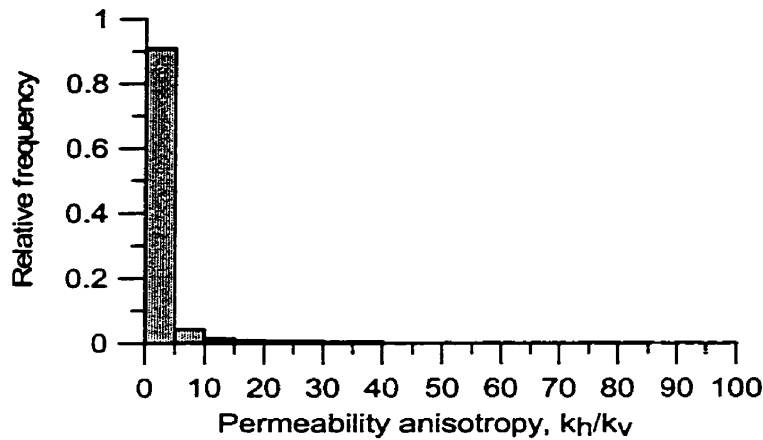


Figure 2.16:

Relative frequency distribution of core-permeability anisotropy from Neogene sandstone reservoirs (data courtesy of MOL, Plc.).

Given the lithologic heterogeneity and structural position of the rock formations in a basin, a distributed analysis of the permeability and porosity distribution is required for adequate characterisation of hydrostratigraphic units. The porosity-depth trend curves (Figure 2.14) and the average permeability-depth trends (Figure 2.15) calculated by Szalay (1982) for shale and sandstone in the study area are the results of lumped data analysis. By virtue of their simplicity, it may be tempting to infer possible porosity and permeability values for mixed sand and shale rocks at any depth within the upper 5000 m depth range of the basin from these trend curves, and assign such values to hydrostratigraphic units. Such a mathematical approach to hydrostratigraphic modelling ignores the geologic reality and leads to definition of meaningless domain characteristics, and ultimately to erroneous results and interpretations. The hydraulic conductivity values assigned to the regional hydrostratigraphic units were not derived from Figure 2.14 and Figure 2.15; instead, they are based on published K-values and geologic descriptions.

Three regional aquifers and two regional aquitards were identified in the Great Hungarian Plain (Figures 2.17 and 2.18). It must be emphasised that these regional hydrostratigraphic units may not apply to local scale (1-100 km²) investigations, and they should be modified or refined according to the scale of future studies, as deemed necessary. An impermeable basal boundary is assumed to exist at a certain depth within the Pre-Neogene basement. Theoretically, this boundary would coincide with a rheological boundary, that is the transition zone from brittle to ductile deformation (Nur and Walder, 1990). Beneath the Pannonian Basin, the depth range of this rheological boundary is conjectural; it is estimated at 10 - 20 km depth, within the Pre-Neogene basement (Horváth, 1993).

The Pre-Neogene basement rocks consist of Mesozoic carbonate rocks, volcano-sediments, and Palaeozoic metamorphic rocks (Fülöp and Dank, 1987). Generally, they are heavily fractured and weathered, the carbonate rocks (limestone and dolomite) are intensively karstified; permeability values in the order of $10^{-12} - 10^{-13} \text{ m}^2$ (correspond to hydraulic conductivity of $\sim 10^{-5} - 10^{-6} \text{ m/s}$) are quite common in the basement rocks. Indeed, this is true for the upper ~ 100 to 1000 m portion of the basement, but the deeper parts are not known from drilling or seismic profiles. The basement rocks are considered to have aquifer properties and are referred to as the *Pre-Neogene aquifer*. The Late Cretaceous-Early Eocene Szolnok-Máramaros Flysch Formation from the northern part of the basin (Figure 2.7 and 2.8) is tentatively included in the Pre-Neogene Aquifer, although very little information is available about the hydraulic properties of this unit because of its limited interest for petroleum exploration (S.Pap, 1997, *personal communication*).

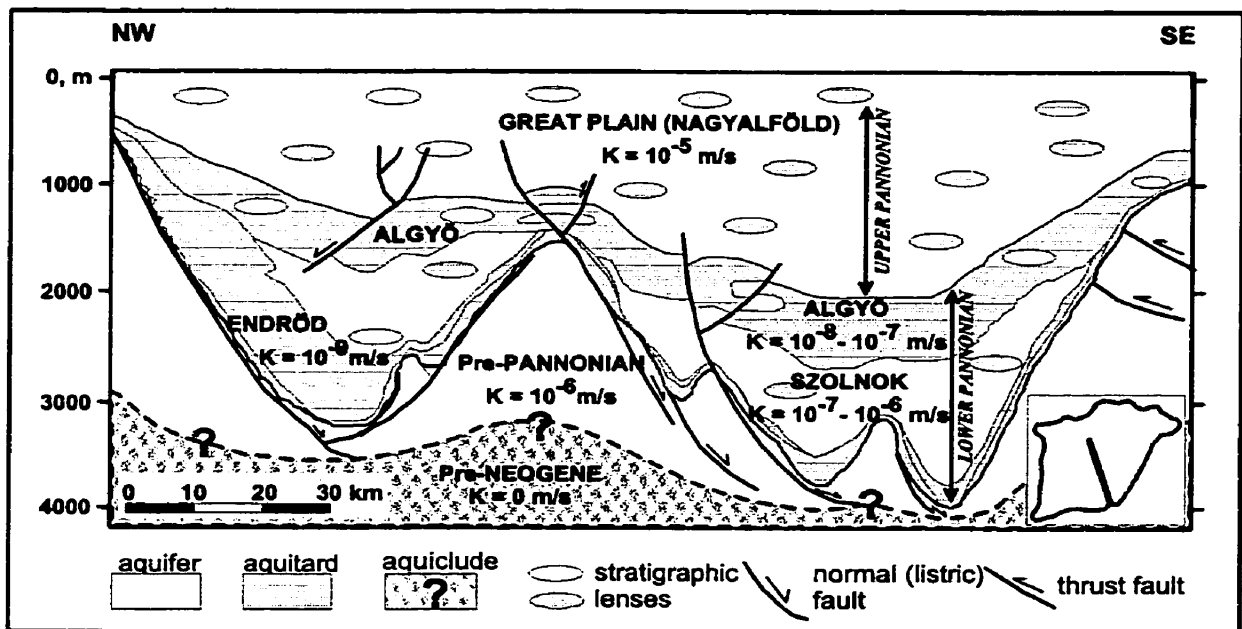
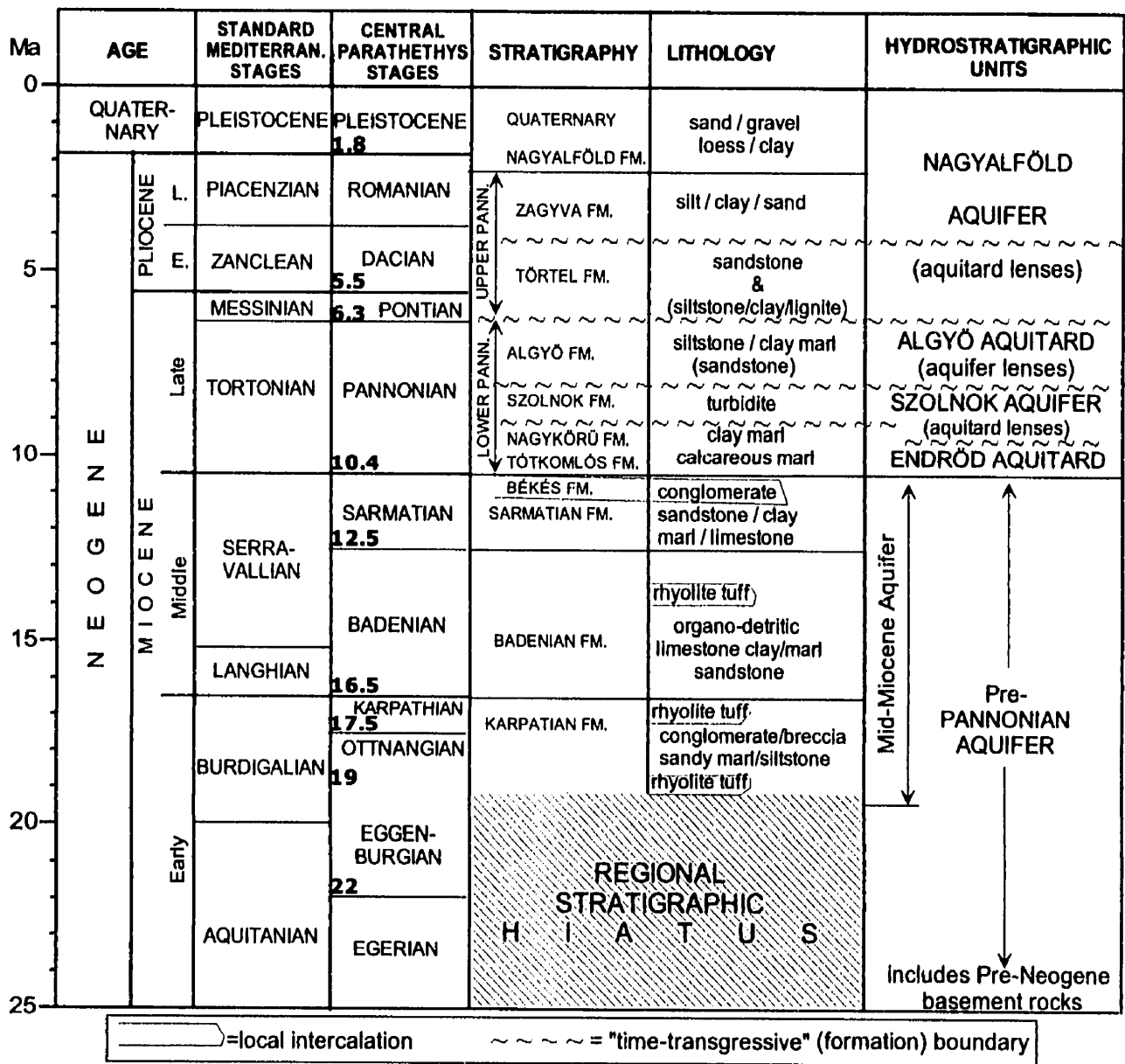


Figure 2.17: Schematic hydrostratigraphic profile across the Great Hungarian Plain. The bulk (regional) hydraulic conductivity values assigned to the hydrostratigraphic units are indicated in [m/s]. The inset in the lower-right corner shows the trace of the schematised cross section.

The Middle Miocene formations (Sarmatian, Badenian, and Karpatian) are usually thin (<300 m) or absent in the Great Hungarian Plain, with the exception of the

Figure 2.18. Hydrostratigraphic chart of the Great Hungarian Plain.



Kiskunhalas Depression (Figure 2.12), where >3000 m sediments were deposited during the Badenian (16.5 to 12.5 Ma) (Horváth, 1995). Generally, they consist of coarse clastics, organo-detritic limestone, and locally (in the northern part of the basin) rhyolite tuff, which have a considerably greater permeability than the overlying deep basin marls.

The presence of Middle Miocene shale and marl bodies is recognised, but their regional significance, as aquitards is believed to be minimal. The basement highs are locally covered by a <100 m thick coastal conglomerate and sand unit, commonly referred to as the “Békés Basal Conglomerate Formation,” of Pannonian age (Gajdos et al., 1983). This formation is grouped into the *Mid-Miocene Aquifer* unit (Figure 2.18). Since the Mid-Miocene formations and the Pre-Neogene basement rocks have similar permeability and they are juxtaposed, although the Mid-Miocene formations are not ubiquitous, the two units are combined into the *Pre-Pannonian Aquifer* (Figures 2.17 and 2.18).

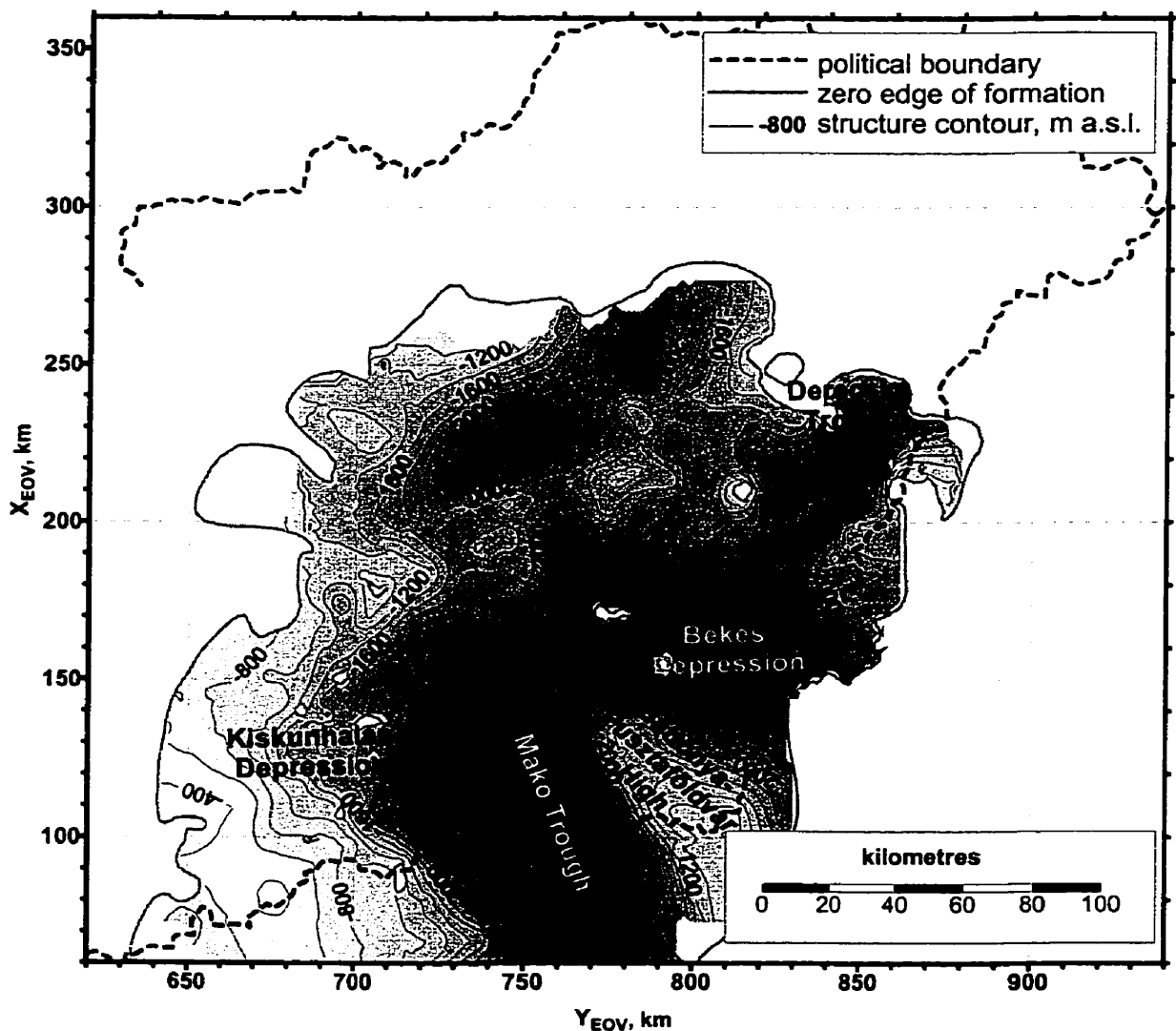


Figure 2.19: Structure contour map of the base of the Szolnok Aquifer / top of the Endrőd Aquitard, with a contour interval of 200 m. Number of control points: 994. Data courtesy of MOL, Plc.

The *Endrőd Aquitard* combines the Tótkomlós Formation and the Nagykőrű Formation; it consists of basal calcareous marls and clay marls (Figure 2.18). The elevation of the top of the Endrőd Aquitard is highly variable because it mimics the complex basement topography (Figures 2.17 and 2.19). The Endrőd Aquitard has a cumulative thickness of 20 to 300 m, which, in isolated locations, may reach up to 800 m (Figure 2.20). Its estimated bulk hydraulic conductivity is $K \approx 10^{-8} - 10^{-10}$ m/s. Above the basement highs, it is directly overlain by the Algyő Aquitard, and within the deep grabens, it is overlain by the Szolnok Aquifer. There are local discontinuities in the Endrőd Aquitard, as indicated by the closed zero-edge curves on the isopach map (Figure 2.20), whereas in the deep basins it shows brittle deformation (Phillips et al., 1994). Water and hydrocarbons may be transmitted across this aquitard along fractures and fault zones. Generally, the basal marls are considered good source rocks for hydrocarbons, and are also excellent cap rocks for petroleum reservoirs of the Middle Miocene and Pre-Neogene age (e.g., Szalay and Koncz, 1993).

The *Szolnok Aquifer* is identical to the Szolnok Formation (prodelta-turbidite facies) (Figure 2.18); it occurs only in the deep sub-basins, always above the deep basin marls; it pinches out along the flanks of the basement highs, and it is covered by the Algyő Aquitard (Figure 2.17). It consists of a cyclic alternation of consolidated light grey sandstone beds, siltstone, and clay marls, and its thickness may reach 1000 m (Juhász, 1991). The estimated bulk hydraulic conductivity of the Szolnok Aquifer ranges $K \approx 10^{-6} - 10^{-7}$ m/s. Important petroleum accumulations are found in the Szolnok Formation, and are located preferentially in regions of stratigraphic pinch-out (e.g., Pusztaföldvár).

The *Algyő Aquitard* is identical to the Algyő Formation (delta slope facies; Figure 2.18), which covers the entire Great Hungarian Plain (Figure 2.21) and its thickness ranges from 100 to 1400 m (Figure 2.22). Its matrix consists predominantly of poorly-to-well consolidated siltstone and clay marl encasing relatively more permeable sand lenses, which were deposited at the base as reworked turbidite or in the upper part as mouth-bar rhythm and submarine channel fill (Pogácsás et al., 1988). Commonly, the strata dip between $5^\circ - 7^\circ$ and often reach $18^\circ - 20^\circ$. Hydraulic communication between the underlying and overlying aquifers across the Algyő Aquitard is enhanced by growth faults that cut across the entire formation or connect isolated sand bodies (Figure 2.17).

Above basement highs, the lithology of Algyő Formation is sand dominated, which locally renders aquifer properties to the formation. As a result, the Algyő Formation can not be considered an efficient regional aquitard. The estimated bulk hydraulic conductivity of the Algyő Aquitard is $K \approx 10^{-8}$ m/s. The top of the Algyő Formation was considered the basal “impermeable” boundary for regional gravity-driven groundwater flow systems (e.g., Erdélyi, 1976; Dövényi and Horváth, 1988; Geiger et al., 1991; Galsa, 1998; Lenkey, 1999). This formation, however, also contains significant petroleum accumulations, and the hydraulic conductivity of the sandstone reservoirs ranges between $K = 10^{-6}$ and 10^{-7} m/s (assuming 100% water saturation).

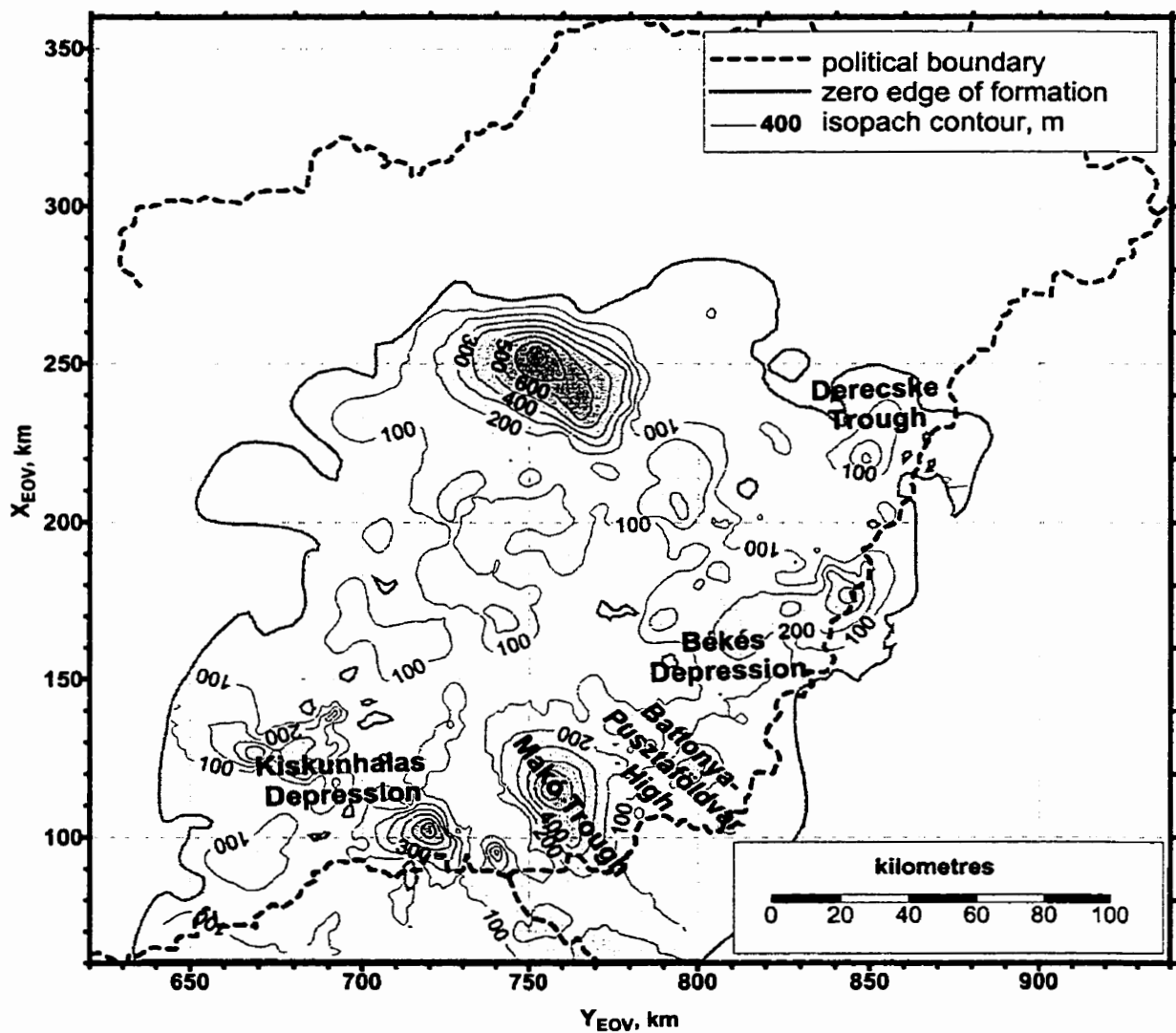


Figure 2.20: Isopach contour map of the Endrőd Aquitard, with a contour interval of 100 m. Number of control points: 994. Data courtesy of MOL, Plc.

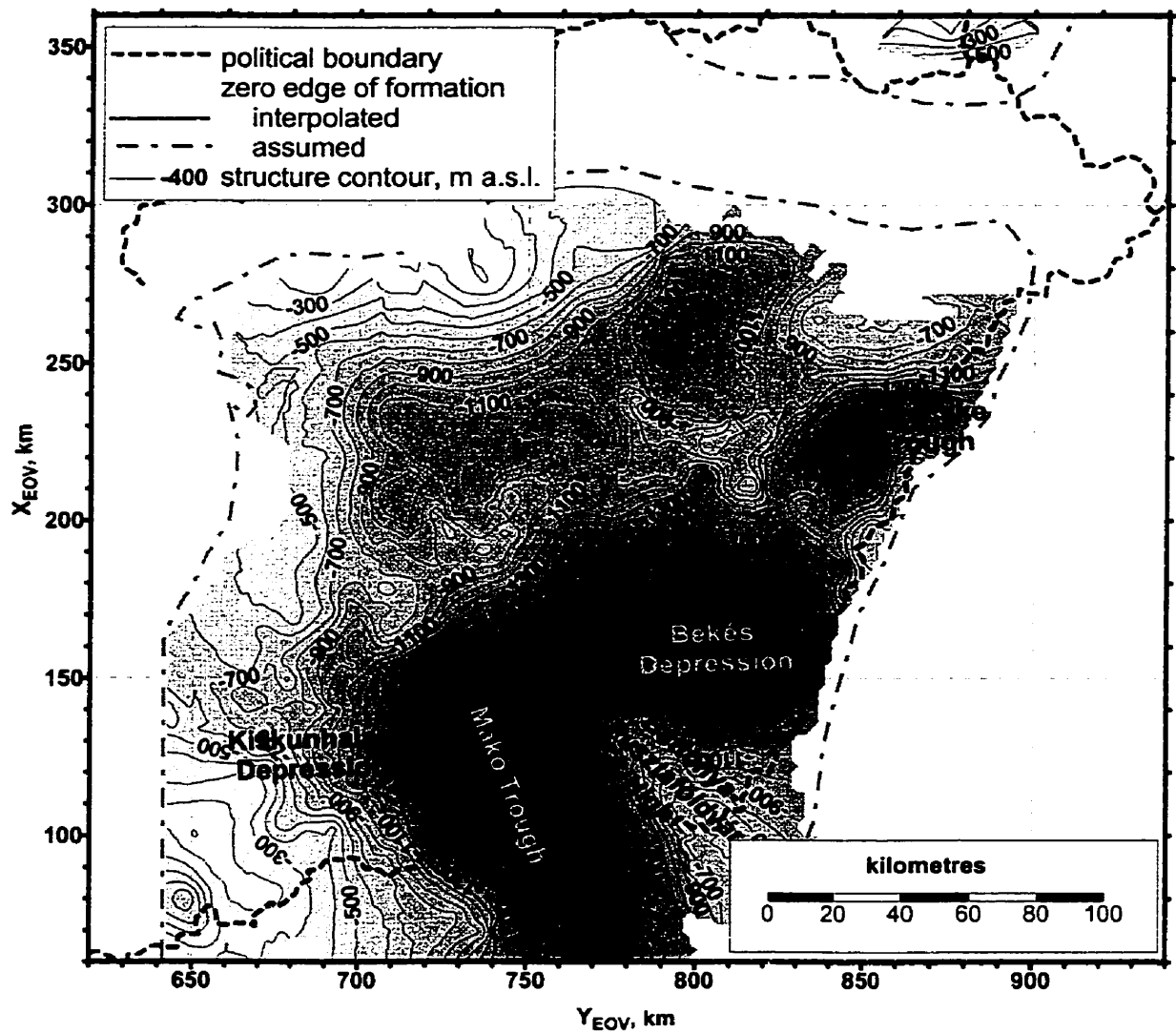


Figure 2.21: Structure contour map of the base of Nagyalföld Aquifer / top of Algyő Aquitard, with a contour interval of 100 m. Number of control points: 1009. Data courtesy of MOL, Plc.

In the northern part of the Great Hungarian Plain, the Oligocene Kiscell Clay Formation has a hydraulic conductivity of $10^{-10} \text{ m s}^{-1}$; this is the tightest clay known in the basin, but it has no regional significance because of its spatially restricted occurrence (Szebényi, 1955). Thus, the estimated bulk hydraulic conductivity values for the regional aquitards, Algyő and Endrőd, seem to be realistic, relative to the Kiscell Clay Aquitard.

The *Nagyalföld Aquifer* comprises the Quaternary sediments, the Nagyalföld Formation, Zagyva Formation, and the Törtel Formation (Figure 2.18); it has a thickness of up to 2400 m and it covers the entire basin. Unconsolidated coarse clastic sediments (sand, gravel, and loess) are dominant in this aquifer. It also contains relatively thin (few

metres) clay and silt beds of varying lateral extent (1 m – 1 km), and, at places, coal measures (Nagyalföld Formation). The alluvial plain deposits (Zagyva Formation) contain thin bedded sequences of sand, silt, and clay, and are dominated by silt (Juhász, 1991). The delta plain and delta front units (Törtel Formation) are rich in sand bodies, which were deposited as distributary mouth bars and channel fill rhythms (Pogácsás et al., 1988). Their thickness commonly reaches 20 - 50 m, and they often merge laterally with one another (Juhász, 1991). At a local scale, the Nagyalföld Aquifer can be conceived of as a layered aquifer system (Halász, 1975; Halász and Szőke, 1992).

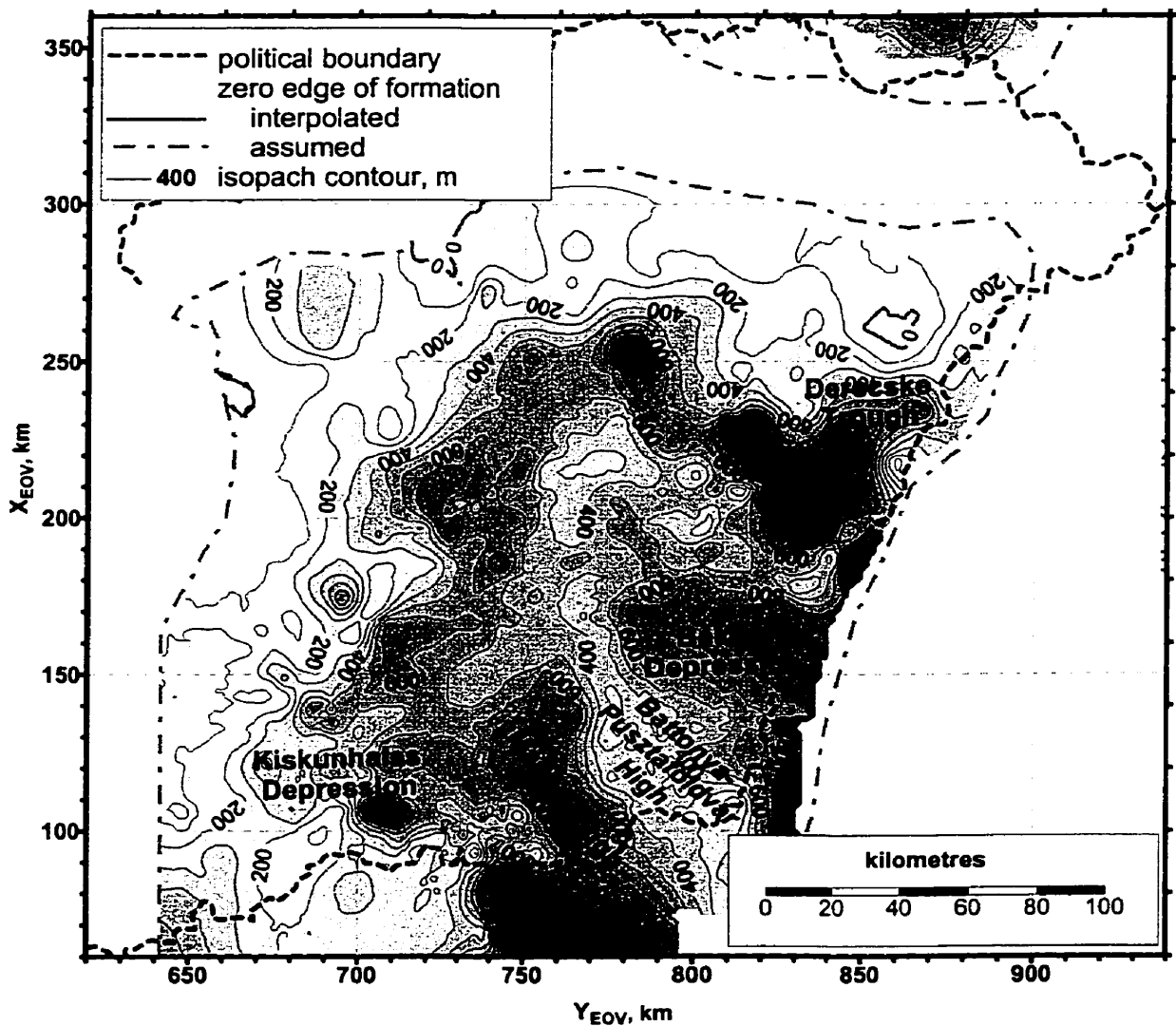


Figure 2.22: Isopach contour map of the Agyó Aquitard, with a contour interval of 100 m. Number of control points: 1009. Data courtesy of MOL, Plc.

In this system, the hydraulic conductivity of the sandy aquifers is in the order of 10^{-3} - 10^{-5} m/s, and that of the clayey aquitards is in the range of 10^{-6} - 10^{-9} m/s (Szebényi, 1955). Due to the predominance and good spatial connectivity of permeable sand bodies, a bulk hydraulic conductivity of $K \approx 10^{-5}$ m/s was adopted for this regional aquifer. Drinking water is produced mainly from the upper part of the Nagyalföld Aquifer (Quaternary and Zagyva Formation), and thermal water is extracted from the underlying Törtel Formation, whereas gas accumulations were discovered in the Zagyva and Törtel Formations.

In summary, the following five regional hydrostratigraphic units were determined in the Great Hungarian Plain, from top to bottom (Figure 2.18): the Nagyalföld Aquifer, the Algyő Aquitard, the Szolnok Aquifer, the Endrőd Aquitard, and the Pre-Pannonian Aquifer. Both the regional aquifers and aquitards consist of an irregularly alternating sequence of smaller (1-100 km² x 1-10 m) 'lenticular' aquifers and aquitards. The Nagyalföld Aquifer is regionally unconfined, while the other two aquifers are regionally confined. Because of the tectonically enhanced hydraulic communication between the regional aquifers across the regional aquitards, it is postulated that the Great Hungarian Plain can be considered a regionally unconfined aquifer over the geologic time scale.

2.6.4 A possible method for enhancing the resolution of regional hydrostratigraphic units

Due to the very nature of the clastic sedimentation in the Great Hungarian Plain, lateral correlation of well logs is quite a difficult and speculative task. On reflection seismic profiles, the lateral continuity of lithologic boundaries (i.e., sand/shale) is indicated by the amplitude contrasts of the reflected seismic waves (Pogácsás et al., 1988). An integrated interpretation of reflection seismic profiles and well logs may facilitate the reconstruction of a two-dimensional stratigraphic architecture, as illustrated in Figure 2.23. It is also possible to infer the permeability of lithologic units from well logs (Schlickenrieder, 1994). Subsequently, a reflection seismic profile can be transformed into a hydrostratigraphic cross section. The level of detail and accuracy of such cross sections is determined by the resolution of the seismic profiles and the available well logs. This way, the relatively fine hydrostratigraphic details of the regional units can be revealed, which is an indispensable prerequisite for local scale

hydrodynamic studies. Unfortunately, no seismic profiles and only a limited number of well logs were available for this study; therefore, the regional hydrostratigraphic units could not be further refined.

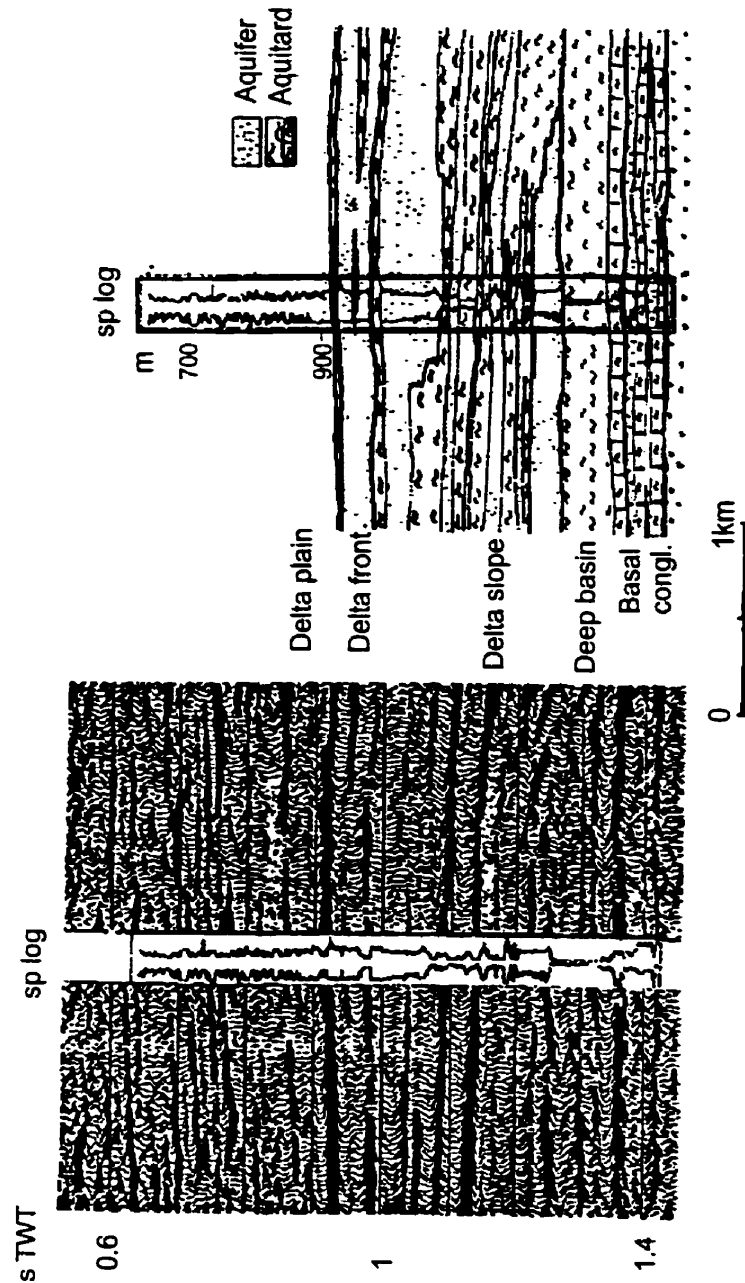


Figure 2.23: Integrated interpretation of a reflection seismic profile and an electric log. The spontaneous potential (sp) and resistivity (r) log from a well is projected onto the seismic profile to identify lithology, sedimentary facies, and lateral extent of individual lithologic units. The reflections with the highest amplitude on the seismic profile coincide with the sand/shale interface (modified from Pogácsás et al, 1988).

2.7 PETROLEUM GEOLOGY

By international standards, Hungary is a small petroleum producer. In the early 1990's, the petroleum industry produced approximately 2×10^6 tons/year of oil, which satisfied only about 10% of the nation's annual demand (Somfai, 1994). Between 1970-1990, the gas production was about $3 - 7.5 \times 10^9$ m³/year, which met the country's annual demand. The oil and gas fields from the Great Hungarian Plain provide about two thirds of the total hydrocarbons produced in Hungary, the remainder comes from the Danube Basin and from the Zala Basin (SW-Hungary). Seven of Hungary's top ten oil fields and nine of the top ten gas fields are in the Great Hungarian Plain. Of these fields, the cumulative amount of original oil in place (OOIP) is 121×10^6 tons (61% of the total), and the original gas in place (OGIP) is 216×10^9 m³ (98% of the total) (Somfai, 1994). According to various estimates, about 55 – 70% of the economically feasible hydrocarbon accumulations have already been found. Therefore, the petroleum exploration risk is increasing and the petroleum potential is decreasing in Hungary (Somfai, 1994). An overview of the history of the Hungarian oil exploration and a map of known hydrocarbon fields were published by Dank (1988) and more recently by Kőrössi (1990, 1992). This section presents an overview of the petroleum geology of the Pannonian basin with emphasis on the Great Hungarian Plain based on a literature review.

2.7.1 Source rocks

According to the Hungarian industrial standards, the rocks containing over 1 mg/g organic carbon are considered “active petroleum source rocks” (Geiger et al., 1991). In the Pannonian Basin, the predominant source rocks are of Middle- and Late Miocene age; these are the *gas-prone terrestrial pelitic rocks* deposited in delta slope and delta plain environment, and the *gas and oil prone marls* deposited in a marine and deep basin environment (Figure 2.18). Generally, the Mesozoic and Paleogene source rocks are ignored because the hydrocarbons generated from them were most likely lost during the process of basin evolution (Somfai, 1994). However, in the western Pannonian Basin the

source rocks of certain oil accumulations are of Triassic age (e.g., Nagylengyel: Clayton and Koncz, 1994). In the Neogene source rocks, 80% of the kerogen is of Type III and 20% is of Type II (Geiger et al., 1991). The average *total organic carbon* (TOC) content of the source rocks is 0.86% (Somfai, 1994) ranging between 0.5 – 1% (Szalay, 1988). Locally, the Middle Miocene source rocks may contain as much as 5.2% TOC (Clayton et al., 1994). Based on geochemical parameters, the quality ranking of potential source rocks deposited in different environments/facies is the following: *Good* (> 1% TOC) = marine and deep basin marls, *Medium* (1 – 0.5% TOC) = delta plain clay-marls, *Poor* (< 0.5% TOC) = delta slope silty clay-marl (Szalay and Koncz, 1991). The hydrocarbons generated from the mature source rocks are ~67% gas (90% CH₄ and 10% is CO₂ + N₂) and ~33% oil (mostly paraffinic, with little S₂, and density in the range of 700 – 900 kg/m³) (Geiger et al., 1991).

2.7.2 Maturation

Maturation of Neogene source rocks in the Pannonian Basin is an ongoing process, which commenced about 9.5 – 6.5 Ma (Szalay, 1988). The process of maturation was accelerated by the large basal heat flow in the basin (Horváth et al., 1988). The source rocks found at depths shallower than 1500 m (Törtel Formation and in some places the upper part of Algyő Formation) are generally immature, with a vitrinite reflectance of $R_0 < 0.4\%$ (Szalay, 1988; Geiger et al., 1991). Currently, the organic matter from these shallow sediments is in the process of biochemical degradation, characteristic for the early stage of diagenesis, during which biogenic gas, peat, and lignite are being generated. Biogenic (microbial) gas accumulations of commercial value are known from Hajdúszoboszló, Tatárüllés, and Kunmadaras (Figure 2.24; Somfai, 1994). Diagenetic gas is being generated from source rocks with a maturation level of $R_0 = 0.4 – 0.6\%$. Commercially significant accumulations of diagenetic gas are known from Battonya, Pusztaföldvár, Tótkomlós, and Endrőd (Figure 2.24; Clayton et al., 1994). Active oil generation by thermal metamorphosis of organic matter (catagenesis) occurs in the depth range of 2000 – 4000 m, where the source rocks have a vitrinite reflectance range of $R_0 = 0.6 – 1.3\%$ (Geiger et al., 1991; Szalay, 1988). The depth to the “oil birth line” (depth where $R_0 = 0.6\%$) is increasing toward the centre of the basement grabens (Figure

2.25; Szalay, 1988). Wet gas is generated in the depth interval of 3400 - 4900 m, where the vitrinite reflectance ranges $R_0 = 1.3 - 2 \%$. The dry gas generation zone is between 4100 - 5600 m depths, where the vitrinite reflectance is $R_0 > 2 \%$ (Geiger et al., 1991). Many reservoirs have high temperatures, ranging between 100 - 180 °C, suggesting that “in-reservoir maturation” may also be an important process (Szalay and Koncz, 1993). However, in some places relatively heavier oils occur (API gravity of 30° - 35°) at temperatures of 100 - 150 °C, therefore, the ‘in-reservoir maturation’ does not seem to be a major process (Clayton et al., 1994).

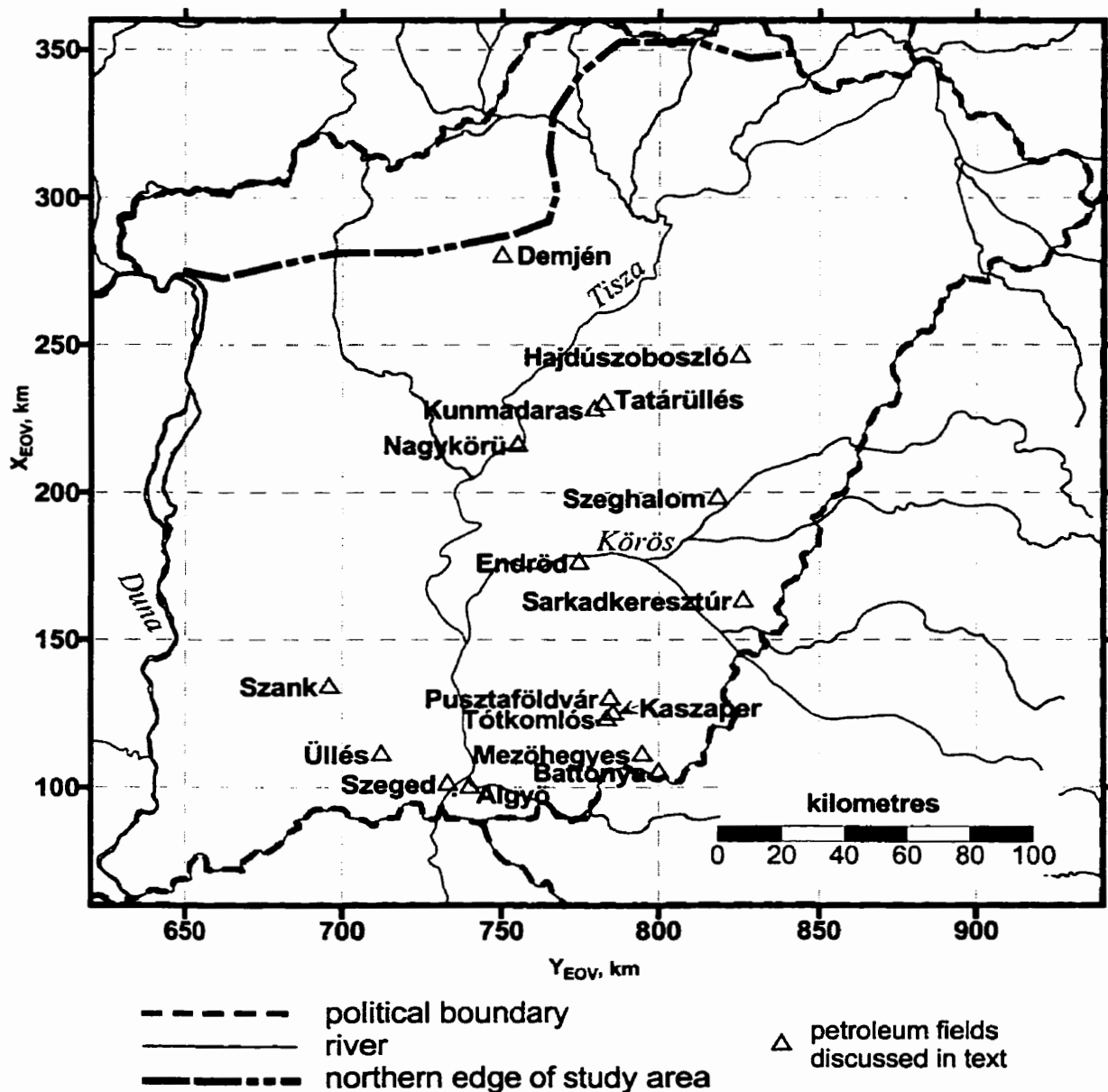


Figure 2.24: Index map of hydrocarbon fields discussed in the text.

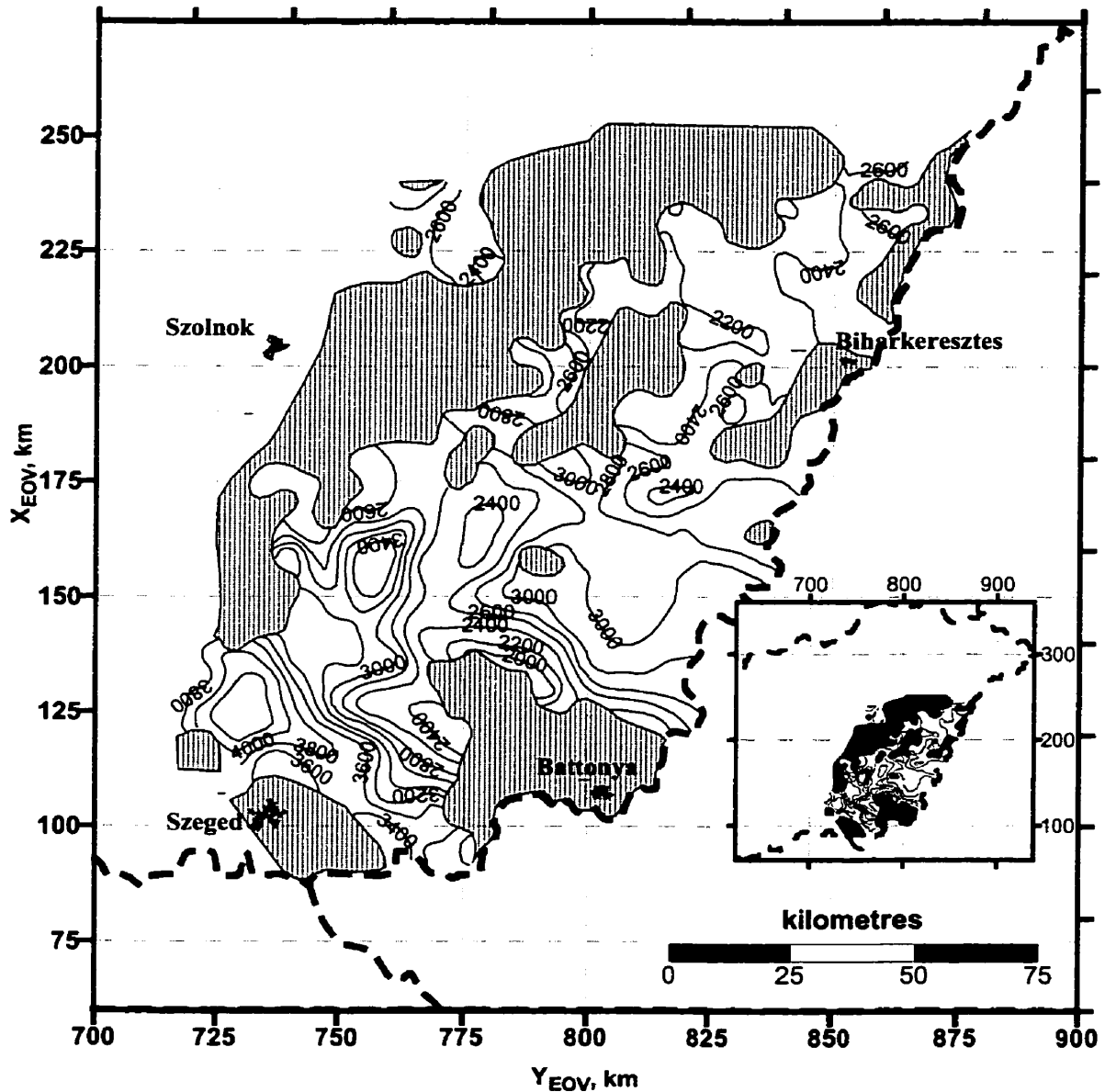


Figure 2.25: Depth to the oil birth line ($R_0 = 0.6\%$ iso-reflectance surface) in the Great Hungarian Plain (after Szalay, 1988). Depth contour lines are drawn at 200 m contour interval. Grey areas represent basement highs covered by immature reservoir and source rocks. The inset map shows the mapped portion of Eastern Hungary.

2.7.3 Carrier beds and reservoirs

In the Pannonian Basin the carrier beds (sandstone, conglomerate, fractured Pre-Neogene basement rocks) also become reservoirs for the migrating hydrocarbons (Pap, 1976). Figure 2.26 is a schematic illustration of possible migration paths and common

reservoir configurations in the Pannonian Basin. The regional unconformity between the Pre-Pannonian and Pannonian units, as well as the Pre-Neogene and Neogene faults are major avenues of hydrocarbon migration (Geiger et al, 1991; Pogácsás et al, 1994).

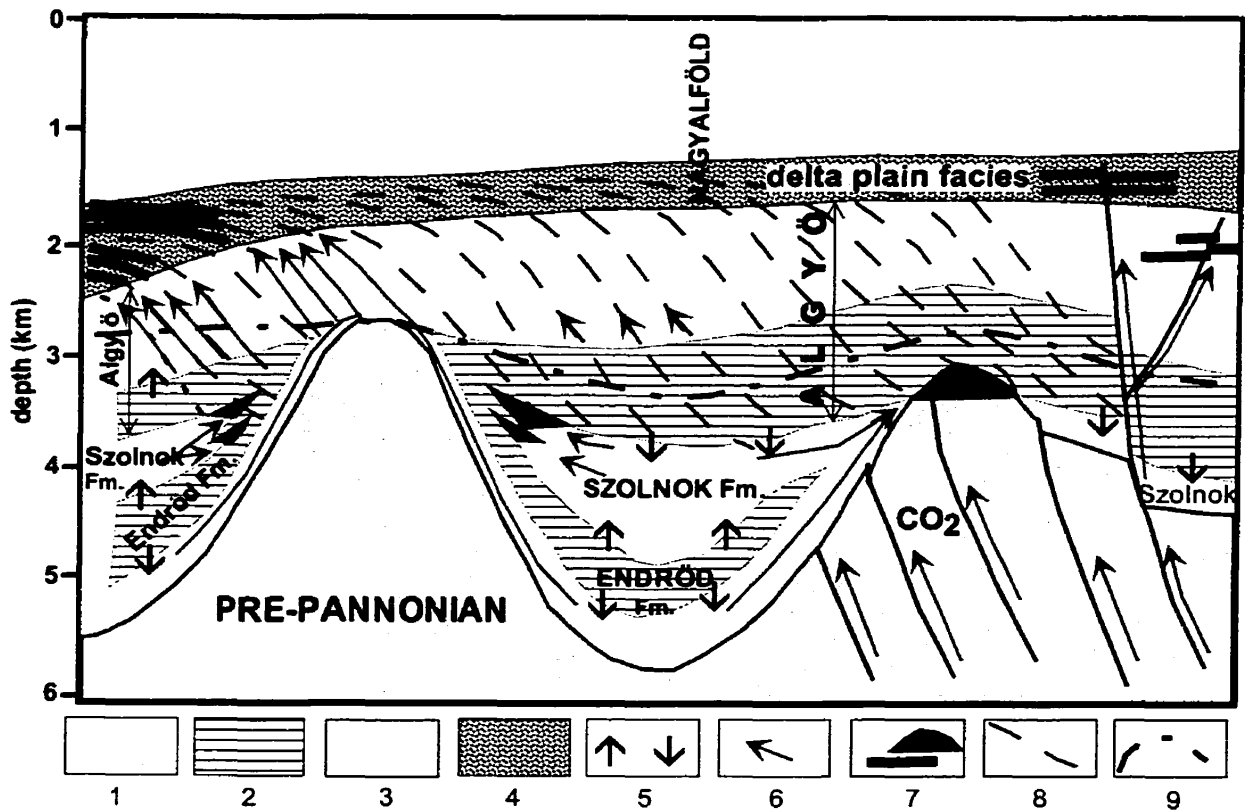


Figure 2.26: Petroleum migration systems in the Great Hungarian Plain postulated by Szalay and Koncz (1993). Symbols: 1 = basement; 2 = source rocks; 3-4 = carrier beds and reservoirs; 5 = primary migration; 6 = secondary migration; 7 = HC-accumulations; 8 = possible migration pathways; 9 = oil birth line, $R_0 = 0.6\%$ iso-reflectance surface; (after Szalay and Koncz, 1993).

The petroleum reservoirs in the Great Hungarian Plain are found in the following regional hydrostratigraphic units (Figure 2.18 and 2.26; Pap, 1976; Szalay and Koncz, 1993):

- Pre-Pannonian Aquifer; in the fractured basement highs, sealed by the Endrőd Aquitard or Algyő Aquitard (e.g., Pusztaföldvár, Algyő, and Sarkadkeresztúr; see location on Figure 2.24).

- Szolnok Aquifer; associated with stratigraphic pinch outs of sandstone into clay-marl in the proximity of the flanks of basement highs (e.g., Pusztaföldvár; see location on Figure 2.24).
- Algyő Aquitard; in sandstone lenses that are often connected by faults and sealed by silty clay-marls (e.g., Mezőhegyes, Endrőd; see location on Figure 2.24).
- Nagyalföld Aquifer; in sandstone lenses sealed by clay layers within the delta plain sediments (e.g., Kaszaper, Mezőhegyes; see location on Figure 2.24).

Often, the sandstone reservoirs are vertically stacked, regardless of which formation they belong to. The thickness of the sandstone layers rarely exceeds 70 m (Geiger et al., 1991). The domed sandstone reservoirs above the basement highs are commonly regarded as folded or compaction anticlines (e.g., Dank, 1988). The characteristic porosity (ϕ) and permeability (k) ranges of the above reservoirs are listed in Table 2.1; data from: Pap (1976), Bérczi and Kókai (1978), Geiger et al. (1991), and Somfai (1994).

Table 2.1. Characteristic porosity (ϕ) and permeability (k) of petroleum reservoir rocks in the Pannonian Basin. Data from: Pap (1976), Bérczi and Kókai (1978), Geiger et al. (1991), and Somfai (1994).

Age of reservoir rock	Porosity, ϕ (%)	Permeability, k (m^2)
Pre-Pannonian	2 - 5	10^{-13} - 10^{-12}
Lower Pannonian	10 - 15	10^{-14} - 10^{-13}
Upper Pannonian	20 - 25	10^{-13} - 10^{-12}

2.7.4 Petroleum accumulations and migration

The areal distribution of known hydrocarbon fields in Hungary, in particular the Great Hungarian Plain, is illustrated in Figure 2.27 and in Dank (1988, Map 4). The pattern of hydrocarbon field distribution in the eastern and south-eastern part of the Great Hungarian Plain correlates remarkably well with the location of basement highs and the associated anticline structures in the Neogene sediments (Szalay and Koncz, 1993). The

wildcat wells were drilled to a depth interval of 600 to ~3200 m, predominantly on basement highs, anticline structures, and stratigraphic traps (e.g., pinch outs) identified on seismic profiles (Körössy, 1990, 1992). Almost every anticline structure in the basin has been tested with drilling, and indeed, many pools were found there. However, the potential reservoir quality strata in the deep basinal structures were ignored (Somfai, 1994).

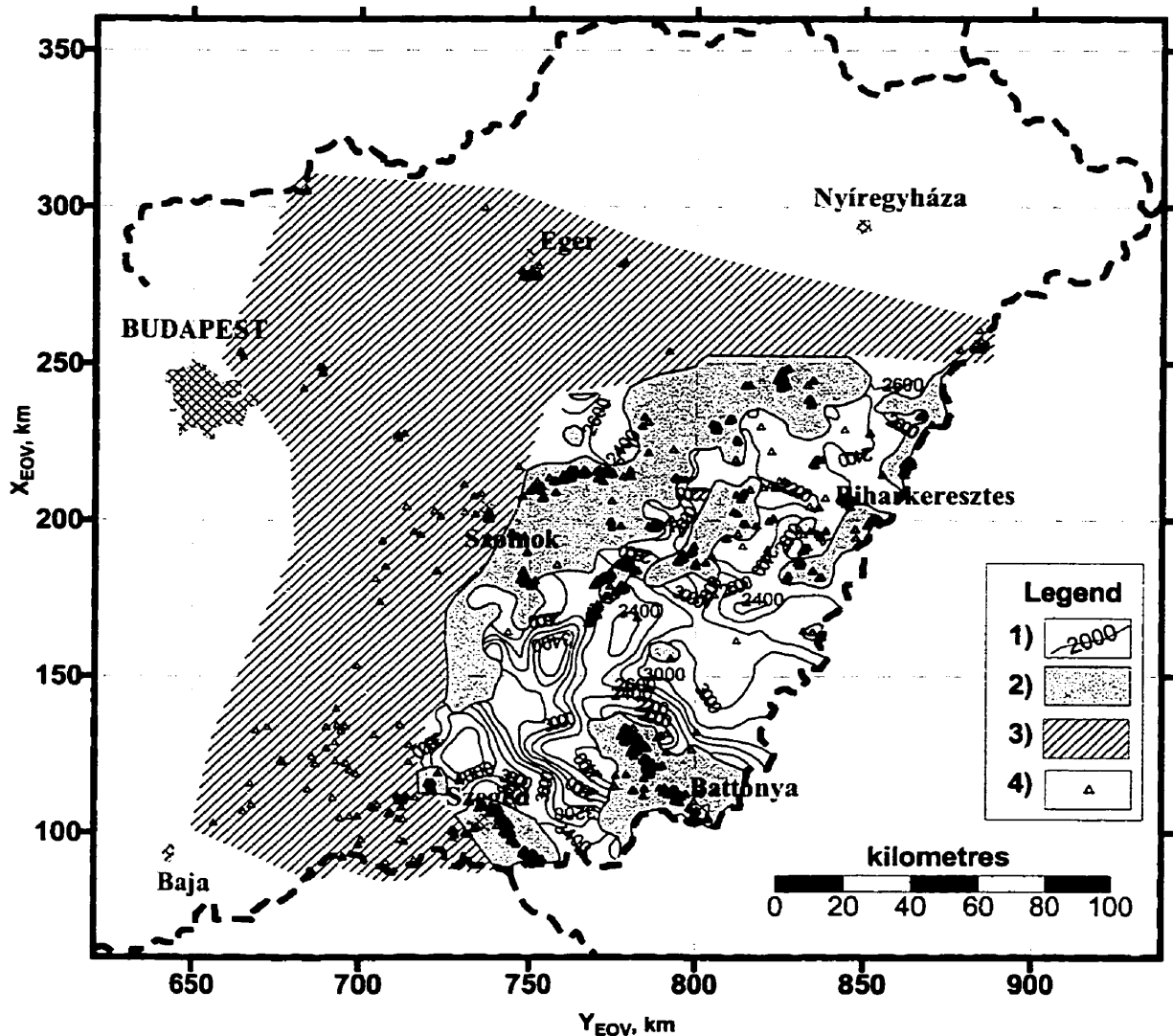


Figure 2.27. Distribution of known petroleum accumulations and their spatial relation with the top of the oil generation zone in the E-SE part of the Great Hungarian Plain. Legend: 1) depth to the oil birth line (m) also shown on Figure 2.25; 2) basement highs covered by immature reservoir and source rocks; 3) areas of un-mapped maturity conditions in the vicinity of petroleum accumulations; 4) petroleum accumulations (contour map of depth to $R_0 = 0.6\%$ after Szalay, 1988).

The known petroleum accumulations consist mainly of gas (often with condensate) and secondarily of oil; mixed, oil and gas, accumulations are also common. Most gas accumulations are characterised by the presence of “inert gases” like CO₂, N₂, and H₂S; CO₂ is the dominant inert gas, which may reach a concentration of 20 - 90 vol.% (Geiger et al., 1991). Large accumulations of CO₂ of inorganic origin are known in the basin, and Kertai (1972) suggested that they are derived from the thermal decomposition of the deeply buried (> 8-10 km) Mesozoic carbonate rocks from the basement. This hypothesis was tested by Koncz (1983) using carbon isotope (¹³C) analysis, who found sufficient circumstantial evidence to support Kertai’s hypothesis. Subsequently, Kertai’s idea was generally accepted in the literature by Szalay (1988), Clayton et al. (1990), Geiger et al. (1991), etc. The origin of N₂ and H₂S is not yet clear (Geiger et al., 1991).

Most of the known petroleum accumulations are located above the oil birth line, suggesting substantial vertical migration (Szalay, 1988). The lack of correlation between the isotopic composition of gas and reservoir depth, as well as the presence of oils with various densities and boiling points derived from different sources in the stacked reservoirs suggest that significant mixing occurred during migration (Szalay and Koncz, 1991; Geiger et al., 1991; Clayton et al., 1994; Clayton and Koncz, 1994). The lighter oils were most likely produced by source rocks buried below ~3000 m, whereas the heavier oils originated from shallow (about 2000 m) source rocks (Clayton et al., 1994). Below a depth of ~1800 m the fluid pressures are abnormally high, i.e., 1 - 15 MPa, or more, above hydrostatic (detailed discussion in Chapter 4). The source rocks are found in this overpressured zone. Given this coincidence, the super-hydrostatic pressures were thought to be the principal driving force for vertical and lateral hydrocarbon migration (Szalay, 1982, 1988; Szalay and Koncz, 1993). Various mechanisms were proposed to explain the generation of overpressures and their role in hydrocarbon migration in the Great Hungarian Plain. For instance: disequilibrium compaction and aquathermal expansion (e.g., Somfai, 1976; Szalay, 1982), hydrocarbon generation (Spencer et al., 1994), and thermal decomposition of carbonate rocks (Clayton et al., 1990; Spencer et al., 1994). Szalay and Koncz (1993) suggested that the hydrocarbons were expelled vertically (upward and downward) from the source rocks into the adjacent carrier beds, in which they were transported radially outward, toward the flanks and tops of basement highs by

the water expelled during compaction (Figure 2.26). Eventually, hydrocarbons were trapped in structural or stratigraphic traps.

The Algyő field (Figure 2.24) is the largest mixed hydrocarbon accumulation in Hungary, which contributes about 50% of the national yearly oil and gas production. At the time of its discovery, in the early 1960's, the estimated amount of "original oil in place" was 76 million metric tons, while the estimated amount of "original gas in place" was 109 billion m³ (Somfai, 1994). The lateral extent of the field is ~80 km². The accumulations are located in the 1600 – 2500 m depth interval, in the fractured basement high, and in stacked sandstone reservoirs from the Békés, Szolnok, Algyő, and Zagyva Formation (e.g., Dank, 1988). Other large oil fields, such as Szeged, Demjén, Szank, Szeghalom, Battonya, and Pusztaföldvár, had each approximately 9 – 6 million metric tons of original oil in place (Figure 2.24). The original gas in place of other important gas fields ranges between 29 – 4 billion m³, each (e.g., Hajdúszoboszló, Pusztaföldvár, Szeghalom, Üllés, Szank, Nagykőrű, Sarkadkeresztúr, and Endrőd; see Figure 2.24). Most of the other known accumulations are about two orders of magnitude smaller than the ones mentioned above.

2.7.5 Hydrocarbon potential

Somfai (1994) predicted that probably 30 to 45% of the economically feasible petroleum fields in Hungary remain to be discovered, and these are thought to be located in "subtle traps" (stratigraphic and tectonic traps) below a depth of 3000 m and related to basement highs. The central parts of the deep sub-basins in the Great Hungarian Plain are weakly explored by drilling, and organic geochemical data are scarce. Therefore, their hydrocarbon potential is subject to speculation based on probabilistic numeric models.

According to a recent organic geochemical study in the Békés Basin (Charpentier et al., 1994), the estimated undiscovered oil is 5.22×10^6 metric tons, while the undiscovered natural gas amounts to 18.05×10^9 m³. The most promising plays are in the delta front sandstones (Törtel Formation) with a mean potential for oil of 1.9×10^6 metric tons, while the prodelta turbidite sandstones (Szolnok Formation) have the greatest potential for natural gas accumulation, 5.22×10^9 m³. Approximately 42% of the predicted recoverable oil and 58% of the predicted recoverable natural gas have been discovered by

1985 (Charpentier et al., 1994). Compared to the volume of hydrocarbons accumulated in the Algyő field, the Békés Basin has a very low potential. In other regions of the Great Hungarian Plain, such as the Makó and Derecske troughs, similar appraisals of the hydrocarbon potential were not available.

3 DATA

The first objective of the present project was to compile a comprehensive database consisting of all the necessary and available data required for a regional petroleum hydrogeological study in the Great Hungarian Plain, from the land surface to the maximum depths of exploration. In Hungary, water exploration data are traditionally acquired from depths shallower than 1000 m, while the oil industry acquires data mostly from the 1000 m to 4000 m depth range. As a result of poor communication between the oil industry and the companies/organisations involved in water exploration, confidentiality reasons, and, to a certain degree, a lack of initiative during the past five decades, it has been practically impossible to consolidate hydrogeological information from all sources in the country. This situation has hindered the preparation of comprehensive regional scale hydrogeological studies that could have encompassed the entire explored extent of the Pannonian Basin. Thus, the first objective of this project was also a first attempt to gather and merge accessible data from as many possible sources.

For this study, data were provided by and gathered from the following sources: Hungarian Oil and Gas Co., Plc. (MOL, Plc.), Hungarian Geological Institute (MÁFI), Water Resources Research Centre, Plc. (VITUKI, Plc.), Mr János Viszok (Petroconsultants S.A., Geneva, Switzerland), Dr. Attila Somfai, Sr. (University of Miskolc), and from refereed publications, atlases, and monographs. The working database prepared for this study is included in digital format on the attached CD-ROM and the required explanatory notes are in Appendix 1.

3.1 STRATIGRAPHY

Stratigraphic information was provided by MOL, Plc. and by Mr. Viszok in electronic format on MSExcel spreadsheets and as hard copies of geologic maps. Ms. Gy. Juhász (MOL, Plc.) identified the elevation of lithostratigraphic formation boundaries from 986 well logs. In addition, stratigraphic data from wells from Serbia (185 wells), Romania (86 wells), Ukraine (9 wells), and Slovakia (28 wells) were included in the database, courtesy Petroconsultants S.A. The original well logs were unavailable;

therefore, a quality check of formation identification could not be performed on these data. The stratigraphic database is included in the digital Appendices on the CD-ROM as ASCII comma delimited text file: *hu_strat.dat*.

3.2 FLUID PRESSURE AND WATER LEVEL DATA

Fluid pressure data from drill-stem tests (DST's) were provided by MOL, Plc. (2436 records) and by Dr. A. Somfai, Sr. (1270 records) in electronic format (MSExcel spreadsheet), and as hard copy of 298 original DST reports. MOL, Plc., also provided 649 records of calculated initial pool pressure data, which were not classified according to any quality criteria.

The original spreadsheets of DST data contained the well names, the maximum recorded pressure values (final shut-in pressures) or the stabilised pressure values extrapolated with the Horner-method (Horner, 1951), the depths of the measurements (usually the depth of a pressure gauge), the depth interval of perforation, and the depth of packers. Essential information not provided with the data received in digital format included the well co-ordinates, date of measurement, technical remarks about the tests, a copy of the recorded pressure build-up curve, and the production history. Information on the type of fluid(s) produced during the DST was often unavailable, and each reported DST-pressure referred to formation water pressure (S. Pap, 1996, *personal communication*). The estimated volume of gas, oil, condensate, or water present in the reservoir was mentioned in most printed DST-reports.

A total of 49 265 stabilised water level data (non-pumping water level) were obtained from VITUKI, Plc. and MÁFI in electronic format. The VITUKI, Plc. database (VIFIR) contained stabilised water level measurements from drilled wells, bored- and hand-dug water table wells, and thermal-water wells, recorded between the years 1800 and 1995. Lithologic information, time-drawdown data from pump or bail tests, and details of well completion are scarce; only the year of water level measurement was contained in the VIFIR. MÁFI provided 519 non-pumping water level data in a similar electronic format and structure as the VITUKI, Plc.

3.2.1 Data processing

With the help of MOL staff, sufficient information was gathered and used to calculate the maximum or stabilised pressure values at the centre of the tested formation interval, that is the middle of perforation or the middle of packers. The well co-ordinates were found in internal reports and spreadsheets of other data types (e.g., stratigraphy), and appended to the corresponding records in the database. Some well co-ordinates were estimated based on information found in reports and the co-ordinates of adjacent wells. The accuracy of these estimates is within 1 km. Well co-ordinates given in a projection system other than the EOV (e.g., stereographic) were converted into the EOV-system with a code designed and provided by MOL, Plc. Wherever possible, missing formation names for the tested intervals were identified from the stratigraphic spreadsheet. There was a significant overlap between the original DST reports and the spreadsheets. Therefore, the overlapping data were retained or eliminated according to the results of evaluation of the reports. 95 tests were reported misrun, 60 tests were technically useless (i.e., incomplete records, the pressure gauge was 100 – 600 m above the test zone, the initial shut-in pressure was >10% larger than the final shut-in pressure, strong negative anomaly) and 143 tests were acceptable. Ideally, there should be an agreement within $\pm 5\%$ between the initial shut-in pressures and the final shut-in pressures (Bair et al., 1985). The fluids produced in the accepted tests always contained some mud, gas and/or oil. Horner-extrapolated stabilised pressure was calculated for all these tests. However, the influence of production and interference between producing or tested wells on every pressure measurement could not be systematically assessed due to lack of production data. Eventually, 647 DST-pressure data were accepted and incorporated in the working-database.

Usually, the DST's performed by MOL, Plc. (and its predecessors) were run for 72 to 168 hours. Due to the fact that the Neogene sediments are poorly consolidated and overpressured, a dense drilling mud (1400 to 2200 kg/m³, occasionally 2400 kg/m³) had to be used to prevent potential blow-outs (I. Horváth, 1996, *personal communication*). The drilling mud often plugged the reservoirs; therefore, the test had to run for several hours in order to unplug and clean the pores, and allow production of formation fluids. During the (unusually) long flow and shut-in periods, the formation pressure could build up and approach its original equilibrium level, which would be approximated with the

Horner-method (Horner, 1951). The *equilibrium pressure* is not necessarily equal to the undisturbed *virgin* formation pressure that existed prior to production, DST, or any other artificial transient effect. The equilibrium pore pressure may be equal to a pressure adjusted to a regime influenced by long lasting fluid production or injection. Therefore, the equilibrium pressure is an underestimate of the virgin formation pressure in a generally overpressured zone influenced by production. On the other hand, in a naturally underpressured regime, long-lasting fluid injection may raise the pore pressure within the zone of influence of the injection wells, whereby the estimated equilibrium pressures will be greater than the original, virgin, formation pressures. Ideally, for the reconstruction of the undisturbed fluid-potential field, virgin formation pressures are required (Tóth, 1978). However, stabilised equilibrium pressure data can also be used for first order approximation of present-day fluid-potential fields, provided the data are consistent.

The initial pool pressure data referred to the depth of the water hydrocarbon interface. Thus, the initial pool pressure was considered to be equal to the equilibrium formation pressure that existed prior to the discovery of the pool. No additional information was available to test the accuracy and validity of these data. Pressure versus depth analysis and mapping of initial pool pressures revealed 201 records showing strong negative anomalies (difference between observed pressure and hydrostatic pressure < -0.5 MPa); these values were attributed to production effects. 448 initial pool pressure data were consistent with the accepted DST data, therefore, they also qualified as “acceptable.” A total of 1298 records were accepted and used throughout this study from the original pressure data received from MOL, Plc. and Dr. Somfai, Sr. The calculated pressure values were converted into freshwater hydraulic heads (Hubbert, 1940):

$$h = z + p/\rho_w g \quad (3.1)$$

where h = hydraulic head (m), z = elevation head (m), or the elevation of the centre of the perforation, p = equilibrium pressure of the formation fluid (MPa), ρ_w = freshwater density (= 1000 kg/m³), g = acceleration due to gravity (= 9.8067 m/s²). Mapping freshwater hydraulic head distribution and pressure-depth profiles aided the identification of dubious DST pressure data. Because of the abundance of anomalously high pressure values (> 1 MPa above hydrostatic) below variable depths, it appeared that anomalous super-hydrostatic values are characteristic in the given tested zones. Thus, sub-hydrostatic pressure values in the generally overpressured test zones were eliminated,

because these measurements were most likely influenced by production. In several instances, the suspicion of production-influence on pressure data was confirmed by MOL, Plc., based on their undisclosed production history data. Given the incomplete information about each DST pressure data, it was impossible to ascertain the quality and reliability of every pressure measurement.

In dealing with the stabilised water level database, all those records were eliminated, which had insufficient information to calculate the hydraulic head. The water levels were measured with reference to the land surface in metres; positive water levels are above- and negative water levels are below the land surface. Thus, the freshwater hydraulic head (h) was calculated from the water level datum (l_w) and the land surface elevation of the well location (z_o):

$$h = l_w + z_o; (l_w > 0 \text{ water level above land surface}) \dots\dots\dots(3.2)$$

For practical purposes, the freshwater pressure at the base of the wells was calculated from the water level data, assuming a water density of $\rho_w = 1000 \text{ kg/m}^3$. The drawdown effects of producing wells adjacent (within 0.1 – 5 km radius) to the wells reported in the database could not be assessed because water production data were not available. Water level data were also culled by mapping their corresponding hydraulic head values and marking those datum points, which are inconsistent with adjacent data (Bair et al., 1985; Bachu et al., 1987). Local pressure-depth [p(d)] and pressure-elevation [p(z)] profiles also aided in identification of dubious data.

The VIFIR database had two inherent problems: first, the measurements were heterochronous (i.e., made in different years, months, and seasons). Secondly, several hundred people contributed measurements to the database, thus it was unrealistic to assume a uniform reliability of every contributor. After sorting and culling, 14 894 water level records were retained. The accepted static, or non-pumping, water level data are suitable for regional scale studies of groundwater flow because the small scale effects of production or of seasonal water level variation are diminished by averaging over the large time span of observations.

In summary, the fresh water hydraulic head database consists of 16 192 records derived from stabilised water level data (14 894 records out of 49 265) and DST-pressure data (1298 records out of 3706) (Figure 3.1). The depth range of pressure measurements ranges between 4 – 4813 m. The overall quality of the database is fair to acceptable,

suitable for mapping fluid-potentials and to infer general regional scale groundwater flow directions. Figure 3.2 illustrates the relative frequency of all the accepted pore-pressure and water level data for 250 m depth intervals. About 90% of the data were measured at depths not exceeding 500 m. The relative frequency of stabilised water well data versus depth at 250 m depth increments is illustrated on Figure 3.3. Similarly, the relative frequency of DST pressure data versus depth is shown on Figure 3.3. The latter two figures clearly illustrate the depth ranges where the water and petroleum industry has thus far concentrated and the importance of combining the data from both sources in order to obtain a new more coherent picture of the hydrodynamic conditions in the Great Hungarian Plain. A digital version of the final hydraulic head database is included in the CD-ROM (Appendix 1); file name: *h_heads.dat*.

3.3 TOPOGRAPHY

The topographic maps provided for the study area were at a 1:500 000 scale or smaller, with elevation-contour intervals of 100 m. The total elevation difference on the study area hardly ever exceeds 150 m; therefore, such maps were inadequate for the purposes of this study. Consequently, a digital topographic map of the study area was prepared 'in-house' based on 15 235 wellhead elevation data (duplicate records were eliminated) in EOVC co-ordinates with the program SURFER 6 (Figure 2.3). This digital map could be reproduced and plotted at any desired scale and preferential contour interval. It proved to be practical to use a 10 m contour interval for regional scale mapping at the 1:500 000 and 1:1 000 000 scale. This topographic map can be regenerated using the well co-ordinates from the hydraulic head data sheet (Appendix 1; CD-ROM: *h_heads.dat*).

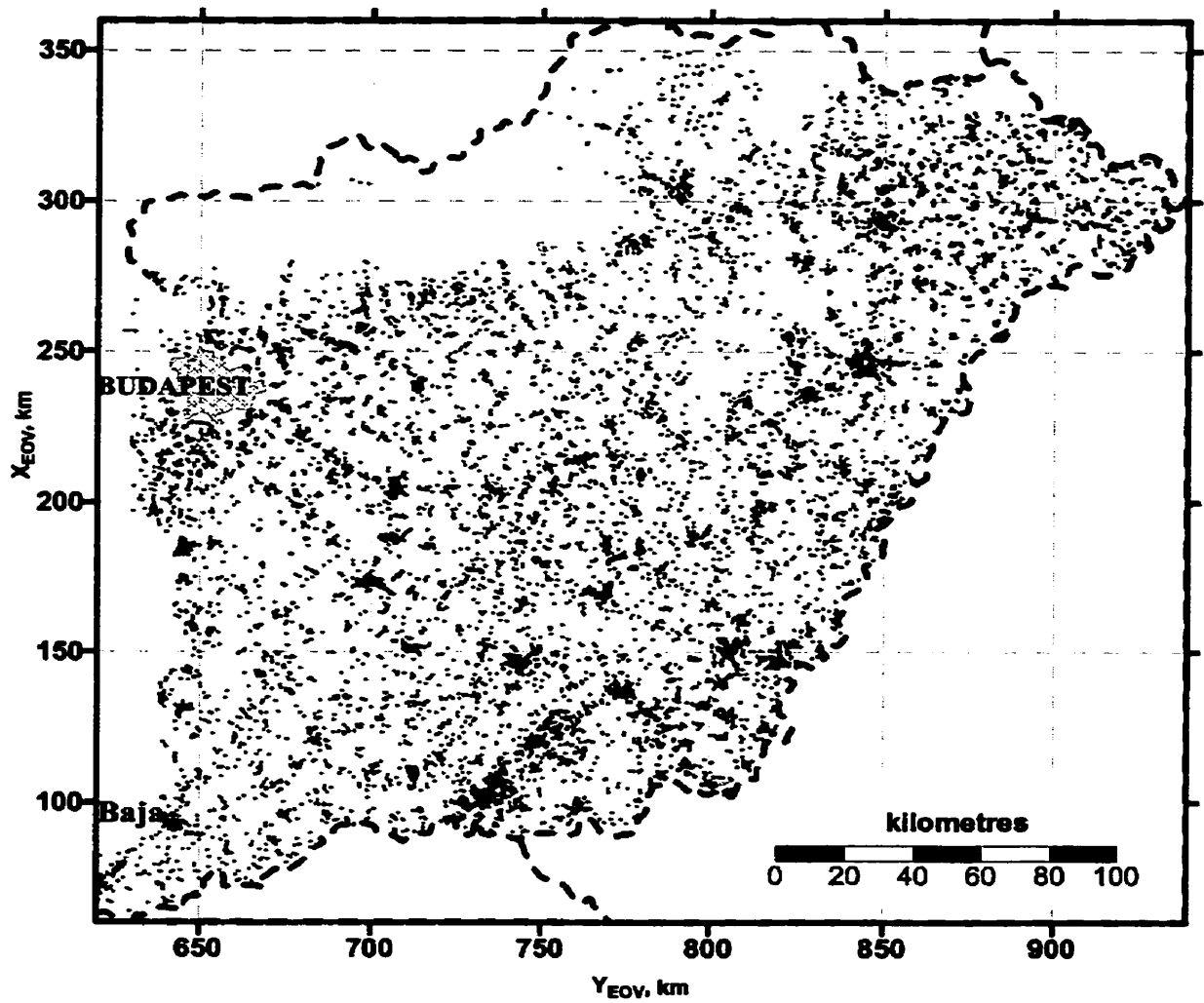


Figure 3.1: Areal distribution of wells with acceptable fluid pressure and stabilised water level measurements in eastern Hungary.

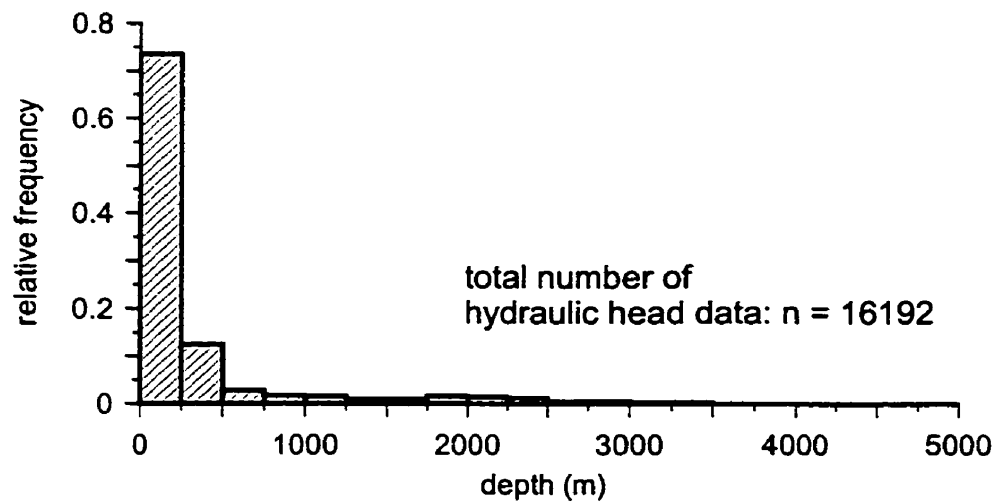


Figure 3.2: Relative frequency versus depth distribution at 250 m depth increments of wells with accepted stabilised water level and DST pressure data from all sources.

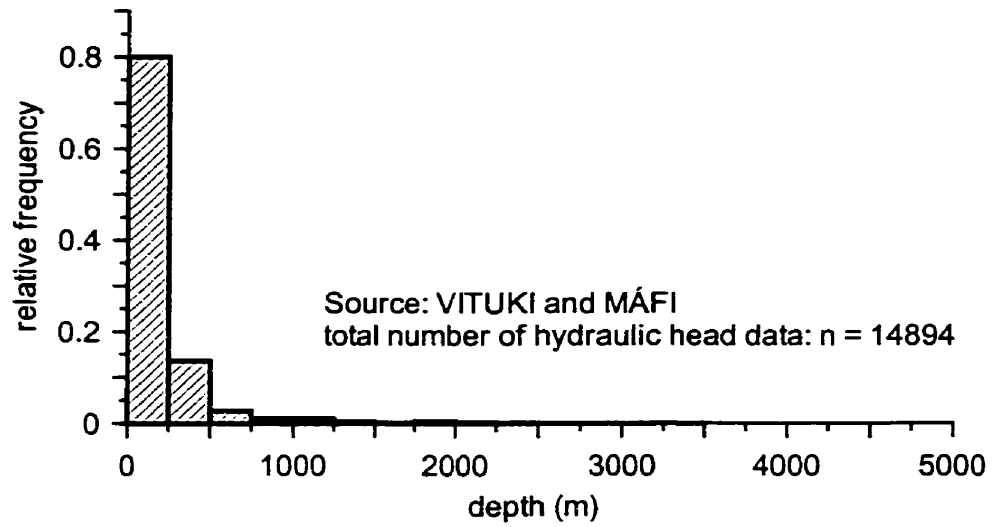


Figure 3.3: Relative frequency versus depth distribution at 250 m depth increments of wells with accepted stabilised water level data from VITUKI, Plc.and MÁFI.

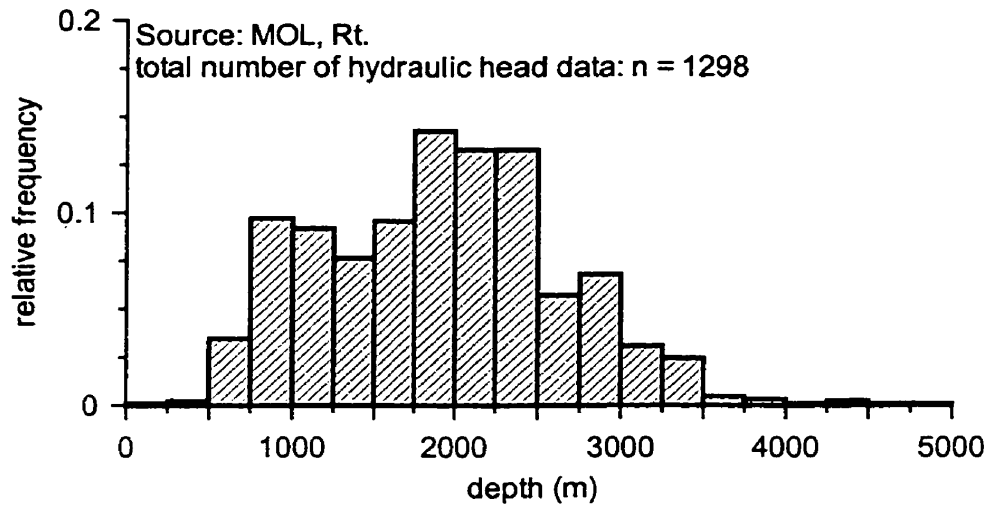


Figure 3.4: Relative frequency versus depth distribution at 250 m depth increments of wells with accepted drill-stem test (DST) pressure data from MOL, Plc.

3.4 SUBSURFACE TEMPERATURE

Two geothermal data sets were available for this study. A published data set (Dövényi and Horváth, 1988) and an industrial one from MOL, Plc. The published data set comprises 2734 reliable and corrected steady-state temperature measurements from Hungary. From this database, 1562 measurements were obtained from the study area (Appendix 1; CD-ROM: *geotherm.dat*). The data base contains measurements of bottom hole temperature (BHT), outflowing water temperature, and temperatures recorded in special geothermal wells and during drill stem tests (DST). The temperature data were corrected and culled by Dövényi and Horváth (1988), and only the steady-state temperature values were retained. Three categories of reliability were determined:

- 1 = best, true steady-state temperature values cross validated by different measuring techniques; the calculated average thermal gradients differ by less than 10%;
- 2 = good, a single steady-state temperature from one hole or from a DST;
- 3 = fair, corrected temperature measurement of outflowing water and any other measurement that may have had errors of more than 10%.

The category of reliability for the measurements made in the special geothermal wells depends on the time of thermal recovery (t_t):

- 1 = best, if $t_t > 45$ days;
- 2 = good, if $20 < t_t < 45$ days;
- 3 = fair, if $5 < t_t < 20$ days.

The thermal gradients were calculated as the difference between the measured formation temperature (T_{obs}) and the corrected mean annual air temperature (T_o) divided by the depth (d) of measurement:

$$grad\ T = (T_{obs} - T_o)/d \dots\dots\dots(3.3)$$

The corrected reference temperatures in Eastern Hungary are between $T_o = 10.5 - 12.5$ °C. All the geothermal gradient values published by Dövényi and Horváth (1988) were calculated using the corrected annual ground surface temperature corresponding to the well location. The well co-ordinates from the Dövényi and Horváth (1988) database were transformed to EOVI with an accuracy of 1 km map for the sake of consistency with the other maps prepared for this study (Figure 3.5).

MOL, Plc. provided 2047 averaged HC-pool temperature data of questionable quality, mainly from DST's, without any technical detail that would enable quality control, culling, or correction. After the elimination of unidentifiable and duplicate records, 654 temperature measurements were retained for preliminary analysis. This data set was inconsistent with the trusted data set of Dövényi and Horváth (1988), therefore, it was attributed less weight during the final mapping and interpretation.

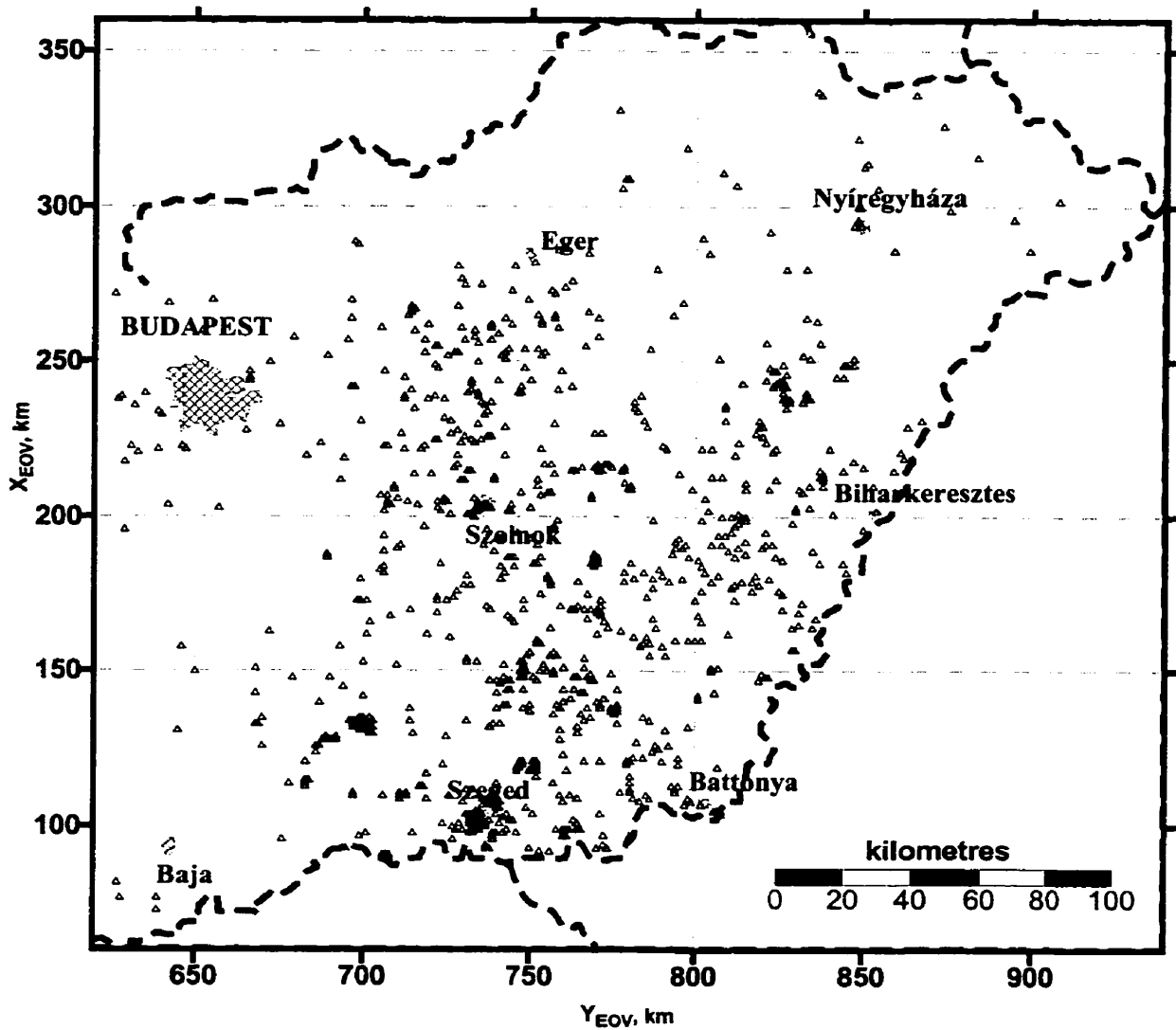


Figure 3.5: Distribution of temperature data from Dövényi and Horváth (1988).

3.5 POROSITY AND PERMEABILITY

MOL, Plc. provided laboratory measurements of porosity and permeability from 689 oil wells on 12 899 core samples. The samples were taken from discovered reservoirs and their cap rocks. Porosity was measured using gas and mercury injection, and the permeability (both horizontal and vertical) was determined for water. Relative permeability values for gas and oil were also calculated. The records included the well name, the name, age, and elevation (top and base) of the tested formations, and depth of core samples. Lithologic information and well co-ordinates were not available and the record fields were often incomplete. These data offered insight into the permeability and porosity distribution within the basin's rock framework, and allowed for estimation of magnitudes of average permeability for most formations. However, they could not be used for regional scale mapping. Published porosity and permeability values, and permeability-depth trend curves were found in the literature (e.g., Pap, 1976; Bérczi and Kókai, 1978; Szalay, 1982; Geiger et al., 1991; Somfai, 1976, 1994).

3.6 STRUCTURAL GEOLOGY

One structural geologic map was available for the study (Fülöp and Dank, 1987), which presents the major tectonic lineaments and the geology of the Pre-Neogene basement of Hungary at a 1:500 000 scale. This map was digitised (Figure 2.12) and the relevant information was extrapolated onto the regional cross sections prepared for this study. The dip of faults was not specified on the map but it was possible to infer the dip-direction from the structural contour lines. Where the sense of offset along faults was not indicated on the map, it was determined from the offset of geologic formations and basement topography. The structural features within the Neogene sedimentary unit can be best revealed by reflection seismic profiles. Although several thousands of kilometres of seismic profiles were shot in the study area, unfortunately, no original seismic information was accessible for this study. Several published seismic line drawing interpretations and a few copies of segments from original seismic profiles were found in the literature (e.g., Royden and Horváth, 1988; Pogácsás et al., 1994; Pap, 1993; Tari,

1994), but only their approximate location was indicated for confidentiality reasons. Even so, these published seismic interpretations provided sufficient support to understand and interpret pressure anomalies in a structural geological context.

3.7 PETROLEUM OCCURRENCE

The spatial distribution of petroleum occurrences in the study area was mapped based on pool location data (X,Y,Z co-ordinates of the geometric centre of water/petroleum interface) and initial pool pressure data, respectively (Appendix 1; CD-ROM: *HC_pool.dat* and *h_head.dat*). The two data sources did not overlap 100%, thus, neither of the two data sheets were exhaustive. The areal distribution of known pools based on the available data is illustrated on Figure 2.27. Production data and petroleum geological information (types of oil, chemistry, boiling point, etc.) about the individual pools were not provided. A limited number of petroleum density data were available. General description of petroleum field/pool characteristics was found in the literature (e.g., Dank, 1988; Körössy, 1990, 1992) and in-house reports of MOL, Plc.

4 REGIONAL GROUNDWATER FLOW SYSTEMS

4.1 CHARACTERISATION OF GROUNDWATER FLOW SYSTEMS

In regions where the water table is a subdued replica of the land surface and the rock framework is hydraulically continuous, groundwater flow is spatially distributed in systems of different hierarchical order (local, intermediate, regional) in function of the complexity of the relief of the water table (Tóth, 1962, 1963). Groundwater flow is directed downward in areas of high elevation (recharge area), upward in areas of low elevation (discharge area), and laterally in regions of intermediate elevation (midline). A flow system consists of a set of streamlines originating in a recharge area and ending in a discharge area. Local flow systems develop when the streamlines connect directly adjacent recharge and discharge areas. A regional flow system develops between the major water divide and the discharge area. Groundwater flow cannot be observed directly, but inferred from observations on the spatial distribution of hydrodynamic parameters and its natural chemical, physical, and biological field-manifestations.

4.1.1 Hydrodynamic parameters^{*}

Steady-state flow in a drainage basin is described by the Laplace equation:

$$\nabla^2 \Phi = 0 \quad (4.1)$$

where Φ is the total mechanical energy per unit mass of fluid [L^2T^{-2}]. According to Hubbert (1940), the fluid-potential (Φ) is:

$$\Phi = g h = \frac{p}{\rho_f} + z g \quad (4.2)$$

where g is acceleration due to gravity [LT^{-2}], h is the hydraulic head [L], p is the pore-pressure [$MT^{-2}L^{-1}$], ρ_f is the fluid density [$M L^{-3}$], and z is the elevation of the point of observation above a datum plane ($z = 0$) [L]. The hydraulic head (h) is the elevation of a

^{*} Sections 4.1.1 and 4.1.2 are based on Tóth and Sheng (1996).

fluid column of density ρ_f due to a pore-pressure p above the point of measurement z with reference to a datum level (commonly the mean sea level):

$$h = \frac{p}{g\rho_f} + z. \quad (4.3)$$

The fluid-potential field can be conveniently characterised by the hydraulic head, which can be determined from pore-pressure and water level measurements. Fluid flow is driven by the hydraulic gradient, which has to overcome the resistance of the medium and the fluid. The relationship among the fluid driving forces, the resistance of the medium (permeability), and the fluid's density and dynamic viscosity is expressed by Darcy's Law as the flow of a fluid volume across a unit surface area per unit time, known as flux or specific discharge (q):

$$q = -K \text{grad}h \quad (4.4)$$

$$K = \frac{k\rho_f g}{\mu} \quad (4.5)$$

Where K is the hydraulic conductivity [LT^{-1}], k is permeability [L^2], ρ_f is fluid density [ML^{-3}], and μ is the dynamic viscosity of the fluid [$ML^{-1}T^{-1}$]. The dimensions of the specific discharge are usually given as velocity [LT^{-1}], although the flux vector q represents rates of discharge of fluid volumes across a unit area in a porous medium. The linear flow velocity (v) can be approximated by dividing the specific discharge (q) with the porosity (ϕ) of the medium (Freeze and Cherry, 1979): $v = \frac{q}{\phi}$.

At hydrostatic equilibrium $q = 0$, thus, the vertical flow component (q_z):

$$q_z = -K \frac{\partial h}{\partial z} = 0, \quad (4.6)$$

where $K > 0$,

Therefore, $\frac{\partial h}{\partial z} = 0$, and by substituting the equation of the hydraulic head (4.3) we get:

$$\frac{\partial h}{\partial z} = 1 + (\rho_f g)^{-1} \frac{\partial p}{\partial z} = 0. \quad (4.7)$$

Thus, the vertical hydrostatic gradient is:

$$\gamma_{st} = \rho_f g = - \left(\frac{\partial p}{\partial z} \right)_{st} = \left(\frac{\partial p}{\partial d} \right)_{st} \quad (4.8)$$

Under hydrodynamic conditions $\mathbf{q} \neq 0$, thus, from equation (4.4), the ‘flow-driving force’ is:

$$\mathbf{grad}h = \left(\frac{\partial h}{\partial x} \mathbf{u}_1 + \frac{\partial h}{\partial y} \mathbf{u}_2 + \frac{\partial h}{\partial z} \mathbf{u}_3 \right) \neq 0 \quad (4.9)$$

where \mathbf{u}_1 , \mathbf{u}_2 , and \mathbf{u}_3 are unit vectors in the x, y, and z direction, respectively.

If the vertical component of the hydraulic gradient is not zero, $\frac{\partial h}{\partial z} \neq 0$, and by ignoring the lateral components of flow, then by substitution of h with p from equation (4.3) we get $\frac{\partial p}{\partial z} \neq (\rho g) = \gamma_{st}$. Thus, the vertical flow component (q_z) is driven by a vertical dynamic pressure gradient (γ_{dyn}):

$$\gamma_{dyn} = - \left(\frac{\partial p}{\partial z} \right)_{dyn} = \left(\frac{\partial p}{\partial d} \right)_{dyn} \quad (4.10)$$

When $\gamma_{dyn} > \gamma_{st}$, flow is directed upward, and when $\gamma_{dyn} < \gamma_{st}$, flow is directed downward.

If the vertical component of the hydraulic gradient is nil, $\frac{\partial h}{\partial z} = 0$, but the lateral components are different from zero, $\left(\frac{\partial h}{\partial x} \text{ and/or } \frac{\partial h}{\partial y} \neq 0 \right)$, then vertical flow does not take place, only horizontal flow. In this case, the vertical pressure gradient is hydrostatic, yet the fluid system is still under dynamic conditions. In practical terms, the apparently hydrostatic vertical pressure distribution observed in adjacent wells does not necessarily imply that fluids are motionless. A combination of pressure vs. depth and pressure vs. elevation profiles should be used to determine the actual state of fluids (Maccagno, 1991). Groundwater flow can be characterised based on observed fluid densities, pore-pressures, water levels, and by calculated hydraulic heads, vertical pressure gradients, potentiometric surfaces, and hydraulic cross sections.

The *vertical pressure gradient*, $\gamma = - \left(\frac{\partial p}{\partial z} \right) = \left(\frac{\partial p}{\partial d} \right)$, is represented on pressure vs. depth, $p(d)$, and pressure vs. elevation, $p(z)$, profiles, where the hydrostatic gradient corresponding to the observed fluid density is used as reference (nominal) gradient. Ideally, to determine a local vertical pressure gradient, simultaneous pressure measurements from a single vertical well at various depths should be plotted on a $p(d)$ or $p(z)$ profile.

The *potentiometric surface*, $h(x,y)$, is represented as a contour map of hydraulic heads in a horizontal plane. The concept of potentiometric surface is rigorously valid for horizontal flow in horizontal confined aquifers with no vertical flow component (Freeze and Cherry, 1979). Such maps show the lateral changes of the fluid-potential in a horizontal flow domain. The lateral components of the driving forces of fluid flow can be deduced from such maps. In an isotropic medium, flow is perpendicular to the hydraulic head contours and is directed from high toward low head values.

A *hydraulic cross section*, $H(L,z)$, shows the contours of hydraulic heads and patterns of flow in a vertical plane chosen in an arbitrary direction. A hydraulic cross section may be misinterpreted if fluids of different densities are present, or if the direction of the cross section is not parallel to the major flow direction. In the latter case, the real flow direction may be oblique or normal to the plane of cross section.

4.1.2 Characterisation of groundwater flow distribution

The two-dimensional steady-state distribution patterns of hydraulic head, flow geometry, and vertical pressure vs. depth profiles in drainage basins with a homogeneous rock framework are illustrated schematically in Figure 4.1a (unit basin) and Figure 4.1b (complex basin). In both models, it is assumed that the flow domain has lateral and basal no-flow boundaries; the upper boundary is the water table, which conforms to the topography (Tóth, 1962, 1963). Under recharge areas (R), the hydraulic heads decrease with depth, flow is directed downward, and the vertical pressure gradient (γ_R) is sub-hydrostatic. In the midline zone (M), the hydraulic head does not change with depth, flow is horizontal, and the vertical pressure gradient (γ_M) is hydrostatic (γ_{st}). Under discharge areas (D), the hydraulic heads increase with depth, flow is directed upward, and the vertical pressure gradient (γ_D) is super-hydrostatic. In the unit basin with a uniformly sloping linear water table (Figure 4.1a), only one flow system develops between the water divide and the valley bottom. In the complex basin with a linearly sloping sinusoidal water table, groundwater flow is spatially distributed in systems of different hierarchical order, i.e., local, intermediate, and regional flow systems (Figure 4.1b; Tóth 1962, 1963). The geometry of the flow systems of different order can be inferred from

the flow pattern. The depths of local flow systems can be approximated from the geometry of the flow lines or the vertical $p(d)$ profiles (Figure 4.1b). In the latter case, the depth of local flow systems is indicated by the reversal of the super-hydrostatic gradient (γ_{Rd}) to the sub-hydrostatic gradient (γ_R).

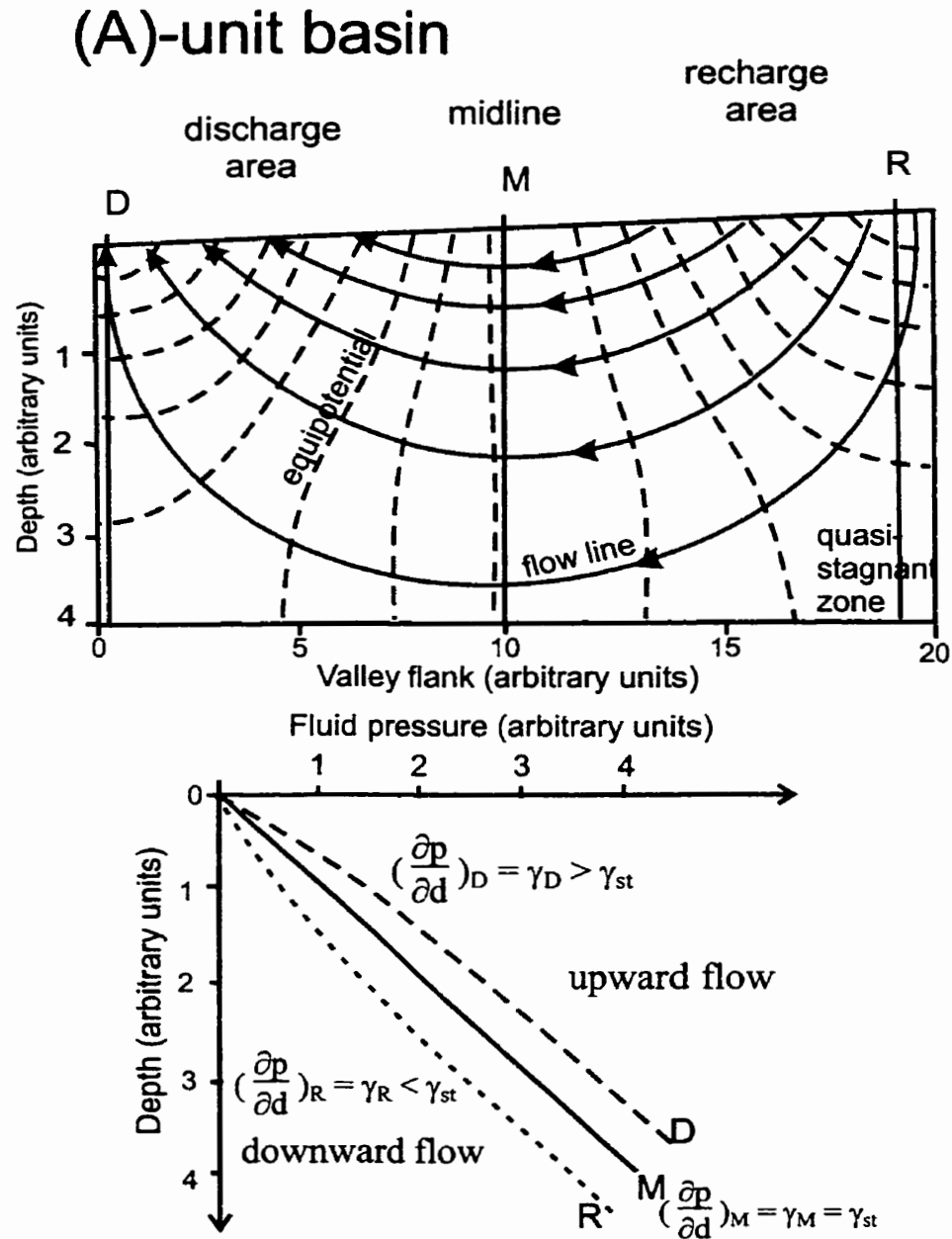


Figure 4.1a: Distribution of hydraulic head, flow systems, and hydraulic regimes, and the corresponding pressure vs. depth profiles in drainage basins with linearly sloping water table ("unit basin"). D, M, and R are observation sites. (after Tóth and Sheng, 1996).

(B)-complex basin

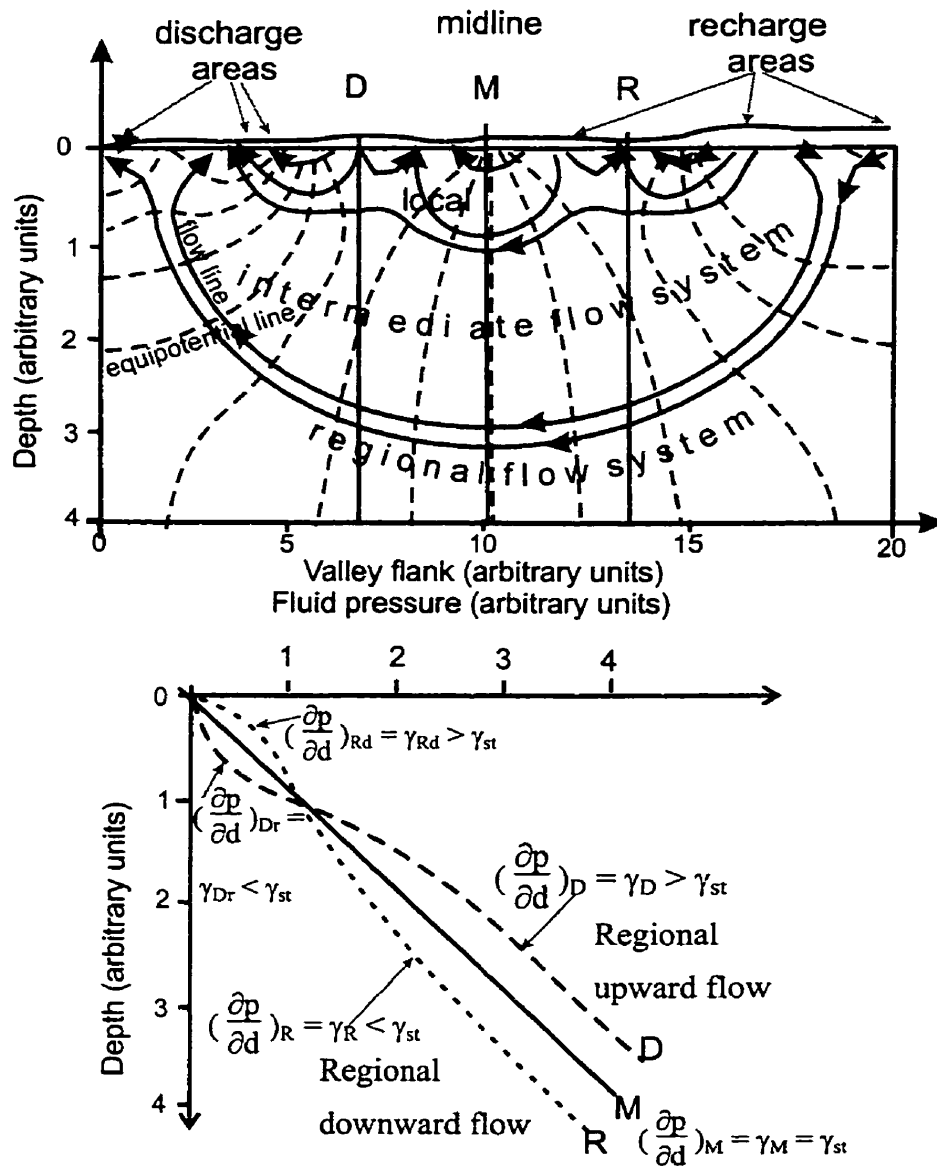


Figure 4.1b: Distribution of hydraulic head, flow systems, and hydraulic regimes, and the corresponding pressure vs. depth profiles in drainage basins with sinusoidally undulating water table superimposed on a linear regional slope (“complex basin”). D, M, and R are observation sites; R_d = Regional Recharge area with local discharge area; D_r = Regional Discharge area with local recharge area (after Tóth and Sheng, 1996).

4.2 GROUNDWATER FLOW SYSTEMS IN THE GREAT HUNGARIAN PLAIN

4.2.1 Methods of characterisation

The fluid-potential field was characterised using $p(z)$ profiles, fluid-potential maps, and hydraulic cross sections.

4.2.1.1 $p(z)$ profiles

The hydrostatic gradient for fresh water ($\gamma_{nom} = \rho_w g = 9.8067 \text{ MPa/km}$) was chosen as reference on the pressure profiles. The error of this approximation is $< \pm 0.8\%$, because the total dissolved solid content of groundwater in the Great Hungarian Plain is generally low; commonly between 0.2 - 10 g/l, never exceeding 55 g/l (MOL, Plc. and MÁFI database, Varsányi et al., 1997, 1999). The stabilised water level values were converted into fresh water pressures to enable their analysis on vertical pressure profiles, $p(d)$ and $p(z)$. The locations of vertical pressure profiles were chosen to best demonstrate regional trends of vertical fluid pressure distribution in the basin, by limiting the plots to areas of minimal topographic relief and sufficient number and range of data (Figure 4.2). Since the wellhead elevation of the well-data plotted on pressure profiles varies only within 10 m, the patterns of $p(d)$ and $p(z)$ profiles are almost identical. Although there is a fundamental difference between $p(d)$ and $p(z)$ profiles (Maccagno, 1991), essentially the same information could be deduced from both profiles constructed for this study. $p(z)$ profiles were chosen to illustrate the vertical pressure distribution patterns in the study area.

4.2.1.2 Fluid-potential maps, $h_{ij}(x,y)$

The freshwater hydraulic heads were mapped on a series of fluid-potential maps. As is discussed in Chapter 2, the regional aquitards in the study area are not ideal confining units, as they permit vertical hydraulic communication between aquifers. A preliminary assessment of fluid-pressure distribution in the basin suggested that strong vertical driving forces are to be expected. Thus, potentiometric mapping in a rigorous sense was not possible in the study area, as it would have yielded misleading results. Instead, the fluid-potential field was portrayed on a series of hydraulic head maps of horizontal flow domains of constant thickness bounded by horizontal planes (Tóth and

Almási, 1998); the same technique was used by Hitchon (1969/a, b) on Tóth's advice. Practically, such horizontal flow domains are horizontal 'tomographic slices' of the basin's rock framework. The elevation interval or thickness of a tomographic slice should satisfy two conditions: 1) it must have sufficient volume and spatial distribution of data; 2) a minimum variability of the vertical pressure gradients, however, the second condition can be treated with flexibility to meet the first condition.

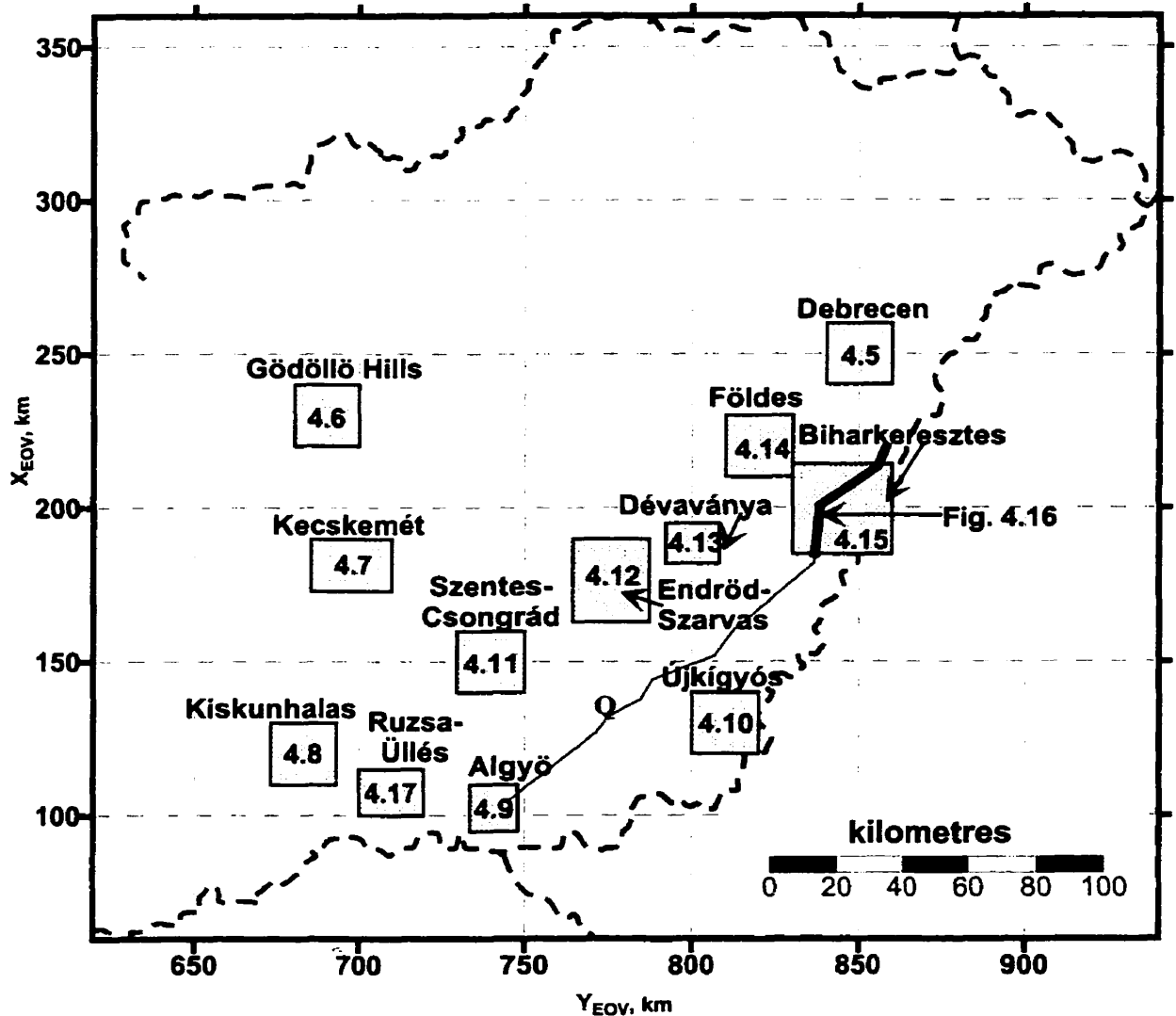


Figure 4.2: Name, extent, and figure number of selected $p(z)$ profiles discussed in text (figure numbers are shown in the boxes). Traces of interpreted seismic cross sections from Tari (1994: Q, Qb, Qc).

Based on the above criteria, eleven (tomographic) elevation intervals were determined from sea level downward (Figure 4.3). Additionally, two hydraulic head maps

were prepared for the basin between the land surface and sea level. The hydraulic head data were grouped according to the elevation range of each tomographic interval based on the elevation head of each datum. They were then projected onto the upper horizontal bounding surface of the appropriate tomographic map, and contoured both automatically (with Surfer) and manually. A code, $h_{i,j}(x,y)$, was assigned to the maps, representing a hydraulic head surface (x,y) in the i -to- j elevation range. The indices ' i ' and ' j ' refer to the *hundreds of metres below sea level of the upper and lower boundary plane, respectively* (Figure 4.3). The uppermost map is based on hydraulic head values from wells shallower than 40 m, $h_{z_0,z_0-40}(x,y)$; its bounding surfaces are parallel to the land surface. This map is neither a water table map nor a potentiometric map, since the data were obtained from different local aquifers from variable depths. However, this map allows a first order comparison of the land surface and the mean fluid-potential surface at shallow depths, and portrays the configuration of the regional hydraulic regime (major recharge and discharge areas). The second map represents a slice bounded by a horizontal plane only at its base ($h_{z_0-40,0}(x,y)$). The other maps represent flow domains bounded by horizontal planes at different elevations below sea level, ranging from 100 to 500 m in thickness.

Several gridding methods were tested for automatic contouring of hydraulic heads, e.g., triangulation, kriging, inverse distance to a power, and natural neighbour. The "natural neighbour" gridding method (Sibson, 1981) was found adequate for generating acceptable contours for almost every data set. This method was particularly effective with irregularly spaced data sets that had large value ranges, such as those in the $z = -600$ to -2800 m elevation range. Wherever it was necessary, the grid files were manipulated (edited) by changing the values of individual grid nodes in order to obtain desired/realistic contour lines. Every map was contoured manually as well, because the interpretative power of manual contouring over automatic is far superior. Subsequently, the manual contours were digitised and reproduced at convenient scales.

From a tomographic fluid-potential map one can infer the horizontal components of the fluid driving forces within the map's elevation range. The sense and strength of the vertical component of fluid driving forces at any site of (X_{EOV}, Y_{EOV}, z_0) co-ordinates can be inferred from the hydraulic head contour values of subsequently deeper elevation

ranges. Directions and magnitudes of horizontal hydraulic gradients were computed for most maps presented in this Chapter.

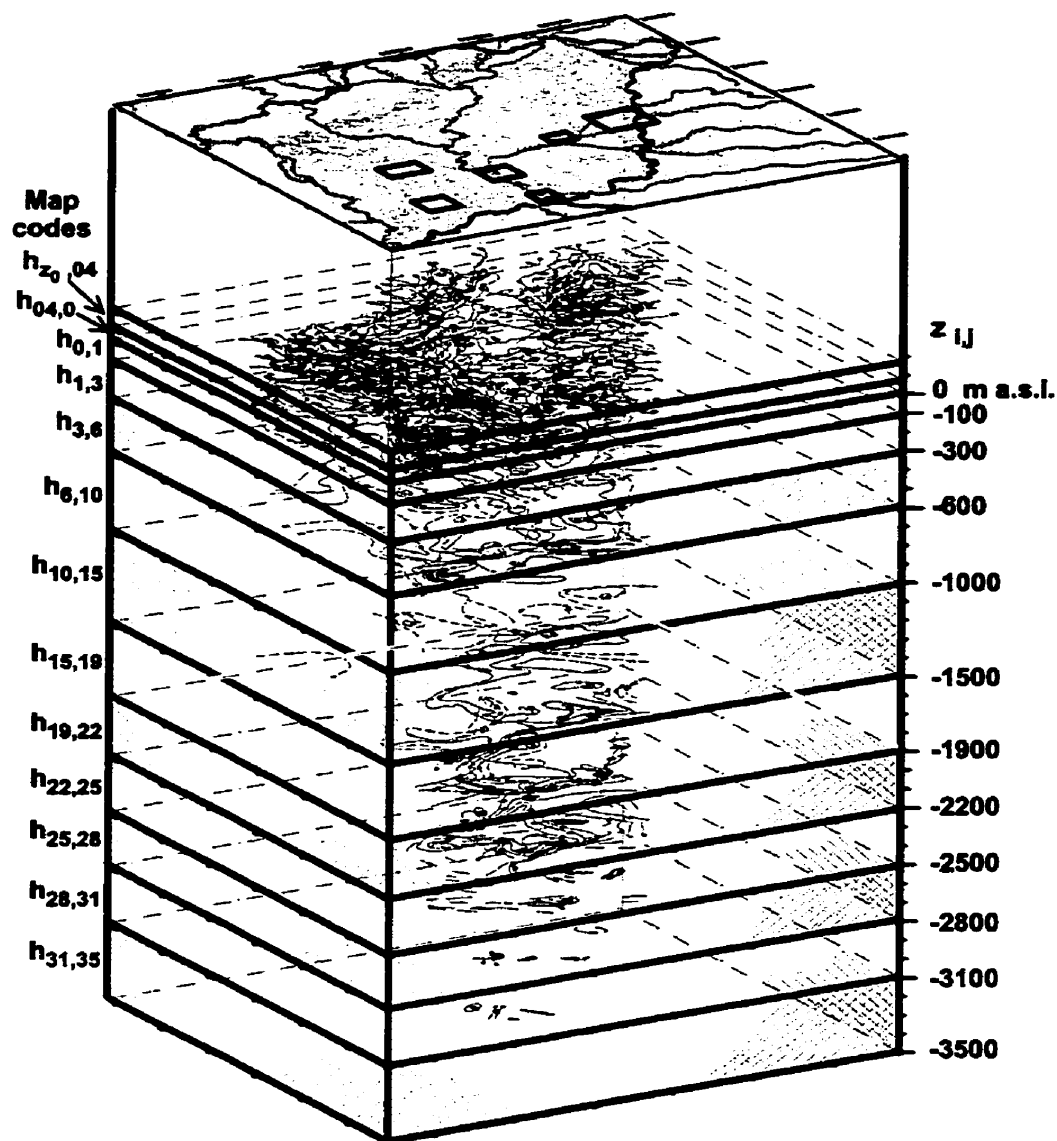


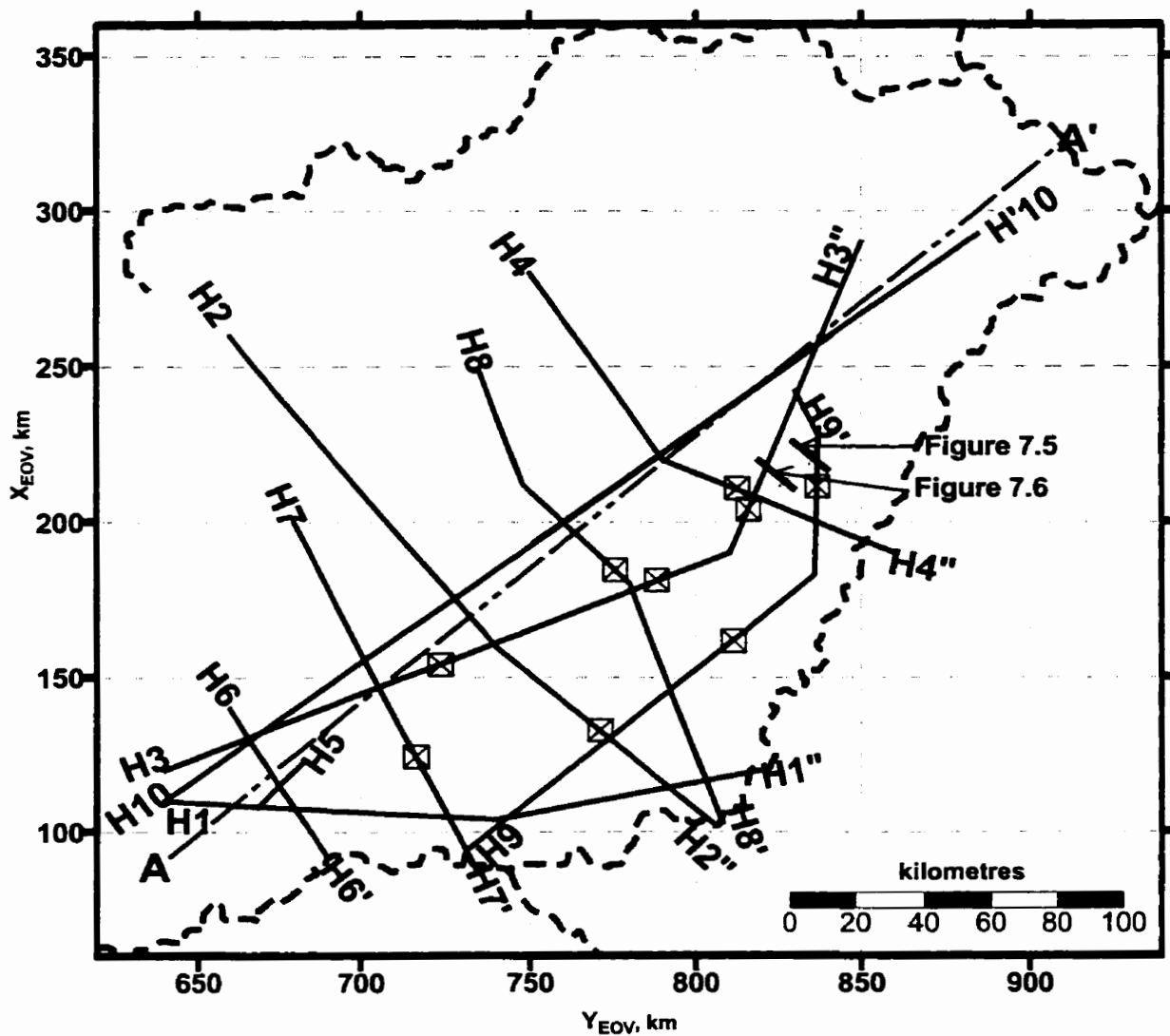
Figure 4.3: Schematic block diagram of the tomographic maps.

4.2.1.3 Hydraulic cross sections; **H_i(L,z)**

Ten regional hydraulic cross sections with a cumulative length of 1725 km were prepared for this study (Figure 4.4, and Figures 4.33 through 4.42). The cross sections were coded as **H_i(L,z)**, where **i** =1, 2,..., 10 is the number of the section; **L** represents horizontal distance along the cross section, and **z** represents elevation. The EOVS coordinates (**Y_{EOV}**, **X_{EOV}**; in kilometres) of end-nodes and breakpoints of cross sections are the following:

H1:	[(640,110); (740, 104); (820, 120)]	Figure 4.33
H2:	[(660, 260); (740, 160); (806, 102)]	Figure 4.34
H3:	[(640, 120); (810, 190); (850, 290)]	Figure 4.35
H4:	[(750, 280); (790, 220); (860, 190)]	Figure 4.36
H5:	[(669, 108); (682, 122)]	Figure 4.37
H6:	[(660, 140); (690, 92)]	Figure 4.38
H7:	[(680, 200); (734, 88)]	Figure 4.39
H8:	[(735, 248); (748, 212); (780, 180); (808, 103)]	Figure 4.40
H9:	[(830, 242); (837, 228); (836, 183); (731, 94)]	Figure 4.41
H10:	[(640, 110); (880, 289)]	Figure 4.42

The original cross sections were prepared at $M_h = 1:250\ 000$ horizontal scale with 1:10 vertical exaggeration. They are reproduced in the thesis at $M_h = 1:500\ 000$ horizontal scale with 1:10 vertical exaggeration. Wherever it was possible, the traces of cross sections were selected parallel to the main horizontal flow directions inferred from the fluid-potential maps. The bases of hydrostratigraphic units were mapped from the stratigraphic data and plotted on the cross sections. The location of fault zones were extracted from the geologic map of Fülöp and Dank (1987) and plotted on each section to aid interpretation. Hydraulic head values and hydrocarbon pool locations, all within a maximum of 2 km distance from the trace of the sections, were horizontally projected onto the cross sections; see Appendix 2 for well selection method. Also, the values of hydraulic head contours (from the tomographic maps) intersected by the cross sections were plotted at the appropriate elevation interval in the vertical plane of the section to complement data coverage, and enable verification of earlier interpretations.



⊠ location of hydraulic head vs. elevation profiles derived from the interpreted hydraulic cross sections

Figure 4.4: Index map of regional hydraulic cross sections prepared for this study, and the location of hydraulic head vs. elevation profiles derived from the interpreted hydraulic cross sections. The EO coordinates (Y_{EOV} , X_{EOV} ; in kilometres) of end-nodes and breakpoints of cross sections are listed in the text. Cross section A-A' is the trace of Erdélyi's model (Erdélyi, 1976) shown on Figure 1.1.

Although the true vertical position of a contour line across the hydraulic head values projected from the maps is uncertain, these interpolated values provide some constraints on the possible magnitude of hydraulic heads in areas where no measurements were available. The data points were contoured manually, then the contours were digitised. The arrows on the cross sections indicate a component of the fluid driving forces in the plane of each cross section. It is recognised that, in reality, the principal flow directions

may be oblique or normal to the chosen planes of cross sections in several instances, as inferred from the tomographic fluid-potential maps.

The importance of using hydraulic cross sections is twofold. First, they provide a vertical perspective to the visualisation of groundwater flow regimes, by which the vertical distribution patterns of fluid-dynamic parameters (pressure, hydraulic head, hydraulic gradient) can be established and interpreted in terms of deduced flow patterns and their hydrostratigraphic, structural controls. Secondly, they allow verification, modification, and clarification of observations, inferences, and working hypotheses formulated based on $p(z)$ profiles and horizontal hydraulic head maps. In light of the latter point, the traces of some cross sections were chosen arbitrarily to dissect areas where potential anomalies were observed on the tomographic fluid-potential maps.

4.2.2 General observations and interpretations

4.2.2.1 $p(z)$ profiles

Twelve areas were selected (Figure 4.2) to illustrate the pressure vs. elevation distribution in the Great Hungarian Plain. These examples are grouped by the elevation range of the chosen regions, starting with the higher elevation one in the north-eastern part of the study area. The pore pressure data obtained from the Pre-Pannonian basement and the Mid-Miocene formations are posted with distinct symbols on the $p(z)$ profiles below (this section and Section 5.1.1). However, recalling Figures 2.17 and 2.18 (pg. 36 and 37), the Pre-Neogene Aquifer and the Mid-Miocene Aquifer are part of the broader Pre-Pannonian Aquifer. This separation of data from the Pre-Pannonian Aquifer is meant to emphasize the possible differences in magnitude and vertical distribution patterns of pore pressures measured in the Pre-Neogene basement and the Mid-Miocene formations relative to those from younger units, and facilitate the evaluation and interpretation of overpressuring mechanisms.

Debrecen region (Figures 4.2 and 4.5): Location: $X_{EOV} = 240 - 260$ km; $Y_{EOV} = 840 - 860$ km; the altitude of the area is $z_0 = 130 - 147$ m a.s.l. The pressure data refer to the Nagyalföld Aquifer.

The fresh water pressures show a steady sub-hydrostatic pressure increase with depth in the $z > -250$ m zone at an average dynamic pressure gradient of $\gamma_{dyn1} = 8.7065$ MPa/km, indicating descending flow. The slight scatter of pressure values may reflect minor permeability heterogeneity, and occasionally production induced drawdown. Two control points are available from the $z = -1600$ to -2000 m range, which plot below the hydrostatic gradient line. Although these two points may not warrant calculation of an actual dynamic gradient, they plot along an apparent super-hydrostatic vertical pressure gradient of $\gamma_{dyn2} = 10.3175$ MPa/km. This indicates ascending flow in the $z = -1600$ to -2000 m elevation interval. The observed change in the vertical pressure gradient indicates vertically convergent flow directions. Owing to the large gap of data between $z = -250$ m to -1600 m, it is not possible to determine the depth where the gradient changes from sub-hydrostatic to super-hydrostatic.

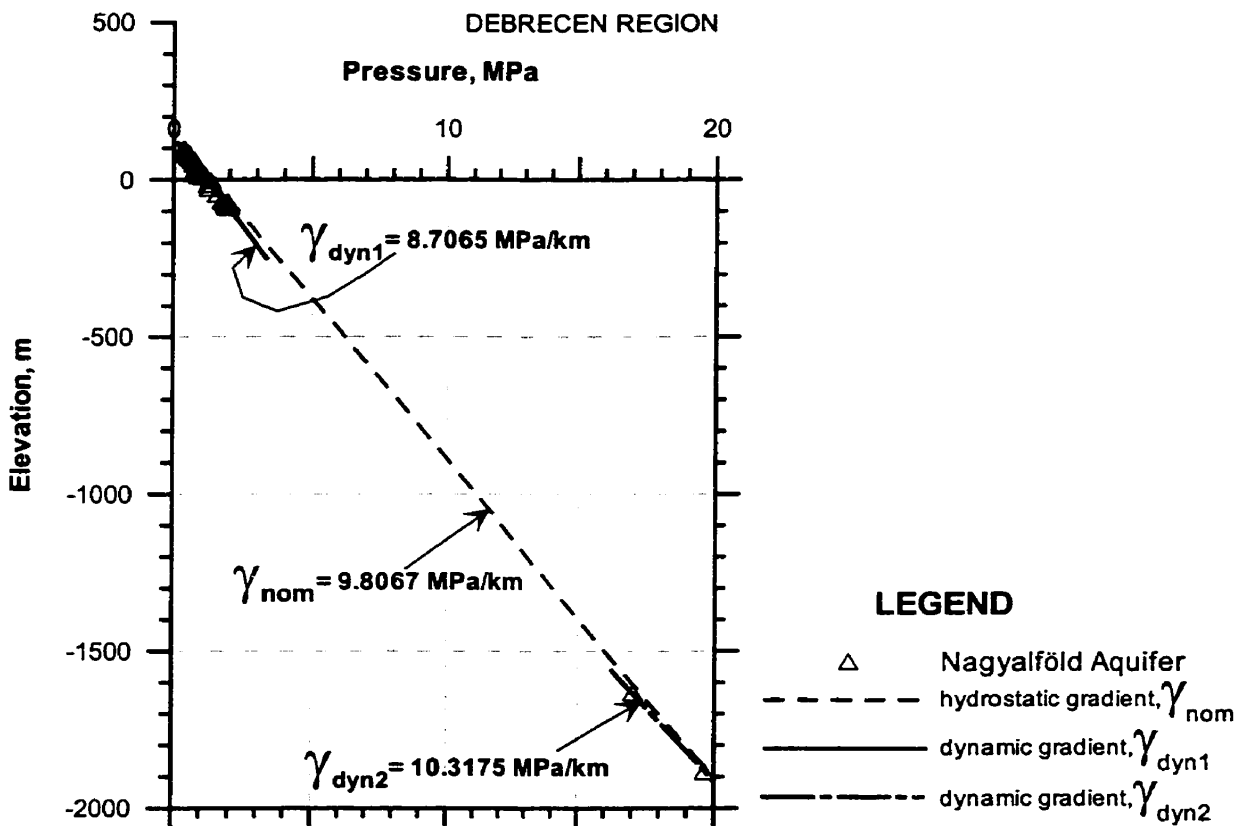


Figure 4.5: $p(z)$ profile in the Debrecen region ($X_{EOV} = 240 - 260$ km; $Y_{EOV} = 840 - 860$ km; $z_0 = 130 - 147$ m a.s.l.). For location see Figure 4.2.

Gödöllő Hills (Figures 4.2 and 4.6): Location: $X_{EOV} = 220 - 240$ km; $Y_{EOV} = 680 - 700$ km; the altitude of the area is $z_0 = 130 - 150$ m a.s.l. The pressure data refer to the Nagyalföld Aquifer.

The fresh water pressures show a steady sub-hydrostatic increase with depth in the $z > -350$ m zone. The average dynamic pressure gradient is $\gamma_{dyn} = 9.3804$ MPa/km, which indicates descending flow.

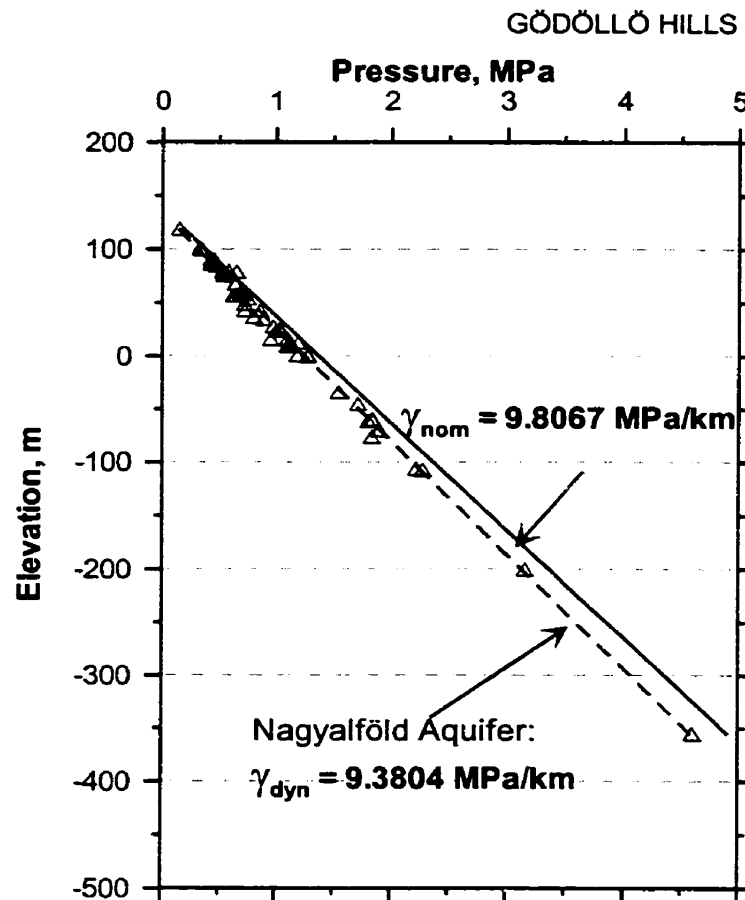


Figure 4.6: $p(z)$ profile in the Gödöllő region ($X_{EOV} = 220 - 240$ km; $Y_{EOV} = 680 - 700$ km; $z_0 = 130 - 150$ m a.s.l.). For location see Figure 4.2.

Kecskemét (Figures 4.2. and 4.7): Location: $X_{EOV} = 173 - 190$ km; $Y_{EOV} = 685 - 710$ km; the altitude of the area is $z_0 = 117 - 135$ m a.s.l. The pressure data refer to the Nagyalföld and to the Mid-Miocene Aquifer.

The fresh water pressures show a steady sub-hydrostatic increase with depth for the whole measured range ($z > -2040$ m). There is a lack of data in the $z = -1055$ m to -2040 m range, and only a single measurement was available at $z = -2040$ m. Therefore, calculation of a dynamic pressure gradient is warranted by the data only for the upper $z > -1055$ m zone. The dynamic pressure gradient is $\gamma_{z > -1055 \text{ m}} = 9.5525$ MPa/km, which indicates descending flow in the upper elevation range. Based on the single measurement at $z = -2040$ m it is not possible to determine the vertical flow direction at that elevation, therefore, the maximum depth of penetration of descending water could not be estimated.

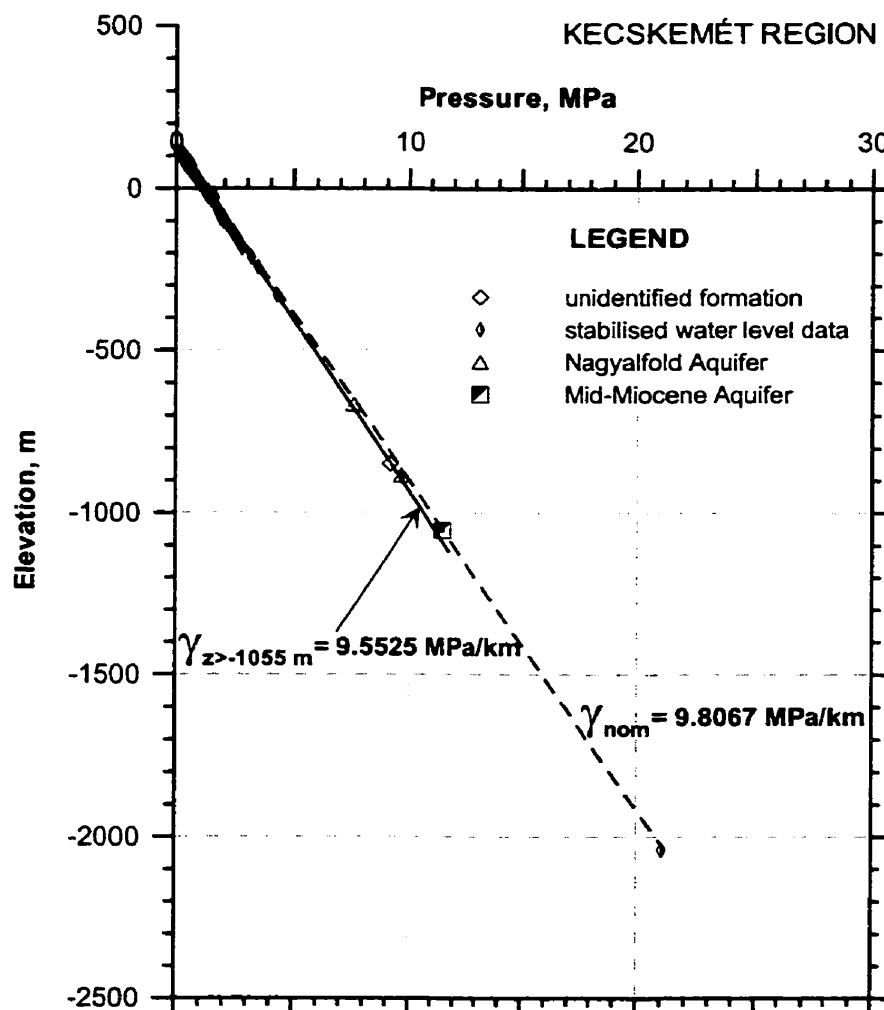


Figure 4.7: $p(z)$ profile in the Kecskemét region ($X_{EOV} = 173 - 190$ km; $Y_{EOV} = 685 - 710$ km; $z_0 = 117 - 135$ m a.s.l.). For location see Figure 4.2.

Kiskunhalas (Figures 4.2 and 4.8): Location: $X_{EOV} = 110 - 130$ km; $Y_{EOV} = 673 - 693$ km; the altitude of the area is $z_0 = 120 - 140$ m a.s.l. Pressure data were available from the Nagyalföld, Mid-Miocene, and the Pre-Pannonian Aquifers.

The fresh water pressures show a steady sub-hydrostatic increase with depth for the $z > -1500$ m range at an average dynamic gradient of $\gamma_{z > -1500 \text{ m}} = 9.5099$ MPa/km indicating descending flow. In the $z < -1700$ m range, the dynamic gradient is $\gamma_{-2500 \text{ m} < z < -1700 \text{ m}} = 11.7425$ MPa/km, i.e., super-hydrostatic, which indicates ascending flow. The change in dynamic pressure gradient from sub-hydrostatic to super-hydrostatic indicates vertically convergent flow. Three measurements from the Pre-Pannonian Aquifer (within the same lithostratigraphic unit) at the Kiskunhalas-South site were ignored in the gradient calculation (Table 4.1). The first two measurements (p_1 and p_2) suggest the existence of a deep-seated high-energy source, which caused the abrupt increase in overpressures from ~14% to above 54%. However, these two control points do not warrant construction of a realistic pressure gradient. The third measurement (p_3) strongly suggested artificial effects, such as production-induced drawdown or instrumentation error – a suspicion later confirmed by MOL, Plc. (p_3 was measured after p_2 in the same well and the same formation, but with technical problems).

Table 4.1: Salient pressure data from the Kiskunhalas region.

Well	Pressure (MPa)	Elevation (m)	pressure difference (MPa) $\Delta p = p_{\text{observed}} - p_{\text{nominal}}$
Kiha-D-1	$p_1 = 41.69$	-2622	14.68
Kiha-D-2	$p_2 = 39.25$	-2656	11.85
Kiha-D-2	$p_3 = 33.78$	-3343	-0.35

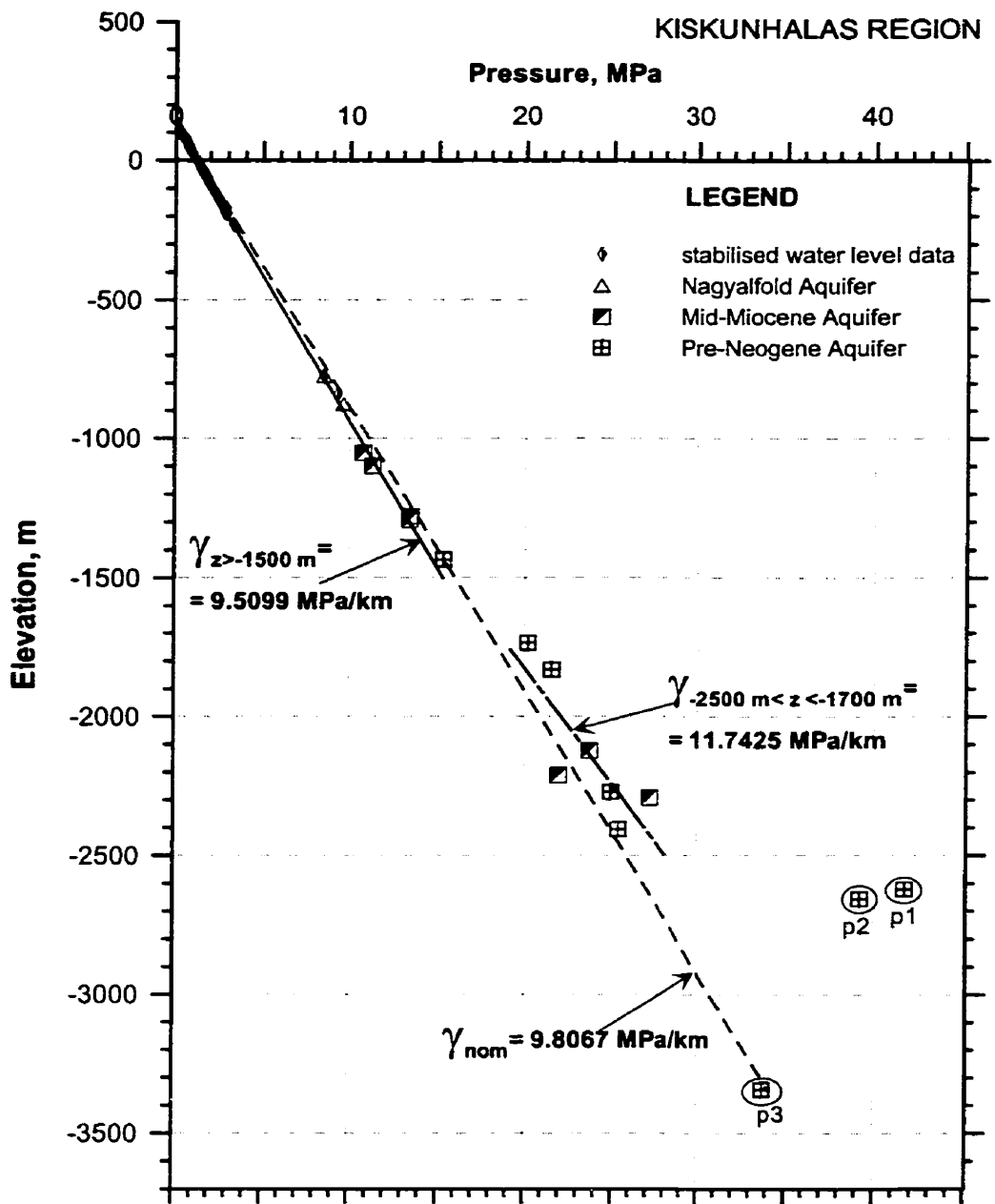


Figure 4.8: $p(z)$ profile in the Kiskunhalas region ($X_{EOV} = 110 - 130 \text{ km}$; $Y_{EOV} = 673 - 693 \text{ km}$; $z_0 = 120 - 140 \text{ m a.s.l.}$). For location see Figure 4.2. Salient data from Table 4.1 are encircled.

Algyő region (Figures 4.2. and 4.9): Location: $X_{EOV} = 95 - 110$ km; $Y_{EOV} = 734 - 748$ km; the altitude of the area is $z_0 = 78 - 85$ m a.s.l. Pressure data were available from every hydrostratigraphic unit.

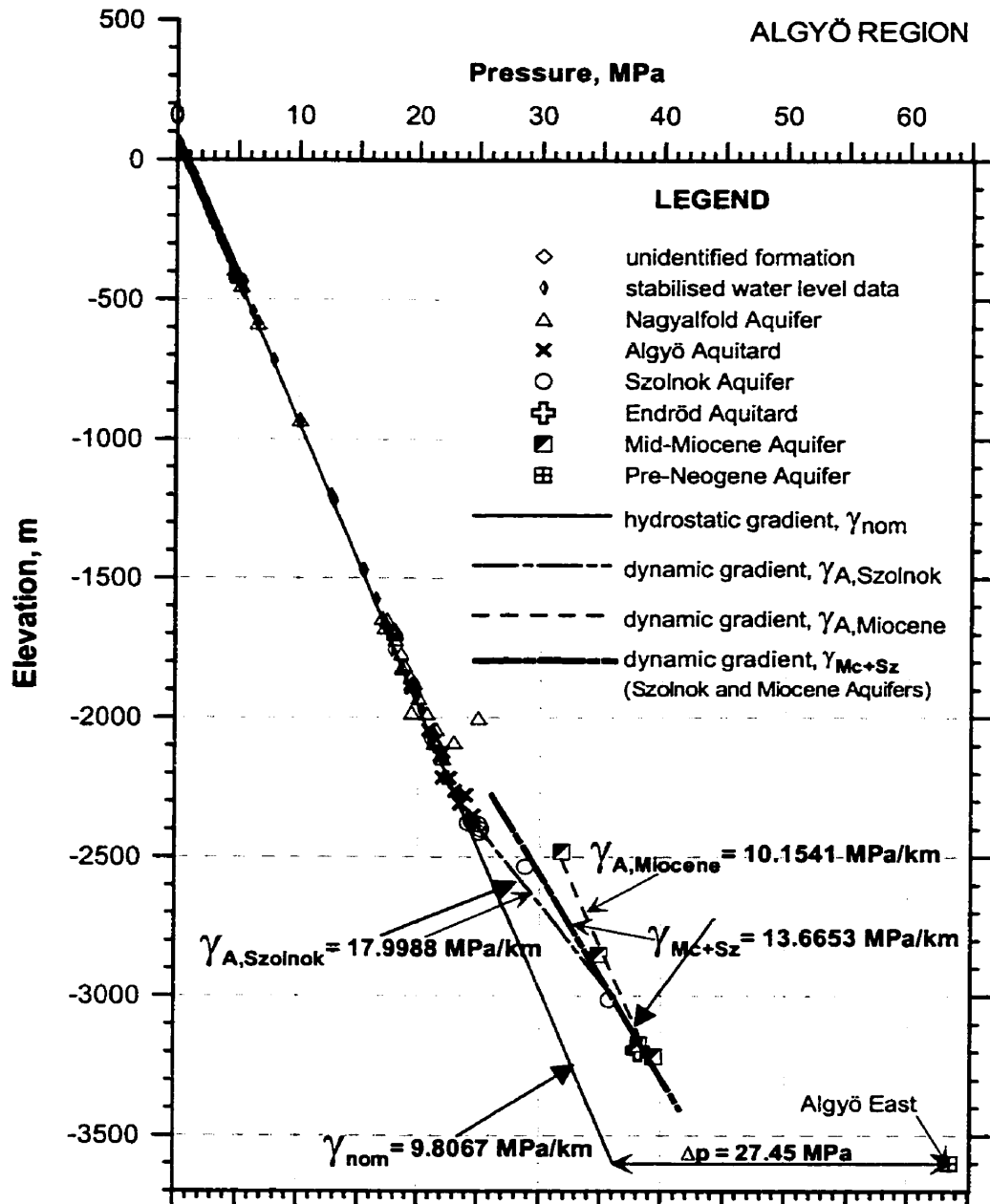


Figure 4.9: $p(z)$ profile in the Algyő region ($X_{EOV} = 95 - 110$ km; $Y_{EOV} = 734 - 748$ km; is $z_0 = 78 - 85$ m a.s.l.). For location see Figure 4.2.

Slight super-hydrostatic pressures prevail above $z = -2400$ m within the Nagyalföld Aquifer, Algyő Aquitard, and the upper part of the Szolnok Aquifer. The

overpressures do not exceed 7 MPa in the $z = -2500 - -3350$ m elevation range. However, the observed vertical dynamic pressure gradient in the Szolnok Aquifer is considerably larger than the one in the Mid-Miocene Aquifer ($\gamma_{A, Szolnok} = 17.9988$ MPa/km; $\gamma_{A, Miocene} = 10.1541$ MPa/km). In the Pre-Neogene basement, there is a single anomalous pressure recorded at Algyő East ($z = -3600$ m, $p = 63.5$ MPa, and $\Delta p = 27.45$ MPa), which indicates a deep pressure-energy source. The large pressure difference between the basement and the Mid-Miocene Aquifer is probably due to the presence of a low permeability unit at the base of the Mid-Miocene beds directly overlying the basement. Within the Mid-Miocene Aquifer, the pressure dissipation by ascending fluid flow is apparently uniform, suggesting homogeneous permeability conditions at the field scale. The relatively steep pressure gradient for the Szolnok Aquifer may indicate the heterogeneous permeability of the turbidites and/or aggressive pressure dissipation along fracture zones that may connect to the base of the Nagyalföld Aquifer. The measurements within the Szolnok and Mid-Miocene Aquifers are at close elevation due to the slope of these formations deposited on the eastern flanks of a basement-high. This is best illustrated on hydraulic cross section **H9** in section 4.2.2.3 (Figure 4.41; see the $L = 15 - 25$ km segment).

An alternative explanation for the observed $p(z)$ distribution patterns is that the spatially adjacent Szolnok and Mid-Miocene Aquifers are most likely connected hydraulically via structural and sedimentological discontinuities, and they act as one large aquifer. For this scenario, the average dynamic pressure gradient across the Mid-Miocene and Szolnok Aquifers is $\gamma_{Mc+Sz} = 13.6653$ MPa/km; it also indicates ascending flow and an abrupt increase in the slope of the pressure gradient approaching the “pressure-energy source” at greater depth.

Újkígyós (Figure 4.2 and 4.10): Location: $X_{EOV} = 120 - 140$ km; $Y_{EOV} = 800 - 820$ km; the altitude of the area is $z_0 = 90 - 100$ m a.s.l., and it is located in the SE part of the Békés basin. The available data are exclusively from the Nagyalföld Aquifer, mostly from the $z = 91$ to -407 m elevation range; there is one measurement at $z = -1209$ m.

In the upper ~ 500 m of the profile, a steady super-hydrostatic pressure increase with an average dynamic gradient of $\gamma_{dyn} = 9.9290$ MPa/km is observed. This suggests modest driving force and upward flow in an unconfined gravity-driven flow regime. The lowest measurement (at $z = -1209$ m) yielded a $\Delta p = 1$ MPa overpressure, which is difficult to interpret. This overpressure may be related to an underlying deep-seated energy source similar to those inferred in other parts of the basin –we do not know.

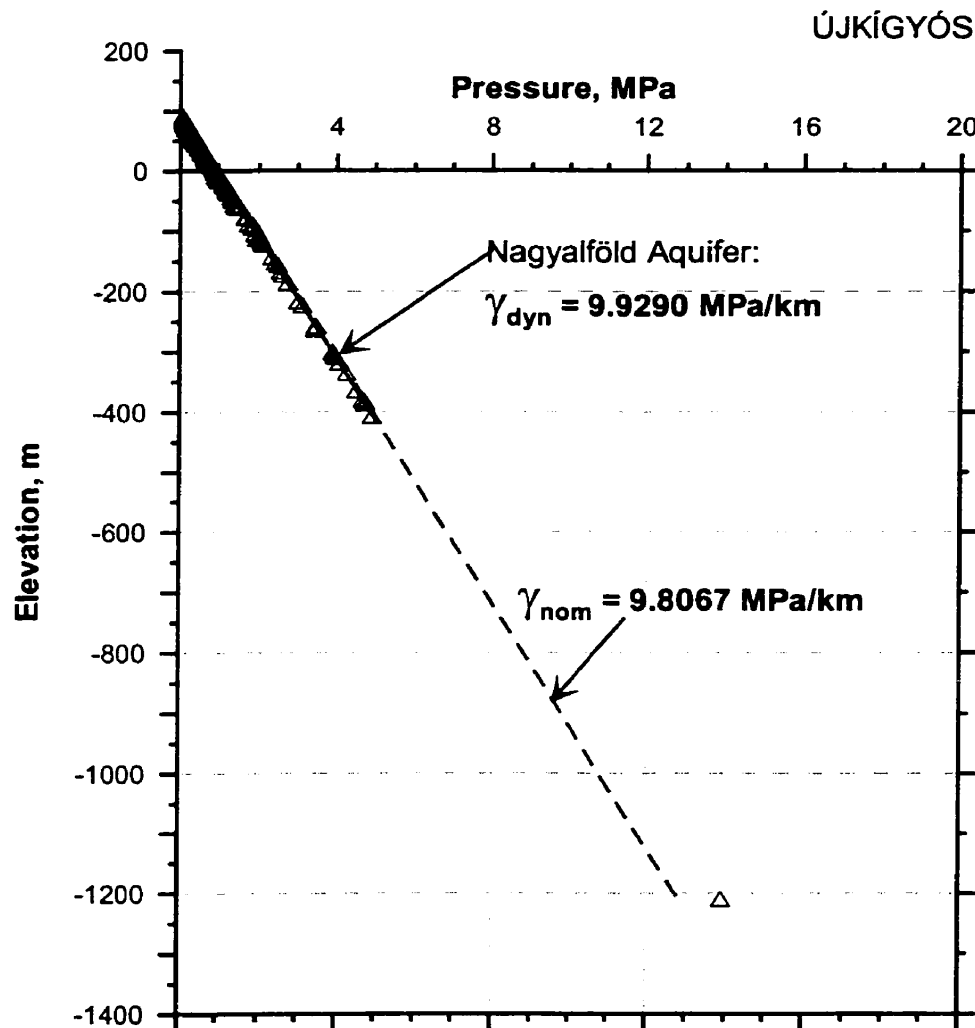


Figure 4.10: $p(z)$ profile in the Újkígyós region ($X_{EOV} = 120 - 140$ km; $Y_{EOV} = 800 - 820$ km; $z_0 = 90 - 100$ m a.s.l.). For location see Figure 4.2.

Szentes – Csongrád (Figure 4.2 and 4.11): Location: $X_{EOV} = 140 - 160$ km; $Y_{EOV} = 730 - 750$ km; the altitude of the area is $z_0 = 80 - 90$ m a.s.l. The majority of the data refer to the Nagyalföld Aquifer, one refers to the Szolnok Aquifer, and another one to the Pre-Pannonian Aquifer.

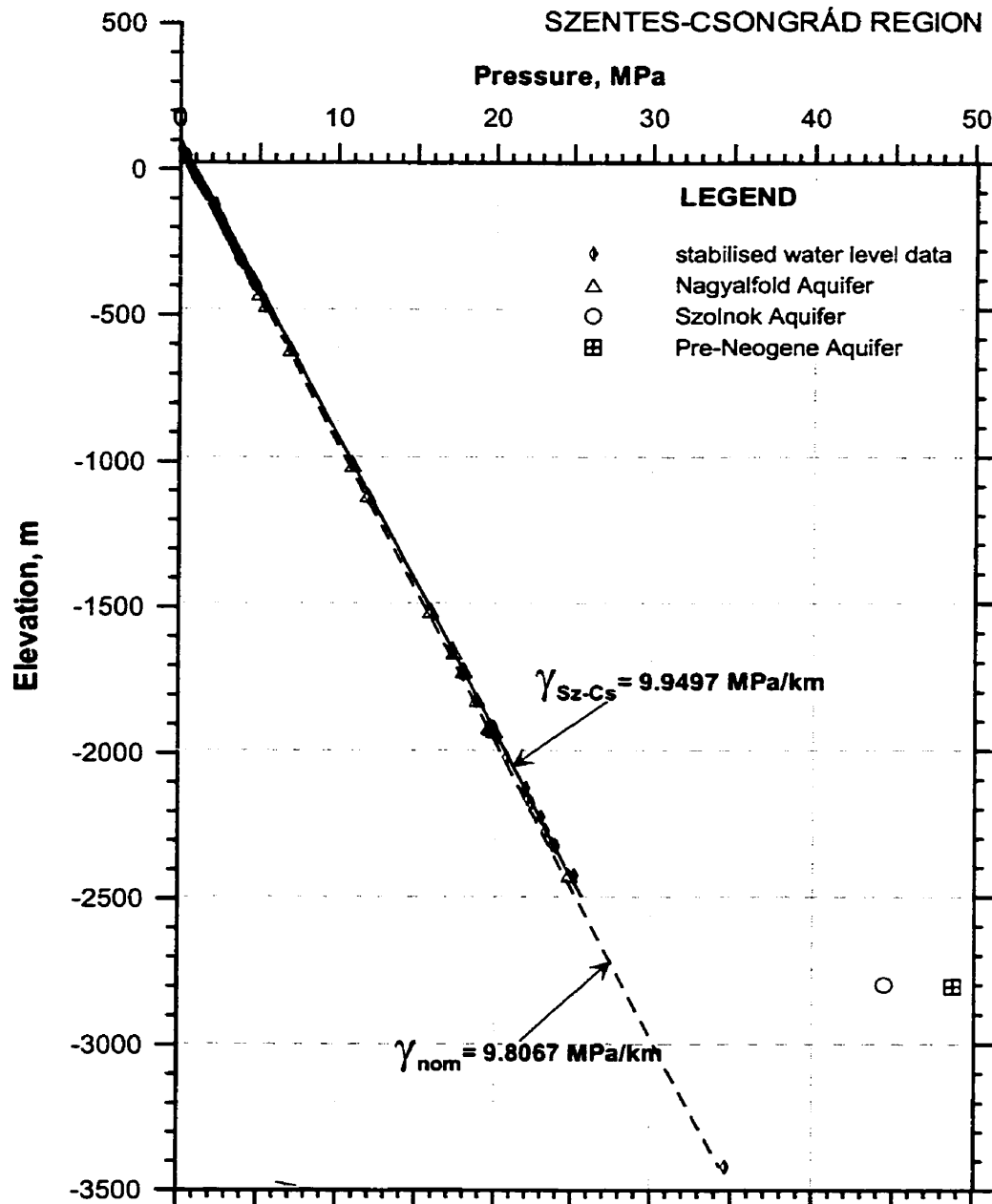


Figure 4.11: $p(z)$ profile in the Szentes - Csongrád region ($X_{EOV} = 140 - 160$ km; $Y_{EOV} = 730 - 750$ km; $z_0 = 80 - 90$ m a.s.l.). For location see Figure 4.2.

Above $z > -2500$ m, slightly super-hydrostatic pressures prevail, which are distributed uniformly within the Nagyalföld Aquifer. The computed hydraulic gradient is $\gamma_{\text{Sz-Cs}} = 9.9497$ MPa/km, which indicates ascending flow. In this region, the Szolnok Aquifer and the Pre-Pannonian Aquifer are overpressured by as much as 16.2 MPa and 20.5 MPa, respectively. Such an abrupt pressure increase over a ~ 350 m elevation difference suggests a high energy source within and/or below these two aquifers and also the presence of a low permeability zone that can impede upward dissipation of excess pressures.

Endrőd-Szarvas (Figures 4.2 and 4.12): Location: $X_{\text{EOV}} = 163 - 190$ km; $Y_{\text{EOV}} = 764 - 787$ km; the altitude of the area is $z_0 = 83 - 101$ m a.s.l. Data are available from every hydrostratigraphic unit.

Three distinctive super-hydrostatic pressure-elevation zones can be observed:

1) an upper zone extending to about $z = -1900$ m characterised by

$$\gamma_{z > -1900 \text{ m}} = 9.8785 \text{ MPa/km};$$

2) a middle zone in the $-1900 \text{ m} > z > -2400 \text{ m}$ elevation range characterised by

$$\gamma_{-1900 \text{ m} > z > -2400 \text{ m}} = 22.9995 \text{ MPa/km}; \text{ and}$$

3) a lower zone in the $-2400 \text{ m} > z_0 > -3400 \text{ m}$ elevation range characterised by

$$\gamma_{-2400 \text{ m} > z_0 > -3400 \text{ m}} = 57.7161 \text{ MPa/km} \text{ (data primarily from the Szolnok Aquifer).}$$

Within the upper super-hydrostatic zone (1) the fluid-pressure data show negligible scatter around the $\gamma_{z > -1900 \text{ m}}$ gradient, which is an indication of the ascending limb of a gravity-driven flow system in a regionally unconfined aquifer. From the abrupt pressure increase in the middle (2) and lower (3) zone a transition from a normally pressured regime to an abnormally overpressured regime is inferred. From the $p(z)$ profile it appears that the transition zone is within and below the Algyő Aquitard. The most likely source of overpressures lies within the Pre-Neogene basement, which is also overpressured by as much as $\Delta p_1 = 22.26$ MPa at $z = -3050$ m and $\Delta p_2 = 28.12$ MPa at $z = -4060$ m. Although the magnitude of the best-fit fluid-pressure gradients in the middle and lower zone seem unrealistically high (≈ 1 to $2 \times \gamma_{\text{lithostatic}}$, respectively), they suggest ascending flow restricted laterally and vertically by fracture zones and low-permeability layers. The $\gamma_{\text{Szolnok, } p > 40 \text{ MPa}} = 19.9606$ MPa/km gradient for the Szolnok

Aquifer was fitted on the $p > 40$ MPa DST data from Szarvas. This pressure gradient can indicate aggressive pressure bleed-off by ascending fluid flow along fracture zones in the $z < -2000$ m domain. Such fluid migration routes are documented from the Szarvas region (e.g., Clayton and Koncz, 1994). Alternatively, the distribution of pressure data from the $z = -1800$ m to -3000 m can indicate severe depressurisation caused by extensive production in the region. This alternative explanation is supported by the hydraulic head contours interpreted on section H3 (Figure 4.35) at $L = 140 - 160$ km, and discussed in Section 4.2.2.3.

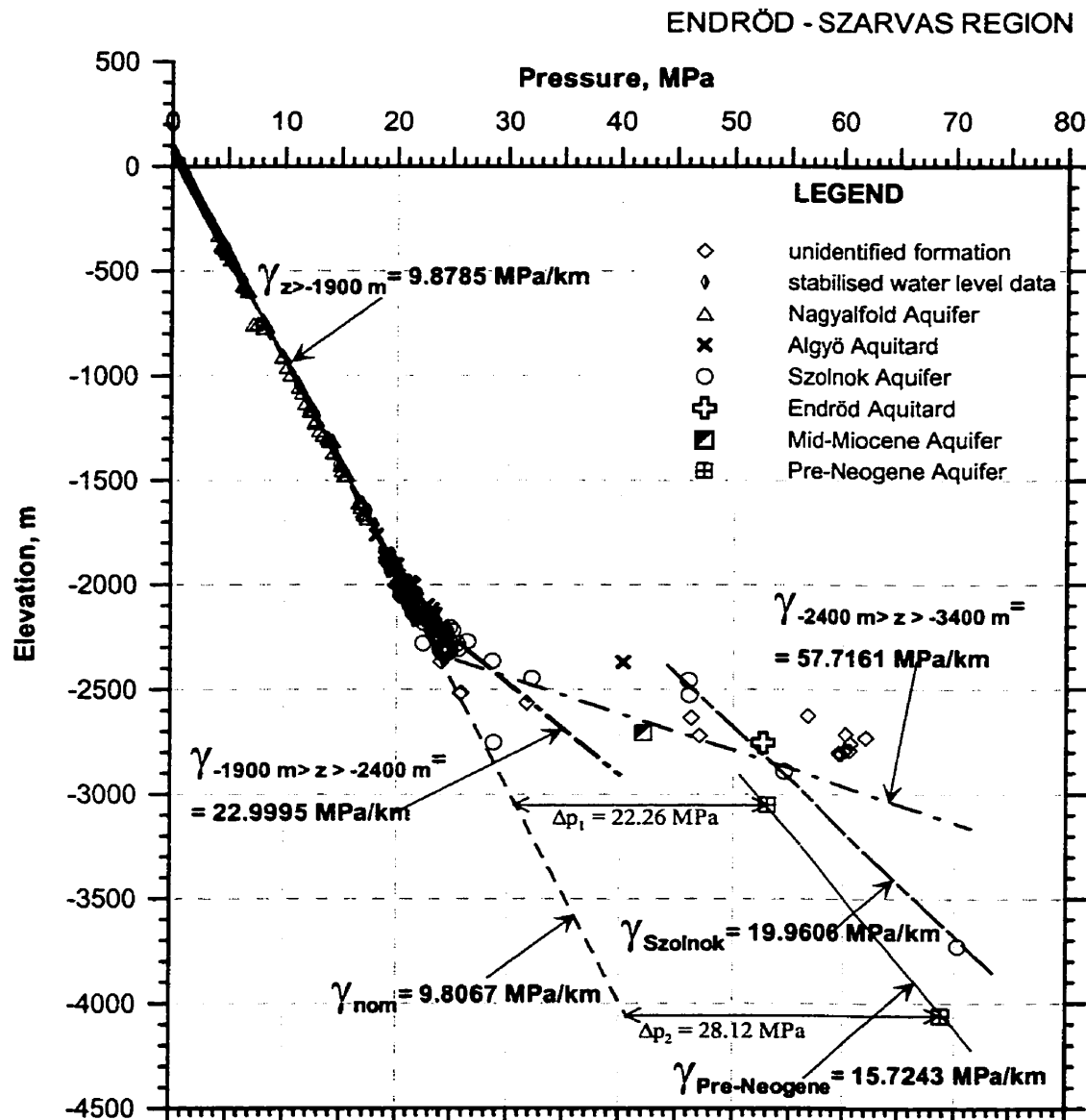


Figure 4.12: $p(z)$ profile in the Endröd-Szarvas region ($X_{\text{EOV}} = 163 - 190$ km; $Y_{\text{EOV}} = 764 - 787$ km; $z_0 = 83 - 101$ m a.s.l.). For location see Figure 4.2.

The $p(z)$ profiles of **Dévaványa** (Figure 4.13; $X_{EOV} = 182 - 195$ km; $Y_{EOV} = 792 - 808$ km; $z_0 = 84 - 92$ m), **Földes** (Figure 4.14; $X_{EOV} = 210 - 230$ km; $Y_{EOV} = 810 - 830$ km; $z_0 = 90 - 100$ m), and **Biharkeresztes** regions (Figure 4.15; $X_{EOV} = 185 - 214$ km; $Y_{EOV} = 830 - 860$ km; $z_0 = 89 - 108$ m) display a pattern similar to the one described above from the Endrőd-Szarvas region (Figure 4.12). On these profiles, the super-hydrostatic pressure gradients indicate ascending flow. Furthermore, the intensity of the vertical pressure gradients increases steadily with depth. This pattern can indicate a deep-seated pressure-energy source and a gradual dissipation of overpressures upward through the middle pressure zone into the upper quasi-hydrostatic fluid pressure zone.

The magnitude of overpressures in these aquifers is similar at about the same elevations. By taking into account the slope of these aquifers over the area of the $p(z)$ plots, it seems that there is hydraulic communication among these ‘overpressured aquifers.’ Interestingly, the Endrőd Aquitard does not seem to have any recognisable effect on the distribution of overpressures within the overlying- and underlying aquifers (i.e., Szolnok Aquifer, and Pre-Pannonian Aquifers, respectively). In the Dévaványa region, the single normal pressure value recorded within the Szolnok Aquifer at -2100 m (Figure 4.13) is in contrast with the overpressures recorded in the same aquifer ~ 200 m deeper. This observation implies that in the Dévaványa region the low-permeability ‘barrier’ or transition zone between the normal- and overpressured regimes is located within the Szolnok Aquifer. Thus, the Szolnok Aquifer is separated into two units of different pressure regimes. At this point we do not know with certainty whether there is any hydraulic communication between the two different pressure regimes across the Szolnok Aquifer, and the $p(z)$ profile alone cannot help us find a definitive answer. Based on the regional lithologic and hydraulic characteristics of the Szolnok Formation (Chapter 2), however, a transition zone of pressure dissipation is more likely to exist rather than a no-flow barrier separating the two pressure regimes.

The abrupt increase in excess pressure by at least 10 MPa observed at Dévaványa ($z < -2100$ m; Figure 4.13) and Földes ($z < -1800$; Figure 4.14) indicates the existence of an anomalous pressure regime underlying the quasi-hydrostatic regime. Such a jump in pressure values also suggests the existence of a low-permeability zone, which delays vertical dissipation of excess pressure, but it is not necessarily an indication for ‘hermetic

isolation' of any given domain in the rock framework. In the case of Dévaványa, overpressures are recorded in the Szolnok-, Mid-Miocene-, and Pre-Pannonian Aquifers.

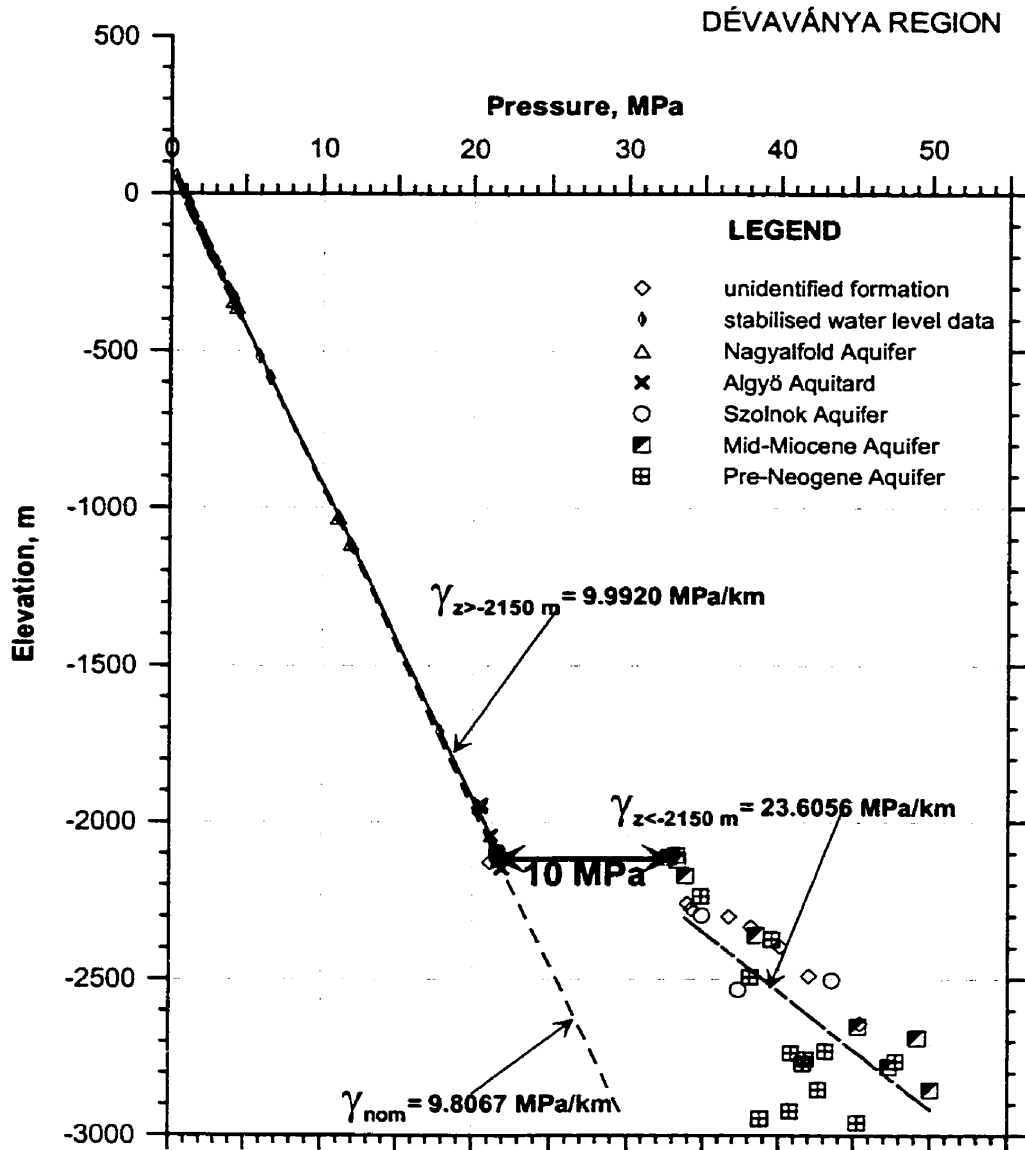


Figure 4.13: $p(z)$ profile in the Dévaványa region ($X_{\text{EOV}} = 182 - 195 \text{ km}$; $Y_{\text{EOV}} = 792 - 808 \text{ km}$; $z_0 = 84 - 92 \text{ m}$). For location see Figure 4.2.

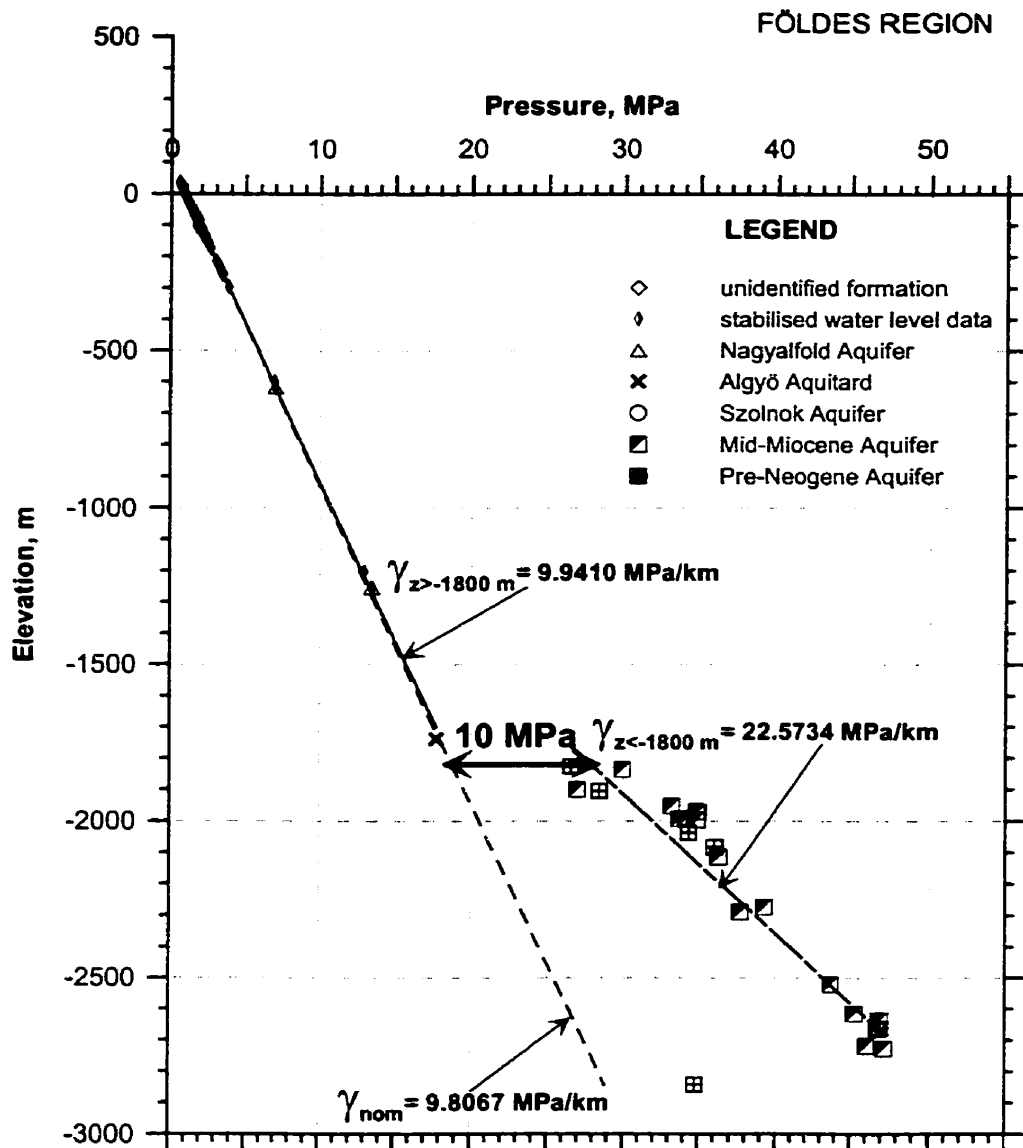


Figure 4.14: $p(z)$ profile in the Földes region ($X_{EOV} = 210 - 230 \text{ km}$; $Y_{EOV} = 810 - 830 \text{ km}$; $z_0 = 90 - 100 \text{ m}$). For location see Figure 4.2.

Two remarkable features can be observed on the $p(z)$ profile of the Biharkeresztes region (Figure 4.15): 1) within the lower overpressured zone ($z < -2150 \text{ m}$) the pore pressures are scattered in a $\sim 10 \text{ MPa}$ wide range, and 2) within the middle and lower zone, the magnitude and range of overpressures is similar in laterally adjacent hydrostratigraphic units (Algyő Aquitard, Szolnok, Mid-Miocene, and Pre-Pannonian Aquifers). These observations can be explained in terms of pressure dissipation along adjacent faults or fault zones of variable hydraulic conductivity crossing low permeability aquitards. Most of the pressure values plotted on this profile were measured in the

central-southern part of the Derecske Trough and the Komádi High (Figure 2.12). In this region, Tari (1994) identified closely spaced (about 1 – 3 km apart) faults within the Pre-Neogene basement and the Neogene sedimentary pile on reflection seismic profiles (Figure 4.16). The coincidence of the seismic and hydrogeologic observations support, but do not necessarily confirm, the above explanation for the pressure distribution in the Biharkeresztes region.

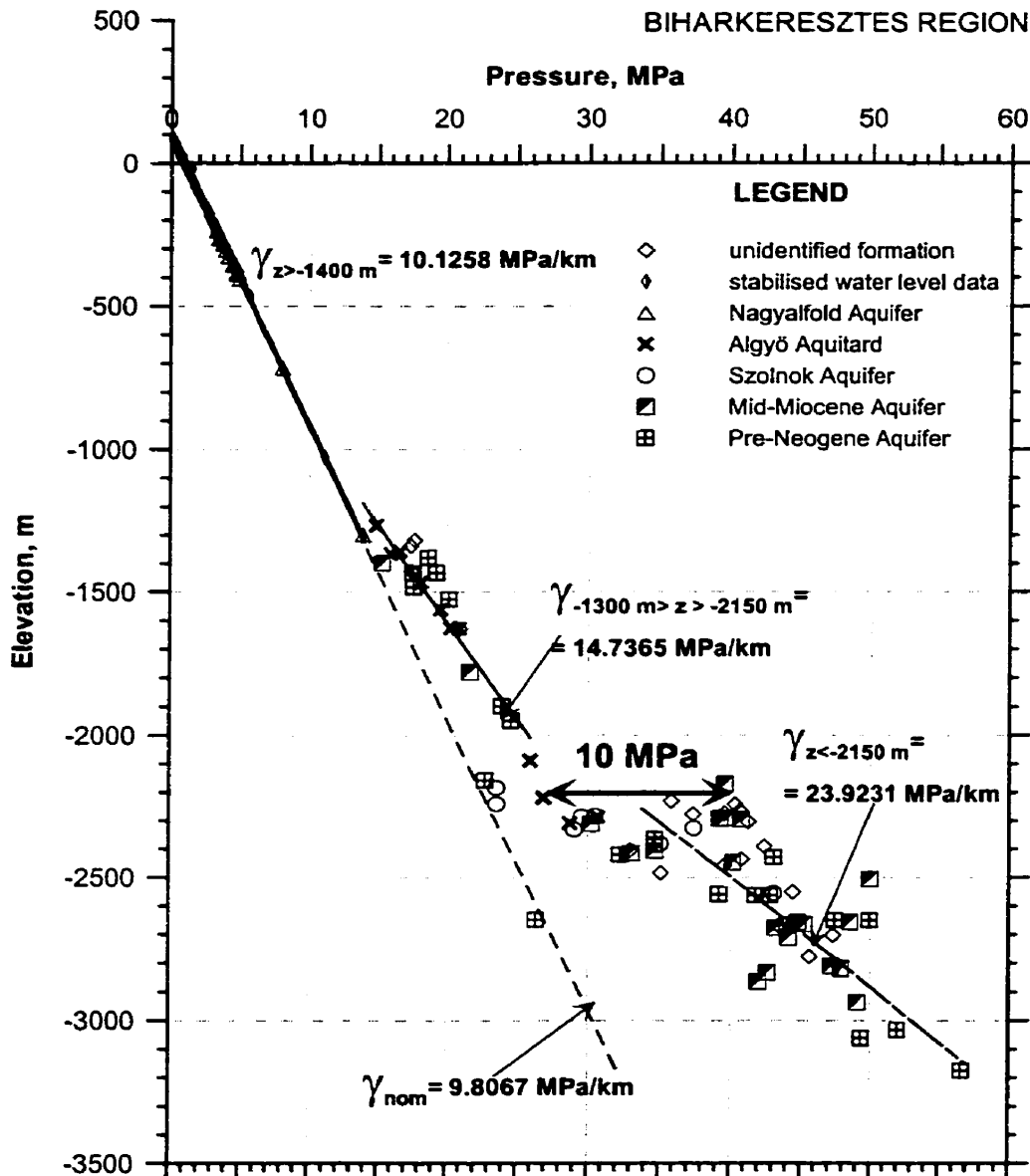


Figure 4.15: $p(z)$ profile in the Biharkeresztes region ($X_{EOV} = 185 - 214$ km; $Y_{EOV} = 830 - 860$ km; $z_0 = 89 - 108$ m). For location see Figure 4.2.

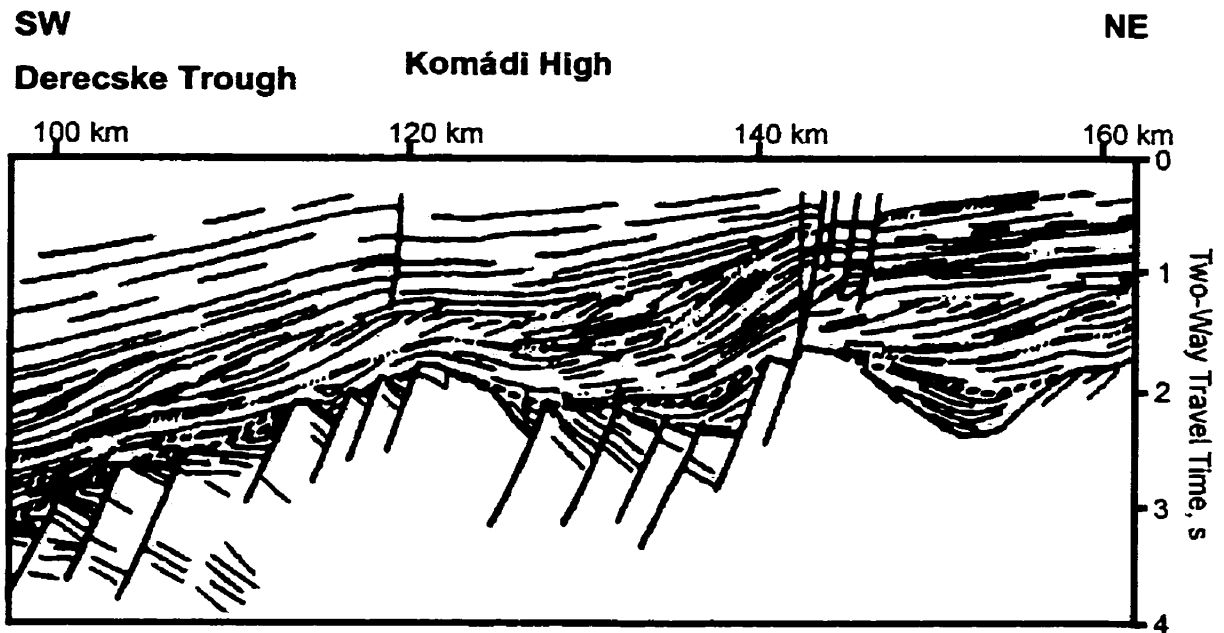


Figure 4.16: Interpreted reflection seismic profile across the Derecske Trough and the Komádi High in the Biharkeresztes region. For location see Figure 4.2. (modified after Tari, 1994; NE part of seismic section Q).

In the **Ruzsa-Üllés region** (Figure 4.2 and 4.17) ($X_{EOV} = 100 - 115$ km; $Y_{EOV} = 700 - 720$ km; $z_0 = 90 - 120$ m) the normal pressures change abruptly within the Pre-Neogene basement ($\gamma_{Pre-Pannonian} = 14.6017$ MPa/km) at about $z = -2000$ m elevation.

The probable cause(s) of overpressure generation in the Pre-Neogene basement is the same as in the other regions described above. The overpressures observed in the Mid-Miocene Aquifer from Üllés are probably due to buoyancy effects, as the control points refer to initial pool pressures of vertically stacked gas accumulations locally with oil. This profile will be discussed in more detail in Chapter 5.

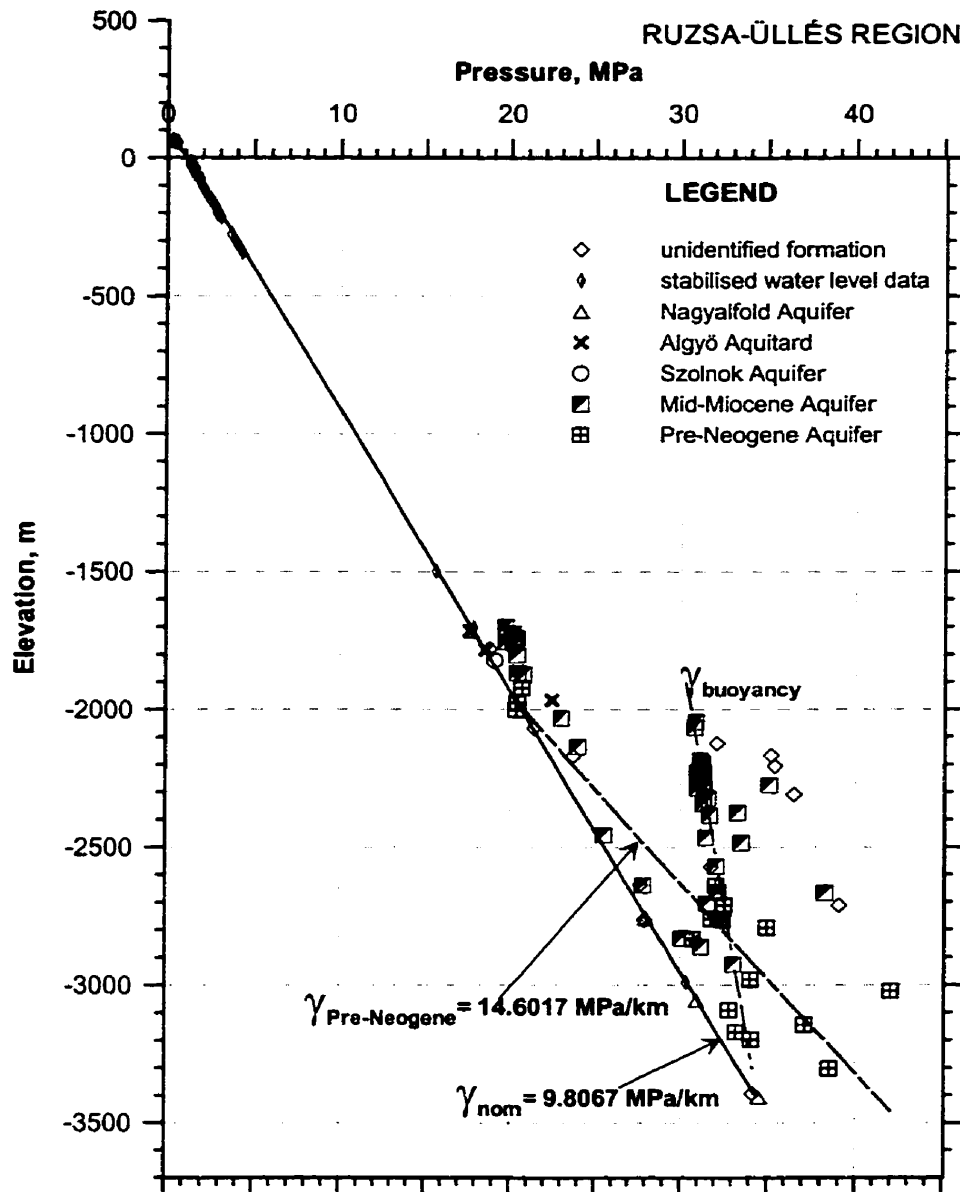


Figure 4.17: $p(z)$ profile in the Ruzsa - Üllés region ($X_{EOV} = 100 - 115$ km; $Y_{EOV} = 700 - 720$ km; $z_0 = 90 - 120$ m). For location see Figure 4.2.

The observations and inferences made from the one-dimensional analysis of vertical pressure distribution ($p(z)$ profiles) are summarised as follows:

1. two regional fluid pressure zones are inferred to exist in the study area: an upper unconfined quasi-hydrostatic zone and an underlying confined overpressured zone. The two pressure zones may be connected by a transition zone or separated by a low-permeability boundary.

2. The quasi-hydrostatic zone extends from the water table to locally variable elevations, i.e., $z = -1500$ m to -2500 m.
3. The regionally unconfined nature of the quasi-hydrostatic zone is inferred from the small deviation of pressure data along straight vertical pressure-gradient lines.
4. The slope of vertical super-hydrostatic gradients increases steadily with depth within the overpressured zone. This indicates the presence of a deep-seated energy source, which generates the overpressures and drives fluids upward.
5. Overpressures within the Pre-Pannonian Aquifer are ubiquitous, which indicates that the 'deep-seated energy source' is located within this hydrostratigraphic unit.
6. The transition zone/boundary between the two pressure zones is not systematically associated with any particular regional hydrostratigraphic unit or depth in the basin. Thus, the upper boundary of the overpressured zone is not controlled by hydrostratigraphy or by depth.
7. Local permeability variations related to lithologic heterogeneity and fracture zones are believed to control pressure dissipation from the overpressured zone and hydraulic communication between the two pressure regimes.
8. Within the upper unconfined zone fluid pressures are adjusted to the topography and flow is driven by gravity, as indicated by the following observations:
 - a) sub-hydrostatic gradients (condition for descending flow, i.e., recharge) are encountered underneath areas of higher topographic elevation, typically where $z_0 > 110$ m (e.g., Figures 4.5, 4.6, 4.7, and 4.8);
 - b) slight super-hydrostatic gradients ($\gamma_{\text{static}} < \gamma_{\text{observed}} < 10$ MPa/km) are systematically encountered underneath areas of low topographic elevation, typically where $z_0 < 110$ m (e.g., Figures 4.9 through 4.15). This is a condition for ascending flow, i.e., discharge.
9. The abrupt change from sub-hydrostatic to super-hydrostatic gradients observed below recharge areas results in vertically convergent flow.

The possible cause(s) of overpressures, i.e., the 'deep-seated energy source,' are discussed in Chapter 7.

4.2.2.2 Tomographic fluid-potential maps ($h_{i,j}(x,y)$)

The tomographic fluid-potential maps are presented on Figures 4.18 through 4.21 and 4.23 through 4.31. On these maps, the direction of the horizontal component of the flow driving forces is posted with arrows. The length of force vectors (arrows) is proportional to the magnitude of the horizontal component of the hydraulic gradient. The arrows do not indicate relative magnitudes of fluid flux or flow velocity, as that also depends on the hydraulic conductivity tensor and porosity. The fluid-potential map codes and corresponding figure numbers are listed in Table 4.2.

Table 4.2. Codes of fluid-potential maps and corresponding figure numbers.

Map code	Figure number	Elevation interval (m a.s.l.)
$h_{z_0,40}$	4.18	z_0 to z_0-40
$h_{04,0}$	4.19	z_0-40 to 0
$h_{0,1}$	4.20	0 to -100
$h_{1,3}$	4.21	-100 to -300
$h_{3,6}$	4.23	-300 to -600
$h_{6,10}$	4.24	-600 to -1000
$h_{10,15}$	4.25	-1000 to -1500
$h_{15,19}$	4.26	-1500 to -1900
$h_{19,22}$	4.27	-1900 to -2200
$h_{22,25}$	4.28	-2200 to -2500
$h_{25,28}$	4.29	-2500 to -2800
$h_{28,31}$	4.30	-2800 to -3100
$h_{31,35}$	4.31	-3100 to -3500

An inspection of the upper four tomographic potential maps, $h_{z_0,04}$, $h_{04,0}$, $h_{0,1}$, and $h_{1,3}$ (Figures 4.18 through 4.21), reveals that the potential surfaces mimic the land surface, $z_0(X_{EOV}, Y_{EOV})$ (Figure 2.3). The hydraulic head ‘mounds’ coincide spatially with the areas of high topographic elevation, while the hydraulic head contours of lower value are located below the regional topographic depressions. Furthermore, beneath the elevated areas the hydraulic heads are decreasing downward, whereas underneath the low-lying areas the hydraulic heads are increasing with depth –as expected from the vertical pressure distribution shown by the $p(z)$ profiles. Such fluid-potential configuration indicates gravity-driven flow regimes in regionally unconfined flow domains (Tóth, 1978). Thus, below the land surface to $z = -300$ m elevation groundwater

flow is clearly gravity-driven in a regionally unconfined flow domain. It must be noted that the $z = -300$ m elevation is not the maximum depth of penetration of gravity-driven flow systems. The fluid-potential surface on $h_{3,6}$ (Figure 4.23) also mimics the land surface.

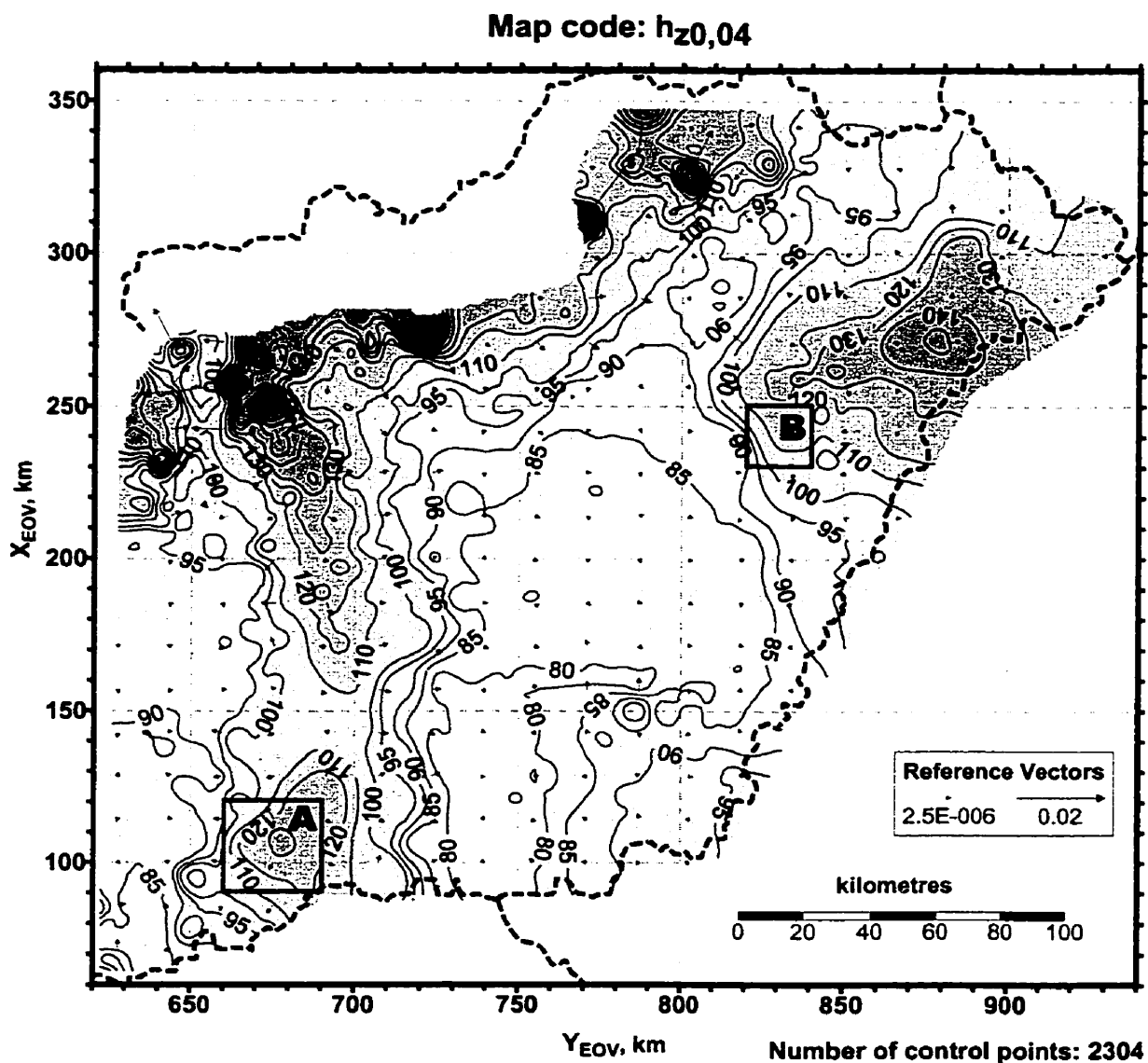


Figure 4.18: Tomographic fluid-potential map based on stabilised water level data from wells shallower than 40 m. Arrows (vectors) indicate the direction and magnitude of the horizontal hydraulic gradients. The hydraulic head contours are in m a.s.l. displayed at a 5 m interval between $h = 80$ to 100 m and at a 10 m interval between $h = 100$ to 220 m

Map code: h04,0

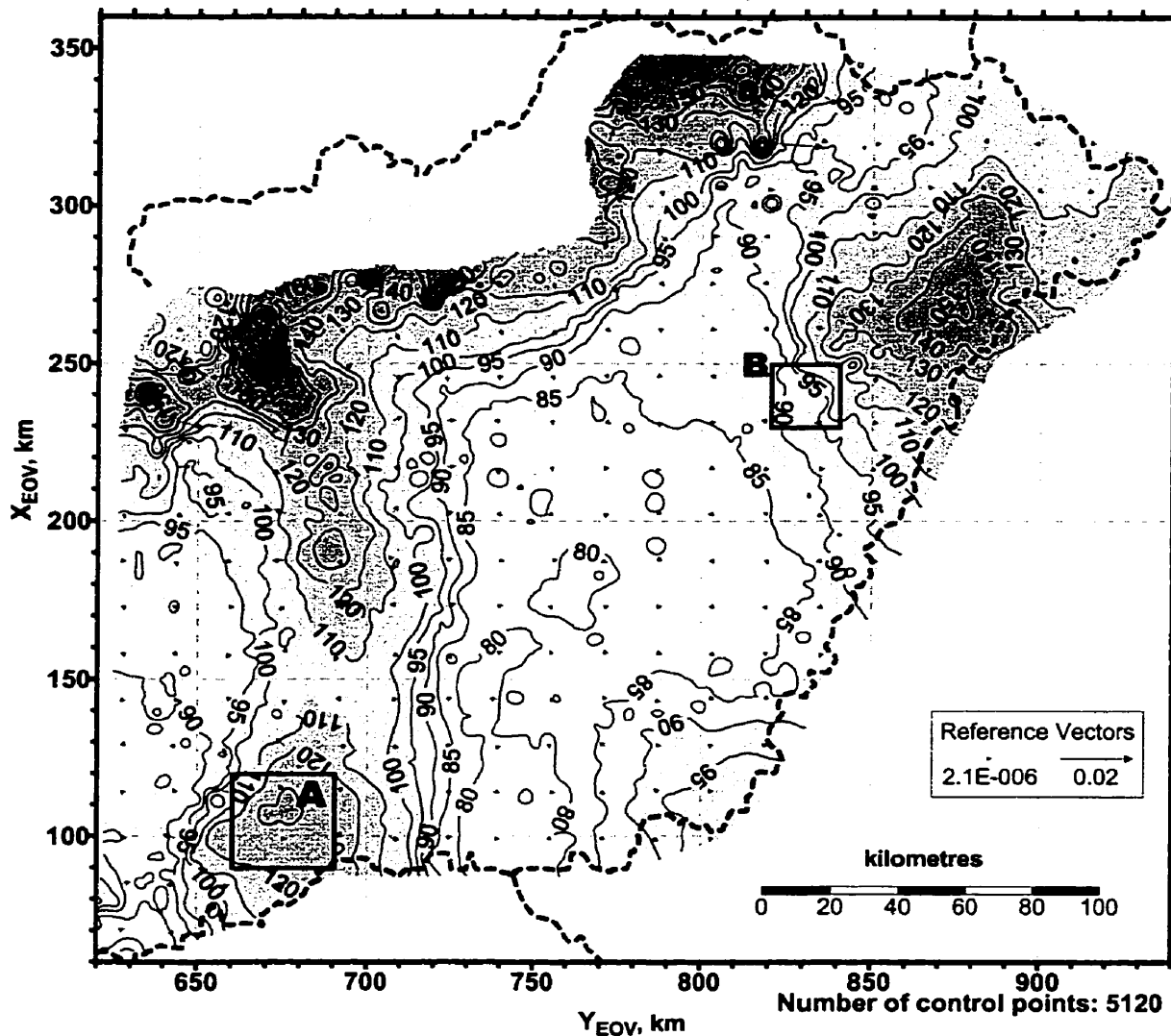


Figure 4.19: Tomographic fluid-potential map based on stabilised water level data from wells deeper than 40 m and elevation heads greater than sea level. Arrows (vectors) indicate the direction and magnitude of the horizontal hydraulic gradients. The hydraulic head contours are in m a.s.l. displayed at a 5 m interval between $h = 80$ to 100 m and at a 10 m interval between $h = 100$ to 210 m.

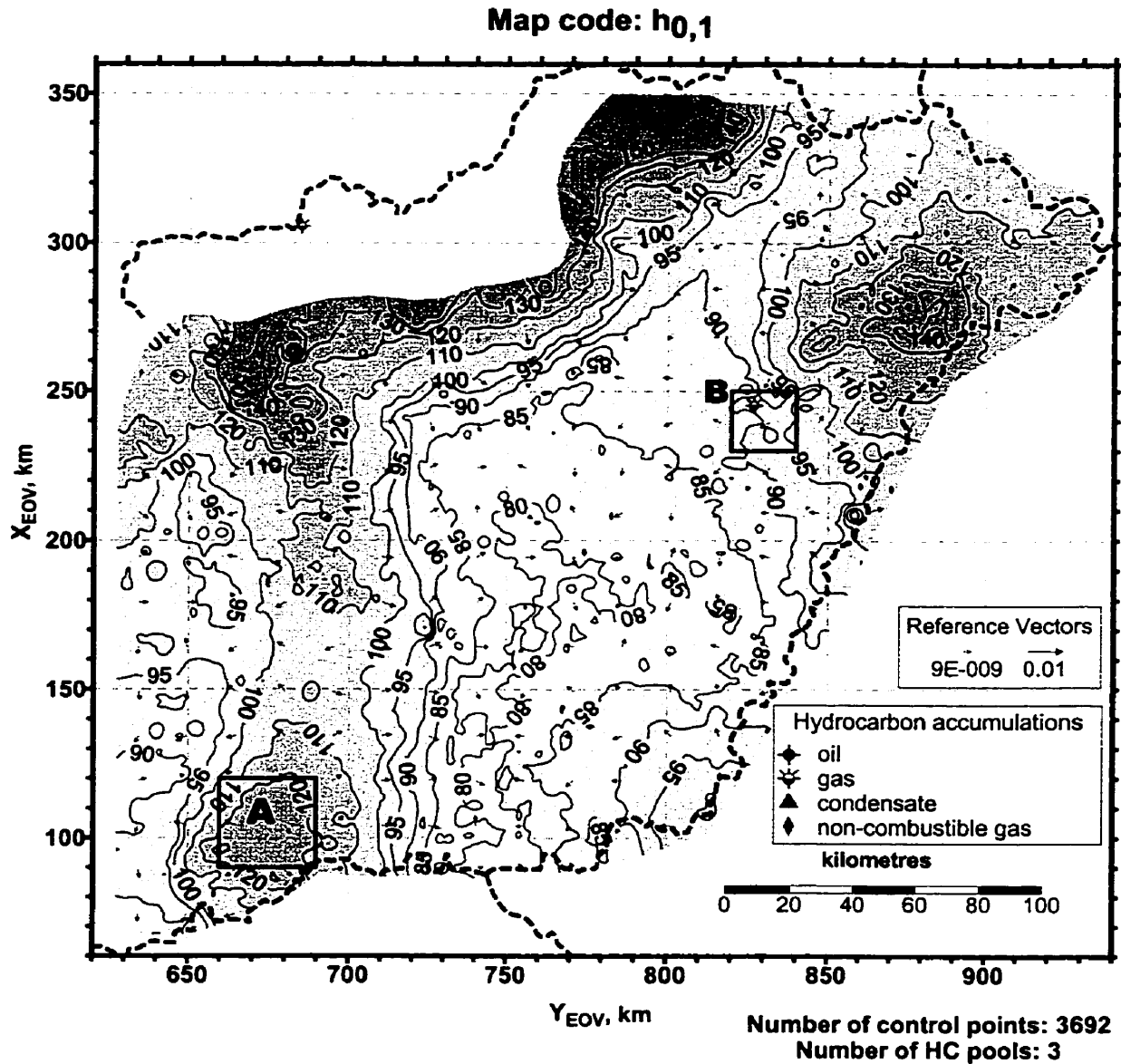


Figure 4.20: Tomographic fluid-potential map based on stabilised water level data and pore pressure (DST) data with elevation heads between $z = 0$ (sea level) to -100 m. Arrows (vectors) indicate the direction and magnitude of the horizontal hydraulic gradients. The hydraulic head contours are in m a.s.l. displayed at a 5 m interval between $h = 80$ to 100 m and at a 10 m interval between $h = 100$ to 170 m. Note: the shallowest commercial gas accumulations are at $(Y_{EOV} = 828 \text{ km}, X_{EOV} = 245 \text{ km})$.

Map code: h1,3

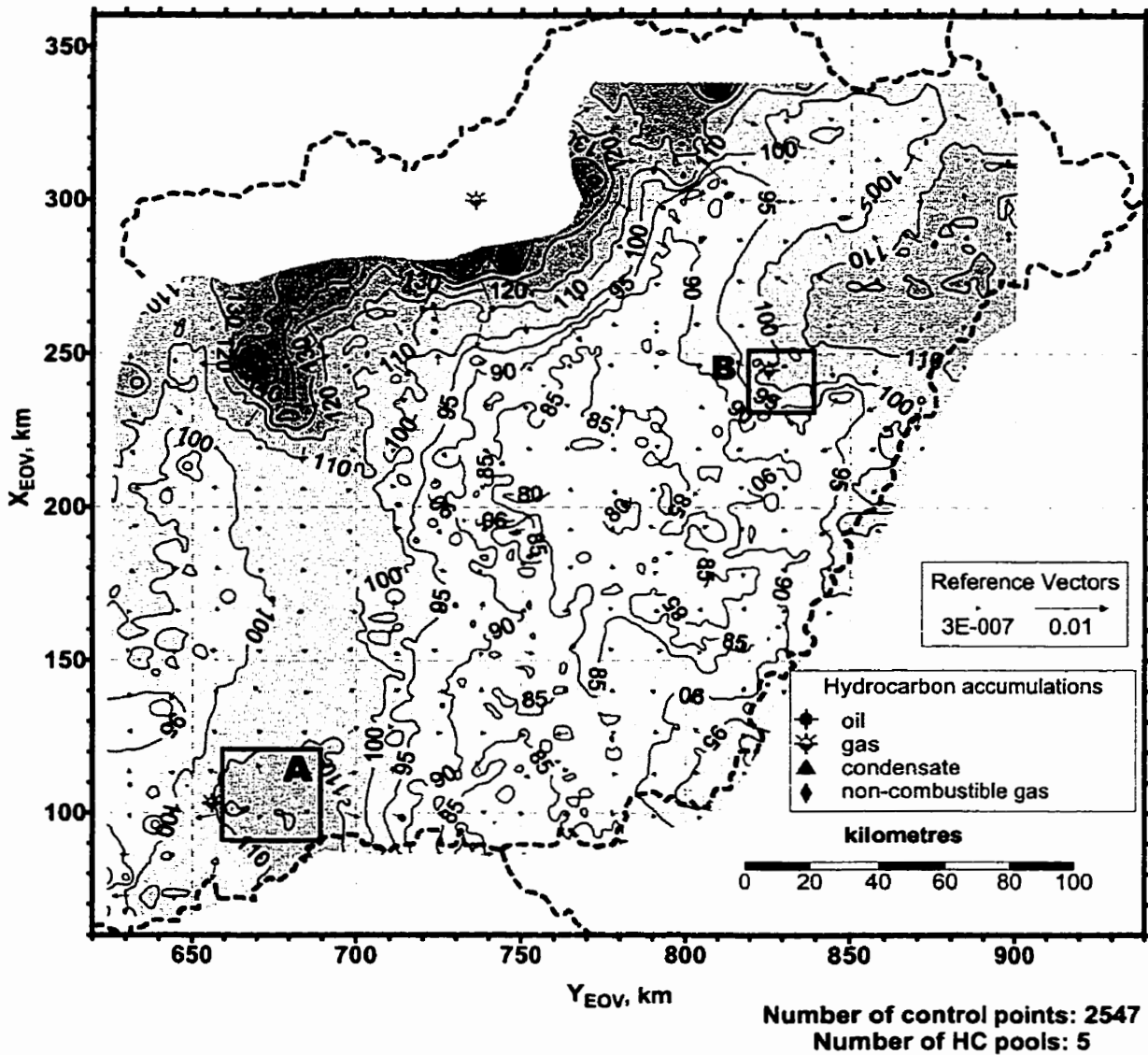


Figure 4.21: Tomographic fluid-potential map based on stabilised water level data and pore pressure (DST) data with elevation heads between $z = -100$ m to -300 m. Arrows (vectors) indicate the direction and magnitude of the horizontal hydraulic gradients. The hydraulic head contours are in m a.s.l. displayed at a 5 m interval between $h = 80$ to 100 m and at a 10 m interval between $h = 100$ to 170 m. Note: commercial hydrocarbon accumulations are displayed.

Based on the tomographic hydraulic head maps for the $z = z_0 - 300$ m elevation interval (Figures 4.18 through 4.21) and the $p(z)$ profiles presented earlier, the regional groundwater regimes within the limits of the study area are generalised as follows (Figure 4.22):

Recharge areas (hydraulic heads decrease downward by up to 20 m or more; descending flow): characteristic land surface elevation is $z_0 \geq 110 - 120$ m a.s.l.; the Duna-Tisza Interfluvium area (Illancs to the S, and Gödöllő Hills to the N), the southern foothills of the North-Central Range and the Nyírség region.

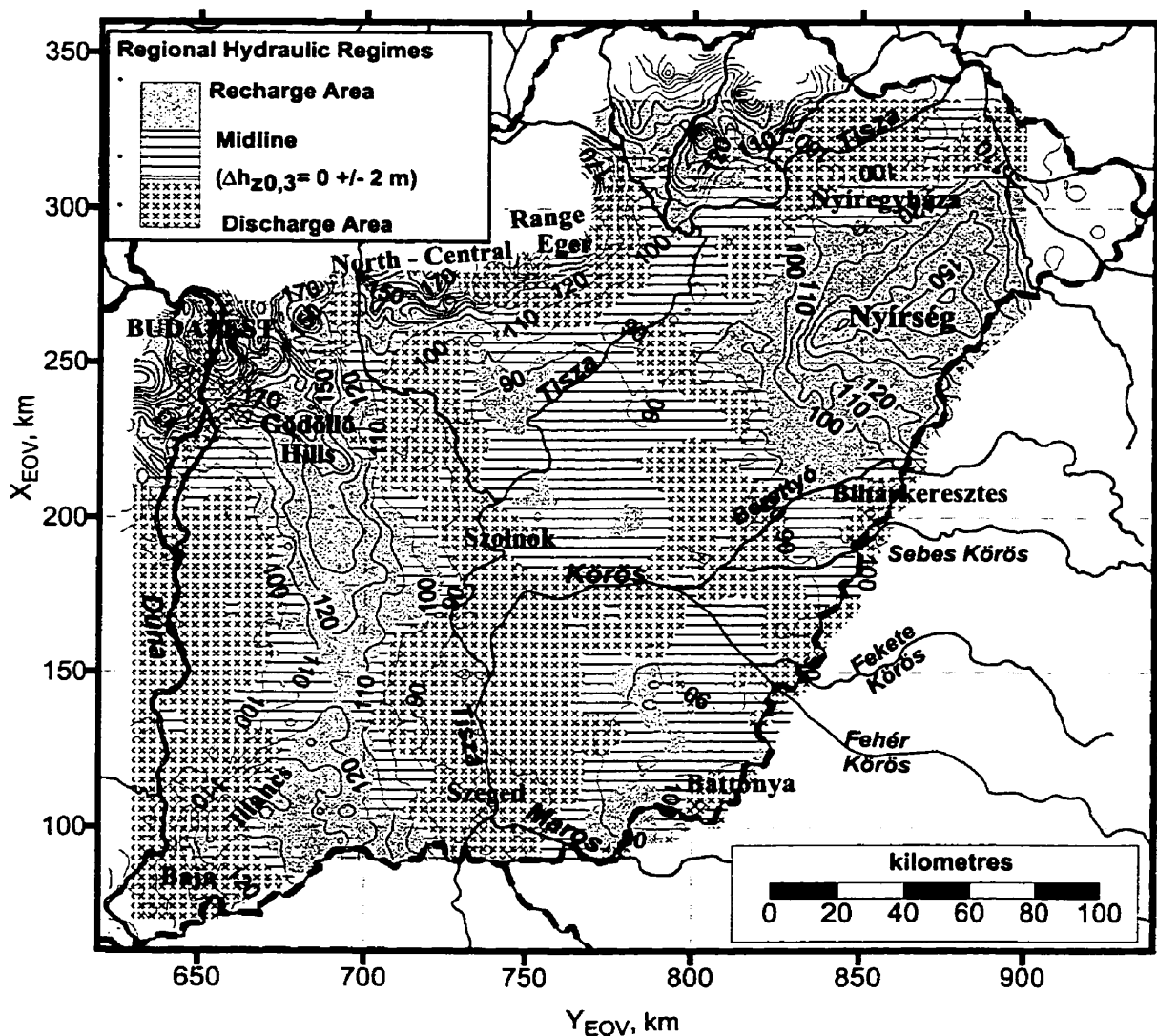


Figure 4.22: Calculated distribution of regional groundwater regimes in eastern Hungary inferred from fluid-potential maps between the land surface (z_0) and $z = -300$ m elevation, and from $p(z)$ profiles. Topographic elevation contours are in metres; C.I. = 10 m.

Midline region: (hydraulic heads barely change with depth; lateral flow): around the Duna-Tisza Interfluvial area, where the vertical hydraulic head difference is $\Delta h \approx 0 \pm 2$ m; it is a narrow zone around the Nyírség, and apparently extended to the north of the Körös River along the Tisza River.

Discharge areas (hydraulic heads increase with depth by up to 10 m or more; ascending flow): characteristic land surface elevation is $z_0 < 100 - 110$ m a.s.l.; the Duna Valley on the western side of the study area, and the lowlands encompassing the Tisza River, the Körös region (the Valleys of Fehér Körös, Fekete Körös, Sebes Körös, and Berettyó) and the Maros-Körös Interfluvial area. The latter broad plain is the very core of the Great Hungarian Plain.

The fluid-potential surface on $h_{3,6}$ (Figure 4.23) mostly mimics the land surface, however, it also shows two anomalies, i.e., fluid-potential mounds. These anomalies are better understood by comparing the upper five tomographic maps ($h_{20,04}$ through $h_{3,6}$, i.e., Figures 4.18, 4.19, 4.20, 4.21, and 4.23). The first anomaly is in the southern part of the Duna-Tisza Interfluvial area (box A: $X_{EOV} = 90 - 120$ km, $Y_{EOV} = 660 - 690$ km): the hydraulic head decreases from 130 m on $h_{20,04}$ (Figure 4.18) to ~ 120 m on $h_{1,3}$ (Figure 4.21), while on $h_{3,6}$ (Figure 4.23) it increases abruptly to $h = 200$ m. The other anomaly is observed in the area bounded by the co-ordinates $X_{EOV} = 230 - 250$ km and $Y_{EOV} = 820 - 840$ km (box B). In this area, the $h \approx 100$ m value hardly changes with depth, indicating lateral flow in the midline zone on $h_{20,04}$ to $h_{1,3}$ (Figures 4.18 through 4.21). However, on $h_{3,6}$ (Figure 4.23) the hydraulic head increases abruptly from $h = 100$ to $h = 140$ m. The location of both fluid-potential anomalies is associated with known gas accumulations. Also, in both locations, the phenomenon is limited to the $z = -300$ m to -600 m elevation interval (Figures 4.22 and 4.23). Therefore, these anomalous hydraulic head mounds are probably due to the density contrast between water and gas, and to the height of the gas columns.

High fluid-potential (high-pressure) anomalies can be observed in increasing number in maps of subsequently deeper domains (i.e., $z < -600$ m a.s.l.). The magnitude of these hydraulic head anomalies exceeds the present topographic elevations in the study area ($z_0 = 76$ to ~ 220 m a.s.l.) by several hundred metres to about 3500 m. From these maps it appears that in the explored part of the Great Hungarian Plain overpressures are ubiquitous, however, they occur with various magnitudes and are detected at different

depths. In other words, the basin is overpressured. If we were to define a constant head upper bounding surface for the overpressured zone, that surface would display a very uneven topography and strong relief.

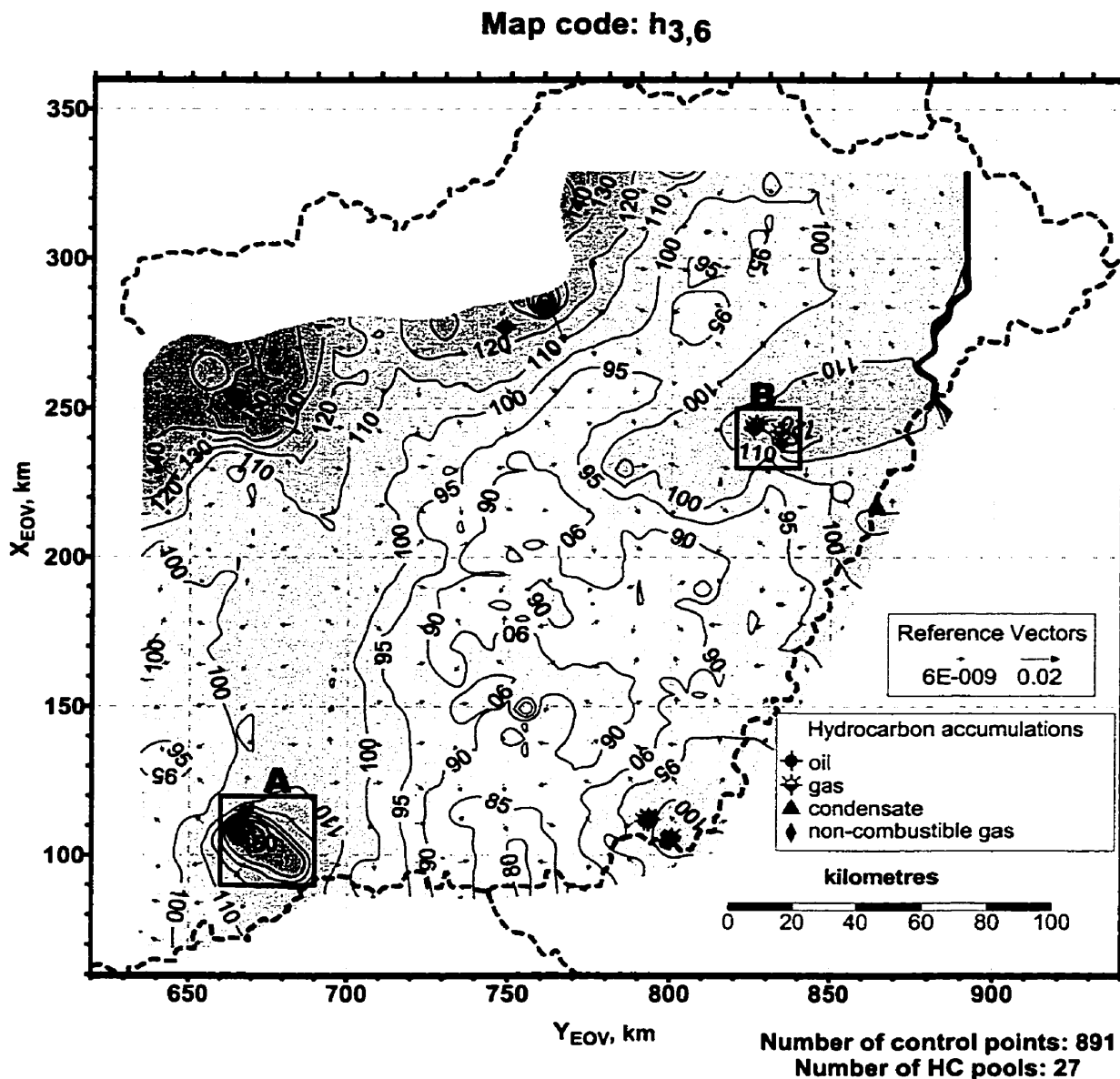


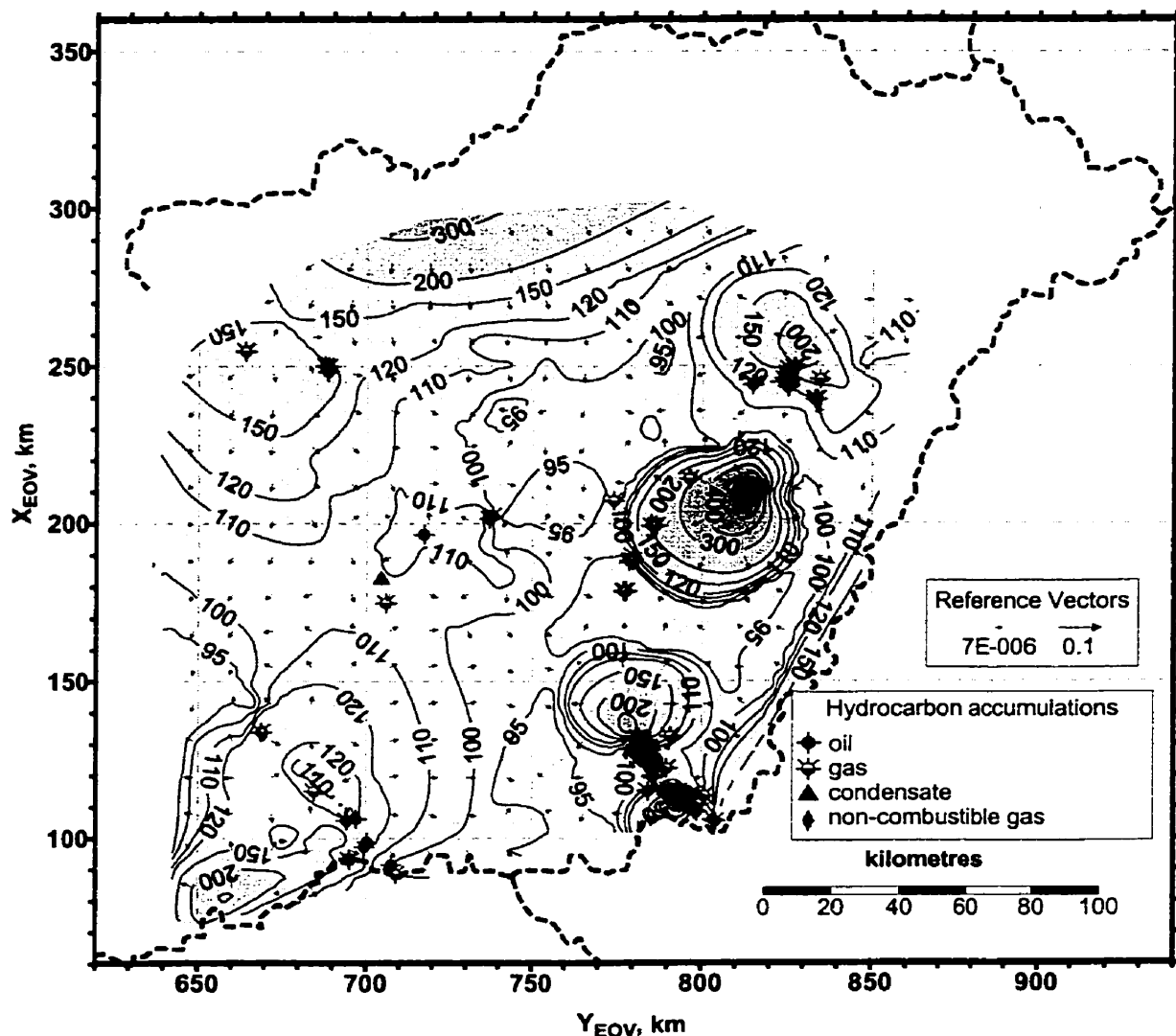
Figure 4.23: Tomographic fluid-potential map based on stabilised water level data and pore pressure (DST) data with elevation heads between $z = -300$ m to -600 m. Arrows (vectors) indicate the direction and magnitude of the horizontal hydraulic gradients. The hydraulic head contours are in m a.s.l. displayed at a 5 m interval between $h = 80$ to 100 m and at a 10 m interval between $h = 100$ to 170 m. Note: commercial hydrocarbon accumulations are displayed

The anomalies first appear as *potentiometric mounds*, i.e., closed high-h contours, for instance, on map **h_{6,10}** (Figure 4.24) and map **h_{10,15}** (Figure 4.25) in the areas bounded by the following co-ordinates: [$Y_{EOV} = 640 - 680$, $X_{EOV} = 70 - 95$], [$Y_{EOV} = 760 - 810$, $X_{EOV} = 100 - 160$], and [$Y_{EOV} = 810 - 852$, $X_{EOV} = 240 - 280$]. In maps of deeper zones, the mounds tend to merge into straight and arched *potentiometric ridges* (e.g., **h_{10,15}**, Figure 4.25, and **h_{15,19}**, Figure 4.26), high-h *plateaus*, and *potentiometric escarpments* bordering *potentiometric depressions* (e.g., **h_{15,19}**, **h_{19,22}**, **h_{22,25}**, and **h_{25,28}**, Figures 4.26 through 4.29). On the ridges, plateaus, and escarpments, the hydraulic head values exceed $h = 500$ m and locally $h > 3000$ m. The high potential mounds, ridges, and escarpments are characterised by high lateral hydraulic gradients, while the plateaus and depressions by low hydraulic gradients. The intensity of the hydraulic gradient does not necessarily imply large flux, as that also depends on the hydraulic conductivity.

There are good examples for *potentiometric ridges* on map **h_{19,22}** (Figure 4.27): the ridges are marked by the $h = 1000$ m contour line, as seen by connecting the following points of co-ordinates Y_{EOV}/X_{EOV} : $835/206 \rightarrow 750/200$ and $710/210 \rightarrow 720/150$. The high-h *plateau* on **h_{22,25}** (Figure 4.28) is marked by $h = 1000$ m and $h = 1500$ m in the central-eastern part of the study area (the area bounded by $Y_{EOV} = 775 - 835$ km; $X_{EOV} = 175 - 220$ km). Also on **h_{22,25}** (Figure 4.28), the high-h *mound* between the points (Y_{EOV}/X_{EOV}) $730/120$ to $755/162$ is marked by the $h = 500 - 2000$ m contours.

The relative *potentiometric depressions* observed in the south-eastern part of the study area on **h_{19,22}** and **h_{22,25}** (Figure 4.27 and 4.28, respectively) are marked by $h < 200$ m and $h < 400$ m. These areas of relative potentiometric minima are directly above the Békés Depression and the Makó Trough (see also Figure 2.19, p.38). Apparently, the overpressures are progressively increasing downward within these troughs (basement grabens), as illustrated on **h_{19,22}**, **h_{22,25}**, **h_{25,28}**, **h_{28,31}**, and **h_{31,35}** (Figures 4.27 through 4.31). However, regional hydraulic head configuration patterns can not be established below $z = -2800$ m (Figures 4.30 and 4.31) due to scarcity of data.

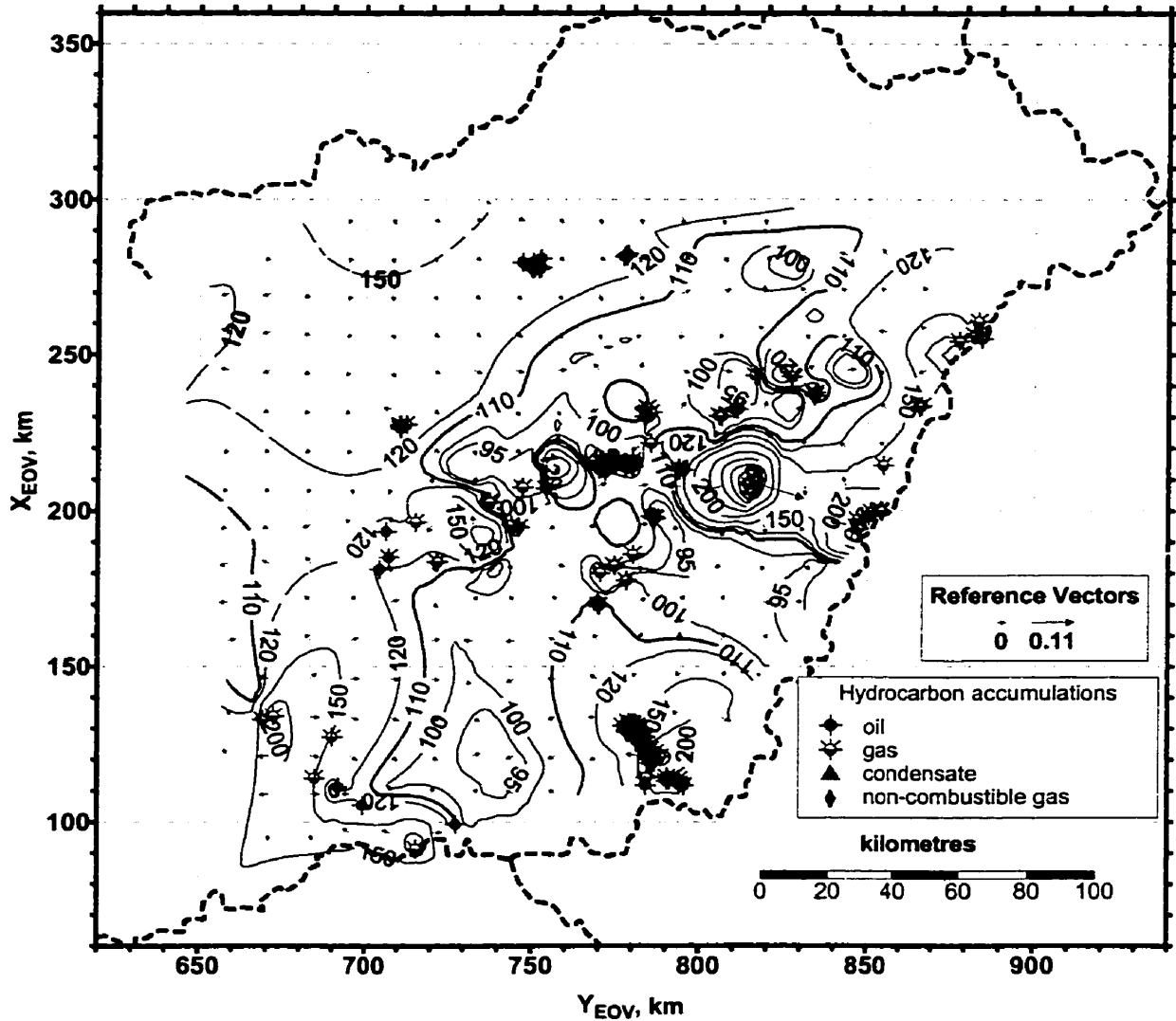
Map code: h6,10



Number of control points used : 375 out of 464
Number of HC pools: 185

Figure 4.24: Tomographic fluid-potential map based on stabilised water level data and pore pressure (DST) data with elevation heads between $z = -600$ m to -1000 m. Arrows (vectors) indicate the direction and magnitude of the horizontal hydraulic gradients. The hydraulic head contours are in m a.s.l. displayed irregularly as $h = 95$ m, 100 m, 110 m, 120 m, 150 m, and 200 m, and regularly at 100 m interval for $h = 200$ m to 300 m. Note: commercial oil and gas accumulations are also displayed.

Map code: h10,15



Number of control points used: 281 out of 339
 Number of HC pools: 174

Figure 4.25: Tomographic fluid-potential map based on stabilised water level data and pore pressure (DST) data with elevation heads between $z = -1000$ m to -1500 m. Arrows (vectors) indicate the direction and magnitude of the horizontal hydraulic gradients. The hydraulic head contours are in m a.s.l. displayed irregularly as $h = 95$ m, 100 m, 110 m, 120 m, 150 m, and 200 m, and regularly at 100 m interval for $h = 200$ m to 900 m. Note: commercial hydrocarbon accumulations are also displayed. From the original 339 data 281 were accepted as representative and 48 data were rejected because of production drawdown effects.

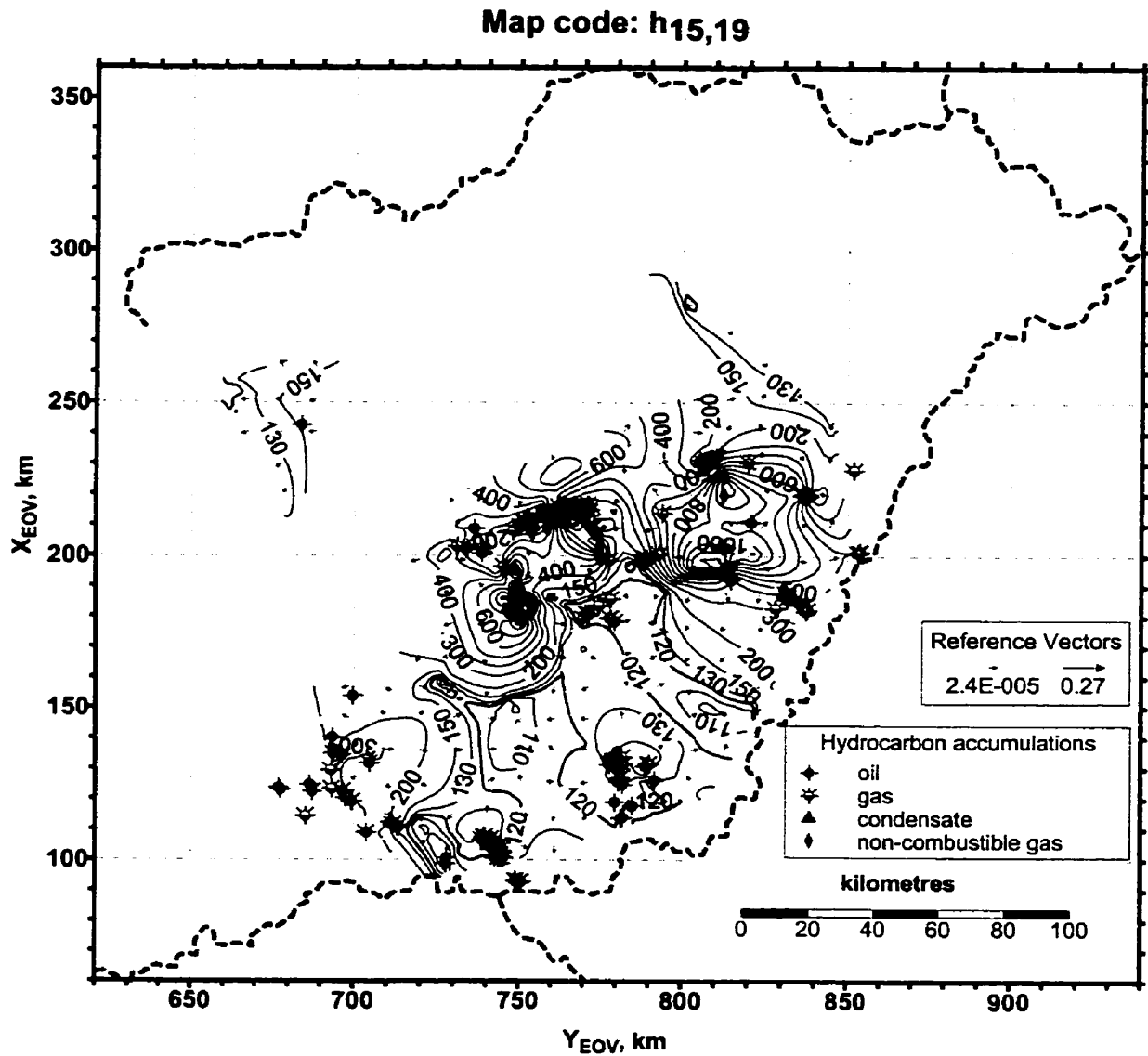
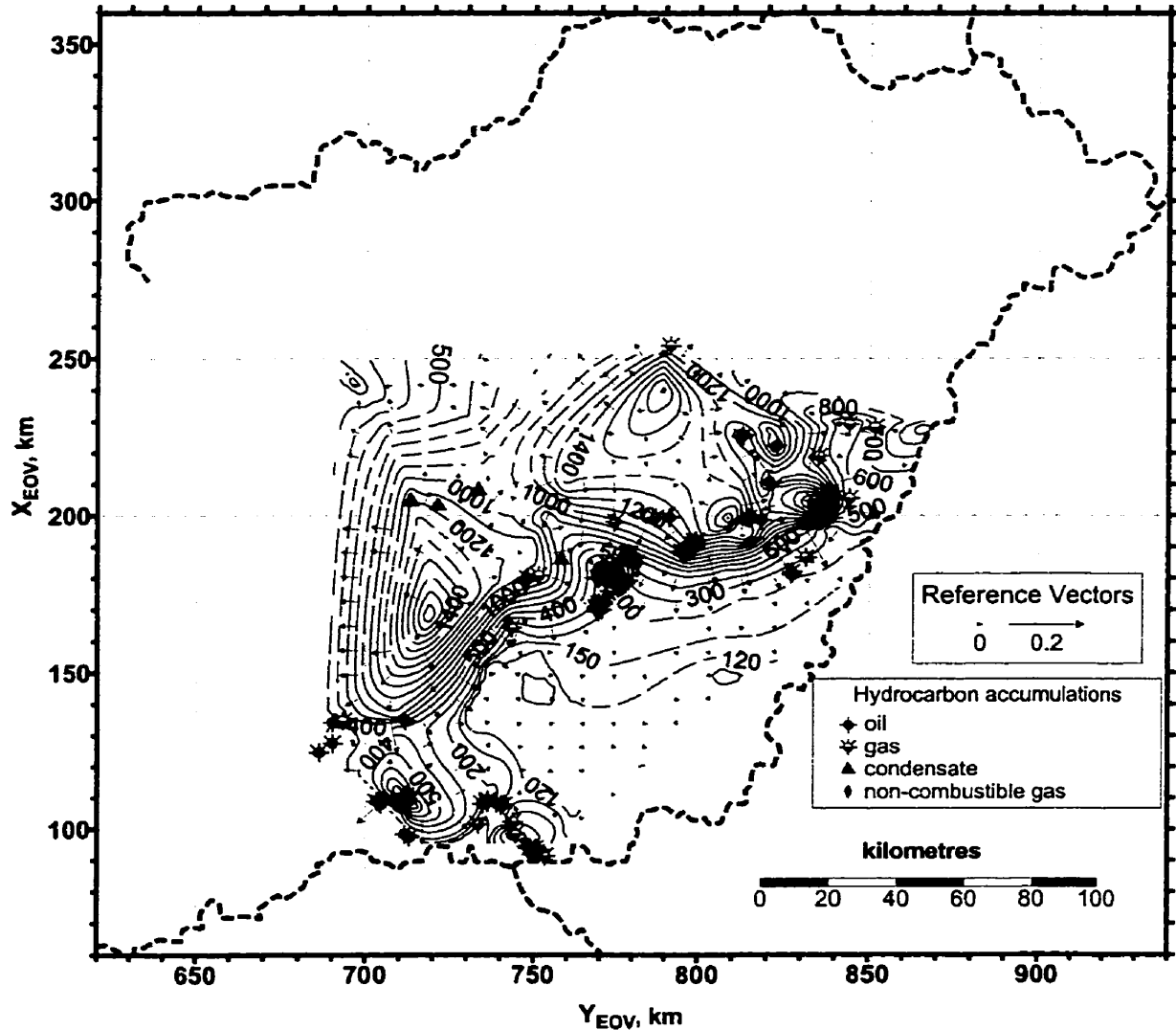


Figure 4.26: Tomographic fluid-potential map based on stabilised water level data and pore pressure (DST) data with elevation heads between $z = -1500$ m to -1900 m. Arrows (vectors) indicate the direction and magnitude of the horizontal hydraulic gradients. The hydraulic head contours are in m a.s.l. displayed irregularly as $h = 95$ m, 100 m, 110 m, 120 m, 150 m, and 200 m, and regularly at 100 m interval for $h = 200$ m to 1400 m. Note: commercial hydrocarbon accumulations are also displayed. From the original 331 data 262 were accepted as representative and 69 data were rejected because of production drawdown effects.

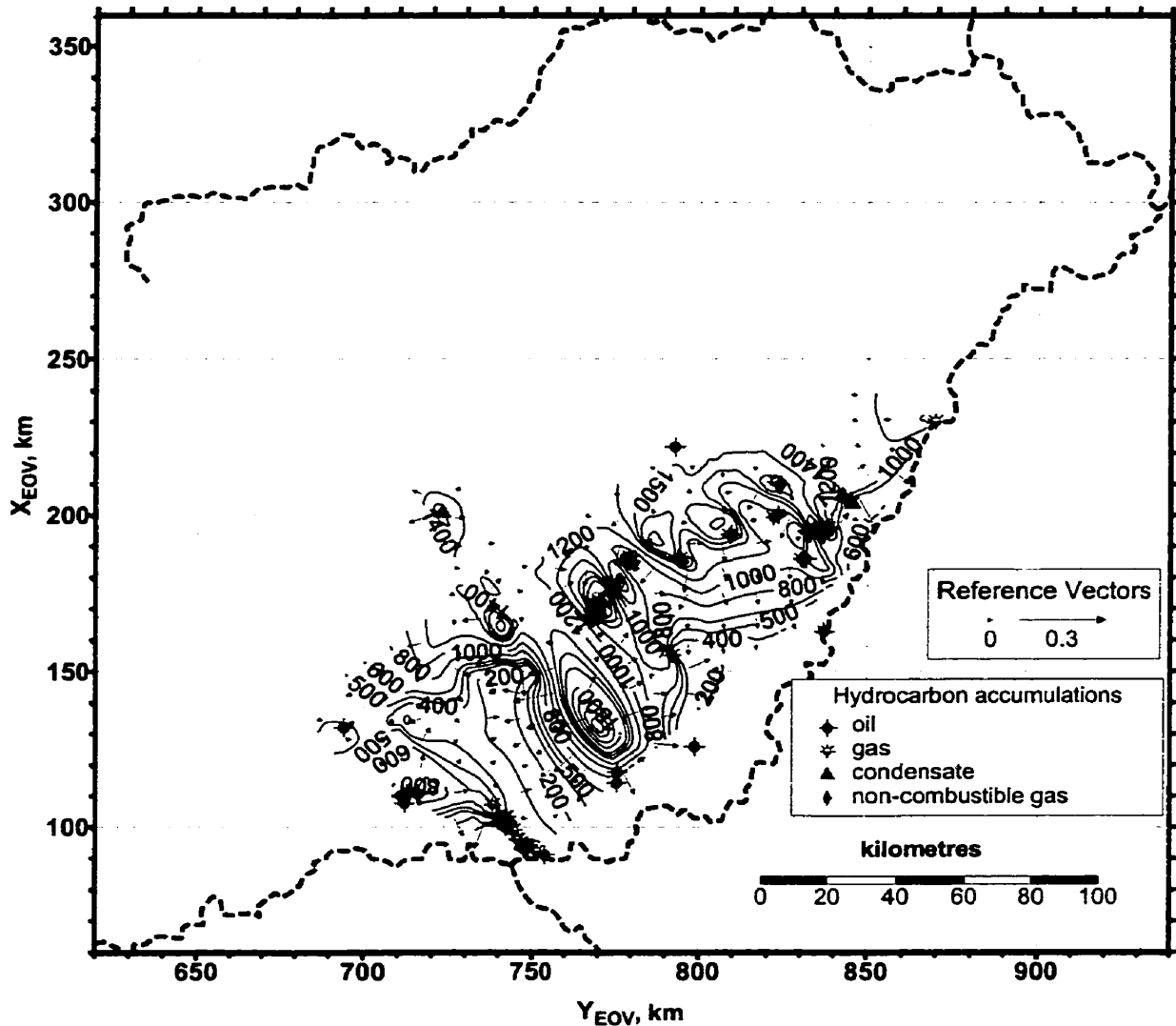
Map code: h19,22



Number of control points used: 180 out of 281
Number of HC-pools: 130

Figure 4.27: Tomographic fluid-potential map based on stabilised water level data and pore pressure (DST) data with elevation heads between $z = -1900$ m to -2200 m. Arrows (vectors) indicate the direction and magnitude of the horizontal hydraulic gradients. The hydraulic head contours are in m a.s.l., displayed irregularly as $h = 100$ m, 120 m, 150 m, and 200 m, and regularly at 100 m interval for $h = 200$ m to 1800 m. Note: commercial hydrocarbon accumulations are displayed. From the original 281 data 180 were accepted and 101 data were rejected on suspicion of production drawdown effects.

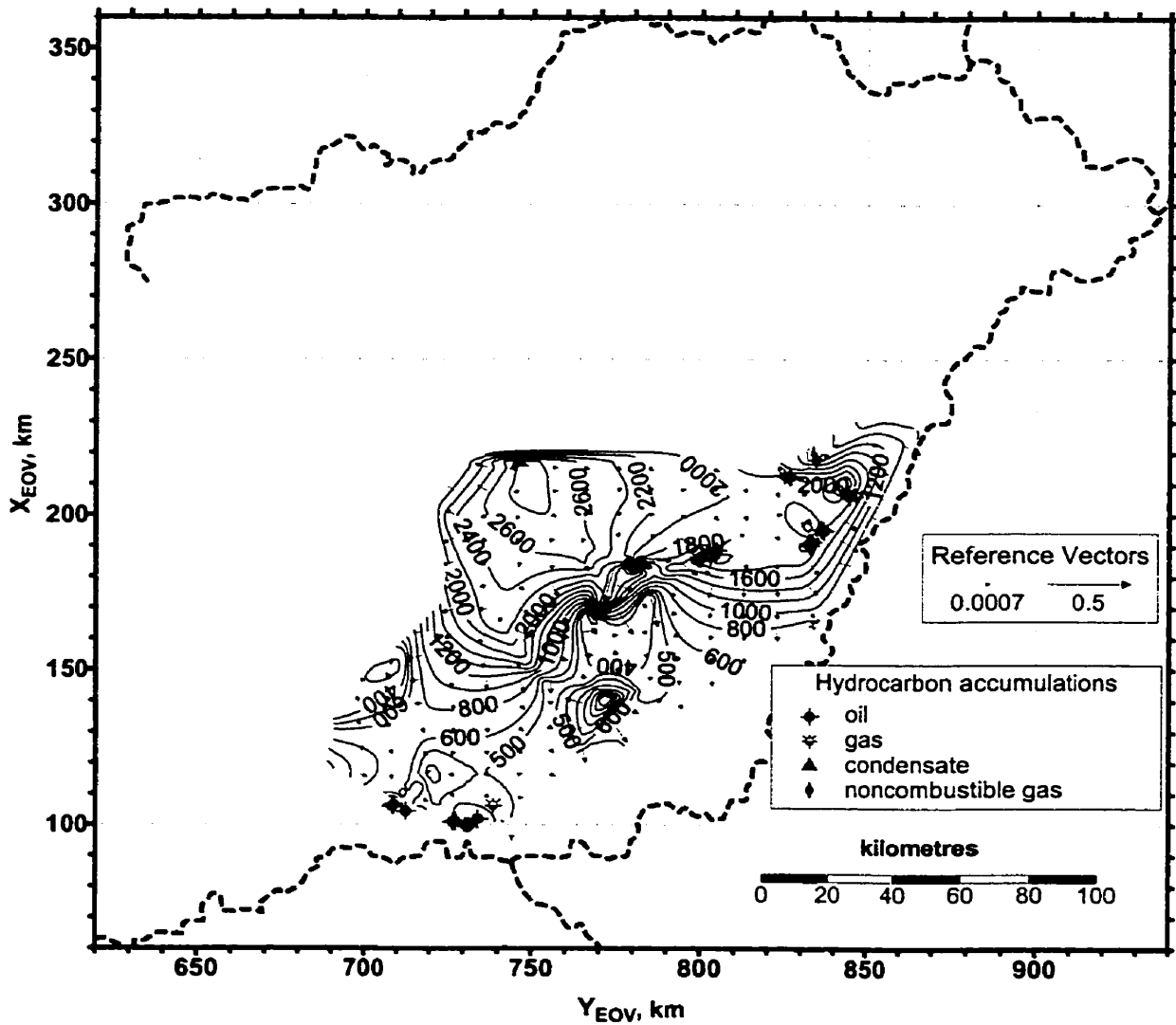
Map code: h22,25



Number of control points used: 140 out of 196
Number of HC pools: 104

Figure 4.28: Tomographic fluid-potential map based on stabilised water level data and pore pressure (DST) data with elevation heads between $z = -2200$ m to -2500 m. Arrows (vectors) indicate the direction and magnitude of the horizontal hydraulic gradients. The hydraulic head contours are in m a.s.l. displayed at a regular interval of 200 m interval for $h = 200$ m to 2600 m; the $h = 500$ m contour is also included. Note: commercial hydrocarbon accumulations are also displayed. From the original 196 data 140 were accepted as representative and 56 data were rejected because of production drawdown effects.

Map code: h25,28



Number of control points used: 96 out of 106
Number of HC-pools: 31

Figure 4.29: Tomographic fluid-potential map based on stabilised water level data and pore pressure (DST) data with elevation heads between $z = -2500$ m to -2800 m. Arrows (vectors) indicate the direction and magnitude of the horizontal hydraulic gradients. The hydraulic head contours are in m a.s.l. displayed at a regular interval of 200 m for $h = 200$ m to 3000 m; the $h = 500$ m contour is also included. Note: commercial hydrocarbon accumulations are also displayed. From the original 106 data 96 were accepted as representative and 10 data were rejected because of production drawdown effects.

Map code: h28,31

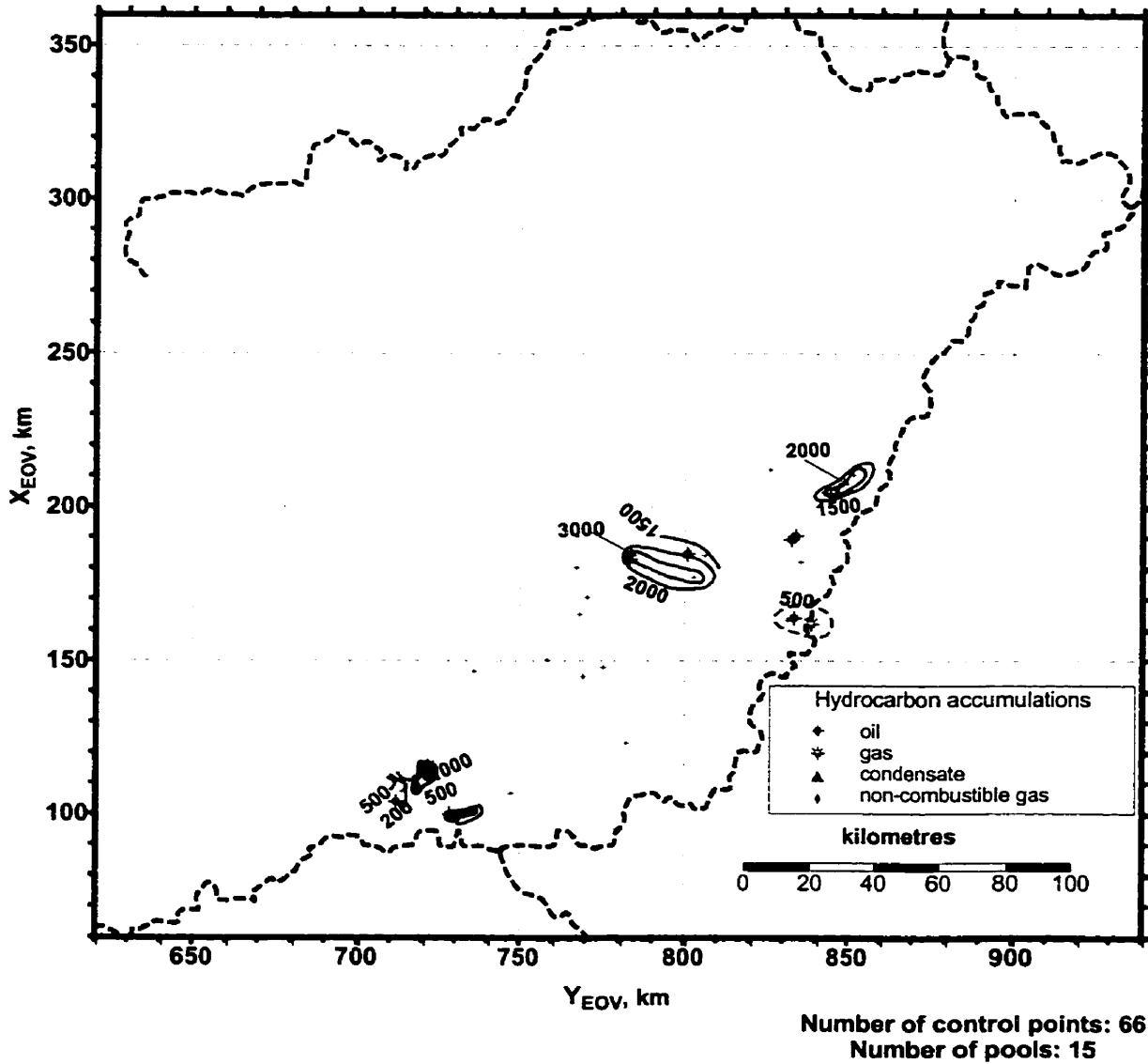


Figure 4.30: Tomographic fluid-potential map based on pore pressure (DST) data with elevation heads between $z = -2800$ m to -3100 m. The hydraulic head contours are in m a.s.l. displayed irregularly. Note: commercial hydrocarbon accumulations are also displayed.

Map code: h31,35

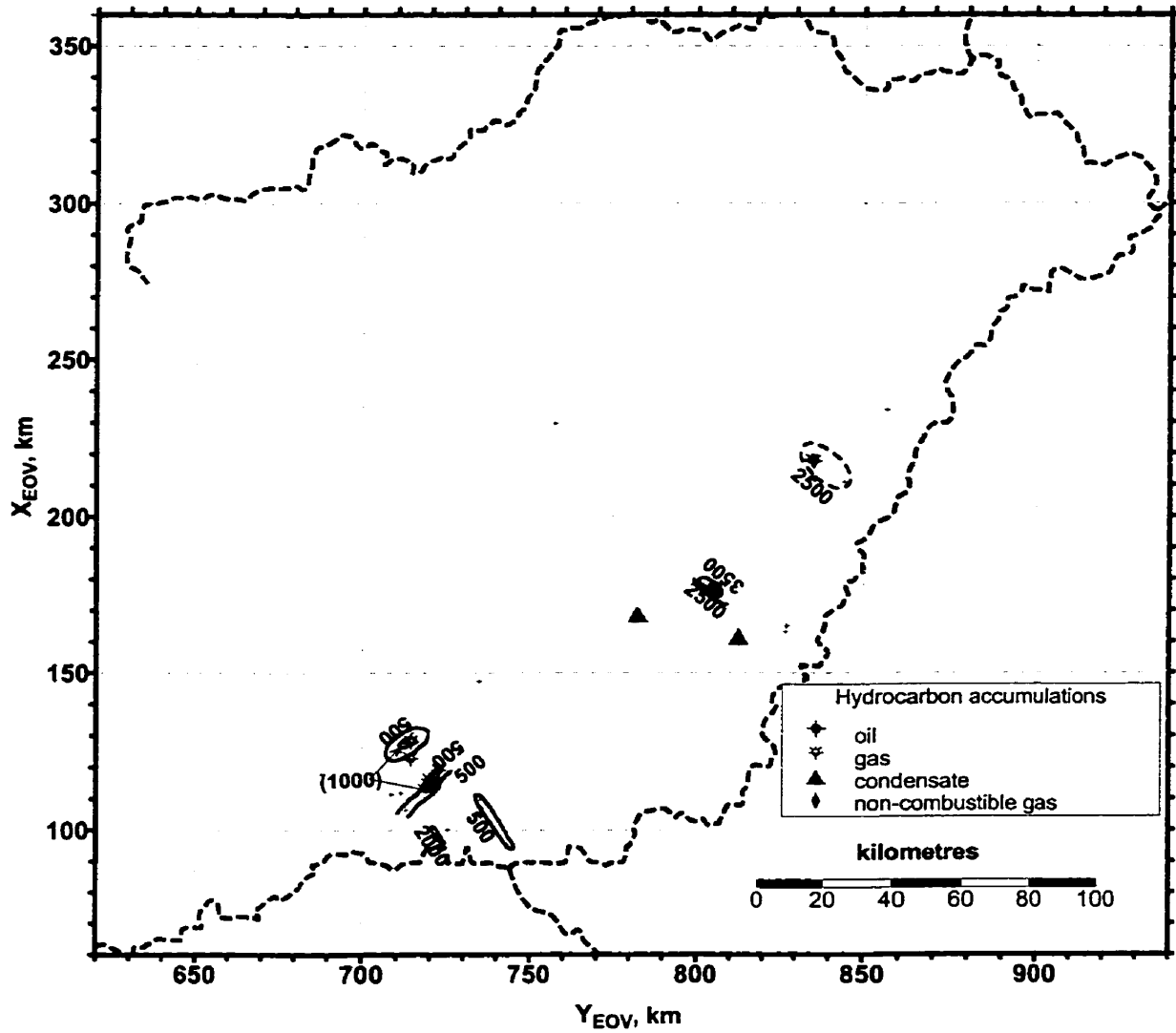


Figure 4.31: Tomographic fluid-potential map based on pore pressure (DST) data with elevation heads between $z = -3100$ m to -3500 m. The hydraulic head contours are in m a.s.l. displayed irregularly. Note: commercial hydrocarbon accumulations are also displayed.

By plotting the boundaries of the intersected hydrostratigraphic units on the tomographic maps (not shown here for the sake of legibility), it appeared that the potentiometric escarpment coincides with the Algyő Aquitard, and locally with the Szolnok Aquifer and Endrőd Aquitard. This may imply that the aquitards act as efficient lateral (not strictly horizontal) buffers for pressure dissipation. Analysis of the spatial coincidence between particular hydraulic head anomaly shapes and structural configurations (fault zones, basement morphology) was also undertaken to search for plausible explanations regarding the cause(s) and distribution of overpressures.

By overlaying the potential maps plotted at 1:500 000 scale on the geologic map of the Pre-Neogene basement (Fülöp and Dank, 1987) it appeared that the overpressures are preferentially located above or within the basement highs and in the vicinity of regional fault zones. The potentiometric escarpments are also sub-parallel to the strike of regional faults in the Pre-Neogene basement. Unfortunately, no structural geologic map of the Neogene units was available. Therefore, a systematic correlation of the hydraulic head anomalies with the precise location of neotectonic features was not possible. The steep lateral gradients may be interpreted as the result of energy loss across fault zones that restrict lateral flow, but allow vertical pressure dissipation.

The observations and inferences made from the tomographic fluid-potential maps prepared for the study area between the land surface (z_0) and $z = -3500$ m elevation are summarised as follows:

1. The fluid-potential surfaces are a subdued replica of the land surface in the $z_0 \leq z \leq -300$ m elevation interval (i.e., to a depth of about 376 - 473 m).
2. In the $-300 \leq z \leq -1000$ m elevation interval, the fluid-potential surfaces still mimic the topographic relief, yet they show a fading tendency, and local super-hydrostatic pressure anomalies occur, which are not related to the topography.
3. In the $z_0 \leq z \leq -300$ m elevation interval, hydraulic head values decrease downward underneath regions of topographic elevation higher than 110 – 120 m, while below areas of $z_0 < 100 - 110$ m hydraulic head values increase downward; beneath areas of $z_0 \approx 100 - 110$ m a.s.l. (locally $z_0 \approx 110 - 120$ m a.s.l.), hydraulic heads barely change with depth.

4. On the fluid-potential maps below $z = -600$ m elevation, potentiometric mounds, ridges, plateaus, escarpments, and depressions are observed, which indicate that
 - a) the basin contains a regionally overpressured zone,
 - b) the spatial distribution of overpressures is not uniform,
 - c) the horizontal components of the flow driving forces are directed from the basement highs toward the centres of the basement grabens filled with sediments, and
 - d) the vertical components of the flow driving forces are directed upwards.
5. Two vertically superposed fluid-pressure regimes are identified: (i.) an upper unconfined regime where fluid flow is driven by gravity and (ii.) an underlying overpressured regime. The elevation (or depth) of the transition zone or boundary between the two pressure regimes is highly variable; generally it is higher above basement highs and lower above/within basement grabens.
6. Below $z \leq -1500$ m elevation, there is a remarkable spatial coincidence between the loci of steep lateral hydraulic gradients and basement faults, as well as between structural basement highs and potentiometric mounds. This implies the possibility of structural control on the pressure distribution in the basin. The steep lateral hydraulic gradients indicate large lateral permeability contrasts related to lithological variation and/or sub-vertical fault splays in a fracture zone.

From the existence of a regionally overpressured zone (4.a) it is inferred that regionally effective mechanisms must be investigated to find the most likely cause(s) of the phenomenon. Regional horizontal tectonic compression of Recent, and perhaps Present, activity seems to be the most likely mechanism able to generate and sustain overpressures of the observed magnitude and distribution (see Chapter 7). The non-uniformity of overpressure distribution (4b) may be due to permeability heterogeneity of the rock framework. Pressure dissipation from the overpressured regime is controlled by local permeability heterogeneity due to lithological heterogeneity, stratigraphic discontinuities, unconformities, and fracture zones. Gradual pressure dissipation is possible across the less tight aquitard layers, whereas across the tight shale aquitards pressure dissipation is abrupt.

4.2.2.3 Hydraulic cross sections ($H_i(L,z)$)

Ten regional hydraulic cross sections of a total length of ~1725 km were constructed for this study and are presented here (Figures 4.33 through 4.42). Details of the cross section construction techniques and coding are discussed in Section 4.2.1.3. A number of hypotheses and conclusions were formulated in the previous two sections regarding the flow regimes, pore-pressure zones, and possible geologic control on their distribution, based on $p(z)$ profiles and horizontal hydraulic maps. The vertical hydraulic cross sections are essential to verify, modify, and clarify the picture of the hydraulic conditions in the study area.

In the previous sections it was concluded that a regionally unconfined gravity-driven flow regime in the upper ~400 to ~2000 m thick part of the basin overlies an overpressured flow regime. The two regional flow regimes do not seem to be sharply separated by a regionally effective aquitard or aquiclude, because the transition between the two flow regimes (locally marked by an abrupt or gradual change in hydraulic gradient) does not coincide systematically with any particular hydrostratigraphic boundary. In this section these conclusions are examined and refined, and the observations complemented with features that can be seen almost exclusively on vertical cross sections.

Gravity-driven flow regime:

Beneath the relative topographic highs in the cross sections **H1**, **H2**, **H3**, **H5**, **H6**, **H7**, and **H10** (Figures 4.33, 4.34, 4.35, 4.37, 4.38, 4.39, and 4.42) the hydraulic head contour values are decreasing downward. This indicates descending flow of infiltrating meteoric water in the recharge areas. The depth of penetration of infiltrating meteoric water is marked by a fluid-potential inversion. The depth of potential inversion strongly varies in function of the local topography and perhaps the local permeability heterogeneity and anisotropy. For example, in section **H1** (Figure 4.33), at $L = 12 - 26$ km segment (Illancs), the potential inversion occurs at $z = -600$ to -1000 m elevation (see $h = 100$ m equipotential). Farther east, at $L = 30 - 40$ km segment, the fluid-potential inversion occurs at ~300 m depth (see $h = 120$ m equipotential). In section **H2** (Figure 4.34), at $L = 10 - 40$ km segment (Gödöllő Hills), the potential inversion occurs at depths of 1500 - 1700 m (see $h = 150$ m equipotential). In the Duna – Tisza Interfluve area

potential inversion occurs in the depth range of 300 to 1000 m (sections **H1**, **H3**, **H5**, **H6**, **H7**, and **H10**, Figures 4.33, 4.35, 4.37, 4.38, 4.39, and 4.42). In the Nyírség region, potential inversion occurs at depths of 200 to 920 m (sections **H3** and **H10**, Figures 4.35 and 4.42). The depth of potential inversion in the foothills of the North Central Range could not be determined because of paucity of data. In the NW end of section **H4** (Figure 4.36), the equipotential lines indicate upward flow in front of the foothills of the North Central Range, SE of Eger, and this flow system is recharged most likely farther NW beyond the cross section. In these hydraulic cross sections we may notice that under the topographic highs the hydraulic head inversion occurs mostly within the Nagyalföld Aquifer. In other words, meteoric water does not seem to be driven downward across the boundary between the Nagyalföld Aquifer and the underlying Algyó Aquitard. One exception was found on the western end of section **H1** under Illancs (Figure 4.33; L = 10 - 20 km).

Groundwater flow is directed upward in the following regions: E of the Duna – Tisza Interfluve area, S-SW of the Nyírség and the North Central Range, and in the central part of the Great Hungarian Plain (the vicinity of the Tisza, Berettyó, Körös, Sebes Körös, Fehér Körös, and Maros Rivers; see Figure 4.22 for location and horizontal plan view).

Examples for shallow (i.e., depth less than 100 to 500 m) local flow systems can be observed in the following locations:

- section **H2**, Figure 4.34; L = 5 - 15 km,
- section **H3**, Figure 4.35; L = 8 - 20 km, L = 130 - 135 km, and L = 238 - 255 km,
- section **H6**, Figure 4.38, and
- section **H7**, Figure 4.39; L = 25 - 35 km and L = 80 - 85 km.

From the fluid-potential distribution, continuous gravity-driven flow can be inferred across the Quaternary/Pliocene chronostratigraphic boundary within the entire Nagyalföld Aquifer. Since the lithology and hydraulic properties of the Quaternary and the directly underlying Pleistocene sediments are generally similar if not identical (Chapter 2), the Quaternary/Pliocene chronostratigraphic boundary can not be a physical boundary between regional flow systems. Local and intermediate gravity-driven flow systems can be spatially limited to the Quaternary, but they are more likely due to

topographic control on the size of flow systems and to a lesser extent due to lithological controls (e.g., Zijl, 1999).

Based on the hydrochemical characteristics of groundwater, Varsányi et al., (1997, 1999) inferred the existence of two regional flow systems in the Great Hungarian Plain. There is a shallow flow system in the Quaternary and Pliocene-age sediments (the Zagyva, Nagyalföld, and Quaternary Formations), which is recharged in the Duna-Tisza Interfluve, and its general flow direction is from west to east (WSW to ENE). The other flow system occupies the deeper sediments of Pontian age (mainly the Törtel Formation), it extends to a depth of about 2500 m, its recharge area is not known, and its general flow direction is from east to west. The hydraulic cross sections **H1** and **H3** (Figures 4.33 and 4.35, respectively) presented here are sub-parallel to the cross section of Varsányi et al. (1999), and they do confirm the existence of the upper flow system, but there is no indication for westward flow in the lower part of the Nagyalföld Aquifer (i.e., Törtel Formation) on the portion indicated by Varsányi et al..

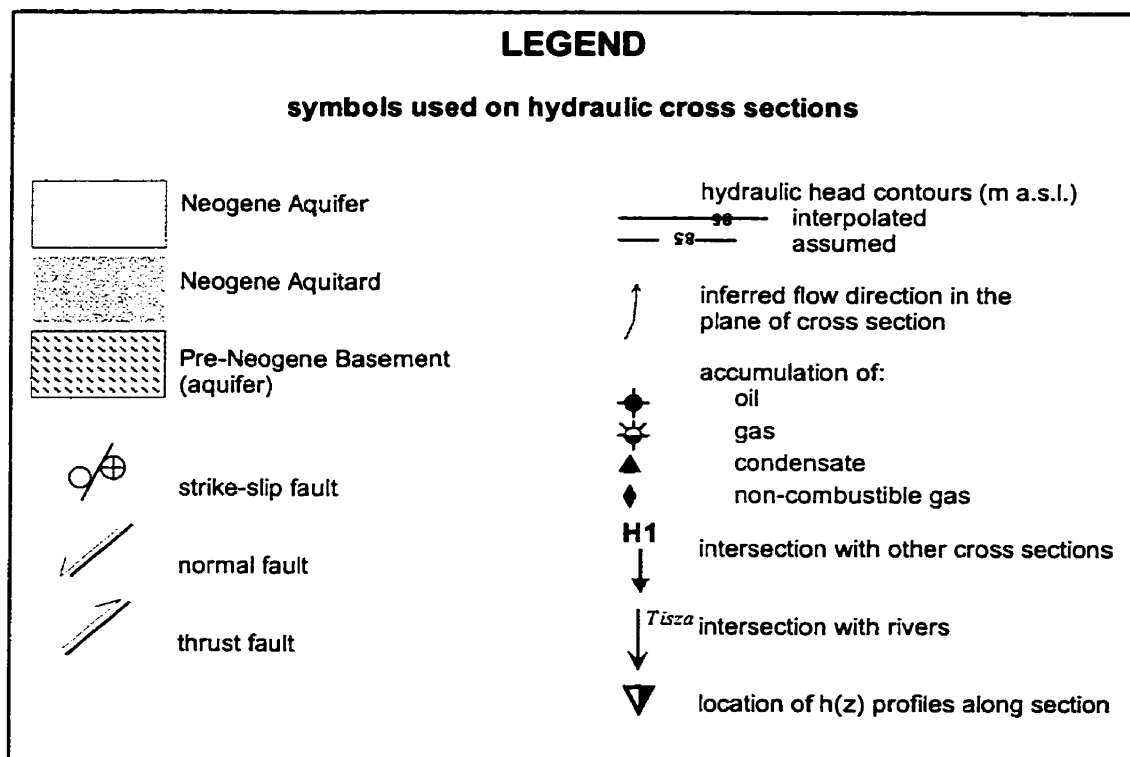


Figure 4.32: Legend of symbols used on the hydraulic cross sections.

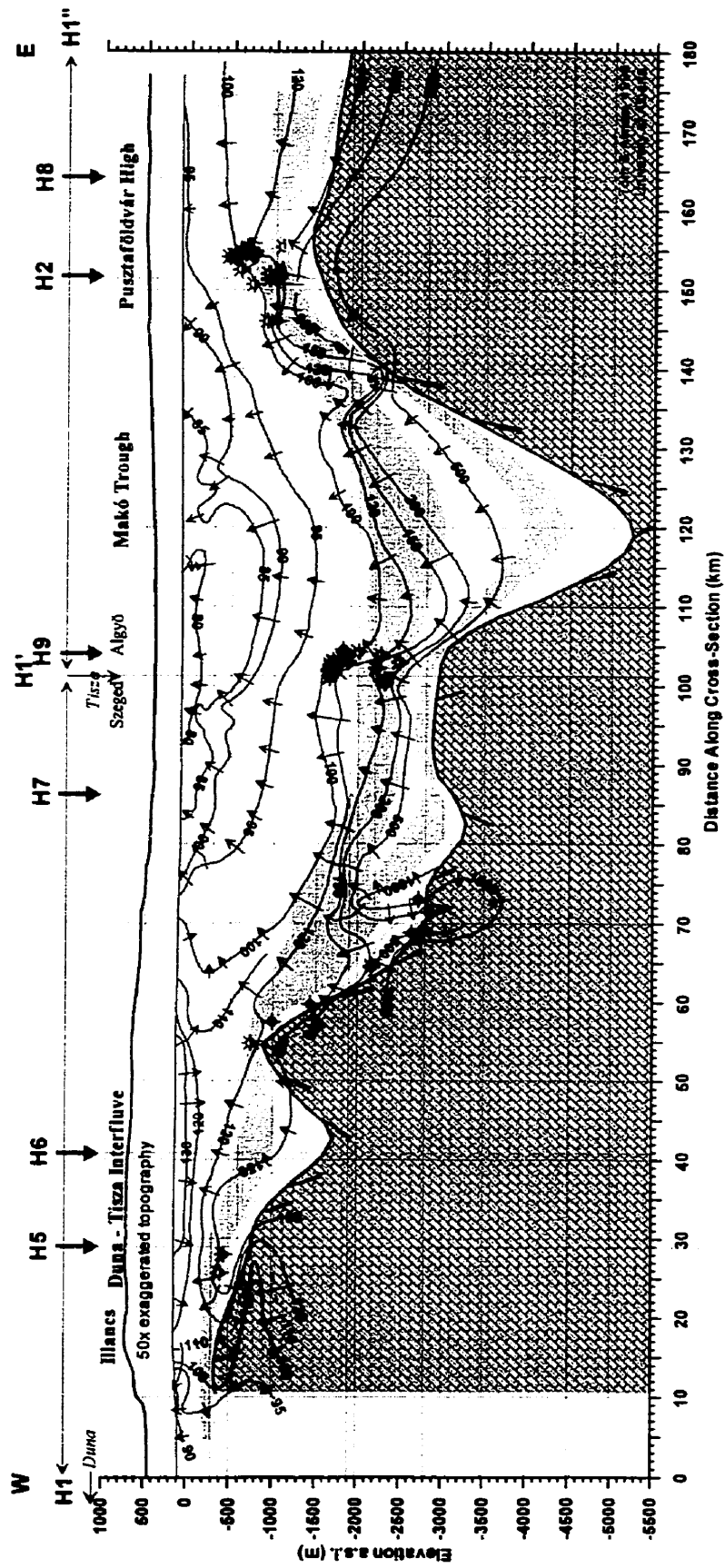


Figure 4.33: Hydraulic cross section H1 and hydrocarbon accumulations within 2 km distance from either side of the section (for location see Figure 4.4). A copy of the cross section at 1:500,000 scale is included in the pocket.

12]

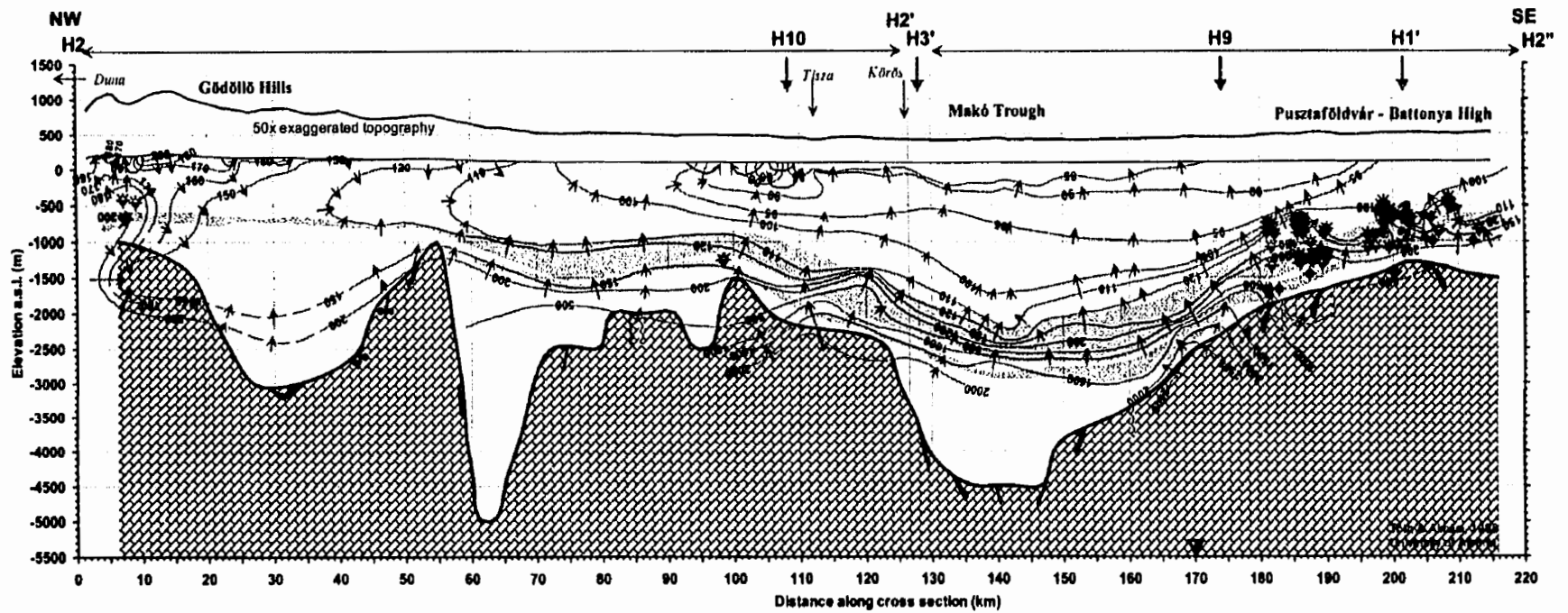


Figure 4.34: Hydraulic cross section H2 and hydrocarbon accumulations within 2 km distance from either side of the section (for location see Figure 4.4). A copy of the cross section at 1:500,000 scale is included in the pocket.

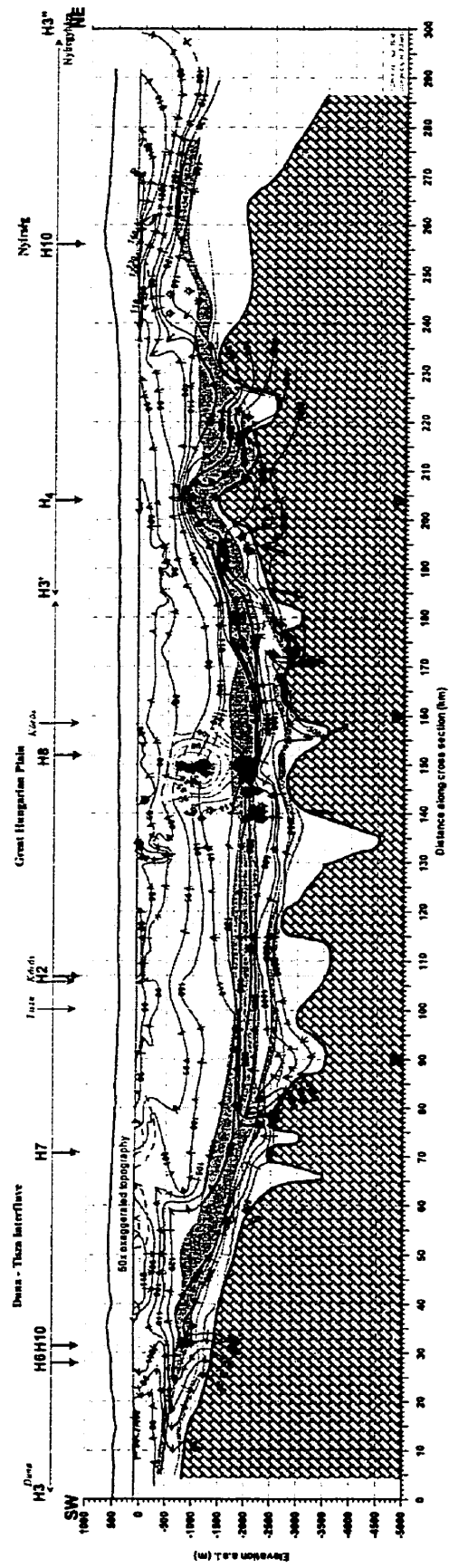


Figure 4.35: Hydraulic cross section H3 and hydrocarbon accumulations within 2 km distance from either side of the section (for location see Figure 4.4). A copy of the cross section at 1:500,000 scale is included in the pocket.

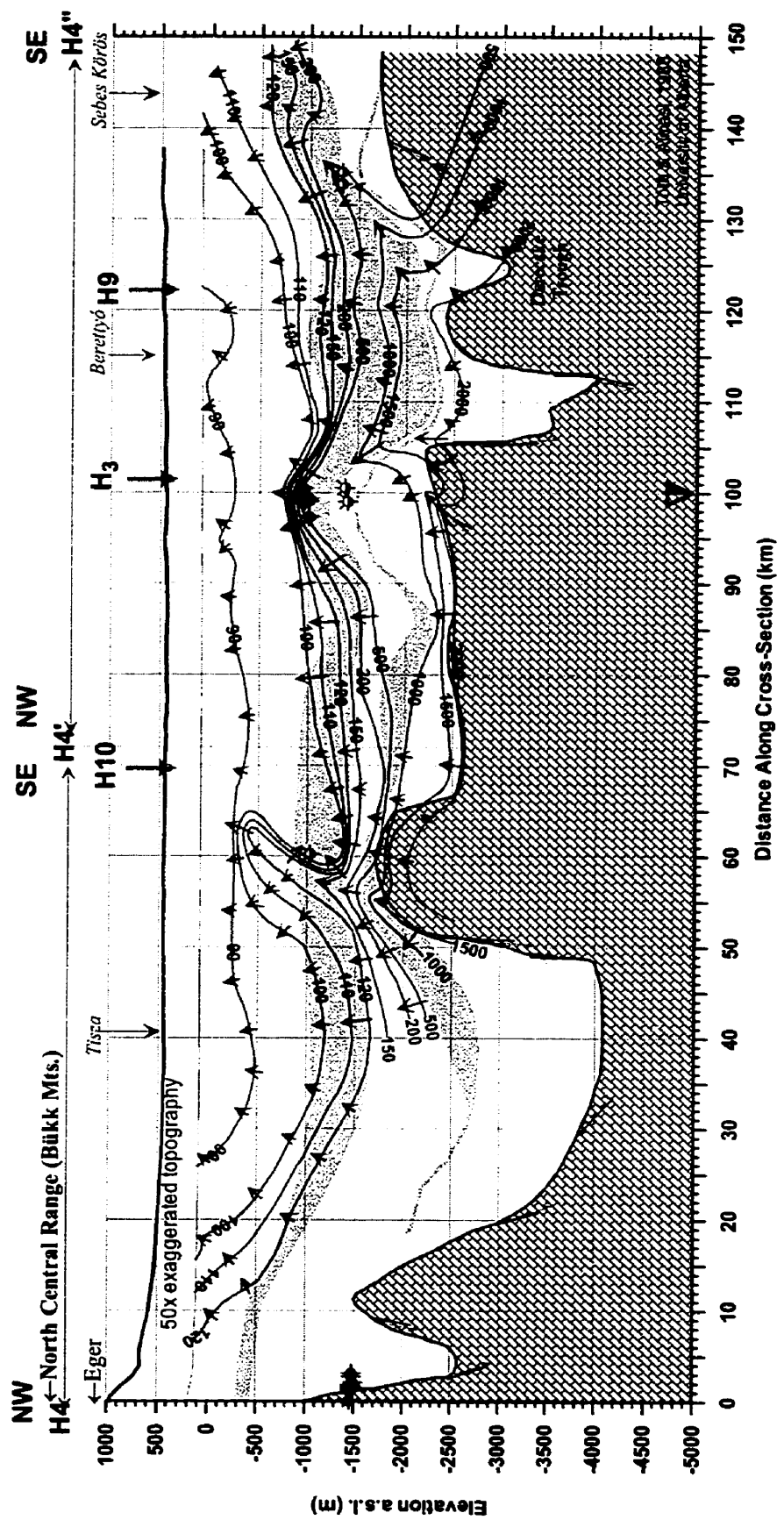


Figure 4.36: Hydraulic cross section H4 and hydrocarbon accumulations within 2 km distance from either side of the section (for location see Figure 4.4). A copy of the cross section at 1:500,000 scale is included in the pocket.

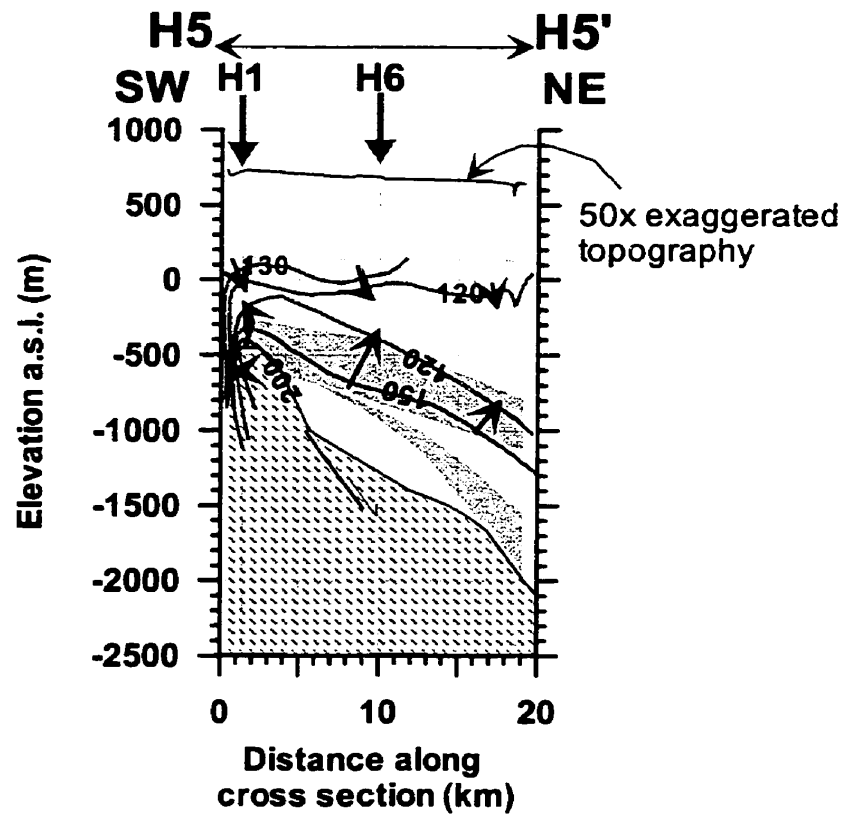


Figure 4.37: Hydraulic cross section H5 (for location see Figure 4.4).

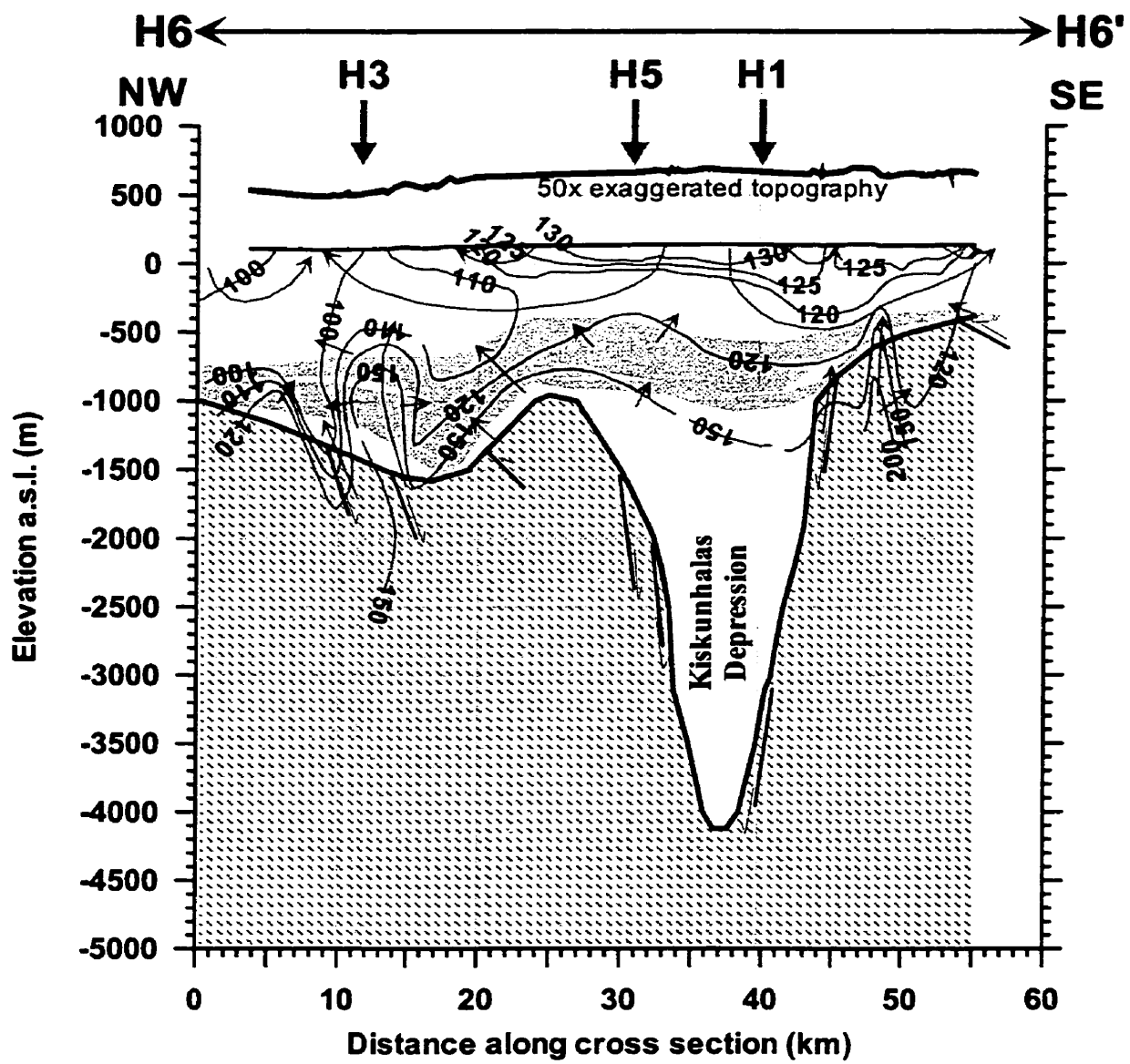


Figure 4.38: Hydraulic cross section H6 (for location see Figure 4.4).

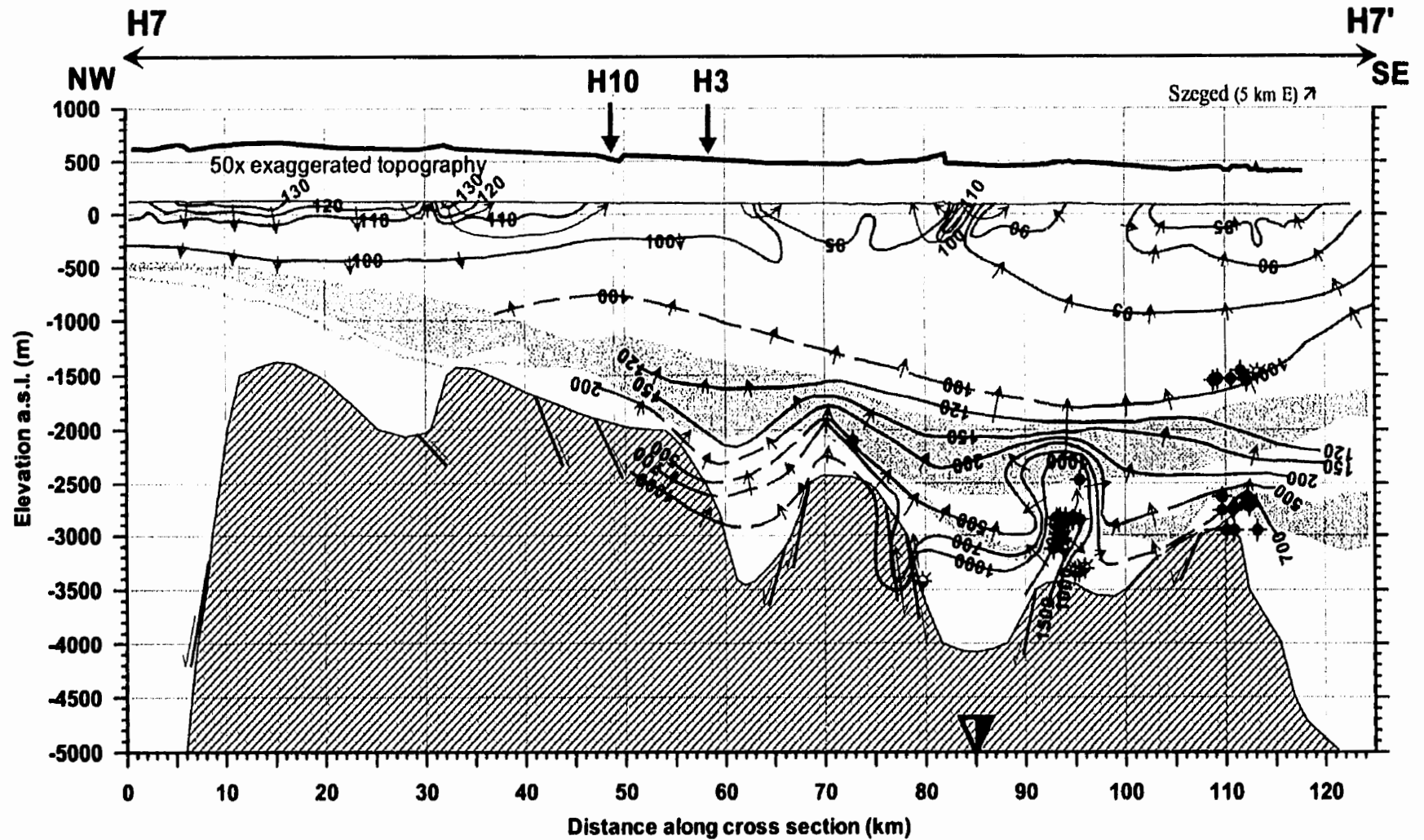


Figure 4.39: Hydraulic cross section H7 and hydrocarbon accumulations within 2 km distance from either side of the section (for location see Figure 4.4). A copy of the cross section at 1:500 000 scale is included in the pocket.

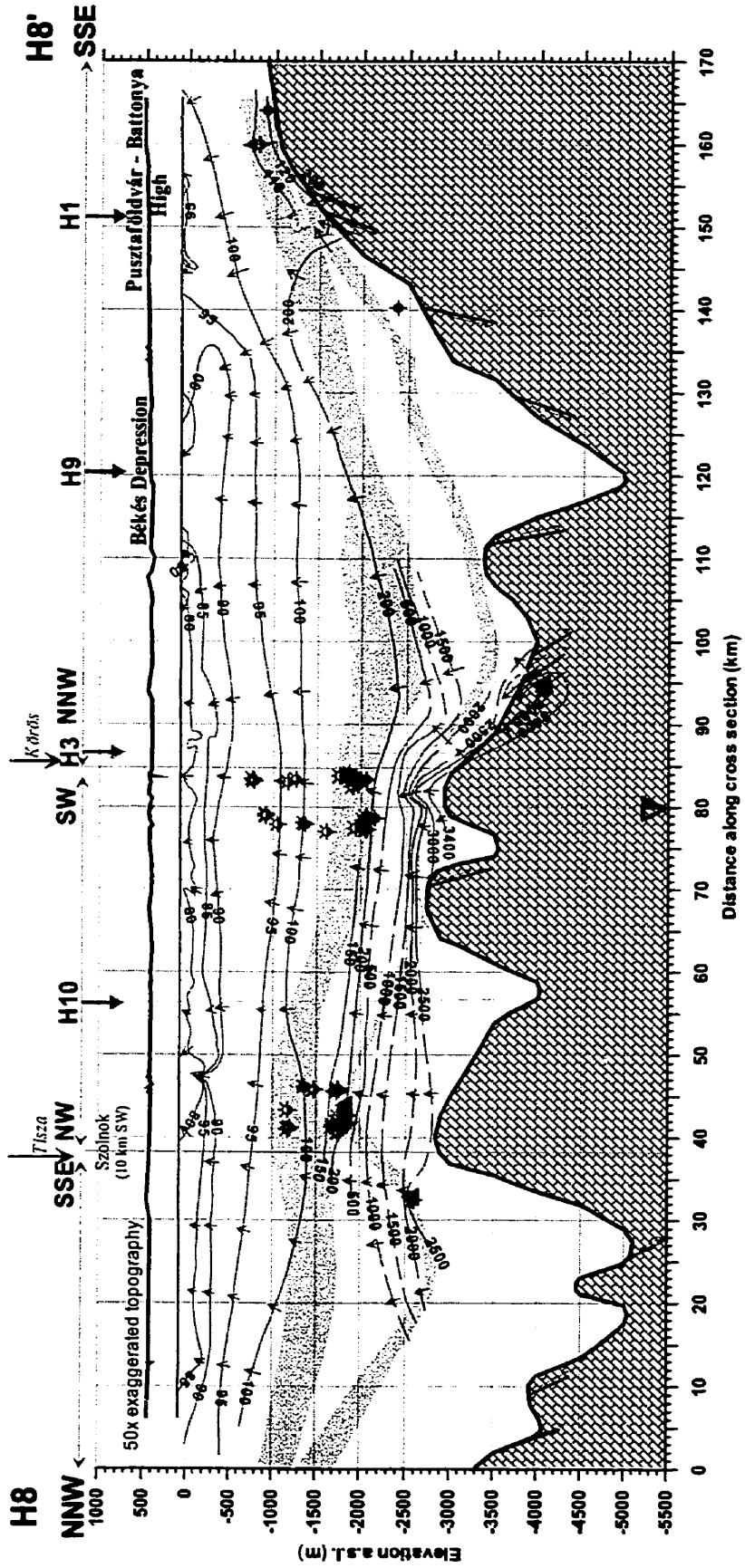


Figure 4.40: Hydraulic cross section H8 and hydrocarbon accumulations within 2 km distance from either side of the section (for location see Figure 4.4). A copy of the cross section at 1:500 000 scale is included in the pocket.

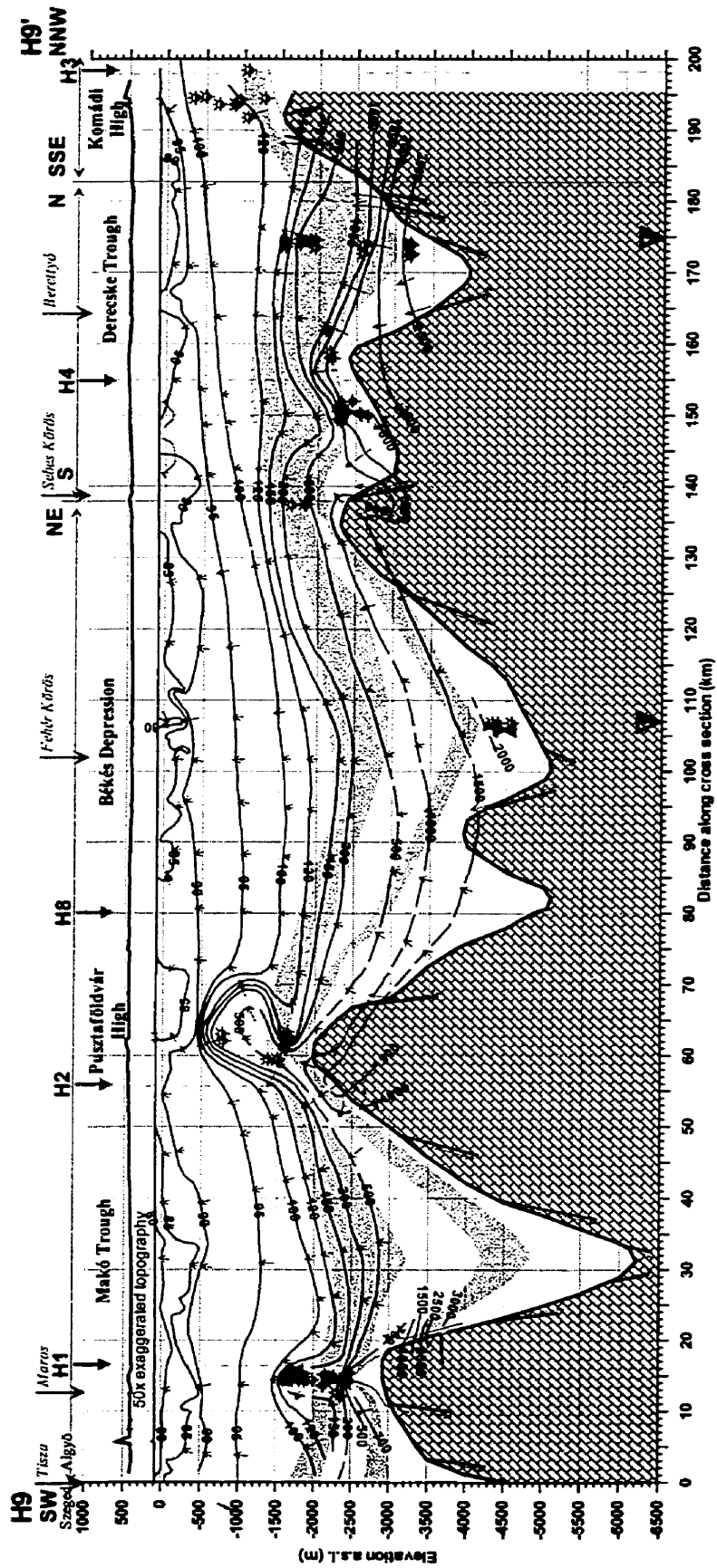


Figure 4.41: Hydraulic cross section H9 and hydrocarbon accumulations within 2 km distance from either side of the section (for location see Figure 4.4). A copy of the cross section at 1:500 000 scale is included in the pocket.

129

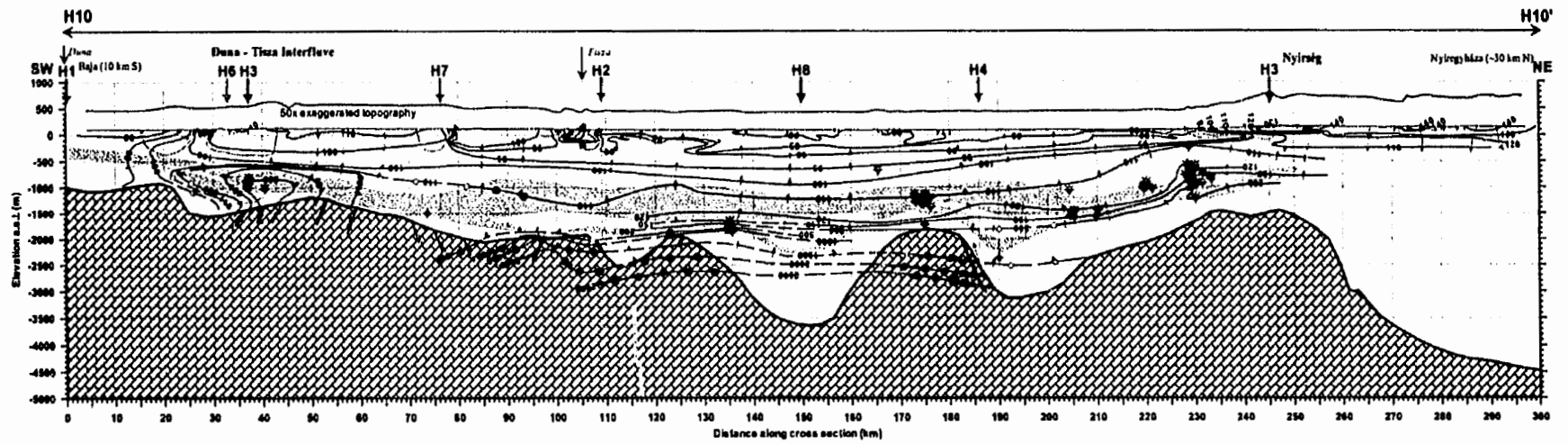


Figure 4.42: Hydraulic cross section H10 and hydrocarbon accumulations within 2 km distance from either side of the section (for location see Figure 4.4). A copy of the cross section at 1:500 000 scale is included in the pocket.

The hydraulic cross sections indicate that the gravity-driven flow regime does not have an impermeable basal boundary, instead, it has a basal 'recharge boundary.' Basal recharge occurs as a result of fluid expulsion from the overpressured regime. Assuming that every layer possesses finite permeability and elasticity, fluids escaping from the overpressured regime must be produced from storage, because this realm can not be recharged with meteoric water from the land surface. It is very difficult, if not impossible, to identify an explicit surface to mark the lower limit of the gravity-driven flow regime in the entire basin, based solely on pressure data, except for the regional recharge areas. Also, on the hydraulic cross sections it is difficult to determine the correct geometry and possible lateral extent of streamlines originating from the surface. This is due to a limitation of the mode of presentation (i.e., vertical exaggeration of the cross section and the hydraulic anisotropy of rocks is not accounted for), and interference of flow lines originating from the two different flow regimes under the lowlands. The lateral extent of regional gravity flow systems can be approximated from the sections **H1** and **H3** (Figures 4.33 and 4.35, respectively).

Section **H1** straddles the southern part of the Danube basin, the entire Duna-Tisza Interfluve area, and the southern part of the Great Hungarian Plain; its trace is parallel to the main lateral flow directions (within reasonable limits) inferred from hydraulic head maps. The recharge area is located between $L = 15$ to 63 km, with a symmetry axis at about $L = 40$ km. Two regional unit basins, each hosting a regional flow system, can be identified on this cross section. The first is across the Danube Valley, on the western end of the section; it is about ~ 40 km long, and the Danube flows southward in its thalweg. In this unit basin, the horizontal component of flow is directed mainly westward. The second one is the Tisza valley, which extends between $L = 40$ to $100 - 110$ km, that is 60 to 70 km long, with a general horizontal flow component directed eastward. The two rivers are not necessarily line sinks of the drainage basins, as none of the cross sections that intersect them offer any reason to exclude lateral flow below these rivers. The total hydraulic head change over the length of these two drainage basins is in the order of 10^{-3} to 10^{-4} m/m. Given the favourable hydraulic properties of the shallow Quaternary sediments in the upper part of the Nagyalföld Aquifer ($K = 10^{-5} - 10^{-6}$ m/s or $k = 10^{-12} - 10^{-13}$ m², and porosity $\phi > 20$ %), a horizontal seepage velocity in the order of at least $1 - 50$ cm/year can be expected. Thus, in the Duna – Tisza Interfluve region, the hydraulic

and hydrodynamic conditions necessary for the development of vertical and horizontal components of groundwater flow driven by gravity are present. This finding is opposite to that of Rónai (1978, 1985), who explained the elevated water table in the recharge area (Duna-Tisza Interfluve) as the result of high pressures from greater depth. Rónai (1978, 1985) excluded the possibility of lateral flow toward the Duna and the Tisza rivers, respectively, even within the shallow sand layers. He argued that the large variability of the groundwater's hydrochemical character is due to the lack of -or very sluggish- horizontal flow.

Section **H3** (Figure 4.35) crosses the study area from the Danube (~30 km N of Baja) to Nyíregyháza. The pattern of the gravity-flow regime observed in its **H3** - **H3'** segment is similar to that described from section **H1** (Figure 4.33). The effects of extensive water and petroleum production on the regional fluid-potential distribution were detected in the vicinity of the Körös river at $L = 140 - 160$ km and at $L = 177 - 184$ km (see Figure 4.35; dark dashed lines). The segment **H3' - H3''** offers insight into the flow regime recharged in the Nyírség region. The major water divide on this cross section is at about $L = 260$ km. A regional flow system is developed in the north-eastern end of the section, which extends beyond Nyíregyháza (the limit of the section). Another regional flow system has developed between $L \approx 150 - 260$ km, with horizontal flow directions oriented toward the south-west. In this flow system, water infiltrated in the Nyírség may be expected to reach the Körös River.

Overpressured flow regime:

Hydraulic head values in excess of $h = 150$ to 200 m (the expected maximum range based on the topographic elevations) reflect fluid-potential conditions, which can not be attributed to the elevation and relief of the water table in the Great Hungarian Plain. Underneath the purely gravity-driven regionally unconfined flow regime, there is a confined overpressured flow regime with hydraulic heads exceeding 200 m and locally even 3000 m. Generally, the $h > 200$ m equipotential lines mimic the undulating surface of the Pre-Neogene basement. Apparently, the amplitude of equipotential lines is smaller within the grabens than above the basement highs. The geometry of the high- h equipotential lines is convex upward above basement highs and convex downward within the grabens. This suggests that the energy source of overpressures lies within the Pre-

Neogene basement highs, and that the driving forces of fluid flow are directed laterally toward the deep grabens and upward into the Neogene sediments. This hydrodynamic pattern is well illustrated in the case of the Makó Trough and the Békés Depression, which are separated by the Pusztaföldvár High, on sections **H1**, **H2**, and **H9** (Figures 4.33, 4.34, and 4.41), and by other smaller sub-basins on sections **H3**, **H6**, **H7**, **H8**, and **H10** (Figures 4.35, 4.38, 4.39, 4.40, and 4.42). In the Derecske Trough, the $h \leq 1800$ m equipotential lines fit into the above described pattern, yet the $h \geq 2000$ m lines are convex upward below $z = -2800$ m elevation (section **H4**, Figure 4.36, $L = 120 - 130$ km; section **H9**, Figure 4.41, $L = 160 - 180$ km).

The above observations support the working hypotheses, i.e., the basin is regionally overpressured and the source of overpressures lies within the more rigid Pre-Neogene basement. As to the cause of overpressures, intuitively, regional lateral tectonic compression of the Pre-Neogene basement is believed to be the main mechanism (see discussion in Chapter 7).

The transition zone between the gravity-driven and compressional flow regimes:

The shape, position, and dynamic characteristics of the transition zone between the two pressure regimes are variable, and depend on the local topographic and geologic conditions. Due to the non-uniform contour intervals used on the cross sections, it is difficult to evaluate intuitively the transition patterns between the two pressure regimes. As a first approximation, the following observations and inferences can be made on the hydraulic cross sections. The transition between the unconfined normally pressured zone and the confined overpressured zone is apparently abrupt or gradual. *Abrupt transition* is inferred from the congestion of hydraulic head contours, whereas *gradual transition* is inferred from a rather even distribution of hydraulic head contours. Abrupt transition zones are preferentially associated with basement highs, while the gradual transition zones are associated with the grabens. A plausible interpretation for the abrupt transition zone is the proximity of the energy source of overpressures and the presence of local aquitards. The transition zone between the two regional flow regimes is apparently diffuse and it does not systematically coincide with a regionally extensive aquitard or aquiclude. The gravity-driven flow regime is mostly accommodated by the Nagyalföld

Aquifer. Fluid-potentials that can be due to topography ($h < 120$) also occur locally within the Algyő Aquitard, Szolnok Aquifer, and the Pre-Pannonian Aquifer. For instance:

- section **H1** (Figure 4.33), $L = 5 - 20$ km segment;
- section **H3** (Figure 4.35), $L = 10 - 30$ km;
- section **H4** (Figure 4.36), $L = 7 - 40$ km; and
- section **H10** (Figure 4.42), $L = 10 - 25$ km.

In contrast, the high-potential *plumes* mostly coincide with basement highs and faults that penetrate into the Nagyalföld Aquifer. The reverse geometry of a plume is the *sac*. Such potentiometric plumes and sacs can indicate dissipation of overpressures by cross-formational fluid flow across the Endrőd and Algyő Aquitards. For example:

- section **H1** (Figure 4.33), $L = 140 - 160$ km, and $L = 65 - 75$ km;
- section **H2** (Figure 4.34), $L = 189 - 190$ km and $L = 197 - 211$ km;
- section **H3** (Figure 4.35), $L = 194 - 213$ km;
- section **H4** (Figure 4.36), $L = 50 - 65$ km;
- section **H6** (Figure 4.38), $L = 10 - 16$ km;
- section **H9** (Figure 4.41), $L = 10 - 20$ km and $L = 55 - 72$ km; and on
- section **H10** (Figure 4.42), $L = 22 - 60$ km.

These *pressure diffusion plumes*, *sacs*, and *ridges* can be explained as the result of leaky aquitards caused by lithologic heterogeneity and/or the presence of stratigraphic unconformity and conduit faults. Hence, it is concluded that the two flow regimes are hydraulically connected and the upper gravity-driven flow regime is recharged by the overpressured regime as well.

A quantitative evaluation of transition patterns was possible by preparing hydraulic head versus elevation profiles, $h(z)$, in selected sample locations along the cross sections. At an arbitrary location along a cross section the values of interpreted hydraulic head contour lines are plotted against their elevation on these $h(z)$ profiles (Figure 4.43). The following viewpoints were considered in the selection of representative places for $h(z)$ profiles: 1) comparison of hydraulic head distribution in deep grabens with those above basement highs; 2) evaluation of locations with apparently congested and evenly distributed h -contours; 3) consideration of places with sufficient control points and/or interpolated contour lines; 4) use of assumed contour values augments the level of

uncertainty; 5) preference for locations with minimal lateral and maximal vertical hydraulic gradient (i.e., almost horizontal segments of contour lines).

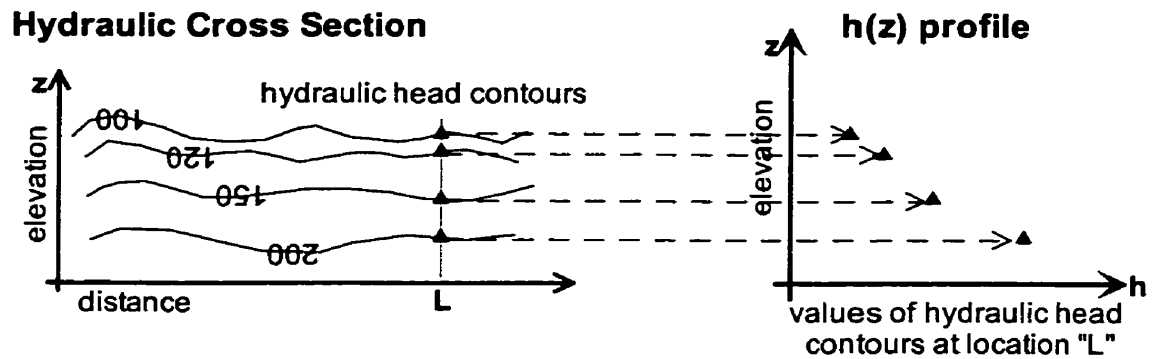


Figure 4.43: Schematic diagram of $h(z)$ profile preparation at a selected location (L) on a hydraulic cross section.

Nine sample locations were selected (Table 4.3 and Figure 4.4) to illustrate patterns of transition between the two regional flow regimes inferred from the hydraulic cross sections (Figures 4.44, 4.45, 4.46, and 4.47). The data extracted from the hydraulic cross sections are grouped according to their position relative to basement highs (horsts; Figures 4.44 and 4.45) and basement depressions (grabens; Figures 4.46 and 4.47).

Table 4.3: Selected location of $h(z)$ profiles along hydraulic cross sections and associated basement morphology. (see Figure 4.4)

Cross section	Sampling location(s) along cross section (km)	Basement morphology	Figure # of $h(z)$ profile
H2	170	Horst	4.4 and 4.5
H3	160	Horst	
H3	204	Horst	
H4	100	Horst	
H8	80	Horst	
H3	90	Graben	4.6 and 4.7
H7	85	Graben	
H9	107	Graben	
H9	175	Graben	

The following patterns can be observed on- and inferences made from the $h(z)$ profiles:

1. the vertical segment of the $h(z)$ lines (figures 4.44 and 4.46) indicates nearly hydrostatic conditions in the upper zone characterised by low average vertical hydraulic gradients (i.e., $|\Delta h/\Delta z| < 0.03$) and interpreted as a regionally unconfined gravity-driven flow regime.
2. The shallowest abrupt change in the slope of the $h(z)$ lines (pseudo-hydraulic gradient) indicates the upper boundary of the overpressured zone. From the enlarged details of the $h(z)$ profiles (Figures 4.45 and 4.47) it is evident that this boundary is below the elevation of the $h = 100$ m hydraulic head contours.
3. The transition zone is in the elevation range of the $h = 100$ to 200 m hydraulic head contours (Figures 4.45 and 4.47).
4. The vertical transition zones are wider ($400 - 800$ m) within basement depressions (i.e., *gradual transition*: $|\Delta h/\Delta z| = 0.25 - 0.06$), and narrower ($50 - 300$ m) above basement highs (i.e., *abrupt transition*: $|\Delta h/\Delta z| = 2 - 0.17$) (Figures 4.45 and 4.47).
5. The boundary/transition zone between the two flow regimes does not correlate with any particular regional hydrostratigraphic unit or elevation.
6. Repeated abrupt changes in the slope of any given $h(z)$ line may be related to boundaries of different hydrostratigraphic units, local permeability variation due to lithology and/or fractures.
7. Within the overpressured zone the slope of the pseudo-hydraulic gradient is generally steeper above basement highs ($|\Delta h/\Delta z| = 3 - 5$) than the basement depressions ($|\Delta h/\Delta z| = 1 - 2$).

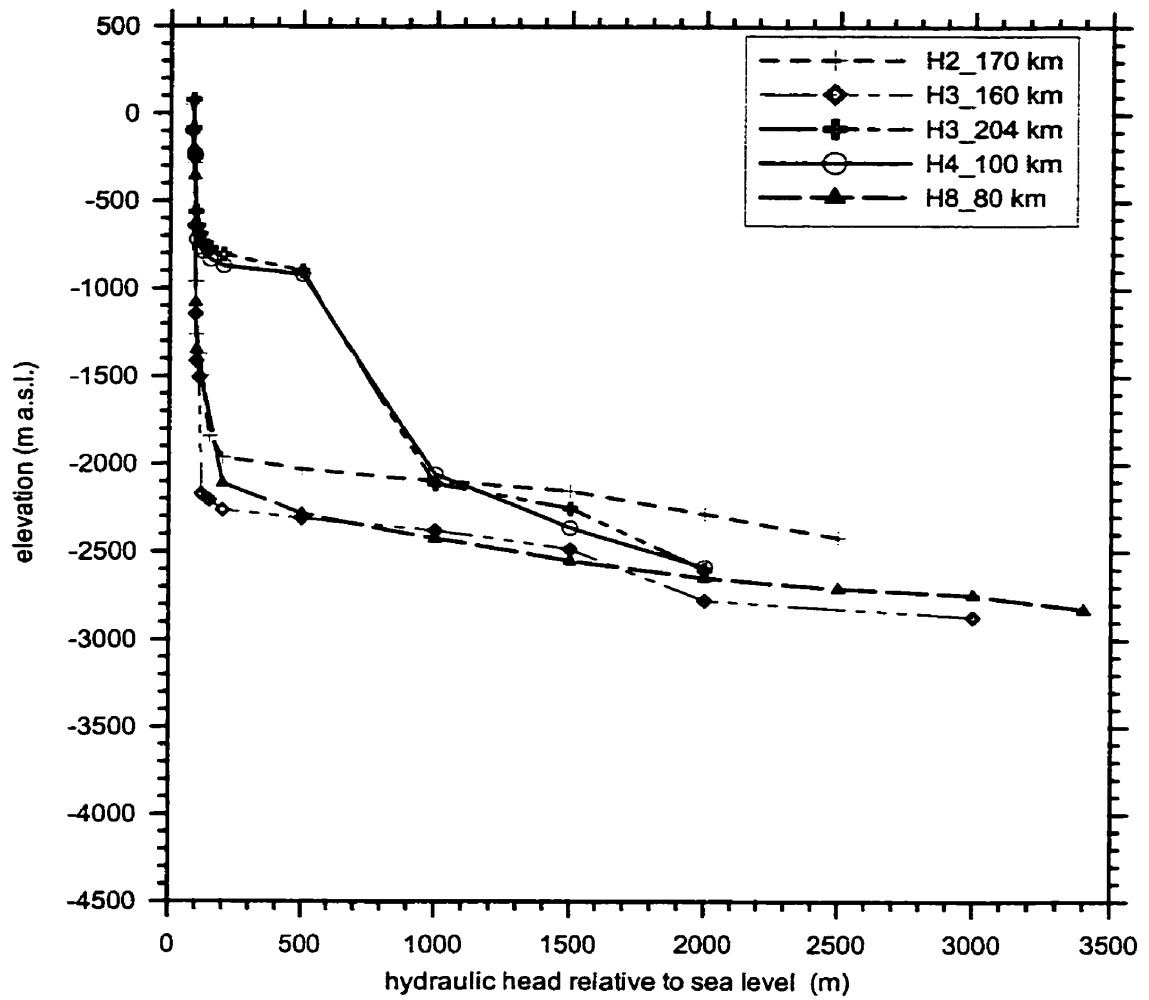


Figure 4.44: Hydraulic head vs. elevation distribution inferred from hydraulic cross sections. The selected samples are associated with basement highs (horsts). Legend: “code of cross section”_”position along cross section in km”.

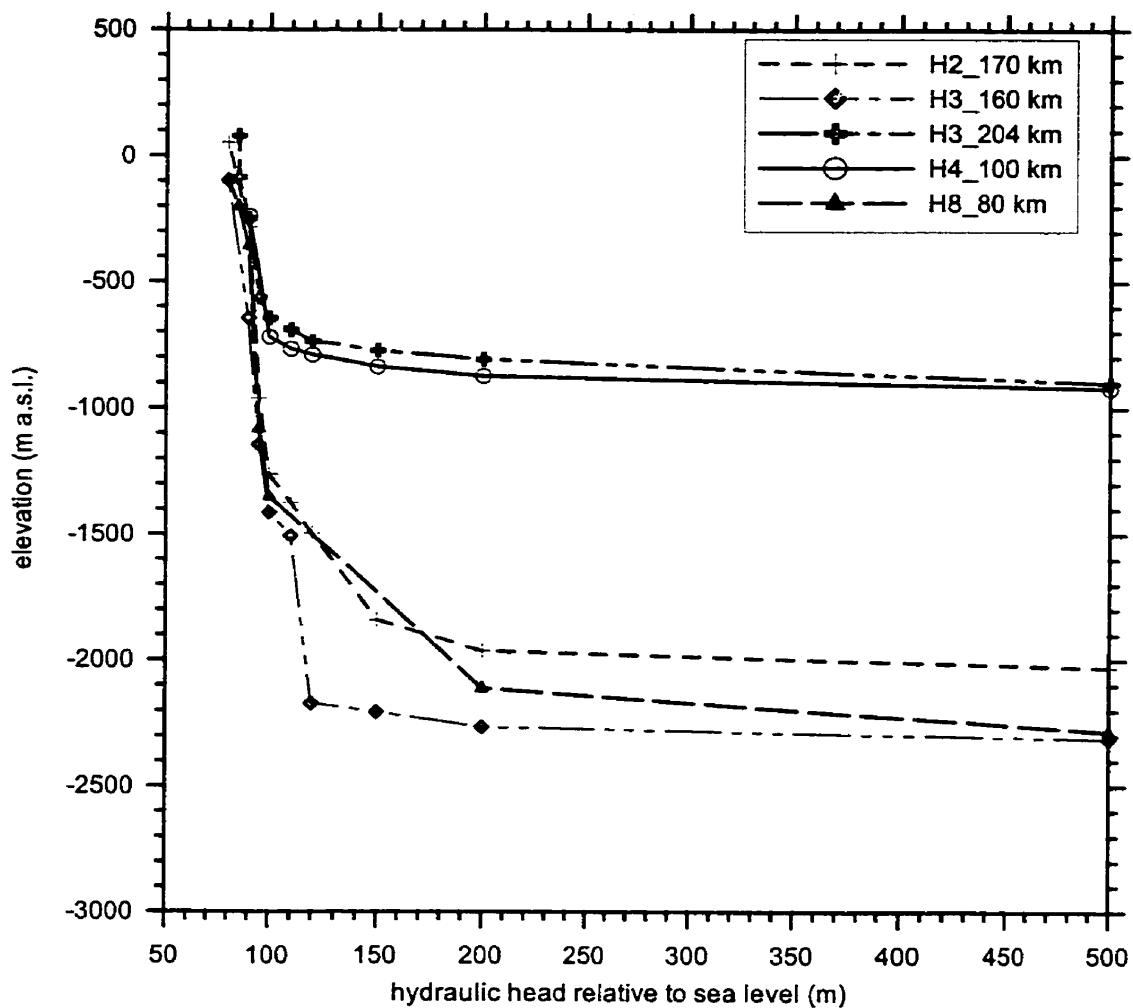


Figure 4.45: Enlarged portion of Figure 4.44: $h = 50$ to 500 m; $z = 500$ to -3000 m. Legend: “code of cross section”_”position along cross section in km”.

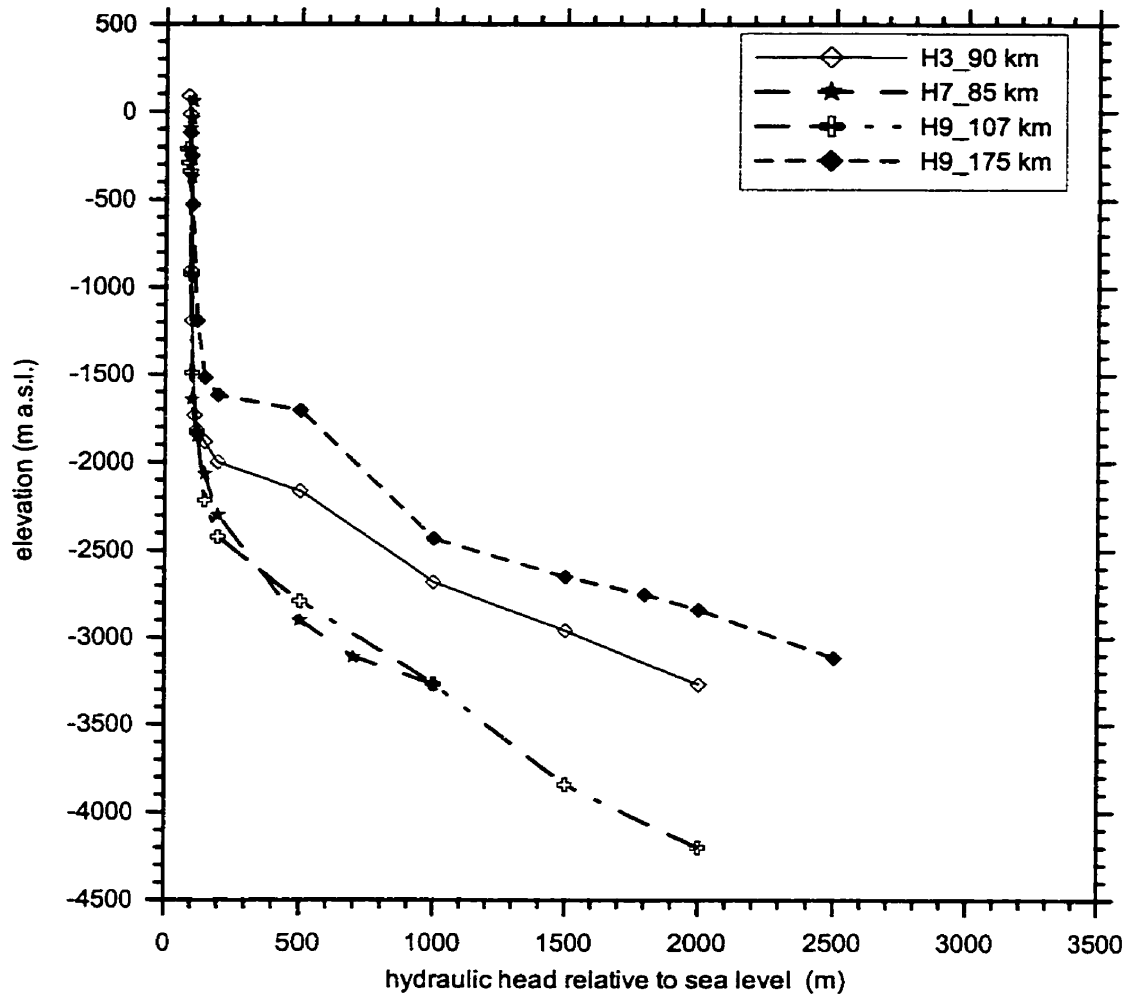


Figure 4.46: Hydraulic head vs. elevation distribution inferred from hydraulic cross sections. The selected samples are associated with basement depressions (grabens). Legend: “code of cross section”_”position along cross section in km”.

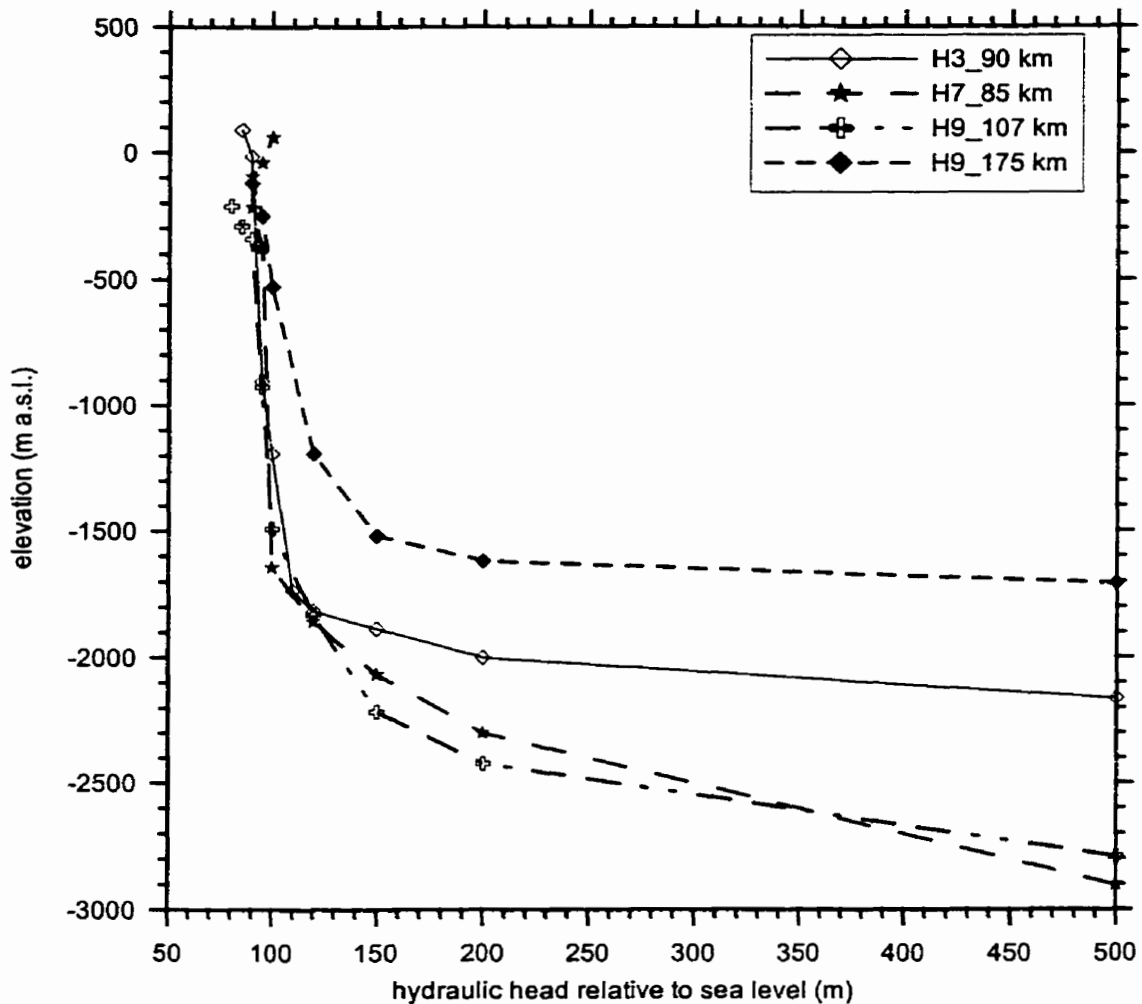


Figure 4.47: Enlarged portion of Figure 4.46: $h = 50$ to 500 m; $z = 500$ to -3000 m. Legend: “code of cross section”_”position along cross section in km”.

The observations and inferences made from the hydraulic cross sections prepared for the study area are summarised as follows:

1. Two major vertically superposed zones with distinct fluid pressure regimes are recognised in the study area: a) an upper ‘normally pressured’ unconfined zone within which flow is driven by gravity and b) a lower confined ‘overpressured’ zone.
2. Within the unconfined gravity-driven flow regime, flow is directed downward beneath topographic highs and upward beneath the low-lying plains
3. Within the confined overpressured zone flow is generally ascending.
4. Infiltrating meteoric water beneath regional recharge areas reaches depths varying between ~ 200 to ~ 1700 m and is generally not driven across the

boundary between the upper regionally unconfined Nagyalföld Aquifer and the underlying Algyő Aquitard.

5. The lower boundary of the gravity-driven flow systems in regional discharge areas can not be established from the hydraulic head data, because their fluid-potential distribution pattern blends into the upper part of the overpressured zone.
6. The vertical transition zones between the two pressure regimes are wider (400 – 800 m) within basement depressions (i.e., *gradual transition*: $|\Delta h/\Delta z| = 0.25 - 0.06$), and narrower (50 – 300 m) above basement highs (i.e., *abrupt transition*: $|\Delta h/\Delta z| = 2 - 0.17$).
7. The boundary/transition zone between the two flow regimes does not correlate with any particular regional hydrostratigraphic unit or elevation.
8. The hydraulic head contours at depth mimic the morphology of the Pre-Neogene basement.
9. The lateral components of the fluid-driving forces at depth are oriented from the basement highs toward the grabens.

4.2.2.4 Hydraulic role of faults:

The hydraulic role of faults depends on several factors, such as: the permeability of the fault gouge; the relative position and geometry of aquifers and aquitards in the foot wall and hanging wall, respectively; the relative orientation of the fault planes and driving forces of fluid flow; the shear strength of faulted rock units; the length of fracture zones, as well as the spatial and temporal variation of all the known and unknown factors within the fault zone. Thus, it is impossible to generalise the hydraulic role of faults as conduits or barriers for fluid flow. Pressure solution or precipitation of diagenetic minerals from the circulating groundwater may locally or totally 'seal' a fracture (Bjørlykke, 1994). Faults can act as lateral flow barriers, or as vertical (i.e., up-dip or down-dip) conduits, and channel flow up-dip in the fault zone, as observed also in the Rhine Graben by Otto (1992). The conductivity of a large fault zone may vary by several orders of magnitude in every direction at different parts of the fault zone. It is possible, though, to infer qualitatively from potentiometric maps and cross sections whether a fault zone acts as conduit or barrier to fluid flow from the geometry of fluid-potential

anomalies and the inferred flow directions. Steep horizontal potential gradients may indicate lateral restriction by a fault/fracture zone. Pogácsás et al. (1994) showed that several petroleum accumulations in the Great Hungarian Plain are related to faults (e.g., Dévaványa, Földes, Algyő; see location in Figure 4.2). Thus, migration into the reservoirs must have been facilitated by up-dip conduit faults.

The location of major faults in the Pre-Neogene basement was extrapolated onto the cross sections from the 1:500 000 scale geologic map of Fülöp and Dank (1987) with an error of about ± 1 km. The dip-direction of the faults was estimated based on the structure contour lines of the basement topography. The hydraulic cross sections **H5** through **H10** (Figures 4.37 through 4.42) are running parallel (within 5 km horizontal distance) to some of the seismic profiles shot by MOL, Plc. and interpreted by Tari (1994). The position in EOVS co-ordinates of these seismic profiles was identified from the seismic network map of MOL, Plc. and compared to the position of the above mentioned hydraulic cross sections. Tari's (1994) interpretations were focussing mainly on basement structures. Therefore, he identified only a few faults in the Neogene unit, which were difficult to project with reasonable accuracy onto the hydraulic cross sections. The depth range of faults in the Neogene unit inferred from the seismic profiles was estimated by assuming that in the Neogene clastic sediments 1 s two-way travel time (TWT) corresponds to ~ 1000 m depth, i.e., the velocity of acoustic waves is ~ 2000 m/s (F. Horváth, 1994, *personal communication*). For instance, a fault inferred to exist at 0.5 to 1.5 s TWT in the Neogene unit is estimated to be at a depth range of ~ 500 to 1500 m. The propagation velocity of acoustic waves in the rigid basement is higher than in the clastic sediments, and it changes non-linearly with depth. Thus, in the absence of original seismic profiles and concrete velocity functions, it was impossible to convert the basement structures interpreted and published by others from length-time sections onto length-length sections. In the case of Tari's interpretations (Tari, 1994) it was possible, however, to determine the horizontal distance along the cross sections to faults, which intersected the basement top; the depth to the basement top at such faults was estimated using the mentioned acoustic velocity value. Only a qualitative appraisal of the hydraulic role of some major faults was possible.

The *equipotential plumes*, *sacs*, and *ridges* associated with faults of known location suggest a tendency for fluid flow channelling, as illustrated on most hydraulic

cross sections presented here. Similar pressure anomaly types and the associated flow patterns were produced also by numerical modelling of fracture flow in sand/shale sequences (Matthäi and Roberts, 1996) (Figure 4.48). The effects of a lenticular body of high permeability on the fluid-potential field studied by Tóth and Rakhit (1988) produce similar anomalies as the potentiometric plumes and sacs.

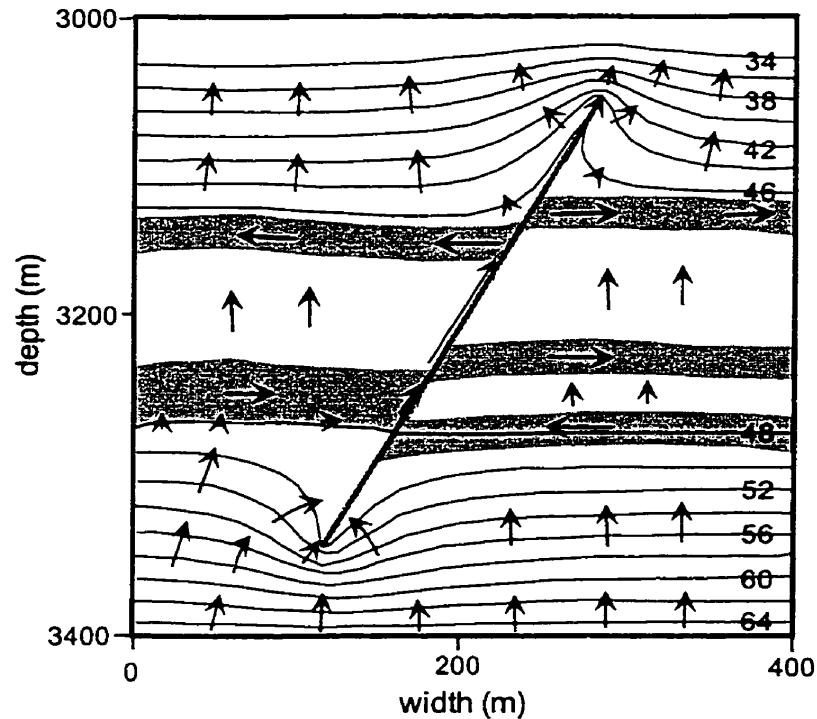


Figure 4.48: Pore pressure (MPa) and fluid flow (arrows) distribution pattern in a sand (white)/clay (grey) sequence containing a conduit fault (after Matthäi and Roberts, 1996).

The steep hydraulic gradients quasi-perpendicular to the basement faults indicate lateral flow barriers due to the permeability difference between the offset layers and the fault walls. These potential anomalies appear as *escarpments* or *isolated mounds* and *ridges* in horizontal plan view. The geometry and size (depth range and horizontal extent) of *equipotential plumes*, *sacs*, and *ridges* associated with basement faults extend across formation boundaries. This suggests that most basement faults are connected to faults in the Neogene formations, which permit dissipation of overpressures and enhance cross-formational flow. Unless the existence of faults in the loci of potential anomalies is ascertained, however, the interpretation remains arguable. An alternative explanation could be lithological/sedimentological control on the hydraulic head distribution pattern.

5 RELATIONS BETWEEN BASIN SCALE FLUID DYNAMICS AND PETROLEUM OCCURRENCES*

5.1 SPATIAL CORRELATION BETWEEN FLUID-POTENTIAL ANOMALIES AND PETROLEUM ACCUMULATIONS

Subsurface fluids migrate along the paths of least hydraulic resistance, and usually they are driven by hydraulic gradients from locations of high fluid potential toward locations of lower fluid potential. In the absence of hydraulic gradients generated by total mechanical energy differences (e.g., gravity potential, compaction, etc.), fluid motion is primarily due to buoyancy forces. If groundwater were motionless, only buoyancy forces would drive migration of hydrocarbons of characteristically lower density than water. As a result, oil and gas accumulations should be found above and at relatively short lateral distances from their source rocks. However, this is not the case in most sedimentary basins. Oil and gas can migrate and accumulate at several tens to hundreds of kilometres laterally from its source rock, as several studies demonstrated it (examples in England and Fleet, 1991). Such long-range migration may not be plausibly explained by invoking only buoyancy forces; a dynamic transport agent must be called upon. Moving groundwater is able to mobilise and transport hydrocarbons and their protoforms towards regions of lower fluid potential. Assuming that the migration paths of groundwater and hydrocarbons are similar, and that groundwater flow plays a principal role in hydrocarbon migration, a cause-and-effect relationship can be established between the fluid-potential field and the spatial distribution of known hydrocarbon accumulations (Hubbert, 1953; Tóth, 1980).

Fluid-potential field anomaly in a drainage basin is understood here as the deviation of the actually existing potential field from an ideal reference potential field. The reference potential field is that established in a 'unit basin' (Figure 4.1a) or 'complex basin' (Figure 4.1b), identical in size to the investigated one. The reference basin is assumed to have lateral and basal no-flow boundaries, a homogeneous and isotropic rock

* Chapter 5 is based on the report of Tóth and Almási, 1998.

framework, and the sole driving force is the relief of the water table, i.e., gravity (Tóth, 1962, 1963). The geometry and magnitude of the fluid-potential anomalies vary according to the changes in boundary conditions and the distribution patterns of permeability in the real basin, relative to the reference basin (e.g., Freeze and Witherspoon, 1967; Tóth and Rakhit, 1988; Bredehoeft et al., 1992; Matthäi and Roberts, 1996). In turn, from the fluid-potential field anomalies it is possible to deduce the presence and combined effects of such changes in the real flow domain relative to the reference domain (e.g., Tóth and Rakhit, 1988). Thus, local potentiometric anomalies may indicate specific local permeability configurations related to lithologic heterogeneities (e.g., high- or low-permeability sedimentary lenses, low-permeability seals) and conduit- or barrier faults. Recognition of such heterogeneities in the rock framework can have economic or practical significance, for example in petroleum migration and entrapment (e.g., Hubbert, 1953; Tóth, 1980; Wells, 1987; Tóth and Rakhit, 1988), heat-flow distribution (e.g., Čermák and Rybach, 1979; Stegena, 1982; Ben Dhia, 1987; Deming, 1994b), surface geochemical exploration for hydrocarbons (e.g., Holysh and Tóth, 1996; Tóth, 1996), formation of ore deposits (e.g., Galloway and Hobday, 1996), etc.

Due to the differences in the physical properties of water and hydrocarbons, the latter may be trapped along migration paths under favourable stratigraphic, structural and hydraulic/hydrodynamic conditions (Hubbert, 1953; Dahlberg, 1995). As a result of their potential economic significance, certain types of fluid-potential anomalies may be diagnostic for preferential migration paths and trapping conditions, hence the term “Diagnostics Potential Anomaly” or “DiPotAn” (Tóth and Almási, 1998). The hydraulic theory of petroleum migration postulates that locations of fluid-potential minima and zones of convergent or divergent flow (discharge areas, stagnation zones) are the hydraulically favourable sites for petroleum accumulation (Tóth, 1978). However, this theory does not exclude entrapment anywhere along the flow paths of gravity flow systems in a basin with complex structure and lithology. In a basin where transient fluid flow conditions dominate the realm of petroleum generation-migration-accumulation, hydrocarbon pools may form in overpressured or underpressured reservoirs (examples in Dahlberg, 1995). Spatial correlation of fluid-potential anomaly patterns with known petroleum accumulations by ways of pressure vs. depth, pressure vs. elevation profiles,

fluid-potential mapping, and hydraulic cross sections can reveal patterns of diagnostic anomalies. The diagnostic potential anomalies provide an empirical/probabilistic tool for predicting prospective sites of petroleum accumulations. Assuming that hydrocarbons share the preferential migration paths with water, the identifiable and identified anomaly patterns can be used individually or in conjunction with one another to delineate prospective accumulation sites. The two-dimensional geometric expression of diagnostic fluid-potential anomalies depends on the permeability heterogeneity of the medium which is determined by geologic factors (e.g., facies boundaries, lenticular structures, fracture zones), spatial distribution of available data, and on the orientation of the plane of representation (map or cross section). As long as the permeability distribution and stratigraphy/structure of an area are not known in sufficient detail, the interpretation of DiPotAn's in a geological context remains speculative, yet they may reveal hydraulic characteristics of rock bodies, which were not documented previously with classical geological methods.

5.1.1 Diagnostic $p(z)$ anomalies

Three patterns of pressure vs. elevation distribution were found diagnostic for petroleum accumulation:

- a) *super-hydrostatic gradient* (upward flow);
- b) *super-hydrostatic gradient with abrupt increase at certain depth* (upward flow and either presence of a flow-barrier or proximity of high energy source, or both);
- c) *sub-hydrostatic gradient changes to super-hydrostatic gradient at certain depth* (hydraulically enhanced trap by vertical convergent flow) (Figure 5.1).

In the Great Hungarian Plain, most of the known petroleum accumulations are found in regions of ascending flow, characterised by super-hydrostatic gradients (Figure 5.1/A), as postulated by Tóth's (1980) hydraulic theory of petroleum migration. Similar basin hydraulic configurations are known from other sedimentary basins, e.g., Rhine Graben (Otto, 1992), and considered favourable for hydrocarbon accumulation (Tóth, 1980; Wells, 1987). $p(z)$ distribution patterns and the elevation ranges of known

petroleum accumulations in the corresponding areas (Figure 4.2) are illustrated on Figures 5.2 through 5.7.

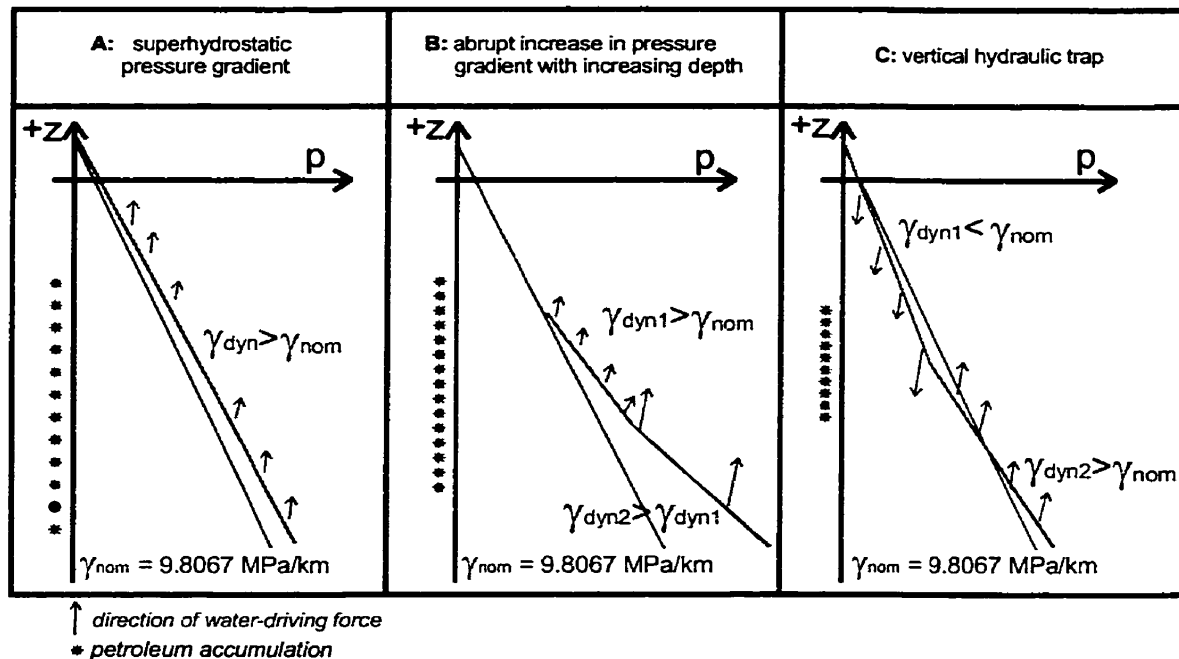


Figure 5.1: Pressure vs. elevation diagnostic anomalies (after Tóth and Almási, 1998)

Essentially, each investigated petroleum field from the regional discharge area presents an example for the first anomaly type, i.e., super-hydrostatic pressure gradient (Figure 5.1/A). The second anomaly type, i.e., abrupt increase in pressure gradient with depth (Figure 5.1/B), is exemplified by the profiles constructed for the Biharkeresztes, Dévaványa, Endrőd, and Ruzsa-Üllés regions (Figures 5.3, 5.4, 5.5, and 5.6). A plausible interpretation of the abrupt increase in pressure gradient could be the presence of an effective “pressure seal” in the form of a very low permeability aquitard. The petroleum accumulations located above the “pressure seal” are still in a super-hydrostatic regime. This may be the result of cross-formational flow across the “seal.” Another possible explanation would be that the “pressure seal” has a limited lateral extent, therefore, the hydrocarbons might have migrated toward shallower traps around the seal. This latter scenario can not be excluded, because the data plotted on the pressure profiles are lumped from areas of 100 – 400 km², which may exceed the extent of the hypothetical pressure seal.

The third anomaly type, i.e., vertical hydraulic trap (Figure 5.1/C), is exemplified by the profile of Kiskunhalas region from the southern part of the Duna – Tisza Interfluve recharge area (Figure 5.7). A sub-hydrostatic regime, which induces downward flow, is indicated by the $\gamma = 9.5099$ MPa/km gradient to a depth of $d \approx 1500$ m. Also, a super-hydrostatic regime, which induces upward flow, is indicated by the $\gamma = 11.7425$ MPa/km gradient at depths greater than 1500 m. In this region, the location of oil and gas pools correlates remarkably well with the vertically convergent flow systems. Therefore, the petroleum accumulations in the Kiskunhalas region are interpreted as the result of vertical hydraulic entrapment.

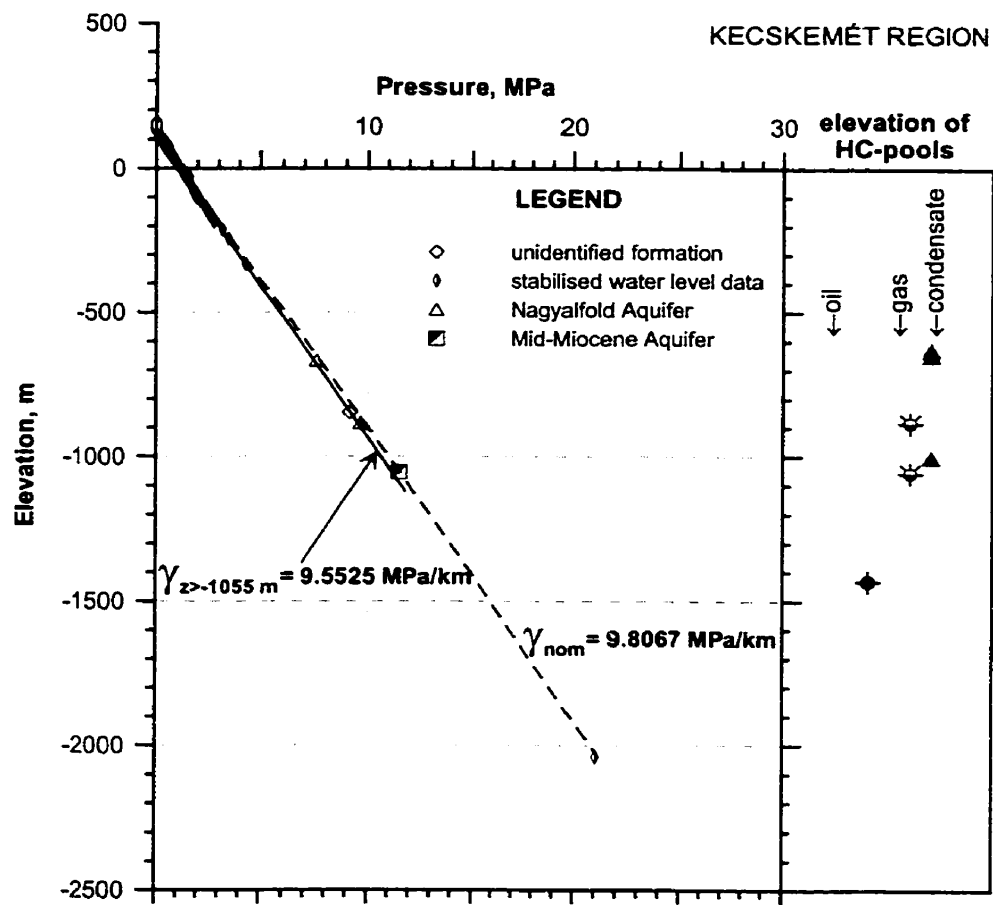


Figure 5.2: $p(z)$ profile and elevation of petroleum accumulations (HC pools) in the Kecskemét region (for location see Figure 4.2).

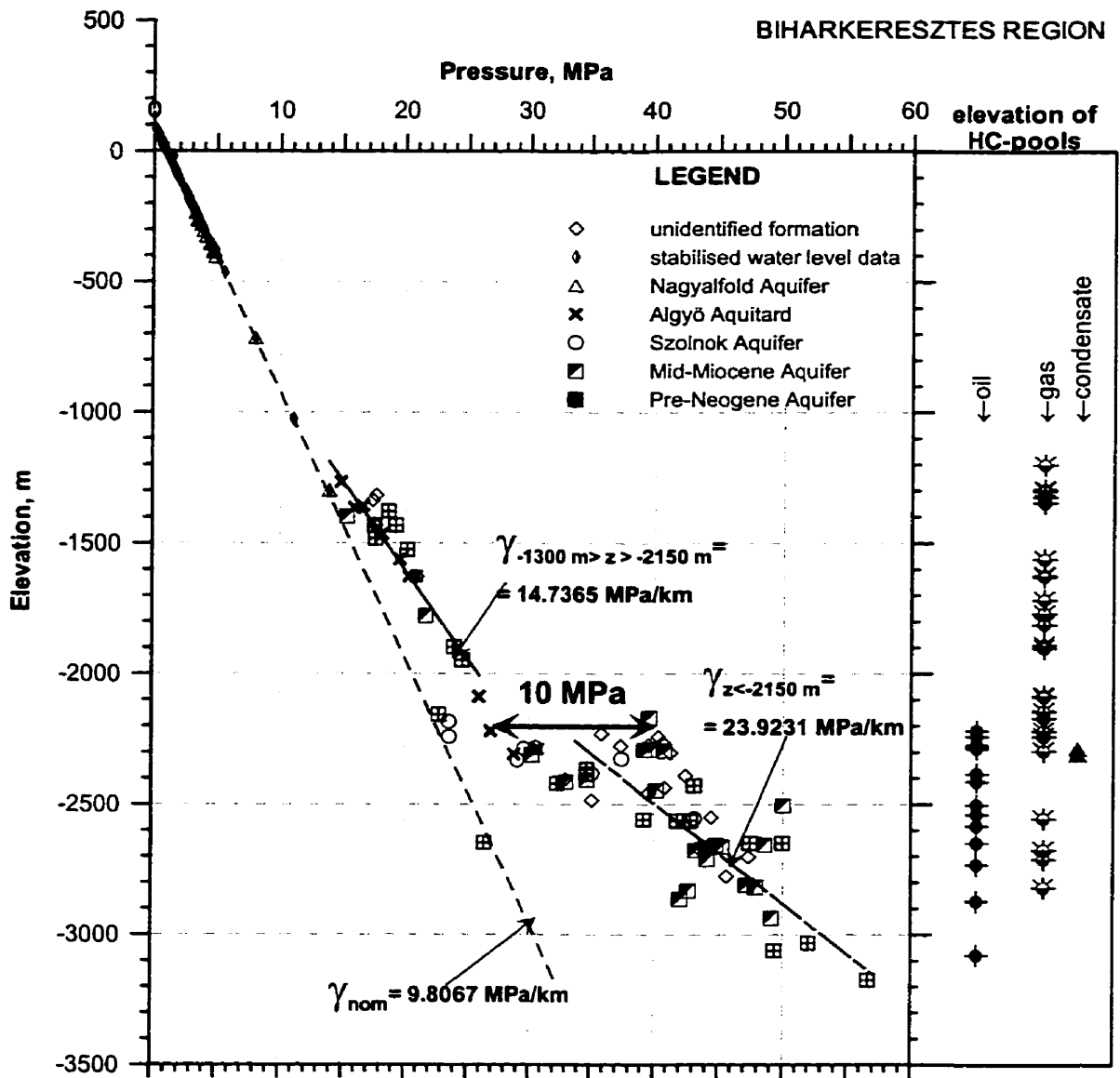


Figure 5.3: $p(z)$ profile and elevation of petroleum accumulations (HC pools) in the Biharkeresztes region (for location see Figure 4.2).

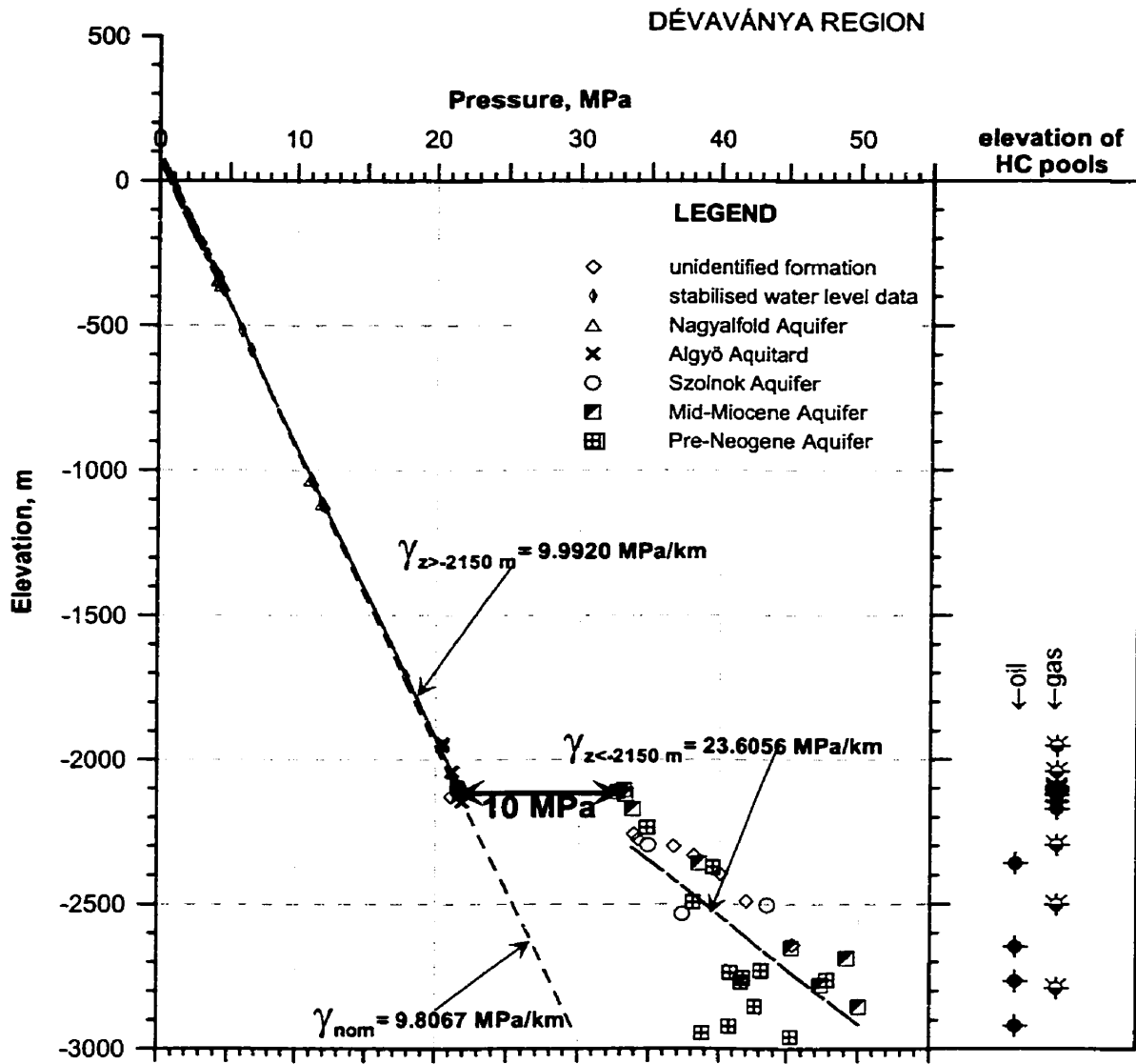


Figure 5.4: $p(z)$ profile and elevation of petroleum accumulations (HC pools) in the Dévaványa region (for location see Figure 4.2).

ENDRŐD - SZARVAS REGION

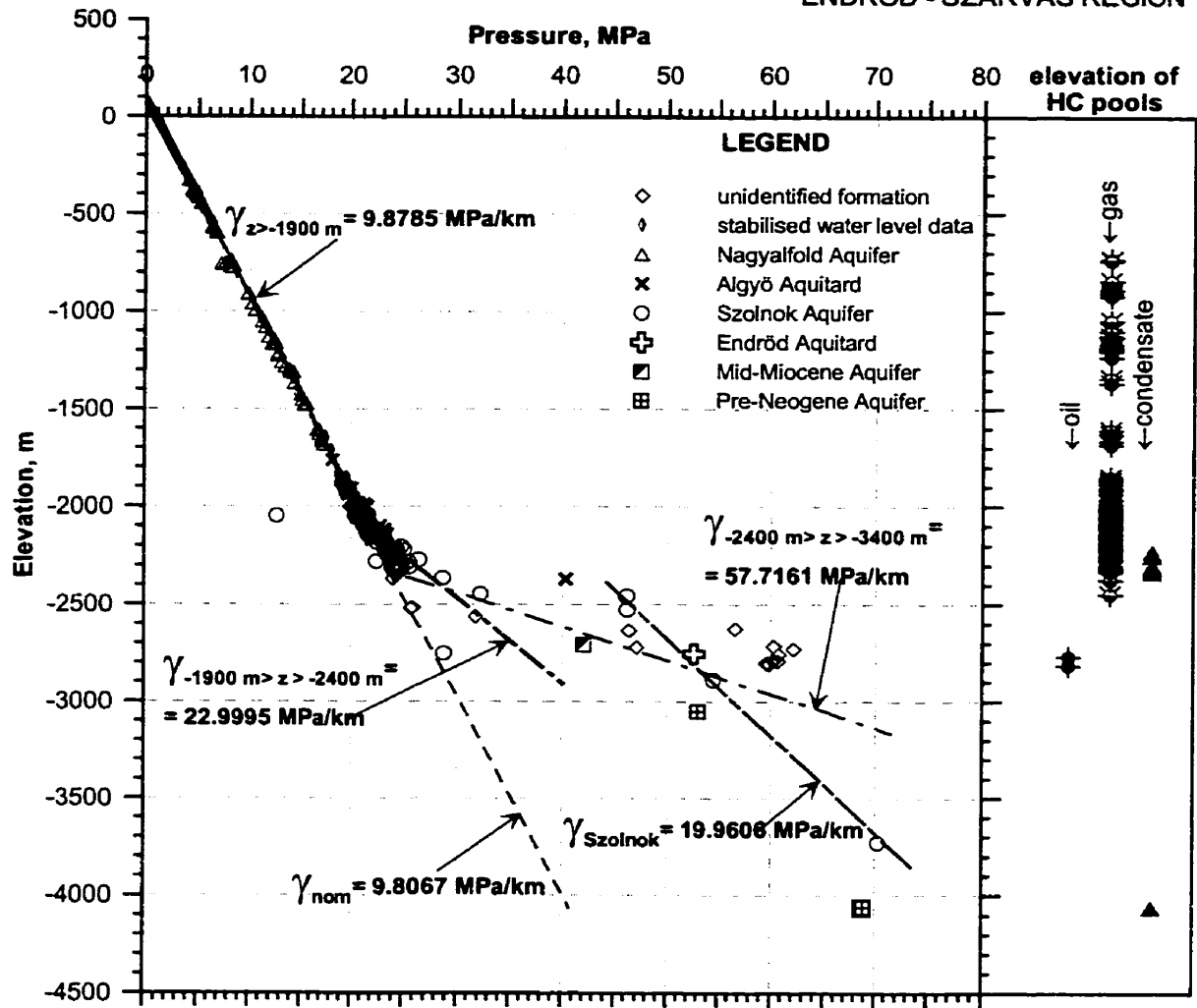


Figure 5.5: $p(z)$ profile and elevation of petroleum accumulations (HC pools) in the Endrőd –Szarvas region (for location see Figure 4.2).

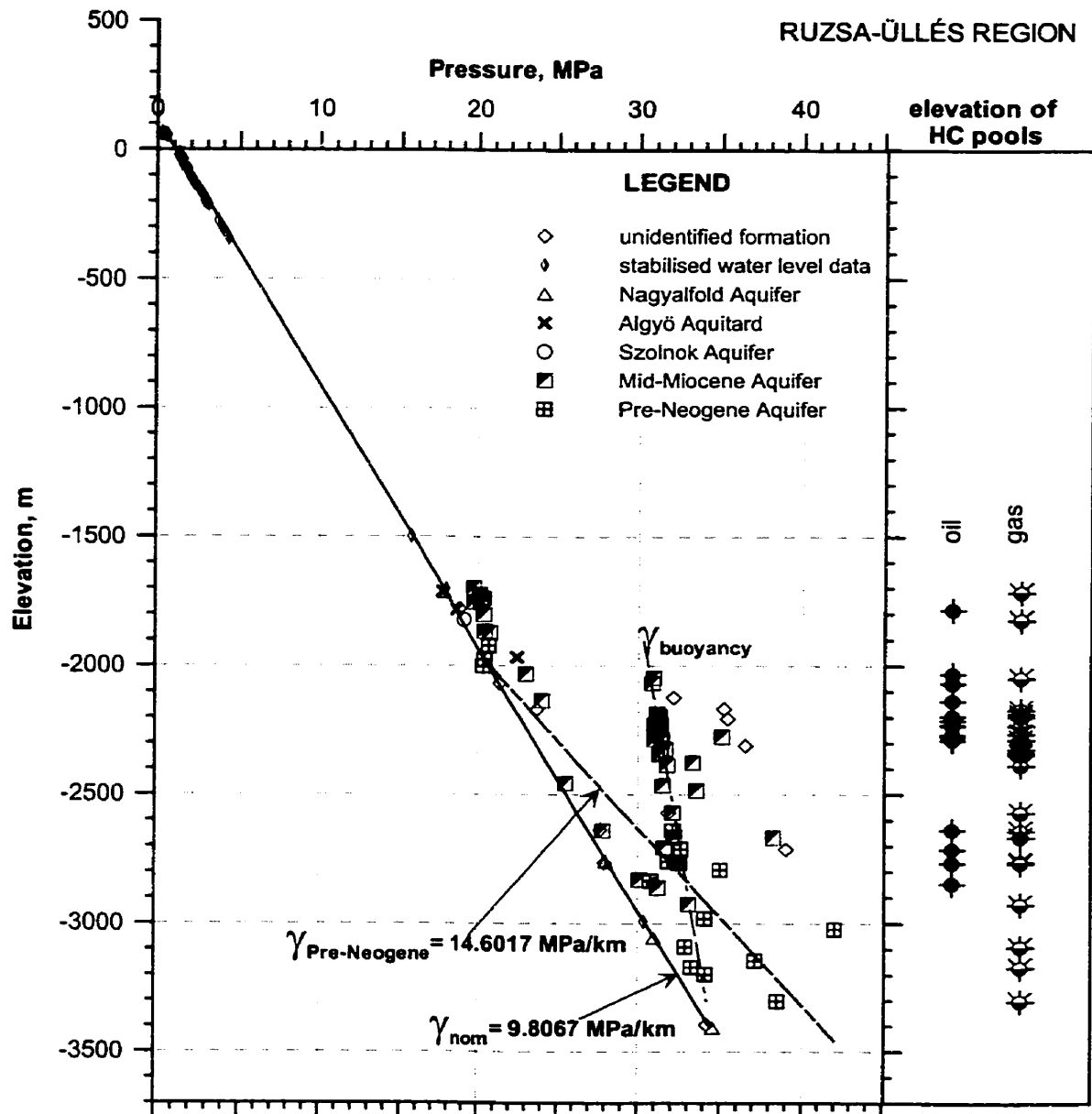


Figure 5.6: p(z) profile and elevation of petroleum accumulations (HC pools) in the Ruzsa - Üllés region. The pressure gradient within the Pre-Neogene basement increases abruptly indicating upward flow.

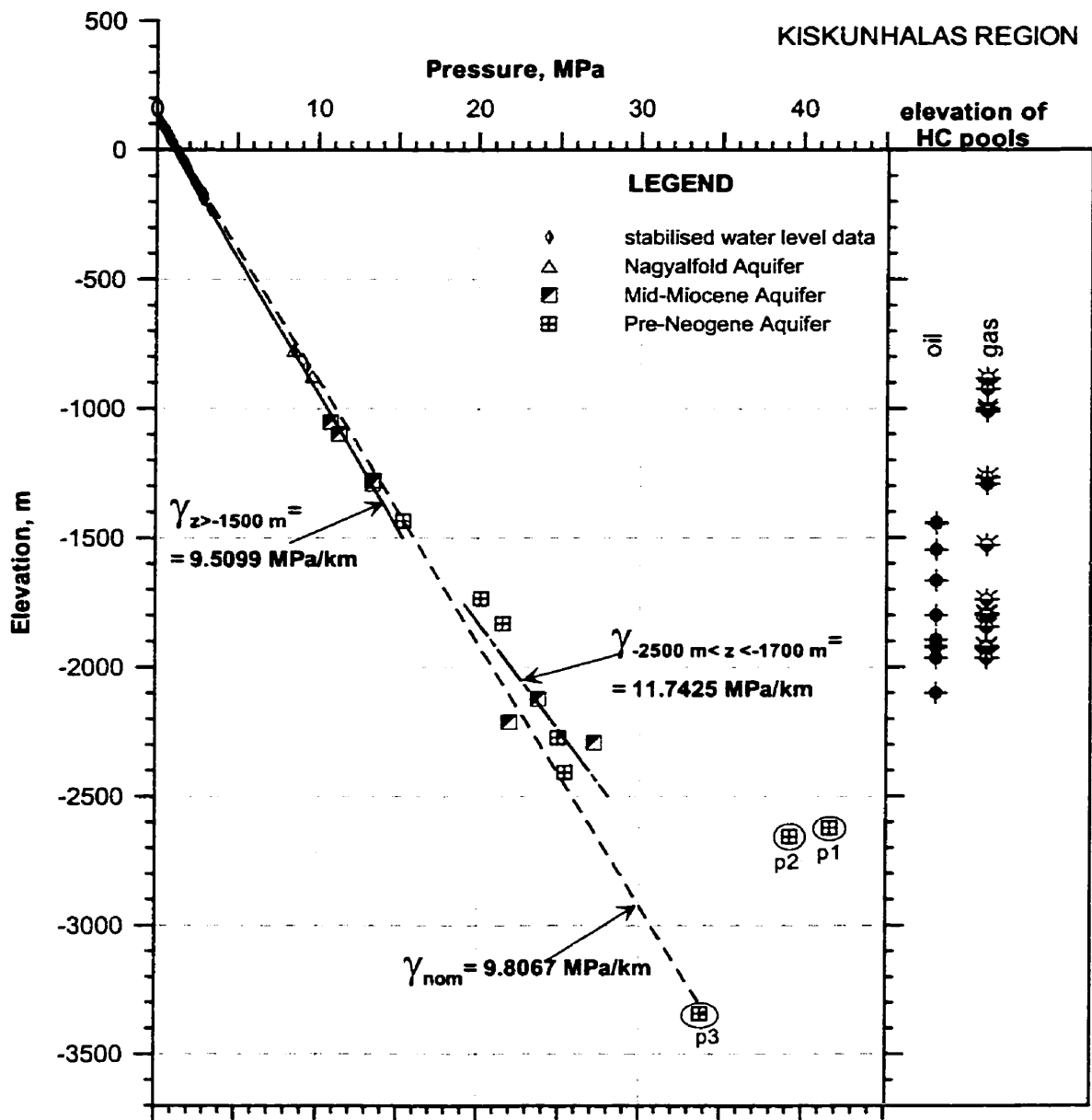


Figure 5.7: $p(z)$ profile and petroleum accumulations (HC pools) in the Kiskunhalas region, located in a regional recharge area (for location see Figure 4.2). Descending gravity-driven meteoric water converges with ascending deep basin fluids squeezed by lateral tectonic stress; an example for vertical hydraulic entrapment.

Figure 5.8 is an example for an exceptionally tall gas pay zone in the Ruzsa-Üllés region giving rise to overpressures due to buoyancy forces resulting from the density difference between gas and water. At the Ruzsa field gas is produced mainly from the fractured Pre-Neogene basement reservoirs, while at the Üllés field the stacked gas pools are in Mid-Miocene reservoirs.

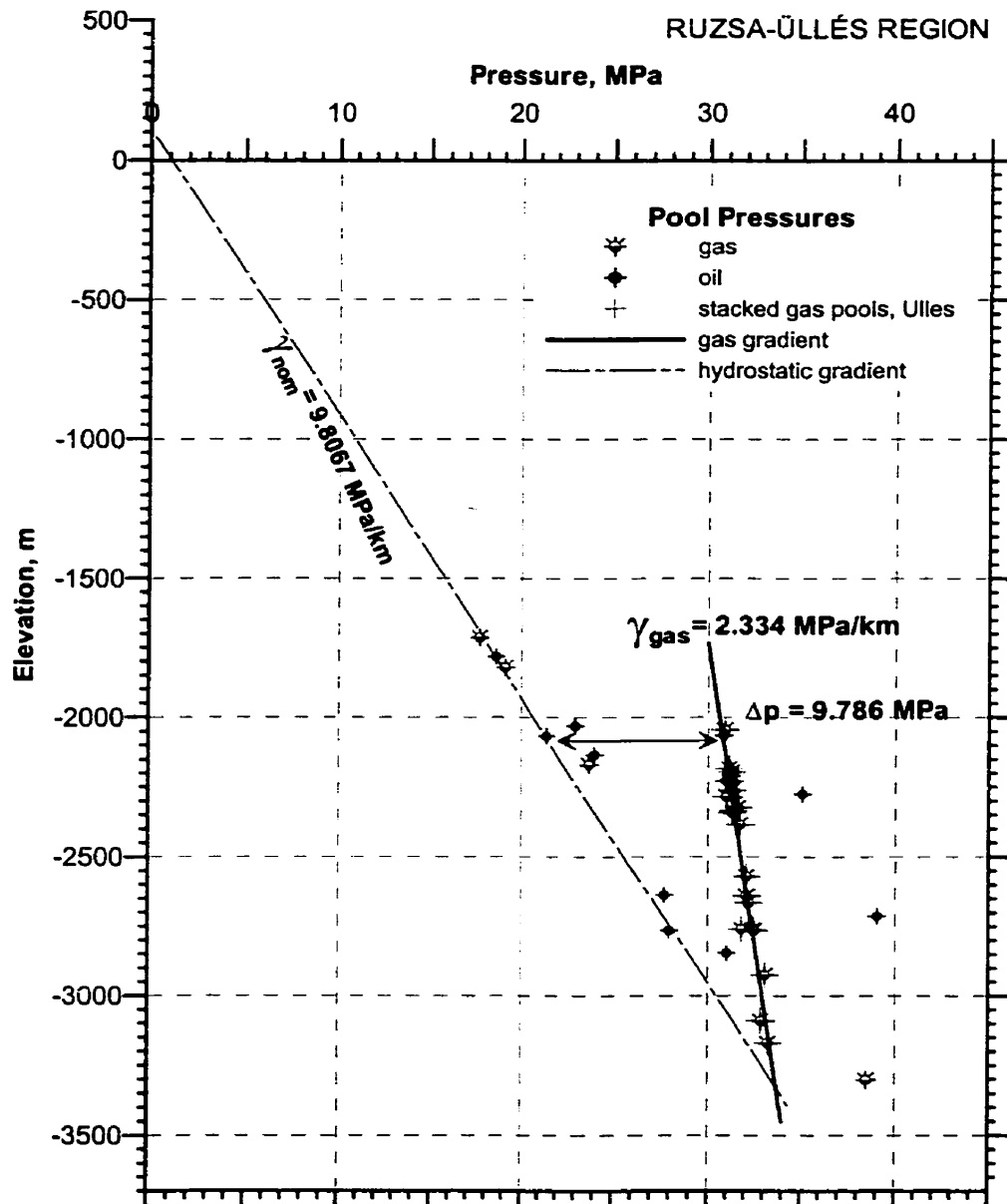


Figure 5.8: $p(z)$ profile of initial pool pressures of oil and gas accumulations in the Ruzsa - Üllés region. Vertically stacked gas pools in the Mid-Miocene reservoirs of Üllés field (B) seem to form a continuous hydrostatic gas column, at the top of which the overpressure due to buoyancy reaches 9.786 MPa (for location see Figure 4.2).

The initial pool-pressure values at Űllés follow a gradient of $\gamma = 2.334$ MPa/km, suggesting the presence of a virtually continuous gas column of ~800 m height above a gas/water contact, where the equilibrium pressure is close to the water's nominal pressure. The "virtual height" of this gas column can be the result of hydraulic communication among the stacked gas pools. Indeed, gas production in this region proved the existence of hydraulic communication among individual pools, and the thickness of the gas column in the Mid-Miocene reservoirs of Űllés field was believed to be of several hundred metres (S. Pap, I. Révész, and A. Somfai, Sr., 1998, 1999, *personal communication*).

Apparently, the initial gas pool pressures from the diagnostic $p(z)$ anomalies may be applied for making first order predictions on prospective depth ranges for exploration, and also for predicting magnitudes of pore pressures, which may be needed for the technical preparation of future drilling. The interpretation of pressure-elevation profiles, however, should be done in conjunction with fluid-potential maps and cross sections.

5.1.2 Diagnostic tomographic fluid-potential map anomalies

In this section those fluid-potential distribution patterns (or configurations) are discussed, which seem to be preferentially related to petroleum accumulations in a horizontal map view. These are the "diagnostic tomographic fluid-potential map anomalies" or " $h_{ij}(x,y) - \text{DiPotAn}$ "-s (Tóth and Almási, 1998). The location of hydrocarbon pools from the $z = -300$ to -3500 m elevation interval and their relation to horizontal hydraulic head configuration is illustrated on the tomographic fluid-potential maps presented above (Figures 4.23 through 4.31). The fluid-potential anomalies were correlated with local tectonic elements (fault zones with en-échelon faults, intersecting faults), by comparing the tomographic maps with the available geologic map of Fülöp and Dank (1987) (Figure 2.12, p. 27) and one confidential structural geologic map of MOL, Plc., which could not be used for this study.

Three major anomaly types are established from the fluid-potential maps: A: *potential high*; B: *potential escarpment*; and C: *potential low* (Figure 5.9). A *potential high* is identified as an area bounded by a closed or semi-closed equipotential line of

higher value relative to its environment and it indicates divergent driving forces (Figure 5.9/A). Within the unconfined flow regime a potential high indicates descending flow,

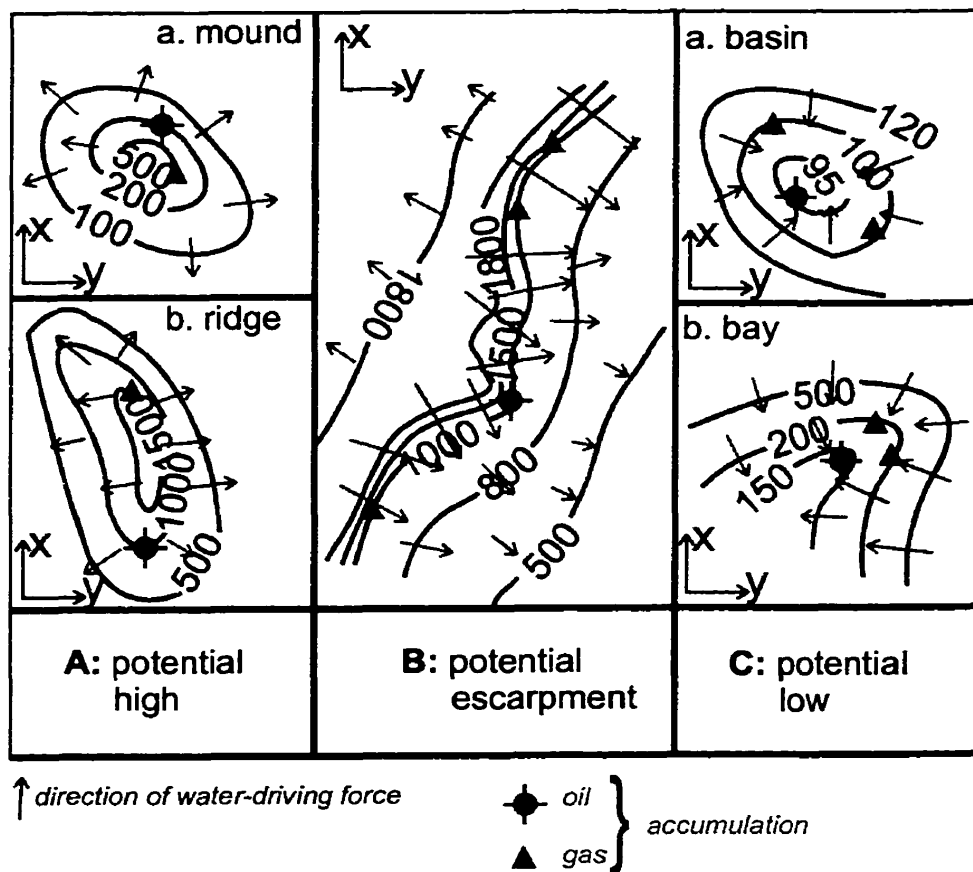


Figure 5.9: Schematic illustration and classification of tomographic fluid-potential map anomalies, $h_{ij}(x,y)$ - DiPotAn-s (after Tóth and Almási, 1998).

while within the confined flow regime it indicates upward flow. Further anomaly subtypes can be defined according to the geometry of the closed high- h lines. Circular or slightly elliptic (length/width < 2) contour lines determine a *mound* or *dome*-shaped anomaly (Figure 5.9/A-a), whereas elliptic contour lines with a length/width > 2 determine a *ridge*-shaped anomaly (Figure 5.9/A-b). Both the mound and the ridge anomalies are characterised by high lateral gradients. A *potential escarpment* is identified as a segment of the potential field outlined by a set of closely spaced, sub-parallel equipotential lines, which indicate a steep lateral gradient (Figure 5.9/B). The probable geologic interpretation of this anomaly is a large lateral permeability contrast due to either lithologic changes (sand/shale or fractured basement/marl contact) or the presence

of a fault zone, which allows up-dip flow, but restricts lateral flow. *Potential lows* (depressions) are delineated by closed or open equipotential lines of relatively low value, which determine two anomaly sub-types, the *basin* and the *bay*, respectively (Figure 5.9/C-a and b). This anomaly type indicates convergent driving forces. The terminology of the anomaly types and sub-types must be applied carefully for unevenly contoured surfaces. The above defined anomaly types and sub-types are considered ‘diagnostic’ for petroleum accumulations, because several known accumulations seem to correlate with one or the other anomaly type.

Vertical hydraulic communication between tomographic slices can be evaluated by comparing maps prepared for subsequent depth intervals. As mentioned earlier, zero-permeability seals are not present (at least not proven so far) in the Great Hungarian Plain, therefore, a non-zero hydraulic head difference between subsequent potential maps implies vertical cross-formational (cross-slice) flow. The location of *potentiometric highs* and *escarpments* coincide with areas of predominantly upward flow. A few representative examples are given below for the map-DiPotAn’s, but the list is not exhaustive (see fluid-potential maps $h_{i,j}(x,y)$ in Chapter 4; the EOv co-ordinates are in km):

A) Potential High

a) mound:

- $h_{3,6}$ (Figure 4.23), the area within $X_{EOV} = 95 - 115$ km, $Y_{EOV} = 660 - 690$ km; boundary: $h = 120$ m; oil and gas pools
- $h_{10,15}$ (Figure 4.25), $X_{EOV}/Y_{EOV} = 135/673$ and $90/715$; boundary: $h = 200$ m; gas pools
- $h_{10,15}$ (Figure 4.25), $X_{EOV}/Y_{EOV} = 210/815$; boundary: $h = 150$ m;

b) ridge:

- $h_{19,22}$ (Figure 4.27), convex southward lines between $X_{EOV}/Y_{EOV} = 95/700$ and $130/730$; boundary: $h = 400$ m
- $h_{22,25}$ (Figure 4.28), NNW-SSE trending zone between $X_{EOV}/Y_{EOV} = 148/770$ to $110/790$; boundary: $h > 800$ m

B) Potential Escarpment

An arched, roughly NE-SW striking, regional escarpment develops from $h_{15,19}$ (Figure 4.26) downward, persists over the $h_{19,22}$ (Figure 4.27), $h_{22,25}$ (Figure 4.28), and $h_{25,28}$

(Figure 4.29) maps in the central-eastern part of the study area, with a lateral gradient in the order of 100 m/km. Primarily gas and secondarily oil accumulations are common both within and at the top of the escarpment.

C) Potential Low (Depression)

a) basin:

- $h_{10,15}$ (Figure 4.25), delimited by the $h = 110$ m equipotential line; gas and oil pools
- $h_{15,19}$ (Figure 4.26), south-eastern part of the study area, delimited by the $h = 120$ m equipotential line; gas and oil accumulations

b) bay:

- $h_{19,22}$ (Figure 4.27), the area within $X_{EOV} = 165 - 190$ km, $Y_{EOV} = 765 - 785$ km, shows a bay delimited by the $h = 500$ m to 200 m equipotential line; gas and condensate pools.

5.1.3 Diagnostic hydraulic cross section anomalies

In this section, those fluid-potential distribution patterns (or configurations) are discussed, which seem to be preferentially related to petroleum accumulations in a vertical plane view. These are the “diagnostic fluid-potential cross section anomalies” or “H(L,z) - DiPotAn-s” (Tóth and Almási, 1998). In several instances, the cross section-DiPotAn-s can be correlated with local tectonic elements as well, by comparing them with available seismic profiles and tectonic features projected from the available geologic map of Fülöp and Dank (1987). Two major types of cross section-DiPotAn-s are established: A: *potential protrusion* and B: *potential depression* (Figure 5.10).

The *potential protrusion* (Figure 5.10/A) indicates axially divergent driving forces, while the *potential depression* (Figure 5.10/B) indicates axially convergent driving forces. The amplitude and slope of the axis of both the equipotential protrusion and depression may vary significantly. However, the geometry of these anomalies is determined not only by geologic, hydraulic, and hydrodynamic factors (e.g., fractures, heterogeneity and anisotropy of hydraulic conductivity of the rock framework, intensity of energy sources), but also by the distortion of their geometric representation (i.e., direction and vertical exaggeration of cross sections, density of contour intervals).

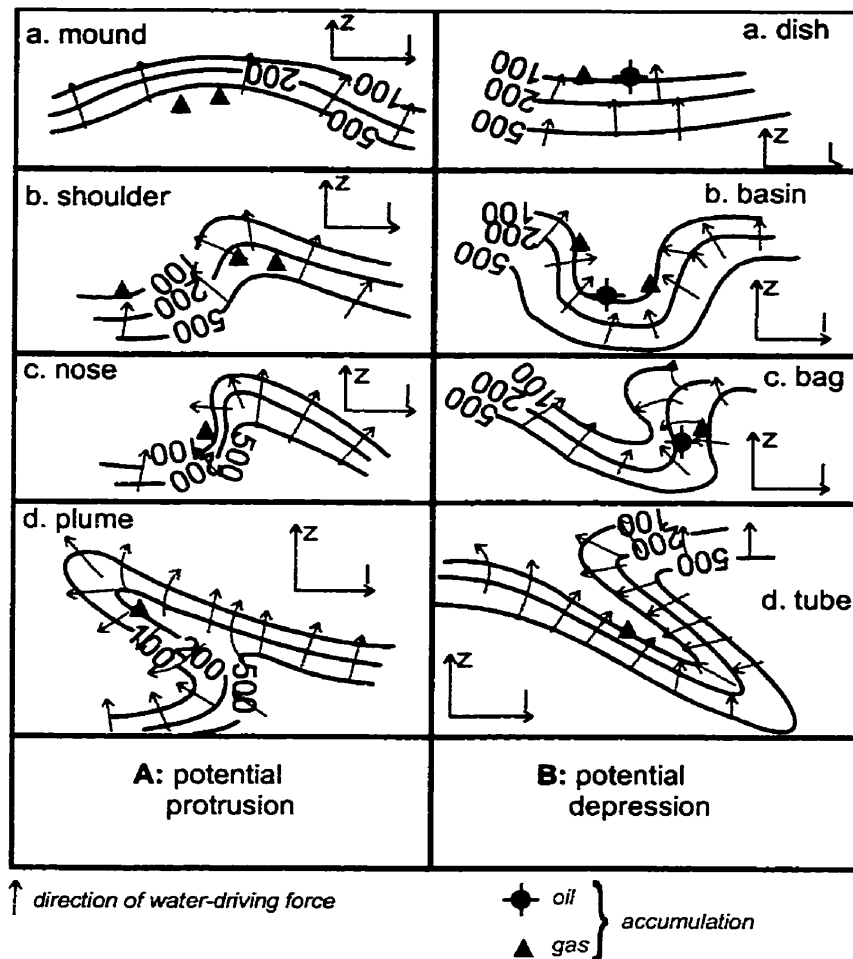


Figure 5.10: Schematic illustration and classification of hydraulic cross section anomalies, $H(L,z)$ -DiPotAn-s (after Tóth and Almási, 1998).

Therefore, further subdivision of major anomaly types is justified only for describing striking differences in their appearance/shape on a given cross section, such as *mound*, *shoulder*, *nose*, *plume*, *dish*, *basin*, *bag*, and *plume* (Figure 5.10). Hydraulic mounds and dishes tend to coincide with the regional aquitards, suggesting laterally extended (about 10 – 30 km) flow barriers for ascending flow. The occurrence of hydrocarbon pools associated with these anomaly types within the Algyő Aquitard seems to prove that these barriers are not impervious seals. The more elongated anomaly patterns (*nose*, *plume*, *bag*, and *tube*) indicate flow channelling along discrete pathways that tend to coincide with basement faults, or they may indicate fault zones within the Neogene sediments that could not be ascertained yet. A few representative examples are given below for the cross section-DiPotAn's, but the list is not exhaustive:

A) Potential Protrusion:

a) *Mound*

- Section **H2**: (Figure 4.34) L = 186 km; h = 200 – 110 m; gas
- Section **H4**: (Figure 4.36) L = 97 – 101 km; h = 500 m; gas and oil

b) *Shoulder*

- Section **H1**: (Figure 4.33) L = 100 – 106 km; h = 100 – 200; gas and oil

c) *Nose*

- Section **H2**: (Figure 4.34) L = 5 – 10 km; h = 180 – 200 m; gas

d) *Plume*

- Section **H1**: (Figure 4.33) L = 25 – 30 km; h = 150 m; gas
- Section **H3**: (Figure 4.35) L = 205; h = 500 m; gas

B) Potential Depression:

a) *Dish*

- Section **H3**: (Figure 4.35) L = 145 – 152 km; h = 120; gas and condensate

b) *Basin*

- Section **H3**: (Figure 4.35) L = 170 – 180 km; h = 1500 m; oil and gas

c) *Bag*

- Section **H2**: (Figure 4.34) L = 203 km; h = 100 - 120 m (tube); oil

d) *Tube*

- Section **H1**: (Figure 4.33) L = 68 – 74 km; h = 500 - 1000 m (tube); oil

5.2 SUMMARY AND DISCUSSION

Based on empirical observations, the most probable pore pressure / fluid-potential anomaly patterns indicative of petroleum accumulations in the Great Hungarian Plain are summarised below.

On pressure-elevation profiles:

- (A) regions of upward flow inferred from super-hydrostatic pressure gradients;

- (B) regions of upward flow characterised by abrupt or gradual increase of super-hydrostatic gradients with depth, suggesting low permeability flow barriers at the elevation range of the gradient-brake;
- (C) vertical hydraulic traps created by vertically convergent flow under recharge areas recognised by a change of pressure gradient from sub-hydrostatic to super-hydrostatic.

On fluid-potential maps:

- (A) closed fluid-potential highs, which indicate laterally divergent and ascending flow along discrete pathways;
- (B) potentiometric escarpments that are recognised as zones of steep lateral hydraulic gradient, which indicate lateral flow barriers due to either lithological changes or fault walls that permit only up-dip flow;
- (C) closed potentiometric depressions, which indicate convergent flow.

On hydraulic cross sections:

- (A) potential protrusions or upwarped hydraulic head contours indicate divergent flow, which may be vertically restricted by laterally extensive aquitards or channelled by discrete pathways;
- (B) potential depressions indicate laterally convergent and ascending flow perhaps into higher permeability zones.

The above fluid-potential anomaly patterns are considered to be diagnostic for hydrocarbon accumulations only, by virtue of the frequency of the observed coincidences. The geometry of permeability contrasts, the density difference between water and hydrocarbons, and the intensity of fluid flow control entrapment of hydrocarbons along the flow paths. The identified fluid-potential anomalies are determined/controlled by the actual energy sources and the hydraulic properties of the porous medium. The steep vertical pressure gradients (from the $p(z)$ profiles) and the vertical hydraulic head gradients (from the regional hydraulic cross sections) indicate generally ascending flow directions. These are considered favourable for entrapment of hydrocarbons (Tóth, 1980). Vertical stacking of oil and gas pools within a field (such as Ruzsa-Üllés (Figures 5.6 and 5.8) is due to the combined effects of ascending flow and buoyancy.

Below recharge areas, gravity-driven flow seems to play an important role in hydrocarbon entrapment, as illustrated by the case of Kiskunhalas region, where a vertical, hydraulically enhanced trapping condition was inferred from the $p(z)$ profile (Figure 5.7). Most petroleum accumulations were discovered below the central discharge area of the study area. A number of such pools were discovered within the quasi-hydrostatic zone under moderate super-hydrostatic conditions (e.g., Endrőd – Szarvas region; Figure 5.5 and on Figure 4.35, section H3, L = 140 – 160 km). Some of these pools are, indeed, associated with ascending limbs of gravity-driven flow systems, yet those found in the lower part of the ‘normal pressured’ zone can not be unequivocally linked to gravity-driven flow systems. As it was shown in Chapter 4, the fluid-potentials of the two regional flow regimes blend into each other at variable depths within the transitional zone.

Two-dimensional numerical models of compaction driven flow in the Great Hungarian Plain (van Balen, 1995; Lenkey, 1999) offer plausible explanation for the vertical and lateral direction of petroleum migration from the deep sub-basins toward basement highs. These models are in agreement with the model of Szalay and Koncz (1993); most discovered hydrocarbon pools are within or above basement highs. However, the present-day fluid flow field in the basin does not seem to be driven by vertical compaction, as shown in Chapter 7. The lateral components of the present-day hydraulic gradients are directing fluids toward the centres of the deep grabens. Hence, the lateral components of groundwater flow could be driving hydrocarbons as well toward the basin centres, where they may accumulate in hydraulically enhanced traps. This mechanism may involve remigration of hydrocarbons from pre-existent accumulations toward new traps, and secondary migration of newly generated hydrocarbons toward traps enhanced by the present-day hydraulic conditions. This scenario is feasible in light of Tóth and Corbet’s (1986) idea about the effects of delayed adjustment of the regional groundwater flow field to the modified boundary conditions on petroleum accumulations. Thus, the internal parts of sub-basins in the Great Hungarian Plain, which were, and still are, avoided as exploration targets (I. Szilágyi, 1999, *personal communication*) should be re-considered in the future.

Geologic interpretation of DiPotAn’s is hypothetical, as we do not have satisfactory data control accessible to evaluate our hypotheses in the required detail. The

hypotheses are based on theoretical studies (e.g., Tóth and Rakhit, 1988; Matthäi and Roberts, 1996) and experience with field examples from other basins (examples presented in Dahlberg, 1995). The “diagnostic fluid-potential anomalies” described here were observed at a regional scale, which bears an inherent limitation of their application to field/local scale, where the potential distribution and the flow pattern may be strongly modified due to the local permeability heterogeneities. The role of the “DiPotAn’s” in the entrapment or destruction of petroleum accumulations can be investigated at local scale with the UVZ-method of Hubbert (1953) (see Dahlberg, 1995, for a discussion), provided that these anomaly types also occur on potentiometric maps constructed in a rigorous sense. Detailed sedimentological and structural information, hydraulic head values, and water/oil/gas density values are required for such studies. The tomographic fluid-potential maps are not “true” potentiometric maps (section 4.2.1.2), therefore, they are inadequate for the UVZ method.

The resolution of the available data did not enable local scale studies. The formation boundaries (top/bottom) from the stratigraphic database are not reliable permeability boundaries. Therefore, a structure contour map of a regional aquitard/aquifer boundary is not an accurate representation of local scale hydraulic conditions. As a result, the Z surface can not be represented. To determine the V surface, hydraulic head values must be selected from within the confined aquifer under investigation limited from above by the Z surface. This was not possible under the present conditions, therefore, the UVZ method could not be applied and the details of map and cross section DiPotAn’s could not be evaluated with the UVZ method.

5.3 CONCLUSIONS

Based on spatial analysis of petroleum accumulations and fluid-potential anomalies characteristic for trapping conditions in the Great Hungarian Plain it is concluded, that:

1. Several petroleum accumulations in the basin can be linked to the present-day flow-field.

2. Gravity-driven flow seems to have a determinant effect on trapping within the quasi-hydrostatic zone, under both recharge and discharge areas.
3. The position of most petroleum accumulations discovered within the overpressured zone can be explained with compactional flow models.
4. Several accumulations within the overpressured zone that are found in regions of dominantly ascending flow can be linked to either, earlier compactional flow directions or present day flow directions.
5. Hydrocarbons could have been- or may be redistributed from above basement highs toward graben centres along the lateral component of regional hydraulic gradients;
6. Internal parts of the grabens seem to be promising prospective areas for hydrocarbon exploration.

6 HYDRO-GEOTHERMAL CONDITIONS

6.1 INTRODUCTION

The Pannonian Basin is well-known for its geothermal anomalies. In 1671, Boyle documented the increase of temperature with depth in coalmines in the north-central part of the basin (Boyle, 1671, in Bullard, 1965, and in Jessop, 1990). The numerous thermal springs that were used for curative purposes over the past centuries are a natural indication of high geothermal gradients and heat flow in this basin. The first three thermal wells were drilled by V. Zsigmondy between 1866 and 1877 in Budapest and Harkány, and these wells are still active today (Ottlik et al., 1981).

Large thermal water reserves are stored in the Neogene sediments and Mesozoic carbonate rocks, which were discovered as a result of petroleum exploration after World War I. Exploration has intensified during World War II; thousands of exploration and production wells were drilled and most of them produced thermal water. Until 1994, there were 1050 registered thermal wells producing water with temperatures above 30 °C at a total output of 500 000 m³/day (Korim, 1994). Thermal water is widely utilised in Hungary in balneology, therapeutics, district and space heating, agriculture, and even for drinking. Most of the actively producing thermal water wells are located in oil/gas producing areas (Radó, 1974a,b,c). Indeed, drilling of a thermal water well led to the discovery of the largest oil and gas accumulation in Hungary (Algyő: ~76x10⁶ metric tons of oil and 109x10⁹ m³ of gas; Kőrössy, 1990). As a result of intensive hydrocarbon and thermal water exploration over the past eight decades, a large number of temperature measurements were recorded as bottom hole temperatures and outflowing water temperatures. Centralised collection of temperature and other relevant data commenced in 1956, and the results were regularly published by the Research Institute for Water Resources (VITUKI, Plc.) in a book series entitled “Thermal Wells of Hungary” (“Magyarország hévízkútjai”). Systematic temperature data collection started in the late 1970’s at the Department of Geophysics, Loránd Eötvös University. The digital temperature database of Hungary consists of 2734 reliable data out of over 10,000

measurements from about 1000 wells (Dövényi and Horváth, 1988); 1562 out of these 2734 reliable data are from the present study area.

6.1.1 Geothermal features of the Pannonian Basin

The first heat flow measurements in Hungary were made by Balyi and Papp (1950) and Boldizsár (1956a,b, 1964, 1966). Currently, there are 28 standard heat flow determinations in the country (Dövényi and Horváth, 1988; Lenkey, 1999). Based on these measurements and hundreds of heat flow estimates, the surface heat flow in the Pannonian Basin generally exceeds 83 mW/m^2 , often it is between $100 - 130 \text{ mW/m}^2$ (Figure 6.1), whereas in the surrounding areas it is $40 - 60 \text{ mW/m}^2$ (Dövényi and Horváth, 1988; Lenkey, 1999). The estimated magnitude of heat flow from the Pre-Neogene basement is about $80 - 100 \text{ mW/m}^2$ (Horváth et al., 1981). The geothermal gradients commonly reach $50 - 60 \text{ }^\circ\text{C/km}$; almost double the value of the average continental thermal gradient ($30 \text{ }^\circ\text{C/km}$) (Ottlik et al, 1981; Dövényi and Horváth, 1988).

The most significant heat source in the Pannonian Basin is related to the thin ($\sim 26 \text{ km}$) continental lithosphere, the upwelling of the hot asthenosphere, and mantle diapirism (Stegena et al., 1975; Horváth et al., 1979). Radioactive heat sources within the Neogene clastic sedimentary unit and the underlying basement are restricted to a few small areas; their regional significance is considered negligible (Lenkey, 1999). In the NE part of Hungary, the observed high heat flow is attributed to the volcanic activity during the Pliocene (Ottlik et al., 1981). The terrestrial heat flow was reduced by approximately $10 - 20 \%$ in western Hungary, and by up to 30% in the south-central part of the Great Hungarian Plain, as a result of the accumulation of up to 7 km thick sedimentary pile during the Neogene and Quaternary (Lenkey, 1999). The annual average surface temperature ranges between $9.5 - 12 \text{ }^\circ\text{C}$ (Radó, 1974a,b,c). During wintertime, the water temperature at- and below the water table (a depth of $\sim 3 - 7 \text{ m}$) is always above freezing point (Rónai, 1985).

The effects of groundwater flow on the temperature and heat flow distribution in Hungary were discussed in several earlier studies, and they were also evaluated quantitatively at local scale (i.e., $< 100 \text{ km}^2$) in thermal karstic aquifers, Quaternary-Neogene sandstone aquifers, and hydrocarbon reservoirs (e.g., Stegena, 1958, 1963,

1982, 1989; Völgyi, 1977; Alföldi et al., 1978; Korim, 1978, 1982, 1994; Horváth et al., 1979; Ottlik et al., 1981; Dövényi et al., 1983; Rónai, 1985). Lenkey (1999) did the first regional scale quantitative modelling study on the effects of groundwater flow on the thermal field. In the literature, the general consensus regarding the effects of groundwater flow on heat distribution in Hungary is that heat transport within the gravity-driven flow regime is predominantly advective in karstic aquifers and in the vicinity of fracture zones (e.g., Stegena, 1989), and it is conductive in the thick Neogene-Quaternary sediments.

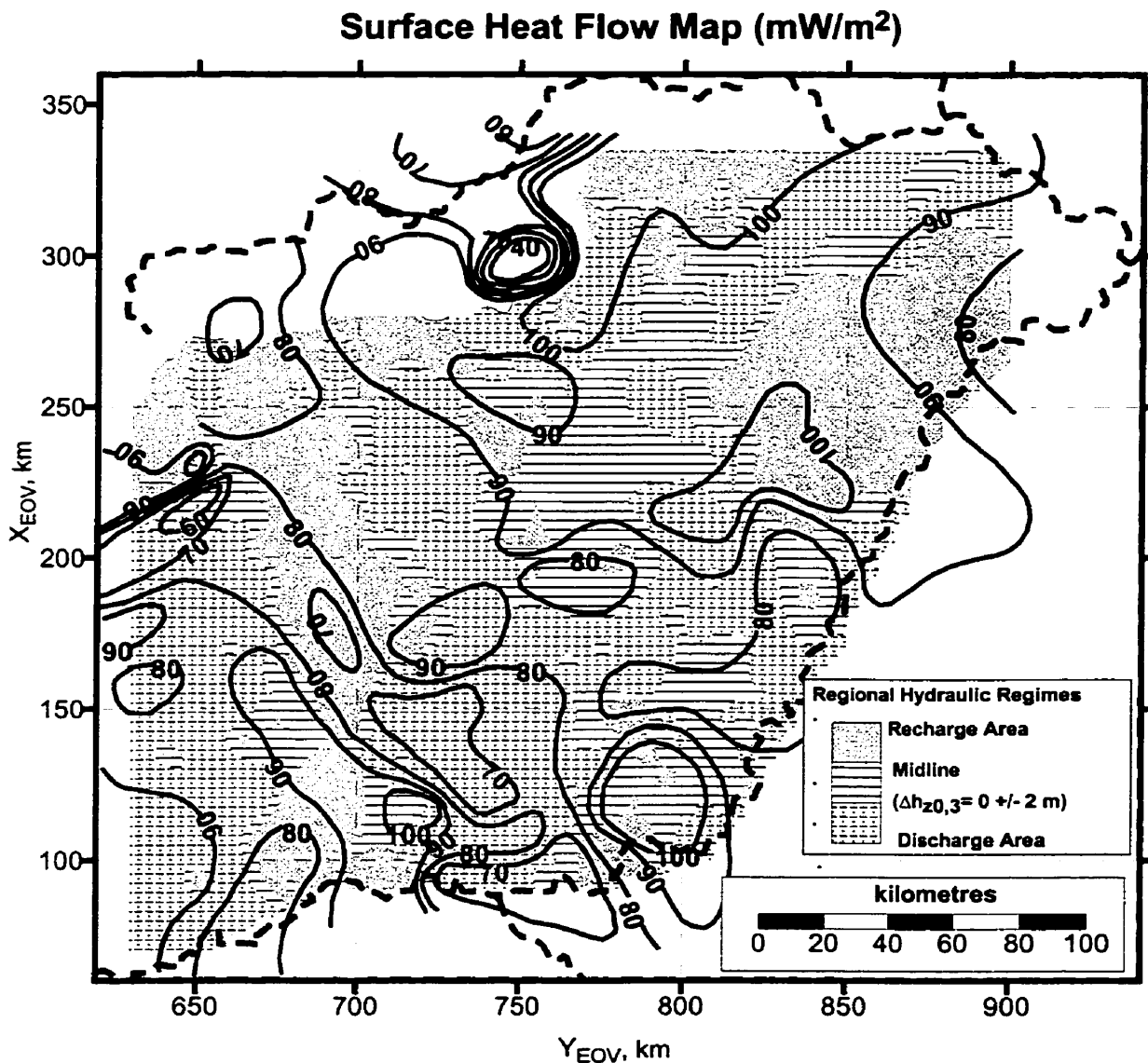


Figure 6.1: Lateral distribution of average surface heat flow (contour interval = 10 mW/m²) in Eastern Hungary (after Dövényi and Horváth, 1988) and the regional hydraulic regimes (this study).

Free convection is documented in a single location in central eastern Hungary (at Tisza-kécske; Alföldi et al., 1978). Within the zone of abnormally high fluid pressures, heat transport is achieved by conduction, assuming that fluid flow is driven by vertical compaction (Lenkey, 1999).

6.1.2 Objectives of present study

Earlier regional scale generalisations regarding the relationship between groundwater flow and the heat distribution in the Pannonian Basin were either based on local scale observations (e.g., Ottlik et al., 1981; Stegena, 1982) or on numerical modelling of compaction- and gravity-driven flow (Lenkey, 1999). The latter relied on the regional hydrodynamic model of Erdélyi (1976) –the only one published so far.

The objectives of this study are: 1) to investigate the possible coupled relations between the geothermal field and the fluid flow field (as described in Chapter 4) at regional scale using our integrated hydraulic head database and the temperature database of Dövényi and Horváth (1988), and 2) to evaluate the possibility of using geothermal information to hydrocarbon exploration in the Great Hungarian Plain.

6.2 THEORETICAL CONSIDERATIONS

6.2.1 Definitions

Heat transfer in saturated porous media is achieved by *conduction*, *convection*, and *radiation*. Purely conductive heat transfer occurs when the pore fluids are static. Heat transport in the presence of fluid flow is called *convection*, and can be of two types, i.e., *forced convection* and *free (or natural) convection*. Forced convection occurs when external forces (e.g., gravity) induce fluid flow. Free convection occurs when buoyancy effects of density gradients caused by temperature gradients induce the flow. The term *advection* is often used as a synonym for forced convection. All these mechanisms may be active simultaneously in a sedimentary basin, however, with varying efficiency. Convection is always accompanied by conduction, although, conductive heat transfer can

act independently from convection. Radiation is effective for temperatures higher than 500 °C, which is uncommon in sedimentary basins (Kappelmeyer and Hänel, 1974).

The thermal gradient, $\nabla T = \mathbf{grad}T = \left(\frac{\partial T}{\partial x} \mathbf{u}_1 + \frac{\partial T}{\partial y} \mathbf{u}_2 + \frac{\partial T}{\partial z} \mathbf{u}_3 \right)$, is a vector, which describes the highest rate of temperature change in space at every point in a medium of a given thermal conductivity (κ) with respect to a reference temperature value (\mathbf{u}_1 , \mathbf{u}_2 , and \mathbf{u}_3 are unit vectors in the x, y, and z direction, respectively). Since the isotherms are quasi-horizontal, the lateral components of the thermal gradient are practically negligible relative to the vertical component, $\left(\frac{\partial T}{\partial x} \text{ and } \frac{\partial T}{\partial y} \ll \frac{\partial T}{\partial z} \right)$. The SI unit for $\mathbf{grad} T$ is [K m^{-1}]; the unit of °C/km is also widely used. The corrected annual average air temperature at the ground surface is commonly used as reference value for the calculation of the vertical $\mathbf{grad} T$. A reasonable estimate of the average ground surface temperature can be obtained by adding 1.1 °C to the average annual air temperature that is measured 2 m above ground surface (Hänel, 1980).

The thermal conductivity, κ , [$\text{W m}^{-1} \text{K}^{-1}$] is a tensor, an internal material-property, which depends on the temperature, mineralogical composition, porosity, and fluid saturation of the rocks. When conduction is at steady state, $\mathbf{grad} T$ is inversely proportional to κ (Jessop, 1990). The SI units for κ is [$\text{W m}^{-1} \text{K}^{-1}$]. For practical purposes it may be assumed that κ is independent from temperature (Jessop, 1990; p. 255). Generally, pelitic rocks have a lower thermal conductivity than psammitic rocks. Therefore, the pelite/psammite ratio of a sedimentary rock also controls its bulk thermal conductivity, which can be estimated at arbitrary depths using porosity and lithologic logs with the formula (Vacquier, 1984; Dövényi and Horváth, 1988):

$$\kappa(d) = \kappa_m^{1-\phi(d)} \kappa_w^{\phi(d)} \quad (6.1)$$

where κ_m and κ_w are the thermal conductivity of the matrix and water, respectively, and $\phi(d)$ is the porosity vs. depth trend function. Usually, it is quite difficult to obtain accurate measurements for κ that are representative for particular field conditions (Jessop, 1990; p. 84). Tabulated values of κ for various rocks can be found in the literature (e.g., Domenico and Mifflin, 1965; Jessop, 1990; p.46); these values can be used for probabilistic modelling or as first order approximations. Thermal conductivity

values of sandstones and shales measured on rock samples from boreholes in Hungary and calculated from porosity-depth trend functions (Figure 2.14, p.32) are illustrated on Figure 6.2.

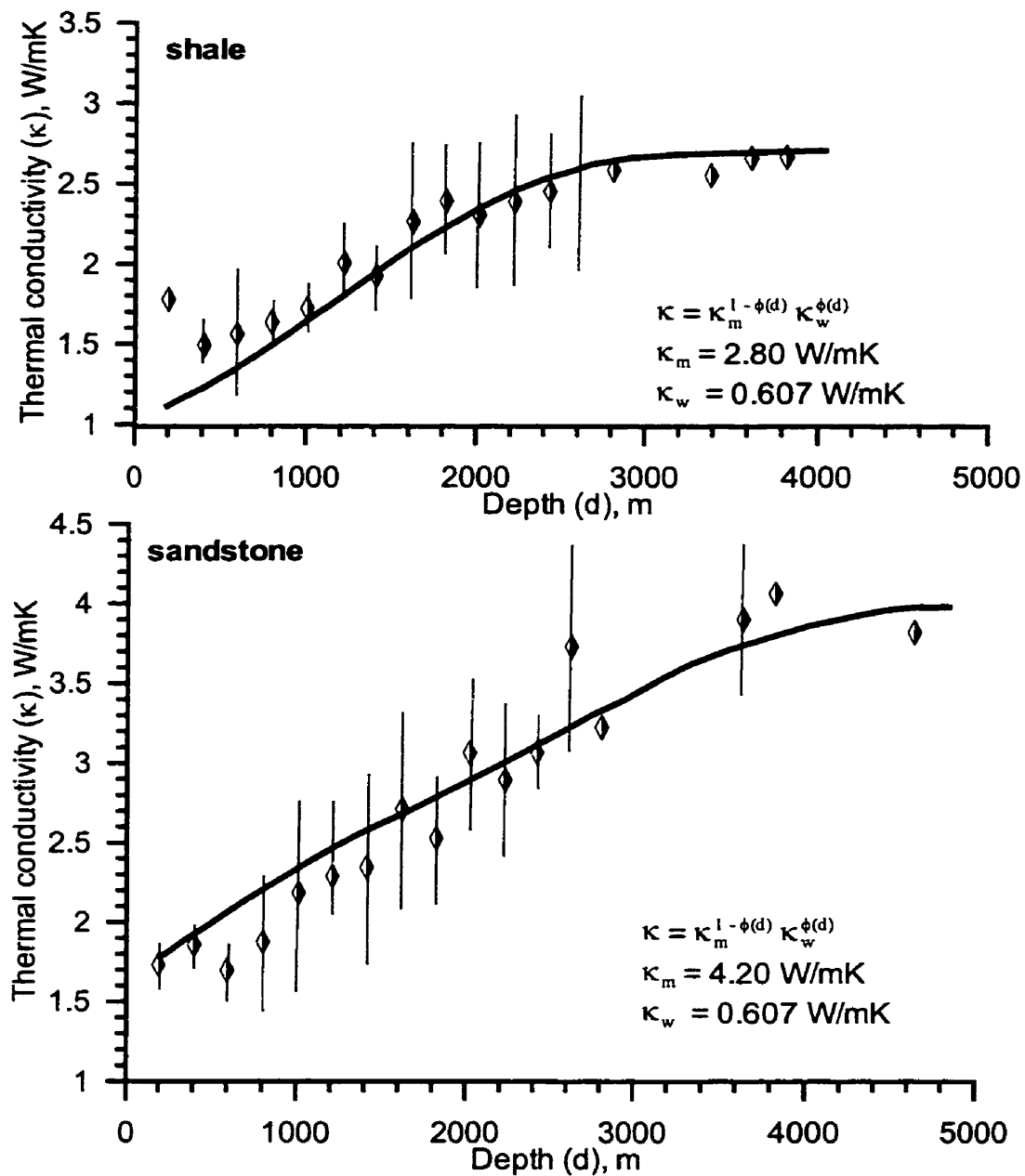


Figure 6.2. Thermal conductivity of sandstones and shales measured on rock samples from boreholes and estimated from porosity-depth trend functions (after Dövényi and Horváth, 1988).

In some respects, thermal conductivity is analogous to the hydraulic conductivity. The bulk thermal conductivity of a rock unit ($\bar{\kappa}$) with layered thermal heterogeneity can be calculated as the harmonic mean of each layer's conductivity (κ_i), weighted by the thickness of each layer (l_i): $\bar{\kappa} = \left(\sum_{i=1}^n l_i \right) / \left(\sum_{i=1}^n (l_i / \kappa_i) \right)$, $i = 1, \dots, n$, for 'n' number of horizontal layers, assuming that heat flow is vertical.

The *conductive heat flow*, θ , is a vector defined as the amount of thermal energy perpendicularly crossing a unit area per unit time with SI units of W m^{-2} :

$$\theta = -\kappa \nabla T \quad (6.2)$$

The negative sign indicates that flow is directed toward the decreasing temperature. If cooling would be purely conductive, then the heat flow should be constant across the overlying strata. Otherwise advection would decrease or increase the heat flow in recharge and discharge areas, respectively. A profile of vertical heat flow variation is a sensitive tool used to ascertain whether or not, the conductive heat flow is affected by advective perturbations (Smith and Chapman, 1983).

The *equation of heat transfer* is (Domenico and Palciauskas, 1973):

$$\nabla(\kappa \cdot \nabla T) - \rho_w C_w \nabla(q \cdot T) + A = \rho_s C_s \frac{\partial T}{\partial t} \quad (6.3)$$

where κ is the bulk thermal conductivity of the solid-fluid complex, ρ_w is the fluid density, ρ_s is the bulk density of the solid-fluid complex, C_w and C_s are the heat capacity of water and solid-fluid complex, respectively [$\text{J/kg } ^\circ\text{C}$], q is the flux:

$$q(x,y,z) = -K \nabla h \quad (6.4)$$

(h is the hydraulic head, K is hydraulic conductivity), A is a source term representing radioactive heat production per unit volume of rock, and t is time. The effectiveness of the advective heat transport depends on the magnitude and sense of the Darcy-flux, hence, on the magnitude and sense of the hydraulic gradient, and the hydraulic conductivity of the rock framework. Since the isotherms are usually almost horizontal, the horizontal component of fluid flow has little or no effect on the lateral temperature distribution (Jessop, 1990; p.255). Therefore, the first and second order derivatives of temperature in the x and y directions can be taken as 0. The vertical flow component in

the z direction is expected to perturb the thermal field, which results in the bending of isotherms in the direction of flow (Domenico and Palciauskas, 1973).

The *temperature anomaly*, ΔT , (in °C or K units) is defined here as the difference between the observed (T_{obs}) and the reference (T_{ref}) temperature (or nominal temperature) at any given depth:

$$\Delta T = T_{obs} - T_{ref}$$

Where the reference temperature is calculated as:

$$T_{ref} = d \cdot grad T_{avg} + T_o$$

(d is depth, T_o is average temperature at the land surface). The measured temperatures are considered *sub-geothermal* ($\Delta T < 0$) or *super-geothermal* ($\Delta T > 0$) if they fall below or above the average geothermal gradient line ($grad T_{avg}$), respectively. The statistical average temperature gradient is used as reference, assuming pure conductive heat transfer and a homogeneous and isotropic medium. Even in unusually hot basins, it is possible to determine geothermal anomalies relative to the average regional or local conditions characteristic to the basin that are assumed to have reached the state of equilibrium over geologic time.

6.2.2 Dimensionless parameters

The relative efficiency (ratio) of advective to conductive heat transfer caused by fluid flow in porous media is expressed by the dimensionless Péclet number (P_e):

$$P_e = \frac{\rho_w C q L}{\kappa} \quad (6.5)$$

where L = length of the flow-domain, the other terms were defined above. For a one-dimensional case the flux is $q = -K \frac{\Delta h}{\Delta z}$; if $L = \Delta z$, the Péclet number can be expressed as (Jessop, 1990; p. 256):

$$P_e = \frac{K \rho_w C \Delta h}{\kappa} \quad (6.6)$$

Forced convection is considered an efficient heat transfer mechanism when $P_e \geq 0.5$ (Bredehoeft and Papadopoulos, 1965), and it becomes dominant over conduction when

$P_e \geq 1$. Bredehoeft and Papadopoulos (1965) presented a one-dimensional solution of the heat transfer equation (6.3), by assuming steady-state conditions $\left(\frac{\partial T}{\partial t} = 0\right)$, negligible radioactive heat contribution ($A = 0$), only vertical fluid and heat flow across a semiconfining layer of thickness L with fixed temperatures at the top (T_0) and bottom (T_L) (Figure 6.2). Thus, the equation to be solved is:

$$\frac{\partial^2 T}{\partial z^2} - \frac{P_e}{L} \frac{\partial T}{\partial z} = 0 \quad (6.7)$$

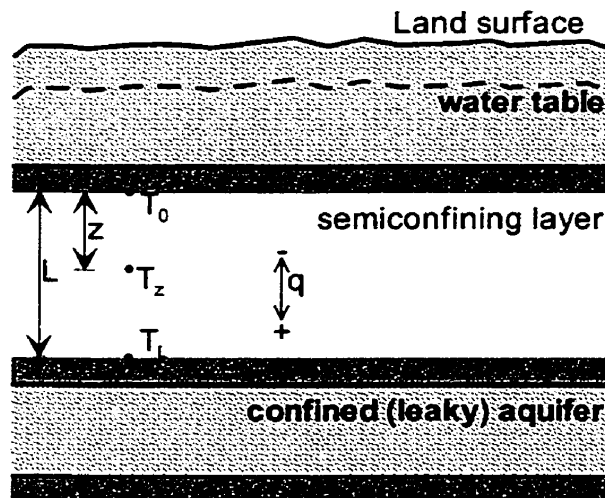


Figure 6.3. Sketch of a leaky aquifer (after Bredehoeft and Papadopoulos, 1965). T_0 , T_z , and T_L are measured temperatures; L is the thickness of the semiconfining layer; q is the vertical seepage across the semiconfining layer.

The solution to this problem is (Bredehoeft and Papadopoulos, 1965):

$$T_z = T_0 + (T_L - T_0) \frac{\exp\left(P_e \frac{z}{L}\right) - 1}{\exp(P_e) - 1} \quad (6.8)$$

where T_z is the temperature at an arbitrary depth z within the semiconfining layer; z ranges from 0 to L (Figure 6.3). They gave a graphical solution for equation (6.8), which consists of a set of type curves representing values of the Péclet number. The vertical seepage velocity can be estimated from a thermal profile of reliable temperature data and adequate values of thermal conductivity by matching plots of $(T_z - T_0)/(T_L - T_0)$ versus z/L to the type curves. The type curves for $P_e = -10, -2, -1.5, -1, -0.5, -0.1, 0, 0.1, 0.5, 1, 1.5, 2,$ and 10 were computed using equation (6.8) and are illustrated on Figure 6.4.

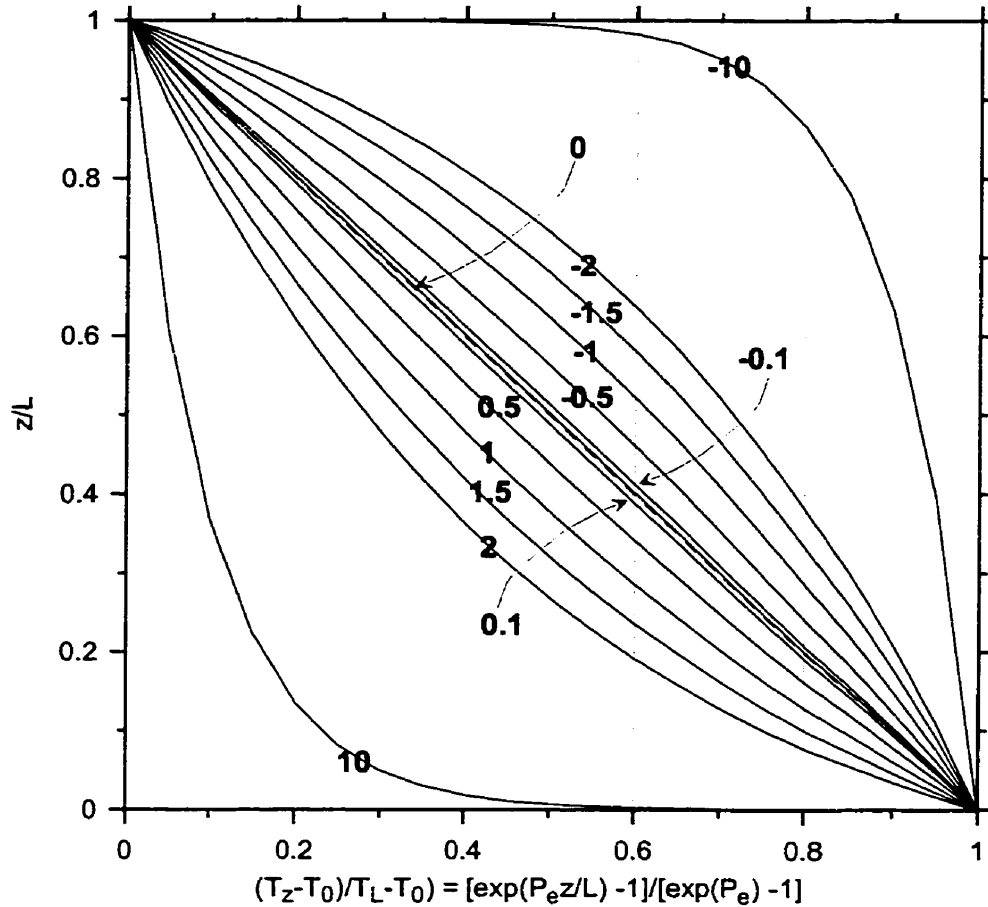


Figure 6.4. Type curves of Péclet numbers computed from equation (6.8).

A two dimensional analytical solution for advective heat transfer was presented by Domenico and Palciauskas (1973) for a homogeneous and isotropic medium, with steady state fluid flow. They showed that the dimensionless Péclet number is a representative relative measure of the advective and conductive flow only if it takes into account the geometry of the fluid flow system (length and depth). Accordingly, the dimensionless group becomes:

$$N_P = \frac{K \rho_w C \Delta h \Delta z_f}{2L\kappa} \dots\dots\dots (6.9)$$

where $\Delta h/2$ is the mean hydraulic head difference (or the mean water table elevation above the discharge area) across the basin of length L and depth Δz_f .

The magnitude of a threshold hydraulic conductivity (K) required for advection to become detectable and effective can be estimated from equation (6.6) and (6.9) as a

function of the total hydraulic head difference (Δh) and the basin geometry, respectively. A robust estimate of the threshold hydraulic conductivity (K) can be obtained by ignoring the fluid density variation caused by thermal expansion, and assuming the following parameter values: $\rho_w = 1000 \text{ kg/m}^3$, $C = 4180 \text{ J/kg } ^\circ\text{C}$; κ ranges between 1 – 4.5 W/m $^\circ\text{C}$, where $\kappa = 3 \text{ W/m } ^\circ\text{C}$ is a reasonable approximation for a porous medium dominated by sandstone; Δh varies between 1 – 1000 m; $\Delta z_f/L = 0.1$ (e.g., 1 km deep and 10 km long flow system) and 0.01 (e.g., 1 km deep and 100 km long flow system); consider P_e and N_p values of 0.1, 0.5, 1, and 10, respectively.

K versus Δh was computed for three scenarios: i) the one-dimensional case, using equation (6.6); and the two-dimensional case, using equation (6.9) for a flow system with ii) $\Delta z_f/L = 0.1$, and iii) $\Delta z_f/L = 0.01$. The results of the calculations are illustrated on Figure 6.5, 6.6, and 6.7, respectively. From these results it was concluded that:

- i) The threshold hydraulic conductivity required for advective heat transfer to become effective decreases as the hydraulic head difference across the domain increases.
- ii) Equation (6.6) underestimates the threshold hydraulic conductivity relative to solutions obtained using equation (6.9) (Domenico and Palciauskas, 1973).
- iii) The lower the depth/length ratio of a flow system in a drainage basin, the higher the threshold hydraulic conductivity necessary for efficient advective heat transfer, in agreement with Smith and Chapman (1983).

The dimensionless Rayleigh number (R_a), expresses the relative efficiency of free convection to conduction, and it is also derived from the heat transfer equation (equation 6.3):

$$R_a = \frac{\alpha K \rho_w C \Delta z^2 \text{grad} T}{\kappa} \quad (6.10)$$

where α denotes the fluid's coefficient of thermal expansion, Δz is the height of the convection cell (Jessop, 1990; p. 256).

For the initiation of natural convection, the Rayleigh number has to exceed a critical value, which depends on the boundary conditions and the hydraulic conductivity anisotropy. The vertical hydraulic conductivity is used for the estimation of R_a . Suggested critical values are $4\pi^2$ for an isotropic medium with isothermal boundaries (Lapwood, 1948; van der Kamp, 1984) and 27.1 for uniform basal heat flux (Deming,

1994/b). In an anisotropic medium, the R_a depends on the average vertical hydraulic conductivity, as it can be deduced from equation (6.10). High values of vertical hydraulic conductivity and geothermal gradient are favourable for the initiation of free convection. Intercalation of low permeability shale layers of >1 m thickness can significantly reduce the vertical permeability of a sandstone body, thus, keeping R_a below the critical value and inhibiting the initiation of free convection (Bjørlykke, 1994; Deming, 1994/b). Therefore, free convection is not believed to be common in sedimentary basins (Bjørlykke, 1994). In basins with indurated rockframework, where fracture networks are abundant, the importance of free convection may exceed the expectations; this topic is controversial yet and subject to ongoing investigation (J. M. Sharp, Jr., 2001, *written communication*).

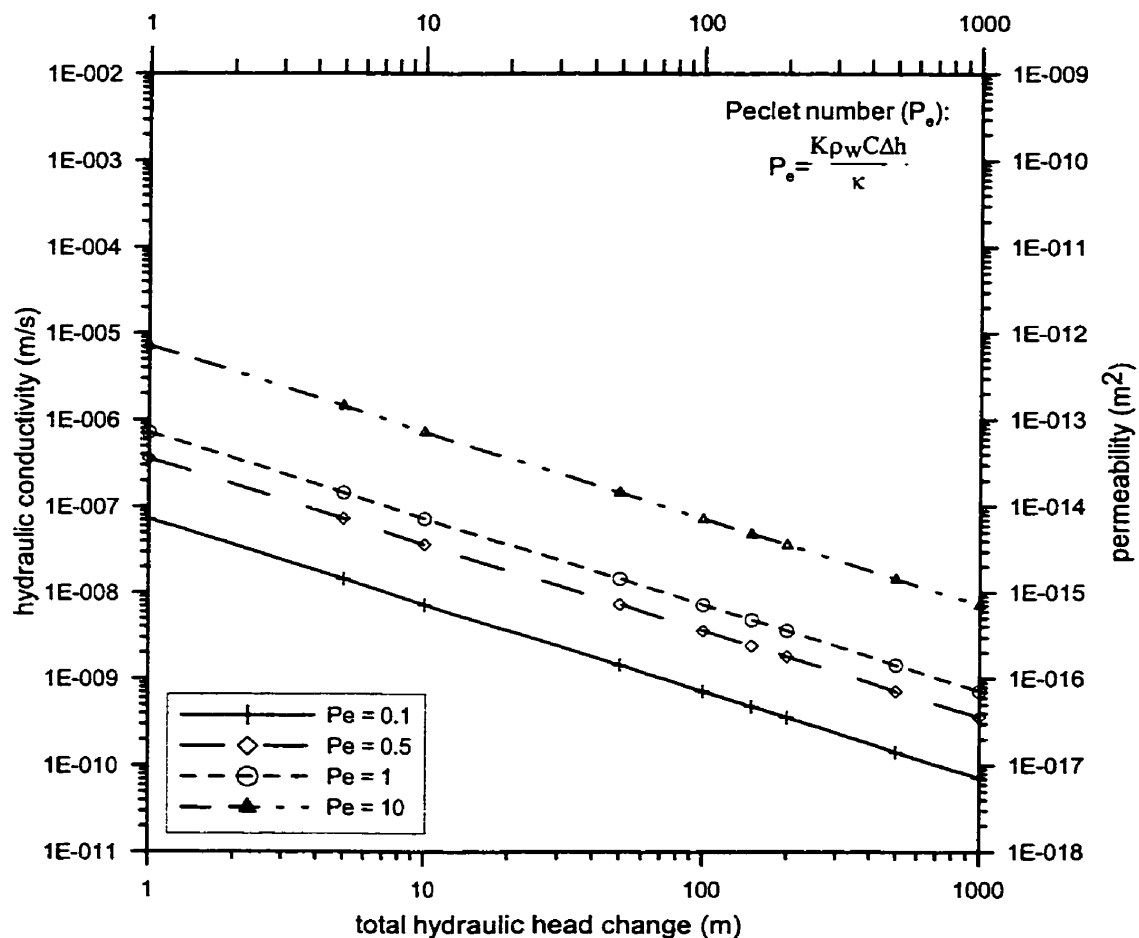


Figure 6.5: Influence of the hydraulic conductivity and total hydraulic head change on the importance of advective heat transfer estimated from the Péclet number (equation 6.6).

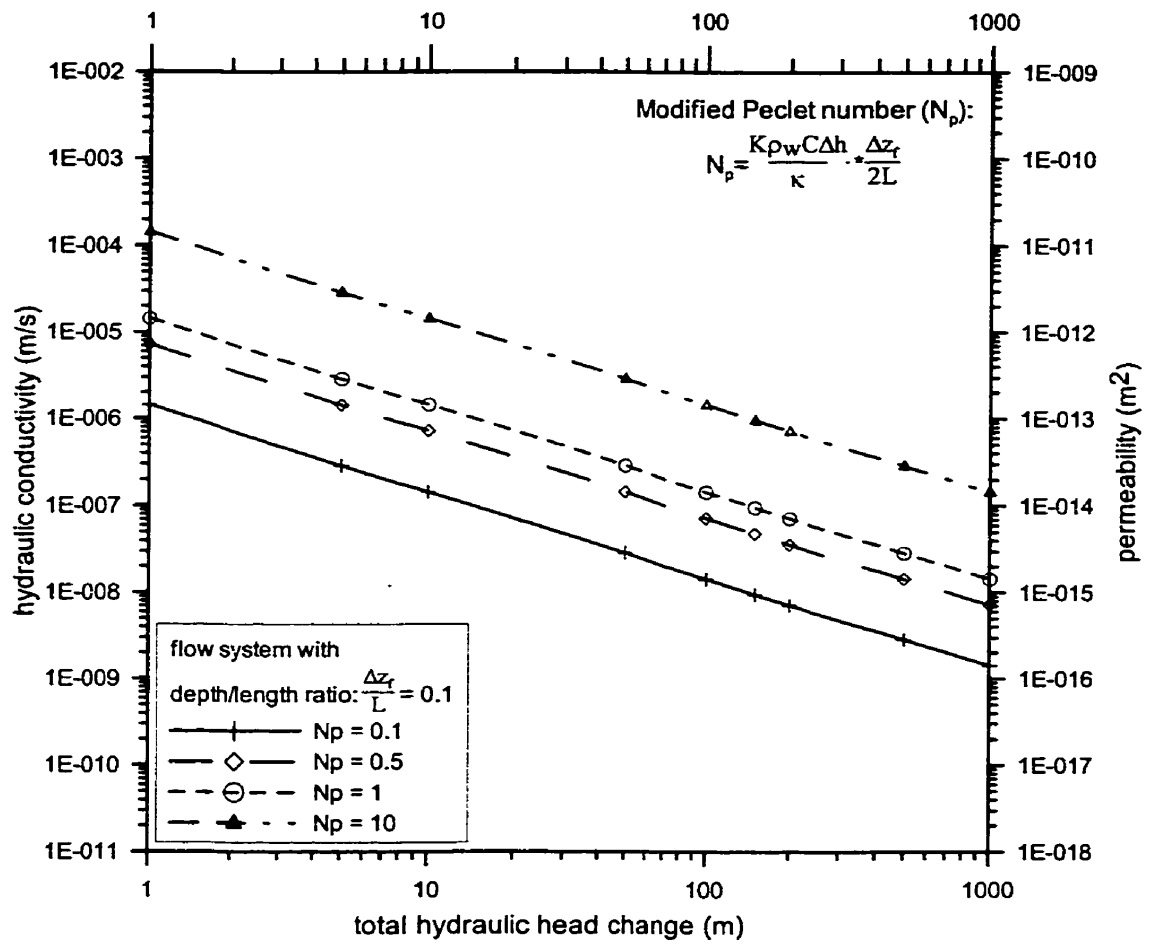


Figure 6.6: Influence of the hydraulic conductivity, total hydraulic head change, and the geometry of a flow system characterised by a depth/length ratio of 0.1 on the importance of advective heat transfer estimated from the modified Péclet number (equation 6.9).

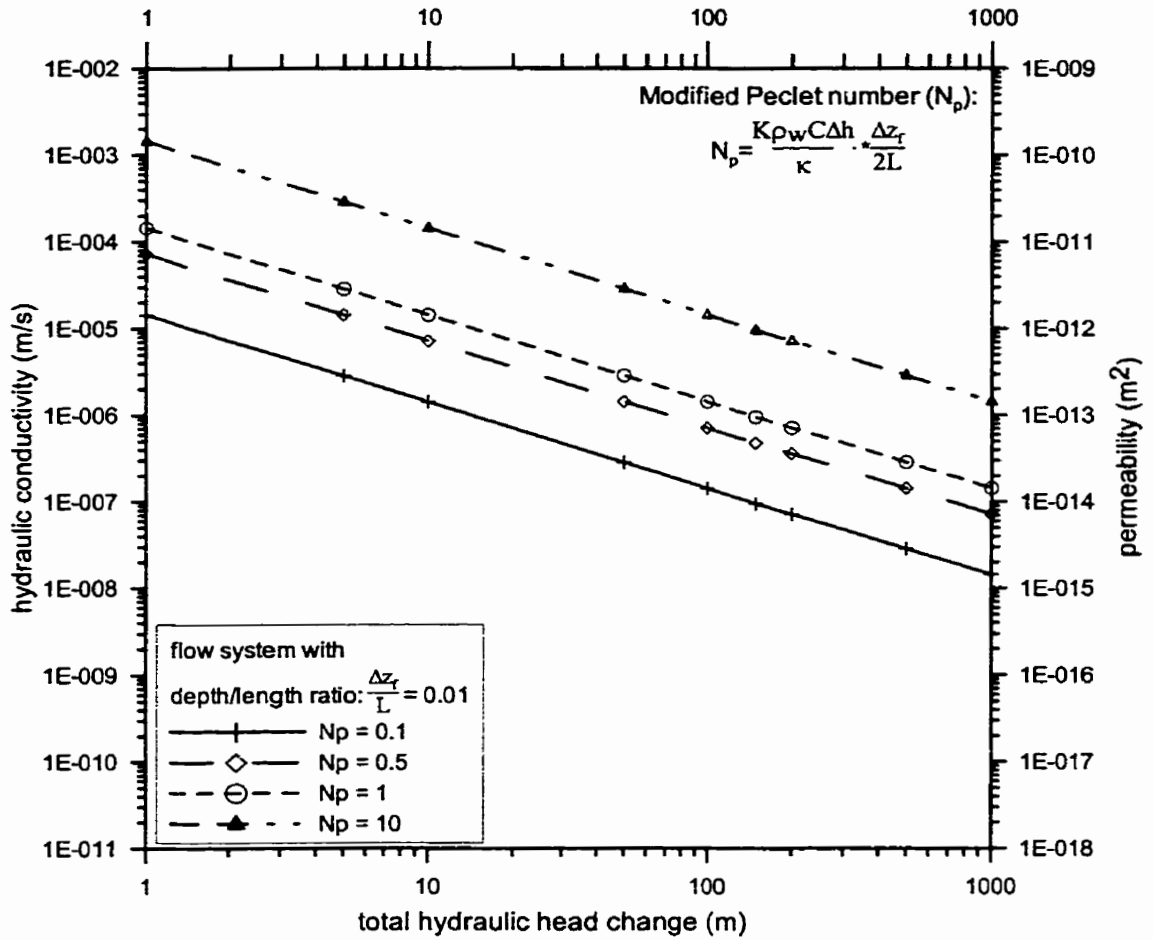


Figure 6.7: Influence of the hydraulic conductivity, total hydraulic head change, and the geometry of a flow system characterised by a depth/length ratio of 0.01 on the importance of advective heat transfer estimated from the modified Péclet number (equation 6.9).

6.2.3 Effects of sedimentation on heat flow

Deposition of cold sediments with low thermal conductivity has a transient cooling effect on the upper part of the crust, which increases with the rate and duration of sedimentation in a basin. The time required for the transient cooling effect to diminish can be approximated by the half-life of the sedimentation process (Lenkey, 1999):

$$t_{1/2} = \frac{\ln 2}{\pi^2 + \frac{P_{es}^2}{4}} \frac{l^2}{\omega} \quad (6.11)$$

where l = constant lithospheric thickness [L]; ω = thermal diffusivity [L^2/T]; P_{es} is the dimensionless Péclet number obtained as the ratio between heat transported by the

moving sediment and by conduction, where advection is caused by the subsidence of the deposited sediment. To approach the stationary state, the duration of sedimentation must be at least double the half-life. For instance, a 7000 m thick clastic layer deposited over 17 – 19 Myr may absorb as much as 30% of the conductive heat flow (Posgay et al., 1995). The half-life of a thermal transient effect caused by an average sedimentation rate of 450 m/Myr is ~32 Myr (Lenkey, 1999). This example is encountered in the deep (>6500 m) sub-basins of the Pannonian Basin. Thus, the Neogene sediments deposited in the Pannonian Basin during the last 17 Myr did not reach thermal equilibrium with their surroundings, i.e., the clastic sedimentary pile did not heat up to the nominal equilibrium temperature (Lenkey, 1999).

6.2.4 Regional scale heat transfer and groundwater flow

Regional scale heat transfer in sedimentary basins is largely controlled by the rates of groundwater flow and uplift or subsidence of the basins (e.g., Ingebritsen and Sanford, 1998; pp. 117-121). In basins with sufficiently low rates of groundwater flow and uplift/subsidence, conductive heat transfer dominates the thermal regime. Domenico and Palciauskas (1973) demonstrated that superposition of a sufficiently vigorous gravity-driven flow field on the thermal field of a basin can perturb the conductive field, rendering significance to advective heat transfer. As a result, the isotherms will be depressed under the elevated recharge areas and raised under the discharge areas. That is, in regions of descending flow, thermal gradients increase with depth causing negative heat-flow anomalies, whereas in regions of ascending flow, they decrease with depth causing positive heat-flow anomalies. Disturbances of the temperature field caused by groundwater flow are usually reflected by the bending of isotherms in the direction of flow and lack of conformity of the isotherms with the land surface (Smith and Chapman, 1983; Garven and Freeze, 1984). However, the two-dimensional geometric pattern of isotherms and thermal gradients may also be influenced by contrasts in the hydraulic and thermal properties of the porous medium. Thus, a simple qualitative interpretation of geothermal maps and cross sections can be quite misleading.

The Péclet number (equation 6.4 or 6.5) and its modified expression (equation 6.9) can be used for quantitative evaluation of the dominant regional and local heat

transfer mechanism, i.e., conductive or advective. In most regional scale field studies there is uncertainty regarding appropriate values of hydraulic conductivity and thermal conductivity of stratigraphic units, as both parameters are scale-dependent. The hydraulic conductivity of rocks can vary within at least thirteen orders of magnitude (Freeze and Cherry, 1979; p. 29, Table 2.2), while the thermal conductivity of rocks merely varies within a factor of 5 (Domenico and Mifflin, 1965). From the expressions of the Péclet number (equation 6.6 and 6.9) it is clear that subjective selection of hydraulic conductivity values of differing order of magnitude greatly influences the final decision about the conductive or advective nature of heat transfer. Thus, interpretation of regional scale heat transfer by groundwater flow and related geologic phenomena are controversial due to these uncertainties (e.g., the Western Canada Sedimentary Basin; Hitchon, 1984; Majorowicz et al., 1985; Bachu, 1988; Garven, 1989; Majorowicz, 1989).

6.2.5 Geologic manifestations of advective heat transport

The geothermal conditions and, implicitly, groundwater flow, as the transport agent of heat and matter, largely control the formation of certain mineral ore deposits, such as lead, zinc, copper, iron, mercury, tin sulphides, uranium, etc. (e.g., Garven et al., 1993, Raffensperger and Garven, 1995), as well as hydrocarbon generation, migration, and accumulation (e.g., Garven, 1989, Person and Garven, 1992). In the Pannonian Basin, the possible relationship between advective heat transport and hydrocarbon generation and accumulation are of particular interest.

Person and Garven (1992) demonstrated that regional groundwater flow could significantly modify the position of the oil-window relative to its position in a conductive regime (i.e., in the absence of groundwater flow). Even for modest flow velocities in the order of 0.4 to 4 mm/a and $P_e = 0.3$, the position of the oil-window can be significantly altered by gravity-driven flow in the recharge versus discharge area, given sufficient time for the process to be completed (Person et al., 1996).

Positive geothermal anomalies observed in the vicinity of hydrocarbon accumulations in regions that are also characterised by ascending or convergent flow can likewise be attributed to advective heat transport (e.g., Stegena, 1963; Ben Dhia, 1987). According to the hydraulic theory of petroleum migration (Tóth, 1980), preferential sites

of petroleum accumulations are the locations of fluid-potential minima, mostly discharge areas, which are expected to be associated with local positive geothermal anomalies.

6.3 METHODS OF CHARACTERISATION OF THE GEOTHERMAL FIELD

The methods applied for the characterisation of the geothermal field are analogous in some respects to those applied for the fluid-potential field described in 4.2.1., i.e., temperature-depth (T(d)) profiles, tomographic temperature distribution maps, and regional geothermal cross sections. In order to identify any potential correlation between the groundwater flow field and the geothermal field, the graphical representation of the two fields has to allow their comparison, i.e., the elevation interval of the tomographic maps, the trace of the cross sections, and the location of profiles ($p(z)$ and $T(d)$) must be the same. The location of sites selected for construction of T(d) profiles is illustrated in Figure 6.8. The sites were selected to illustrate temperature versus depth distribution patterns observed in elevated recharge areas (Kecskemét and Kiskunhalas-Tázlár), low-lying discharge areas (Szeged-Algyő, Szentes – Csongrád, Endrőd – Szarvas, Dévaványa, Biharkeresztes), and zones with contrasting thickness of Neogene clastic sediments. T(d) profiles permit a one-dimensional analysis of the thermal field. Regression lines fitted on a plot of spatially scattered data do not yield a rigorously valid temperature gradient, similar to the $p(d)$ and $p(z)$ profiles (Maccagno, 1991). Data from several wells can be plotted on the same profile for a lumped T(d) profile analysis, whereas for a distributed T(d) profile analysis, data from a single well should be used. Lumped analysis of a parameter may yield qualitative information, while a distributed analysis permits derivation of meaningful qualitative and quantitative results.

The tomographic isotherm and the thermal gradient maps were prepared for the same elevation intervals as the fluid-potential maps (Figure 4.3). Because of the limitations of the temperature data distribution, only the $z = -100$ to -2800 m elevation interval was mapped. A code was assigned to each map according to the elevation of its bounding surfaces, $T_{i,j}$ and $\text{grad } T_{i,j}$, where i and j represent the *hundreds of meters below sea level of the top and the bottom boundary surface, respectively* of each slice (Table 6.1) and the maps are referred to by their codes hereafter.

Only discrete temperature values were available for this study (Chapter 3), although temperature logs would have been ideal. Temperature and geothermal gradient values for each slice were posted with SURFER 6 using distinctive symbols according to the quality class of the data (1 = best, 2 = good, and 3 = average; after Dövényi and Horváth, 1988) to facilitate their interpretation during manual contouring. Subsequently, the contour lines were digitised to enable their reproduction at any desired scale.

On the thermal gradient maps the posted *grad T* values were calculated with reference to the corrected mean annual temperature at the land surface taken from Pécsi (1989). The average thermal gradients calculated for the elevation intervals of the tomographic maps are listed in Table 6.1.

Table 6.1: Codes of geothermal maps with mean temperature and mean gradient values.

Elevation interval (m a.s.l.)	Isotherm Map	grad T Map	Mean T (°C)	Mean grad T (°C/km)
-100 to -300	T _{1,3}	Grad T _{1,3}	30.1	57.5
-300 to -600	T _{3,6}	Grad T _{3,6}	36.5	52
-600 to -1000	T _{6,10}	Grad T _{6,10}	58.9	54.8
-1000 to -1500	T _{10,15}	Grad T _{10,15}	81.2	53.5
-1500 to -1900	T _{15,19}	Grad T _{15,19}	104.7	51
-1900 to -2200	T _{19,22}	Grad T _{19,22}	112.4	47.7
-2200 to -2500	T _{22,25}	Grad T _{22,25}	126.2	47.3
-2500 to -2800	T _{25,28}	Grad T _{25,28}	139	47.3
Z < -2800			157.8	42.1

The traces of the geothermal cross sections **T1(L,z)**, **T2(L,z)**, **T3(L,z)**, and **T4(L,z)** (Figures 6.34, 6.35, 6.36, and 6.37) coincide with the traces of the hydraulic cross sections **H1**, **H2**, **H3**, and **H4**, respectively, presented in Chapter 4 (Figures 4.33, 4.34, 4.35, and 4.36). The temperature values were projected onto the geothermal cross sections from a maximum of 5 km horizontal distance from either side of the cross section. This relatively large projection distance was a necessity imposed by the scarcity

of data. The boundaries of the hydrostratigraphic units and the location of major faults dissected by the cross sections also are plotted on each geothermal cross section.

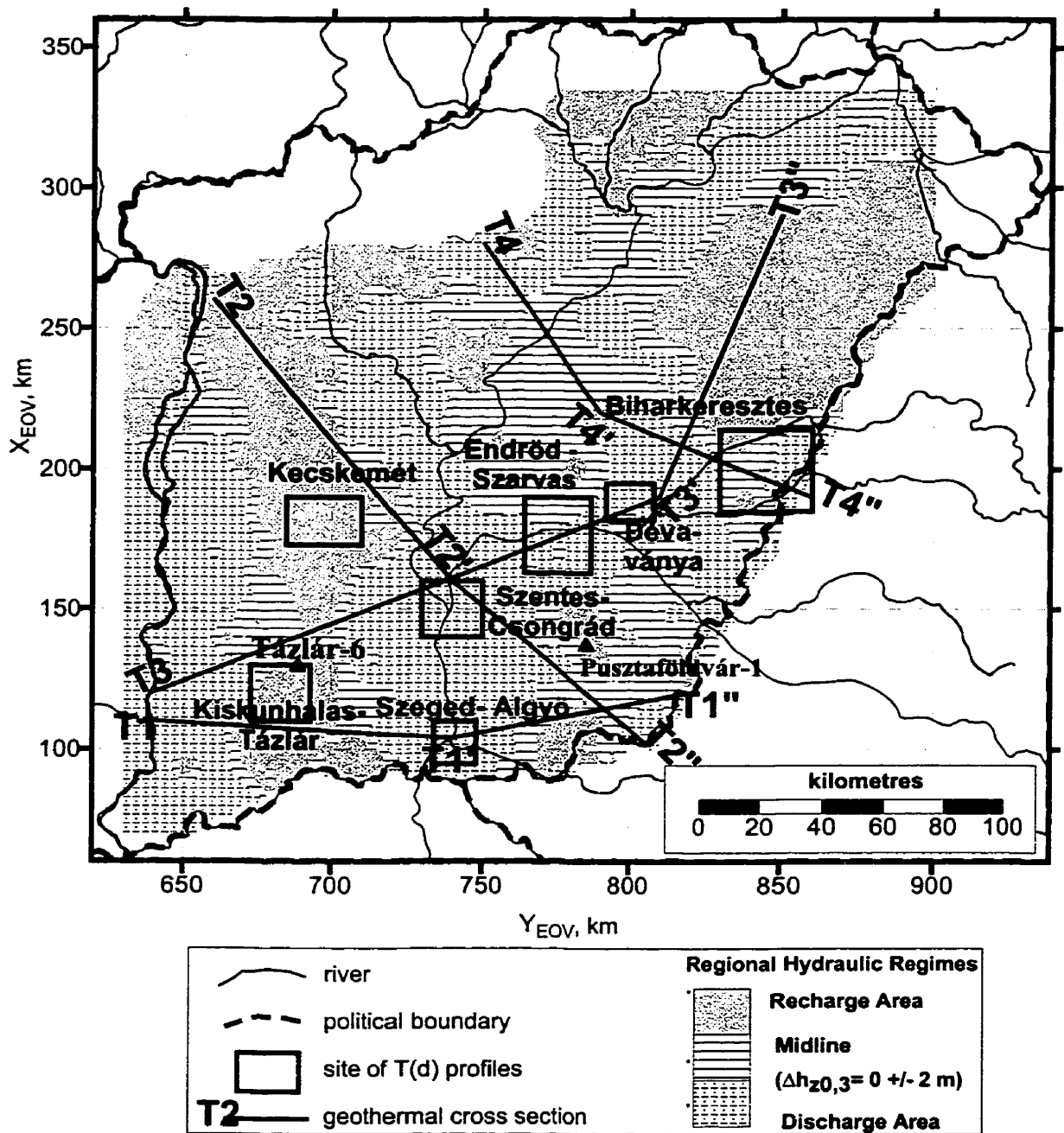


Figure 6.8. Index map of temperature versus depth profiles and traces of geothermal cross sections.

6.4 RESULTS AND DISCUSSION

6.4.1 General observations and interpretations

The regional geothermal field of the Great Hungarian Plain is presented below on eight selected temperature-depth profiles (Figures 6.10 through 6.17), eight tomographic isotherm maps (Figures 6.18 through 6.25) and geothermal gradient maps (Figures 6.26 through 6.33), and four regional geothermal cross sections (Figures 6.34 through 6.37).

6.4.1.1 Temperature vs. depth profiles ($T(d)$):

The average geothermal gradient in the Great Hungarian Plain is $50\text{ }^{\circ}\text{C}/\text{km}$ (Figure 6.9), based on 1562 measurements from the basin. This average thermal gradient is used as reference (or nominal) gradient on the $T(d)$ profiles presented below.

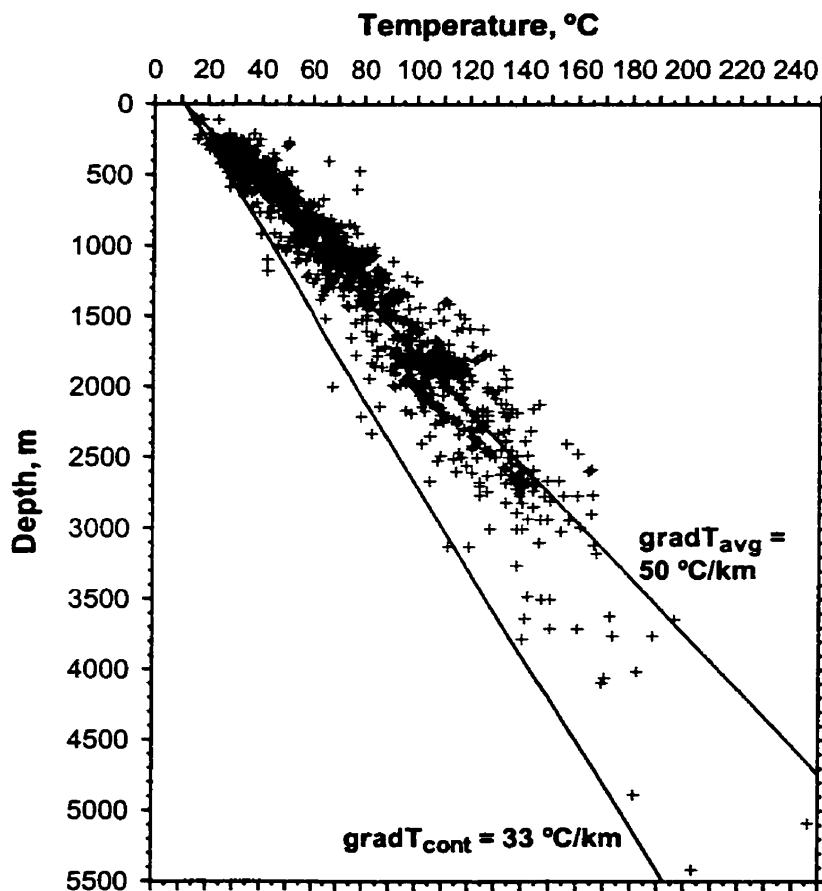


Figure 6.9 :

Temperature vs. depth plot, Eastern Hungary; coordinates: $X_{EOV} = 60 - 360$ km; $Y_{EOV} = 620 - 940$ km; $z_0 = 78 - 250$ m a.s.l. (data from Dövényi and Horváth, 1988). $grad T_{cont}$ is the continental average thermal gradient; $grad T_{avg}$ is the mean thermal gradient in Eastern Hungary.

Kecskemét region (Figures 6.8 and 6.10): Location: $X_{EOV} = 173 - 190$ km; $Y_{EOV} = 685 - 710$ km; the altitude of the area is $z_0 > 117$ m a.s.l., and it is located in the Duna – Tisza Interfluve region, a regional recharge area (Chapter 4). The temperatures were measured in the Nagyalföld and Mid-Miocene Aquifers. The top of the Pre-Neogene basement is at a depth of 1100 to 1600 m at most tested wellsites.

The measured temperature values plot below the nominal gradient line; the best-fit thermal gradient for this region is 48 °C/km. In the 600 to 1100 m depth interval three measurements are below the nominal value by $\Delta T = T_{nom} - T_{obs} = -10$ to -15 °C. This anomaly may be the result of cooling caused by descending meteoric water, or that of thermal disequilibrium, i.e., the measurements were made relatively soon after well completion, thus, the formation fluids could not reach thermal equilibrium. The latter possibility is most likely not valid, because only steady-state temperature values were retained in the database (Section 3.4 and Dövényi and Horváth, 1988). The average thermal gradients calculated from the data obtained in different wells and lumped on this profile are between 35 and 50 °C/km, suggesting cooling by meteoric water, in support of the first possible explanation mentioned above.

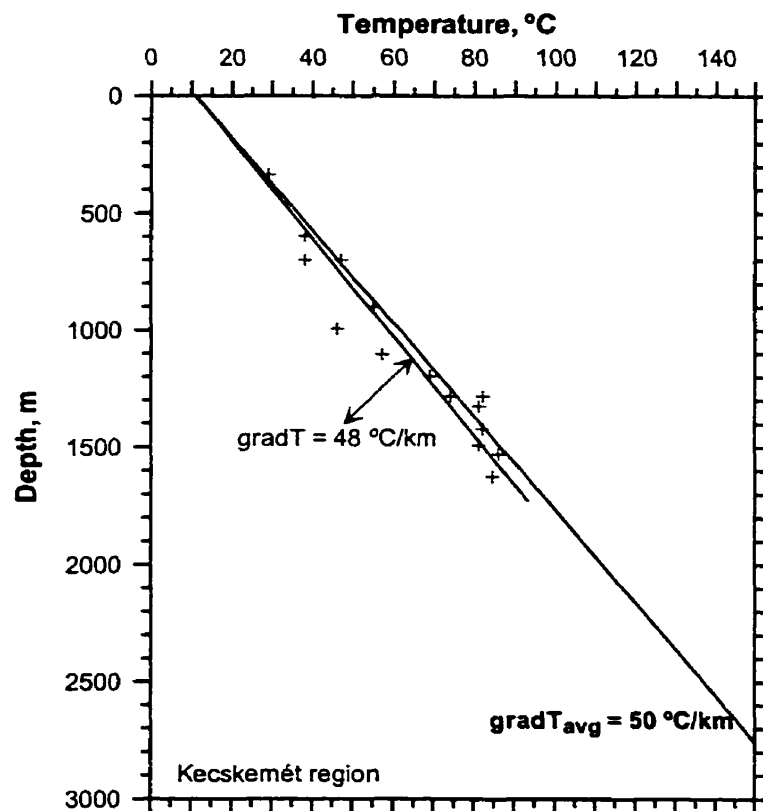


Figure 6.10:
Temperature vs. depth plot, Kecskemét region (coordinates: $X_{EOV} = 173 - 190$ km; $Y_{EOV} = 685 - 710$ km; $z_0 > 117$ m a.s.l. Data from Dövényi and Horváth, 1988. For location see Figure 6.8.

Kiskunhalas – Tázlár region (Figures 6.8 and 6.11): Location: $X_{EOV} = 110 - 130$ km; $Y_{EOV} = 673 - 693$ km; the altitude of the area is $z_0 = 120 - 140$ m a.s.l. and it is located in the Duna – Tisza Interfluve region, a regional recharge area (Chapter 4). The temperatures were measured in the Nagyalföld Aquifer, Algyő and Endrőd Aquitards, and the Mid-Miocene Aquifer. The top of the Pre-Neogene basement is at a depth of 1800 to 2700 m at most tested wellsites.

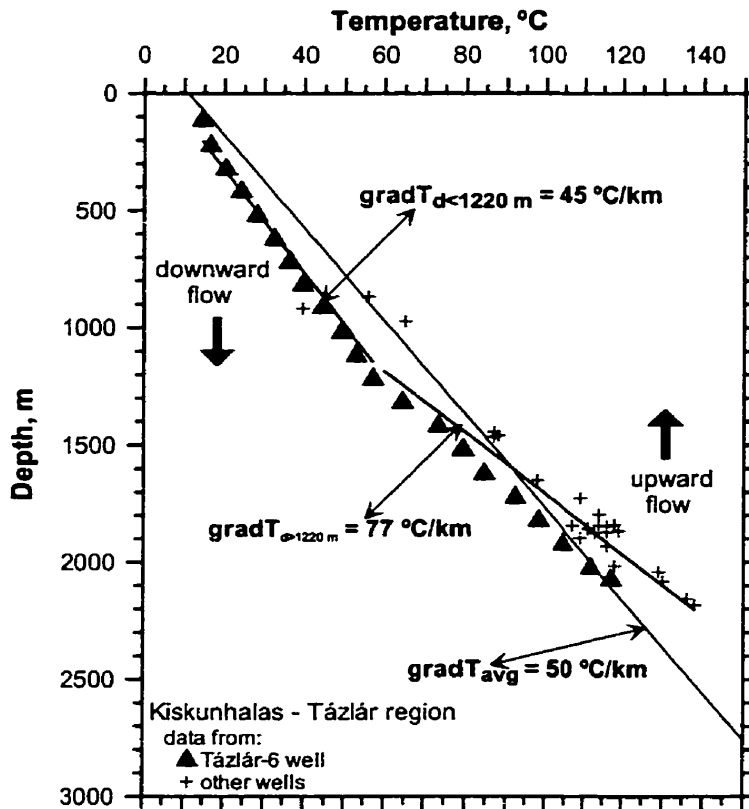


Figure 6.11:

Temperature vs. depth plot, Kiskunhalas - Tázlár region (co-ordinates: $X_{EOV} = 110 - 130$ km; $Y_{EOV} = 673 - 693$ km; $z_0 = 120 - 140$ m a.s.l.). Data from Dövényi and Horváth, 1988. For location see Figure 6.8. Tázlár-6 well: $X_{EOV} = 128$ km; $Y_{EOV} = 688$ km; $z_0 = 120$ m a.s.l.

The temperatures increase steadily at an average thermal gradient of $\text{grad } T_{d < 1220 \text{ m}} = 45 \text{ °C/km}$ to a depth of ~ 1220 m, where the thermal gradient increases abruptly to $\text{grad } T_{d > 1220 \text{ m}} = 77 \text{ °C/km}$. Under steady state conditions, assuming that heat transfer is achieved by pure conduction, such an abrupt increase in $\text{grad } T$ would require a commensurate decrease in thermal conductivity of the deeper rocks. Thus, the conductive heat flow should be the same in the two depth intervals. We obtain (from equation 6.2):

$$\frac{K_{d < 1220 \text{ m}}}{K_{d > 1220 \text{ m}}} = \frac{\text{grad } T_{d > 1220 \text{ m}}}{\text{grad } T_{d < 1220 \text{ m}}} = \frac{77}{45} = 1.71$$

where $\kappa_{d < 1220m}$ and $\kappa_{d > 1220m}$ are the average thermal conductivities of rocks in the upper 0 to 1220 m depth interval and below 1220 m depth, respectively. This requirement is not satisfied in reality, because the thermal conductivity of deeper rocks actually increases (e.g., Dövényi and Horváth, 1988). Therefore, the observed temperature distribution pattern is most likely caused by advective heat transport, provided there is vertical groundwater flow of sufficient vigour. Indeed, there is vertical groundwater flow in this region, as it was deduced from the $p(z)$ profile of the Kiskunhalas region (Figure 4.8, p. 84). It was shown in Chapter 4, that in the zone of $z > -1700$ m elevation ($\sim d < 1560$ m depth range), groundwater flow is directed downward, whereas below $z = -1700$ m, groundwater flow is directed upward. Thus, the most plausible explanation of the observed temperature – depth distribution pattern in the Kiskunhalas-Tázlár region is advective heat transport, i.e., in the upper zone ($d < 1220$ m) descending meteoric water caused cooling (sub-nominal thermal gradient), while the deeper super-nominal gradient is the result of ascending water.

Szeged – Algyő region (Figures 6.8 and 6.12): Location: $X_{EOV} = 95 - 110$ km; $Y_{EOV} = 734 - 748$ km; the altitude of the area is $z_0 = 78-85$ m a.s.l. The temperatures were measured in the Nagyalföld Aquifer, Algyő Aquitard, and the Szolnok Aquifer. The top of the Pre-Neogene basement is at a depth of 2500 to 3400 m at most tested wellsites.

The temperature data plot predominantly below the reference thermal gradient line. Apparently, there is a difference in the rate of temperature increase with depth between the $d = 0$ to 1200 m and the $d > 1500$ m depth ranges. In the upper zone, the best-fit thermal gradient is $\text{grad } T_{d < 1200 \text{ m}} = 46$ °C/km, while in the lower zone, it is $\text{grad } T_{d > 1500 \text{ m}} = 55$ °C/km. Assuming steady state conditions and pure heat conduction, this abrupt change in the slope of the thermal gradient would imply that the thermal conductivity of the lower zone must be about 0.84 times that of the upper zone. This requirement is not satisfied, therefore, advective heat transport and/or artificial perturbations of the thermal field can be invoked to explain the observed $T(d)$ pattern. It was shown in Chapter 4 (Figure 4.9, p. 85) that this region is characterised by ascending flow –it is in a regional discharge area (Figure 6.8). Here, the thermal gradient should increase upward, if ascending groundwater flow is sufficiently vigorous to advect heat (Domenico and Palciauskas, 1973), yet the thermal gradient decreases upward.

Differences in measured temperatures as large as $\Delta T = 10 - 30 \text{ }^\circ\text{C}$ can be observed below $d = 1900 \text{ m}$. Such magnitude of temperature differences at similar depths and within less than 15 km lateral distance is most likely the result of advective heat transport by water ascending at different rates along discrete pathways, such as fracture zones or faults, provided local heat sources can be excluded. To explain the up to $15 \text{ }^\circ\text{C}$ difference in measured temperatures at about the same depths within the $d = 0$ to $\sim 1200 \text{ m}$ depth interval, it is also important to consider the possibility of artificial perturbation of the thermal field caused by extensive production of thermal water and injection of water. Indeed, in the Szeged - Algyő region, thermal water is being extracted for wide public, agricultural, and industrial use since the late 1950's (e.g., Liebe, 1993), and water injection in the petroleum production wells is also common practice, which started in the 1970's (I. Révész, 1999, *personal communication*).

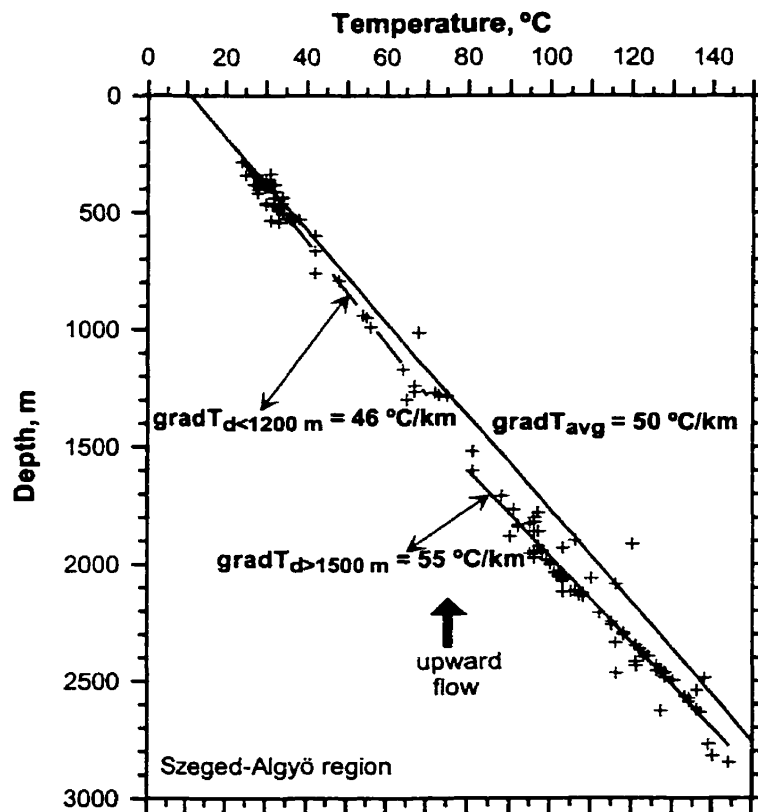


Figure 6.12:

Temperature vs. depth plot, Szeged-Algyő region (coordinates: $X_{EOV} = 95 - 110 \text{ km}$; $Y_{EOV} = 737 - 748 \text{ km}$; $z_0 = 78-85 \text{ m a.s.l.}$). Data from Dövényi and Horváth, 1988. For location see Figure 6.8.

Szentes – Csongrád region (Figures 6.8 and 6.13): Location: $X_{EOV} = 140 - 160$ km; $Y_{EOV} = 730 - 750$ km; the altitude of the area is $z_0 = 80 - 90$ m a.s.l. The majority of the data were measured in the Nagyalföld Aquifer. The top of the Pre-Neogene basement is at a depth of 3200 to 3300 m at most tested well-sites.

The majority of temperature measurements plot below the nominal gradient line and show a steady increase with depth at an apparent average gradient of $grad T = 44$ °C/km, suggesting steady state conditions. The $\Delta T = 23$ °C wide scatter of temperature data at depths below $d = 1700$ m is intriguing; it is difficult to explain this in terms of steady state conductive heat transport, yet it leads to uncertainty regarding its possible causes. Perhaps the combined effect of thermal conductivity heterogeneity and advection caused by vertical fluid movement along adjacent fracture zones may explain the observed anomalous phenomenon.

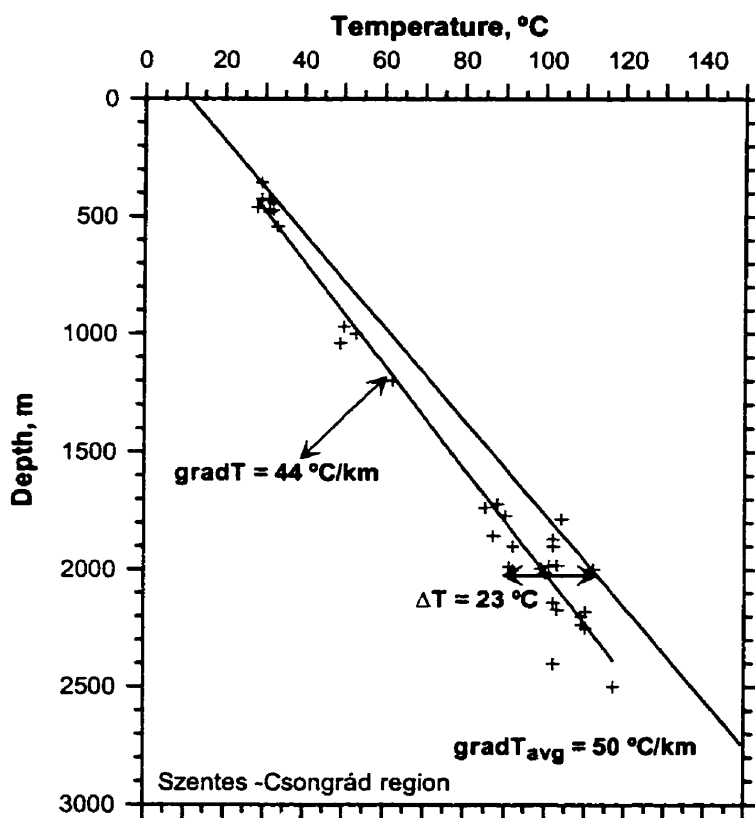


Figure 6.13:

Temperature vs. depth plot, Szentes -Csongrád region (coordinates: $X_{EOV} = 140 - 160$ km; $Y_{EOV} = 730 - 750$ km; $z_0 = 80 - 90$ m a.s.l.). Data from Dövényi and Horváth, 1988. For location see Figure 6.8.

Endrőd – Szarvas region (Figures 6.8 and 6.14): Location: $X_{EOV} = 163 - 190$ km; $Y_{EOV} = 764 - 787$ km; the altitude of the area is $z_0 = 83 - 101$ m a.s.l. The temperatures were measured in every hydrostratigraphic unit. The top of the Pre-Neogene basement is at a depth of 2700 to 3300 m at most tested wellsites.

In the upper $d = 0$ to 1600 m depth range, the measurements plot above the reference temperature gradient line, and they show a steady increase versus depth at a best fit gradient of $\text{grad } T_{d < 1600 \text{ m}} = 56 \text{ }^\circ\text{C/km}$. At depths greater than $d = 1700$ m, the measurements from wells drilled at Szarvas and Gyoma plot predominantly below the mean thermal gradient line, while those from Endrőd plot above the mean gradient line. The apparent thermal gradient at Szarvas is approximately $\text{grad } T_{\text{app}} = 36 \text{ }^\circ\text{C/km}$. At Szarvas, the difference between temperatures measured at $d = 2600$ m and at $d = 3000$ m is $\Delta T = 26 \text{ }^\circ\text{C}$.

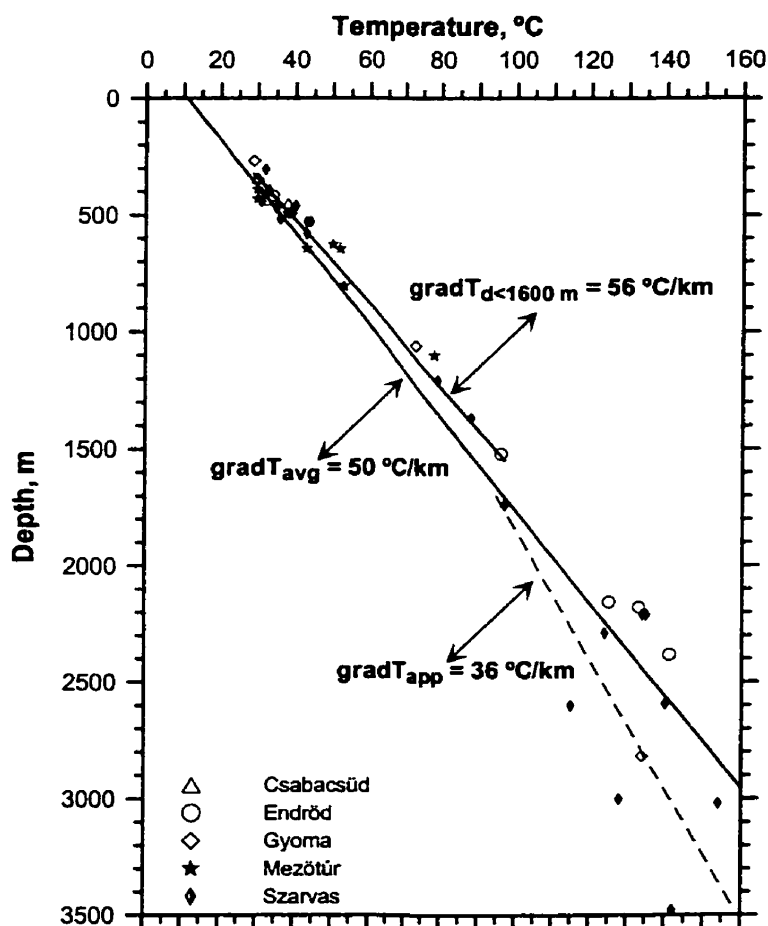


Figure 6.14:

Temperature vs. depth plot, Endrőd-Szarvas region. (coordinates: $X_{EOV} = 163 - 190$ km; $Y_{EOV} = 764 - 787$ km; $z_0 = 83 - 101$ m a.s.l.). Data from Dövényi and Horváth, 1988. For location see Figure 6.8.

The dramatic upward increase in the slope of the apparent thermal gradient lines suggests advective heat transport by ascending fluid flow. The $T(d)$ pattern of data from Szarvas at depths greater than 2000 m suggests advective heat transport by water ascending with different seepage rates along discrete pathways, most probably along connected fractures or faults. Indeed, the $p(z)$ profile prepared for this region (Figure 4.12, p. 90) indicated ascending fluid flow in the entire tested elevation (depth) range, i.e., gravity-driven ascending flow in the upper 0 to ~2000 m depth range and from the underlying confined overpressured zone. Although the vertical seepage velocity could not be estimated from the $p(z)$ profile for any elevation range, the hydrodynamic conditions for ascending fluid flow are ascertained here. In conclusion, advection seems to be an important mechanism in the local heat distribution, yet conduction may be the dominant heat transfer mechanism here.

Déaványa region (Figures 6.8 and 6.15): Location: $X_{EOV} = 182 - 195$ km; $Y_{EOV} = 792 - 808$ km; the altitude of the area is $z_0 = 84 - 92$ m a.s.l. The temperatures were measured in the Nagyalföld, Szolnok, and mid-Miocene Aquifers. The top of the Pre-Neogene basement is at a depth of 2200 to 2900 m at most tested wellsites.

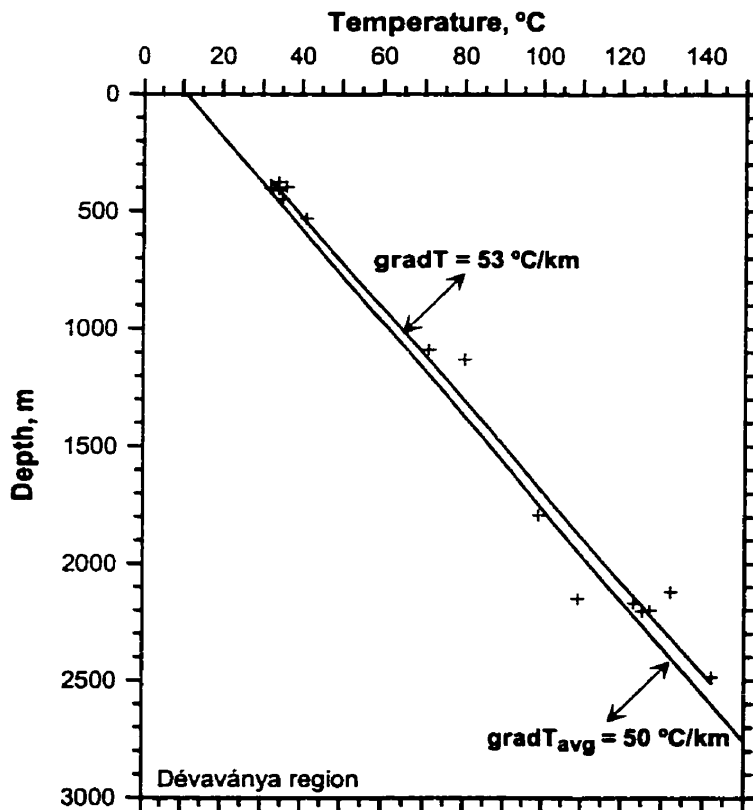


Figure 6.15:

Temperature vs. depth plot, Déaványa region (co-ordinates: $X_{EOV} = 182 - 195$ km; $Y_{EOV} = 792 - 808$ km; $z_0 = 84 - 92$ m a.s.l.). Data from Dövényi and Horváth, 1988. For location see Figure 6.8.

The measurements plot predominantly (with two exceptions) above the reference thermal gradient line; the best-fit average thermal gradient of this region is $\text{grad } T = 53 \text{ }^\circ\text{C}/\text{km}$. In the upper $\sim 1000 \text{ m}$ depth range, only a slight scatter of data along the local average gradient can be observed; this scatter augments to about $\Delta T = 26 \text{ }^\circ\text{C}$ at $\sim 2100 \text{ m}$ depth. The minor scatter of data in the upper zone is most likely due to thermal conductivity heterogeneity and minor advective perturbations. The large scatter of data at depths greater than $d = 1700 \text{ m}$ is due to locally significant advection caused by water ascending along discrete pathways. The hydrodynamic conditions necessary for water flow are given in this region (Chapter 4, Figure 4.13); thus, it is plausible to explain local anomalies in terms of advective perturbation.

Biharkeresztes region (Figures 6.8 and 6.16): Location: $X_{\text{EOV}} = 185 - 214 \text{ km}$; $Y_{\text{EOV}} = 830 - 860 \text{ km}$; the altitude of the area is $z_0 = 87 - 100 \text{ m a.s.l.}$ The temperatures were measured in the Nagyalföld Aquifer. The top of the Pre-Neogene basement is at a depth of 2300 to 2800 m at most tested wellsites.

The measurements are scattered in a $\Delta T \approx 15 \text{ }^\circ\text{C}$ wide band along the reference thermal gradient line; the best-fit average gradient is $56 \text{ }^\circ\text{C}/\text{km}$ in this region. The data from the Ártánd well show an increase of the thermal gradient upwards, suggesting advective effects of ascending water flow superimposed on conductive heat transfer. The thermal gradients calculated relative to the mean surface temperature also show a tendency of increasing upward, which suggests advection. The hydrodynamic conditions required for ascending groundwater flow are given here (Chapter 4, Figure 4.15, p. 94); the dynamic pressure gradient in the upper $\sim 1500 \text{ m}$ zone is slightly super-hydrostatic ($\gamma_{z > -1400 \text{ m}} = 10.1258 \text{ MPa}/\text{km}$). The vertical seepage velocity is probably not sufficiently high to cause predominantly advective heat transfer in this region, yet advection is detectable whereas conductive heat transfer is the dominant mechanism.

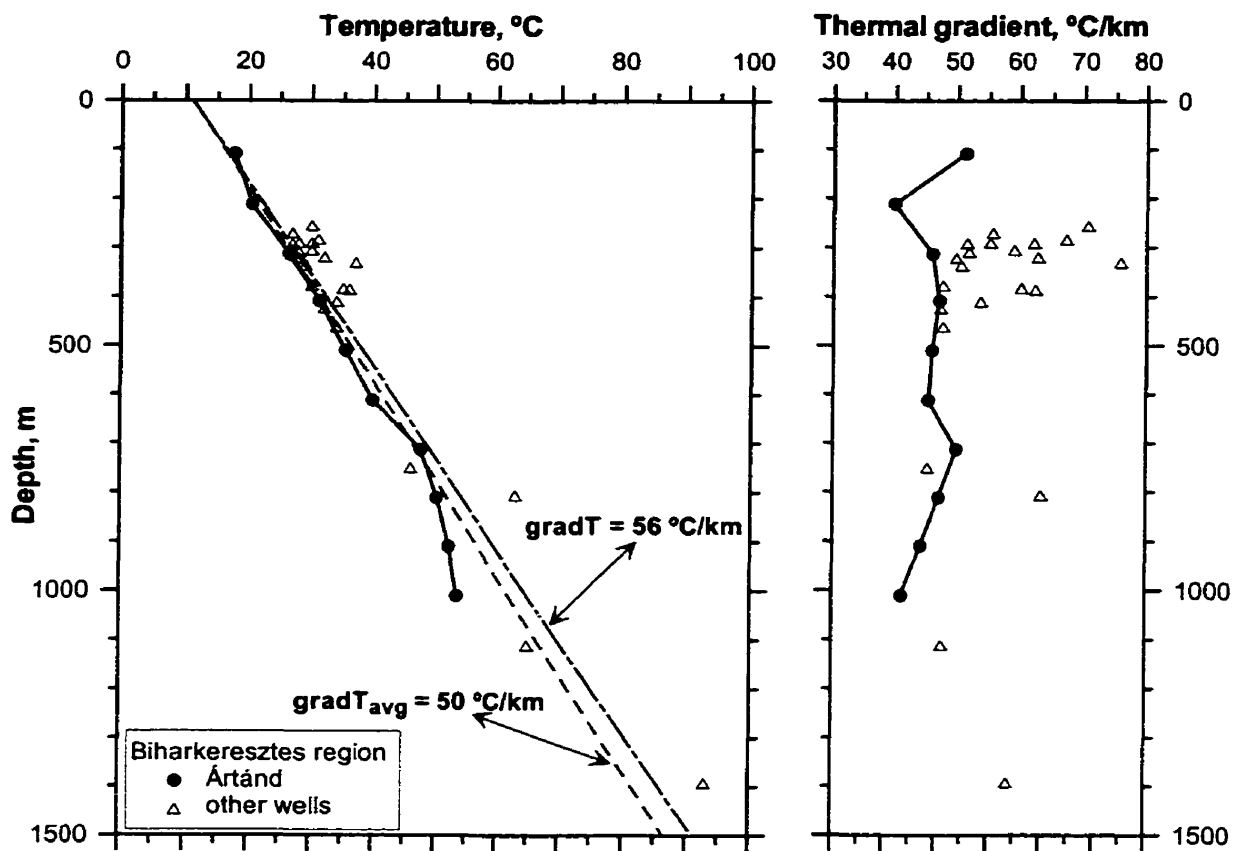


Figure 6.16: Temperature vs. depth plot, Biharkeresztes region (co-ordinates: $X_{EOV} = 185 - 214$ km; $Y_{EOV} = 830 - 860$ km; $z_0 = 87 - 100$ m a.s.l.). Data from Dövényi and Horváth, 1988. For location see Figure 6.8.

Pusztaföldvár-1 well (Figures 6.7 and 6.16): Location: $X_{EOV} = 135$ km; $Y_{EOV} = 784$ km; the altitude of the area is $z_0 = 92$ m a.s.l. The temperatures were measured in the Nagyalföld Aquifer. The top of the Pre-Neogene basement is at a depth of 1800 m.

Every measurement plots above the reference thermal gradient line; the average thermal gradient in the well is 69 °C/km. The thermal gradient vs. depth plot shows a general upward-increase of thermal gradients, which is characteristic for advective effects of ascending groundwater. The Pusztaföldvár-1 well is in the central-south-eastern part of the regional discharge area (Figure 6.8) where the hydrodynamic conditions necessary for advection are given.

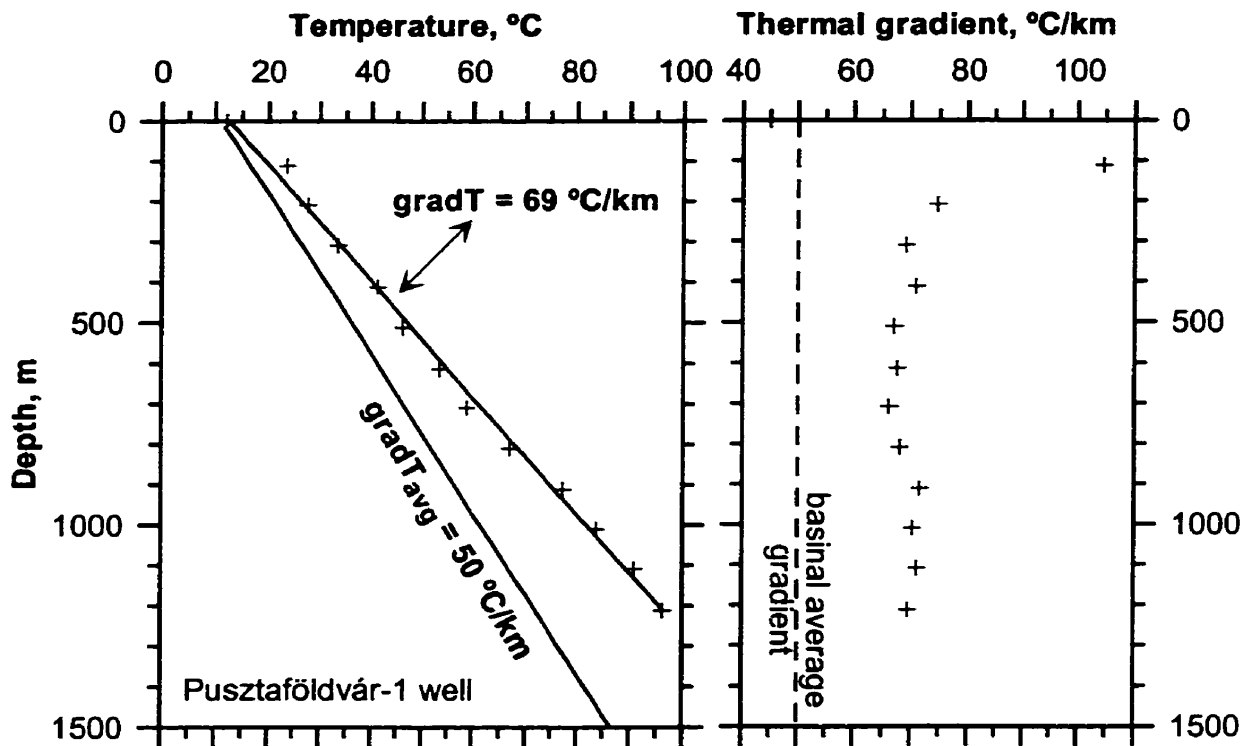


Figure 6.17: Temperature vs. depth and thermal gradient vs. depth plot, Pusztaföldvár-1 well (coordinates: $X_{EOV} = 135$ km; $Y_{EOV} = 784$ km; $z_0 = 92$ m a.s.l.). For each measurement the thermal gradient is calculated as the difference between the measured and the mean surface temperature divided by the depth of measurement. Data from Dövényi and Horváth, 1988. For location see Figure 6.8.

The observations and inferences made from the vertical temperature-depth profiles and their correlation with vertical fluid flow directions inferred from pressure-elevation profiles can be summarised as follows:

1. The vertical temperature distribution and variation of thermal gradients correlates moderately well with the vertical direction of groundwater flow; i.e., downward increasing thermal gradients correlate with descending fluid flow, and downward decreasing gradients correlate with ascending fluid flow. Remarkably good correlation between groundwater flow direction and thermal gradient change was observed in the southern part of the Duna Tisza Interfluve at Kiskunhalas and Tázlár, in the south-eastern part of the study area at Pusztaföldvár, in the central part of the study area at the Endrőd – Szarvas region, and at Biharkeresztes.
2. Local advective perturbations were inferred from the large scatter of temperature measurements made at tight vertical and lateral distances within the low-thermal

conductivity Neogene sediments. The magnitude of the observed local thermal anomalies can not be attributed only to the variation of thermal conductivity.

3. The local average thermal gradients for the measured depth intervals are generally higher than the basinal average (50 °C/km) above basement highs (thin sedimentary cover) and lower than the basinal average within/above basement depressions (thick sedimentary cover). Thus, the local average temperature gradients also are controlled by the thickness of the low-thermal conductivity Neogene sediments.

6.4.1.2 Isotherm ($T_{ij}(x,y)$) and isograd maps ($\text{grad } T_{ij}(x,y)$):

By comparing the isotherm maps ($T_{1,3}$, through $T_{25,28}$; Figures 6.18 through 6.25) with the corresponding fluid-potential maps ($h_{1,3}$, through, $h_{25,28}$; Figures 4.21 through 4.28), no unequivocal correlation between the horizontal temperature distribution and the horizontal groundwater flow directions (inferred from the hydraulic head distribution) could be revealed. Local positive and negative temperature anomalies are associated both with fluid-potential lows and highs, i.e., convergent and divergent fluid-flow patterns, respectively. Thus, it is concluded that the horizontal fluid flow components have a negligible effect on the thermal field, in agreement with the previously mentioned theoretical assumption of Jessop (1990; p. 255), and the general observations discussed by Rónai (1985; p. 178-185). Namely, the first and second order derivatives of the temperature in the horizontal directions can be assumed to be nil because the isotherms are almost horizontal. Local congestion of isotherms (i.e., domes or depressions) is rather due to advection caused by vertical fluid flow than to horizontal fluid flow.

The vertical temperature and thermal gradient variation with depth can be observed in maps of successively lower elevation intervals. For instance, consider the areas bounded by the following co-ordinates and compare the isotherms and isogradients shown on the maps in Figures 6.26 through 6.33):

A = [$Y_{EOV} = 650 - 700$ km, $X_{EOV} = 100 - 150$ km],

B = [$Y_{EOV} = 720 - 750$ km, $X_{EOV} = 90 - 140$ km],

C = [$Y_{EOV} = 750 - 810$ km, $X_{EOV} = 100 - 150$ km], and

D = [$Y_{EOV} = 800 - 850$ km, $X_{EOV} = 200 - 250$ km].

In area **A**, the thermal gradient slightly increases with depth, while in the examples **B**, **C**, and **D**, the thermal gradient slightly decreases with depth in the $z = -100$ to -1000 m

elevation interval. This pattern of vertical thermal gradient variation can be due to advective heat transport by gravity-driven flow systems (Domenico and Palciauskas, 1973). Indeed, the area of upward decreasing thermal gradient coincides with the regional recharge area (see Figure 6.8), whereas the areas with downward decreasing thermal gradients are in the central discharge area, i.e., the Great Hungarian Plain (Alföld; Figure 2.3). Thus, some of the positive and negative thermal anomalies can be correlated with the vertical components of groundwater flow within the gravity-driven flow regime, as it was also concluded from the vertical $T(d)$ profiles (section 6.4.1.1).

The locations of known hydrocarbon accumulations seem to preferentially coincide with positive thermal anomalies. For instance (Figures 6.18 through 6.33): the Pusztaföldvár-Battonya field in area C, and the Hajdúszoboszló field in the northern part of area D. Stegena (1963) documented similar anomalies in oil fields from western Hungary. Most hydrocarbon accumulations are, indeed, in regions with steep vertical hydraulic gradients (ascending flow; within the overpressured zone), but also in regions with large lateral hydraulic gradients, where potentiometric mounds, ridges, and escarpments were mapped (see discussion in Section 5.1.2, p. 154-157, examples on Figures 4.22 through 4.30). The fluid flow velocity in the overpressured zone is not known with acceptable accuracy, and there are very few proper temperature logs in the study area (Lenkey, 1999). Therefore, no estimates of the Péclet number are available to ascertain the degree of advective perturbation caused by fluid flow in this zone. In the Great Hungarian Plain, the positive thermal anomalies apparently related to hydrocarbon accumulations are not necessarily an indication of advective heat transport, because most of the accumulations are also situated above relatively hot basement highs. Therefore, such positive anomalies may as well be attributed to the proximity of a hot basement high, which -by virtue of its high thermal conductivity- acts as a protruding heat source. The horizontal temperature distribution below $z = -600$ m elevation (Figures 6.20 through 6.25 and 6.28 through 6.33) and the surface heat flow distribution (Figure 6.1) correlates remarkably well with the basement topography. By overlaying the geothermal maps onto Figure 2.19 (p. 38) it will be readily apparent that the location of isotherm and heat flow *domes* generally coincides with basement highs, whereas isotherm and heat flow *depressions* seem to preferentially coincide with basement grabens. The vertical

component of fluid flow may cause diagnostic thermal anomalies that are less noticeable on horizontal maps than on vertical cross sections.

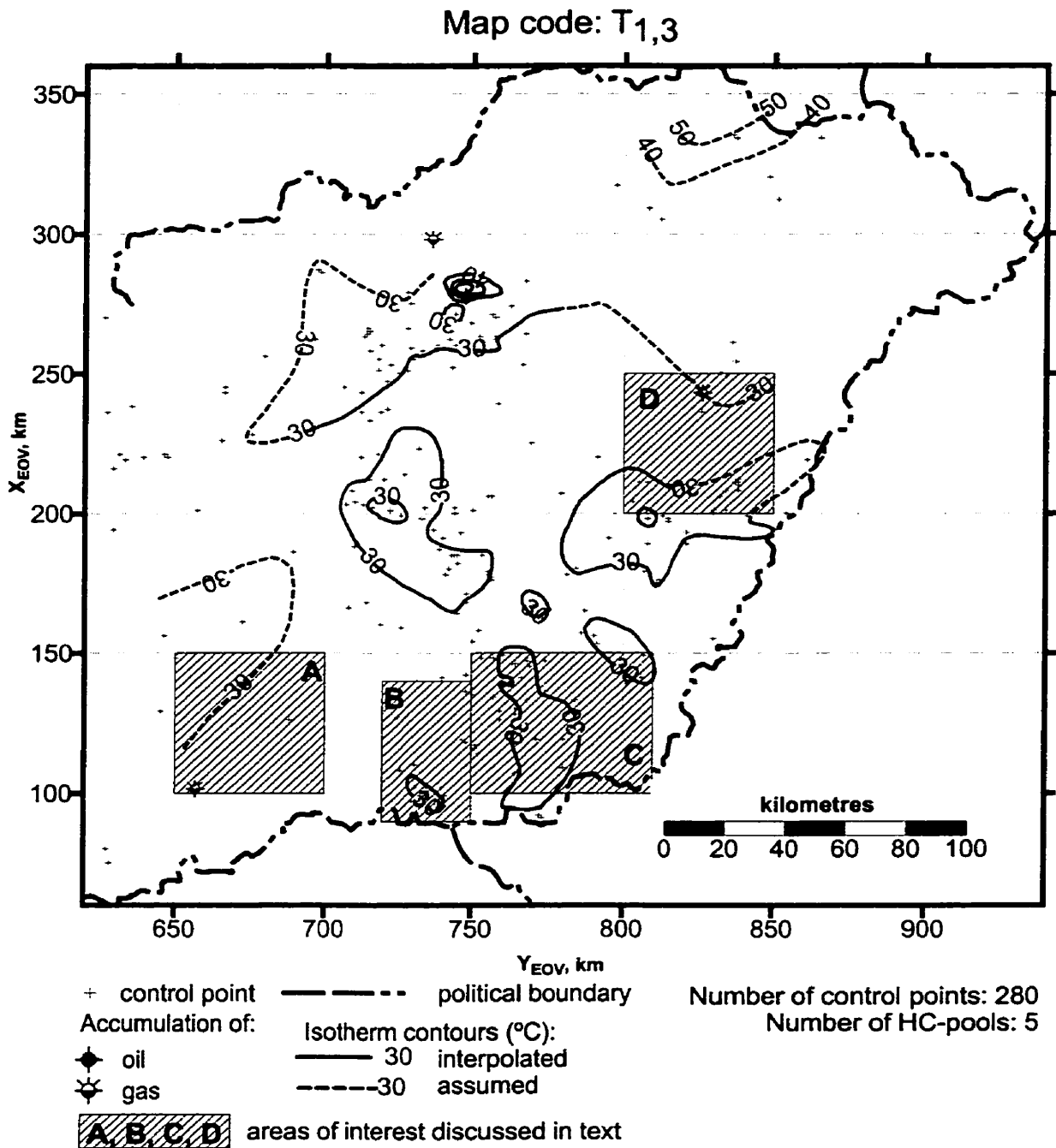


Figure 6.18: Distribution of subsurface temperature and hydrocarbon accumulations. Elevation range of measurements and hydrocarbon accumulations: $z = -100$ to -300 m a.s.l. Map code: T_{1,3}. Contour interval of isotherms: 10 °C.

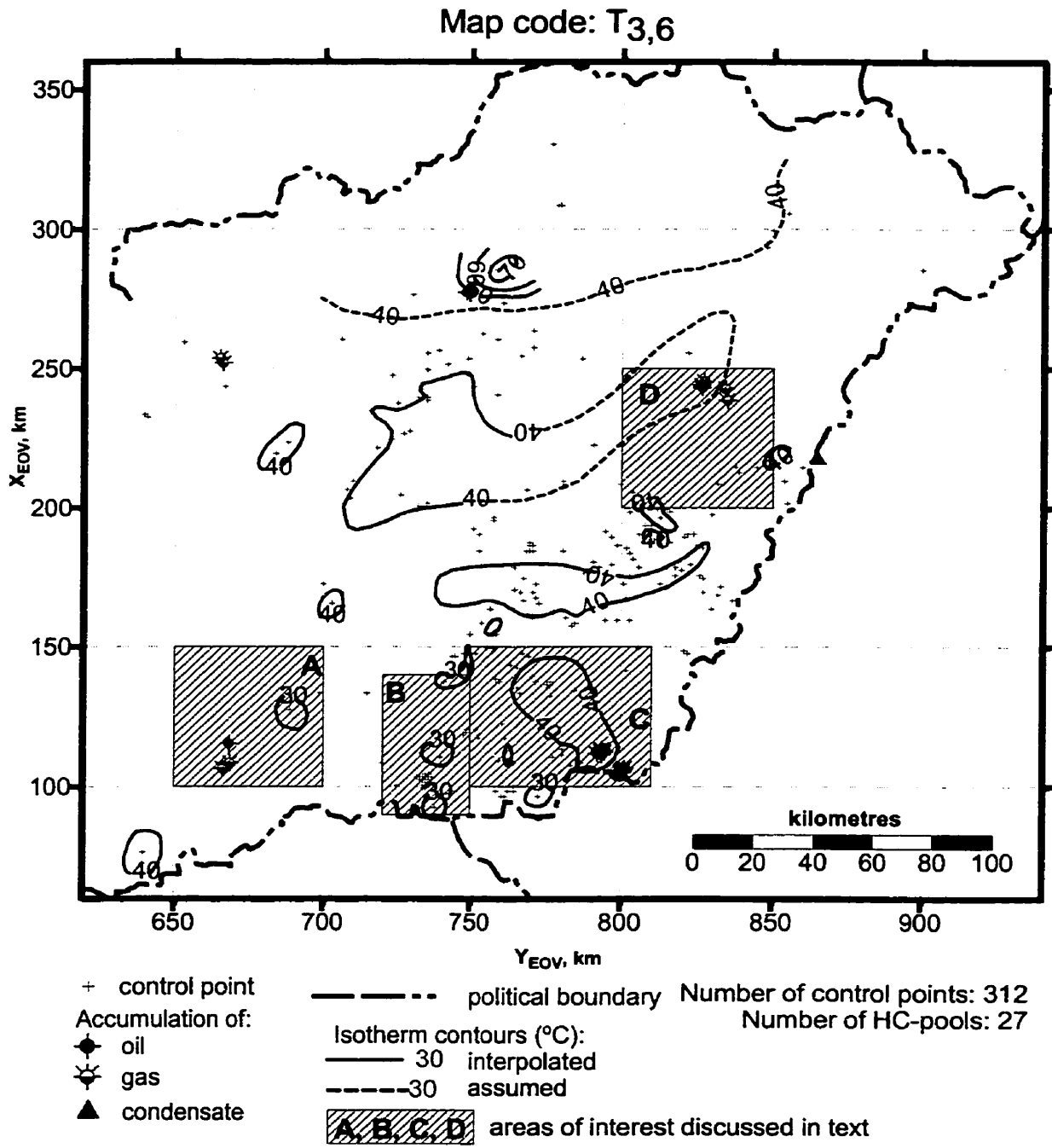


Figure 6.19: Distribution of subsurface temperature and hydrocarbon accumulations. Elevation range of measurements and hydrocarbon accumulations: $z = -300$ to -600 m a.s.l. Map code: T_{3,6}. Contour interval of isotherms: 10 °C.

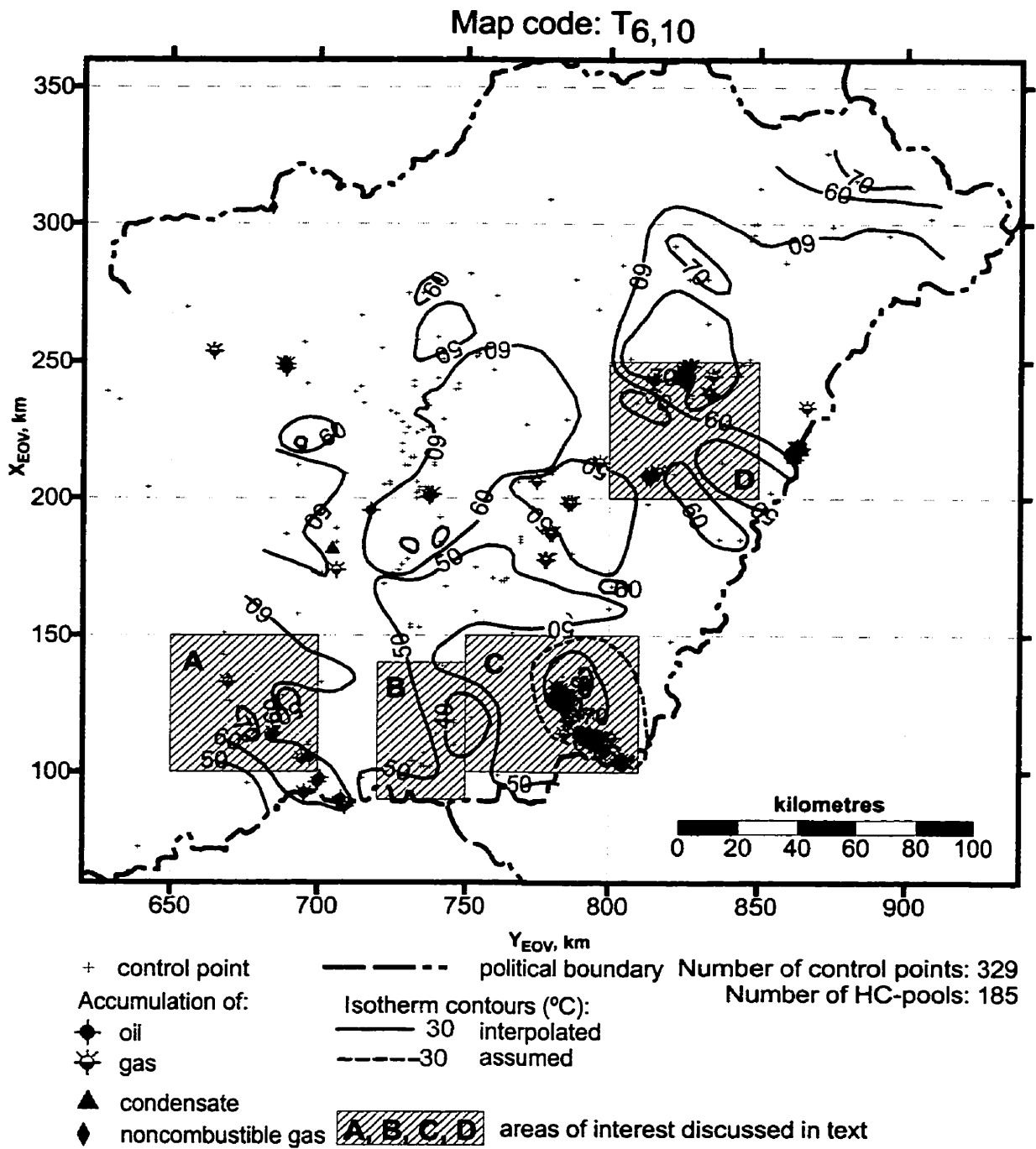


Figure 6.20: Distribution of subsurface temperature and hydrocarbon accumulations. Elevation range of measurements and hydrocarbon accumulations: $z = -600$ to -1000 m a.s.l. Map code: T_{6,10}. Contour interval of isotherms: 10 °C.

Map code: T_{10,15}

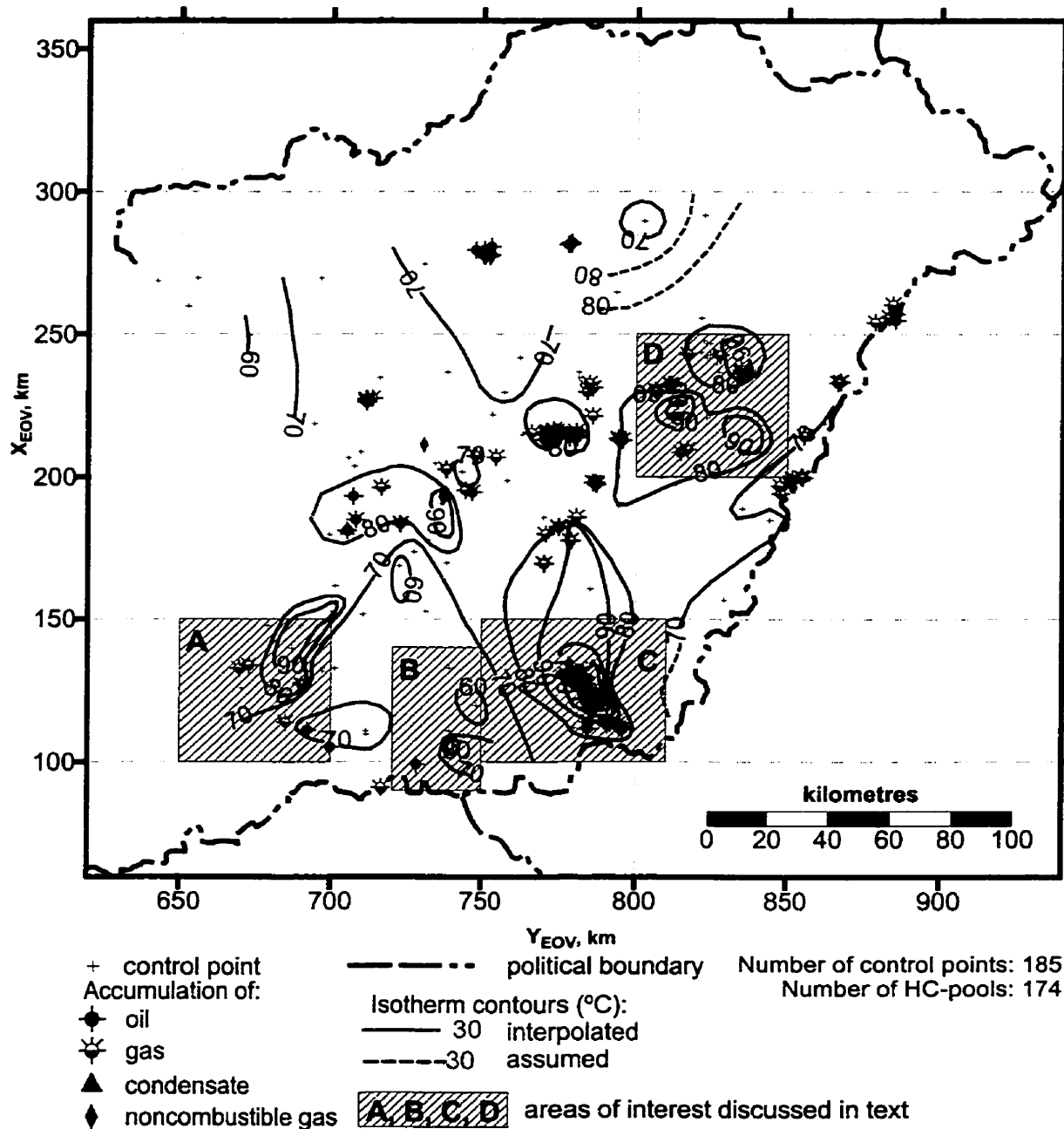


Figure 6.21: Distribution of subsurface temperature and hydrocarbon accumulations. Elevation range of measurements and hydrocarbon accumulations: $z = -1000$ to -1500 m a.s.l. Map code: T_{10,15}. Contour interval of isotherms: 10 °C.

Map code: T_{15,19}

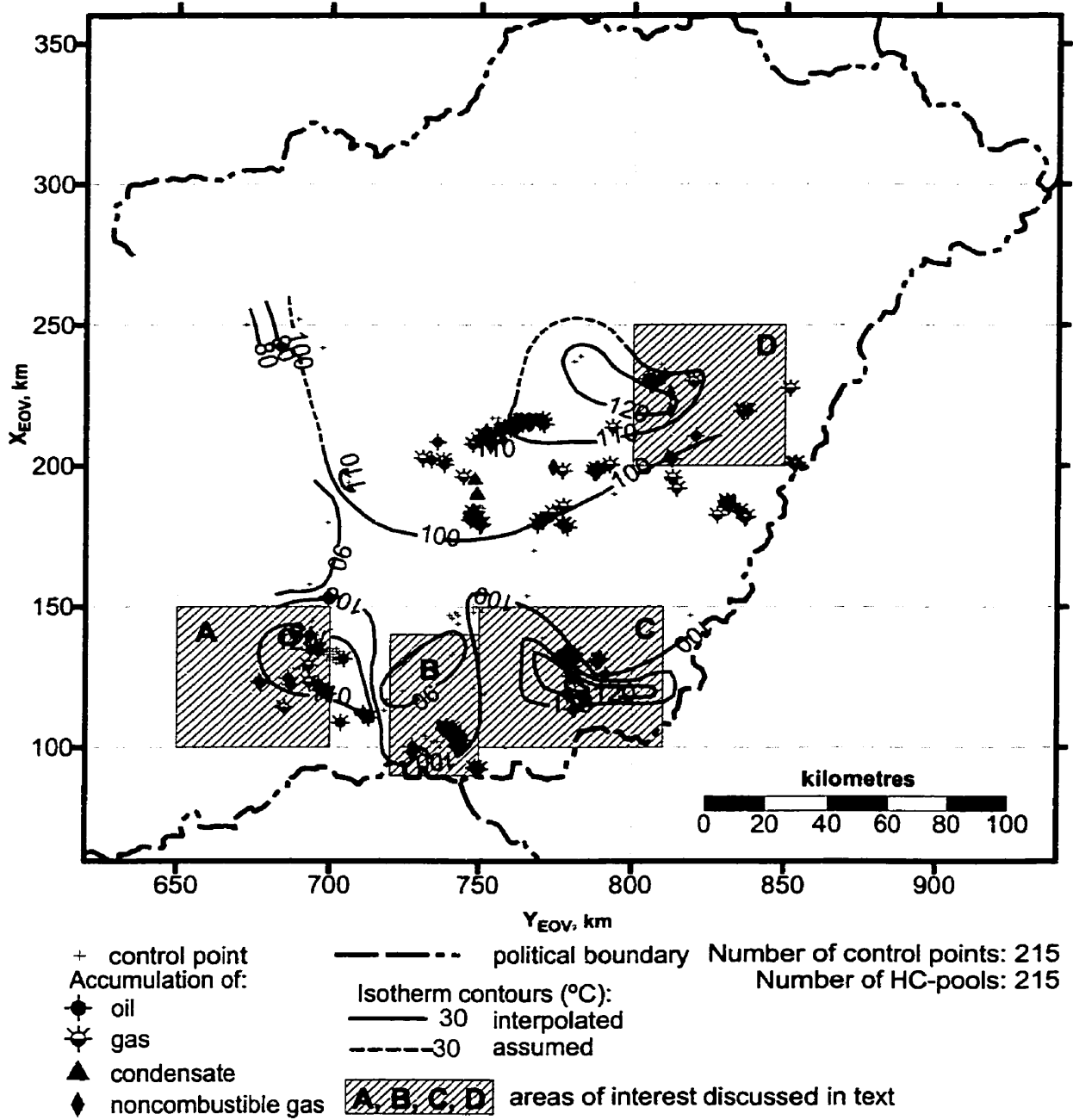


Figure 6.22: Distribution of subsurface temperature and hydrocarbon accumulations. Elevation range of measurements and hydrocarbon accumulations: $z = -1500$ to -1900 m a.s.l. Map code: T_{15,19}. Contour interval of isotherms: 10 °C.

Map code: T19,22

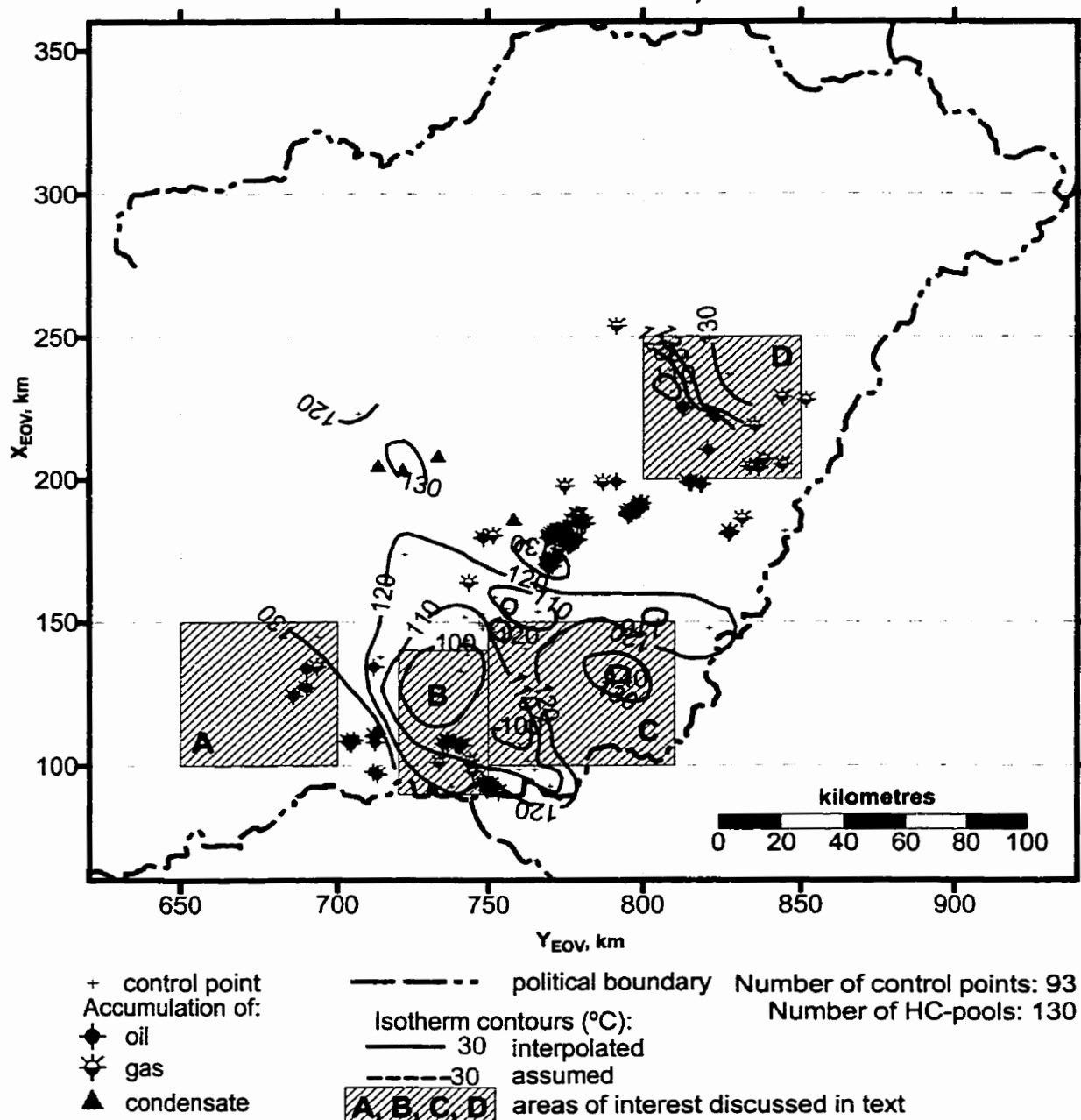


Figure 6.23: Distribution of subsurface temperature and hydrocarbon accumulations. Elevation range of measurements and hydrocarbon accumulations: $z = -1900$ to -2200 m a.s.l. Map code: T_{19,22}. Contour interval of isotherms: 10 °C.

Map code: T22,25

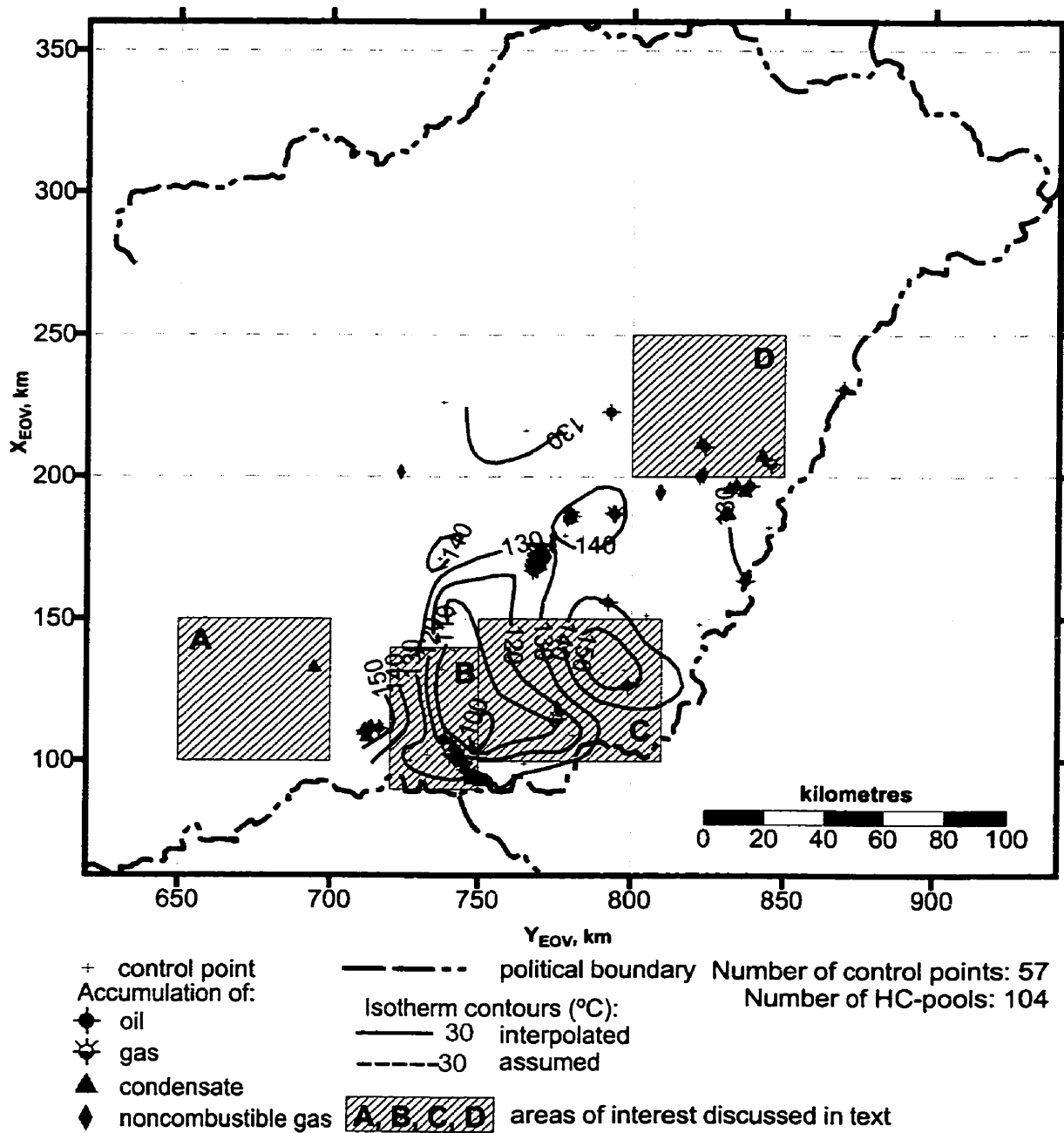


Figure 6.24: Distribution of subsurface temperature and hydrocarbon accumulations. Elevation range of measurements and hydrocarbon accumulations: $z = -2200$ to -2500 m a.s.l. Map code: T_{22,25}. Contour interval of isotherms: 10 °C.

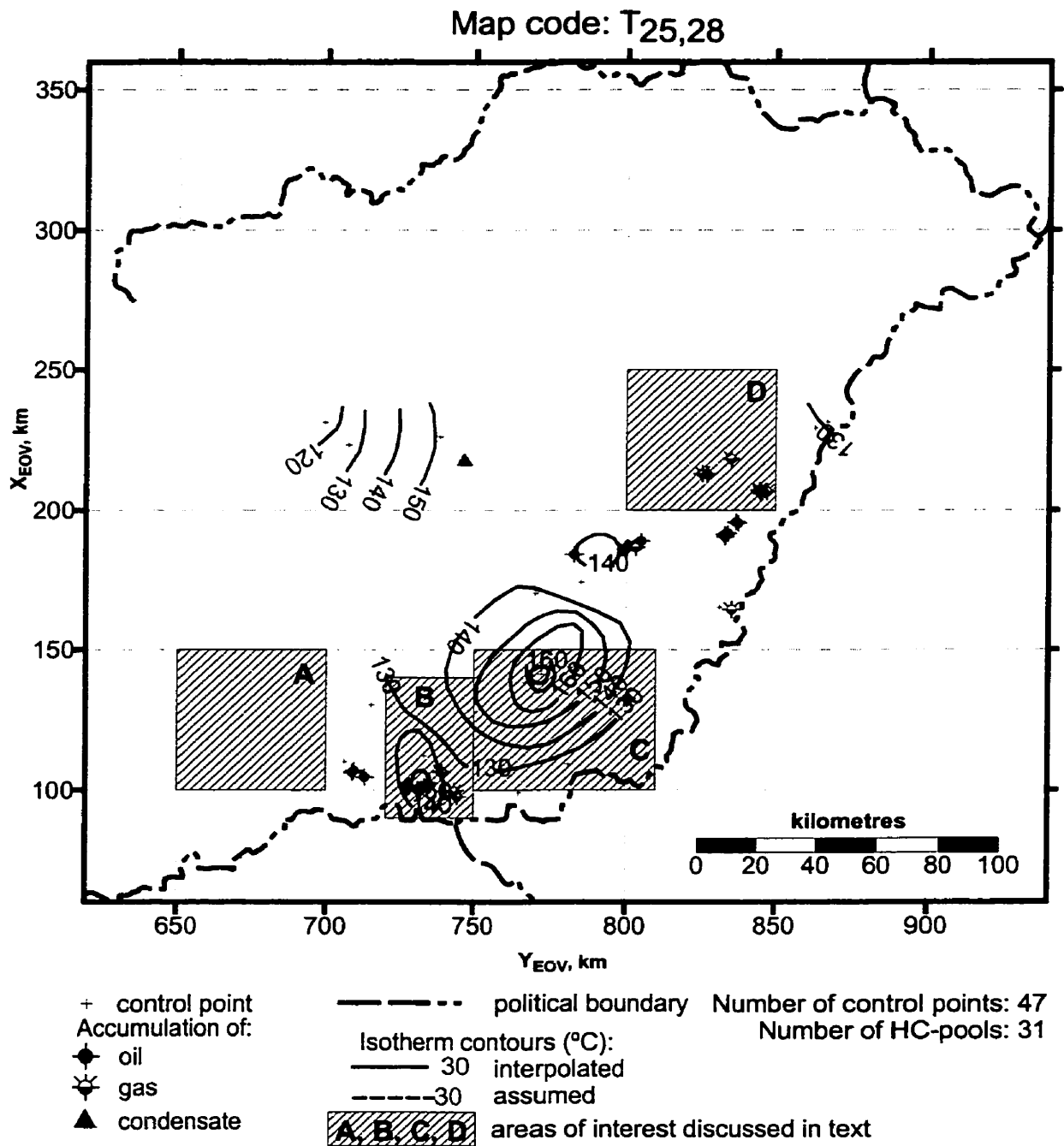


Figure 6.25: Distribution of subsurface temperature and hydrocarbon accumulations. Elevation range of measurements and hydrocarbon accumulations: $z = -2500$ to -2800 m a.s.l. Map code: T_{25,28}. Contour interval of isotherms: 10 °C.

Map code: gradT_{1,3}

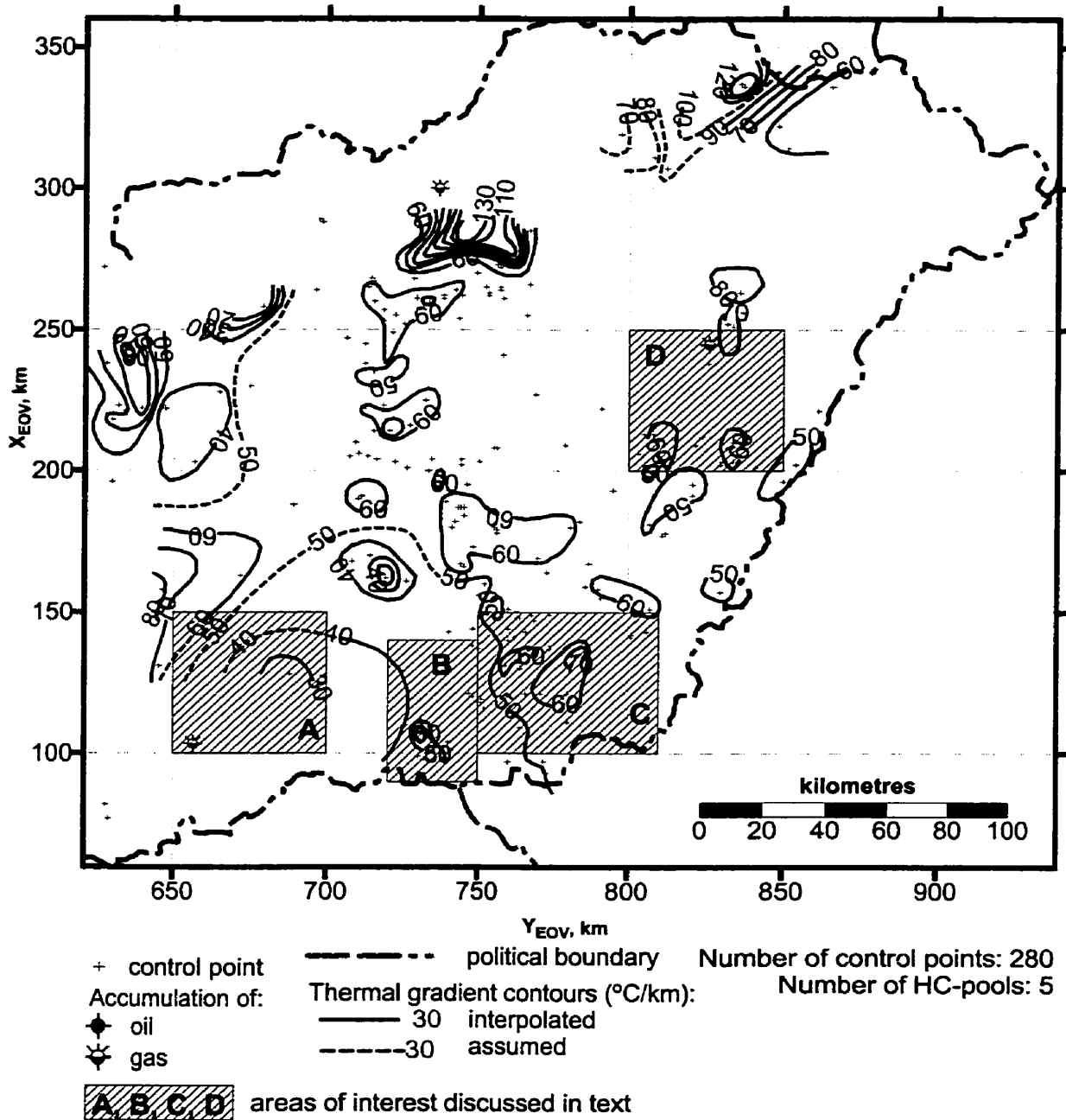


Figure 6.26: Distribution of subsurface thermal gradient and hydrocarbon accumulations. Elevation range of measurements and hydrocarbon accumulations: $z = -100$ to -300 m a.s.l. Map code: grad T_{1,3}. Isogradient contour interval: 10 °C/km. Thermal gradient values are calculated based on the difference between the measured and the mean surface temperature (11 °C) divided by the depth of measurement.

Map code: gradT_{3,6}

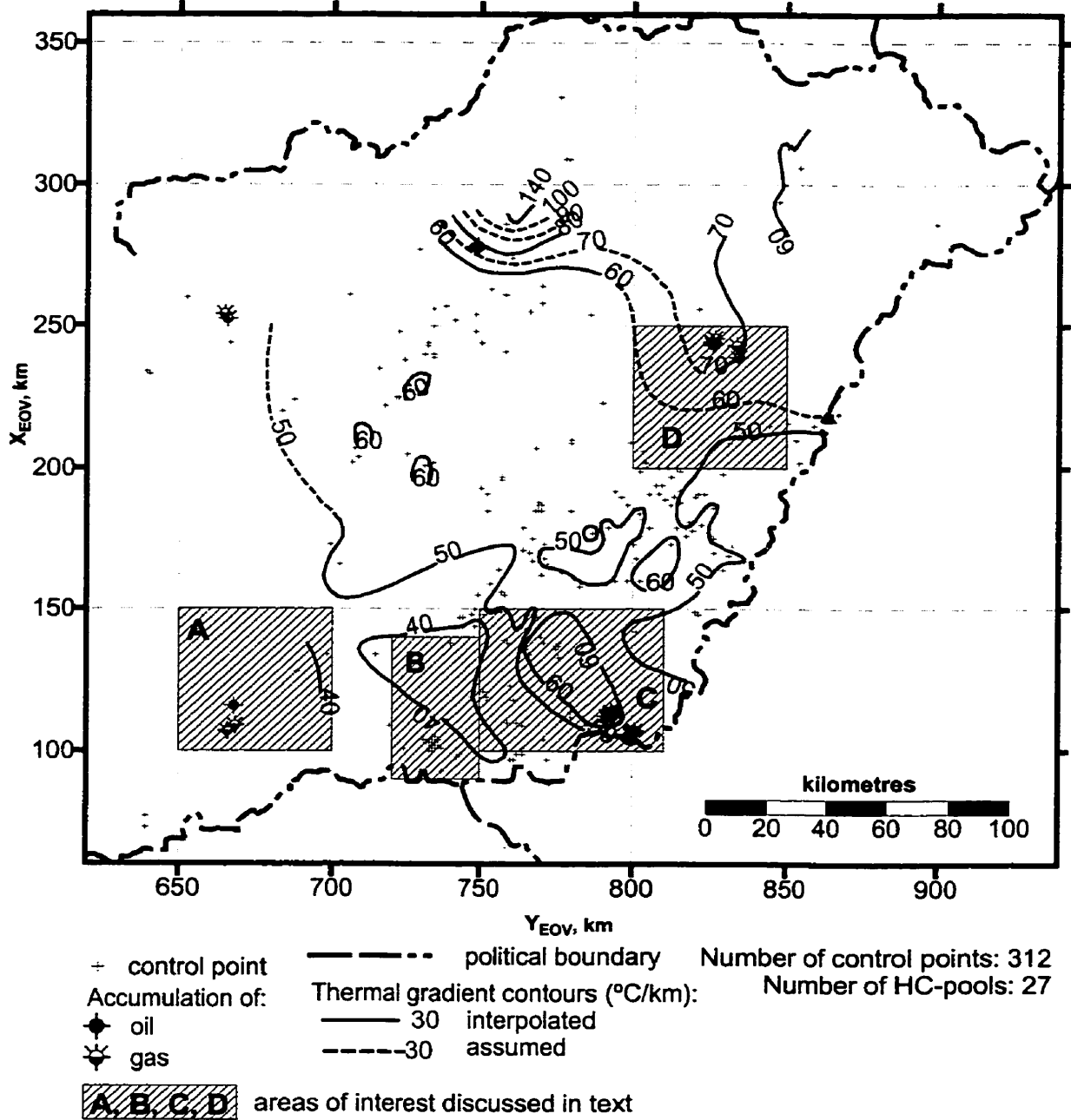


Figure 6.27: Distribution of subsurface thermal gradient and hydrocarbon accumulations. Elevation range of measurements and hydrocarbon accumulations: $z = -300$ to -600 m a.s.l. Map code: grad $T_{3,6}$. Isogradient contour interval: 10 °C/km. Thermal gradient values are calculated based on the difference between the measured and the mean surface temperature (11 °C) divided by the depth of measurement.

Map code: gradT_{6,10}

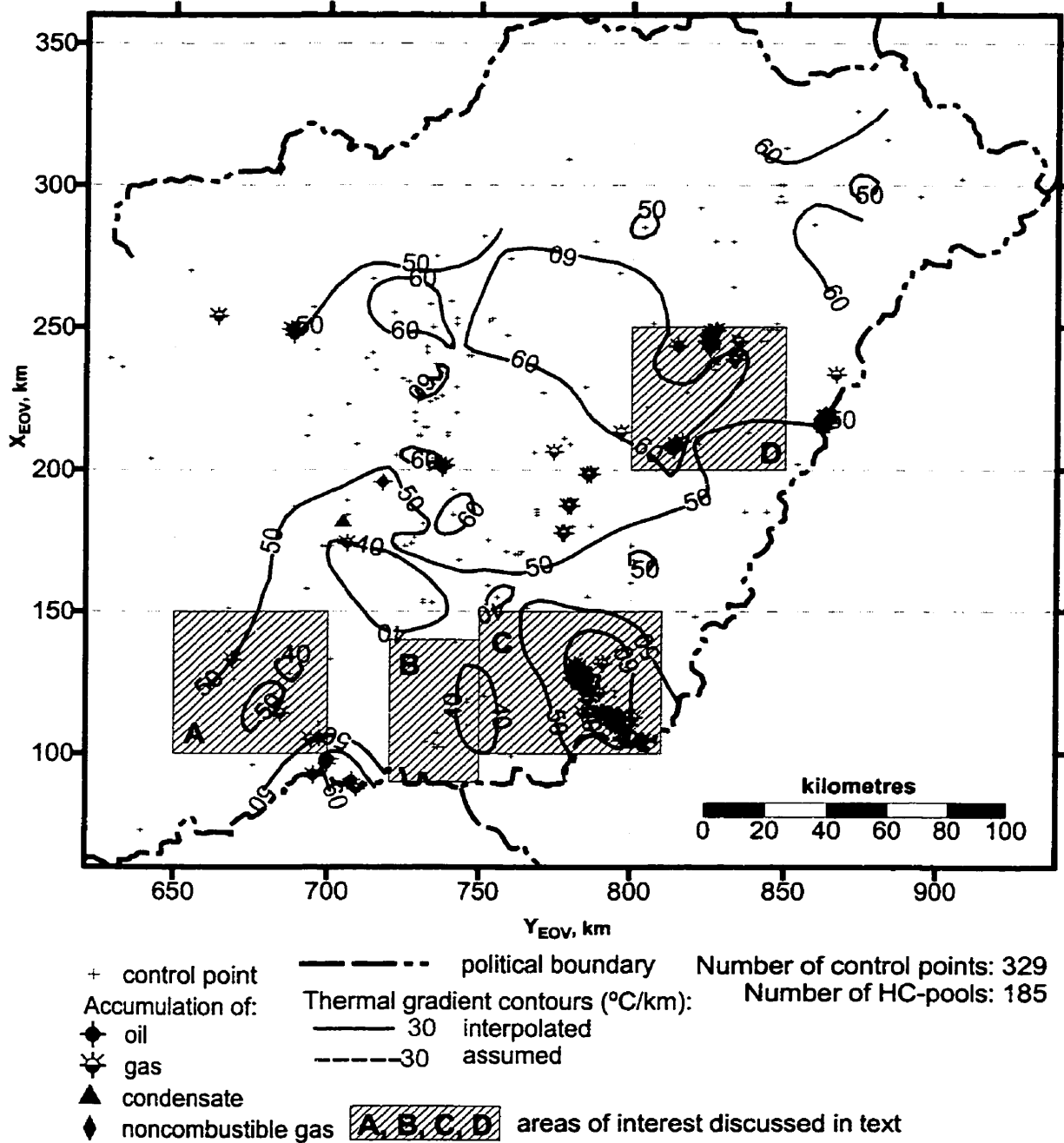


Figure 6.28: Distribution of subsurface thermal gradient and hydrocarbon accumulations. Elevation range of measurements and hydrocarbon accumulations: $z = -600$ to -1000 m a.s.l. Map code: grad T_{6,10}. Isograd contour interval: 10 °C/km. Thermal gradient values are calculated based on the difference between the measured and the mean surface temperature (11 °C) divided by the depth of measurement.

Map code: gradT_{10,15}

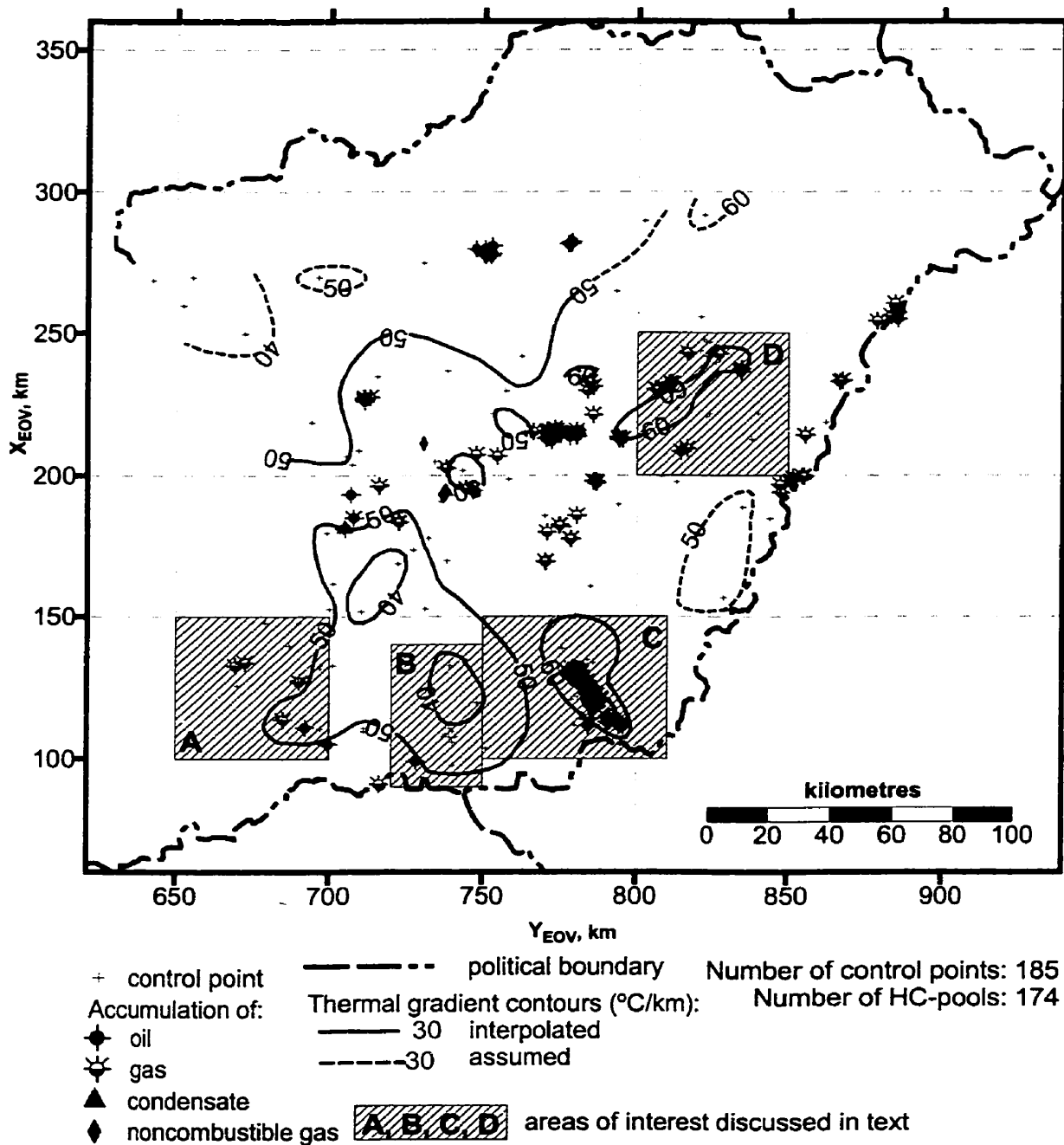


Figure 6.29: Distribution of subsurface thermal gradient and hydrocarbon accumulations. Elevation range of measurements and hydrocarbon accumulations: $z = -1000$ to -1500 m a.s.l. Map code: grad $T_{10,15}$. Isogradients contour interval: 10 °C/km. Thermal gradient values are calculated based on the difference between the measured and the mean surface temperature (11 °C) divided by the depth of measurement.

Map code: gradT_{15,19}

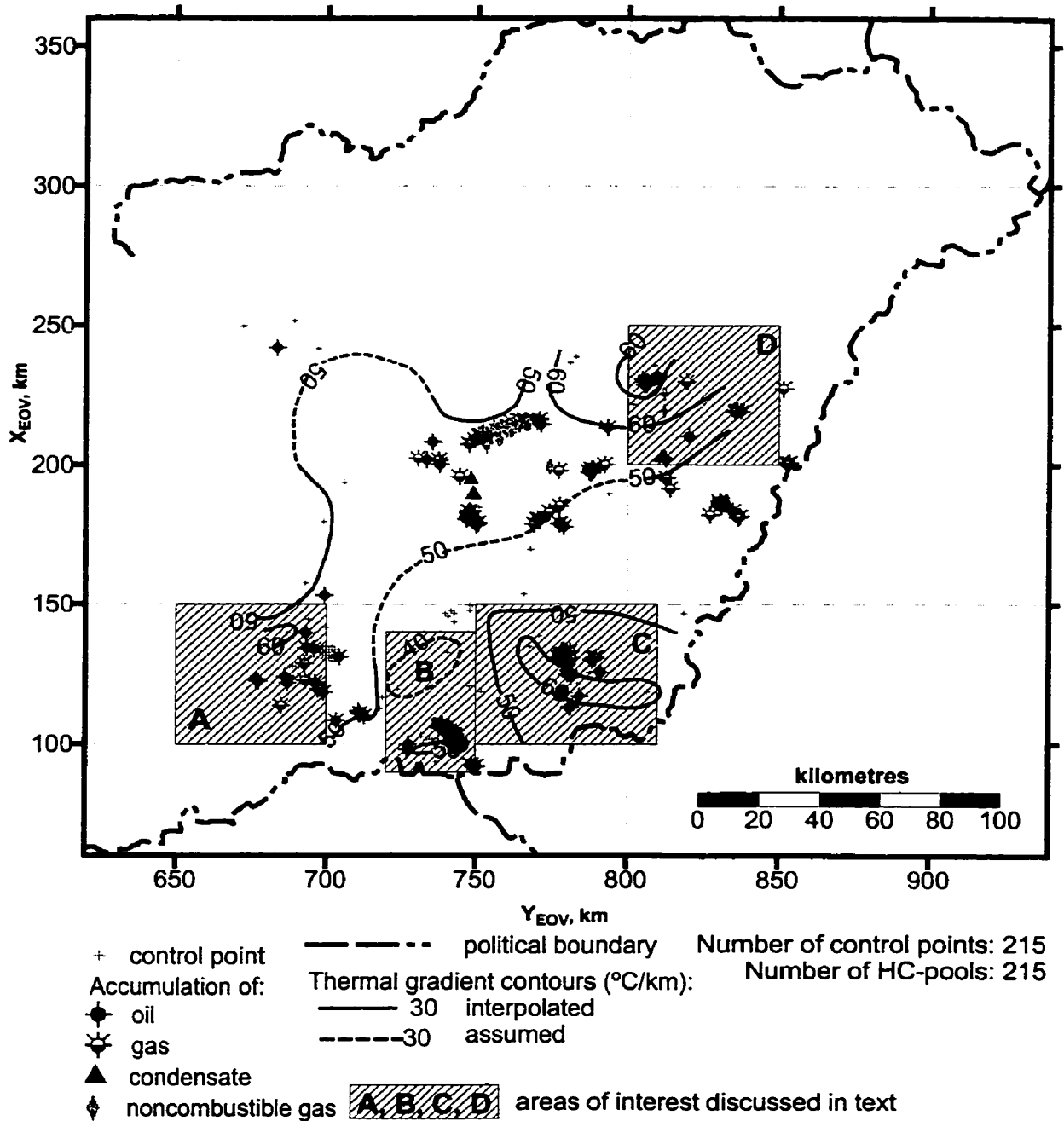


Figure 6.30: Distribution of subsurface thermal gradient and hydrocarbon accumulations. Elevation range of measurements and hydrocarbon accumulations: $z = -1500$ to -1900 m a.s.l. Map code: grad $T_{15,19}$. Isograd contour interval: 10 °C/km. Thermal gradient values are calculated based on the difference between the measured and the mean surface temperature (11 °C) divided by the depth of measurement.

Map code: gradT_{19,22}

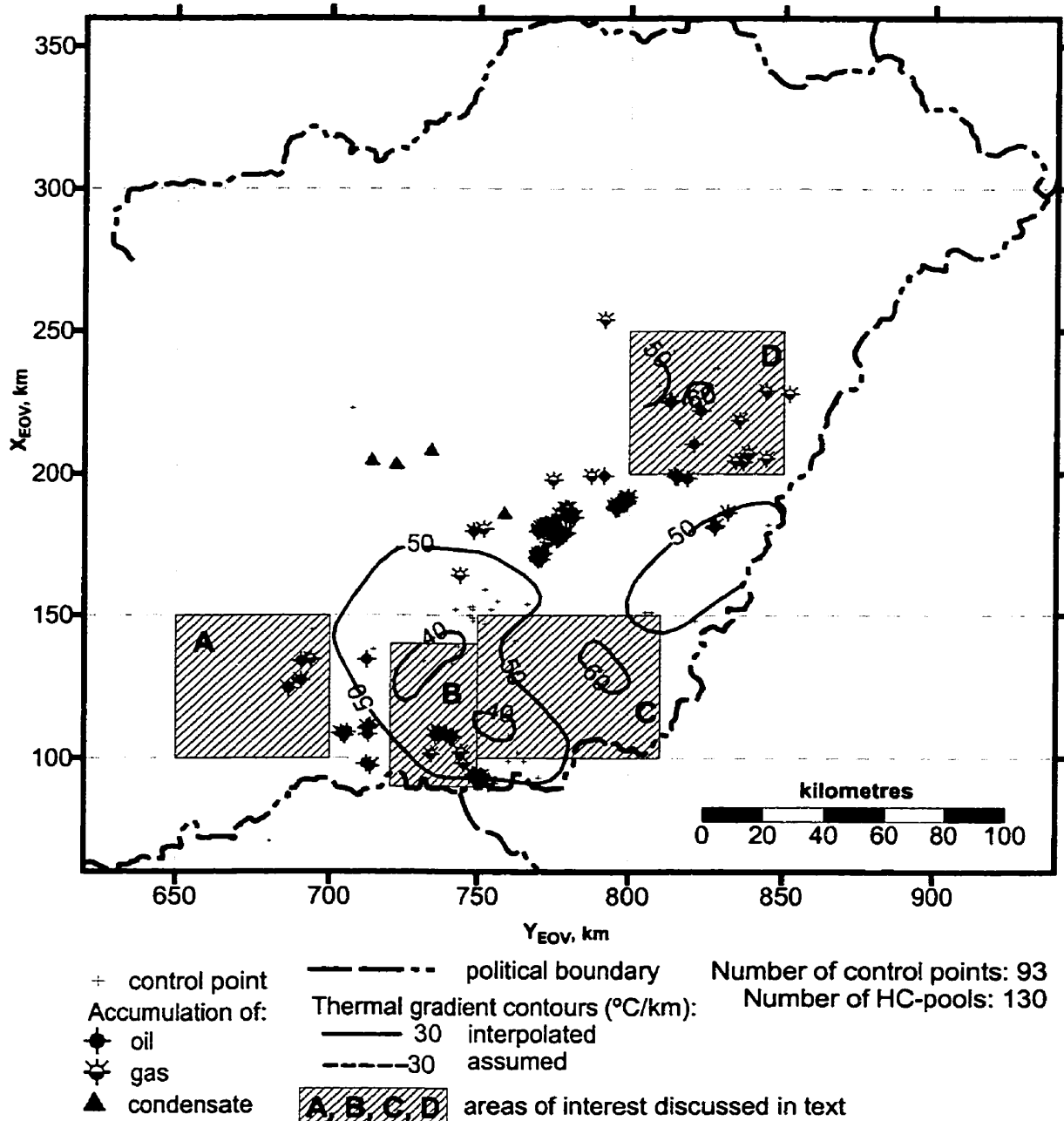


Figure 6.31: Distribution of subsurface thermal gradient and hydrocarbon accumulations. Elevation range of measurements and hydrocarbon accumulations: $z = -1900$ to -2200 m a.s.l. Map code: grad T_{19,22}. Isogradient contour interval: 10 °C/km. Thermal gradient values are calculated based on the difference between the measured and the mean surface temperature (11 °C) divided by the depth of measurement.

Map code: gradT22,25

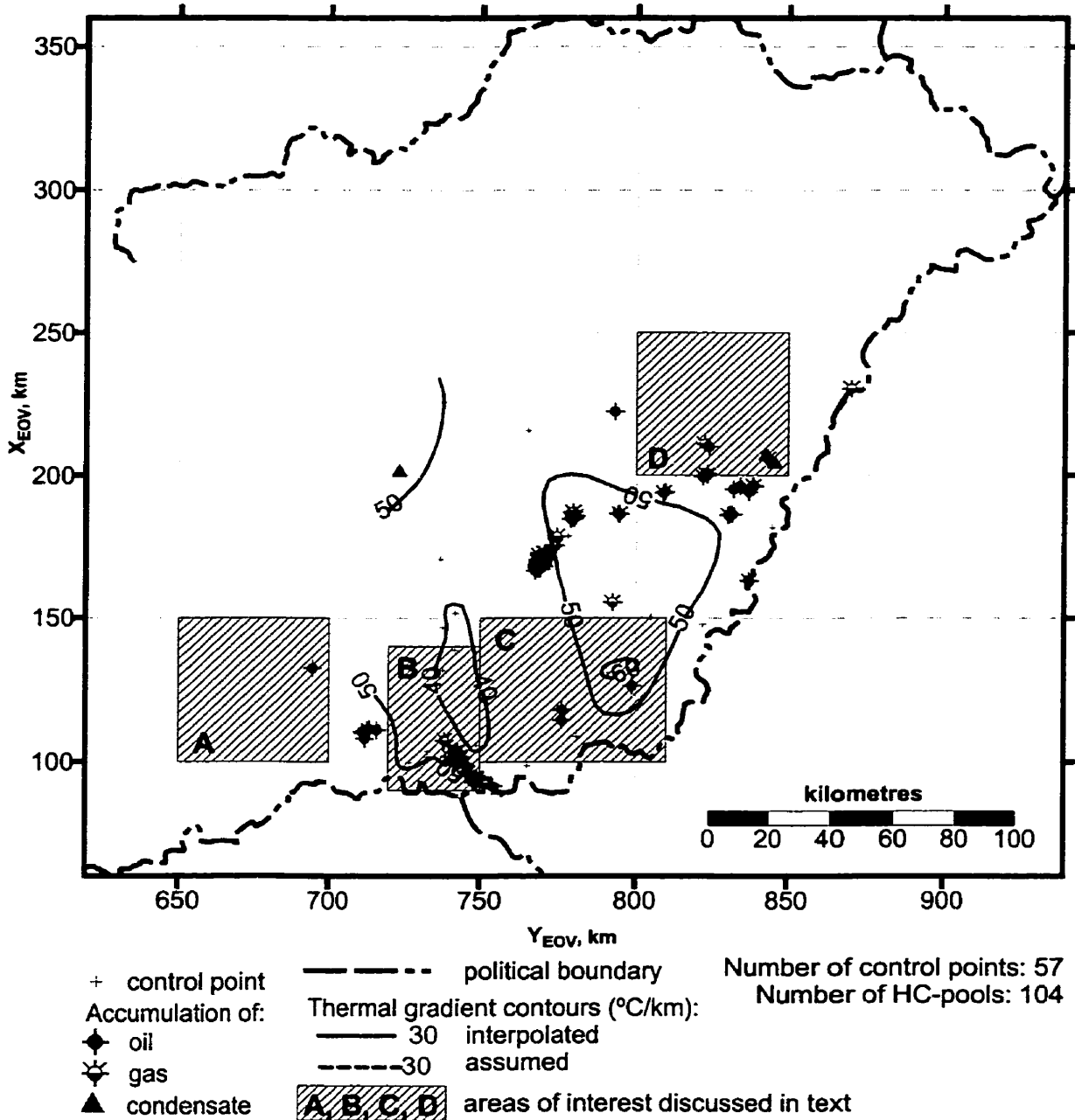


Figure 6.32: Distribution of subsurface thermal gradient and hydrocarbon accumulations. Elevation range of measurements and hydrocarbon accumulations: $z = -2200$ to -2500 m a.s.l. Map code: grad $T_{22,25}$. Isogradient contour interval: 10 °C/km. Thermal gradient values are calculated based on the difference between the measured and the mean surface temperature (11 °C) divided by the depth of measurement.

Map code: gradT_{25,28}

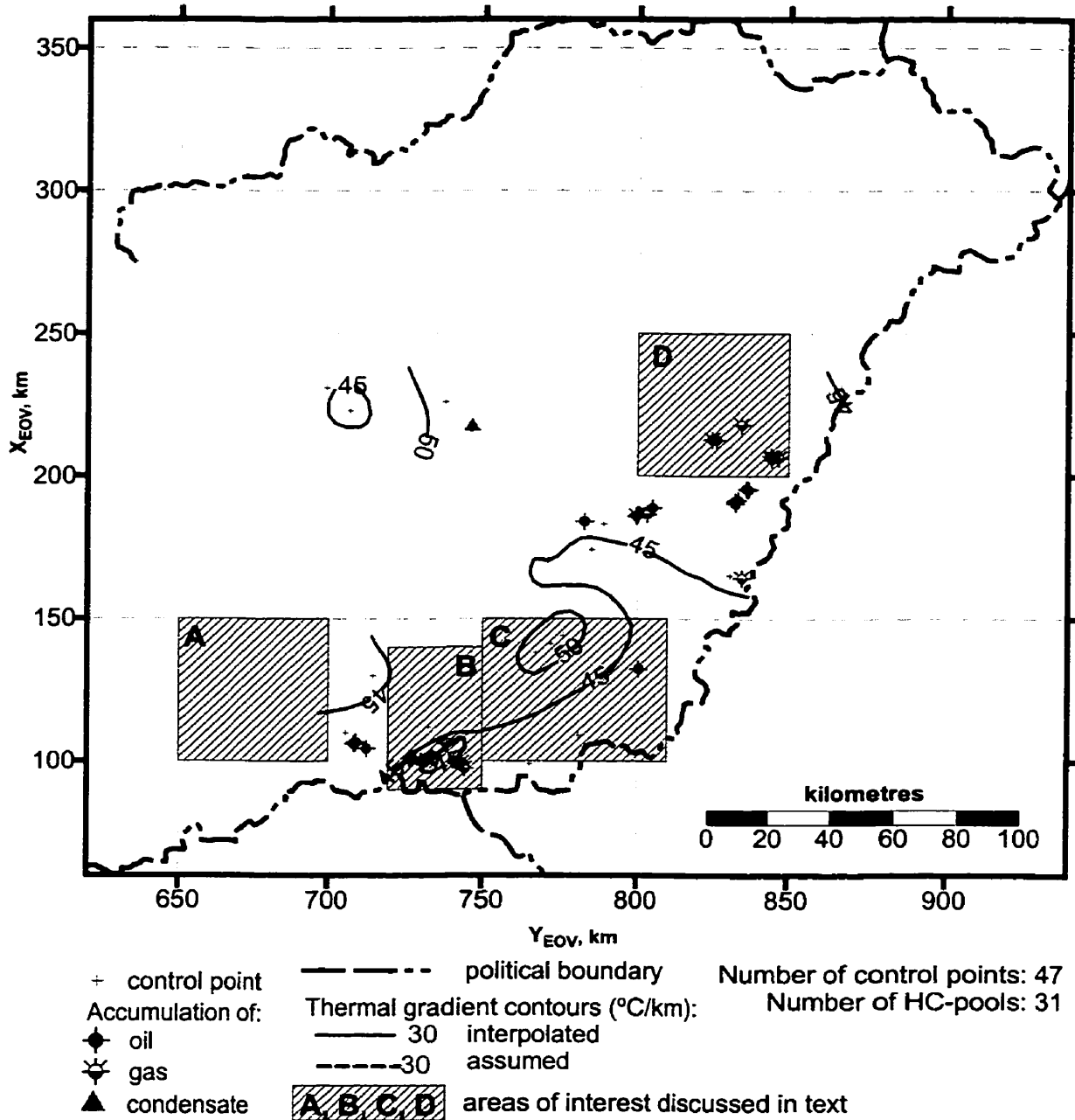


Figure 6.33: Distribution of subsurface thermal gradient and hydrocarbon accumulations. Elevation range of measurements and hydrocarbon accumulations: $z = -2500$ to -2800 m a.s.l. Map code: grad T_{25,28}. Isogradient contour interval: 10 °C/km. Thermal gradient values are calculated based on the difference between the measured and the mean surface temperature (11 °C) divided by the depth of measurement.

6.4.1.3 Regional geothermal cross sections ($T_i(L,z)$):

On the regional thermal cross sections **T1-T1'-T1''**, **T2-T2'-T2''**, and **T3-T3'-T3''** (Figures 6.34, 6.35, and 6.36) the geometric pattern of the isotherms seems to mimic the thermal conductivity contrast between the Pre-Neogene basement and the Neogene clastic sediments. Also, the isotherms appear to bend in the direction of groundwater flow inferred from the hydraulic cross sections (compare Figure 4.33 with 6.34, Figure 4.34 with 6.35, Figure 4.35 with 6.36, and Figure 4.36 with 6.37). On the western end of **T1-T1'-T1''** (Figure 6.34; $L = 50 - 70$ km segment), between the surface and a depth of ~1700 m, the depressed isotherms correlate well with the topography driven descending flow in a regional recharge area (see also Figure 4.33; southern part of the Duna-Tisza Interfluve). A similar isotherm pattern, and a good correlation between vertical temperature distribution and fluid flow, can be observed on the NW end of the cross section **T2-T2'-T2''** (Figure 6.35; Gödöllő Hills). The isotherm domes observed on section **T1-T1'-T1''** (Figure 6.34: $L = 55 - 105$ km segment), section **T2-T2'-T2''** (Figure 6.35: $L = 45 - 60$ km segment and $L = 175 - 210$ km segment), and the central part of **T3-T3'-T3''** (Figure 6.36: $L = 110 - 185$ km segment) correlate well with the regionally ascending flow inferred from the corresponding hydraulic cross sections, i.e., **H1**, **H2**, and **H3**, respectively (Figures 4.33, 4.34, and 4.35).

Within the deep sub-basins, the isotherms are domed to a depth of 500 – 1500 m, and they are depressed below a depth of 1500 m (e.g., **T1-T1'-T1''**, $L = 110 - 140$ km segment; **T2-T2'-T2''**, $L = 125 - 175$ km segment; **T3-T3'-T3''**, $L = 210 - 230$ km segment). By expanding the scale of observation from that of the sub-basin to a scale that includes the adjacent basement horsts as well, it is readily apparent that the isotherms mimic the topography of the high thermal conductivity basement. The isotherm domes in the upper part of the basin (depth of 500 – 1500 m) are probably the result of ascending groundwater, while the general depression of isotherms within the sub-basins is most likely due to the great thickness of the low thermal conductivity sediments. It was shown on the hydraulic cross sections that in these areas flow is ascending. This should have a detectable effect on the geometry of isotherms, if forced convection were a significant mechanism, i.e., the water flow velocity would be sufficiently high. Indeed, advective perturbations of these depressed isotherms, probably caused by upward flow, are apparent on section **T2-T2'-T2''** within the $L = 135 - 150$ km segment.

214

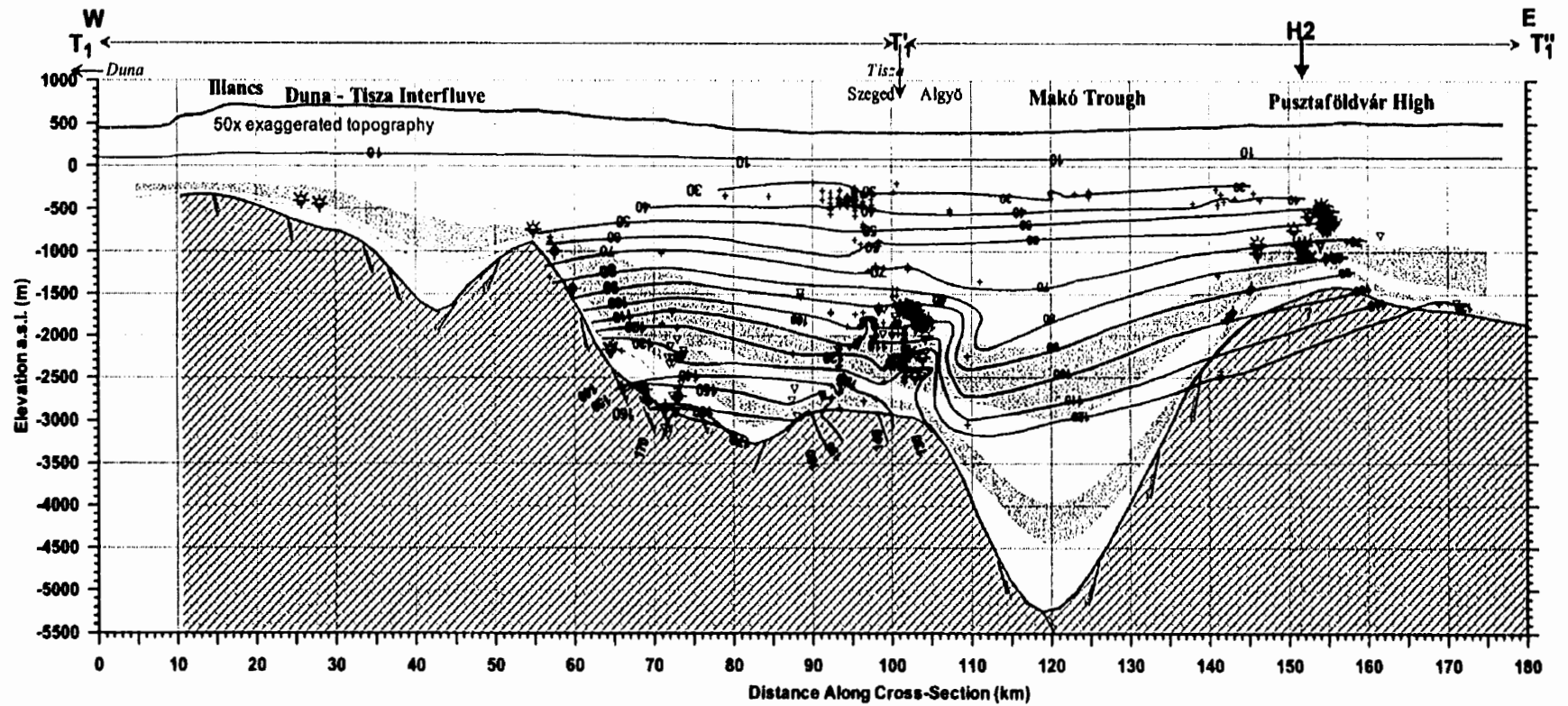


Figure 6.34. Geothermal cross section T1-T1'-T1'' (for location see figure 6.7). EOVS co-ordinates in kilometres of end-nodes and break-point: T1(640, 110), T1'(740, 104), and T1''(820, 120). A copy of the cross section at 1:500 000 scale is included in the pocket.

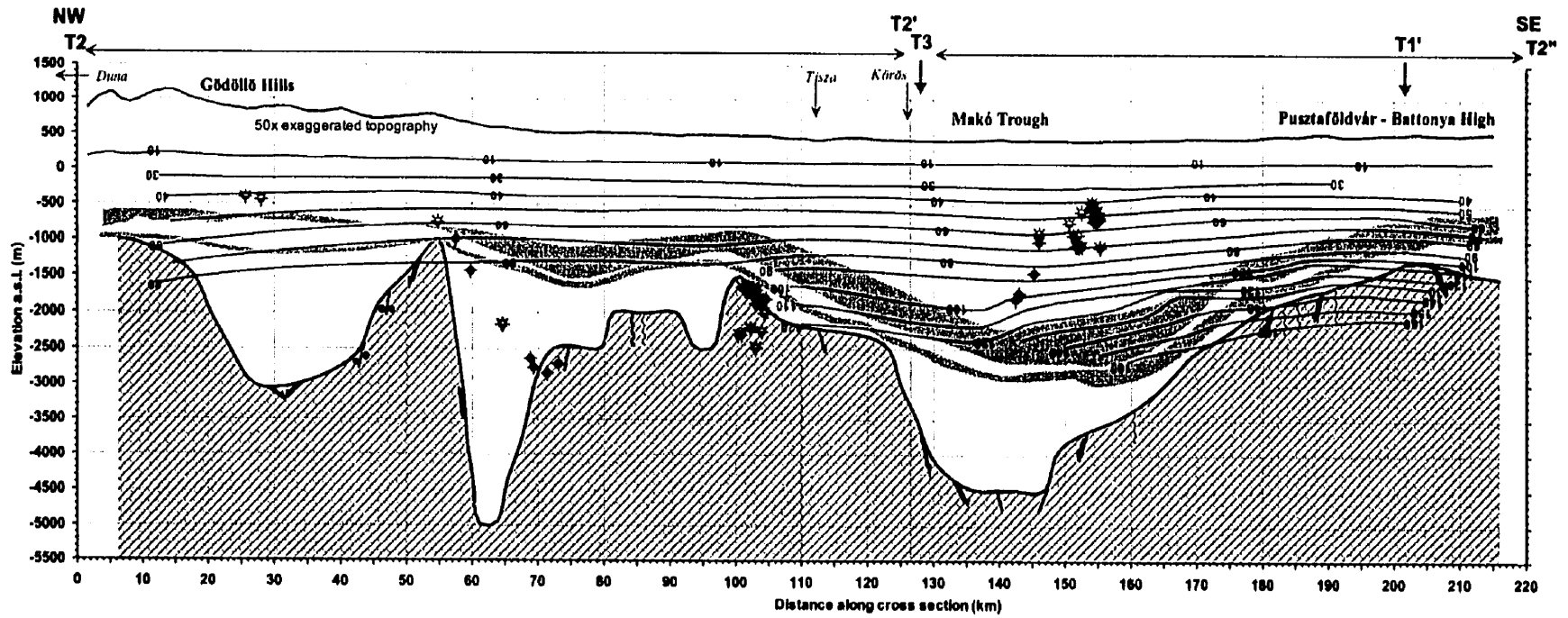


Figure 6.35. Geothermal cross section T2-T2'-T2'' (for location see figure 6.7). EOv co-ordinates in kilometres of end-nodes and break-point: T1(660, 260), T2'(740, 160), and T2''(806, 102). A copy of the cross section at 1:500 000 scale is included in the pocket.

216

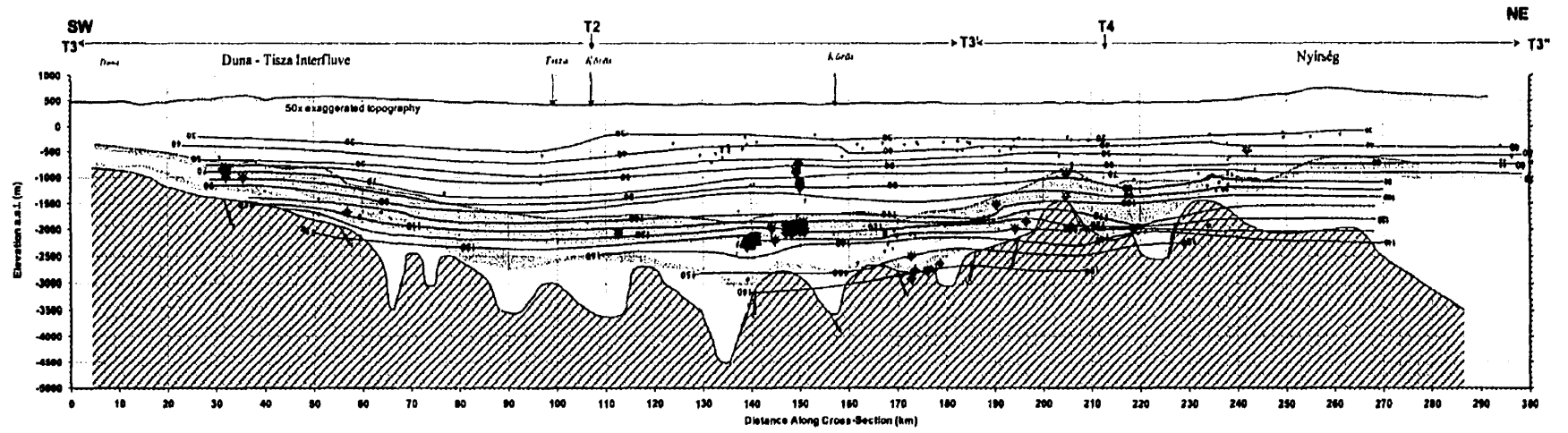
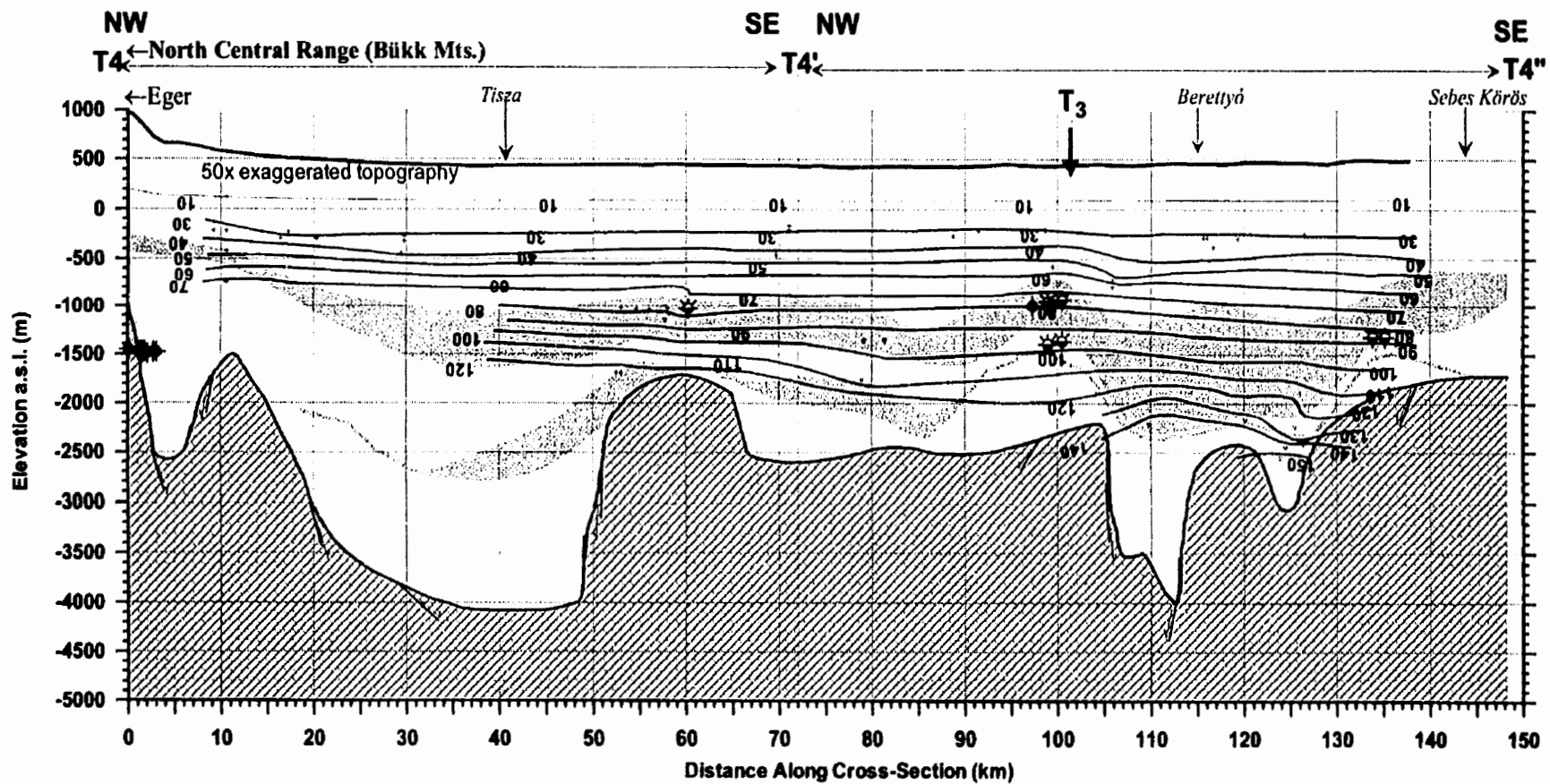


Figure 6.36. Geothermal cross section T3-T3'-T3'' (for location see figure 6.7). EOv co-ordinates in kilometres of end-nodes and break-point: T3(640, 120), T3'(810, 190), and T3''(850, 290). A copy of the cross section at 1:500 000 scale is included in the pocket.



217

Figure 6.37. Geothermal cross section T4-T4'-T4'' (for location see figure 6.7). EOv co-ordinates in kilometres of end-nodes and break-point: T4(750, 280), T4'(790, 220), and T4''(860, 190). A copy of the cross section at 1:500 000 scale is included in the pocket.

An isotherm plume can be observed on **T1-T1'-T1''**, $L = 90 - 110$ km segment (Szeged, Algyő), which is tentatively interpreted as the result of advective perturbation caused by groundwater flow channelling (a potentiometric plume) along a conduit fault, which extends from the basement into the Nagyalföld Aquifer. This thermal anomaly spatially coincides with a *potentiometric shoulder* anomaly (Section 5.1.3, Figure 5.10, p. 158) observed on the corresponding hydraulic cross section **H1** (Figure 4.33), as well as with the Pre-Neogene basement faults extrapolated from the lineament map of Fülöp and Dank (1987). The published structural geological maps of this region (Bérczi and Kókai, 1978) also support this interpretation. Farther west on the same cross section, at the $L = 65 - 80$ km segment, the apparent congestion of isotherms in the $z = -2400$ to -3200 m elevation range spatially coincides with a *potentiometric plume & tube* anomaly-combination. These coincidences of fluid-potential and geothermal anomalies suggest a remarkably good correlation between fluid flow and temperature distribution, i.e., certain diagnostic fluid potential anomalies seem to induce advective perturbations of the thermal field.

The relatively sparse data coverage of section **T4-T4'-T4''** (Figure 6.37) warrants only a first order approximation and interpretation of the thermal regime, because the isotherm contours are mostly assumed. A positive anomaly (isotherm dome) can be observed on the NW-SE segment of the section between $L = 100 - 140$ km at $z = -1500 - -3000$ m elevation, within/above the Derecske trough. Generally, this section suggests pure conduction as dominant heat transfer mechanism.

6.4.2 Heat transfer in the gravity flow region

The $T(d)$ profiles and the isotherm cross sections presented above suggest that advective heat transport may be significant in the Great Hungarian Plain. However, according to the heat flow modelling results of Lenkey (1999), the regional gravity-driven flow causes a maximum of only $\pm 10\%$ heat flow anomaly (+10% in discharge area, -10% in recharge area). Therefore, Lenkey (1999) concluded that forced convection due to regional scale gravity-driven flow is insignificant relative to the conductive heat flow. The surface heat flow map (Figure 6.1) also appears to support this conclusion,

inasmuch as no unequivocal differences in surface heat flow pattern can be discerned between the regional discharge and recharge areas.

The vertical hydraulic gradients in the upper unconfined groundwater flow regime were estimated from the hydraulic cross sections (Figures 4.32 through 4.41), and they are about 5 m/500 m. For a vertical hydraulic conductivity of $K_{vertic} = 10^{-5} - 10^{-6}$ m/s (realistic in the Nagyalföld Aquifer) the Darcy-flux is $q = 10^{-7} - 10^{-8}$ m/s, and for a porosity of $\phi = 20\%$, the flow velocity is approximately $v = 5 \times 10^{-9} - 5 \times 10^{-10}$ m/s $\approx 15 - 1.5$ cm/a. In the Quaternary sediments, flow velocities in the order of $v = 10 - 100$ cm/a were also determined from radiocarbon dating (J. Deák, 1997, *personal communication* and I. Forró, 1999, *written communication*). Flow velocity in the order of 1 – 10 cm/a is usually sufficient to cause significant advective perturbations (Smith and Chapman, 1983; Deming, 1994/b).

Another way to estimate the predominance of advective or conductive heat transfer is to calculate the dimensionless Péclet number using equation 6.9 (Domenico and Palciauskas, 1973). For a model calculation, consider on the hydraulic cross section **H1** (Figure 4.33) the segment $L = 40 - 110$ km, which corresponds to a *unit basin*. In this unit basin, the gravity-driven flow system in the Nagyalföld Aquifer penetrates to an average depth of ~ 1500 m. The total hydraulic head drop in this unit basin is $\Delta h = 130 \text{ m} - 80 \text{ m} = 50 \text{ m}$. Assuming that $C = 4180 \text{ J/kg } ^\circ\text{C}$; $K = 10^{-6}$ m/s is isotropic; $\rho_w = 1000 \text{ kg/m}^3$; $\kappa = 1.8 \text{ W/m K}$; $\Delta z_f = 1500 \text{ m}$; and $L = 70 \text{ km}$; from equation (6.9) the modified Péclet number is $N_P = 1.24$. This means that heat transfer in the Nagyalföld Aquifer is predominantly advective. The error induced by the assumed thermal conductivity is negligible compared to the effect of hydraulic conductivity, because a one order of magnitude change in the bulk hydraulic conductivity modifies N_P by an order of magnitude. Hence, for $K = 10^{-7}$ m/s, we get $N_P = 0.124$, which means that forced convection is neither dominant nor a negligible mechanism. Lenkey (1999) assumed a horizontal hydraulic conductivity value of $K_{horiz} = 3.32 \times 10^{-6}$ m/s and an anisotropy coefficient of $K_{horiz}/K_{vertic} = 30$ in his regional scale models, and concluded that advective heat transport in the gravity-driven flow regime is negligible.

In the Great Hungarian Plain, the depth-to-length ratio of regional flow systems is on the order of 0.01. Thus, from Figure 6.7, it is concluded that the threshold hydraulic

conductivity required for advection to become noticeable is approximately $K \approx 3 \times 10^{-7}$ m/s, and advection may become dominant if $K > 3 \times 10^{-6}$ m/s.

6.4.3 Heat transfer in the overpressured regime

6.4.3.1 Vertical seepage velocities estimated from the dimensionless Péclet number:

The velocity of groundwater flow within/across the Algyő and Endrőd Aquitards was assumed to be sufficiently low to cause advection (Dövényi and Horváth, 1988). This assumption was later confirmed by results of two-dimensional numerical modelling calculations of compaction driven flow, which took into consideration the rate of basin subsidence, the rate of porosity decrease, and porosity-depth trend functions for sandstone and shale (Figure 2.14, p. 33; Lenkey, 1999). It is possible, however, to test the general validity of the above assumption and conclusion by estimating the Péclet number (equation 6.6) from T(d) profiles. Data from well Tázlár-6 (Figure 6.10) was chosen for estimation of the dimensionless Péclet-number and the vertical seepage velocity using the method of Bredehoeft and Papadopoulos (1965). A sufficient number of good quality data (steady state temperature measurements) is available from each formation to allow performing the calculations. Also, the well is located in a region with expectedly high advective perturbation. The thermal conductivity was estimated with the method described above, assuming 30% sand and 70% shale for the Algyő Aquitard, and 10% sand and 90% shale for the Endrőd Aquitard, based on published well logs. The harmonic mean thermal conductivity values calculated for each formation are listed in Table 6.2. Assuming a fresh water density of $\rho_w = 1000 \text{ kg/m}^3$ and specific heat of water of $C = 4180 \text{ J/kg } ^\circ\text{C}$, the Péclet number was estimated using equation (6.6) and the type curves in Figure 6.7; the results are listed in Table 6.2. Since the estimated Péclet number is 1.5 and 1 for the Algyő and Endrőd Aquitards, respectively, it can be concluded that forced convection is the dominant heat transfer mechanism across these hydrostratigraphic units in the vicinity of the investigated well. Such an advective anomaly can be caused by channelling of fluid flow along high permeability fractures dissecting the tight aquitards. The magnitude of the computed seepage velocity is two orders of magnitude higher than that estimated by Lenkey (1999) from compaction

models, which is realistic for flow across the above aquitards. These results do not contradict Lenkey's general conclusion regarding the dominant regional scale heat transfer mechanism in the overpressured part of the basin. Instead they highlight locally significant advective anomalies caused by locally high fluid fluxes, and provide indirect evidence for vertical cross-formational flow across the two regional aquitards.

Table 6.2: Estimated vertical seepage velocity and Péclet number across the Algyó and Endrőd Aquitards from well Tázlár-6.

Well / Locality	Temperature °C	Depth, m	Estimated thermal conductivity, W/m K	Estimated vertical seepage velocity v_z (cm/year)	Estimated Péclet number	Hydrostratigraphic unit
Tázlár-6	53.0	1120	2.14	12.17	1.5	Algyó
	57.2	1219				
	64.4	1318				
Tázlár-6	104.6	1922	2.4	11.9	1	Endrőd
	111.8	2024				
	117.2	2074				

6.5 CONCLUSIONS

The dominant heat transfer mechanism at the regional scale in the Great Hungarian Plain is conduction, while the role of forced convection varies throughout the basin. Advective perturbations of the thermal field are noticeable on T(d) profiles and geothermal cross sections in certain parts of the upper unconfined gravity-driven flow regime. Estimates of the modified Péclet number (equation 6.9; Figure 6.7) suggest that advection would be dominant in the study area under the given topographic conditions, if the thermal and hydraulic properties of the rock framework were isotropic, and if the hydraulic conductivity were $K > 3 \times 10^{-6}$ m/s. This ideal condition is not satisfied in the basin. Within the deep overpressured zone, heat transfer is also dominated by conduction,

while advective thermal anomalies occur as *isotherm plumes* or *domes* in the vicinity of faults, along which flow channelling is observed from hydraulic cross sections.

Heat distribution in the study area is controlled by the morphology of the high thermal conductivity basement, by the thickness of the overlying clastic sediments with low thermal conductivity, and by the regional and local groundwater flow systems. Generally, the average surface heat flow correlates well with the complex topography of the Pre-Neogene basement. In the vicinity of basement highs underneath recharge areas, the surface heat flow may not always reflect possible cooling effects of descending meteoric water compared to adjacent areas, because of the overwhelming influence of the proximity of the basal heat source. Thus, it may not be appropriate to define thermal anomalies as differences between actual measured values and some regional average reference (nominal) value of temperature (calculated from a regional mean thermal gradient) in the context of the Pannonian Basin, due to the large range of variation of these parameters.

Hydrocarbon accumulations in the Great Hungarian Plain are often associated with positive thermal anomalies, yet the actual nature of these anomalies is not always advective. From the geothermal cross sections it can be observed that the geothermal anomalies in the vicinity of hydrocarbon accumulations are generally attenuated within the upper gravity-driven flow regime, and they are not detectable in the upper $z = -100$ to -600 m elevation range. Thus, shallow geothermal surveys are not expected to reveal the existence of deep lying thermal anomalies that could be indicative of hydrocarbon accumulation. An exception to this general statement is the south-eastern part of the basin (Pusztaföldvár – Battonya region), where the positive thermal anomalies persist within the $z = -100$ to -2500 m elevation range, and where significant oil and gas accumulations were discovered.

7 EVALUATION OF THE POSSIBLE MECHANISMS ABLE TO GENERATE AND MAINTAIN THE OVERPRESSURED REGIME IN THE PANNONIAN BASIN

7.1 INTRODUCTION

Systematic mapping of pressure distribution to a depth of ~3700 m revealed the existence of two regional flow regimes in the Great Hungarian Plain (Chapter 4). An upper unconfined regime, characterised by quasi-hydrostatic pressures, extends to depths of ~300 to ~1800 m. This is underlain by a confined flow regime, where pressures in excess of hydrostatic commonly reach 10 – 35 MPa, locally approaching lithostatic values (see Chapter 4 for details). In the unconfined flow regime, the non-hydrostatic pressures appear to be in hydrodynamic equilibrium with the present hydrogeologic environment, i.e., flow is at steady-state driven by gravity. The regional occurrence of the overpressured regime (i.e., overpressures are ubiquitous throughout the study area) reflects hydrodynamic disequilibrium, which must be due to regionally effective geologic processes or energy sources that were or presently are active in the basin. The non-uniform distribution of overpressures (i.e., overpressures are observed everywhere, but at different depths and with variable magnitude) may be explained in terms of permeability heterogeneity at regional and local scales, by the contribution of locally effective energy sources and sinks, and also by the spatial and temporal variation of pressure generating and dissipating factors. Maintenance of anomalous pressures depends on the ‘lifetime’ and spatial distribution of the pressure-energy sources (Neuzil, 1995), and the hydraulic resistance of the rock framework (Tóth and Millar, 1983).

The objective of this Chapter is to evaluate the probable contribution/efficiency of overpressuring mechanisms potentially present in the Great Hungarian Plain, and to determine those likely to explain the anomalous pressure regime. As a corollary, the probability of the existence of paleo-flow systems is evaluated. The working hypothesis is that a recent increase in the magnitude of lateral tectonic compression is the principal cause of present day overpressures in the Great Hungarian Plain. Overpressures are

envisaged here as transient hydrodynamic phenomena (Bredehoeft and Hanshaw, 1968, Hanshaw and Bredehoeft, 1968; Bethke, 1989; Neuzil, 1995).

7.2 OVERPRESSURES AND RELATED HYDRODYNAMIC EQUATIONS

7.2.1 Overpressuring mechanisms

Overpressure is defined as fluid pressure in excess of hydrostatic for a fluid of density ρ_f . Several natural mechanisms can generate overpressures, and these mechanisms can be divided into three categories (Osborne and Swarbrick, 1997):

- a) increase in compressive stress (i.e., pore volume reduction), caused by disequilibrium compaction and/or lateral tectonic compression;
- b) changes in fluid volume, due to thermal expansion (aquathermal pressuring), diagenesis (mineral phase transformation), hydrocarbon (gas and oil) generation;
- c) fluid movement and processes related to density differences between fluids and/or gases caused by hydraulic gradients, buoyancy forces, and osmosis.

The mechanisms from category a) and b) are related to ongoing geologic processes, which generate *disequilibrium-type overpressures* (i.e., pore pressures not adjusted to their hydrogeologic environment), while those from c) generate *equilibrium-type overpressures* (i.e., pore pressures are adjusted to their hydrogeologic environment), as defined by Neuzil (1995).

Usually, overpressures are generated by the coupled action of some of the above forces (Neuzil, 1995). The relative efficiency of coupled forces may vary significantly in space and time, having the effect of distributed sources or sinks for fluid flow in any sedimentary basin. Hence, the pore pressure distribution reflects the complex signature of the superposition of hydraulic stresses of different age in a heterogeneous medium with finite permeability (Parks and Tóth, 1995). The geological, geophysical, and geochemical characteristics of a sedimentary basin control which overpressuring mechanisms could be operative during the different evolutionary stages of a basin, and also the relative efficiency of each mechanism (Neuzil, 1995). Maintenance of overpressures is a function of the hydraulic properties of the porous medium (hydraulic conductivity and specific storage) and of the vigour and lifetime of the pressure-energy sources. Overpressures are

created whenever the rate of pressure generation exceeds the rate of pressure dissipation. The rate of fluid-pressure dissipation across a porous medium is inversely proportional to that medium's hydraulic conductivity. Therefore, low-conductivity regions are essential for the generation and maintenance of both equilibrium- and disequilibrium-type overpressures (Neuzil, 1995). In the absence of a continuous pressure-energy source, the overpressures would dissipate over time until hydrodynamic equilibrium with the hydrogeologic environment is reached. Therefore, problems related to pressure-maintenance are best approached by that of transient flow. This, already classical, hydrodynamic approach was taken by Hubbert and Rubey (1959), Bredehoeft and Hanshaw (1968), Hanshaw and Bredehoeft (1968), Tóth and Millar (1983), Domenico and Palciauskas (1988), Ge and Garven (1989, 1992, 1994), Tóth et al. (1991), Corbet and Bethke (1992), Parks and Tóth (1995), to enumerate only a few. Earlier studies in the Great Hungarian Plain (e.g., Somfai, 1976; Szalay, 1982, 1983, 1988) favoured the 'static' approach of Powers (1967), Barker (1972), and Magara (1976) to explain the occurrence and magnitude of observed overpressures. Neuzil (1995) offers a conceptual hydrodynamic framework for, and discusses the mathematical aspects of, overpressuring mechanisms. A detailed description and critical evaluation of overpressuring mechanisms can be found in Gretener (1981) and Osborne and Swarbrick (1997). The equations of fluid flow and transport, as well as the limitations of some mathematical models developed for analysing fluid flow and pressure anomalies, are reviewed by Person et al. (1996).

7.2.2 Equation of fluid flow in deforming porous media

The governing equation of fluid flow in a deforming porous medium is based on the mass conservation principle, which relates the net mass flux to the change in mass storage, and is expressed with reference to non-fixed co-ordinates as (after Domenico and Palciauskas, 1979):

$$\rho_f S_s \frac{\partial h}{\partial t} - \rho_f \left(\phi \alpha_T \frac{\partial T}{\partial t} + \alpha_P \frac{\partial \sigma_T}{\partial t} - \phi \alpha_c \frac{\partial C}{\partial t} \right) = -\text{div}(\rho_f \mathbf{q}) \quad (7.1)$$

Where ρ_f is fluid density [kg m^{-3}], S_s specific storage [m^{-1}], h hydraulic head [m], t time [s], ϕ porosity, α_T coefficient of thermal expansion of porous medium [$^{\circ}\text{C}^{-1}$], T temperature [$^{\circ}\text{C}$], α_P compressibility of porous medium due to changes in total stress [$\text{m s}^2 \text{kg}^{-1}$], σ_T total stress [N m^{-2}], α_C density coefficient due to salinity changes [L mg^{-1}], C concentration of total dissolved solids [mg L^{-1}], and \mathbf{q} is the Darcy-flux vector [m s^{-1}].

The terms on the left side of equation (7.1) represent the time rate change in fluid mass storage within a deforming unit volume of rock due to changes in hydraulic head $\left(\rho_f S_s \frac{\partial h}{\partial t}\right)$, thermal expansion $\left(\rho_f \phi \alpha_T \frac{\partial T}{\partial t}\right)$, mechanical loading $\left(\rho_f \alpha_P \frac{\partial \sigma_T}{\partial t}\right)$, and the effects of salinity on density $\left(\rho_f \phi \alpha_C \frac{\partial C}{\partial t}\right)$, respectively. The latter three terms represent the sources and sinks for fluid flow, i.e., the *geologic forcing*, Γ (Neuzil, 1995). The right side of equation (7.1) stands for the net mass flux of fluid across a unit volume of porous rock. Equation (7.1) can account for groundwater flow inducing mechanisms such as compaction, thermal expansion, variable density, and topography-driven flow. Neuzil (1995) demonstrated through a non-dimensional analysis of equation (7.1) that overpressures preferentially develop in low-conductivity (K) rocks, and also the size of the domain (L) and the strength of the geologic forcing are important controls on the efficiency of overpressuring mechanism. By defining the dimensionless geologic forcing is defined as $\Gamma_D = \frac{L}{K} \Gamma$, significant overpressures can develop, whenever $\Gamma_D > 1$.

According to Luo and Vasseur (1992), mechanical loading is the most significant mechanism in the creation of excess pressures approaching lithostatic values. Thus, in equation (7.1) the terms of thermal expansion and fluid density may be negligible relative to the mechanical loading term. For evaluating the probable magnitude of overpressures generated by mechanical loading with equation (7.1), it is assumed that the deformation is poro-elastic, the medium is fully saturated, and the strain is infinitesimal. Basin scale processes, however, involve large-scale three-dimensional strains and non-linear elastic-plastic deformations over geologic time. To account for the effects of mechanical loading, additional equations are required to describe the force balance and stress equilibrium within the deforming porous media, such as:

$$\text{div}[\boldsymbol{\sigma}] = -\mathbf{F} \quad (7.2)$$

where $[\sigma]$ is the internal stress tensor and F is the force vector, which may include body forces, external tectonic forces, and the weight of overburden. The relationship between the stress and strain ($[\varepsilon]$) can be established by constitutive equations, which incorporate the effects of pore pressure (p) (Jaeger and Cook, 1972):

$$[\varepsilon] = \frac{1}{E} ((1+\nu)[\sigma] - \nu \text{Tr}[\sigma] \delta_i^j) + \frac{p}{3H} \delta_i^j \quad (7.3)$$

where E is the Young's modulus, ν is the Poisson ratio, $\text{Tr}[\sigma] = \sigma_T$, δ_i^j is the Kronecker delta (=1, if $i = j$; =0, if $i \neq j$), and H is Biot's bulk modulus for porous medium. The time-derivative ($\partial/\partial t$) of equation (7.3) expresses the relationship between the rate of applied stress and the rates of deformation and pore pressure changes. The vigour of the mechanical loading term is a function of the stress rate (Neuzil, 1995).

According to the consolidation theory of Terzaghi (1925), also known as the principle of effective stress, the total mechanical stress (σ_T) acting upon a porous medium saturated with fluid is born by the fluid and the solid rock:

$$\sigma_T = \sigma_e + p \quad (7.4)$$

where σ_e is the effective stress in the solid framework and p is the pore pressure. This equation implies that under conditions of constant total stress, i.e., $\Delta\sigma_T = 0$, any change in fluid pressure will be accompanied by an equal change in effective stress with opposite sign, i.e., $\Delta\sigma_e = -\Delta p$.

7.2.3 Lifetime of transient overpressures

In the absence of a continuous pressure-energy source, disequilibrium overpressures dissipate until equilibrium with the environment is reached (Neuzil, 1995). The time needed for a pressure (or hydraulic head) transient to dissipate across a layer of thickness z and hydraulic diffusivity K/S_s can be calculated from a particular solution of equation (7.1), following the analysis of Bredehoeft and Hanshaw (1968; p. 1101). Assuming a stepwise head change at the boundary of a semi-infinite layer with uniform hydraulic characteristics, the time of dissipation is (from the solution of Carslaw and Jaeger, 1959):

$$t = \frac{S_s z^2}{4K} \quad (7.5)$$

From equation (7.5) it can be seen that the time of dissipation is directly proportional to the square of the layer's thickness and inversely proportional to the layer's hydraulic conductivity. In the case of layered hydraulic systems (sequence of aquitards alternating with aquifers), dissipation of excess pressure in a basin is controlled by the least permeable aquitards with the highest 'hydraulic resistance' ($= z/K$) (Tóth and Millar, 1983).

7.3 RESULTS AND DISCUSSION

The total elevation difference in the Great Hungarian Plain is ~ 100 m. Hence, the excess pore pressure possibly due to the topographic relief (i.e., gravity) is < 0.5 MPa, or the excess hydraulic head is < 50 m. Thus, for practical purposes, hereafter we shall refer to overpressures (p_o) in the study area as those pore pressures, which exceed the nominal pore pressure by at least 0.5 MPa:

$$p_o = p - p_n \geq 0.5 \text{ MPa}, \quad (7.6)$$

or expressed as *excess hydraulic head* (h_o):

$$h_o = h - h_n = \left(z + \frac{p}{\rho_f g} \right) - \left(z + \frac{p_n}{\rho_f g} \right) = \frac{p_o}{\rho_f g} \geq 50 \text{ m} \quad (7.7)$$

Where p is the actual measured pressure at elevation z , p_n is the hydrostatic (nominal) pressure at the same point, h is the actual hydraulic head, and h_n is the hydrostatic (nominal) hydraulic head at the same point of observation. The advantage of this modification is that it facilitates recognition of pore pressures that are higher than the pressures possibly due to gravity. On the other hand, subtle overpressuring mechanisms, which generate modest overpressures ($p_o < 0.5$ MPa) and are superimposed on topography-controlled overpressures, remain undetected. Since the central issue in this study is to determine the most probable causes of overpressures ranging between $p_o = 1$ and 35 MPa, the above modification seems justified.

7.3.1 Compaction due to vertical loading

7.3.1.1 Overview of the mechanism

Accumulation of sediments in a subsiding sedimentary basin increases the overburden stress, which results in compaction of sediments by porosity reduction and fluid expulsion (Bethke, 1989). When the rate of fluid expulsion exceeds the rate of porosity reduction as a result of a restriction imposed by low-permeability layers (commonly shale), significant overpressures may develop. Thus, the fluids are bearing a substantially larger proportion of the overburden weight than they would in a fully compacted (consolidated) rock framework under equilibrium conditions (Bethke, 1989).

The magnitude of excess pressure due to sedimentation can be estimated from an analytical solution of equation (7.1), by considering only the mechanical loading term as 'geologic forcing', Darcy's Law, and the equation of state for slightly compressible fluid and solid (e.g., Gibson, 1958; Bredehoeft and Hanshaw, 1968). The assumptions of this solution are: continuous sedimentation at constant rate, incompressible fluids and solids, constant hydraulic diffusivity (i.e., the incurring changes in hydraulic conductivity are compensated for by changes in specific storage), vertical stress and flow, zero lateral strain, and lateral and basal no-flow boundary. Thus, the equation describing excess pressure due to compaction within the sediments is:

$$\frac{\partial^2 p_o}{\partial z^2} = \frac{S_s}{K} \frac{\partial p_o}{\partial t} - \gamma' \frac{\partial l}{\partial t} \quad (7.8)$$

Boundary conditions:

$$l = 0 \quad \text{for } t = 0 \text{ (0 sediment thickness at the start of accumulation)}$$

$$\left(\frac{\partial p_o}{\partial z} \right)_{z=0} = 0 \quad \text{for } t \geq 0 \text{ (basal no-flow boundary)}$$

$$p_o(l, t) = 0 \quad \text{for } t > 0 \text{ (hydrostatic pressure at the top of sediments).}$$

Where $\gamma' = (\rho_s - \rho_f)g$; ρ_s is the bulk density of the sediments, ρ_f is fluid density, S_s is specific storage, l is the sediment thickness, t is time since deposition, and p_o is super-hydrostatic pressure. Bredehoeft and Hanshaw (1968) presented a graphic solution for equation (7.8) (Figure 7.1), which allows the calculation of a compactional pressure-depth curve. For the calculation of a compactional $p(d)$ curve using the graphical solution

of equation (7.8), the dimensionless time, $\frac{t}{T^*} = \frac{S_s l^2}{K t}$, must be computed first, where t is the total time of deposition, $l/t = \omega$ is the rate of sedimentation, and $T^* = K/\omega^2 S_s$ is a time-constant for the basin (Domenico and Schwartz, 1998; p. 176). The excess pressure vs. depth curve is calculated from the dimensionless pressure values corresponding to the dimensionless depth values, z/l , ($= 0$, at the bottom, and $= 1$ at the top of the sedimentary pile). For $t/T^* < 0.1$ no significant excess pressure can develop, whereas pore pressure values approaching lithostatic values can develop for values of t/T^* ranging between 10 and 100. From the expressions of the dimensionless time and dimensionless pressure as well as Figure 7.1 it can be seen that the higher the sedimentation rate, the larger overpressures can develop.

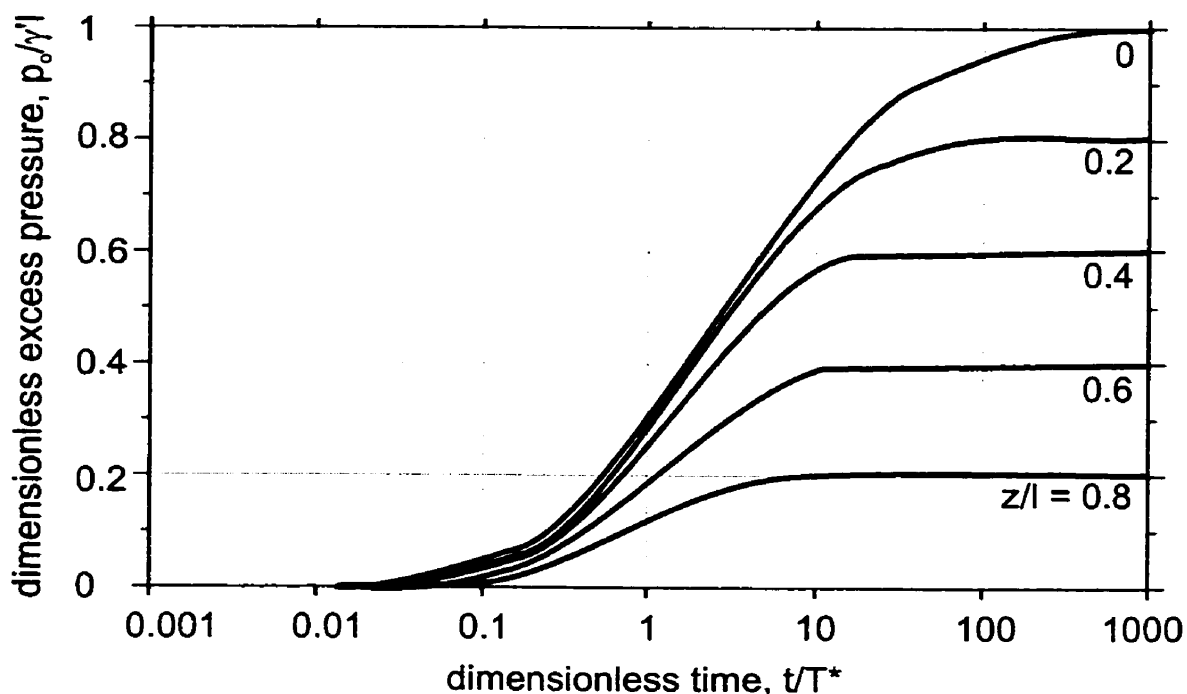


Figure 7.1: Graphic solution of the flow equation for vertical loading of Bredehoeft and Hanshaw (1968). L is the thickness of the accumulated sediments, and z/l is a dimensionless depth ranging from 0 at the bottom of the sediments to 1 at the top. The dimensionless time, t/T^* , and the dimensionless pressure are discussed in text.

Person et al. (1996) demonstrated that the above graphical solution systematically overestimates excess pressures compared to the numerical models, which incorporate porosity-depth trend functions. Hence, the graphical solution is only suitable for order-of-magnitude estimates, as needed for this study. Two-dimensional numerical models of

compaction in the Viking Graben and the Gulf Coast by Bethke et al. (1988) and Harrison and Summa (1991) showed that the top of overpressured zone shallows toward the deeper parts of the sedimentary basin. Also, maximum overpressures are observed in the core of depositional centres of sedimentary basins, where the steady increase of fluid pressure gradient versus depth is reversed toward the basement.

Results of a one-dimensional analysis of compaction for distinct locations in a basin may be difficult to generalise in three-dimensions, because it is hard to link the effects of spatially and temporally variable factors, such as the distribution of deposition rate. However, one-dimensional analytical methods still offer a good insight into the magnitude and efficiency of burial compaction. For instance, this approach is suitable for examining the effects of variable sedimentation rate on overpressuring by compaction. Both tectonic movements and climatic changes control the rates of erosion, sediment transport, deposition, and basin subsidence (Allen and Allen, 1990). These two controlling factors vary over time. Therefore, the rate of sedimentation also varies over extended time periods during a basin's evolution. Such fluctuations in sedimentation rates are reflected by the variable thickness of the sediments deposited over discrete time intervals. During periods of peak deposition rates, the vertical stress rate $\left(\frac{\partial^2 \sigma_v}{\partial t^2}\right)$ may dramatically increase, which ultimately leads to rapid increase of compactional overpressures.

7.3.3.2 The role of compaction in overpressure generation in the Great Hungarian Plain

Compaction has been considered the most plausible explanation for the observed overpressures in the Great Hungarian Plain. Earlier studies (e.g., Somfai, 1976; Szalay, 1982, 1983, 1988) relied on lumped pressure-depth analysis, and followed the 'static' approach of Powers (1967), Barker (1972), and Magara (1976). More recently, van Balen (1995) and Lenkey (1999) prepared two-dimensional numerical models of compactional fluid flow, which also involved forward modelling of sedimentation in the Great Hungarian Plain. In these latter models, the overpressure generation was calibrated using pressure measurements from the deepest borehole (Hód-I) drilled in the central part of the Makó Trough. The pattern of pore pressure and fluid flow distribution obtained by their models was similar to that obtained by Harrison and Summa (1991) for a simpler basin

geometry in the Gulf Coast. A common drawback of these earlier studies on overpressures in the Great Hungarian Plain is the lack of distributed analysis of pressure distribution.

In order to evaluate the role of compaction in the Great Hungarian Plain, the following questions need to be answered:

- a) Was the rate of sedimentation sufficiently high everywhere in the basin to create overpressures of the observed magnitude and spatial distribution, given the hydraulic conductivity values measured on the deposited sediments?
- b) What are the maximum values of overpressure that could have been generated by compaction in the basin, and are such values confirmed by direct field evidence?
- c) How would a continuous sedimentation of non-uniform rate affect compactional overpressures?
- d) Is it plausible to attribute the overpressures encountered in Neogene sediments above the basement highs to compaction?
- e) Are the assumed hydraulic conductivity values realistic at a regional scale?
- f) For how long could these overpressures be maintained, i.e., how long would it take to dissipate such overpressures?
- g) Does the distribution of fluid potential anomalies and the flow directions inferred from both fluid-potential maps and cross sections match the flow directions calculated by compactional models?
- h) Are the overpressures within the relatively rigid basement highs due to vertical compaction (i.e., due to elastic or plastic porosity reduction in the Pre-Neogene consolidated rocks caused by vertical loading)?

In the Great Hungarian Plain, the thickness of clastic sediments deposited during the last 17 Myr varies between ~1000 m above basement highs to ~7000 m in the deep basement grabens. Thus, the average rate of deposition varies between ~59 m/Myr to ~412 m/Ma. Previous studies from other basins have demonstrated that continuous deposition of over 5000 m of sediments with low hydraulic conductivity ($<10^{-11}$ m/s) at such average depositional rates can generate large compactional overpressures (Bredehoeft and Hanshaw, 1968; Bethke, 1985, 1989). The maximum compactional overpressures are expected in the deepest part of the basins, because those regions have

experienced the highest rate of sedimentation, in contrast to the regions above the flanks toward the edges of the basins.

In the deep sub-basins of the Great Hungarian Plain, the average rate of sedimentation might have been sufficiently high to generate compactional overpressures approaching lithostatic values, if the bulk hydraulic conductivity of the deposited sediments were $K \leq 10^{-11}$ m/s. Above the basement highs, the sediment thickness is generally less than 2000 – 2500 m, and the depositional rates averaged over 17 Myr are less than 117 or 147 m/Ma. The hydraulic conductivity of these sediments is commonly $K \geq 10^{-10}$ m/s (Figure 2.15; Szabó, 1955; Szalay, 1982). Whether or not significant compactional overpressures may develop under these conditions must be evaluated quantitatively. A quick order of magnitude estimate can be obtained using the one-dimensional graphical solution of Bredehoeft and Hanshaw (1968), as shown below.

Assuming that the total sediment thickness is $l_1 = 2000$ m above a basement high, and $l_2 = 6500$ m in a basement depression, the hydraulic conductivity is $K = 10^{-10}$ m/s, the duration of sedimentation $t = 17$ Ma, the specific storage is $S_s = 0.003$ m⁻¹ (Appendix 3), and $\gamma' = (\rho_s - \rho_f)g = (2700 \text{ kg/m}^3 - 1000 \text{ kg/m}^3) \cdot 9.8 \text{ m/s}^2 = 16.7 \text{ MPa/km}$, we obtain for the dimensionless time at the top of the basement high (H):

$$\left(\frac{t}{T^*}\right)_H = \frac{S_s l_1^2}{K t} = \frac{3 \cdot 10^{-3} \text{ m}^{-1} \cdot 4 \cdot 10^6 \text{ m}^2}{10^{-10} \text{ m/s} \cdot 17 \cdot 10^6 \text{ a}} = \frac{12 \text{ m}}{17 \cdot 10^{-1} \text{ m/s} \cdot 31.536 \cdot 10^6 \text{ s}} = \frac{12}{53.6112} = 0.22$$

and at the base of basement grabens (G):

$$\left(\frac{t}{T^*}\right)_G = \frac{S_s l_2^2}{K t} = \frac{3 \cdot 10^{-3} \text{ m}^{-1} \cdot 42.25 \cdot 10^6 \text{ m}^2}{10^{-10} \text{ m/s} \cdot 17 \cdot 10^6 \text{ a}} = \frac{126.75 \text{ m}}{17 \cdot 10^{-1} \text{ m/s} \cdot 31.536 \text{ s}} = \frac{126.75}{53.6112} = 2.36$$

Thus, from Figure 7.1, the corresponding values of the dimensionless pressure at the bottom of the sedimentary piles (at $z/l = 0$) are: $\left(\frac{p_o}{\gamma' l_1}\right)_H \approx 0.09$, and $\left(\frac{p_o}{\gamma' l_2}\right)_G \approx 0.46$, respectively. The resultant overpressures at the bottom of the sedimentary piles above the basement highs will be: $p_{oH} = 0.09 \cdot 16.7 \text{ MPa/km} \cdot 2 \text{ km} = 3.01 \text{ MPa}$, under 2000 m of sediments, and $p_{oG} = 0.46 \cdot 16.7 \text{ MPa/km} \cdot 6.5 \text{ km} = 49.9 \text{ MPa}$, under 6500 m of sediments. Such estimates indicate that significant compactional overpressures might

have developed throughout the basin, if the sedimentation rates are averaged over the entire duration of the basin infilling, and the lowest documented hydraulic conductivity value is considered representative for the entire sedimentary pile. Whether or not it is reasonable to consider long-term averages of depositional rates, and if the magnitude of the resultant overpressures can be presently encountered in the study area, needs further attention.

The Great Hungarian Plain was filled by prograding delta systems, and the depositional centres shifted through time from the north and north-east toward south and south-west, respectively (Section 2.5). Hence, the deep sub-basins in the southern and south-eastern part of the study area (i.e., the Makó Trough and the Békés Depression; Figure 2.19) were the last to be filled. Therefore, the total duration of sedimentation in these two sub-basins was less than 17 Ma. Nevertheless, the basement highs in the southern part of the Great Hungarian Plain were buried probably during an even shorter time period than the adjacent grabens. Under these circumstances, it does not seem reasonable to consider depositional rates averaged over the entire duration of the basin infilling, i.e., over ~17 Ma, for evaluating the role of compaction as a potentially efficient overpressuring mechanism throughout the Great Hungarian Plain.

Owing to the time-transgressive nature of the Lower and Upper Pannonian formation boundaries (Section 2.5), it is difficult to establish the variation of sedimentation rate during the past 10.4 Myr throughout the basin. The turbidites and the delta slope sediments (i.e., the Szolnok Formation and the Algyő Formation, respectively) were probably deposited at peak rates, because of the very nature of their high-energy depositional process. Indeed, based on van Balen's (1995) forward modelling of sedimentation and his computed decompaction curves, the Algyő Formation was deposited over a period of 1 to 2 Myr in the Makó Trough and its pre-compaction thickness reached ~2400 m. Van Balen (1995) and Lenkey (1999) also calculated the possible depositional history for the Makó Trough. According to their results, the peak depositional rate in the Makó Trough was 4000 m/Myr between 7 and 5.5 Ma; this was preceded by a rate of 600 m/Myr and followed by a rate of 1000 m/Myr between 5.5 and 2.4 Ma. Horváth et al. (1988) calculated subsidence history curves for five deep wells in the Great Hungarian Plain, north of the Makó Trough, using a combination of

stratigraphic data, porosity data, seismic profiles, paleo water depth data, vitrinite reflectance data, temperature-depth profiles, and heat flow values. Their results show peak subsidence and depositional rates of 500 to 700 m/Myr during the past 12 to 10 Myr. The last sedimentation period took place in the Quaternary, i.e., during the last 1.8 Myr (Figure 2.9). This time, the depositional rates varied between ~50 to 370 m/Ma. The distribution of Quaternary sedimentation rates was calculated as the ratio between the thickness of layers and 1.8 Ma, using the available stratigraphic data; the results are illustrated in Figure 7.2. This map shows that the regions above the deep sub-basins show the fastest depositional rates (up to 370 m/Ma). It is beyond doubt that such peak depositional rates could have significantly contributed to overpressuring in the study area. However, there are two peculiarities related to areas where peak depositional rates were calculated. First, these areas do not systematically coincide with the loci of maximum overpressures; second, even if the magnitude of overpressures encountered in these areas can be reproduced with compactional models, the maintenance of such overpressures over geologic time is questionable.

Estimating the magnitude of overpressures generated by peak sedimentation rates is subjective, as the results strongly depend on the choice of hydraulic conductivity and specific storage values. For instance (by repeating the steps of the above sample calculations for new parameters): deposition of $l = 1000$ m sediments with $S_s = 0.003$ m⁻¹ and $K_1 = 10^{-10}$ m/s during $t = 1$ Ma, can generate $p_{o1} = 5.01$ MPa overpressure at the base of the pile. If $K_2 = 10^{-11}$ m/s is chosen, the resulting overpressure is $p_{o2} = 12.56$ MPa. As long as there is a lack of adequate knowledge of the hydraulic conductivity distribution in these sediments, prediction of compactional overpressure magnitudes remains speculative.

Hydraulic conductivity values ranging between 10^{-11} to 10^{-13} m/s are realistic for shales (Freeze and Cherry, 1979; p. 29, Table 2.2). However, judging from the average permeability values measured on shales in the Great Hungarian Plain (Figure 2.15, p. 34), it seems unlikely that such values would be representative for regionally effective pressure “seals¹” in this basin. The technical detection limit of permeability

¹ A pressure seal is defined by Hunt (1990, p. 2) as “...a zone of rocks capable of hydraulic sealing, that is, preventing the flow of oil, gas, and water ... the term refers to seals that prevent essentially all pore fluid movement over substantial intervals of geologic time.”

measurements in MOL, Plc. labs is 10^{-17} m^2 (B. Kiss, 1996, *personal communication*), which approximately corresponds to a hydraulic conductivity of $K = 10^{-10} \text{ m/s}$. Therefore, shale permeability values below the detection limit are prone to subjective speculation.

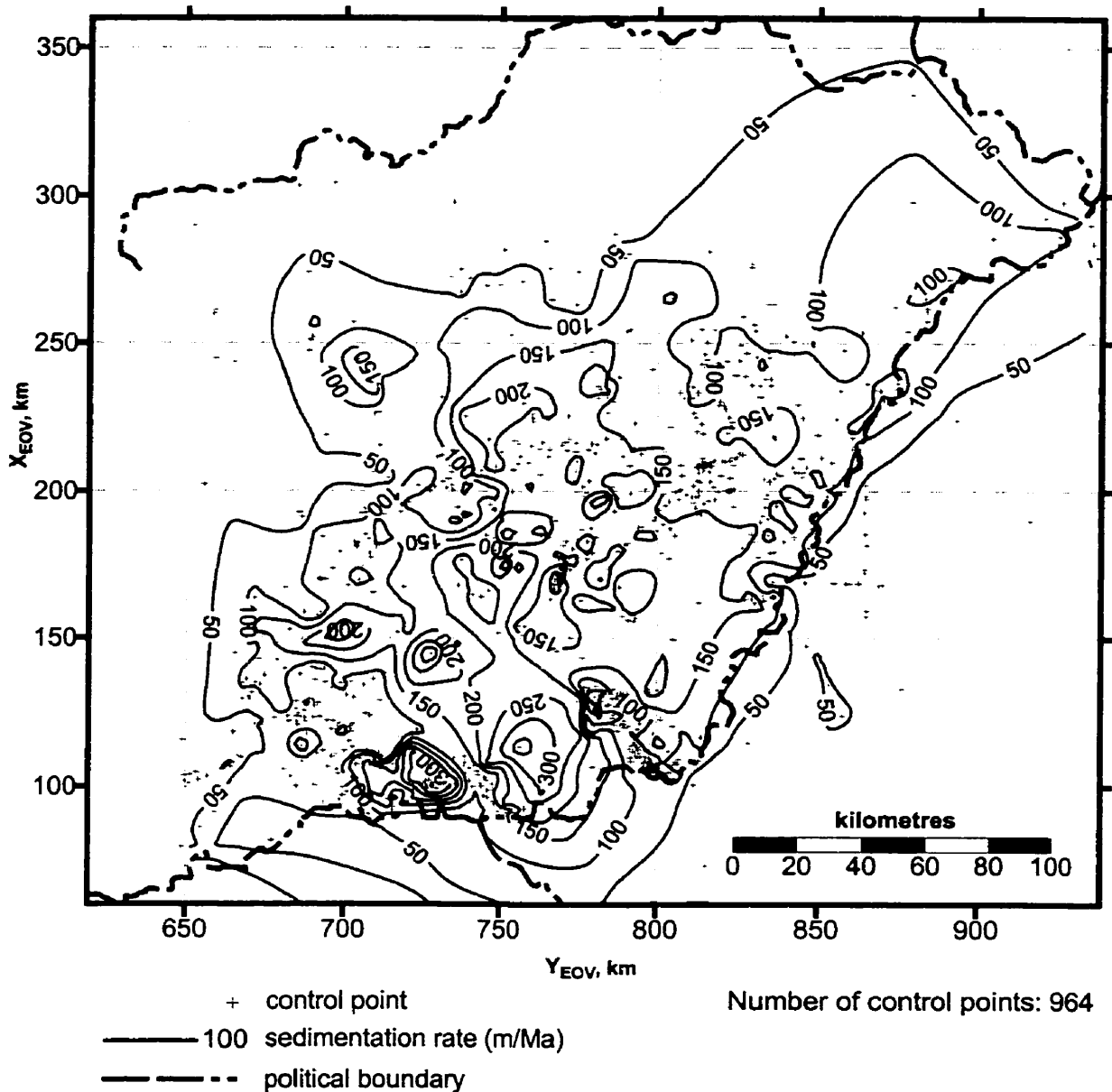


Figure 7.2: Contour map of sedimentation rate during the Quaternary (1.8 Ma) in the Great Hungarian Plain. Contour interval: 50 m/Ma.

The regional vertical conductivity of the two regional aquitards might be significantly higher than that required by the calibration of compactional flow models (e.g., van Balen, 1995; Lenkey, 1999). This is supported by the lithologic heterogeneity

of the Algyő Aquitard, local absence (Juhász, 1992, and Figure 2.20) and brittle deformation of the Endrőd Aquitard observed from core cuttings (Phillips et al., 1994), and the relatively high measured core permeability values (MOL, Plc. database).

According to the studies on scale effect of Bredehoeft et al. (1983), the vertical hydraulic conductivity of the Cretaceous Pierre Shale can be up to three orders of magnitude higher at the regional scale than the values obtained from laboratory measurements. It seems reasonable, therefore, to assume that the shale/marl aquitards in the Great Hungarian Plain might present similar scale effects.

In the Great Hungarian Plain, the hydraulic conductivity values of psammitic rocks are in the range of $K = 10^{-5} - 10^{-7}$ m/s. The hydraulic conductivity of the Algyő Aquitard is known to vary within $K = 10^{-6} - 10^{-11}$ m/s, it contains important hydrocarbon reservoirs, and it is known to leak hydrocarbons through breaches above basement highs (Mátyás and Matter, 1997). Thus, the magnitude of regional hydraulic conductivity ($K \leq 10^{-11}$ m/s) required for compaction to be an effective cause of overpressures in the Great Hungarian Plain is not supported by direct observations/measurements nor by theoretical considerations, i.e., scale effects. This implies that a sedimentation rate of at least 3000 to 4000 m/Myr would be required to compensate for the low hydraulic resistance, and generate large overpressures of the observed magnitude. For instance (using the graphical solution of Bredehoeft and Hanshaw, 1968 in Figure 7.1): generation of an overpressure of 25 MPa at the base of 2500 m sediments with $K = 10^{-10}$ m/s, and $S_s = 0.003$ m⁻¹, requires a sedimentation rate of $\omega = 4000$ m/Ma. Such sedimentation rates are not characteristic for the whole basin, neither as averages over 17 Ma, nor as peaks, over shorter time periods.

The lifetime of overpressures within the Great Hungarian Plain was estimated with equation (7.5). The maximum time required for a pressure transient to dissipate across the Endrőd Aquitard at its thickest ($z_{\max} = 300$ m) and lowest conductivity ($K = 10^{-10} - 10^{-11}$ m/s) zones, assuming that $S_s = 0.003$ m⁻¹, is $t_E \approx 22\ 200$ to $222\ 000$ years. In the case of the Algyő Aquitard, the pressure dissipation time across 1000 m consolidated shale (a rare occurrence!) with $K = 10^{-8} - 10^{-10}$ m s⁻¹ is $t_A \approx 2400$ to $240\ 000$ years. The dissipation time across the aquifers is < 1 to 1000 years, owing to their high hydraulic conductivity ($K = 10^{-5} - 10^{-8}$ m s⁻¹). Based on equation (7.5), Deming (1994a; p. 1008) prepared a nomogram to estimate the time over which a layer of

a given thickness and permeability can act as a pressure seal. From Deming's nomogram it appears that the two major aquitards in the Great Hungarian Plain could maintain overpressures for more than 10^6 years, if their permeability would be in the order of $k = 10^{-21}$ to 10^{-23} m² (or hydraulic conductivity of $K = 10^{-14}$ – 10^{-16} m/s). These estimates imply that overpressures generated 5 – 8 Ma (Szalay, 1988) would not be detectable today, if the true conductivity of the two major aquitards is, indeed, in the order of $K = 10^{-8}$ – 10^{-11} m/s. Thus, compaction-induced overpressures can not be maintained over geologic time scale by the two major aquitards, which implies that the present day overpressures can not be attributed to vertical compaction, if vertical loading ceased within the past 3×10^4 to 3×10^5 years. The short pressure diffusion times also suggest that the probability of preservation of paleo-flow systems that might have developed earlier (> 1 Ma) in the study area is very low.

Horizontal flow directions calculated by two-dimensional compactional flow models indicate flow from the centre of the basin toward its flanks and upwards (e.g., Bethke, 1985; van Balen, 1995; Lenkey, 1999). Below a certain depth in the core of the depocentres, the reversal of pressure gradients induces downward flow (Harrison and Summa, 1991). Based on fluid-potential contours from actual data, below a depth of ~2000 m the horizontal components of groundwater flow are directed toward the centre of the sub-basins (Figures 4.27 through 4.29, and 4.33 through 4.42). These flow directions are opposite to those expected from idealised compactional models.

The ubiquity of overpressures within the rigid Pre-Neogene basement rocks can not be due to vertical sedimentary loading because of several reasons. 1) Large overpressures (up to 34 MPa) are common in basement highs, which experienced the least vertical stress (shown above). 2) The elastic response of the basement to high vertical loading rates would be significantly lower than that of the clastic sediments, due to its lower compressibility relative to the sand-shale sequences. 3) The excess pressure possibly generated by vertical loading would have had dissipated already across the overlying aquitards. 4) Fluid escape from basement rocks is also facilitated by secondary permeability increase due to hydraulic fracturing, documented by Horváth and Cloetingh (1996). 5) Infiltration of meteoric water across the overlying lower Pannonian units into the basement has also been documented (e.g., Juhász et al., 2000); 6) a presently active

mechanism is required to explain the actual pressure distribution in the basement, and sedimentary loading does not seem to be the one.

In summary, compaction does not appear to be the dominant regional overpressuring mechanism in the Great Hungarian Plain, because the observed spatial distribution of overpressures and the relatively low hydraulic resistance of sediments do not support the theoretically expected parameter values and pore pressure distribution patterns. The Quaternary-to-Recent subsidence and sedimentation in the Great Hungarian Plain may have contributed to the increase in pressure within the Makó Trough and perhaps the Békés Depression (areas of maximum burial stress rate, >300 m/Ma). However, vertical loading alone can not adequately explain the observed magnitude of excess pressures and inferred flow directions in these sub-basins.

7.3.2 Aquathermal pressuring

7.3.2.1 Overview of the mechanism

Barker (1972) introduced the term “aquathermal pressuring” to describe the pore pressure variation in an isolated volume of porous medium due to temperature gradients greater than ~ 15 °C/km. In order for aquathermal pressuring to be effective, the pore volume expansion due to heating must be less than the volumetric expansion of the fluids, and the medium must be perfectly sealed, i.e., zero-permeability seal. None of the permeability reducing processes (diagenesis or gas capillary seals) can produce sufficiently low or demonstrable zero permeability to satisfy this requirement (Osborne and Swarbrick, 1997). According to Barker (1972), aquathermal pressuring is scale invariant, i.e., at basin scale it would require a regionally extensive zero permeability seal at a certain depth. If such perfect seals did exist, then the pressure vs. depth profiles would present an abrupt increase in pressure at the depth of the seal from quasi-hydrostatic to quasi-lithostatic, without any transition. In fact, a gradual increase in pressure gradient within the depth range of the seal implies flow through a medium with finite permeability.

Luo and Vasseur (1992) demonstrated through a one-dimensional sensitivity analysis that aquathermal pressuring has a negligible efficiency as an overpressuring mechanism compared to disequilibrium compaction even in rocks with unrealistically low hydraulic conductivity ($K = 3 \times 10^{-20}$ m/s) and thermal gradients of 50 °C/km. Corbet and Bethke (1992) arrived at similar conclusion in their study on disequilibrium pressures in the Western Canada Sedimentary Basin. Their study also demonstrated that aquathermal pressuring is significant only where subsidence is not accompanied by compaction, and if Darcy flow does not occur. McPherson and Garven (1999) arrived to identical conclusion as Luo and Vasseur (1992) and Corbet and Bethke (1992), by analysing the effect of thermal loading in a two-dimensional numerical model for the Sacramento basin, California. Furthermore, McPherson and Garven (1999) observed a decrease in pressure due to heating, which they attributed to the decrease in density and viscosity of water.

7.3.2.2 The possible role of aquathermal pressuring in the Great Hungarian Plain

The generally high average geothermal gradients (~50 °C/km; Chapter 6) and the presence of abnormally high pore pressures within and below the two regional aquitards offered some hope for solution of the enigma of overpressuring mechanisms in the Great Hungarian Plain (e.g., Somfai, 1976, 1994) by invoking aquathermal pressuring. The coincidence of abrupt increases in pore pressure with positive geothermal anomalies was interpreted in terms of “hermetic isolation” of highly porous rocks by perfect shale seals, and subsidence of such “isolated compartments” without compaction and fluid flow accompanied by a high thermal gradient (Somfai, 1976; Szalay, 1982). The lack of Darcy-flow required for this mechanism to be effective implies that the pressure gradient should be hydrostatic within the “isolated compartment” although the absolute pressure values are abnormally high. The $p(z)$ profiles constructed in various parts of the study area (see Chapter 4) do not confirm this expectation, instead they show super-hydrostatic gradients, which imply ascending fluid flow. This would explain the associated positive thermal anomalies as the result of advective heat transport by ascending water from deeper overpressured zones. The basic requirement of aquathermal pressuring, i.e., existence of perfectly closed systems, is clearly not satisfied or supported by field

evidence in the Great Hungarian Plain, hence it is concluded that aquathermal pressuring is unimportant in this basin.

7.3.3 Osmosis

7.3.3.1 Overview of the mechanism

Osmosis can generate overpressures in a layered porous medium when a semi-permeable membrane, like clay, separates two aqueous solutions of different salinity. The concentration difference will drive the electro-neutral water molecules across the membrane from the low-salinity zone to the high-salinity zone. If the high salinity zone is a closed system, the hydraulic head would increase to a critical level beyond which further water intake is impossible (Domenico and Schwartz, 1990). If the low-salinity zone were a closed system, then the hydraulic head would decrease in it (Freeze and Cherry, 1979). The maintenance of the hydraulic head differential thus created would require continuous recharge on the high-salinity side and discharge on the low-salinity side. Once the two zones are closed the possibility of external recharge/discharge is excluded –one of the arguments against this mechanism (Osborne and Swarbrick, 1997). The other contra-argument is that osmosis can be effective only at local scale (Parks and Tóth, 1995). The equilibrium osmotic pressure requires a head differential of 10 m for every 1000 mg/l concentration difference across the semi-permeable shale (Domenico and Schwartz, 1990, p. 565). Neuzil (2000) presented evidence for semi-permeable shale membranes generating up to ~20 MPa osmotic overpressures. The conditions for generating significant osmotic overpressures require large salinity contrasts (on the order of 10^5 mg/l) and very low shale porosity (< 5%). Salinity contrasts on the order of 10 000 to 50 000 mg/l may result in 1 to 5 MPa osmotic overpressures (Neuzil, 2000).

7.3.3.2 The possible role of osmosis as an overpressuring mechanism in the Great Hungarian Plain

The salinity of groundwater in the Great Hungarian Plain is fresh to brackish, with total dissolved solid contents commonly between 500 to 20 000 mg/l, never exceeding 55 000 mg/l (Rónai, 1985; Varsányi et al., 1997, 1999). Based on the published water

salinity data, the maximum concentration difference conceivable in the Great Hungarian Plain is approximately 35 000 mg/l, which requires ~350 m hydraulic head differential (~3.5 MPa overpressure). The hydraulic head differential between the gravitational and the overpressured flow regime in the basin is in the order of 500 – 1000 – 1500 m, or more. This would imply a salinity contrast in the order of 50 000 – 100 000 – 150 000 mg/l and an ideal semi-permeable membrane between the two flow regimes. None of these requirements are supported by field evidence in the basin. The relative contribution of osmosis to the generation of overpressures would be minimal due to the dilute groundwater. Hence, osmosis can be ignored as a regionally efficient overpressuring mechanism in the Great Hungarian Plain. However, local salinity increases in the overpressured regime may be attributed to ultrafiltration (Back and Hanshaw, 1965).

7.3.4 Hydrocarbon generation

7.3.4.1 Overview of the mechanism

Thermal maturation of kerogen results in transformation of solid kerogen into liquid hydrocarbons, gas, solid residue, and other by-products, accompanied by an increase in porosity and pore fluid volume (Tissot and Welte, 1984). This process could generate overpressures, if the increase of pore fluid volume would exceed the increase of porosity. The relative change in fluid vs. pore volume is a function of the amount and type of kerogen available, the intensity of the maturation process, and temperature, among others (such as compressive stress). Thermal cracking of oil to gas in reservoirs may also create abnormally high pressures (Barker, 1990). The overpressures thus created and buoyancy (section 7.3.6) are important driving forces of primary migration. Hydrocarbon generation as an overpressuring mechanism is most effective when large volumes of liquid hydrocarbon are generated over short time periods in low-permeability rocks where primary migration is restricted (Osborne and Swarbrick, 1997). Additionally, regions of active hydrocarbon generation usually coincide with the top of the overpressured zone (Spencer, 1987). For this mechanism to be regionally effective, a thick source rock of basin-wide extent is required, which is rich in organic carbon (high TOC). Otherwise only local pressure anomalies may occur. Based on the idealistic

assumption of instantaneous transformation of an extremely rich source rock with ~ 8 wt.% kerogen resulting in a 5 vol.% increase in effective porosity, the estimated maximum overpressure that could be generated by this mechanism is 7.6 MPa (Osborne and Swarbrick, 1997). The magnitude of overpressures thus created is controlled by the distribution of overburden stress between the solid framework and the pore fluid.

7.3.3.1 The possible role of hydrocarbon generation as overpressuring mechanism in the Great Hungarian Plain

The source rocks in the Great Hungarian Plain are of poor quality, with average TOC dominantly in the 0.5 – 1% range, and local peak values of 5.2% (Section 2.7). The mature Neogene source rocks (Endrőd and Algyő Formation) and the known petroleum accumulations below the “oil birth line” ($R_0 = 0.6\%$ iso-reflectance surface; at depths > 2300 m) are located mostly in the overpressured zone. Thermal conditions in the basin are favourable for maturation even above the presently known depth range of the “oil birth line” and already within the overpressured regime, due to the high heat flux (Chapter 6). Therefore, Spencer et al. (1994) concluded that hydrocarbon generation has a significant contribution to the generation and maintenance of overpressures in the Great Hungarian Plain. Yet this conclusion is arguable, as shown below.

The problems with the efficiency of this mechanism in the Great Hungarian Plain stem from the overall low total organic carbon (TOC) content of potential source rocks, their spatial distribution, the duration of the maturation process (the past 6.5 to 9.5 Ma; Szalay, 1988), and the magnitude of excess pore pressures (commonly >10 MPa). Maturation of the source rocks in the Great Hungarian Plain may generate only a fraction of the maximum possible overpressures (7.6 MPa). In the absence of ideal seals, the overpressures would dissipate over time (e.g., Deming, 1994a). Furthermore, it is still not entirely clear whether the pressure build-up facilitates or inhibits the reaction rate of kerogen transformation. Price and Wenger (1992; in Osborne and Swarbrick, 1997) found that under laboratory conditions pressure build-up inhibited all organic transformation. Also, the threshold overpressure that can be created prior to the inhibition of the maturation process is generally not known yet (Osborne and Swarbrick, 1997). Geological evidence that could support the above finding would be immature overpressured source rock at temperatures favourable for maturation, e.g., the immature

delta plain and delta slope sediments found in the overpressured zone at temperatures favourable for maturation ($T = 80 - 100 \text{ }^{\circ}\text{C}$). Further research is needed to ascertain whether these rocks are immature as a result of the inhibited maturation process due to overpressuring or because of the basin's thermal evolution.

The geothermal conditions in the Great Hungarian Plain are favourable for thermal cracking of oil to gas too, which is documented to occur in some pools (Somfai, 1994). However, this would explain only local pressure anomalies. Many of the DST's that recorded abnormally high pressures recovered water without any trace of hydrocarbons. Thus, these records also refute the regional significance of this mechanism. In conclusion, the role of hydrocarbon generation in overpressuring is ambiguous and it is not likely that this mechanism would have regional significance in the Great Hungarian Plain, but its local importance can not be ruled out.

7.3.5 Diagenesis

Diagenesis may contribute to overpressuring directly through dewatering reactions (e.g., smectite dehydration, gypsum transformation), or indirectly by destruction of permeability through cement precipitation (e.g., Neuzil, 1995). The magnitude of overpressures due to diagenetic processes is generally not known. Smectite dehydration is unlikely to be a primary cause of overpressuring, because the volume of released water is small and the reaction is inhibited by pressure build-up (Osborne and Swarbrick, 1997). Precipitation of diagenetic cements may act to reduce permeability, thus enhance fluid retention and, ultimately, facilitate maintenance of overpressures created by other mechanisms (Neuzil, 1995).

Smectite dehydration may be an important diagenetic process in the Great Hungarian Plain worthy of further research, but as a pressure-generating mechanism is probably unimportant. Transformation of gypsum to anhydrite occurs at $40 - 60 \text{ }^{\circ}\text{C}$ during shallow burial and results in the loss of 39 vol.% water; hence it is thought to create significant overpressures in evaporite sections (Osborne and Swarbrick, 1997). Overpressures measured at depths greater than 1000 m are not likely to be related to this process. Gypsum and evaporite beds are not abundant in the Great Hungarian Plain, and overpressures occur mostly at depth and temperature ranges where gypsum

transformation would not occur, anyway. Hence this process can be discarded from future analysis.

Diagenetic processes are not likely to be significant primary causes of overpressuring in the Great Hungarian Plain, however, indirectly they may have an important role in the maintenance of overpressures or local control on pressure dissipation by porosity/permeability reduction. For example, diagenetic processes may also be invoked to explain the presence of low-permeability barriers inferred from the abrupt pressure increase observed on the $p(z)$ profiles of Endrőd - Szarvas (Figure 4.12, p.90), Dévaványa (Figure 4.13, p. 92), Földes (Figure 4.14, p. 93), and Biharkeresztes regions (Figure 4.15, p. 94).

7.3.6 Buoyancy

7.3.6.1 Overview of the mechanism

Fluid density contrasts caused by salinity differences or by different fluid phases (e.g., water/oil/gas) can produce overpressures without flow, as a result of hydrostatic phenomena (Dahlberg, 1995; Neuzil, 1995). The hydrostatic pressure gradients of brines are steeper than that of fresh water. Significant hydrostatic overpressures develop in hydrocarbon accumulations of large vertical extent trapped in geologic structures by capillary forces, as illustrated on Figure 7.3. At the interface of two distinct fluid phases, the pressure in both fluids is equal. At the top of the lighter fluid, the pore pressure will exceed the hydrostatic pressure of the denser fluid expected at that depth by an amount proportional to the density (or specific gravity, γ) contrast and the height of the lighter fluid column. Overpressures due to buoyancy are characteristic to hydrocarbon provinces, they are spatially limited to the volume of pay zone in a reservoir, yet such pressure anomalies have no regional (i.e., basin wide) significance, when groundwater salinity differences are minimal.

7.3.6.2 The role of buoyancy in overpressure generation in the Great Hungarian Plain

In the Great Hungarian Plain, the height of gas and oil columns in the majority of pools is less than 100 m. Thus, overpressures attributable to buoyancy at the top of pools

are < 0.18 MPa for oil ($\gamma_{oil} \sim 8$ MPa/km) and < 0.86 MPa for gas ($\gamma_{gas} \sim 1.2$ MPa/km) accumulations. If, however, stacked gas pools are in direct hydraulic communication over >1000 m depth interval, via stratigraphic or fault connections, then at the top of the shallowest pools the hydrostatic overpressure can reach 10 MPa. Direct hydraulic communication between stacked pools can be inferred from pressure vs. depth profiles; the gas pressures from each 'individual pool' plot along a common gas hydrostatic gradient. In the study area, two examples are documented for hydrostatic overpressuring:

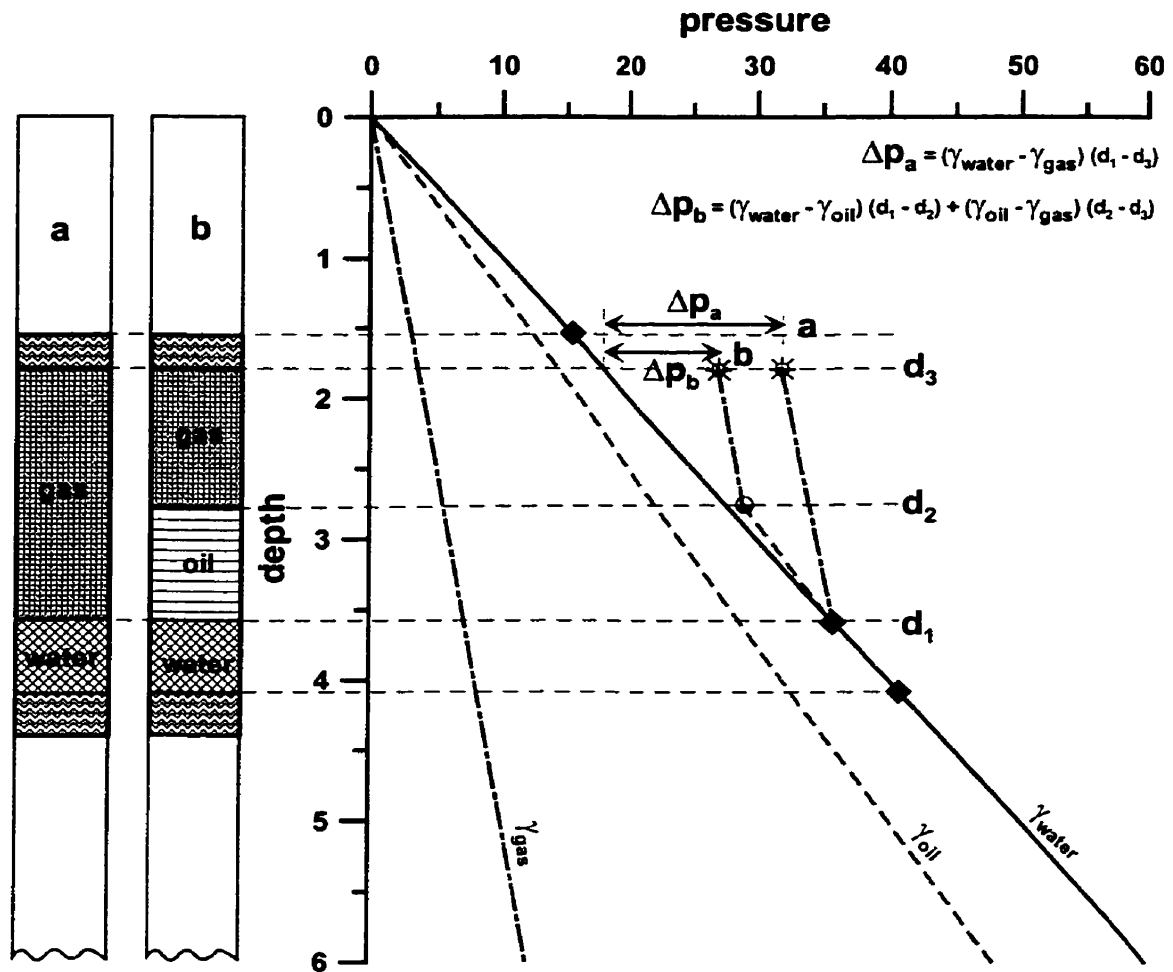


Figure 7.3: Schematic diagram of hydrostatic overpressuring due to buoyancy in a) gas accumulation and b) oil + gas accumulation. The pressure and depth units are arbitrary; γ = specific gravity or hydrostatic gradient of fluids.

- i) from the Middle-Miocene and Pre-Neogene reservoirs of the Ruzsa - Üllés fields (Figures 4.17, p. 96, and Figure 5.8, p. 153) (confirmed by S. Pap, I. Révész, and A. Somfai, Sr., 1998, 1999, *personal communication*);

- ii) from the Middle-Miocene and Pannonian reservoirs of the Sarkadkeresztúr field ($X_{EOV} \approx 835$, $Y_{EOV} \approx 175$) a 500 m high 'column' of gas and condensate with $\Delta p = 6.5$ MPa at the top (Spencer et al., 1994).

In both instances the formation water at the bottom of the petroleum accumulations is 'slightly' overpressured, i.e., 2-3 MPa above hydrostatic, probably due to hydraulic communication with deeper overpressured aquifers.

Based on the distributed pressure-depth analyses carried out for several regions in the study area it appears that significant overpressures (~9 MPa) attributable clearly to buoyancy are uncommon. The phenomenon observed in the Ruzsa-Üllés and Sarkadkeresztúr fields is rather the exception than the rule. The overall contribution of buoyancy to the observed overpressures in hydrocarbon fields is estimated to be low, and its regional significance is negligible.

7.3.7 Horizontal tectonic compression

7.3.7.1 Overview of the mechanism

In some respects, the overpressuring effect of horizontal compression is analogous to that of vertical burial compaction, the difference being that the horizontal principal stress exceeds the vertical stress due to the weight of the overburden (Domenico and Schwartz, 1998). Numerical modelling studies of Ge and Garven (1989, 1992, and 1994) and McPherson and Garven (1999) have shown that a rapid increase in the magnitude of tectonic compression can create significant overpressures and transient flow in foreland and forearc basins. These overpressures dissipate in about 10^4 years and a new steady state can be reached in about 10^5 years (Ge and Garven, 1989). The anomalously high fluid-potentials observed in the California Coast Ranges (Sacramento Basin) were explained as the result of recent tectonic compression of shales squeezed by two granitic blocks (Berry, 1973). Based on these studies, it seems reasonable to hypothesise that a recent rapid increase in magnitude of the lateral compression in the Pannonian region could be responsible for the creation of the observed excess pore pressures, without the need to increase vertical stress by additional sedimentary loading. The estimated pressure dissipation times across the two important aquitards in the Great

Hungarian Plain are short over geologic time scale (section 7.3.3.2), which justifies the need to consider very young mechanical loading to explain the present day pressure anomalies.

7.3.7.2 The role of compressive stress in overpressure generation in the Great Hungarian Plain

Based on the evaluation of potential alternative causes of overpressuring and the observed spatial distribution of pore pressures, tectonic compression appears to be the only plausible regional mechanism left to explain the anomalous pressure regime in the Great Hungarian Plain (Tóth and Almási, 1998). To test this hypothesis the following questions need to be answered:

- Are there deformation patterns and seismicity indicating compressive stress regime in the Great Hungarian Plain?
- What is the age and duration of the compressive stress regime?
- Can the overpressures be correlated with geologic structures?
- What is the magnitude of stress and the corresponding shortening rate required for producing the observed pore pressures?
- Was tectonic forcing sufficiently vigorous to generate and maintain the observed pore pressures?

The compressive nature of the present-day stress regime of the Pannonian Basin was recognised relatively recently from borehole breakout analysis, *in situ* stress measurements, and earthquake focal mechanism solutions (Dövényi and Horváth, 1990; Gerner, 1992, Gerner et al., 1999). Only the orientation of the mean trend of the stress axis was determined. Within the Great Hungarian Plain, the mean trend of the axis of maximum horizontal compression, σ_1 , is NE-SW (Gerner et al., 1999) (Figure 7.4). According to Horváth (1995), the dominant character of the regional stress field in the Pannonian Basin has been compressional since the Late Miocene to the Recent. The magnitude of the compressive stress might have fluctuated dramatically over this time period (from 10.4 Ma to Present), especially during the past 2.4 Ma, which is suggested by the episodic fluctuation of uplift and subsidence inferred from the sedimentary record (van Balen and Cloetingh, 1994). Several mild earthquakes (magnitude < 3 on the Richter scale) with epicentres in the southern part of the Pannonian Basin were recorded during

the last decade, which are a direct indication of fault activity probably caused by compressive stress regime.

In a recent study based on high-precision geodetic surveys, Grenczy et al. (2000) provided new evidence to show that the Alpine-Pannonian-Dinaric system is a region of active present shortening. The calculated relative crustal velocities are in the range of 4 to 7 mm/a, while the shortening rates are 10 – 12 ppb/a (ppb = parts per billion) along presently active strike-slip faults and less further away from the active faults.

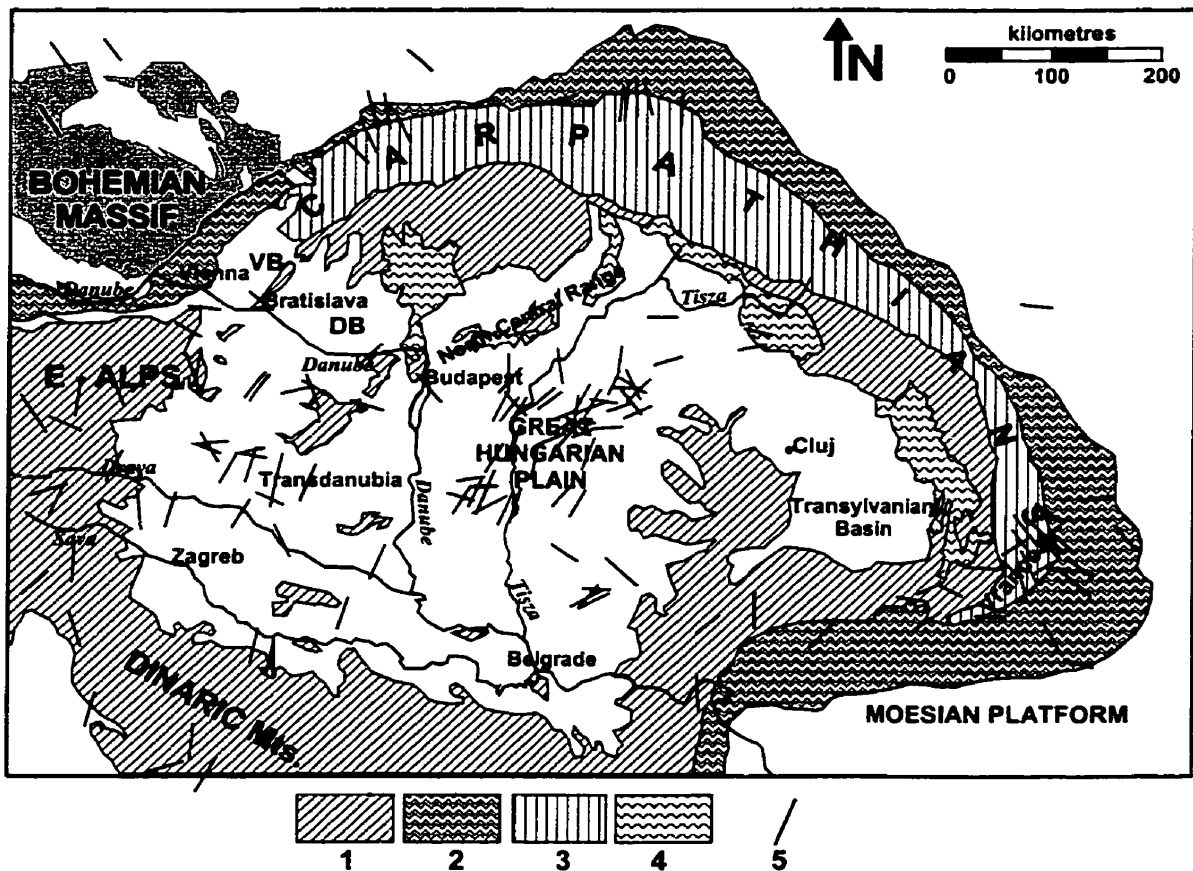


Figure 7.4: Orientation of the Recent maximum horizontal compressive stress (σ_1) axis in and around the Pannonian Basin based on field observations (data from Gerner et al., 1999). Legend: 1 = inner Alpine mountains; 2 = molasse foredeep; 3 = flysch belt; 4 = Neogene calc-alkaline volcanic rocks; 5 = σ_1 axis.

There is no compilation of tectonic field data available on recent shortening for the Pannonian Basin (L. Fodor, 1999, *personal communication*). Deformation patterns

clearly indicating young (Quaternary to Recent) regional tectonic compression in the Pannonian Basin are scarcely documented in the literature, and limited to the following:

- In the early 1920's, F. Pávai Vajna observed thrust faults and folds at shallow depths in the Quaternary sediments around Hajdúszoboszló (EOV co-ordinates: ~825/245), which he attributed to lateral tectonic compression (Rónai, 1985, p. 178).
- Flower structures, thrust faults, anticlines, and folds were observed on seismic reflection profiles in the Little Hungarian Plain and in the Great Hungarian Plain, which apparently affected Upper Pannonian and Quaternary strata (Rumpler and Horváth, 1988, Tari, 1994; the author's own interpretations of seismic profiles in 1995; L. Fodor, 1995, and L. Csontos, 1998, *personal communication*; G. Tari, 1999, *written communication*).
- Gerner et al. (1999) found evidence for recent horizontal displacement along the mid-Hungarian tectonic lineament from *in situ* stress measurements.
- Flower structure indicating strike-slip faulting (i.e., compressive stress), which apparently involved the basement and the entire overlying sedimentary pile, was interpreted on seismic profiles for the Derecske Trough, Figure 7.5, and the adjacent Földes area, Figure 7.6 (Rumpler and Horváth, 1988; Pogácsás et al. 1994).
- Folded anticline structures in the Upper Pannonian and Quaternary sediments were observed on seismic profiles above the Pusztaföldvár - Battonya High (EOV co-ordinates: $Y_{EOV} = 760-810$ km; $X_{EOV} = 100-140$ km) that may be due to recent compression (Gajdos and Pap, 1977; Tari, 1994).

The sources of recent tectonic stress were inferred from stress measurements and modelling of intraplate stress distribution (Bada et al., 1998). The results show that the Pannonian Basin is being laterally pushed by the rotating Adriatic microplate from the SW, by the Vrancea zone from E, and, to a much lesser extent, by the Bohemian Massif from NW (Figure 7.7). In the N-NE, the Western and North-Eastern Carpathians seem to act as unconstrained zones, while the Moesian platform in the SE acts as a rigid buttress. Therefore, the compressional stress field in the Pannonian Basin is analogous to a circular vise or a grip. The "tectonic vise" model for the Sacramento Basin, California, proposed by Berry (1973) and tested by McPherson and Garven (1999), seems to apply for the Pannonian Basin at a large regional scale, and to the deep sub-basins within the Great

Hungarian Plain at intermediate scale, with the necessary modifications of the boundary conditions.

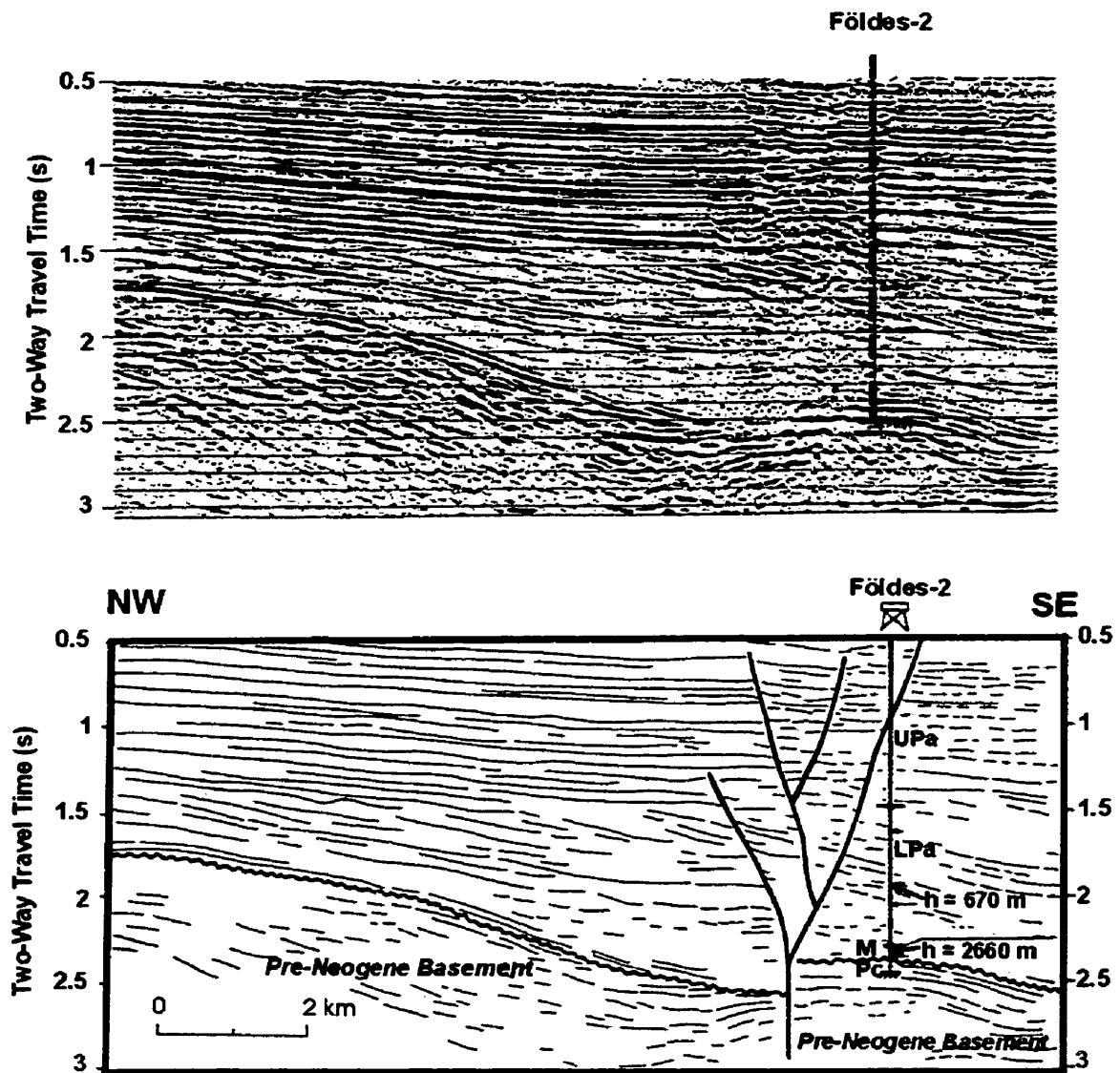


Figure 7.5: Dercske Trough. Uninterpreted migrated 24-fold seismic profile (top), and interpretation of profile (bottom). A well-developed flower structure can be identified on the SE-side of the profile above 2.5 s TWT. The wavy line represents the unconformity between the Neogene sedimentary pile and the Mesozoic-Precambrian basement complex. PC = Precambrian; M = Middle-Miocene rocks; LPa = Lower Pannonian; UPa = Upper Pannonian (modified after Pogácsás et al., 1994). The approximate vertical position of the two hydraulic head values available from this well are $h = 670$ m at $z = -1937$ m in Lower Pannonian/Algyó Fm. \sim TWT = 1.9 s; $h = 2660$ m at $z = -3151$ m in Middle-Miocene, TWT \approx 2.3 s. The trace of the cross section and well location is shown on Figure 4.4, p. 78.

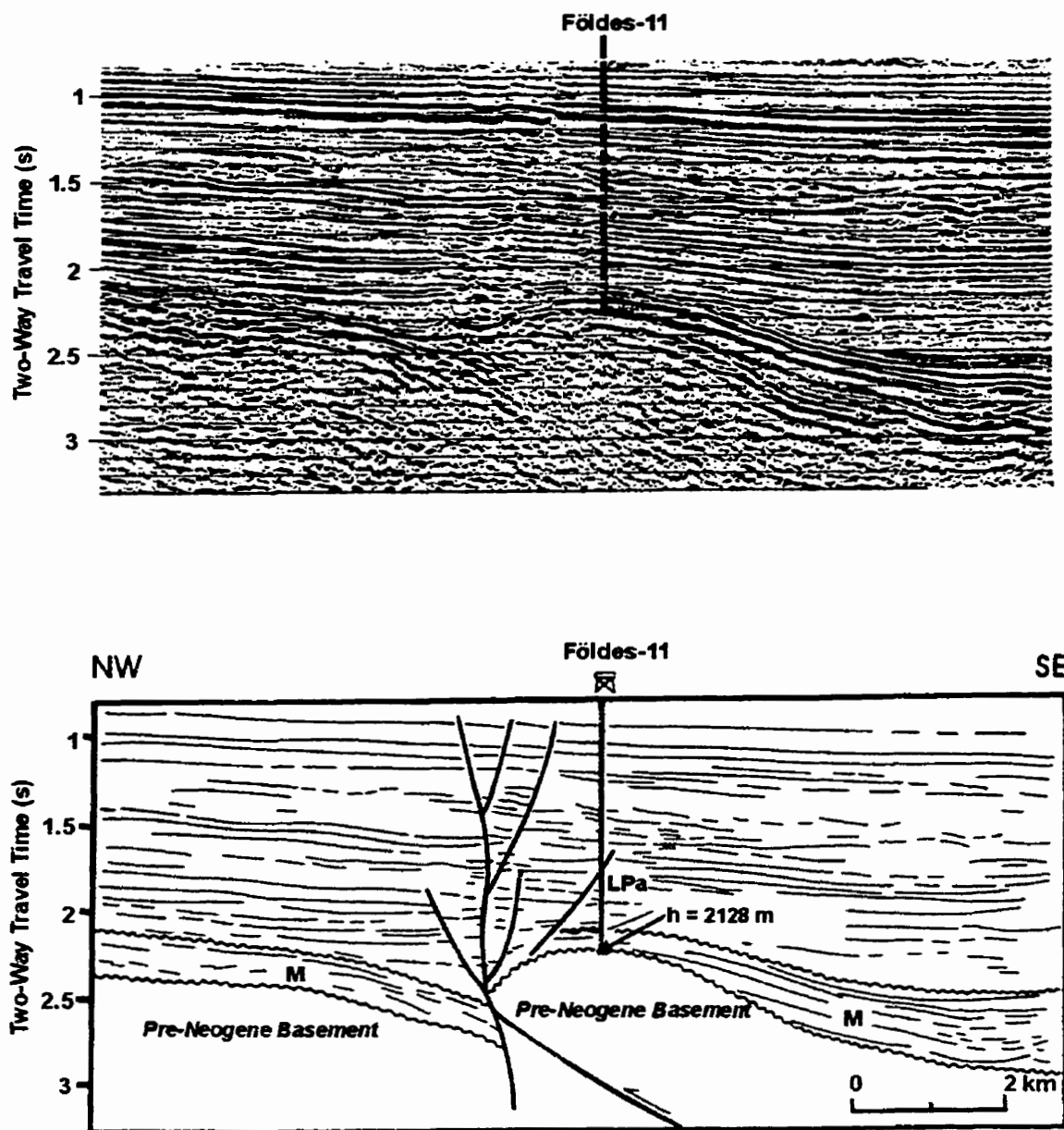


Figure 7.6: Földes region. Uninterpreted migrated 24-fold seismic profile (top), and its line-drawing interpretation (bottom). A well-developed flower structure related to a strike-slip fault can be identified in the centre of the profile above 2.5 s TWT, which is connected to a thrust fault in the basement. The age of thrusting is probably Cretaceous or Miocene. The wavy lines represent unconformity between the Middle Miocene and Lower Pannonian sediments (upper line), and the Precambrian basement and the Middle Miocene sedimentary pile (lower line). PC = Precambrian; M = Middle-Miocene rocks; LPa = Lower Pannonian (modified from Pogácsás et al., 1994). The approximate vertical position of the single hydraulic head value available from Földes-11 well are posted ($h = 2128$ m at $z = -2662$ m in the Precambrian basement, $TWT \approx 2.25$ s. Trace of the cross section and well-location is shown on Figure 4.4, p. 78.

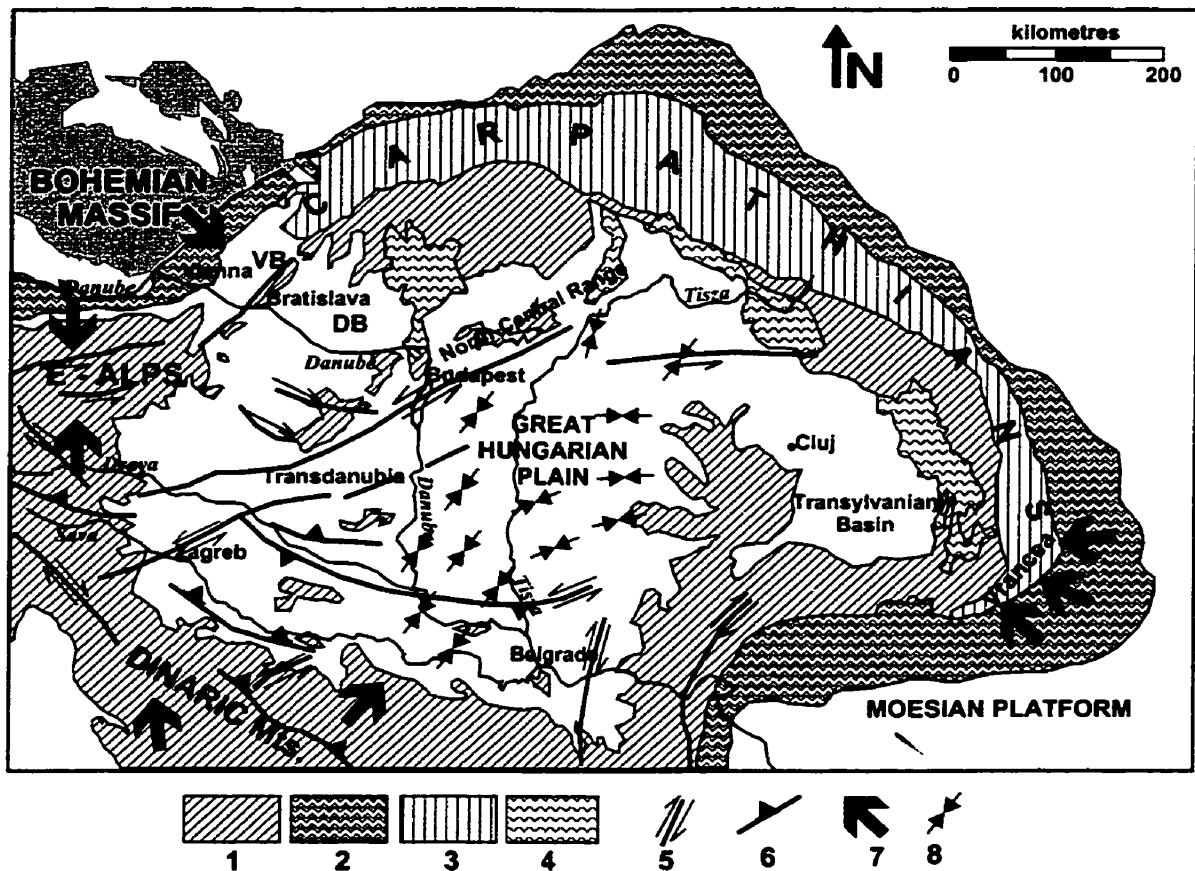


Figure 7.7: Sources of recent compressive stress in the Pannonian region (after Bada et al., 1998). Legend: 1 = inner Alpine mountains; 2 = molasse foredeep; 3 = flysch belt; 4 = Neogene calc-alkaline volcanic rocks; 5 = strike-slip fault; 6 = thrust fault; 7 = direction of present-day tectonic push; 8 = maximum compressive stress axis in the Great Hungarian Plain.

The intensity of lateral stress may be buffered through deformation of the surrounding mountains (Dinarids and Carpathian Arc). Thus, stress is transferred to the interior parts of the Pannonian Basin at a lower rate and magnitude, which still must be sufficiently high to cause deformation and increase pore pressure. Stress transfer is controlled by the rheological heterogeneity and the morphology of the deforming tectonic units (Ramsay, 1967) while the pore-pressure distribution will depend on the distribution of hydraulic diffusivity (K/S_v) within the rock framework (from equation 7.1 and 7.8). The pore pressure merely has to exceed the sum of the minimum principal stress and the tensile strength of a rock for hydraulic fracturing to occur (Secor, 1965). Compressional

overpressures may dissipate very quickly because of secondary porosity increase due to fracturing.

The Pre-Neogene basement rocks are more rigid than the overlying consolidated Lower Pannonian sediments and the poorly- to unconsolidated clastic sediments of the Upper Pannonian and Quaternary. Therefore, the mode of deformation of basement rocks is more likely poro-elastic/brittle, while the relatively softer clastic rocks are prone to plastic deformation. The compressibility of rocks is inversely proportional with their rigidity. As a result, the rate of pore pressure increase induced by sudden increases in total stress is relatively lower in the softer sediments than in the more rigid rocks. The location of the above mentioned deformation patterns coincides with fluid-potential anomalies illustrated on tomographic fluid-potential maps, hydraulic cross sections, and $p(z)$ profiles discussed in Chapter 4. Thus, there is sufficient circumstantial evidence to suggest that the present day abnormally high pore pressures may be, indeed, directly related to the very young compressional stress regime of the Pannonian Basin.

The problem of compressional overpressuring consists of two components: a mechanical problem of the stress – strain redistribution in the basin, and a hydrodynamic component which involves transient fluid flow in response to changes in boundary conditions and deformation of the porous medium. The governing force-equilibrium equations needed for the analysis of stress – strain redistribution are well known (e.g., Jaeger and Cook, 1976; Ge and Garven, 1992), while the pressure variation can be calculated from equation (7.1) by ignoring the thermal and chemical loading terms for simplicity's sake. The relationship between stress-strain-pore pressure for poro-elastic deformation is described by equation (7.3). There is no analytical solution for the system of equations describing the interrelation among tectonic stress, strain, and fluid flow (Bethke, 1989). Quantitative evaluation of the process using numerical solutions is possible for complex basin morphology and lithologic heterogeneity (Ge and Garven, 1989). Input parameters for numerical models include: basin geometry, boundary conditions regarding the deformation and flow field, material properties (permeability, porosity, compressibility, Poisson's ratio, Young's modulus), pore pressure, and the mechanical loading history (Ge and Garven, 1989). The unknown magnitudes of stress and volumetric strain can be approximated through iterative calculations, by using the observed pore pressure distribution and reasonable permeability values for calibration.

Numerical modelling of compression driven fluid flow is beyond the scope of this thesis. However, a rough estimate of the magnitudes of vertical vs. lateral loading rates is useful for the purposes of the present study. The magnitude of the mean stress is difficult and not necessary to determine, because the rate of stress is important in overpressuring. The rate of mean stress can be approximated from the vertical stress rate (rate of sedimentation). One possible way to approach this problem is to consider the stress rate, $(\partial\sigma_T/\partial t)$, from equation (7.1) the result of a mean principal stress (σ_m) (Domenico and Schwartz, 1998) and solve an appropriate variant of equation (7.8) for horizontal tectonic compression.

The mean principal stress is:

$$\sigma_m = \frac{\sigma_1 + \sigma_2 + \sigma_3}{3} \quad (7.9)$$

Assuming that $\sigma_1 = \sigma_2 = \sigma_h$ are the principal horizontal stresses and $\sigma_3 = \sigma_v$ is the principal vertical stress, equation (7.9) can be written as:

$$\sigma_m = \frac{2\sigma_h + \sigma_v}{3} \quad (7.10).$$

If the deformation of the medium is poro-elastic, then it is possible to assume that

$$\sigma_h = M \sigma_v \quad (7.11)$$

where $M > 0$ is a dimensionless constant (Jaeger and Cook, 1976); when $M = 1$, the state of stress is hydrostatic; when $0 < M < 1$, the weight of the overburden is the main principal stress; $M > 1$ indicates lateral compression induced by forces other than the weight of the overburden (Domenico and Palciauskas, 1988). By substituting equation (7.11) into (7.10) the mean stress becomes:

$$\sigma_m = \frac{2M + 1}{3} \sigma_v \quad (7.12)$$

The equation to be solved for calculating the pore pressure generated by vertical loading and horizontal tectonic compression is (Domenico and Schwartz, 1998):

$$\frac{\partial p_o}{\partial t} = \frac{K}{\rho_w \cdot g \cdot R} \cdot \frac{\partial^2 p_o}{\partial z^2} + \frac{1 + 2M}{3} \cdot \gamma \cdot \omega \cdot \left(\frac{R}{H}\right) \quad (7.13)$$

where $1/R$ and $1/H$ are Biot's coefficients of elasticity, the other terms were defined in Section 7.3.3.1. $1/R$ is the change in fluid mass due to change in fluid pressure at constant stress [Pa^{-1}]; $1/H$ is the pore compressibility [Pa^{-1}]; R/H expresses the change in fluid

pressure with stress at constant fluid mass; and $\gamma' \omega \left(\frac{R}{H} \right)$ is the effective rate of vertical loading. The graphical solution of equation (7.13) is very similar to that of equation (7.8) by Bredehoeft and Hanshaw (1968) shown on Figure 7.1, but in this case the ordinate is $p_o' / \left(\gamma' l \cdot \frac{1 + 2M R}{3 H} \right)$, instead of $p_o' / \gamma' l$. For a reference case, the basinal average sedimentation rate and $M = 1$ and $R/H = 1$ (for shale) can be used, and the procedure is identical to that used for compactional overpressures (Sections 7.3.3.1 and 7.3.3.2).

In the Great Hungarian Plain, the rate of mean stress required to produce the observed overpressures should vary between 2 and 4 times the vertical stress rate, that is, $M = 2.5 - 5.5$ (see model calculation in Appendix 4). Based on equation (7.11), the horizontal stress rate must exceed 1030 to 2266 m/Ma. Such stress rates were not common throughout the basin during the Late Pliocene-Quaternary sedimentation period. In order to assess whether the required rate of horizontal stress is realistic, the regional shortening rate must be estimated by geodetic means.

7.4 SUMMARY

Lateral tectonic compression is the most plausible explanation for the cause of regional scale overpressuring in the Great Hungarian Plain. Other potential overpressuring mechanisms either require physical conditions that are not satisfied in the basin, or the hydraulic head distribution pattern does not match the theoretically expected patterns (i.e., little or no field evidence to support other mechanisms). Buoyancy may create only local yet significant hydrostatic overpressures. The time span of pressure diffusion for the known (realistic) permeability ranges was estimated to vary between $t_E = 22\ 200$ to $222\ 000$ years across the Endrőd Aquitard and $t_A = 2400$ to $240\ 000$ years across the Algyő Aquitard. This implies that recent accumulation of up to 700 m thick sediments during the Quaternary (i.e., over ~ 1.8 Ma) could not have generated the observed overpressures. In turn, the present day overpressures must be due to recent increase in the lateral compressive stress rate. Paleo-flow systems are not likely to be preserved in the basin because of the relatively large diffusivity of the porous medium.

8 SYNTHESIS

The primary goal of the project was to reconstruct and characterise the regional groundwater flow field in the Great Hungarian Plain based on field data (stabilised water level and pore pressure measurements). Additionally, an attempt was made to evaluate the relationships between the established regional flow field on the one hand, and the hydrocarbon accumulations and the geothermal field, on the other. The observations, their interpretation, and the conclusions presented above are integrated in this Chapter.

8.1 HYDROSTRATIGRAPHY

Five regional hydrostratigraphic units were identified in the Great Hungarian Plain based on regional lithologic and stratigraphic characteristics of the rock framework, core permeability data, and empirical observations on the relative hydraulic conductivity of rock formations during water and hydrocarbon exploration and production. These units are from bottom to top: the Pre-Pannonian Aquifer ($K = 10^{-6}$ m/s), Endrőd Aquitard ($K = 10^{-9}$ m/s), Szolnok Aquifer ($K = 10^{-7}$ to 10^{-6} m/s), Algyő Aquitard ($K = 10^{-8}$ to 10^{-7} m/s) and the Nagyalföld Aquifer ($K = 10^{-5}$ m/s). Both the regional aquifers and aquitards consist of an irregularly alternating sequence of smaller (1-100 km² x 1-10 m) lenticular aquifers and aquitards. The Nagyalföld Aquifer is regionally unconfined, while the other two aquifers are regionally confined. All these hydrostratigraphic units are dissected by several faults. Geologic mapping of the Endrőd Aquitard revealed eleven locations of “breaches” (Figures 2.19 and 2.20; p. 38 and 40, respectively), i.e., zero thickness over an area of at least 25 km². These hydrostratigraphic hiatuses permit vertical hydraulic communication between the aquifers situated below and above the Endrőd Aquitard.

8.2 FLUID-POTENTIAL FIELD

The fluid-potential field between the land surface and a depth of ~3600 m was characterised based on 16 192 hydraulic head data derived from stabilised water levels

measured in drilled wells with tubing, and pore pressure measurements from drill-stem tests. The fluid-potential field was characterised by means of $p(z)$ profiles, tomographic fluid-potential maps, and vertical regional hydraulic cross sections.

The total elevation difference in the study area is ~ 100 m. Hence, the maximum hydraulic head difference possibly due to topographic control is $\Delta h \approx 50$ m, or in terms of fresh water pressure, the maximum pressure difference is $\Delta p \approx 0.5$ MPa ($\rho_w = 1000$ kg/m³). Two vertically superimposed flow regimes of basinwide extent were identified. An upper unconfined quasi-hydrostatic zone and an underlying confined overpressured zone, where pressures in excess of hydrostatic are $p_o > 0.5$ MPa and commonly reach 10 – 35 MPa. In the upper zone groundwater flow is driven by gravity, while in the lower zone the overpressures are generated by tectonic compression. The existence of a gravity-driven flow regime and an overpressured flow regime in the Great Hungarian Plain was recognised earlier by Erdélyi (1976) and Somfai (1970), respectively. The only regional hydrodynamic model for the Great Hungarian Plain prepared so far is that of Erdélyi (1976). However, the spatial extent and cross-formational hydraulic connection of these flow regimes was not well understood. Gravity-driven flow systems were believed to be limited to the Quaternary and Pliocene sediments (Erdélyi, 1976; Rónai, 1978), and the top of the Algyő Formation was considered an impermeable basal boundary for gravity flow (e.g., Erdélyi, 1976; Galsa, 1998; Lenkey, 1999). These earlier concepts are revised and updated below.

8.2.1 Gravity-driven flow regime

From the $p(z)$ profiles it was observed that within the unconfined zone the magnitude of sub-hydrostatic gradients beneath topographic highs and that of super-hydrostatic gradients beneath topographic depressions is consistent with the topographic relief of the basin. On the tomographic fluid-potential maps prepared for the $z = z_0$ to – 600 m elevation range, the hydraulic head contours display a surface, which is a subdued replica of the land surface (Figures 4.18 through 4.21, and 4.23). These maps show that the hydraulic head values gradually decrease with depth beneath topographic highs, whereas they increase with depth beneath the plains. These features are characteristic for gravity-driven flow regimes (Tóth, 1962, 1963). Thus, groundwater flow is driven by gravity in the upper zone. The regional hydraulic regime was determined by calculating

the vertical hydraulic gradient based on the hydraulic head distribution within the land surface and $z = -300$ m elevation (Figure 4.22, p. 103). In *regional recharge areas*, the hydraulic heads are decreasing downward by up to 20 m or more, and groundwater flow is directed downward. The typical land surface elevation of recharge areas is $z_0 \geq 110 - 120$ m a.s.l. The regional recharge areas in the study area are the Duna-Tisza Interfluve area (between Illancs to the S, and Gödöllő Hills to the N), the southern foothills of the North-Central Range, and the Nyírség region. In the *midline regions*, hydraulic heads barely change with depth and groundwater flows mainly laterally. Such areas are identified around the Duna-Tisza Interfluve area at $\Delta h \approx \pm 2$ m, and a narrow zone around the Nyírség, north of the Körös River, and along the Tisza River. *Regional discharge areas* are characterised by hydraulic heads increasing with depth by up to 10 m or more, and by ascending groundwater flow direction. The typical land surface elevation of these areas is $z_0 < 100 - 110$ m a.s.l. The main discharge areas are: the Duna Valley on the western side of the study area, and the lowlands encompassing the Tisza River, the Körös region (the Valleys of Fehér Körös, Fekete Körös, Sebes Körös, and Berettyó), and the Maros-Körös Interfluve area. The latter broad plain is the very core of the Great Hungarian Plain. The outline of these hydraulic regimes is in very good agreement with the map of vertical pressure gradient distribution of Rónai (1985), which is not surprising, because the two maps were based on largely the same VITUKI, Plc.-data. For the present study an updated data set was available from VITUKI, Plc.

From the $p(z)$ profiles, the regionally unconfined nature of the quasi-hydrostatic zone is inferred from the small deviation of pressure data along straight vertical pressure-gradient lines. This zone encompasses the Upper Pannonian and Quaternary formations, which act as one regionally unconfined aquifer, i.e., the Nagyalföld Aquifer. At the local scale, these formations show characteristics of layered hydraulic systems. These systems are hydraulically continuous due to the lateral and vertical communication between confined aquifers along lithologic and/or structural contacts, as shown by Halász and Szőke (1992). Within the overpressured zone, fluids are driven upward everywhere, which is best illustrated on the ten hydraulic cross sections; Figures 4.33 through 4.42. Thus, the boundary between the two pressure zones is well-constrained under recharge areas by vertical hydraulic head inversion and convergent flow.

Beneath regional recharge areas, infiltrating meteoric water reaches depths varying between ~200 to ~1700 m and it is rarely driven across the boundary between the upper Nagyalföld Aquifer and the underlying Algyő Aquitard. The lower boundary of the regional gravity-driven flow systems in regional discharge areas can not be established from the hydraulic head data, because their fluid-potential distribution pattern blends into the upper part of the overpressured zone. From the hydraulic head distribution in the Great Hungarian Plain it appears that the gravity-driven flow regime has a basal recharge boundary instead of a no-flow boundary. Water is produced from storage in the overpressured zone, and the rate of fluid expulsion must be in equilibrium with the rate of pore volume reduction. Generally, fluid flow rates estimated from compactional models are very low (Bethke, 1985); in the Great Hungarian Plain they are < 2.2 mm/a (Lenkey, 1999).

Hierarchically nested flow systems are another characteristic of gravity-driven flow regimes in basins with complex topography (Tóth, 1963). Several shallow local flow systems can be observed on the hydraulic cross sections. For instance: Figure 4.33: $L = 0 - 20$ km and $L = 100 - 110$ km; Figure 4.38; Figure 4.39: $L = 20 - 40$ km and $L = 75 - 90$ km; Figure 4.40: $L = 143 - 156$ km, and Figure 4.42: $L = 15 - 45$ km and $L = 100 - 115$ km). The spatial extent of these local flow systems varies in function of the local topographic relief and permeability distribution.

8.2.2 Overpressured zone

The overpressured zone is recognised from $p(z)$ profiles by the $p > 0.5$ MPa fluid pressure values and by the initially abrupt, then monotonic increase in the slope of vertical super-hydrostatic gradients with depth. This indicates the presence of a “deep-seated energy source,” which generates the overpressures and drives fluids upward. Overpressures within the Pre-Pannonian Aquifer are ubiquitous, which indicates that the deep-seated energy source is located within this hydrostratigraphic unit. On the fluid-potential maps below $z = -600$ m elevation, potentiometric mounds, ridges, plateaus, escarpments, and depressions are observed, which indicate that:

- i) the basin contains a regionally overpressured zone,
- ii) the spatial distribution of overpressures is not uniform,

- iii) the horizontal components of the flow driving forces are directed from basement highs toward the centres of the basement grabens filled with sediments,
- iv) the vertical components of the flow driving forces are directed upwards

Below $z \approx -1500$ m elevation, there is a remarkable spatial coincidence between the loci of steep lateral hydraulic gradients and basement faults, as well as between structural basement highs and potentiometric mounds. This implies the possibility of structural control on the pressure distribution in the basin. The steep lateral hydraulic gradients indicate large lateral permeability contrasts related to lithologic variation and/or sub-vertical fault splays in a fracture zone. In a vertical perspective of the flow field, i.e., on hydraulic cross sections, the hydraulic head contours mimic the morphology of the Pre-Neogene basement and reinforce the observation made on $p(z)$ profiles and fluid-potential maps.

8.2.3 Transition between the regional pressure regimes

The boundary between the gravity flow regime and overpressured regime is generally diffuse, locally abrupt, and it does not correlate with any particular regional hydrostratigraphic unit or elevation. The latter observation is opposite to the conclusion of Somfai (1994). In his view, there is an upper hydrostatic zone within the Quaternary and Pliocene sediments, underlain by an “upper overpressured” zone within the upper part of the Lower Pannonian strata, and a “lower overpressured” zone within the Lower Pannonian and the Pre-Neogene basement. The transition zone is generally in the elevation range of the $h = 100$ to 200 m hydraulic head contour interval; it is wide ($\Delta z = 400$ to 800 m) and gradual ($|\Delta h/\Delta z| = 0.25$ to 0.06) within basement depressions (Figure 4.46 and 4.47), whereas it is narrow ($\Delta z = 50$ to 300 m) and abrupt ($|\Delta h/\Delta z| = 2$ to 0.17) above basement highs (Figures 4.44 and 4.45). Repeated abrupt changes of the vertical hydraulic gradient versus depth (Figure 4.44 and 4.45) are believed to indicate local permeability variation caused by lithologic variation and/or faults. This conclusion is based on the inverse parametrisation problem studied by Tóth and Rakhit (1988). The lack of correlation between the transition zone of the two pressure zones and a particular hydrostratigraphic boundary observed at regional scale is probably due to the lithologic heterogeneity of the Late Miocene stratigraphic formations (Phillips et al., 1994) used as

reference. The Late Miocene lithostratigraphic units are delineated according to deltaic facies boundaries (Gajdos et al., 1983). These formation boundaries do not necessarily reflect the bulk hydraulic properties assigned to the formation (I. Révész, 1996, *personal communication*). For instance, the lower and upper part of the delta slope facies (Algyő Formation) is frequently dominated by high-permeability sandstone, yet the entire sequence is considered an aquitard because it is dominated by siltstone and clay marl of lower permeability.

8.3 ORIGIN OF OVERPRESSURES

The overpressured regime ($p_o > 0.5$ MPa) in the Great Hungarian Plain is of regional extent. Hence, only regionally effective mechanisms can explain the primary cause of overpressuring. The non-uniform distribution of overpressures is interpreted as the result of permeability heterogeneity in the rock framework, differences between the rheological properties of the rigid basement rocks and the 'soft' Neogene clastic sediments displaying various levels of consolidation, and the complex basement morphology. Burial-compaction and lateral tectonic compression are the potential, regionally effective, energy sources. Other potential mechanisms that may contribute to the generation of overpressures are aquathermal pressuring, kerogen transformation, diagenesis, osmosis, and buoyancy (Bredehoeft and Hanshaw, 1968; Neuzil, 1995).

Earlier interpretations for the origin of overpressures invoked vertical compaction and aquathermal pressuring (Somfai, 1970; Szalay, 1982, 1983), and kerogen maturation (Spencer et al., 1994). Lateral tectonic compression was invoked as an indirect cause to explain vertical compaction induced by increased subsidence and sedimentation rate in the central part of the basin, and uplift and erosion on its flanks during the Late Pliocene – Quaternary (van Balen and Cloetingh, 1994). These interpretations were based on geological (rapid subsidence and sedimentation; erosion of Pliocene sediments), geophysical (high terrestrial heat flow), and geochemical evidence (organic matter distribution and maturation conditions) required for the onset of each mechanism. Other common element of these models is the assumption of very low-permeability seals,

which permit preservation of overpressures over millions of years, and the lack of a three-dimensional picture of the fluid-potential distribution.

In the Great Hungarian Plain, there is evidence in favour of most of the above mechanisms to explain the onset of overpressuring. However, there is little evidence in support of the maintenance of overpressures over millions of years. Furthermore, the spatial distribution of present-day fluid pressures and the resulting fluid flow directions do not fit the patterns, which are theoretically expected from any of these mechanisms, or any combination thereof.

In the Great Hungarian Plain, the sedimentation rates averaged over 17 Myr (up to 412 m/Ma) would result in compactional overpressures of comparable magnitude to those observed today in deep sub-basins, only if the regional permeability of the accumulated sediments were 10^{-20} to 10^{-21} m² (or $K = 10^{-13}$ to 10^{-14} m/s). Peak depositional rates that probably occurred in the basin's history were in the range of 500 to 4000 m/Ma, and lasted for about 1 to 2 Ma. During the stages of such rapid deposition, overpressures of the observed magnitude could have been generated, if the lowest documented hydraulic conductivity value ($K = 10^{-10}$ m/a) were representative for the entire sedimentary pile. However, the maximum overpressures encountered in the $z = -2500$ to -3500 m elevation range could be generated by compaction only if a sedimentation rate on the order of 4000 m/Myr and the minimum known hydraulic conductivity were assumed. Such overpressures could be maintained over 1 Ma, if the permeability of the regional aquitards were 10^{-21} to 10^{-23} m² (or $K = 10^{-14}$ to 10^{-16} m/s). These permeability thresholds are not met by the shale aquitards from the Great Hungarian Plain. Based on the permeability ranges documented from the Algyő and Endrőd Aquitards, the overpressures would dissipate across these units within 2377 to 237 750 years and 22 190 to 221 900 years, respectively (calculated with equation 7.5). The direction of the horizontal components of fluid driving forces inferred from both the hydraulic cross sections and tomographic hydraulic maps is from the basement highs toward the centre of the deep sub-basins. These directions are opposite to those expected from two-dimensional compactional models (Harrison and Summa, 1991; Lenkey, 1999). Reversal of pressure gradients at greater depth below the depocentres was also not observed; yet another expectation of compactional models (Harrison and Summa, 1991) is not satisfied.

The ubiquity of overpressures within the rigid Pre-Neogene basement rocks can not be due to vertical sedimentary loading because:

- 1) Large overpressures (up to 20 MPa) are common in basement highs, which experienced the least vertical stress during the last 1.8 Ma.
- 2) The elastic response of the basement to vertical loading at rates of at least 400 m/Myr would be significantly lower than that of the clastic sediments due to its lower compressibility.
- 3) The excess pressure possibly generated by vertical loading would have dissipated already across the overlying aquitards. Fluid escape from basement rocks is also facilitated by secondary permeability increase due to hydraulic fracturing. Hydraulic fracturing and infiltration of meteoric water across the overlying lower Pannonian units into the basement has been documented (e.g., Horváth, 1996; Juhász et al., 2000).
- 4) Maintenance of overpressures in the basement and across the overlying aquitards over geologic time scales (> 1 Ma) is not warranted by the permeability of overlying rocks. Therefore, a presently active mechanism is required to explain the actual pressure distribution in the basement, and sedimentary loading does not seem to be sufficient.

Aquathermal pressuring has a negligible contribution to overpressuring even for high thermal gradients (50 °C/km) and unrealistically low permeability (Luo and Vasseur, 1992). Aquathermal pressuring could be an efficient overpressuring mechanism within ideally closed systems (Barker, 1972). In the Pannonian Basin, there is no documented field evidence to support assumptions that it behaves as a closed system, contrary to earlier model assumptions (e.g., Szalay, 1983). The conditions required by osmosis and kerogen maturation to generate significant overpressures are also not met. Diagenetic processes are not considered to have a significant contribution to overpressuring. Buoyancy was found plausible to explain two local excess pressure anomalies: one at Ruzsa-Üllés (Figure 5.8, p.153) and one at Sarkadkeresztúr (Spencer et al., 1994). The vertical distribution of gas pressure values measured in Middle-Miocene reservoirs plot along a gas-hydrostatic gradient at Ruzsa-Üllés. This is interpreted as the result of direct hydraulic communication between the vertically stacked gas pools. An 800 m tall gas

column was inferred from the data, and later confirmed by MOL exploration geologists (I. Révész, 1999, *personal communication*).

Present-day lateral tectonic compression is the most probable cause of overpressures, because of the following reasons:

1) The Quaternary-to-Recent regional stress regime in the Pannonian region is compressional. This was inferred from the stratigraphic record (van Balen and Cloetingh, 1994), *in situ* stress measurements, borehole breakout analysis, and earthquake focal mechanism solutions (Dövényi and Horváth, 1990; Gerner, 1992; Becker, 1993; Gerner et al., 1995), and shortening rates calculated from high resolution GPS-observations (Grenerczy et al., 2000).

2) The spatial distribution of overpressures and the resulting flow patterns correlate well with deformation patterns that are due to compressive stress. Nevertheless, the fluid-potential distribution alone implies a force field generated by a circular “tectonic vise,” analogous with the mechanism proposed by Berry (1973) for the California Coast Ranges and the flow patterns modelled by McPherson and Garven (1999).

3) Significant overpressures of the observed magnitude cannot be sustained over geologic time scale in the Great Hungarian Plain’s rock framework in the absence of an active energy source. This was inferred from estimates of pressure dissipation time based on the lowest recorded permeability values of shales (Chapter 7).

The presently active compressive regime in the Pannonian region was established in the Late Pliocene - Quaternary, i.e., about 2.4 to 1.8 Ma. If the magnitude of compressive stress would have been constant over this time period, the excess pore pressure would have dissipated and the fluid-potential field would have reached equilibrium with the crustal stress field – provided the estimated dissipation times (<0.3 Ma) across the lowest permeability aquitards are realistic. Intraplate stresses, however, have a finite duration and can be reactivated with different magnitudes (van Balen and Cloetingh, 1994). This may induce pulsatory changes in the fluid flow field (van Balen and Cloetingh, 1994). Thus, the present day overpressures in the Pannonian region and particularly in the Great Hungarian Plain are apparently due to a recent increase in intraplate compressive stress.

8.4 PETROLEUM GEOLOGY

From the spatial analysis of presently known hydrocarbon accumulations and fluid-potential anomalies characteristic for trapping conditions in the Great Hungarian Plain it is concluded that a causal link between hydrocarbon accumulations and the present-day flow field exists. The determinant role of gravity-driven flow in hydrocarbon trapping within the quasi-hydrostatic zone is recognisable under both recharge and discharge areas (e.g., Kiskunhalas, Figure 5.7 and Endrőd – Szarvas, Figure 5.5). The position of most hydrocarbon accumulations discovered within the overpressured zone above basement highs could be explained with compactional flow models, such as that of Szalay and Koncz (1993). However, several accumulations within the overpressured zone, which are found in regions of dominantly ascending flow, can be linked to either earlier compactional flow directions or present day tectonically induced flow directions. Based on the study of Tóth and Corbet (1986) on the geologic effects of flow field adjustment due to changing boundary conditions, it is postulated that hydrocarbons could have been, or may be, redistributed from above basement highs toward graben centres along the lateral component of recent regional hydraulic gradients. As a potential practical consequence, the internal parts of the grabens seem to be promising prospective areas for petroleum exploration in the future, as it was also recommended by Spencer et al. (1994).

8.5 GEOTHERMICS

Based on several temperature-depth profiles, tomographic isotherm- and thermal gradient maps, regional geothermal cross sections, and estimates of the modified Péclet number, it is concluded that the dominant heat transfer mechanism in the Great Hungarian Plain is conduction –in agreement with Dövényi and Horváth (1988) and Lenkey (1999). It appears that the relief of the water table is insufficient to induce a fluid flow velocity that could render predominance to advective heat transfer within the gravity-driven flow regime of the basin. However, advective anomalies were observed in several locations, both within the overpressured zone and the upper gravity-driven flow

regime. These anomalies seem to be related to flow channelling along structural or lithologic discontinuities, or to the locally pronounced topographic relief. Estimates of the Péclet number from one well within the two regional aquitards indicate a substantial advective anomaly. This result is interpreted as a local indirect evidence for cross-formational flow directed upwards across the regional aquitards within the overpressured zone with a vertical seepage velocity of approximately 12 cm/a. Positive thermal anomalies observed in conjunction with hydrocarbon accumulations could not generally be attributed to advection. Due to the overwhelming effect of the hot basement on the temperature and heat flow distribution in the basin, as well as the proximity of most hydrocarbon accumulations to the basement highs, it is difficult to establish the role of advective heat transfer, until reliable fluid flux estimates can be obtained.

8.6 CROSS-FORMATIONAL FLOW

Cross-formational flow across the Lower/Upper Pannonian boundary (i.e., top of Algyő Aquitard) can be inferred from the hydraulic cross sections, the mere presence of hydrocarbons generated from deeper source rocks within and above the Algyő Aquitard, from the mixing of paleometeoric water with deep basin water of NaCl-type (Varsányi et al., 1999), and local advective perturbations of the thermal field (Chapter 6). Thus, the Algyő Aquitard can not be a regionally effective barrier to hydraulic communication between the gravity-driven flow regime and the overpressured zone. The Endrőd Aquitard is considered the only regionally effective aquitard in the Great Hungarian Plain. Cross-formational flow between the Pre-Neogene basement and the Nagyalföld Aquifer is possible due to the finite permeability of the Endrőd Aquitard (MOL database), which is locally enhanced by brittle deformation; facies and lithologic boundaries (Phillips et al., 1994); through the mapped stratigraphic breaches (Chapter 2); and the large vertical hydraulic gradients (Chapter 4). Further indirect evidence for regional cross-formational flow across the major aquitards is offered by the presence of hydrocarbons generated from Mid-Miocene and Lower Pannonian source rocks in the Upper Pannonian Törtel Formation (Clayton and Koncz, 1994), and the proportion of He derived from the Mantle (1-16 %) in the shallow gravity-driven flow systems (Lenkey,

1999). In conclusion, there is sufficient direct and indirect evidence to prove that regionally the rock framework of the Great Hungarian Plain is hydraulically continuous. Several basement faults appear to channel fluid flow in the fault plain and restrict flow perpendicular to the fault walls permitting pressure relaxation toward the Neogene units (Chapter 4).

8.7 THESES

1. Two regional flow regimes are established in the Great Hungarian Plain: -an upper regionally unconfined gravity-driven flow regime and a lower confined regionally overpressured regime.
2. The transition zone/boundary between the two flow regimes does not correlate with any particular regional stratigraphic or hydrostratigraphic formation boundary, contrary to earlier suggestion by Somfai (1970, 1976, and 1994).
3. The present-day overpressures are caused directly by a recent (<0.3 Ma) increase in regional compressive stress in the lithosphere, and not indirectly, as postulated by van Balen and Cloetingh (1994).
4. The widely accepted mechanisms, i.e., vertical compaction and aquathermal pressuring (Somfai, 1976, Szalay, 1982, 1988) as possible overpressuring mechanisms are not supported by the three-dimensional picture of the fluid-potential field nor by the hydraulic properties of the rock framework.
5. The Upper Pannonian and Quaternary sedimentary units act as one regionally unconfined aquifer.
6. None of the two regional aquitards (Algyő and Endrőd) is an effective 'impermeable seal' of the overpressured regime.
7. The regional gravity-driven flow regime has a basal recharge boundary, and not a no-flow boundary, contrary to earlier assumptions (e.g., Galsa, 1998; Lenkey, 1999).
8. Hydraulic communication between the two flow regimes is achieved by vertical cross-formational flow across the two regional aquitards (Algyő and Endrőd).

9. Gravity-driven groundwater flow has a determinant effect on hydrocarbon accumulation within the upper regionally unconfined pressure regime under both regional recharge and discharge areas.
10. Forced convection is not the dominant regional heat transfer mechanism in the Great Hungarian Plain, in agreement with Dövényi and Horváth (1988) and contrary to the original working hypothesis.

8.8 RECOMMENDATIONS

One of the limitations of this study was the insufficient information for detailed characterisation of the rock framework in three-dimensions. The tremendous amount of seismic data, well logs, permeability measurements from both core plugs and DST's, that are available - but are presently inaccessible - for the Pannonian Basin should be used for integrated hydrostratigraphic studies both at regional and local scales. Without adequate knowledge about the architecture of clastic deposits and structural discontinuities in the basin, it is very difficult to continue expanding the possibilities of petroleum exploration in the basin, and to test the hypotheses formulated in this thesis.

The industrial fluid-pressure database could be improved by updating it with new measurements, and by addition of adequate information about production history. It would be beneficial to include photocopies of original pressure build-up curves, which may provide valuable information for every skilled interpreter.

The water well database of VITUKI should be updated; for instance, the coordinates of tens of thousands of water wells are still not surveyed. Thus tremendous amounts of written records could be lost in oblivion. Use of Geographic Positioning Systems would be an efficient and cost effective remedy to this problem.

Ultimately, creation of a national geological – hydrogeological database using modern Geographic Information Systems would be extremely beneficial for future research and exploration. This should consolidate the information acquired over the past century from all sources, i.e., government, industry, and private sector.

The suggested explanation for the cause of overpressures, i.e., horizontal tectonic compression, could be tested in the future by numerical flow modelling. However, such

an undertaking should be preceded by a detailed hydrostratigraphic study on the one hand, and a rock-rheological study, on the other. The boundary conditions of potential numerical models and the basic equations relating stress, strain, and fluid pressure cannot be adequately formulated, unless the nature of deformation of the rock-framework is known with reasonable detail.

The timing of overpressure generation and the position of the transition zone between the gravity driven flow regime and the overpressured regime could be constrained by isotopic analysis of water samples taken from both domains and by diagenetic studies such as that of Juhász et al., 2000.

FOOTNOTES

Page 67: ² Sections 4.1.1. and 4.1.2. are based on Tóth and Sheng (1996).

Page 143: ² Chapter 5 is based on the report of Tóth and Almási, 1998.

Page 236: ¹ A pressure seal is defined by Hunt (1990, p. 2) as “...*a zone of rocks capable of hydraulic sealing, that is, preventing the flow of oil, gas, and water ... the term refers to seals that prevent essentially all pore fluid movement over substantial intervals of geologic time.*”

BIBLIOGRAPHY

- Alföldi, L., Erdélyi, M., Gálfi, J., Korim, K., and Liebe, P., 1978, A geothermal flow system in the Pannonian Basin; case history of a complex hydrogeological study at TiszaKécske: *in* Konda, J., editor, Hydrogeology of great sedimentary basins; conference of Budapest: Memoires - International Association of Hydrogeologists, p. 716-732.
- Allen, P.A. and Allen, J. R., 1990, Basin analysis: principles and applications; Oxford, England, 451 p.
- Bachu, S., 1988, Analysis of heat transfer processes and geothermal pattern in the Alberta basin, Canada: *Journal of Geophysical Research*, v. 93, p. 7767-7781.
- Bachu, S., Sauveplane, C. M., Lytviak, A. T., and Hitchon, B., 1987, Analysis of fluid and heat regimes in sedimentary basins; techniques for use with large data bases: *American Association of Petroleum Geologists Bulletin*, v. 71, p. 822-843.
- Bada, G., Cloetingh, S., Gerner, P., and Horváth, F., 1998, Sources of recent tectonic stress in the Pannonian region; inferences from finite element modelling: *Geophysical Journal International*, v. 134, p. 87-101.
- Bair, E. S., O'Donnell, T. P., and Picking, L. W., 1985, Potentiometric mapping from incomplete drill-stem test data; Palo Duro basin area, Texas and New Mexico: *Ground Water*, v. 23, p. 198-211.

- Báldi, T., 1986, Mid-Tertiary stratigraphy and paleogeographic evolution of Hungary: Budapest, Akadémiai Kiadó, 201 p.
- Balla, Z., 1984, The Carpathian loop and the Pannonian Basin: a kinematic analysis: Geophysical Transactions, v. 30, p. 313-353.
- Bally, A.W. and Snelson, S., 1980, Realms of subsidence, *in* Miall, A. D., editor, Facts and principles of World petroleum occurrence: Canadian Society of Petroleum Geologists Memoir 6, p. 9-94.
- Balyi, K., and Papp, F., 1950, Kőzeteink hővezetőképessége (Thermal conductivity of rocks in Hungary), Földtani Közlöny, v. LXXX, p. 10-12.(in Hungarian)
- Barker, C., 1972, Aquathermal pressuring - Role of temperature in development of abnormal-pressure zones: American Association of Petroleum Geologists Bulletin, v. 56, p. 2068-2071.
- Barson, D., 1993, The hydrogeological characterisation of oil fields in north central Alberta for exploration purposes: Ph.D. thesis, University of Alberta, Edmonton, 301 p.
- Becker, A., 1993, Contemporary state of stress and neotectonic deformation in the Carpathian-Pannonian region: Terra Nova, v. 5, p. 375-388.
- Ben Dhia, H., 1987, The geothermal gradient map of central Tunisia; comparison with structural, gravimetric, and petroleum data: Tectonophysics, v. 142, p. 99-109.
- Bérczi, I., 1988, Preliminary sedimentological investigation of a Neogene depression in the Great Hungarian Plain, *in* Royden, L. H., and Horváth, F., editors, The Pannonian Basin; a study in basin evolution: American Association of Petroleum Geologists Memoir 45, p. 107-116.

- Bérczi, I., Hámor, G., Jámor, A., and Szentgyörgyi, K., 1988, Neogene sedimentation in Hungary, *in* Royden, L. H., and Horváth, F., editors, The Pannonian Basin; a study in basin evolution: American Association of Petroleum Geologists Memoir 45, p. 57-67.
- Bérczi, I., and Kókai, J., 1978, Hydrogeological features of some deep-basins in SE-Hungary as revealed by hydrocarbon exploration, *in* Konda, J., editor, Hydrogeology of great sedimentary basins; conference of Budapest: Memoires - International Association of Hydrogeologists, p. 69-93.
- Bergerat, F., 1989, From pull-apart to the rifting process; the formation of the Pannonian Basin: Tectonophysics, v. 157, p. 271-280.
- Berry, F., 1973, High Fluid-potentials in California Coast Ranges and Their Tectonic Significance, Abnormal Subsurface Pressure: American Association of Petroleum Geologists Bulletin, v.57, p. 1219-1249.
- Bethke, C. M., 1985, A numerical model of compaction-driven groundwater flow and heat transfer and its application to the paleohydrology of intracratonic sedimentary basins: Journal of Geophysical Research, v. B90, p. 6817-6828.
- Bethke, C. M., 1989, Modeling subsurface flow in sedimentary basins: Geologische Rundschau, v. 78, p. 129-154.
- Bethke, C. M., Harrison, W. J., Upson, C., and Altaner, S. P., 1988, Supercomputer analysis of sedimentary basins: Science, v. 239, p. 261-267.
- Bjørlykke, K., 1994, Fluid-flow processes and diagenesis in sedimentary basins, *in* Parnell, J., editor, Geofluids: origin, migration and evolution of fluids in sedimentary basins: Geological Society Special Publications: London, United Kingdom, Geological Society of London, v. 78, p. 127-140.

- Boldizsár, T., 1956a, Measurement of terrestrial heat flow in the coal mining district of Komló: Acta Technica Academiae Scientiarum Hungaricae, v. 15, p. 219-227.**
- Boldizsár, T., 1956b, Terrestrial heat flow in Hungary: Pure and Applied Geophysics, v. 34, p. 66-70.**
- Boldizsár, T., 1959, Terrestrial heat flow in the Nagylengyel oil field: Publication of the Mining Faculty of Sopron, v. XX, p. 27-34.**
- Boldizsár, T., 1964, Geothermal measurements of the twin shafts of Hosszúhetény: Acta Technica Academiae Scientiarum Hungaricae, v. 47/3-4, p. 467-476.**
- Boldizsár, T., 1966, Heat flow in the natural gas field of Hajdúszoboszló: Pure Applied Geophysics, v. 64, p. 121-125.**
- Boyle, R., 1671, Of the temperature of the subterranean regions as to heat and cold. Tracts written by the Honourable Robert Boyle etc. (usually called Cosmical Qualities), Davis, Oxford.**
- Bredehoeft, J. D., Belitz, K., and Sharp, H. S., 1992, The hydrodynamics of the Big Horn Basin; a study of the role of faults: American Association of Petroleum Geologists Bulletin, v. 76, p. 530-546.**
- Bredehoeft, J. D., Blyth, C. R., White, W. A., and Maxey, G. B., 1963, Possible mechanism for concentration of brines in subsurface formations: American Association of Petroleum Geologists Bulletin, v. 47(2), p. 257-269.**
- Bredehoeft, J. D., and Hanshaw, B. B., 1968, On the maintenance of anomalous fluid pressures; 1, Thick sedimentary sequences: Geological Society of America Bulletin, v. 79, p. 1097-1106.**
- Bredehoeft, J. D., Neuzil, C. E., and Milly, P. C. D., 1983, Regional flow in the Dakota Aquifer; a study of the role of confining layers: U.S. Geological Survey Water-Supply Paper 2237, 45 p.**

- Bredehoeft, J. D., and Papadopoulos, I. S., 1965, Rates of vertical groundwater movement estimated from the Earth's thermal profile: *Water Resources Research*, v. 1, p. 325-328.
- Bullard, E. C., 1965, Historical introduction to terrestrial heat flow, *in* Lee, W. H. K., editor, *Terrestrial heat flow: American Geophysical Union Monograph*, p. 1-6.
- Carslaw, H. S., and Jaeger, J. C., 1959, *Conduction of heat in solids*: Oxford, Clarendon Press, 510 p.
- Čermák, V., and Rybach, L., 1979, *Terrestrial heat flow in Europe*: New York, Springer-Verlag, ix, 328 p.
- Charpentier, R., Völgyi, L., Dolton, G., Mast, R., and Pályi, A., 1994, Undiscovered recoverable oil and gas resources, *in* Teleki, P. G., Mattick, R. E., and Kókai, J., editors, *Basin analysis in petroleum exploration; A case study from the Békés Basin, Hungary*: Kluwer Academic Publishers, printed in the Netherlands, p. 305-319.
- Clayton, J. L., and Koncz, I., 1994, Geochemistry of natural gas and carbon dioxide in the Békés Basin - implications for exploration, *in* Teleki, P. G., Mattick, R. E., and Kókai, J., editors, *Basin analysis in petroleum exploration; A case study from the Békés Basin, Hungary*: Kluwer Academic Publishers, printed in the Netherlands, p. 187 - 199.
- Clayton, J. L., Koncz, I., King, J. D., and Tatár, É., 1994, Organic geochemistry of crude oils and source rocks, Békés Basin, *in* Teleki, P. G., Mattick, R. E., and Kókai, J., editors, *Basin analysis in petroleum exploration; A case study from the Békés Basin, Hungary*: Kluwer Academic Publishers, printed in the Netherlands, p. 161 - 185.

- Clayton, J. L., Spencer, C. W., Koncz, I., and Szalay, A., 1990, Origin and migration of hydrocarbon gases and carbon dioxide, Békés Basin, southeastern Hungary: *Organic Geochemistry*, v. 15, p. 233-247.
- Corbet, T. F., and Bethke, C. M., 1992, Disequilibrium fluid pressures and groundwater flow in the western Canada sedimentary basin: *Journal of Geophysical Research*, v. B97, p. 7203-7217.
- Csató, I., 1993, Neogene sequences in the Pannonian Basin, Hungary: *Tectonophysics*: v. 226, p. 377-400.
- Csontos, L., Nagymarosy, A., Horváth, F., and Kovač, M., 1992, Tertiary evolution of the intra-Carpathian area; a model: *Tectonophysics*: v. 206, p. 221-241.
- Csontos, L., Tari, G., Bergerat, F., and Fodor, L., 1991, Evolution of the stress fields in the Carpatho-Pannonian area during the Neogene: *Tectonophysics*, v. 199, p. 73-91.
- Dahlberg, E. C., 1995, *Applied hydrodynamics in petroleum exploration*: New York, Springer Verlag, 295 p.
- Dank, V., 1988, Petroleum geology of the Pannonian Basin, Hungary; an overview, *in* Royden, L. H., and Horváth, F., editors, *The Pannonian Basin; a study in basin evolution*: American Association of Petroleum Geologists Memoir 45, p. 319-331.
- Deming, D., 1994a, Factors necessary to define a pressure seal: *American Association of Petroleum Geologists Bulletin*, v. 78, p. 1005-1009.

- Deming, D., 1994b, Fluid flow and heat transport in the upper continental crust, *in* Parnell, J., editor, *Geofluids: origin, migration and evolution of fluids in sedimentary basins: Geological Society Special Publications: London, United Kingdom, Geological Society of London*, v. 78, p. 27-42.
- Domenico, P. A., and Mifflin, M. D., 1965, Water from low-permeability sediments and land subsidence: *Water Resources Research*, v. 1, p. 563-576.
- Domenico, P. A., and Palciauskas, V. V., 1973, Theoretical analysis of forced convective heat transfer in regional groundwater flow: *Geological Society of America Bulletin*, v. 84, p. 3803-3814.
- Domenico, P. A., and Palciauskas, V. V., 1979, Thermal expansion of fluids and fracture initiation in compacting sediments: *Geological Society of America Bulletin*, v. 90, p. 518-520.
- Domenico, P. A., and Palciauskas, V. V., 1988, The generation and dissipation of abnormal fluid pressures in active depositional environments, *in* Back, W., Rosenshein, J. S., and Seaber, P. R., editors, *Hydrogeology: Boulder, CO, United States, Geological Society of America*, p. 435-445.
- Domenico, P. A., and Schwartz, F. W., 1990, *Physical and chemical hydrogeology: New York, John Wiley & Sons*, 824 p.
- Domenico, P. A., and Schwartz, F. W., 1998, *Physical and chemical hydrogeology: New York, John Wiley & Sons*, 506 p.
- Dövényi, P., and Horváth, F., 1988, A review of temperature, thermal conductivity, and heat flow data for the Pannonian Basin, *in* Royden, L. H., and Horváth, F., editors, *The Pannonian Basin; a study in basin evolution: American Association of Petroleum Geologists Memoir 45*, p. 195-233.

- Dövényi, P., and Horváth, F., 1990, Determination of contemporary crustal stress regime in Hungary: *Acta Geodetica Geophysica Montanistica Hungarica*, v. 25, p. 257-266.
- Dövényi, P., Horváth, F., Liebe, P., Gálfí, J., and Erki, I., 1983, Geothermal conditions of Hungary: *Geophysical Transactions*, v. 29, 84 p.
- Erdélyi, M., 1976, Outlines of the hydrodynamics and hydrochemistry of the Pannonian Basin: *Acta Geologica Academiae Scientiarum Hungaricae*, v. 20, p. 287-309.
- England, W. A., and Fleet, A. J., editors, 1991, *Petroleum migration: Geological Society Special Publication No. 59*, London, p. 280.
- Freeze, R. A., and Cherry, J. A., 1979, *Groundwater: Englewood Cliffs, N.J., Prentice-Hall*, xvi, 604 p.
- Freeze, R. A., and Witherspoon, P. A., 1967, Theoretical analysis of regional groundwater flow: 2. Effect of water-table configuration and subsurface permeability variation: *Water Resources Research*, v. 3, p. 623 – 634.
- Fülöp, J., and Dank, V., 1987, Magyarország földtani térképe a kainozoikum elhagyásával (Geologic map of the Pre-Neogene basement, Hungary, scale 1:500 000): Hungarian Geological Institute (MÁFI), Budapest, Hungary.
- Gajdos, I., and Pap, S., 1977, Töréses formaalakulás lehetőségei az alföldi pliocén üledékekben (Possibilities of brittle deformation in the Pliocene sediments of the Great Hungarian Plain): *Földtani Közlöny*, v. 107, p. 437-456, (in Hungarian).

- Gajdos, I., Pap, S., Somfai, A., and Völgyi, L., 1983, Az alföldi Pannóniai (s.l.) képződmények litosztatigráfiai egységei (Lithostratigraphic units of the Pannonian (s.l.) in the Great Hungarian Plain): Hungarian Geological Institute (MÁFI), Budapest, 70 p, (in Hungarian).
- Galloway, W. E., and Hobday, D. K., 1996, Terrigenous clastic depositional systems: applications to fossil fuel and groundwater resources: New York, Springer, 489 p.
- Galsa, A., 1998, Felszín alatti vízmozgás modellezése egy alföldi szelvényen, fúrólukokban mért víznyomások felhasználásával (Modelling subsurface water flow on a cross section across the Great Hungarian Plain using pressure data from water wells): Magyar Geofizika, v. 38, p. 245-256 (in Hungarian).
- Garven, G., 1989, A hydrogeologic model for the formation of the giant oil sands deposits of the Western Canada sedimentary basin: American Journal of Science, v. 289, p. 105-166.
- Garven, G., and Freeze, R. A., 1984, Theoretical analysis of the role of groundwater flow in the genesis of stratabound ore deposits; 1, Mathematical and numerical model: American Journal of Science, v. 284, p. 1085-1124.
- Garven, G., Ge, S., Person, M. A., Sverjensky, D. A., 1993, Genesis of stratabound ore deposits in the mid-continent basins of North America. 1. The role of regional groundwater flow: American Journal of Science, v. 293, p. 497-568.
- Ge, S., and Garven, G., 1989, Tectonically induced transient groundwater flow in foreland basin, *in* Price, R. A., editor, Origin and evolution of sedimentary basins and their energy and mineral resources: Geophysical Monograph 48, IUGG, Washington, D.C., United States, American Geophysical Union, p. 145-158.

- Ge, S., and Garven, G., 1992, Hydromechanical modeling of tectonically driven groundwater flow with application to the Arkoma foreland basin: *Journal of Geophysical Research*, v. B97, p. 9119-9144.
- Ge, S., and Garven, G., 1994, A theoretical model for thrust-induced deep groundwater expulsion with application to the Canadian Rocky Mountains: *Journal of Geophysical Research*, v. B99, p. 13 851 - 13 868.
- Geiger, J., Hajdúné Molnár, K., Jám bor, Á., Koncz, I., Pogácsás, G., Révész, I., Somfai, A., Szalay, Á., and Szentgyörgyi, K., 1991, A Pannon medence fejlődéstörténeti rekonstrukciója és a fejlődéstörténeti modellek alkalmazása a szénhidrogén prognózisban (The evolution of the Pannonian Basin and the application of evolutionary models for hydrocarbon prognosis)[internal report]: Hungarian Institute of Petroleum Exploration and Development, Szeged, Hungary, p. 1055, (in Hungarian).
- Gerner, P., 1992, Recent stress field of Transdanubia, Western Hungary: *Földtani Közlöny*, v. 122, p. 89-105.
- Gerner, P., Bada, G., Dövényi, P., Mueller, B., Oncescu, M. C., Cloetingh, S., and Horváth, F., 1999, Recent tectonic stress and crustal deformation in and around the Pannonian Basin, data and models, *in*: Durand, B., Jolivet, L., Horváth, F. és Séranne, M., editors, *The Mediterranean basins: Tertiary extension within the Alpine orogen*. Geological Society London Special Publication, v. 156, p. 269-294.
- Gerner, P., Dövényi, P., Horváth, F., and Müller, B., 1995, State of recent stress and seismotectonics in the Pannonian Basin and surrounding area: *Terra Abstracts*, v. 7, p. 123.
- Gibson, R. E., 1958, The progress of consolidation in a clay layer increasing in thickness with time: *Géotechnique*, v. 8, p. 171-182.

- Grenerczy Gy., Kenyeres, A., and Fejes, I., 2000, Present crustal movement and strain distribution in Central Europe inferred from GPS measurements: *Journal of Geophysical Research*, v. 105, p. 21 835-21846.
- Greener, P. E., 1981, Pore pressure: fundamentals, general ramifications, and implications for structural geology (revised): *American Association of Petroleum Geologists Education Course Note Series #4*, 131 p.
- Halász, B., 1975, A rétegzett hidrológiai rendszerek sajátosságai (Particularities of layered hydraulic systems): *Hidrológiai Közlöny*, No. 11, p. 505–507 (in Hungarian).
- Halász, B., and Szőke, S., 1992, Nem-lineáris vízgazdálkodási modell rétegzett hidrogeológiai rendszerekben (Non-linear water management model in layered hydrogeologic systems): *Hidrológiai Közlöny*, v. 72, p. 332-337 (in Hungarian).
- Hänel, R., 1980, Atlas of subsurface temperatures in the European Community: Luxembourg, Commission of the European Community, 36 p.
- Hámor, G., Ravasz-Baranyai, L., Balogh, K., and Árva-Sós, E., 1979, K/Ar dating of Miocene pyroclastic rocks in Hungary: *Annales Géologiques Helleniques*, Tome Hors Séries II., p. 491-501.
- Hanshaw, B. B., and Bredehoeft, J. D., 1968, On the maintenance of anomalous fluid pressures; 2, Source layer at depth: *Geological Society of America Bulletin*, v. 79, p. 1107-1122.
- Harrison, W. J., and Summa, L. L., 1991, Paleohydrology of the Gulf of Mexico basin: *American Journal of Science*, v. 291, p. 109-176.

- Hitchon, B., 1969a, Fluid flow in the western Canada sedimentary basin; 1. Effect of topography: *Water Resources Research*, v. 5, p. 186-195.
- Hitchon, B., 1969b, Fluid flow in the western Canada sedimentary basin; 2. Effect of geology: *Water Resources Research*, v. 5, p. 460-469.
- Hitchon, B., 1984, Geothermal gradients, hydrodynamics, and hydrocarbon occurrences, Alberta, Canada: *American Association of Petroleum Geologists Bulletin*, v. 68, p. 713-743.
- Holysh, S., and Tóth, J., 1996, Flow of formation waters; likely cause for poor definition of soil gas anomalies over oil fields in east-central Alberta, Canada, *in* Schumacher, D., and Abrams, M. A., editors, *Hydrocarbon migration and its near-surface expression: American Association of Petroleum Geologists Memoir 66*, p. 255-277.
- Homer, D. R., 1951, Pressure build-up in wells: *Proceedings of the 3rd World Petroleum Congress, Section II*, Leiden, Holland, E. J. Brill, p. 503-521.
- Horváth, F., 1988, Neotectonic behavior of the Alpine-Mediterranean region, *in* Royden, L. H., and Horváth, F., editors, *The Pannonian Basin; a study in basin evolution: American Association of Petroleum Geologists Memoir 45*, p. 49-55.
- Horváth, F., 1993, Towards a mechanical model for the formation of the Pannonian Basin: *Tectonophysics*, v. 226, p. 333-357.
- Horváth, F., 1995, Phases of compression during the evolution of the Pannonian Basin and its bearing on hydrocarbon exploration: *Marine and Petroleum Geology*, v. 12(8), p. 837-844.
- Horváth, F., and Berckhemer, H., 1982, Mediterranean back-arc basins: *Geodynamics Series*, v. 7, p. 141-173.

- Horváth, F., Bodri, L., and Ottlik, P., 1979, Geothermics of Hungary and the tectonophysics of the Pannonian Basin "Red Spot", *in* Cermak, V., and Rybach, L., editors, *Terrestrial heat flow in Europe: Berlin, Federal Republic of Germany, Springer-Verlag*, p. 206-217.
- Horváth, F., and Cloetingh, S., 1996, Stress-induced late-stage subsidence anomalies in the Pannonian Basin: *Tectonophysics*, v. 266, p. 287-300.
- Horváth, F., Dövényi, P., Erki, I., Liebe, P., Gálfi, J., and Markó, L., 1981, A Pannon medence geotermikus viszonyai. Kutatási Jelentés az MTA részére a 109/78-I. sz. megbízás alapján (Geothermal conditions of the Pannonian Basin. Research Report to the Hungarian Academy of Sciences, Budapest): Department of Geophysics, Loránd Eötvös University, Budapest, 100 p.
- Horváth, F., Dövényi, P., Szalay, A., and Royden, L. H., 1988, Subsidence, thermal, and maturation history of the Great Hungarian Plain, *in* Royden, L. H., and Horváth, F., editors, *The Pannonian Basin; a study in basin evolution: American Association of Petroleum Geologists Memoir 45*, p. 355-372.
- Horváth, F., and Pogácsás, G., 1988, Contribution of seismic reflection data to chronostratigraphy of the Pannonian Basin, *in* Royden, L. H., and Horváth, F., editors, *The Pannonian Basin; a study in basin evolution: American Association of Petroleum Geologists Memoir 45*, p. 97-105.
- Hubbert, M. K., 1940, The theory of ground-water motion: *Journal of Geology*, v. 48, p. 785-944.
- Hubbert, M. K., 1953, Entrapment of petroleum under hydrodynamic conditions: *American Association of Petroleum Geologists Bulletin*, v. 37, p. 1954-2026.

- Hubbert, M. K., and W. W. Rubey, 1959, Mechanics of fluid-filled porous solids and its application to overthrust faulting, [Part] 1 of Role of fluid pressure in mechanics of overthrust faulting: Geological Society of America Bulletin, v. 70, p. 115-166.
- Hunt, J.M., 1990, Generation and migration of petroleum from abnormally pressured fluid compartments: American Association of Petroleum Geologists Bulletin, v. 74, p. 1-12.
- Ingebritsen, S. E., and Sanford, W. E., 1998, Groundwater in geologic processes: Cambridge, Cambridge University Press, 341 p.
- Jaeger, J. C., and Cook, N. G. W., 1976, Fundamentals of rock mechanics: London, Methuen, 593 p.
- Jessop, A. M., 1990, Thermal geophysics: Developments in Solid Earth Geophysics: Amsterdam, Elsevier, 306 p.
- Juhász A., M Tóth, T., Ramseyer, K., and Matter, A., 2000, Connected fluid evolution in fractured crystalline basement and overlying sediments, Pannonian Basin, SE Hungary, Chemical Geology (*in press*).
- Juhász, G., 1991, Lithostratigraphical and sedimentological framework of the Pannonian (s.l.) sedimentary sequence in the Hungarian Plain (Alföld), eastern Hungary: Acta Geologica Hungarica, v. 34, p. 53-72.
- Juhász, G., 1992, A pannoniai (s.l.) formációk térképezése az Alföldön; elterjedés, fácies és üledékes környezet (Mapping of Pannonian (s.l.) formations in the Great Hungarian Plain; distribution, facies, and depositional environments): Földtani Közlöny, v. 122, p. 133-165, (in Hungarian).

- Kappelmeyer, O., and Hänel, R., 1974, Geothermics with special reference to application: Berlin, Gebrüder Borntraeger, 238 p.
- Kázmér, M., 1990, Birth, life and death of the Pannonian Lake: *Palaeogeographia, Palaeoclimatologia, Palaeoecologia*, v. 79, p. 171-188.
- Kertai, Gy., 1972, A kőolaj és földgáz vegyi összetétele (Chemical composition of oil and natural gas): Budapest, Akadémiai Kiadó, 112 p.
- Koncz, I., 1983, The stable carbon isotope composition of the hydrocarbon and carbon dioxide components of Hungarian natural gases: *Acta Mineralogica – Petrographica*, Szeged, Hungary, v. 26(1), p. 33-49.
- Korim, K., 1978, Hydrogeologic factors governing thermal water occurrences and recovery in the Pannonian Basin, *in* Konda, J., editor, Hydrogeology of great sedimentary basins; conference of Budapest: *Memoires - International Association of Hydrogeologists*, p. 756-764.
- Korim, K., 1982, Main types of thermal water reservoirs in the Pannonian Basin, *in* Čermák, V., and Hänel, R., editors, Geothermics and geothermal energy; symposium held during the joint general assemblies of EGS and ESC: Stuttgart, Federal Republic of Germany, E. Schweizer Verlagsbuchhandlung (Naegele u. Obermiller), p. 203-209.
- Korim, K., 1994, The hydrogeothermal systems in Hungary: *International Association of Hydrogeologists, International contributions to hydrogeology*, v. 15: Hamburg, Verlag Heinz Heise, 43-55 p.
- Körössy, L., 1990, A délkelet-Alföld kőolaj- és földgázkutatásának földtani eredményei (Results of petroleum exploration in the south-eastern part of the Great Hungarian Plain): *Általános Földtani Szemle*, v. 25, p. 3-53, (in Hungarian).

- Körössy, L., 1992, A Duna-Tisza köze kőolaj- és földgázkutatásának földtani eredményei (Results of petroleum exploration in the Duna-Tisza Interfluve area): General Geological Review, v. 26, p. 3-162, (in Hungarian).
- Lapwood, E. R., 1948, Convection of a fluid in a porous medium, Proceedings of the Cambridge Philosophical Society, v.44, p.508-521.
- Lenkey, L., 1999, Geothermics of the Pannonian Basin and its bearing on the tectonics of basin evolution: Ph.D. thesis, Vrije Universiteit, Amsterdam, 215 p.
- Liebe, P., 1993, Drinking water and thermal water bearing formations in the Great Hungarian Plain, *in* 8th Meeting of the Association of European Geological Societies, 19 –26 September, Budapest: Excursion Guide, Field Trip C, p.33-35.
- Liebe, P., 1994, Assessment of the state of water resources of Hungary: Budapest, Institute of Hydrology of the Water Resources Research Centre Plc., 101 p.
- Luo, X., and Vasseur, G., 1992, Contributions of compaction and aquathermal pressuring to geopressure and the influence of environmental conditions: American Association of Petroleum Geologists Bulletin, v. 76, p. 1550-1559.
- Maccagno, M. D., 1991, The combined use of pressure-depth and pressure-elevation plots to analyze groundwater flow fields: M.Sc. thesis, University of Alberta, Edmonton, 179 p.
- Magara, K., 1976, Water expulsion from clastic sediments during compaction – direction and volumes: American Association of Petroleum Geologists Bulletin, v. 4, p. 453-553.
- Majorowicz, J. A., Jones, F. W., Lam, H. L., and Jessop, A. M., 1985, Terrestrial heat flow and geothermal gradients in relation to hydrodynamics in the Alberta Basin, Canada, *in* Rybach, L., editor, Heat flow and geothermal processes; proceedings; IUGG inter-disciplinary symposium No. 10: Journal of Geodynamics: Oxford - New York, International, Pergamon Press, p. 265-283.

- Majorowicz, J. A., 1989, The controversy over the significance of the hydrodynamic effect on heat flow in the Prairies Basin, *in* A. E. Beck, G. Garven, and L. Stegena, editors, Hydrogeological regimes and their subsurface thermal effects.: Geophysical Monograph. 47; IUGG Vol, v. 2: Washington, DC, United States, American Geophysical Union, p. 101-105.
- Matthäi, S. K., and Roberts, S. G., 1996, The influence of fault permeability on single-phase fluid flow near fault-sand intersections: results from steady-state high-resolution models of pressure-driven fluid flow: American Association of Petroleum Geologists Bulletin, v. 80, p. 1763-1779.
- Mattick, R. E., Phillips, L.R., and Rumpler, J., 1988, Seismic stratigraphy and depositional framework of sedimentary rocks in the Pannonian Basin, in southeastern Hungary, *in* Royden, L. H., and Horváth, F., editors, The Pannonian Basin; a study in basin evolution: American Association of Petroleum Geologists Memoir 45, p. 117-146.
- Mátyás, J., and Matter, A., 1997, Diagenetic indicators of meteoric flow in the Pannonian Basin, SE Hungary, *in* Montañez, I.P., Gregg, J.M., and Shelton, K.L., editors, Basin-wide diagenetic patterns: Integrated petrologic, geochemical, and hydrologic considerations: Tulsa, Oklahoma, Society for Economic Palaeontologists and Mineralogists Special Publication 57, p. 281-296.
- Maxey, G. B., 1964, Hydrostratigraphic units: Journal of Hydrology, v. 2, p. 124-129.
- McPherson, B. J. O. L., and Garven, G., 1999, Compressional tectonics, hydrodynamics and overpressure mechanisms in the Sacramento Basin, California: American Journal of Science, v. 295, p. 742-786.
- Neuzil, C. E., 1995, Abnormal pressures as hydrodynamic phenomena: American Journal of Science, v. 295, p. 742-786.

- Neuzil, C. E., 2000, Osmotic generation of 'anomalous' fluid pressures in geological environments: *Nature*, v. 403, p.182-184.
- Neuzil, C. E., and Pollock, D. W., 1983, Erosional unloading and fluid pressures in hydraulically "tight" rocks: *Journal of Geology*, v. 91, p. 179-193.
- Nur, A. M., Walder, J. S., 1990, Time-dependent hydraulics of the Earth's crust, *in* Bredehoeft, J.D., and Norton, D.L., editors, *The role of fluids in crustal processes*: Washington, D.C., National Academy Press, p. 113-127.
- Osborne, M. J., and Swarbrick, R. E., 1997, Mechanisms for generating overpressure in sedimentary basins; a reevaluation: *American Association of Petroleum Geologists Bulletin*, v. 81, p. 1023-1041.
- Ottlik, P., Galfi, J., Horváth, F., Korim, K., and Stegena, L., 1981, The low enthalpy geothermal resource of the Pannonian Basin, Hungary, *in* Rybach, L., and Muffler, L. J. P., editors, *Geothermal systems; principles and case histories*: Chichester, United Kingdom, John Wiley & Sons, p. 221-245.
- Otto, C. J., 1992, Petroleum hydrogeology of the Pechelbronn - Soultz basin in the Upper Rhine Graben: Ph.D. thesis, University of Alberta, Edmonton, 357 p.
- Pap, S., 1976, Alföldi és Északi-középhegységi kőolaj-földgáztároló kőzetek (Petroleum reservoir rocks of the Great Hungarian Plain and the North Central Range): *Földtani Közlöny*, v. 106, p. 555-580, (in Hungarian).
- Pap, S., 1993, Fábiánsebestyén-Nagyszénás-Orosháza környékének mélyföldtana (Subsurface geology of the Fábiánsebestyén-Nagyszénás-Orosháza region): *Földtani Közlöny*, v. 123, p. 69-98, (in Hungarian).

- Parks, K. P., and Tóth, J., 1995, Field evidence for erosion-induced underpressuring in Upper Cretaceous and Tertiary strata, west central Alberta, Canada: *Bulletin of Canadian Petroleum Geology*, v. 43, p. 281-292.
- Pécsi, M., 1989, National atlas of Hungary: Budapest, Cartographia on behalf of the Hungarian Academy of Sciences and the Ministry of Agriculture and Food, 395 p.
- Peresson, H., and Decker, K., 1997, Far-field effects of Late Miocene subduction in the Eastern Carpathians: E-W compression and inversion of structures in the Alpine-Carpathian-Pannonian region: *Tectonics*, v. 16, p. 38-56.
- Person, M., and Garven, G., 1992, Hydrologic constraints on petroleum generation within continental rift basins; Theory and application to the Rhine Graben: *American Association of Petroleum Geologists Bulletin*, v. 76, p. 468-488.
- Person, M., Raffensperger, J. P., Ge, S., and Garven, G., 1996, Basin-scale hydrogeologic modeling: *Reviews of Geophysics*, v. 34, p. 61-87.
- Phillips, L. R., Révész, I., and Bérczi, I., 1994, Lower Pannonian deltaic-lacustrine processes and sedimentation, Békés Basin, *in* Teleki, P. G., Mattick, R. E., and Kókai, J., editors, *Basin analysis in petroleum exploration; A case study from the Békés Basin, Hungary*: Kluwer Academic Publishers, printed in the Netherlands, p. 67-82.
- Pogácsás, G., Lakatos, L., Újszászi, K., Vakarcs, G., Várkonyi, L., Várnai, P., and Révész, I., 1988, Seismic facies, electro facies and Neogene sequence chronology of the Pannonian Basin: *Acta Geologica Hungarica*, v. 31, p. 175-207.

- Pogácsás, G., Mattick, R. E., Tari, G., and Várnai, P., 1994, Structural control on hydrocarbon accumulation in the Pannonian Basin, Hungary, *in* Teleki, P. G., Mattick, R. E., and Kókai, J., editors, Basin analysis in petroleum exploration; A case study from the Békés Basin, Hungary: Kluwer Academic Publishers, printed in the Netherlands, p. 221-235.
- Posgay, K., Bodoky, T., Hegedűs, E., Kovácsvölgyi, S., Lenkey, L., Szafián, P., Takács, E., Tímár, Z., and Varga, G., 1995, Asthenospheric structure beneath a Neogene basin in SE Hungary: *Tectonophysics*, v. 252, p. 467-484.
- Powers, M. C., 1967, Fluid release mechanisms in compacting marine mudrocks and their importance on oil exploration: *American Association of Petroleum Geologists Bulletin*, v.51, p. 1240-1254.
- Price, L. C., and Wenger, L. M., 1992, The influence of pressure on petroleum generation and maturation as suggested by aqueous pyrolysis: *Organic Geochemistry*, v. 19, p. 141-159.
- Radó, S., 1974a, Az Észak-Alföld atlasza: Magyarország tervezési- gazdasági körzetei (Atlas of the northern part of the Great Hungarian Plain): Budapest, Ministry of Agriculture and Food, National Land and Cartographic Institute, (in Hungarian).
- Radó, S., 1974b, A Dél-Alföld atlasza: Magyarország tervezési- gazdasági körzetei (Atlas of the southern part of the Great Hungarian Plain): Budapest), Ministry of Agriculture and Food, National Land and Cartographic Institute, (in Hungarian).
- Radó, S., 1974c, A központi körzet atlasza: Magyarország tervezési- gazdasági körzetei (Atlas of the central district): Budapest, Ministry of Agriculture and Food, National Land and Cartographic Institute, (in Hungarian).

- Raffensperger, J.P., and Garven, G., 1995, The formation of unconformity-type uranium ore deposits 1. Coupled groundwater and heat transport modeling: *American Journal of Science*, v. 295, p. 581-636.
- Ramsay, J. G., 1967, *Folding and fracturing of rocks*: New York, McGraw-Hill, 568 p.
- Ratschbacher, L., Frisch, W., Linzer, H. G., and Merle, O., 1991, Lateral extrusion in the Eastern Alps, part 2: Structural analysis: *Tectonics*, v. 10, p. 257-271.
- Rónai, A., 1961, Az Alföld talajvíztérképe – térkép magyarázó (Watertable map of the Great Hungarian Plain - explanatory notes): Hungarian Geological Institute, Budapest, 102 p, (in Hungarian).
- Rónai, A., 1978, Caractère hydrogéologique essentiel de la Grande Plaine Hongroise, *in* Konda, J., editor, *Hydrogeology of great sedimentary basins; conference of Budapest: Memoires - International Association of Hydrogeologists*, p. 462-483 (in French with English abstract).
- Rónai, A., 1985, Az Alföld negyedidőszaki földtana (The Quaternary of the Great Hungarian Plain): *Geologica Hungarica, Serie Geologica*, v. 21: Hungarian Geological Institute, Budapest, 446 p, (in Hungarian).
- Rostron, B. J., 1995, Cross-formational fluid flow in Upper Devonian to Lower Cretaceous strata, West-Central Alberta: Ph.D. thesis, University of Alberta, Edmonton, 195 p.
- Royden, L. H., 1988, Late Cenozoic tectonics of the Pannonian Basin system, *in* Royden, L. H., and Horváth, F., editors, *The Pannonian Basin, a study in basin evolution*, American Association of Petroleum Geologists Memoir 45, p. 27-48.

- Royden, L. H., and Dövényi, P., 1988, Variation in extensional styles at depth across the Pannonian Basin system, *in* Royden, L. H., and Horváth, F., editors, The Pannonian Basin, a study in basin evolution, American Association of Petroleum Geologists Memoir 45, p. 195-235.
- Royden, L., Horváth, F., Nagymarosy, A., and Stegena, L., 1983, Evolution of the Pannonian Basin system; 2, Subsidence and thermal history: *Tectonics*, v. 2, p. 91-137.
- Royden, L. H., and Horváth, F., editors, 1988, The Pannonian Basin; a study in basin evolution: American Association of Petroleum Geologists Memoir 45: Tulsa, OK, United States, American Association of Petroleum Geologists, 394 p.
- Rumpler, J., and Horváth, F., 1988, Some representative seismic reflection lines from the Pannonian Basin and their structural interpretation, *in* Royden, L. H., and Horváth, F., editors, The Pannonian Basin, a study in basin evolution, American Association of Petroleum Geologists Memoir 45, p. 153-171.
- Schlickenrieder, L., 1994, Geophysical well-log analysis in shaly sandstone for hydrogeological purposes: M.Sc. thesis, University of Alberta, Edmonton, 190 p.
- Schmidt, E. R., editor, 1962, Magyarország vízföldtani atlasza (Hydrogeological atlas of Hungary): Hungarian Geological Institute, Budapest, p.102, (in Hungarian with English and German explanatory notes).
- Secor, D.T., 1965, Role of fluid pressure in jointing: *American Journal of Science*, v. 263, p. 663-646.
- Sibson, R., 1981, A brief description of Natural Neighbour Interpolation, *in* Barnett V., editor, *Interpreting Multivariate Data*, John Wiley & Sons, New York, p. 21-36.

- Smith, L., and Chapman, D. S., 1983, On the thermal effects of groundwater flow. 1. Regional scale systems: *Journal of Geophysical Research*, v. 88, p. 593-608.
- Somfai, A., 1970, Examination of overpressured reservoirs in the Great Hungarian Plain: A classification of the causes of overpressure: *Acta Mineralogica-Petrographica*, Szeged, v. XIX, p. 173-194.
- Somfai, A., 1976, Pressure conditions and causes of fluid pressures in hydrocarbon reservoirs in the Great Hungarian Plain: Budapest, Hungarian Academy of Sciences, 145 p.
- Somfai, A., 1994, Hungary, *in* Kulke, H., editor, Regional petroleum geology of the world, Part I: Europe and Asia: Berlin, Gebrüder Borntraeger, p. 277-285.
- Spencer, C. W., 1987, Hydrocarbon generation as a mechanism for overpressuring in Rocky Mountain region: *American Association of Petroleum Geologists Bulletin*, v. 71, p. 368-388.
- Spencer, C. W., Szalay, Á., and Tatár, É., 1994, Abnormal pressure and hydrocarbon migration in the Békés Basin, *in* Teleki, P. G., Mattick, R. E., and Kókai, J., editors, Basin analysis in petroleum exploration; A case study from the Békés Basin, Hungary: Kluwer Academic Publishers, printed in the Netherlands, p. 201-219.
- Stegena, L., 1958, A Nagyalföld geotermikus viszonyai (Geothermal conditions of the Great Hungarian Plain): *Geofizikai Közlöny*, v. VII, p. 3-4, (in Hungarian).
- Stegena, L., 1963, A magyarországi földi hőáram kérdéséhez (About the problem of heat flow in Hungary): *MTA Műszaki Tudományos Osztály Közleményei*, v. 32, p. 151-158, (in Hungarian).

- Stegena, L., 1966, Migration und Geothermik im Ungarischen Becken: Proceedings of the 4th International Conference on Chemistry and Physics, Problems of research and exploration for oil and natural gas, Prague, vol. 1, p. 115-119, (in German).
- Stegena, L., 1982, Water migration influences on the geothermics of basins: Tectonophysics, v. 83, p. 91-99.
- Stegena, L., 1989, Thermal effect of hydrogeology in closed basins, *in* Beck, A. E., Garven, G., and Stegena, L., editors, Hydrogeological regimes and their subsurface thermal effects: Geophysical Monograph 47, IUGG v. 2, Washington, D.C., American Geophysical Union, p. 81-86.
- Stegena, L., Géczy, B., and Horváth, F., 1975, Late Cenozoic evolution of the Pannonian Basin: Tectonophysics, v. 26, p. 71-90.
- Steininger, F. F., Müller, C., and Rögl, F., 1988, Correlation of Central Paratethys, Eastern Paratethys, and Mediterranean Neogene stages, *in* Royden, L. H., and Horváth, F., editors, The Pannonian Basin, a study in basin evolution: American Association of Petroleum Geologists Memoir 45, p. 79-88.
- Szalay, Á., 1982, A túlnyomás okai és a paleopórusnyomás becslése (Causes of overpressures and estimation of paleo-pore pressures): Kőolaj és Földgáz, v. 115, p. 41-46, (in Hungarian).
- Szalay, Á., 1983, A nyomásgátak szerepe a szénhidrogén-migrációs folyamatokban (The role of pressure barriers in hydrocarbon migration processes): Kőolaj és Földgáz, v. 16, p. 363-371, (in Hungarian).
- Szalay, Á., 1988, Maturation and migration of hydrocarbons in the southeastern Pannonian Basin, *in* Royden, L. H., and Horváth, F., editors, The Pannonian Basin; a study in basin evolution: American Association of Petroleum Geologists Memoir 45, p. 347-354.

- Szalay, Á., and Koncz, I., 1991, Genetic relations of hydrocarbons in the Hungarian part of the Pannonian Basin, *in* Spencer, A. M., editor, Generation, accumulation, and production of Europe's hydrocarbons: Special Publication of the European Association of Petroleum Geoscientists, Federal Republic of Germany, p. 317-322.
- Szalay, Á., and Koncz, I., 1993, Migration and accumulation of oil and natural gas generated from Neogene source rocks in the Hungarian part of the Pannonian Basin, *in* Spencer, A. M., editor, Generation, accumulation, and production of Europe's hydrocarbons III: Special Publication of the European Association of Petroleum Geoscientists, Federal Republic of Germany, p. 303-309.
- Szalay, Á., and Szentgyörgyi, K., 1988, A method for lithogenetic subdivision of Pannonian (s.l.) sedimentary rocks, *in* Royden, L. H., and Horváth, F., editors, The Pannonian Basin; a study in basin evolution: American Association of Petroleum Geologists Memoir 45, p. 89-96.
- Szebényi, L., 1955, Ártézi vizeink függőleges irányú mozgásáról (On the vertical motion of artesian waters): *Hidrológiai Közlöny*, v. 35, p. 437-439, (in Hungarian).
- Tari, G., 1994, Alpine tectonics of the Pannonian Basin, Hungary: Ph.D. thesis, Rice University, Houston, Texas, 501 p.
- Tari, G., Báldi, T., and Báldi-Beke, M., 1993, Paleogene retroarc flexural basin beneath the Neogene Pannonian Basin; a geodynamic model: *Tectonophysics*, v. 226, p. 433-455.
- Tari, G., Horváth, F., and Rumpler, J., 1992, Styles of extension in the Pannonian Basin: *Tectonophysics*, v. 208, p. 203-219.
- Terzaghi, K., 1925, *Erdbaumechanik auf Bodenphysikalischer Grundlage*: Vienna, Franz Deuticke, 399 p. (in German)

- Tissot, B. P., and Welte, D. H., 1984, Petroleum formation and occurrence, 2nd ed.: Berlin, Springer Verlag, 699 p.
- Tóth, J., 1962, A theory of groundwater motion in small drainage basins in central Alberta, Canada: *Journal of Geophysical Research*, v. 67, p. 4375-4387.
- Tóth, J., 1963, A theoretical analysis of groundwater flow in small drainage basins: *Journal of Geophysical Research*, v. 68, p. 4795-4812.
- Tóth, J., 1967, Ground water in sedimentary (clastic) rocks: Symposium on ground-water hydrology, San Francisco, Calif., 1967; Proceedings Series - American Water Resources Association, Minneapolis, MN, United States, p. 91-102.
- Tóth, J., 1970, A conceptual model of the groundwater regime and the hydrogeologic environment: *Journal of Hydrology*, v. 10, p. 164-176.
- Tóth, J., 1978, Gravity-induced cross-formational flow of formation fluids, Red Earth region, Alberta, Canada; analysis, patterns, and evolution: *Water Resources Research*, v. 14, p. 805-843.
- Tóth, J., 1980, Cross-formational gravity-flow of groundwater; a mechanism of the transport and accumulation of petroleum; the generalized hydraulic theory of petroleum migration, *in* Roberts, W. H., III, and Cordell, R. J., editors, Problems of petroleum migration: Studies in Geology No.10: Tulsa, OK, United States, American Association of Petroleum Geologists, p. 121-167.
- Tóth, J., 1984, The role of regional gravity flow in the chemical and thermal evolution of ground water, *in* Hitchon, B., and Wallick, E. I., editors, Proceedings of the First Canadian - American conference on hydrogeology; practical applications of ground water geochemistry: Worthington, OH, United States, National Water Well Association, p. 3-39.
- Tóth, J., 1995, Hydraulic continuity in large sedimentary basins: *Hydrogeology Journal*, v. 3, p. 4-16.

- Tóth, J., 1996, Thoughts of a hydrogeologist on vertical migration and near-surface geochemical exploration for petroleum, *in* Schumacher, D., and Abrams, M. A., editors, Hydrocarbon migration and its near-surface expression: American Association of Petroleum Geologists Memoir 66, p. 279-283.
- Tóth, J., 1999, Groundwater as a geologic agent: An overview of the causes, processes, and manifestations: *Hydrogeology Journal*, v. 7, p. 1-15.
- Tóth, J., and Almási, I., 1998, Szénhidrogén kutatás az Alföldön hidrogeológiai szempontok figyelembevételével: Zárójelentés -A Magyar Olaj- és Gázipari Rt. megbízásából és számára (Hydrocarbon exploration using hydrogeological principles on the Great Hungarian Plain -Final report)[confidential report]: University of Alberta, Edmonton, 63 p, (in Hungarian).
- Tóth, J., and Corbet, T., 1986, Post-Paleocene evolution of regional groundwater flow-systems and their relation to petroleum accumulations, Taber area, southern Alberta, Canada: *Bulletin of Canadian Petroleum Geology*, v. 34, p. 339-363.
- Tóth, J., Maccagno, M.D., Otto, C.J., and Rostron, B.J., 1991, Generation and migration of petroleum from abnormally pressured compartments: Discussion: *American Association of Petroleum Geologists Bulletin*, v.75, p. 331-335.
- Tóth, J., and Millar, R. F., 1983, Possible effects of erosional changes of the topographic relief on pore pressures at depth: *Water Resources Research*, v. 19, p. 1585-1597.
- Tóth, J., and Rakhit, K., 1988, Exploration for reservoir quality rock bodies by mapping and simulation of potentiometric surface anomalies: *Bulletin of Canadian Petroleum Geology*, v. 36, p. 362-378.

- Tóth, J. and Sheng, G., 1996, Enhancing safety of nuclear waste disposal by exploiting regional groundwater flow: the Recharge Area Concept: *Hydrogeology Journal*, v. 4(4), p. 4-25.
- Trümpy, R., 1973, *The Timing of Orogenic Events in the Central Alps, Gravity and tectonics*: John Wiley & Sons, New York, p. 229-251.
- Urbancsek, J., 1963, A földtani felépítés és rétegvíznyomás közötti összefüggés az Alföldön (Relationship between the geologic framework and the formation water pressure in the Great Hungarian Plain): *Hidrológiai Közlöny*, v. 3, p. 205-218, (in Hungarian).
- Urbancsek, J., 1978, Formation water pressure in the Quaternary sediments of the Great Hungarian Plain, *in* Konda, J., editor, *Hydrogeology of great sedimentary basins; conference of Budapest: Memoires - International Association of Hydrogeologists*, p. 257-267.
- Vacquier, V., 1984, Oil fields – a source of heat flow data: *Tectonophysics*, v. 103, p. 81-89.
- van Balen, R. T., 1995, Tectonic control on the hydrodynamics and sedimentary record of extensional basins; inferences from numerical modelling and analysis of the Pannonian Basin: Ph.D. thesis, Vrije Universiteit, Amsterdam, 202 p.
- van Balen, R. T., and Cloetingh, S., 1994, Tectonic control of the sedimentary record and stress-induced fluid flow; constraints from basin modelling, *in* Parnell, J., editor, *Geofluids: origin, migration and evolution of fluids in sedimentary basins*: Geological Society Special Publications: London, United Kingdom, Geological Society of London, v. 78, p. 9-26.

- van der Kamp, G., 1984, Evaluating the influence of groundwater flow systems on geothermal conditions, *in* Curtis, F. A., editor, *Energex '84, Energy developments: new forms, renewable, conservation*: Regina, Saskatchewan, Pergamon Press, p. 297-301.
- Varsányi, I., Mátray, J.-M., and Ó Kovács, L., 1997, Geochemistry of formation waters in the Pannonian Basin (Southeast-Hungary): *Chemical Geology*, v. 140, p. 89-106.
- Varsányi, I., Matray, J.-M., and Ó Kovács, L., 1999, Hydrogeochemistry in two adjacent areas in the Pannonian Basin (Southeast-Hungary): *Chemical Geology*, v. 156, p. 25-39.
- Völgyi, L., 1977, Hazai geotermikus viszonyok szerepe a szénhidrogénprognózisban (The role of geothermics in prediction of prospective areas of HC-accumulations in Hungary -research report for the Hungarian Petroleum Research Company, p.52, (in Hungarian).
- Wells, P. R. A., 1987, Hydrodynamic trapping of oil and gas in the Cretaceous Nahr Umr lower sand of the North area, offshore Qatar, *in* Kazmawi, F. J., editor, *Proceedings; Society of Petroleum Engineers 5th Middle East oil show*: Richardson, TX, United States, Society of Petroleum Engineers, p. 17-26.
- Zentay, L., 1996, Digital maps of Hungary: <http://lazarus.elte.hu/gb/maps/karpat.htm>.
- Zijl, W., 1999, Scale aspects of groundwater flow and transport systems: *Hydrogeology Journal*, v. 7, p. 139-150.

APPENDIX 1: EXPLANATORY NOTES TO THE DATABASE CREATED AND USED FOR THIS STUDY INCLUDED ON THE ATTACHED CD-ROM.

The hardcopy of the database compiled for this study would need over 1000 pages to print and it would be of little use for potential future research. Therefore, a digital version of the database is included on a CD-ROM. All the data files are saved as ASCII text files. The data are tabulated; columns are delimited by commas (,) and quotation marks (“”) are used as text delimiters. Spaces in the text strings are replaced with underscore () signs, because some computer applications may consider spaces as column delimiters, thus data import errors are prevented. This file structure can be imported into applications running on most computer platforms, such as Microsoft Windows 95/98/NT/2000, Apple Macintosh, and UNIX. An ASCII text (*.txt) and Rich Text Format (*.rtf) version of Chapter 3 from the thesis is also included with the data files, as supporting information.

List of files on the CD-ROM:

Necessary background information:

Explanatory notes to the data files: readme.txt

Extract of Chapter 3 from the thesis in ASCII format: Almasi_ch3.txt

Data:

Hydraulic head data: h_heads.dat

Stratigraphic data: hu_strat.dat

Geothermal data from Dövényi and Horváth (1988): geotherm.dat

Hydrocarbon pool depths: HC_poold.dat

Thesis:

Electronic versions of the present thesis are included in original Microsoft Word97 format (almasi-PhD.doc) and in Adobe Portable Document Format (almasi-PhD.pdf). A current copy of “Adobe Acrobat Reader 4.0” self-extracting installation file is also included.

APPENDIX 2: METHOD OF WELL-DATA SELECTION FOR CROSS SECTION CONSTRUCTION

Manual selection of wells from a large data set, which fall within a certain distance from the trace of a cross section, may impose a serious practical problem, i.e., it is extremely time consuming. To avoid this problem, the author developed an efficient solution, which can be used with any spreadsheet and may spare several weeks or months of tedious work. The method is primarily applicable for data sets where the point (well) co-ordinates are Cartesian (linear and orthogonal), such as the EOVS (Hungarian National Projection System). It is also applicable for data with Universal Transversal Mercator (UTM) co-ordinates, which fall within one zone, and it is ideal on scales not exceeding 1:100 000.

The criteria for well data selection from a tabular data set along any given linear direction are: (1) the maximum distance of wells from either side of the section, and (2) the limits of the cross section's length. The basic idea of the method is to rotate the original Cartesian co-ordinate axes of the points around the origin so that one of the rotated axes becomes parallel to the direction of the cross section, thus the other axis is perpendicular to it (Figure A2.1). As a result, the projection distance of wells from the cross section and their lateral distance along the cross section can be computed with high accuracy.

Rotation of co-ordinates is achieved by the rotation matrix. Using the symbols from Figure A2.1, the equations of the rotated axes are written as:

$$X' = X \cdot \cos \alpha - Y \cdot \sin \alpha \quad (\text{A2.1})$$

and

$$Y' = Y \cdot \cos \alpha + X \cdot \sin \alpha \quad (\text{A2.2})$$

where X and Y are the original northing and easting co-ordinates, respectively; X' and Y' are the rotated northing and easting, respectively, and α is the angle of rotation or the angle between the cross section and the original easting co-ordinate axis (Figure A2.1).

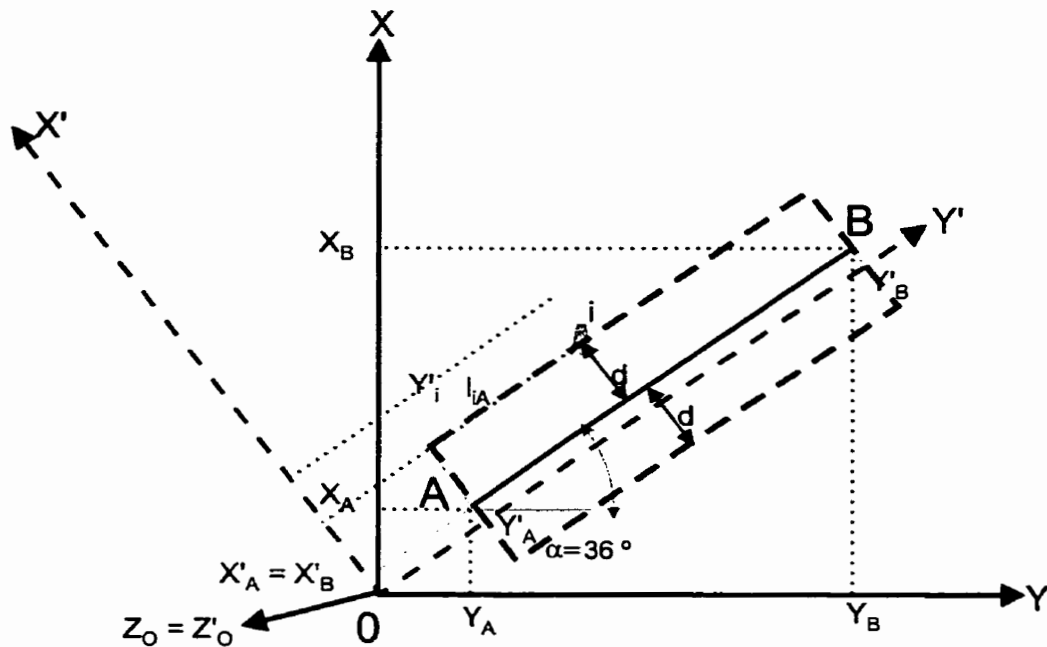


Figure A2.1: Schematic diagram of co-ordinate rotation and calculation of well location along and from a cross section (AB). To construct a cross section AB select wells with coordinates that fall within $X'_i \leq X'_A \pm d$ or $X'_i \leq X'_B \pm d$

Application of the selection method using EOV co-ordinate conventions (X = northing; Y = easting; distance measured in metres):

1. choose end-nodes of cross section to be constructed: **A**(Y_A, X_A), **B**(Y_B, Y_B).
2. Calculate the rotation angle (α) between the trace of cross section and Y axis

$$\tan \alpha = \frac{X_B - X_A}{Y_B - Y_A}$$

3. In the data table, calculate the co-ordinates of every well in the rotated co-ordinate system in new columns using the equations (A2.1) and (A2.2).
Note: - for reference, include the co-ordinates of the end-nodes (**A** and **B**) as fictitious wells in the table.

4. If the calculations are correct, $X'_A = X'_B$, and the length of the cross section is

$$L_{AB} = Y'_B - Y'_A$$

5. Filter the data based on the column of rotated northing (X') according to the maximum projection distance d from X'_A (or X'_B); retain those records, for which the criterion $X'_A - d \leq X'_i \leq X'_A + d$ is satisfied (where X'_i is the rotated northing co-ordinate of the i -th well in the table; $i = 1, 2, \dots$)
6. Filter data based on the column of rotated easting (Y') according to the limits of the cross section, i.e., retain those points which fall between **A** and **B** for which the criterion $Y'_A \leq Y'_i \leq Y'_B$ must be satisfied (where Y'_i is the rotated easting co-ordinate of the i -th well in the table; $i = 1, 2, \dots$)
7. Calculate distance of points along cross section with reference to **A** in a separate column: $L_i = Y'_i - Y'_A$

If a complex cross sections is to be constructed with one or more breakpoints and segments of different angles relative to the map axis, the above steps (1. → 7.) have to be applied repetitively for each segment. For computation of the distance along cross section beyond the first break point, make sure to add the total length of the previous segments. To avoid duplicates in the vicinity of breakpoints check the wells within the projection distance from the breakpoint and decide which one to retain.

APPENDIX 3: CALCULATION OF SPECIFIC STORAGE

The specific storage, $S_s = \rho g(\alpha + \phi\beta)$, changes with depth in function of the porosity, compressibility, and density of sediments (Freeze and Cherry, 1979). S_s can be calculated from average porosity-depth trend curves using compressibility values that are appropriate for the lithology. For a first approximation one-dimensional study, it is practical to consider an average porosity of $\phi = 20\%$, a compressibility value typical for medium clay and loose sand of $\alpha = 1.3 \times 10^{-2} \text{ Pa}^{-1}$ (Bredehoeft and Hanshaw, 1968). The compressibility of water is $\beta = 4.4 \times 10^{-10} \text{ Pa}^{-1}$. The bulk density of the saturated porous medium is calculated with the formula $\rho = \phi\rho_{\text{water}} + (1-\phi)\rho_{\text{solid}}$. For a porous medium with density of solid part $\rho_{\text{solid}} = 2700 \text{ kg m}^{-3}$ and porosity $\phi = 20\%$ saturated with fresh water of density $\rho_w = 1000 \text{ kg m}^{-3}$, the bulk density is $\rho = 2360 \text{ kg m}^{-3}$. Thus, the average specific storage of the total sediment sequence is $S_s = 0.003 \text{ m}^{-1}$. Values of specific storage of hydrostratigraphic units used for sample calculations were taken from the table compiled by Domenico and Mifflin (1965) (in Bredehoeft and Hanshaw, 1968; p. 1100 Table 1, or Domenico and Schwartz, 1998).

APPENDIX 4: ESTIMATION OF THE HORIZONTAL TO VERTICAL STRESS RATIO

Knowing the magnitude of overpressure (p_o) at the bottom of the sedimentary pile of thickness l , specific storage S_s , and hydraulic conductivity K , deposited at a rate ω during time t , it is possible to estimate the relative contribution of the horizontal and vertical stress rates to overpressuring from the graphical solution of equation (7.8) (Bredehoeft and Hanshaw, 1968) shown in Figure 7.1, and its modified version according to the solution of equation 7.13 (Domenico and Schwartz, 1998).

For the graphical solution of equation (7.13), the ordinate on Figure 7.2 is $\frac{p_o}{\gamma \cdot l \cdot \frac{1 + 2M}{3} \cdot \left(\frac{R}{H}\right)}$

instead of $p_o/\gamma l$. Thus the overpressures resulting from the combined effect of sedimentary loading and lateral tectonic compression are $\frac{1 + 2M}{3} \frac{R}{H}$ times greater than those due to only vertical loading.

For a model calculation, assume the following parameter values, which are common in the Great Hungarian Plain:

$p_o = 25$ MPa overpressure observed at the base of $l = 2500$ m thick shale unit deposited during $t = 10$ Myr (approximate duration of the post-rift phase and deltaic sedimentation in the southern part of the basin), at an average rate of $\omega = l/t = 250/\text{Ma}$. The hydraulic conductivity value if the shale is the lowest documented in the basin, $K = 10^{-10}$ m/s, and the assumed specific storage at 20 % porosity is $S_s = 0.003 \text{ m}^{-1}$. The elastic coefficient $R/H = 1$ for clay (= 0.83 for mudstone; = 0.67 for sandstone; Domenico and Schwartz, 1998).

The dimensionless time is $t/T^* = S_s l \omega / K = 0.6$. At the bottom of the sedimentary pile for the $z/l = 0$ curve the dimensionless pressure is $\frac{p_o}{\gamma \cdot l \cdot \frac{1 + 2M}{3} \cdot \left(\frac{R}{H}\right)} = p^* = 0.2$. In Section

7.3.3.2 it was shown that $\gamma' = 16.7 \text{ MPa/km}$. Thus $M = \frac{1}{2} \left(\frac{3p_o}{p^* \gamma' l \frac{R}{H}} - 1 \right) \approx 4$. From equation

(7.11) it results that the horizontal stress must be 4 times greater than the vertical stress due to sedimentary loading, and from equation (7.12) the mean stress would be 3 times greater than the vertical stress in order to generate an overpressure of the observed magnitude.

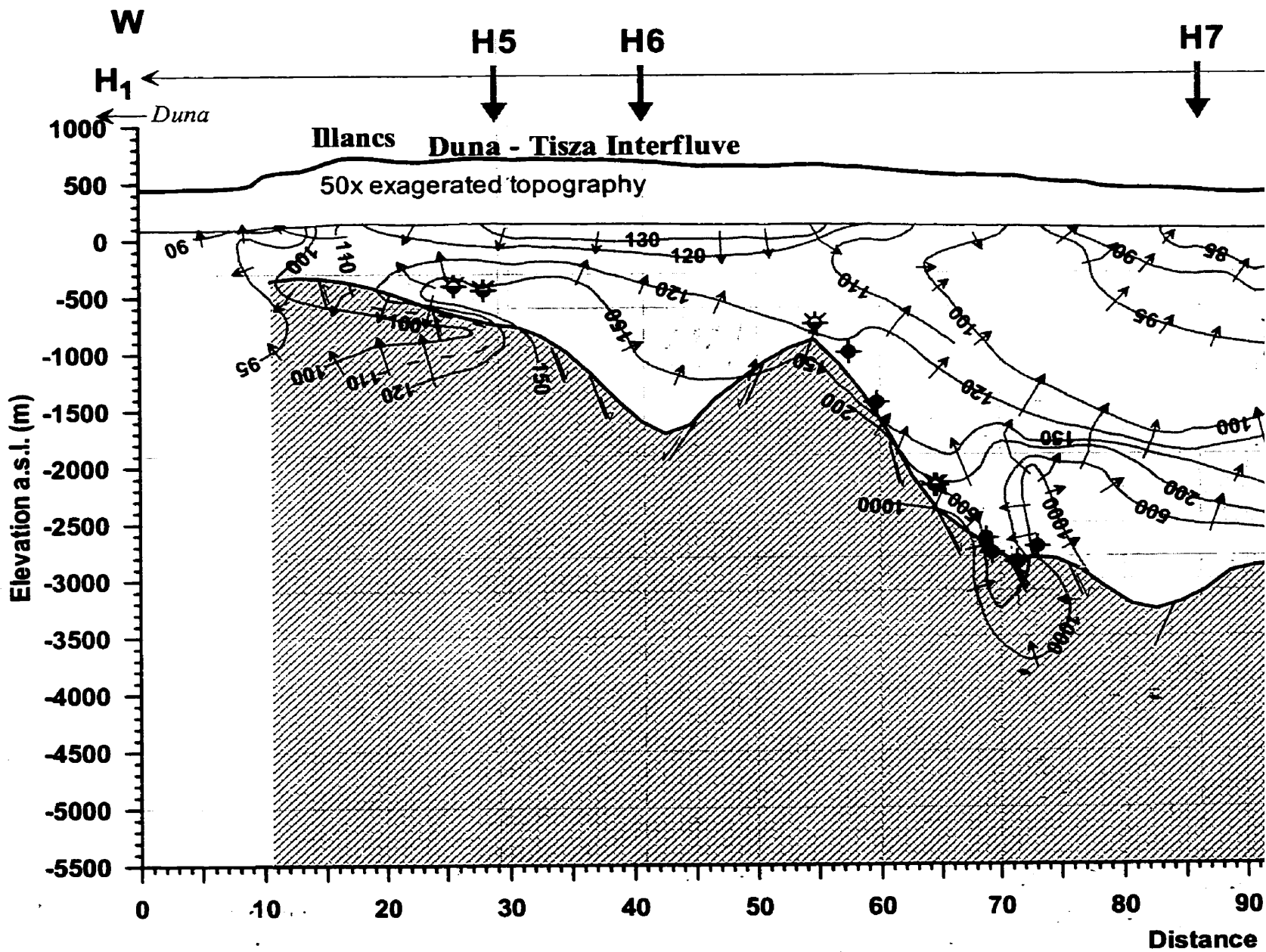
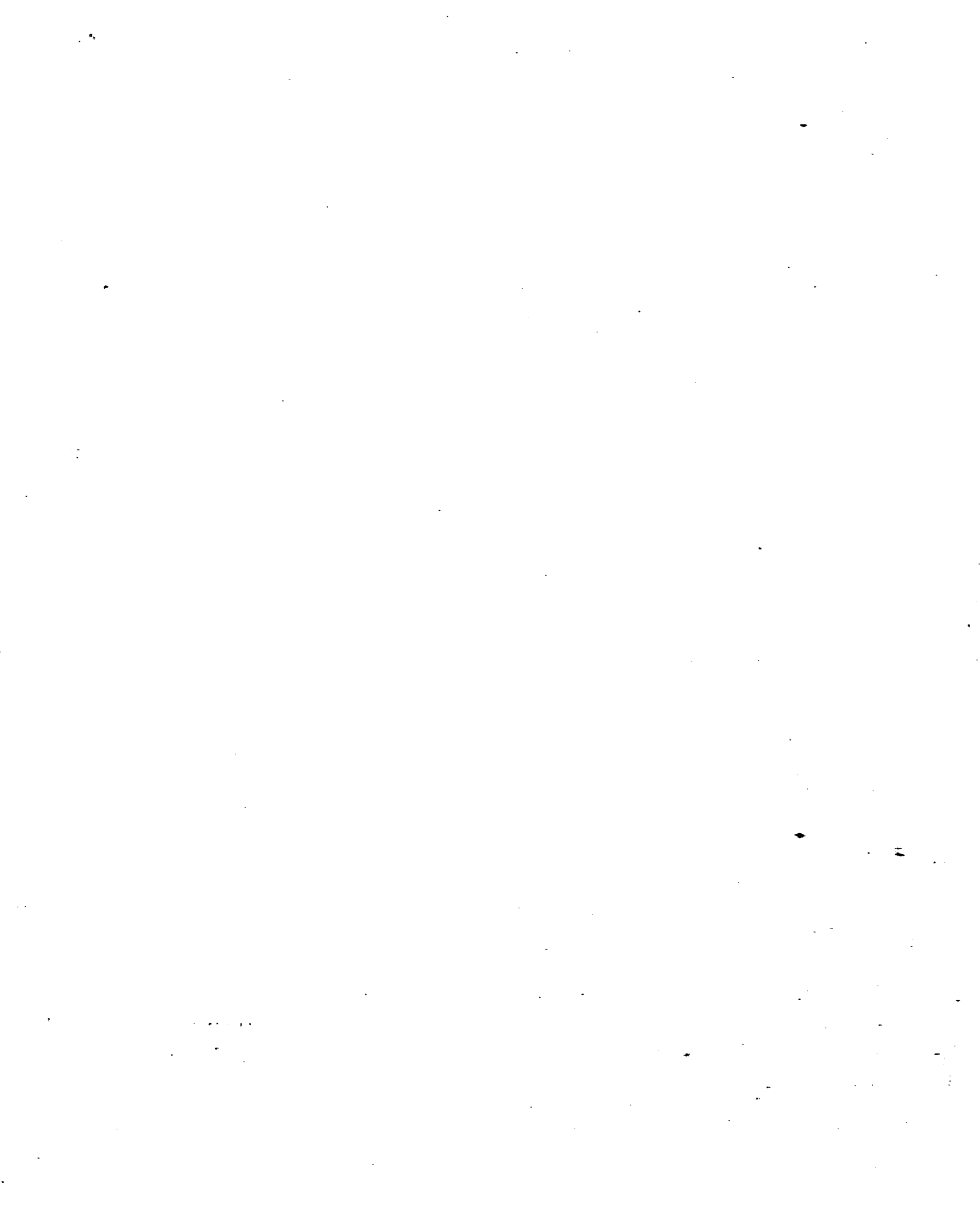
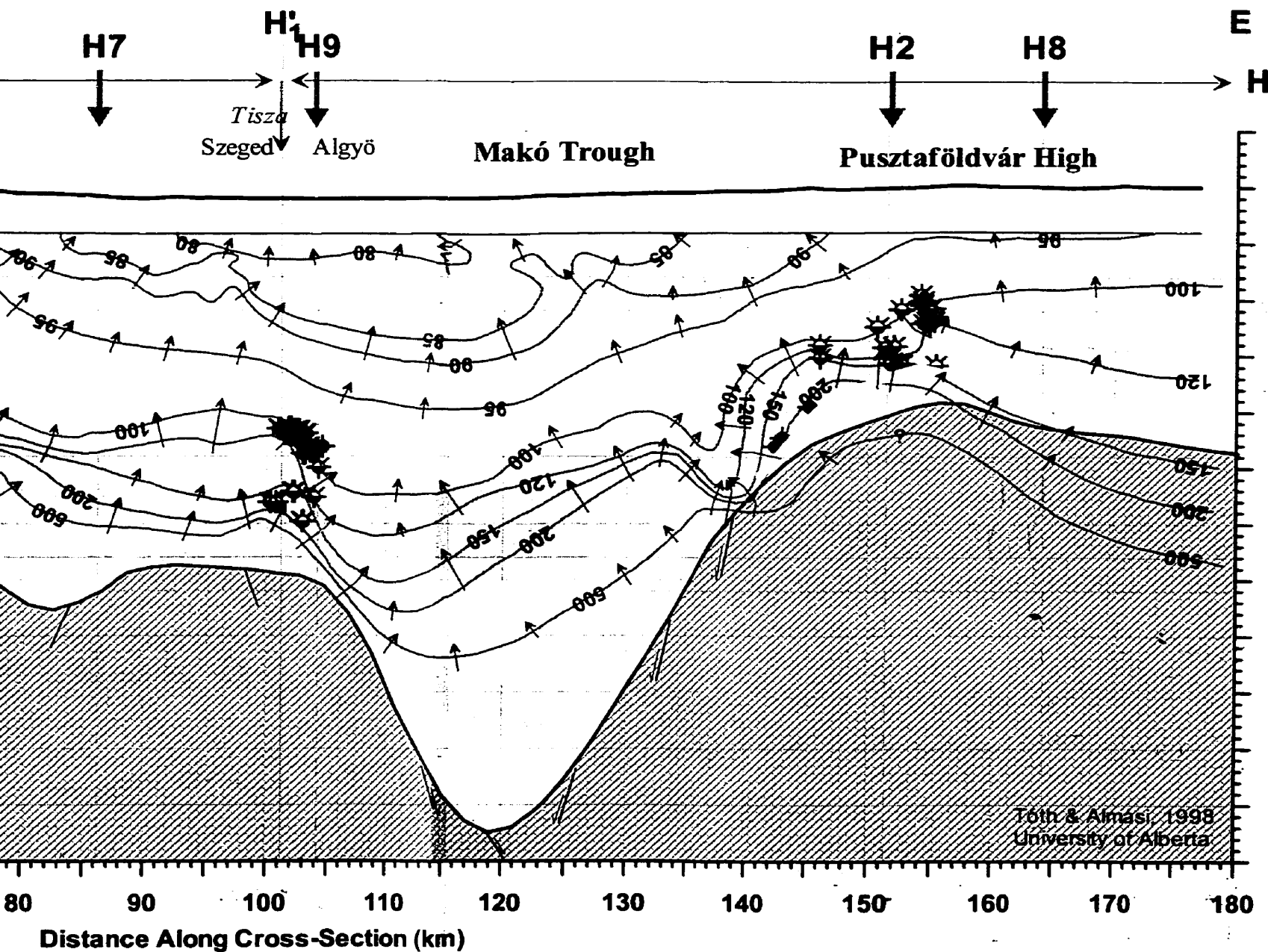
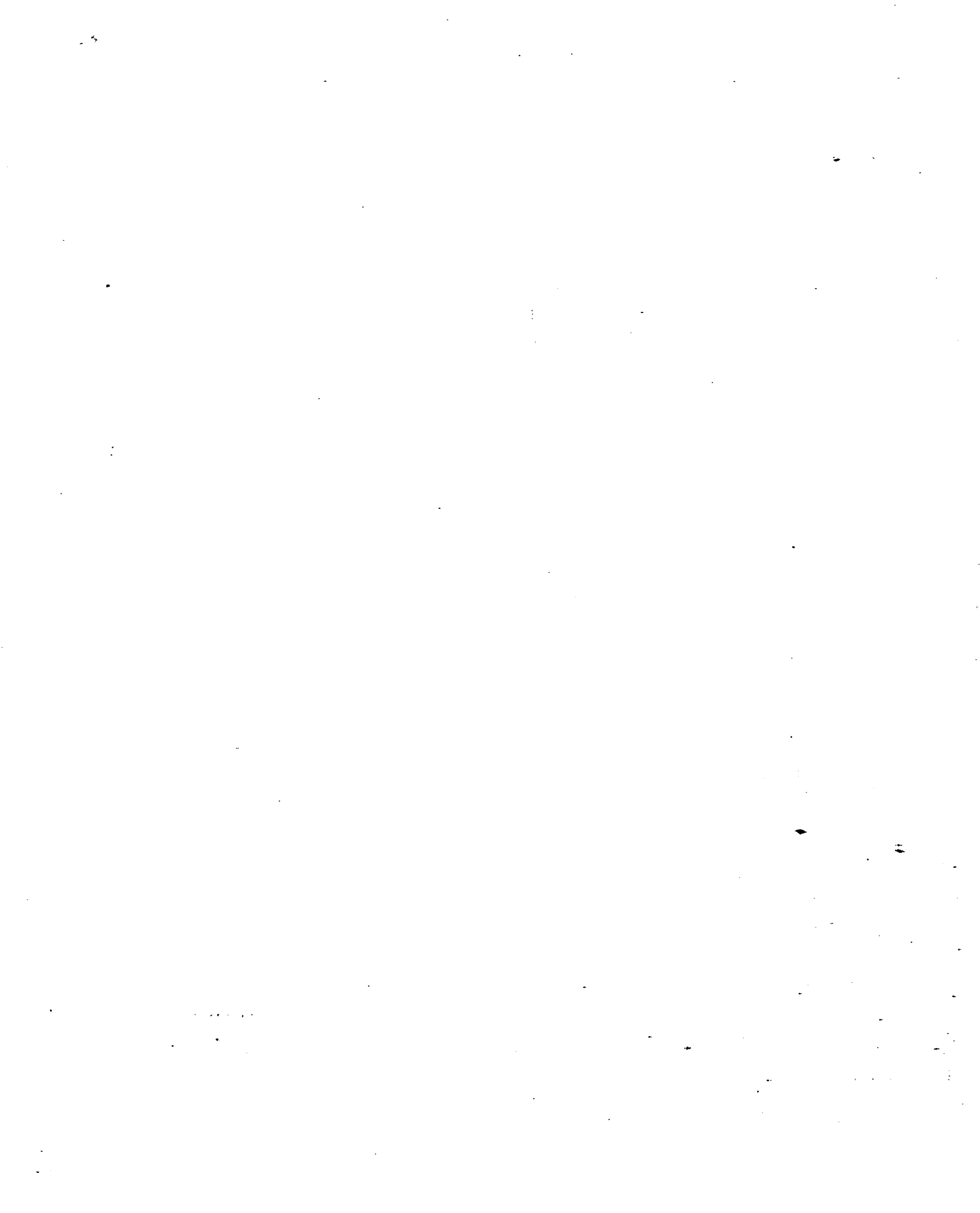


Figure 4.33. Hydraulic cross section H1 and hydrocarbon accumulations distance from either side of the section (for location see





simulations within 2 km
 location see Figure 4.4).



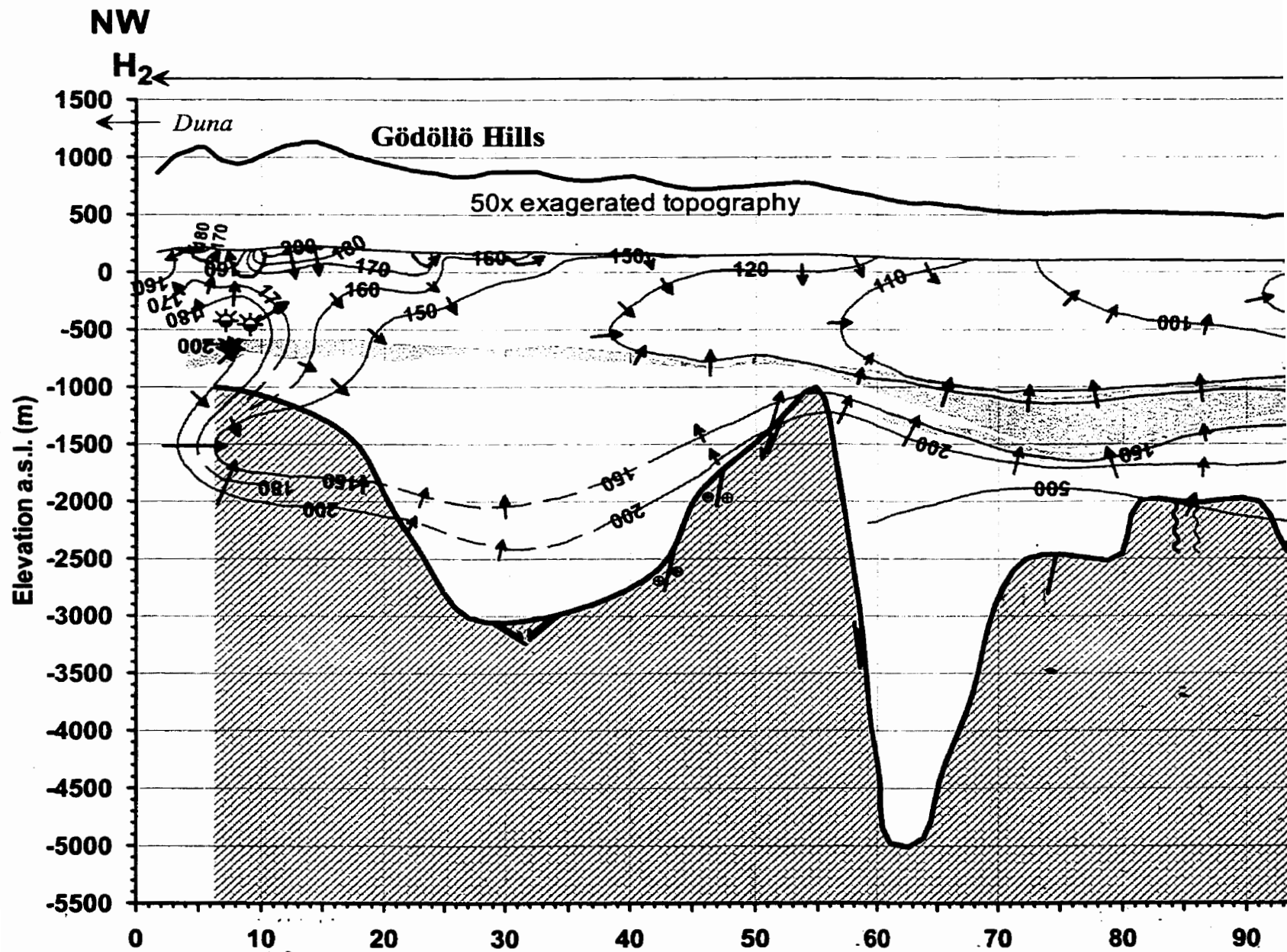
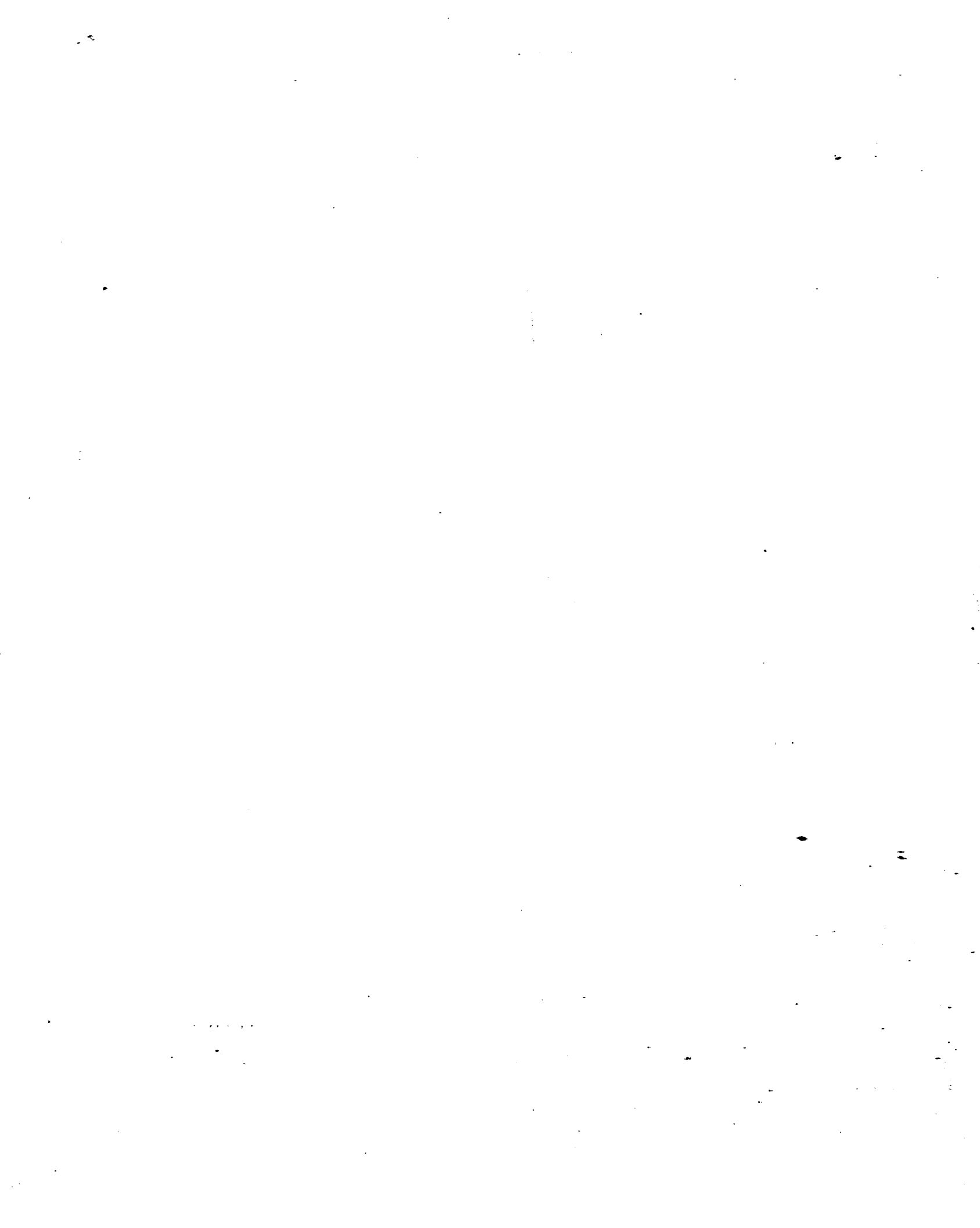
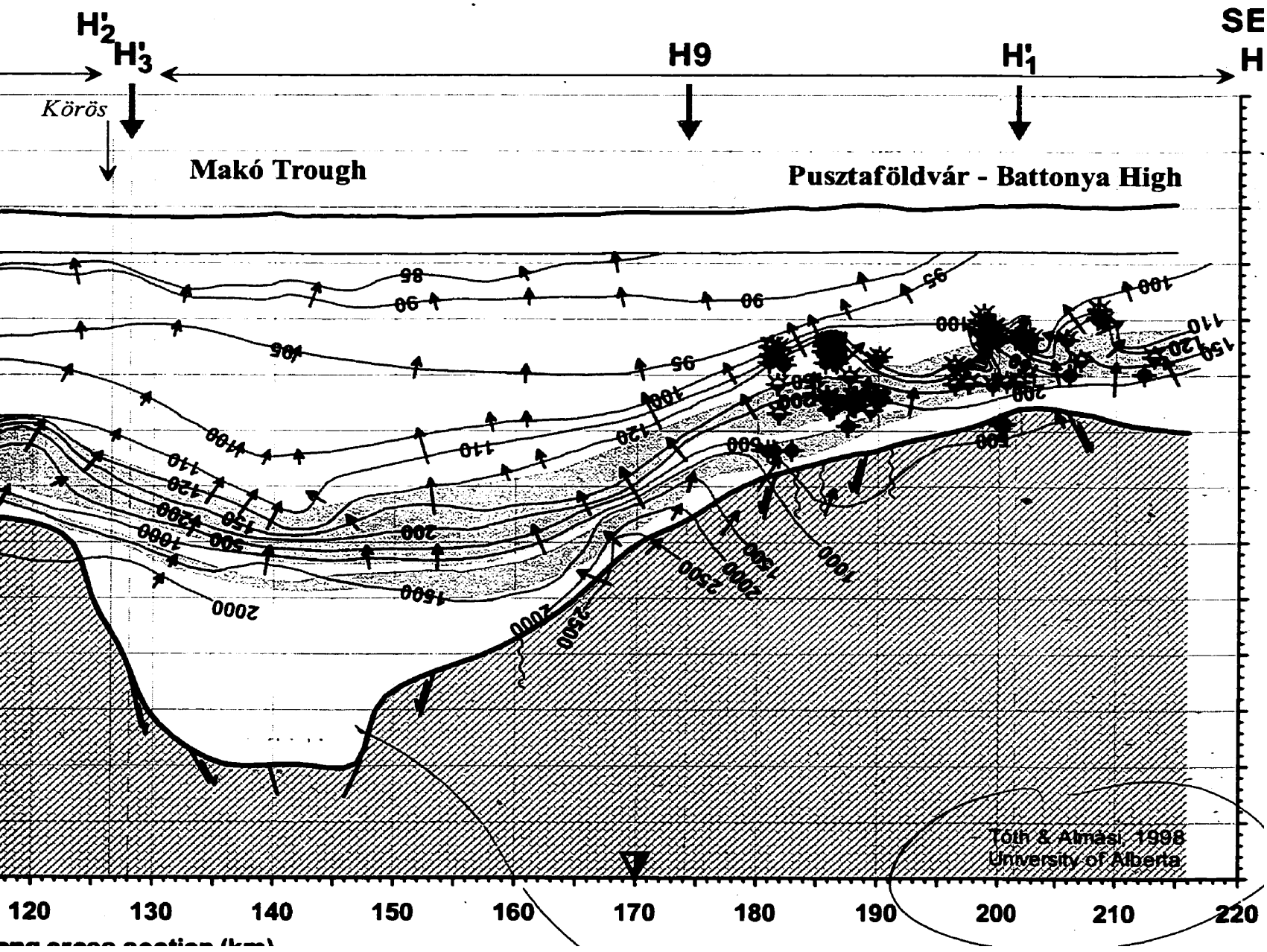
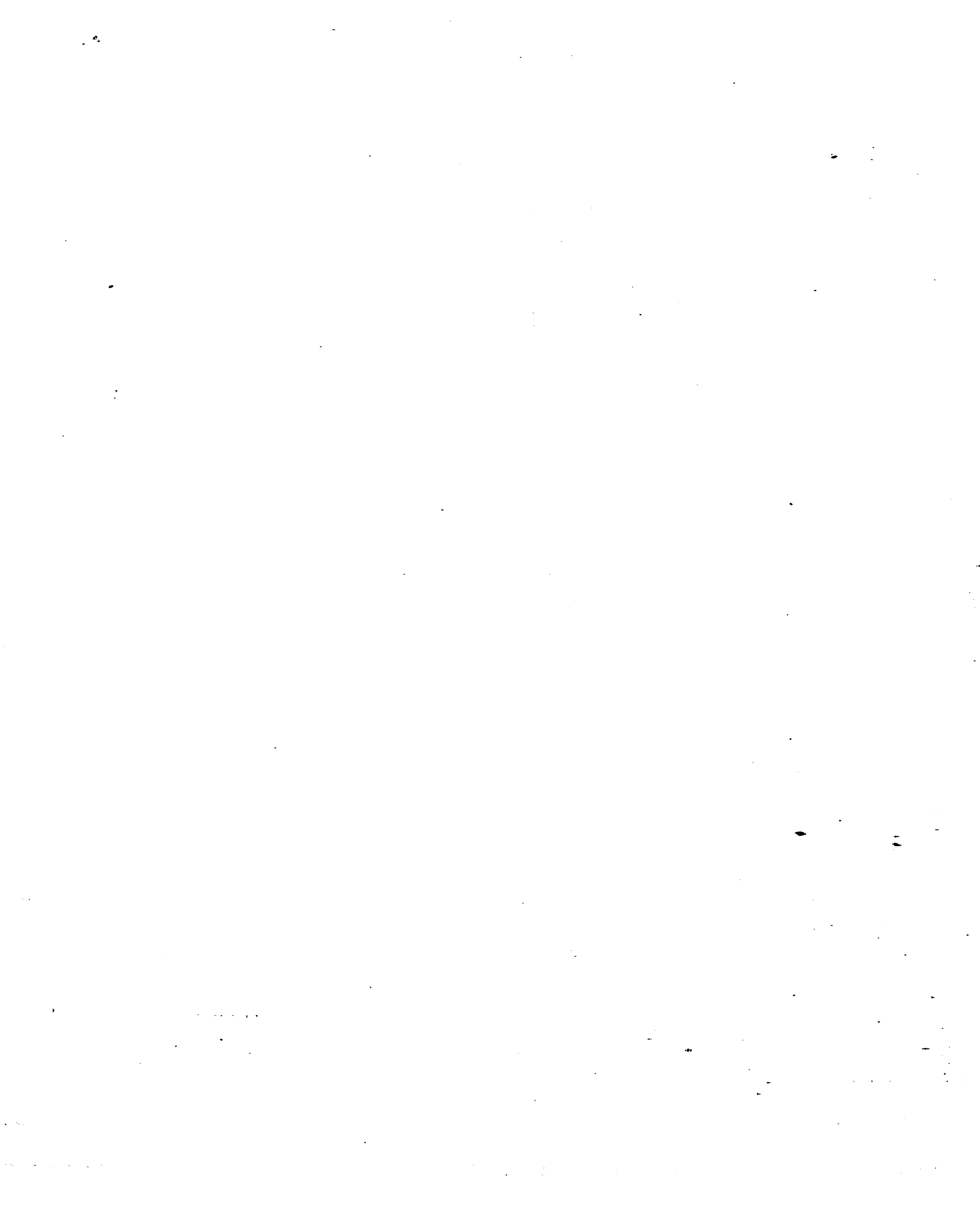


Figure 4.34. Hydraulic cross section H₂ and hydrocarbon accumulation distance from either side of the section (for location see F







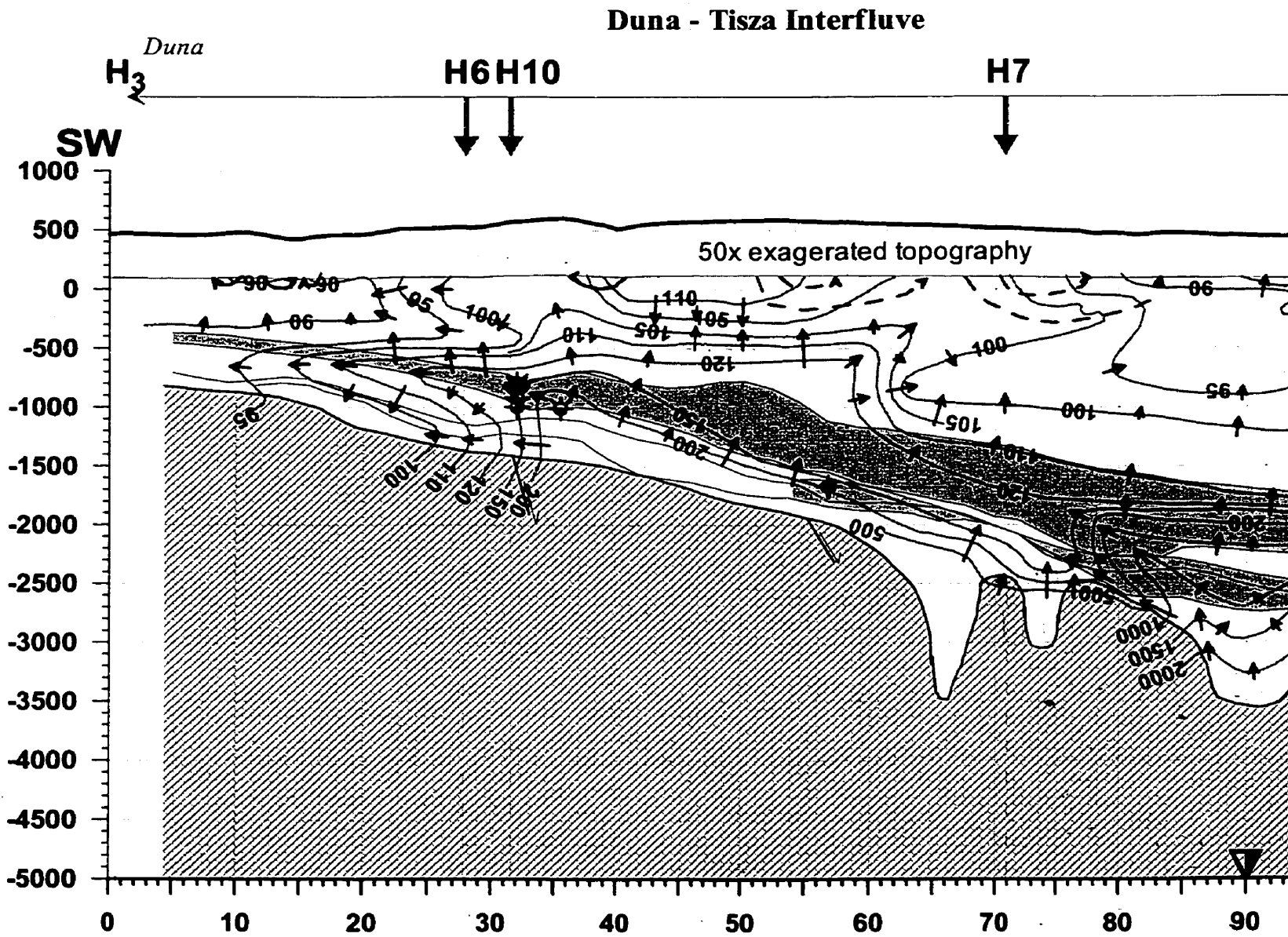
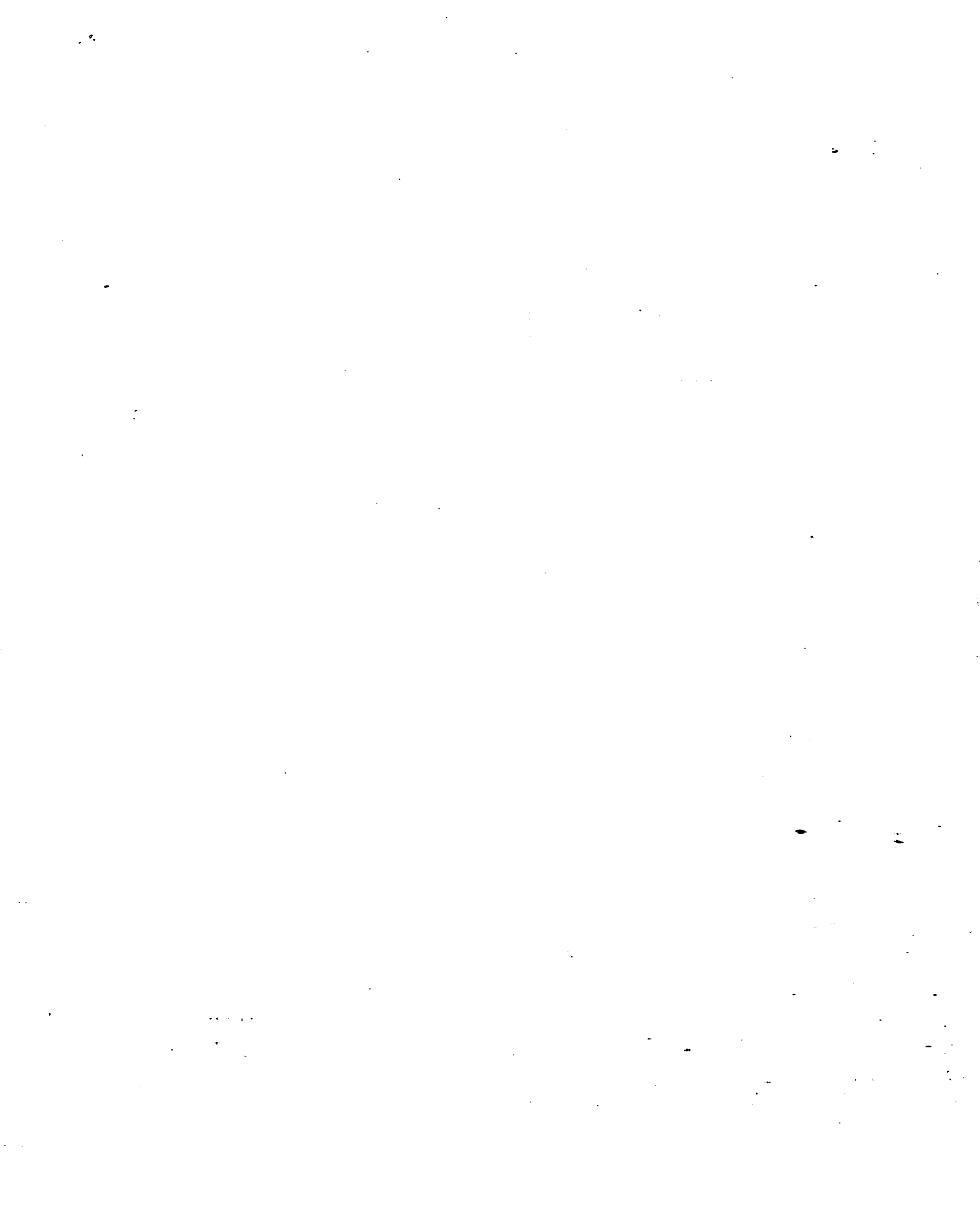
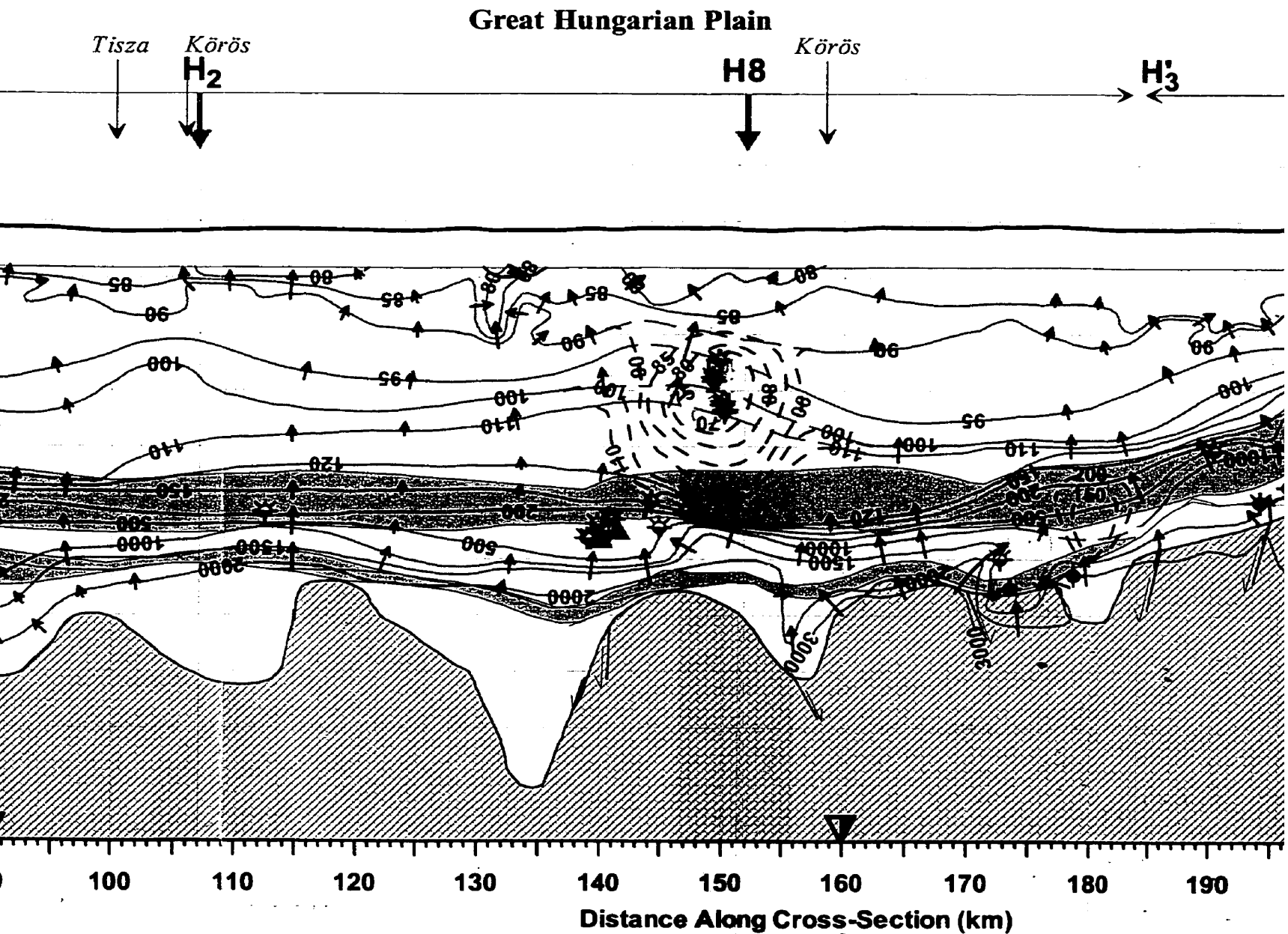
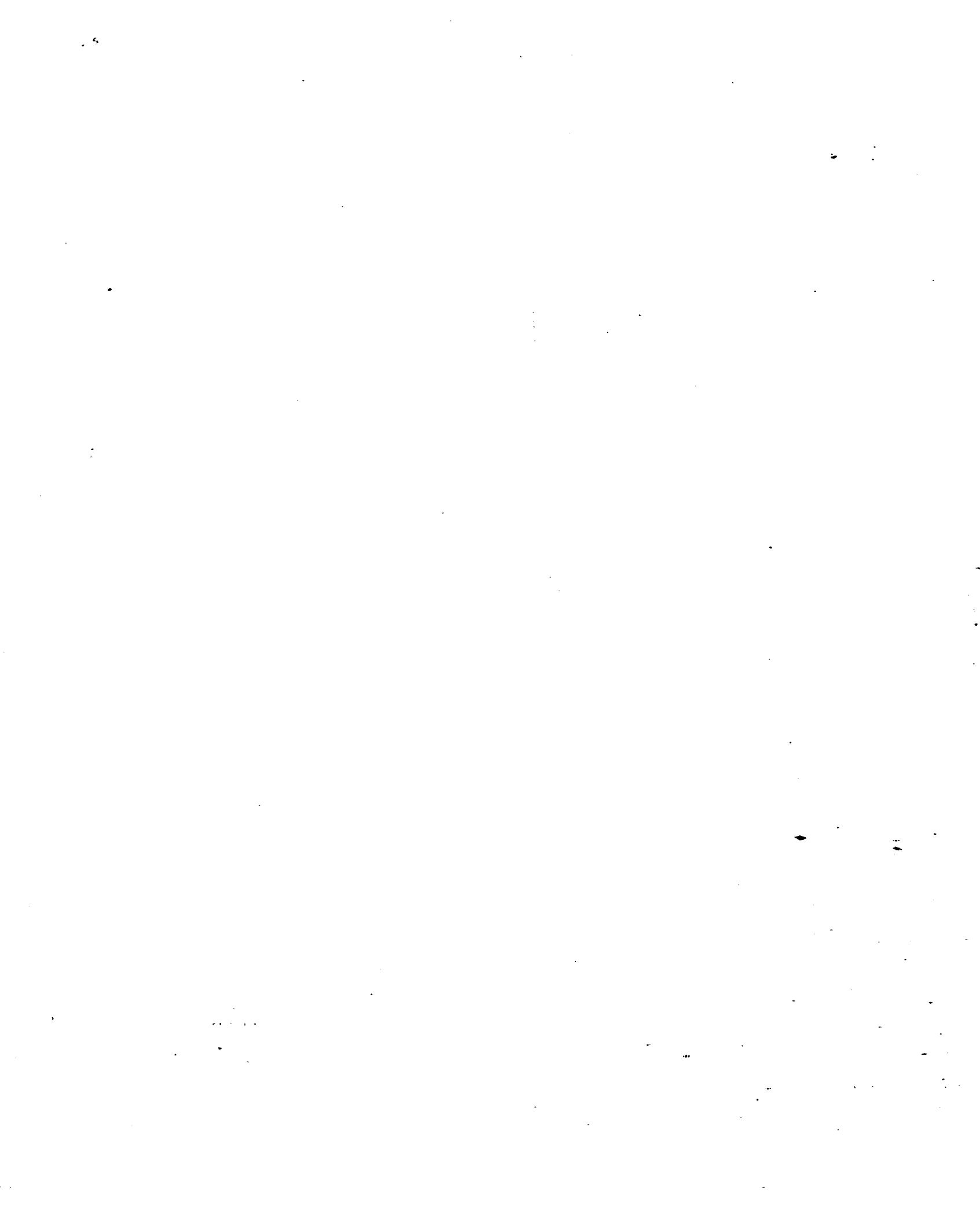


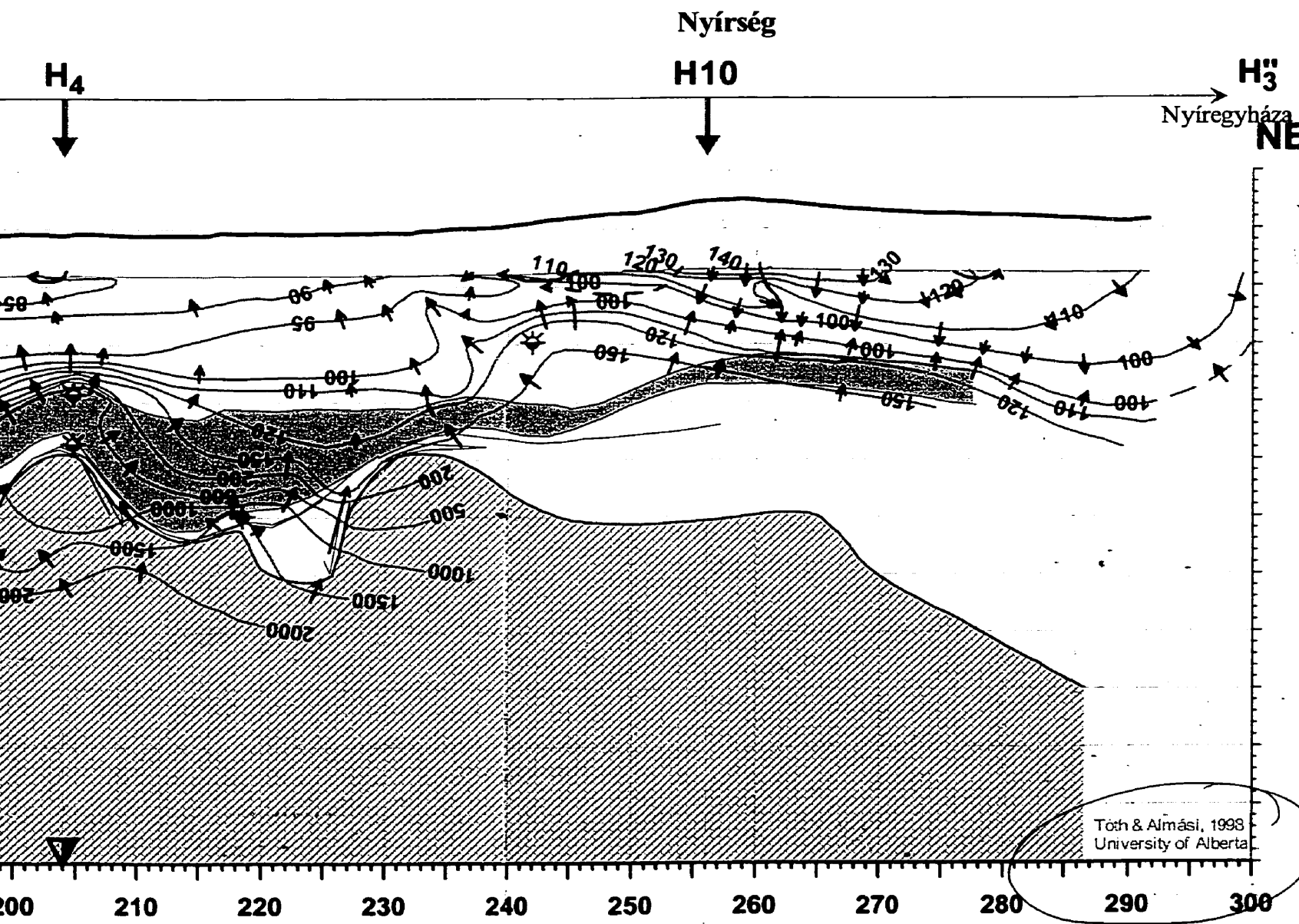
Figure 4.35: Hydraulic cross section H3 and hydrocarbon accumulation



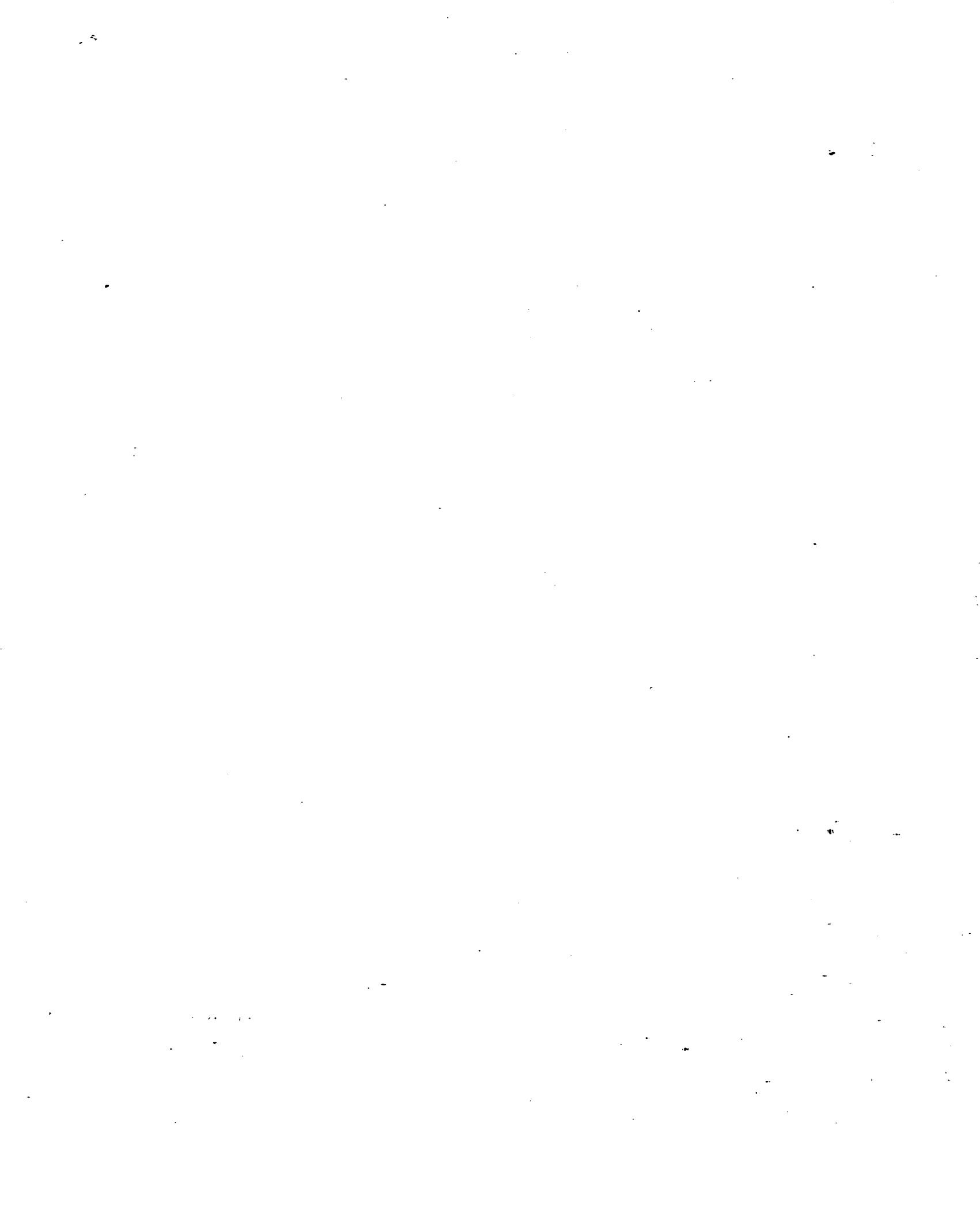


ons within 2 km distance from either side of the section (for location see Figure





4).



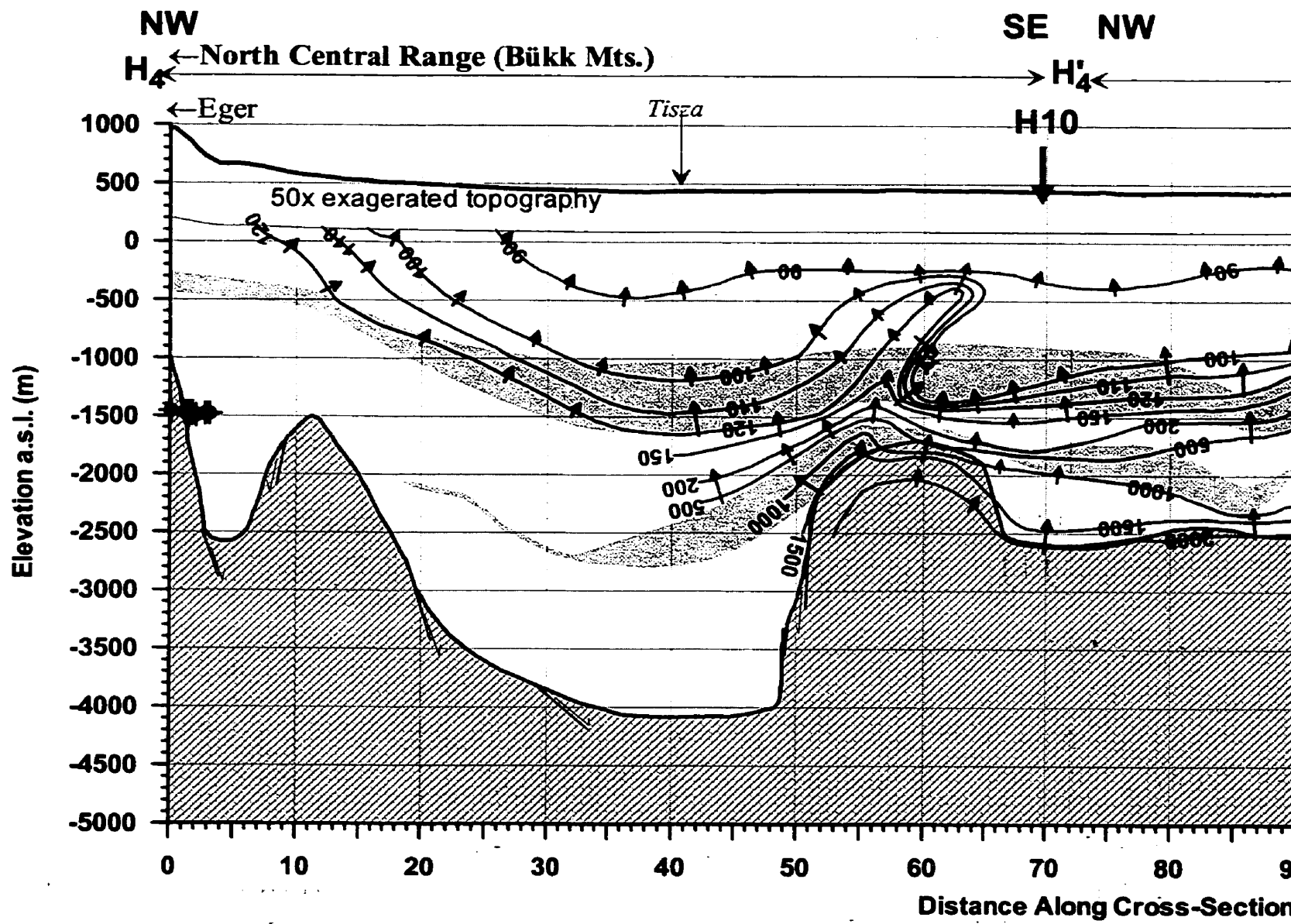
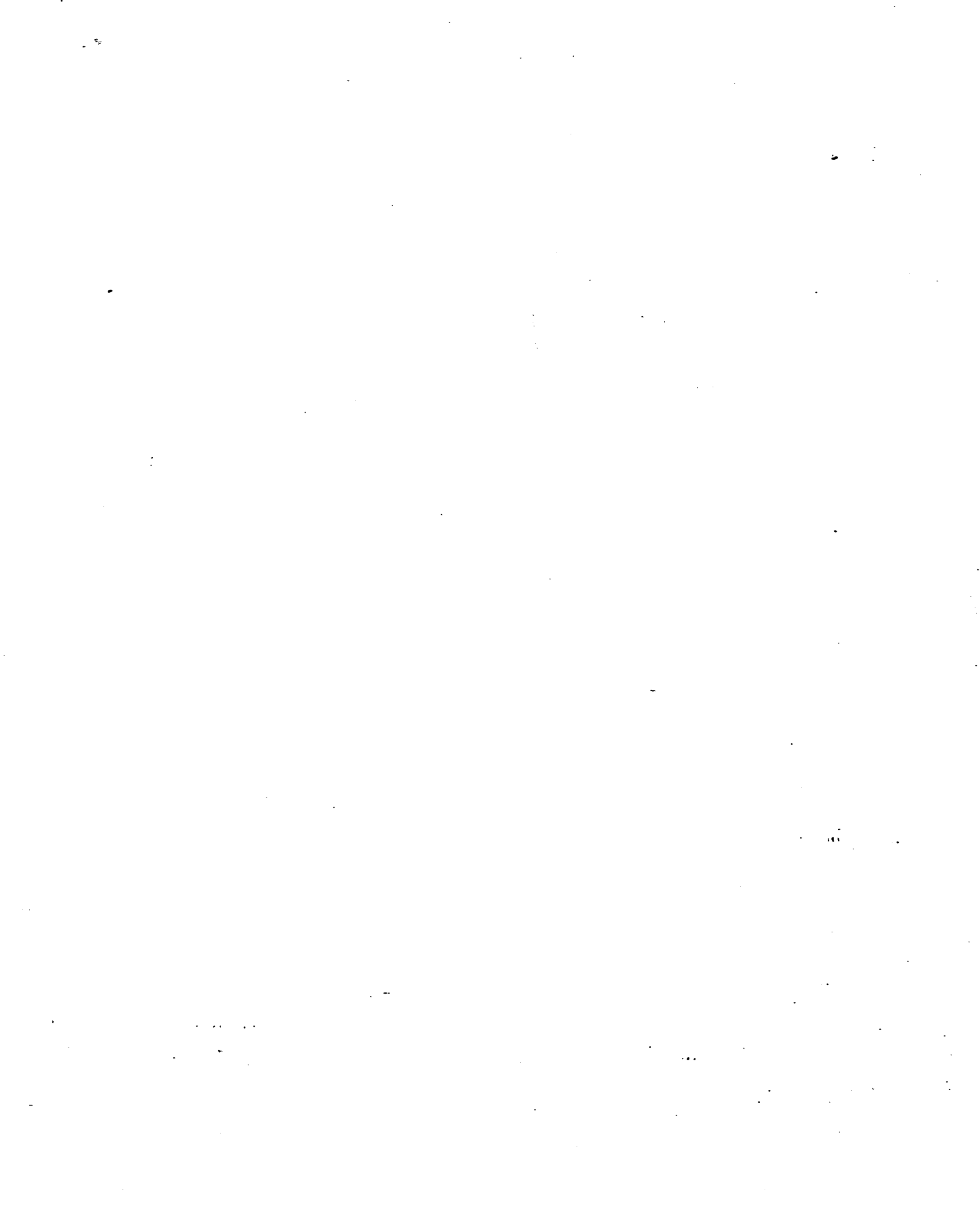
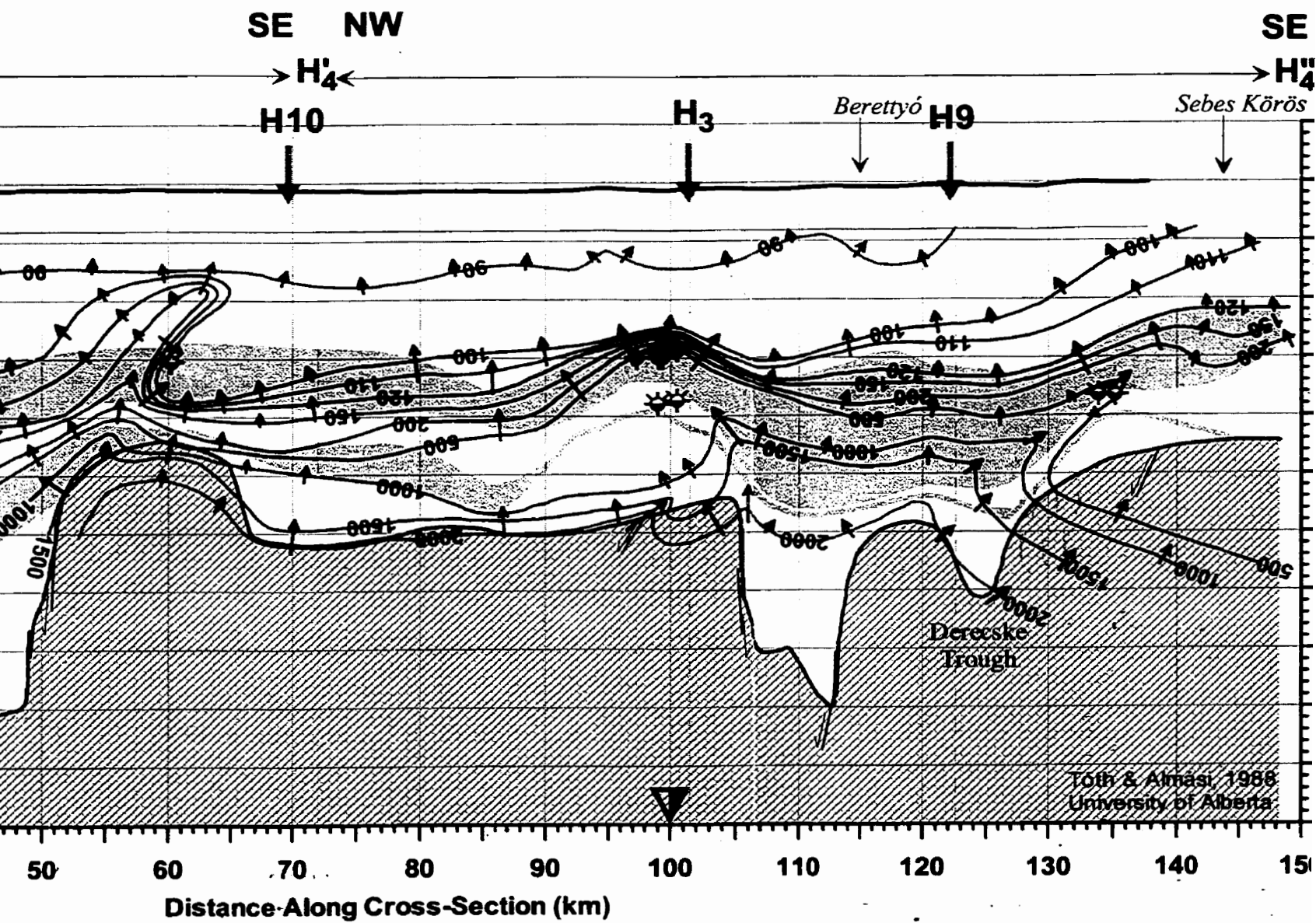
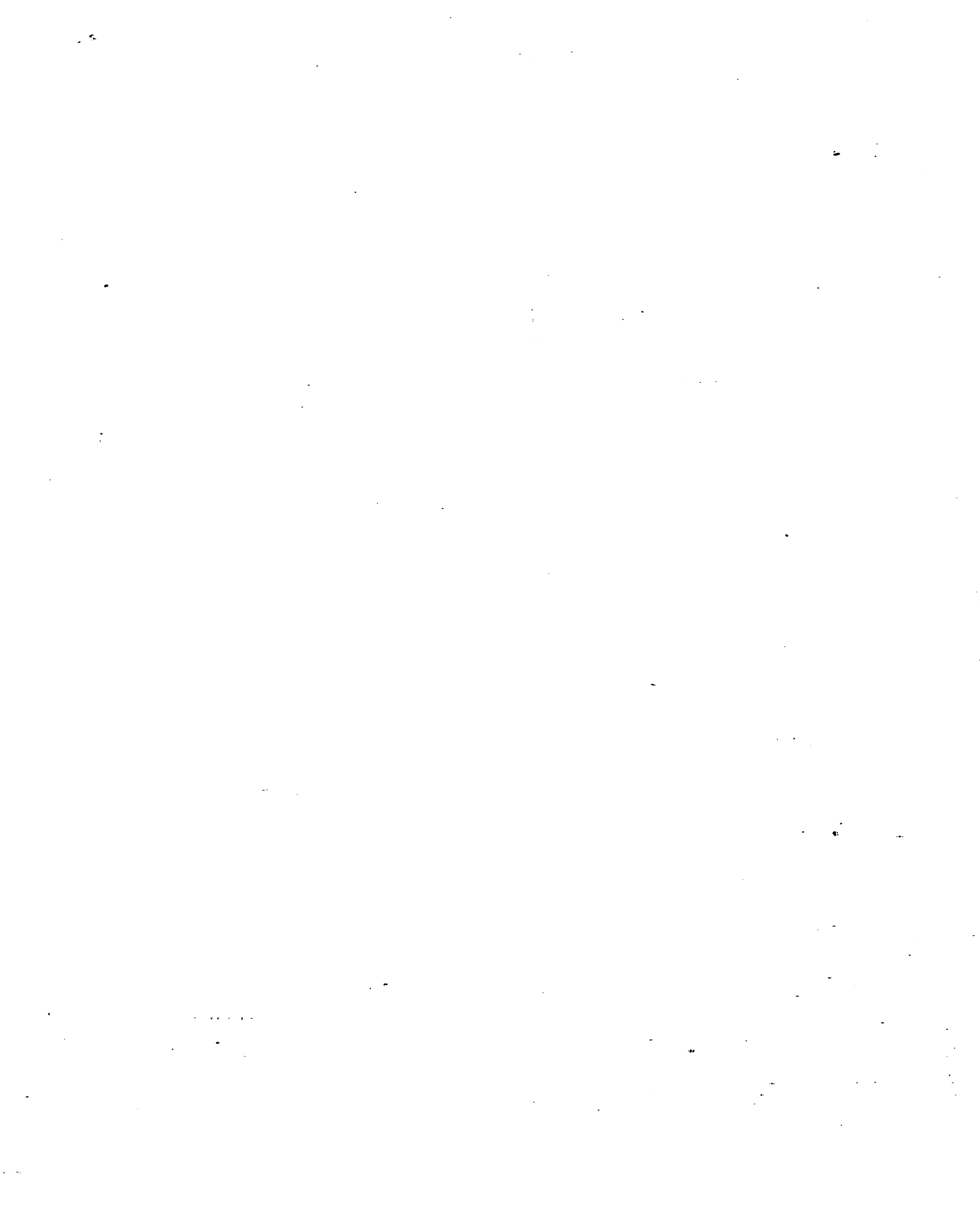


Figure 4.36. Hydraulic cross section H4 and hydrocarbon accumulation from either side of the section (for location see Figure 4.4)





H4 and hydrocarbon accumulations within 2 km distance section (for location see Figure 4.4).



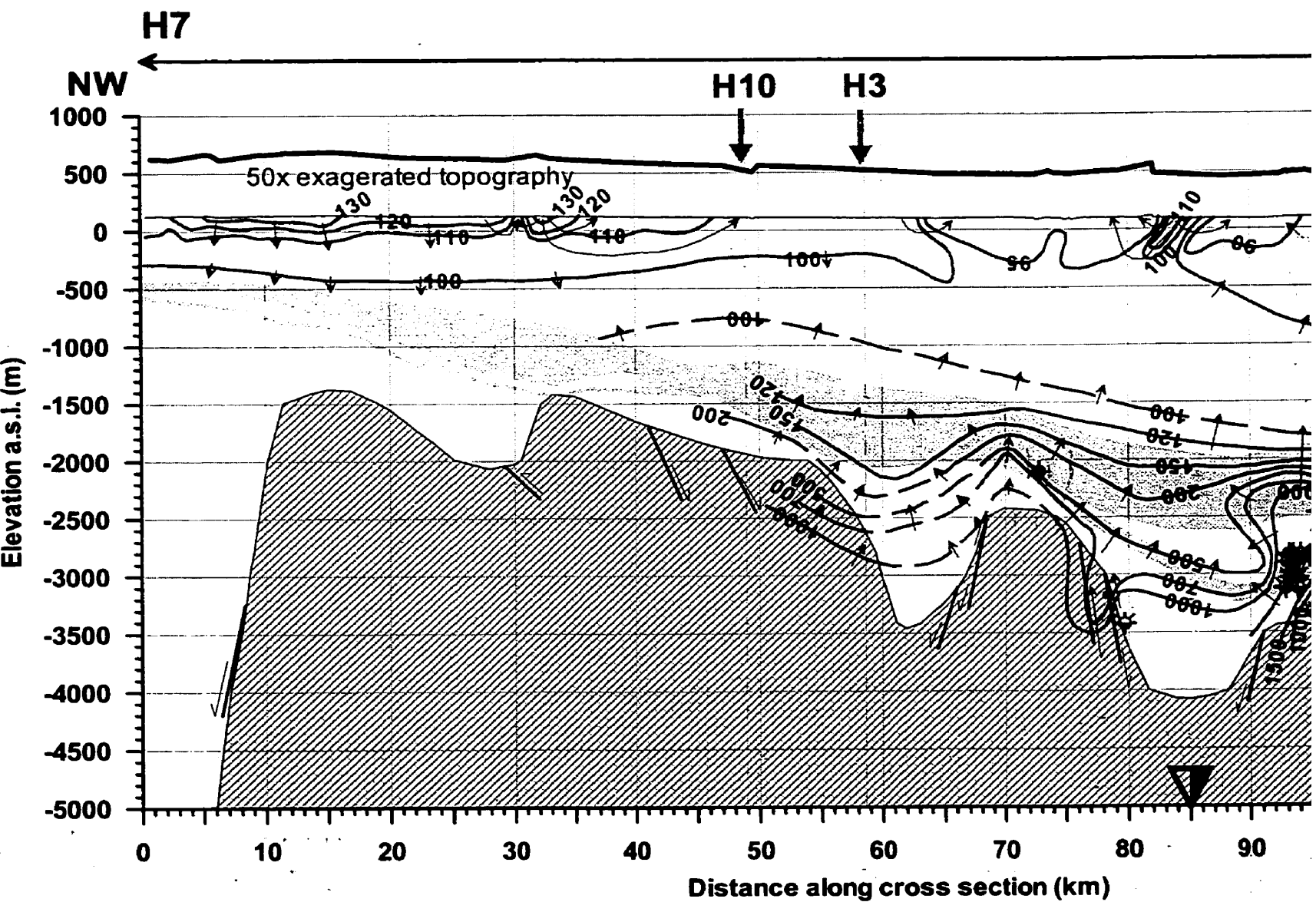
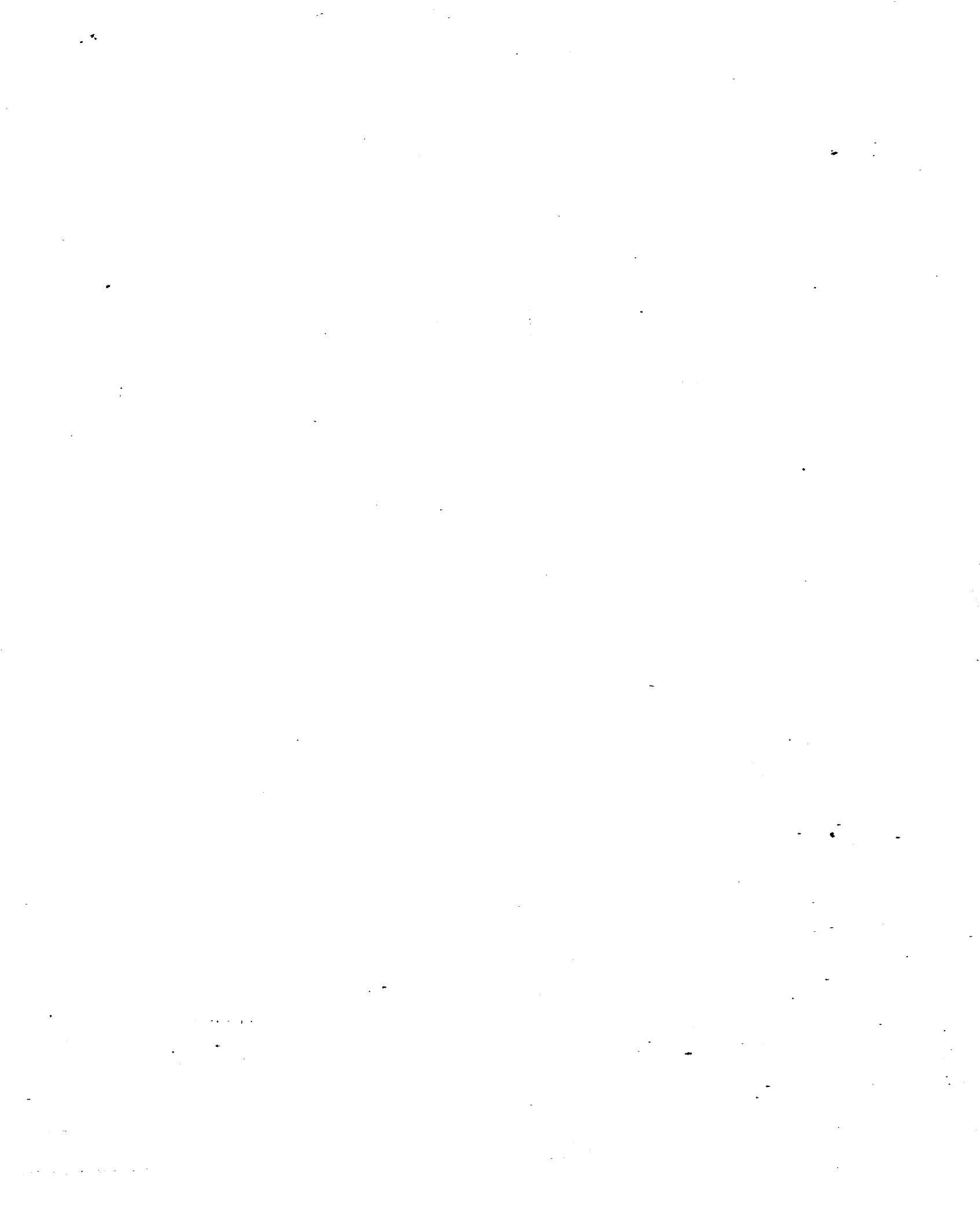
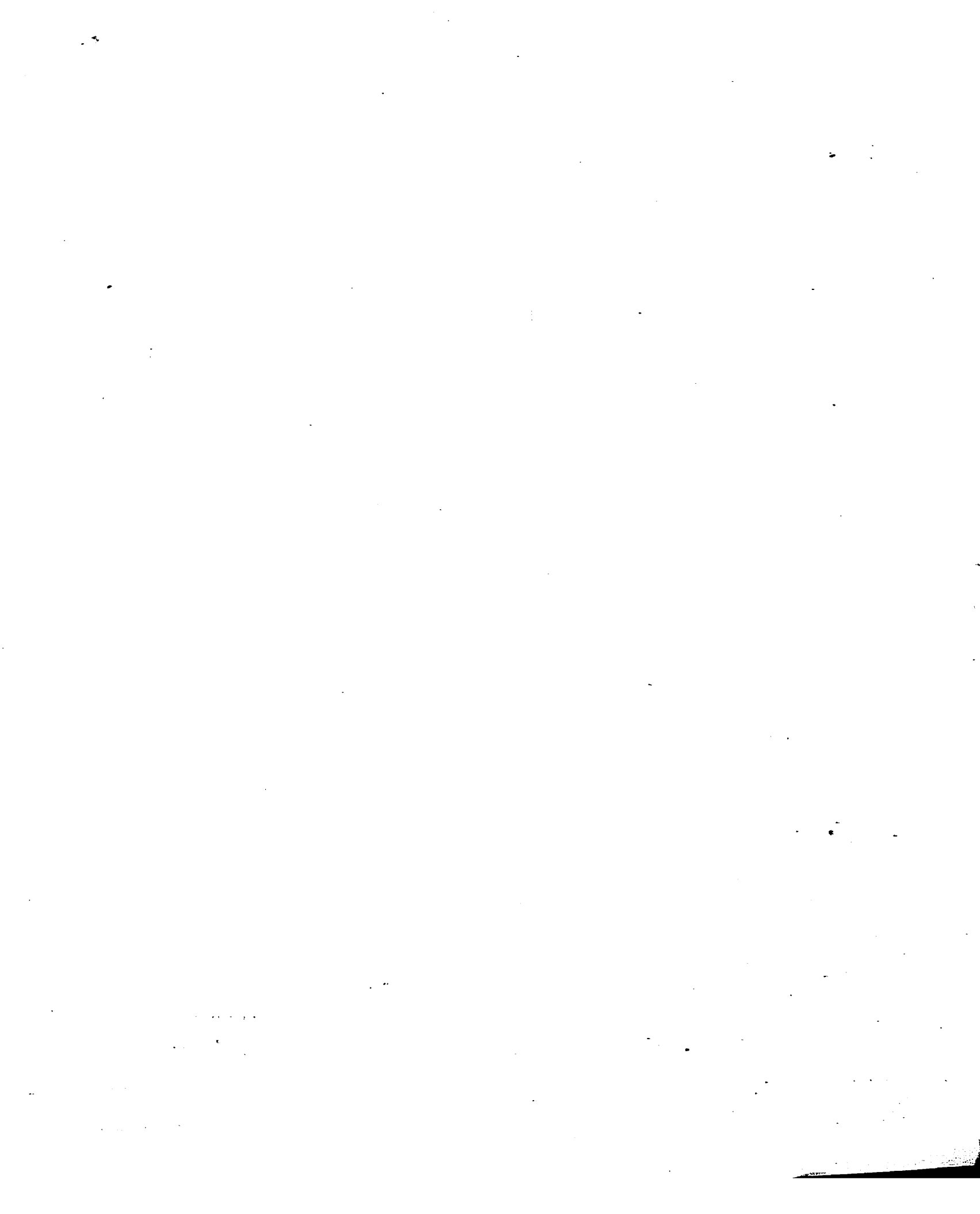


Figure 4.39. Hydraulic cross section H7 and hydrocarbon accumulations from either side of the section (for location see Figure 4.4).





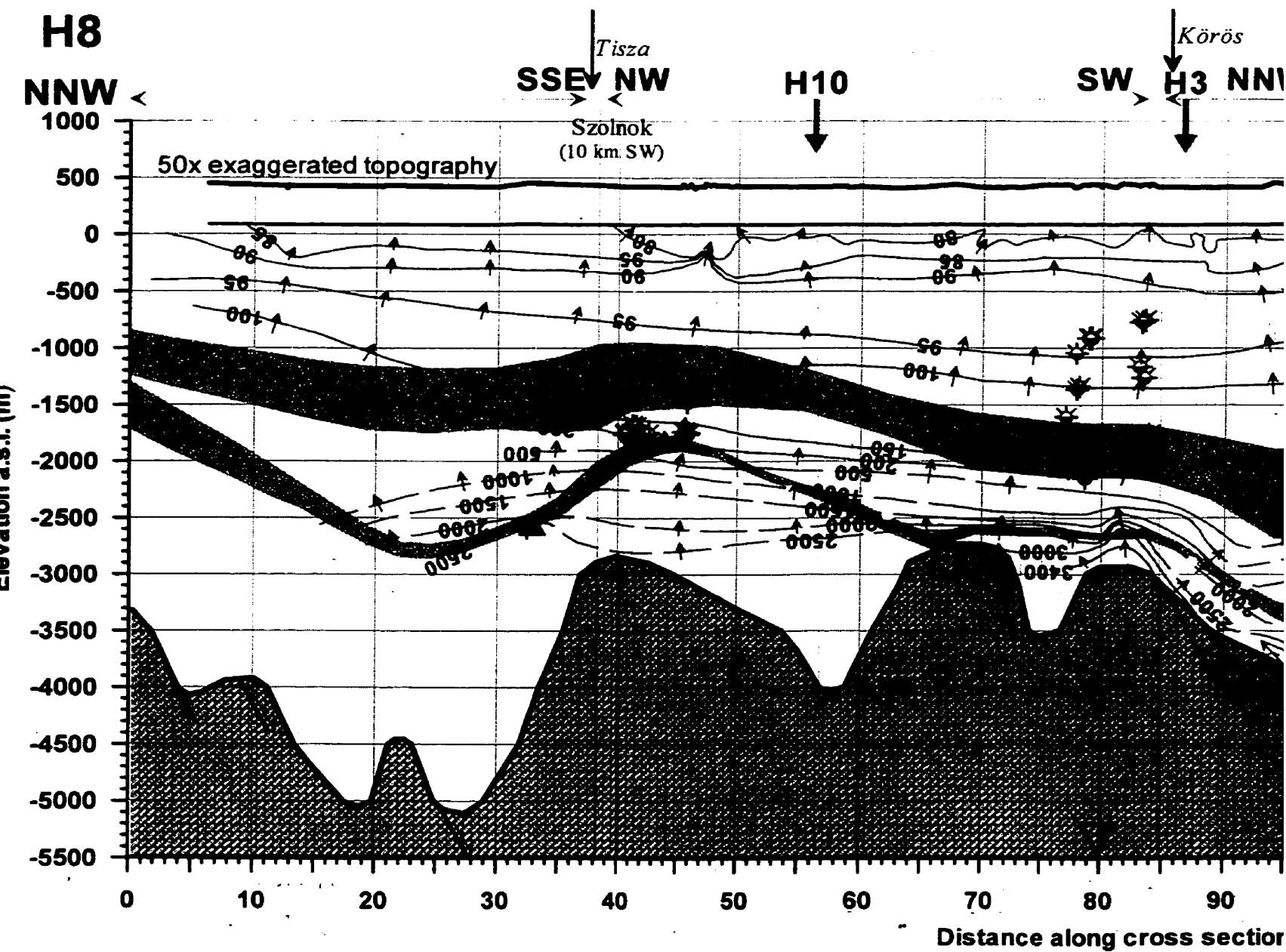
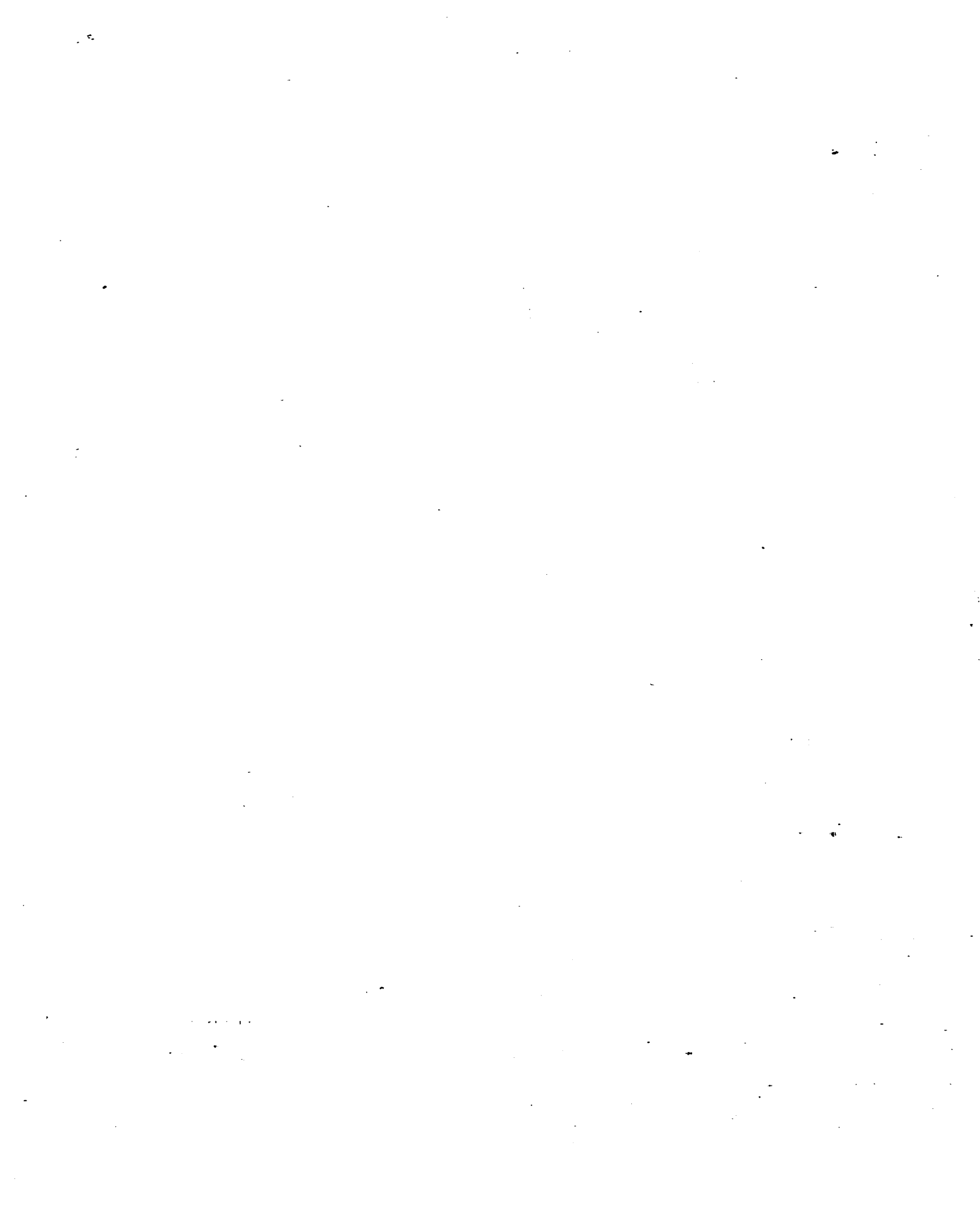
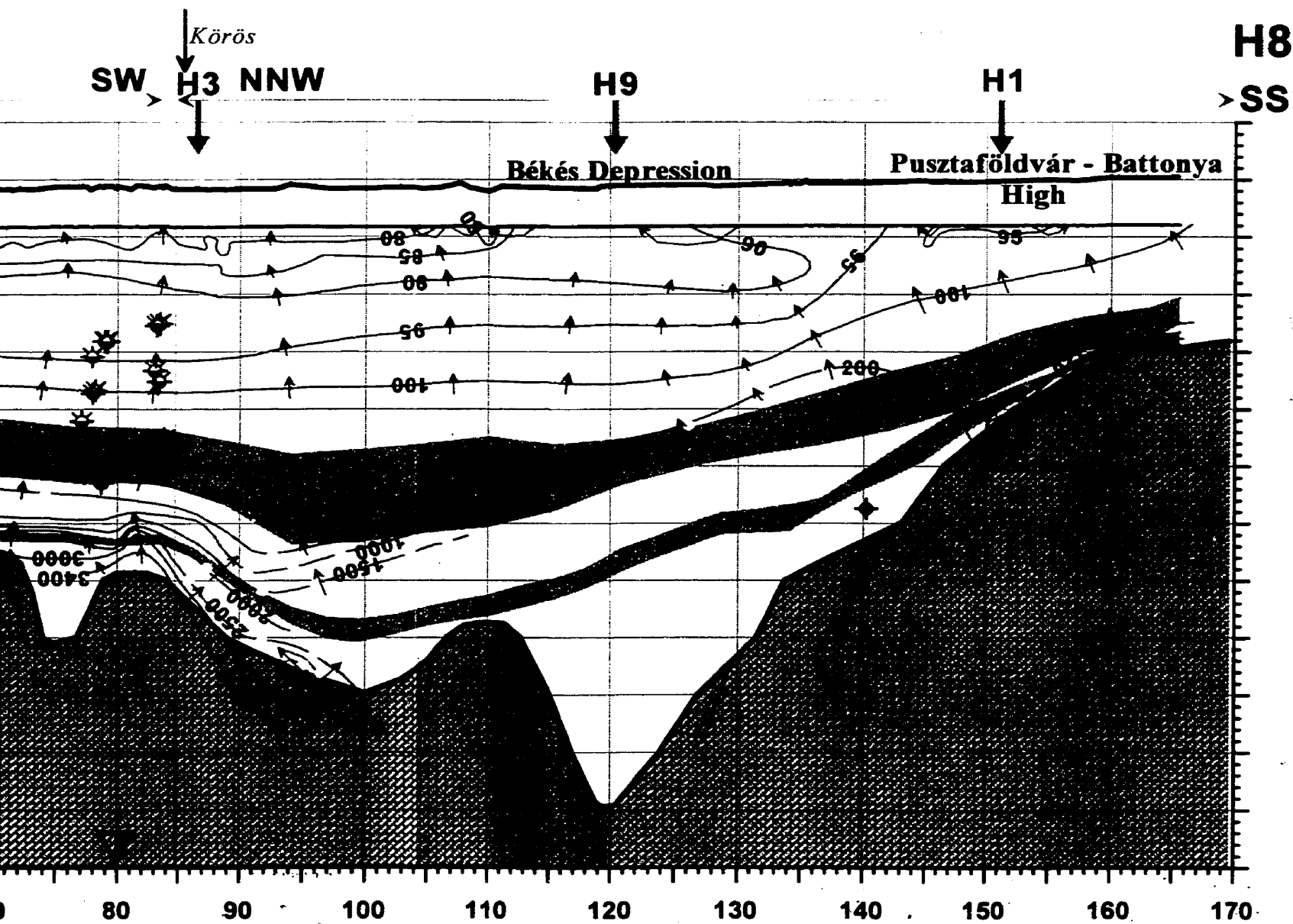
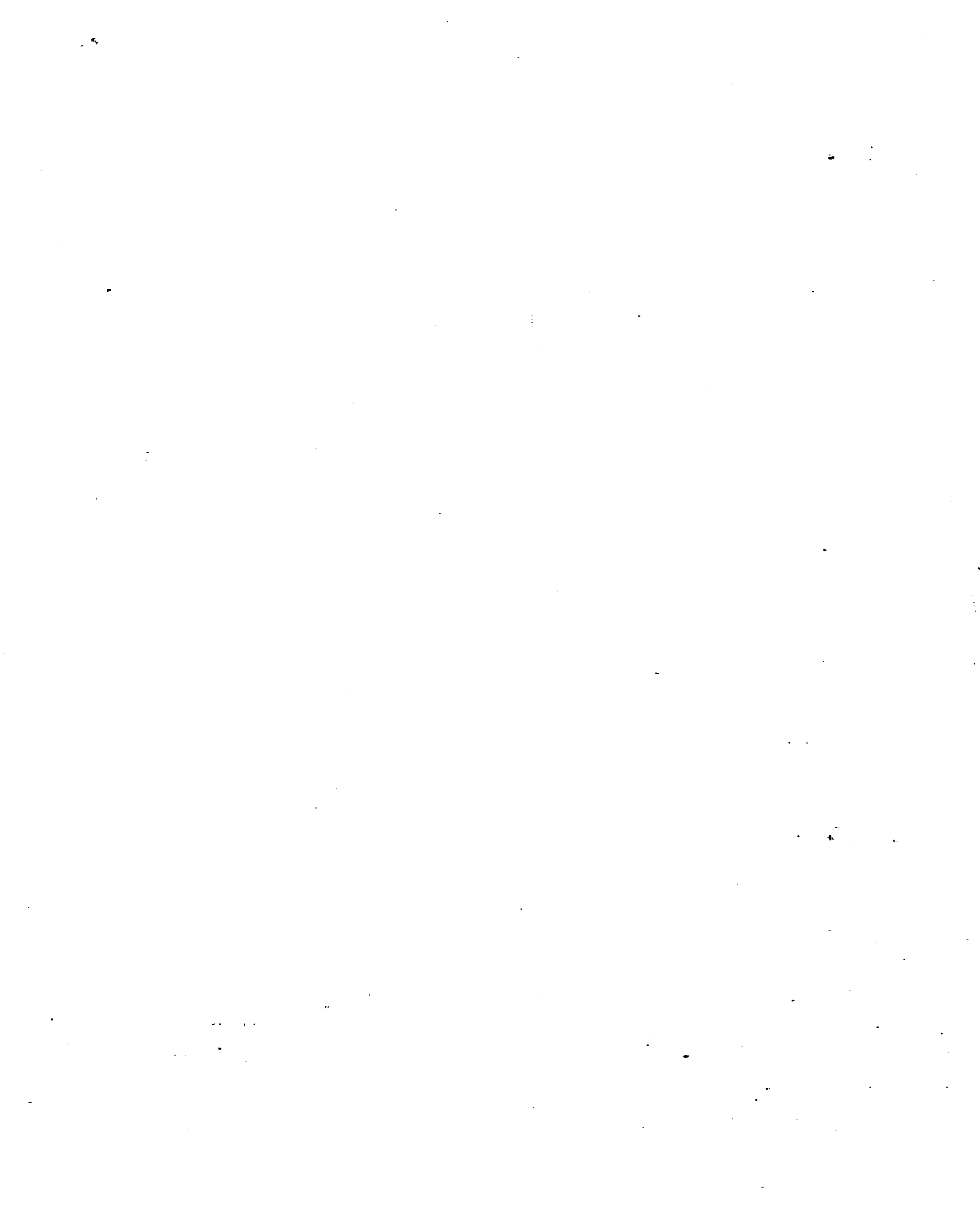


Figure 4.40. Hydraulic cross section H8 and hydrocarbon accumulation:
(for location see Figure 4.4).





Carbon accumulations within 2 km distance from either side of the section



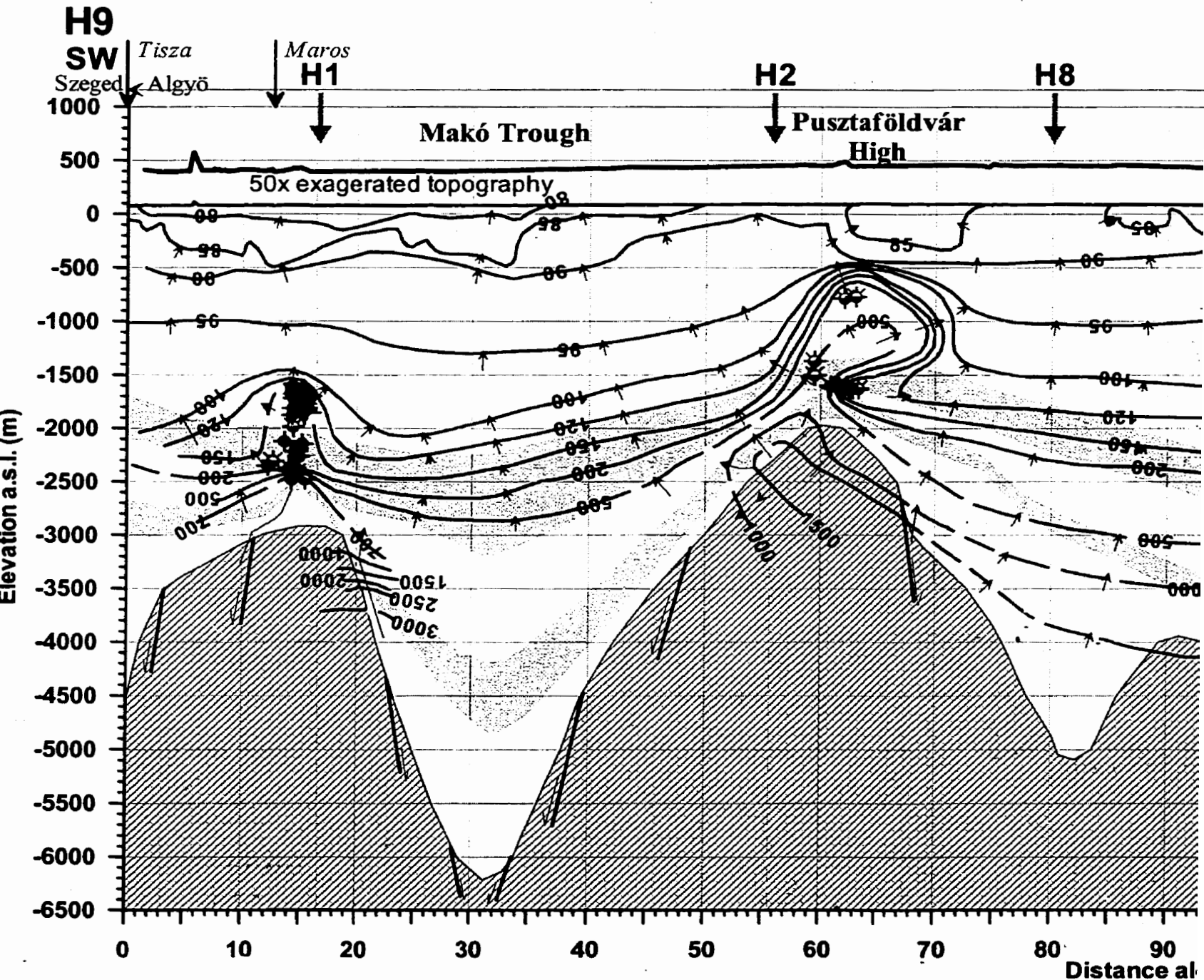
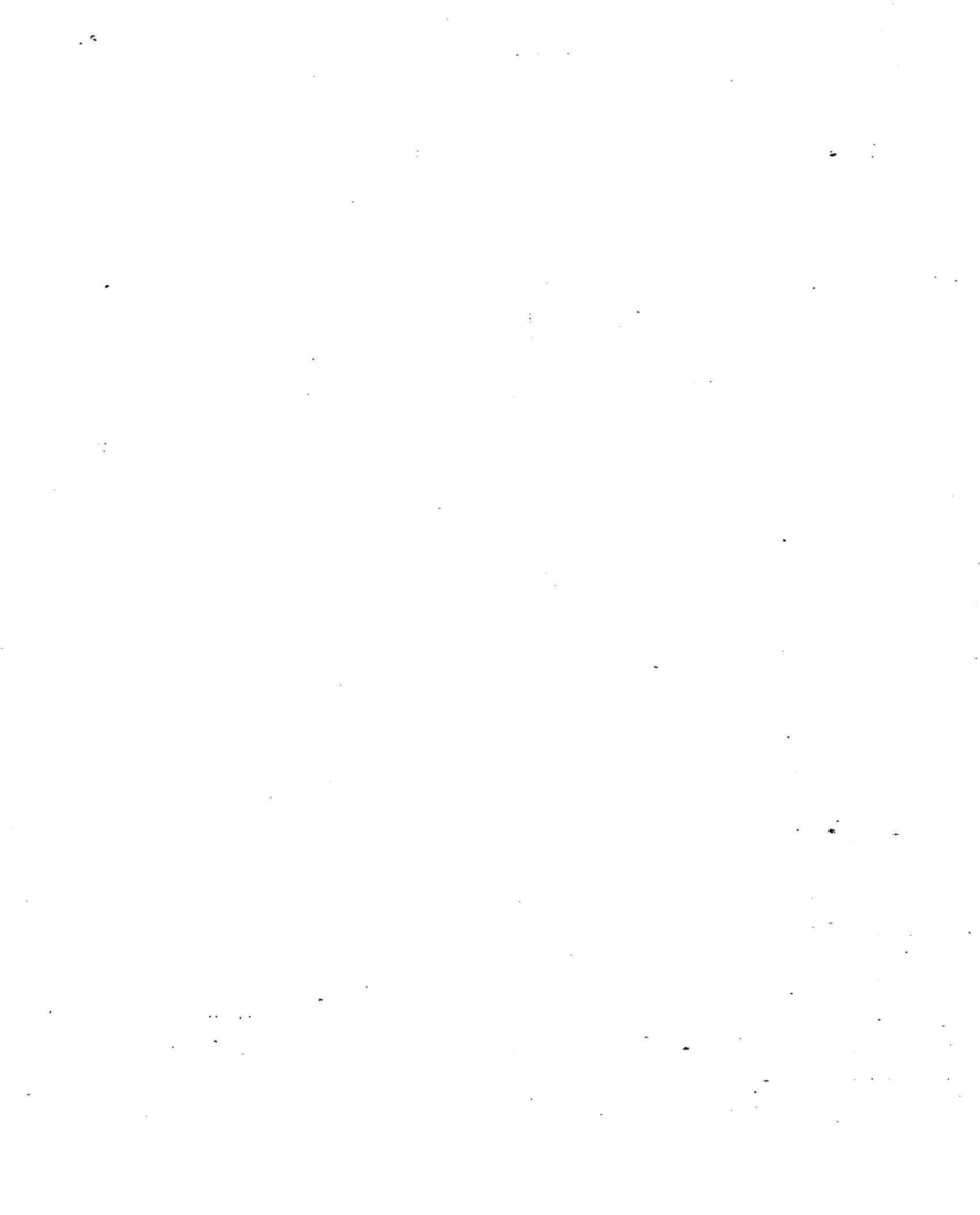
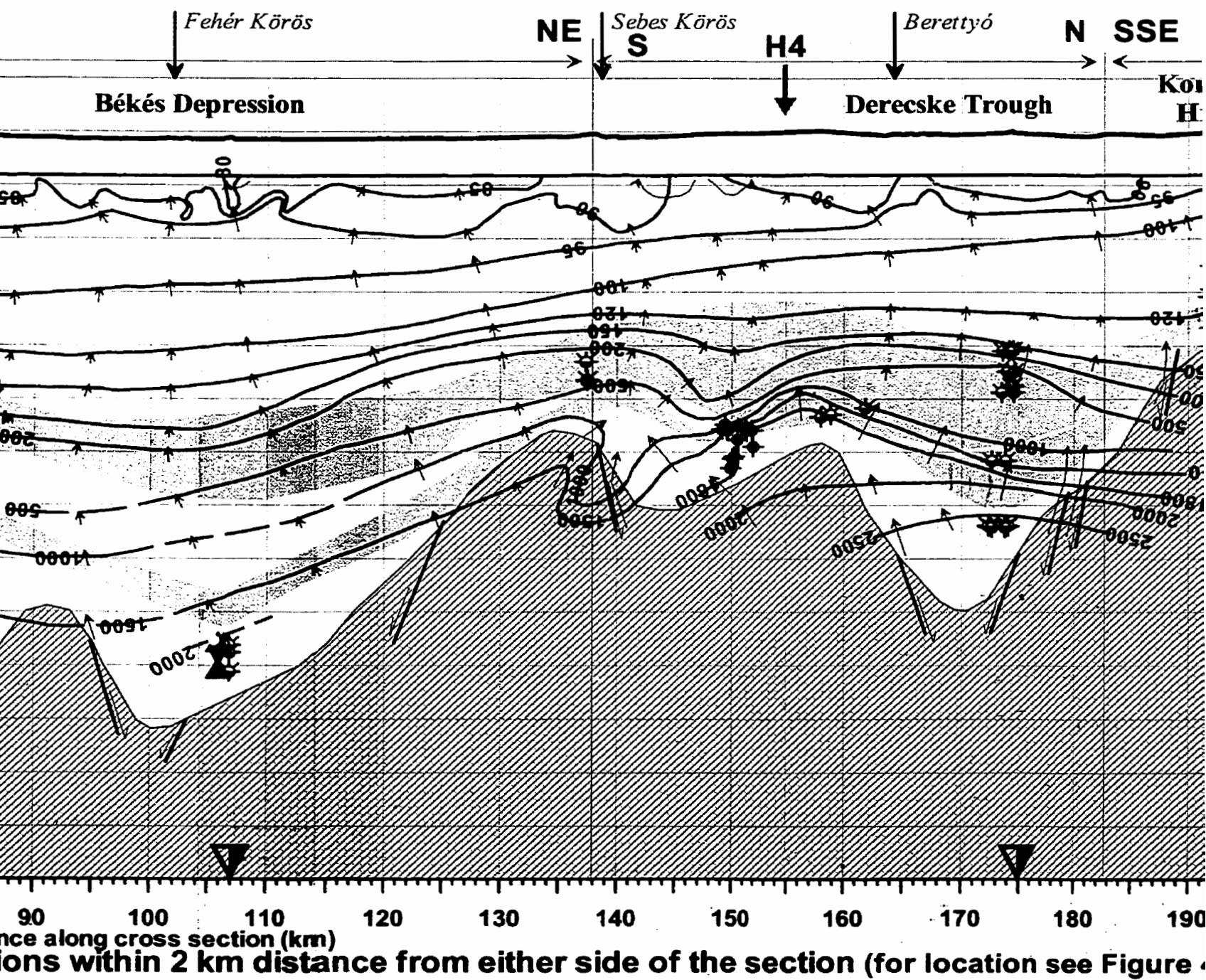
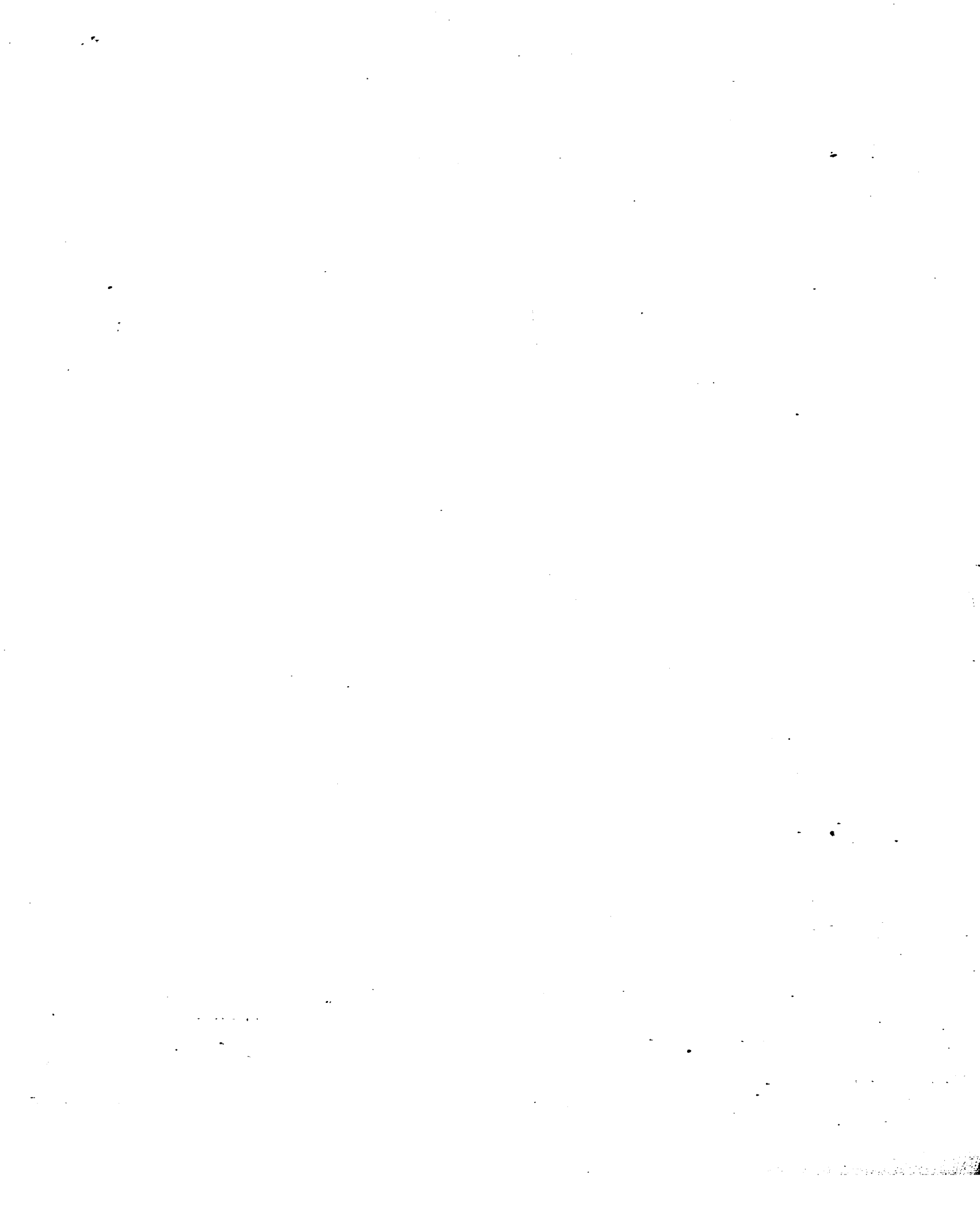


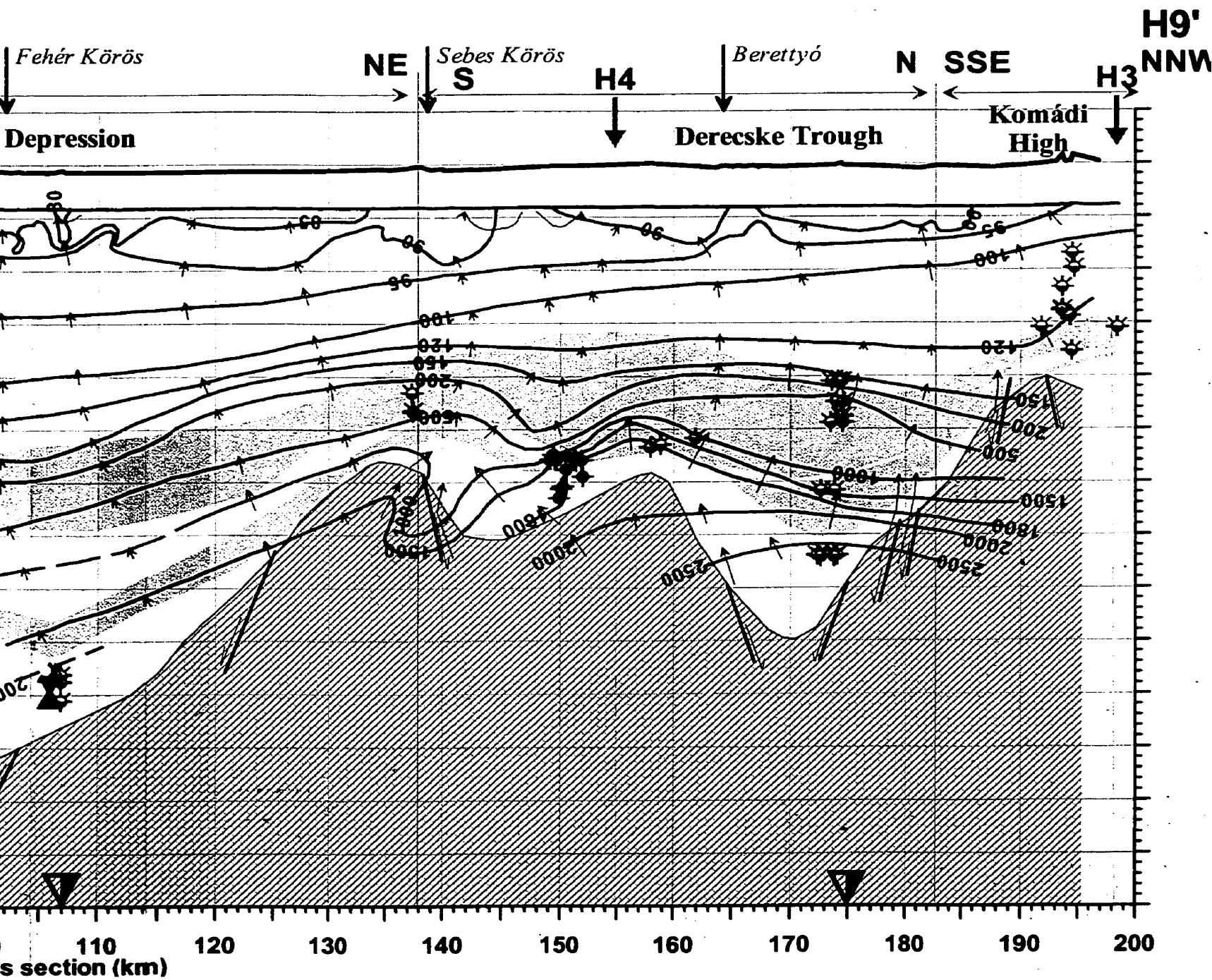
Figure 4.41: Hydraulic cross section H9 and hydrocarbon accumulations

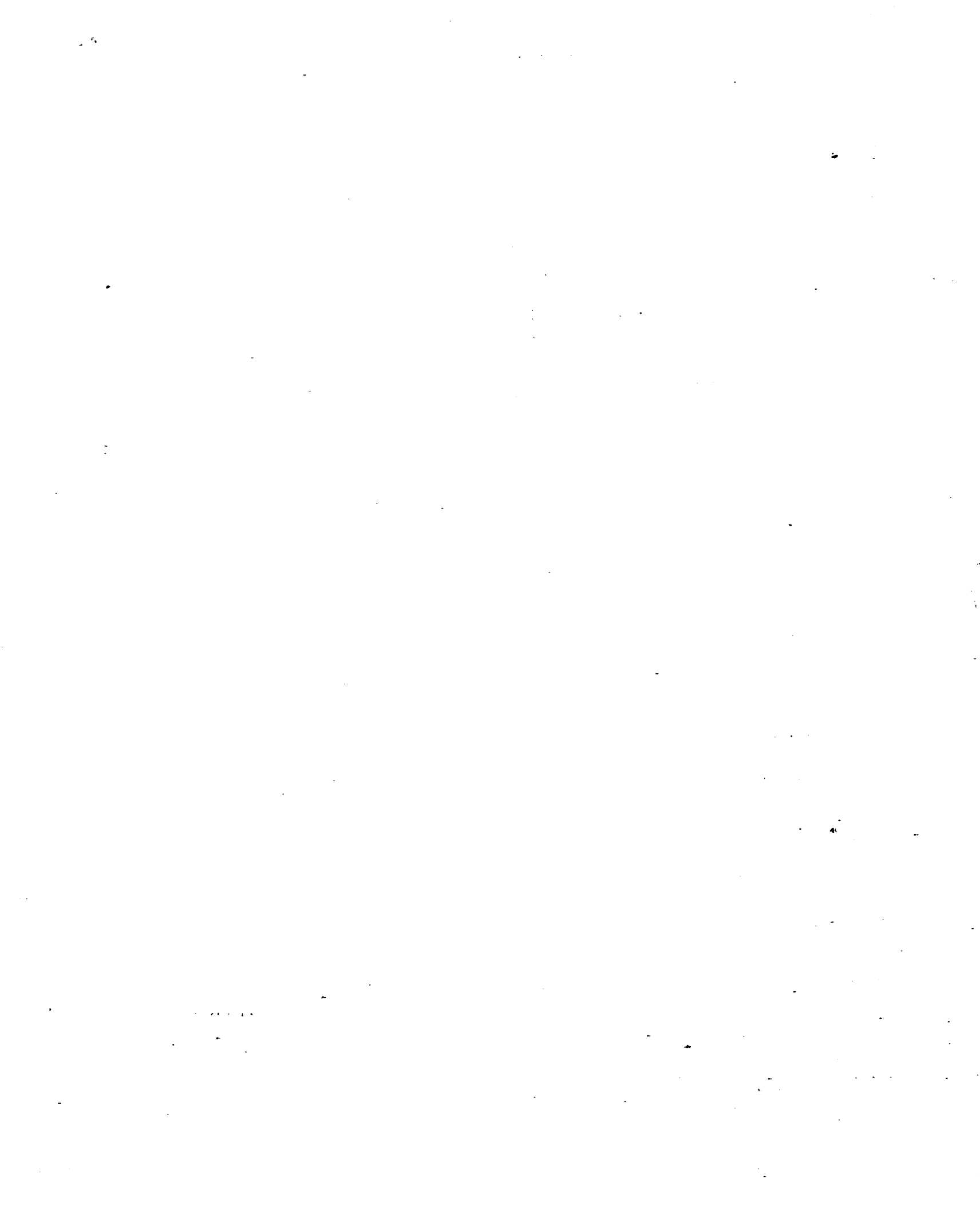




Distance along cross section (km)
 Stations within 2 km distance from either side of the section (for location see Figure 4)







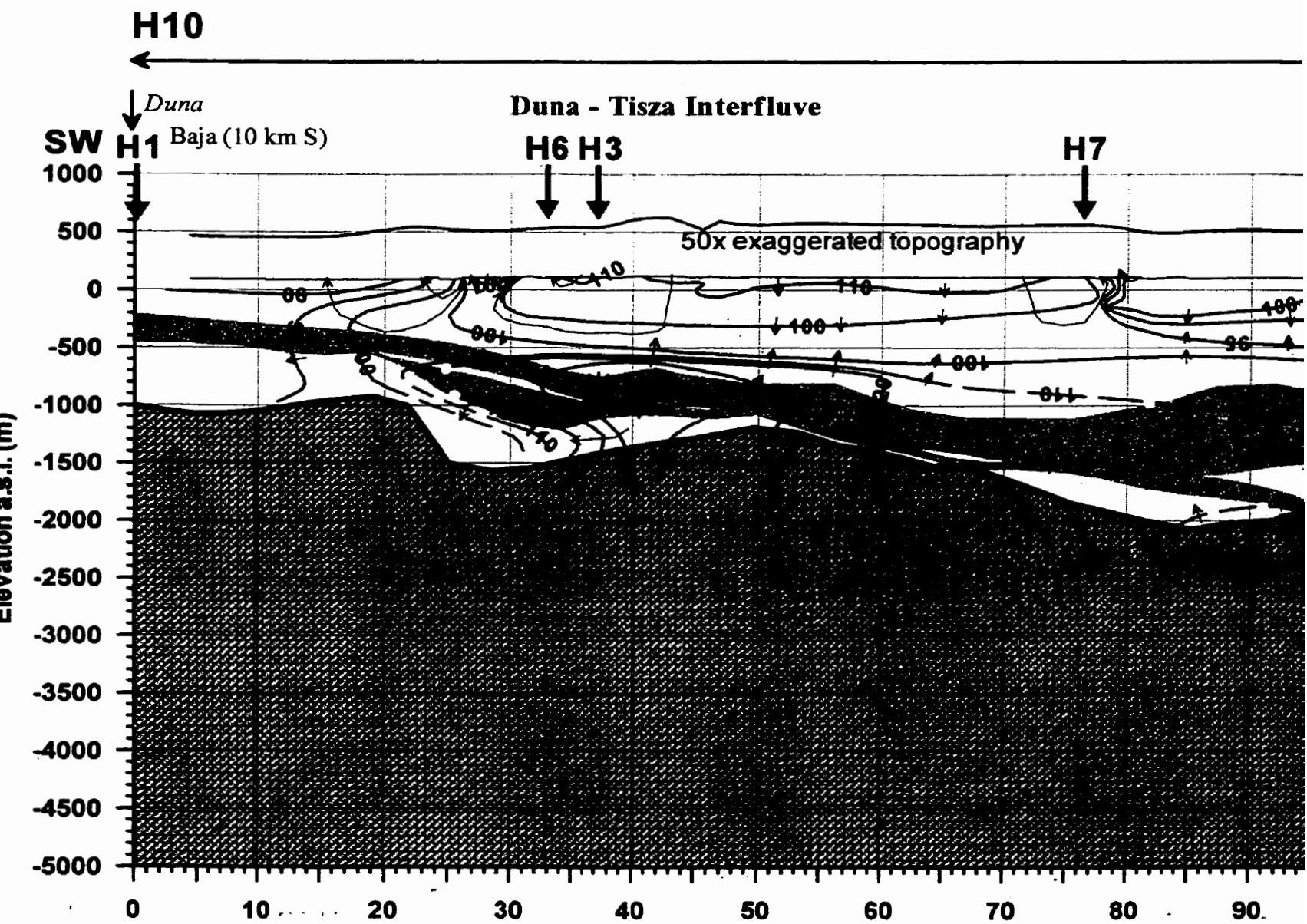
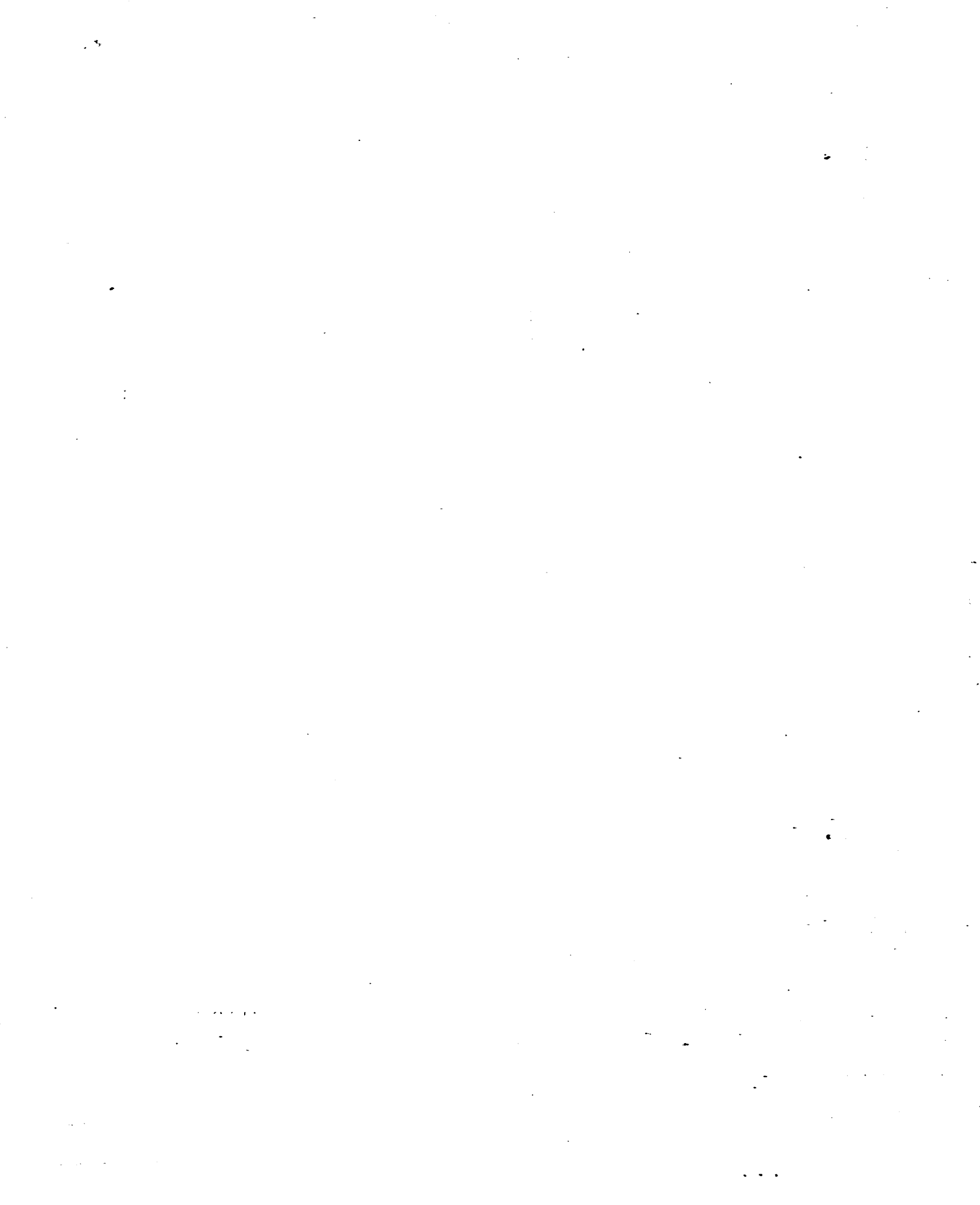
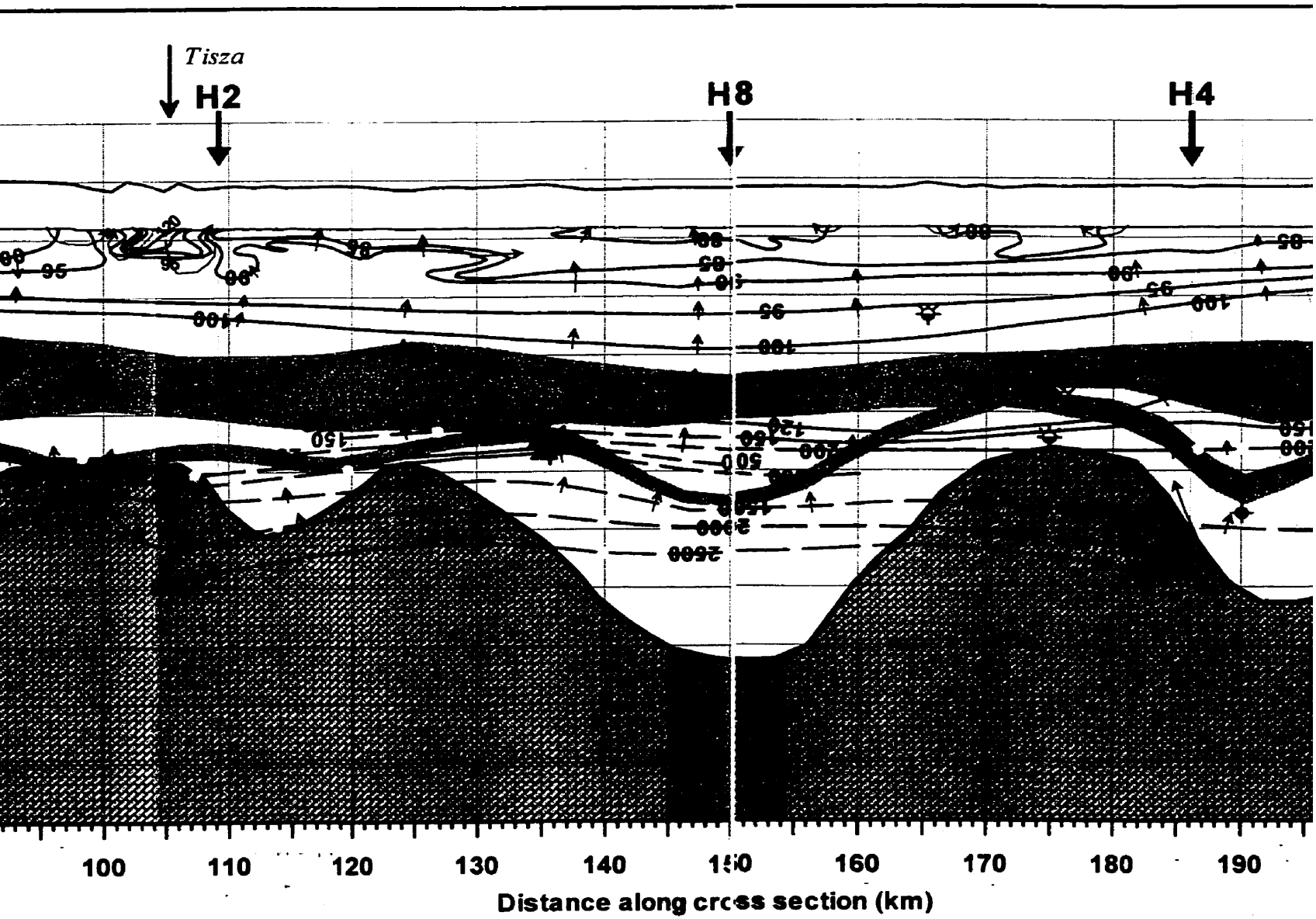


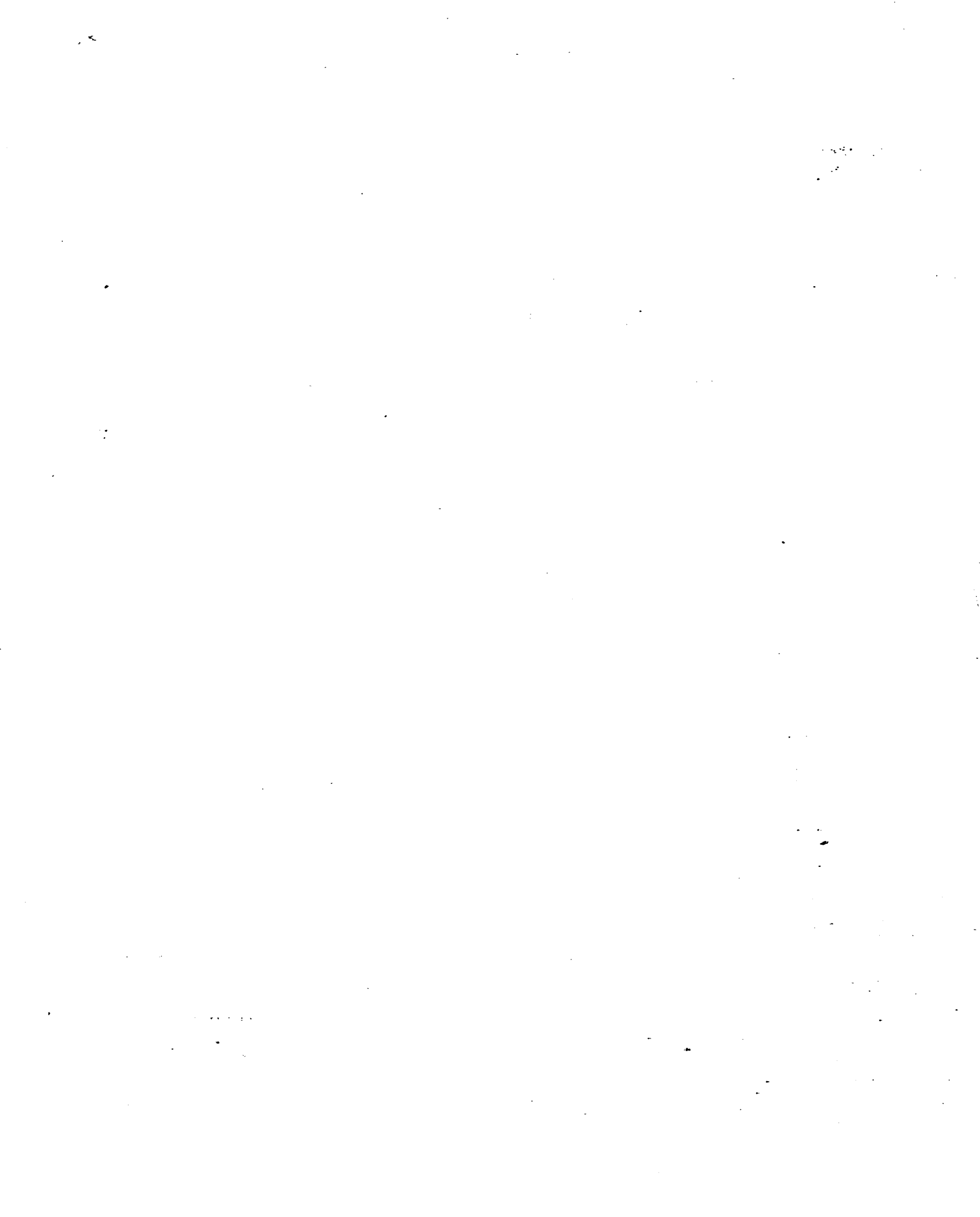
Figure 4.42: Hydraulic cross section H10 and hydrocarbon accumulations

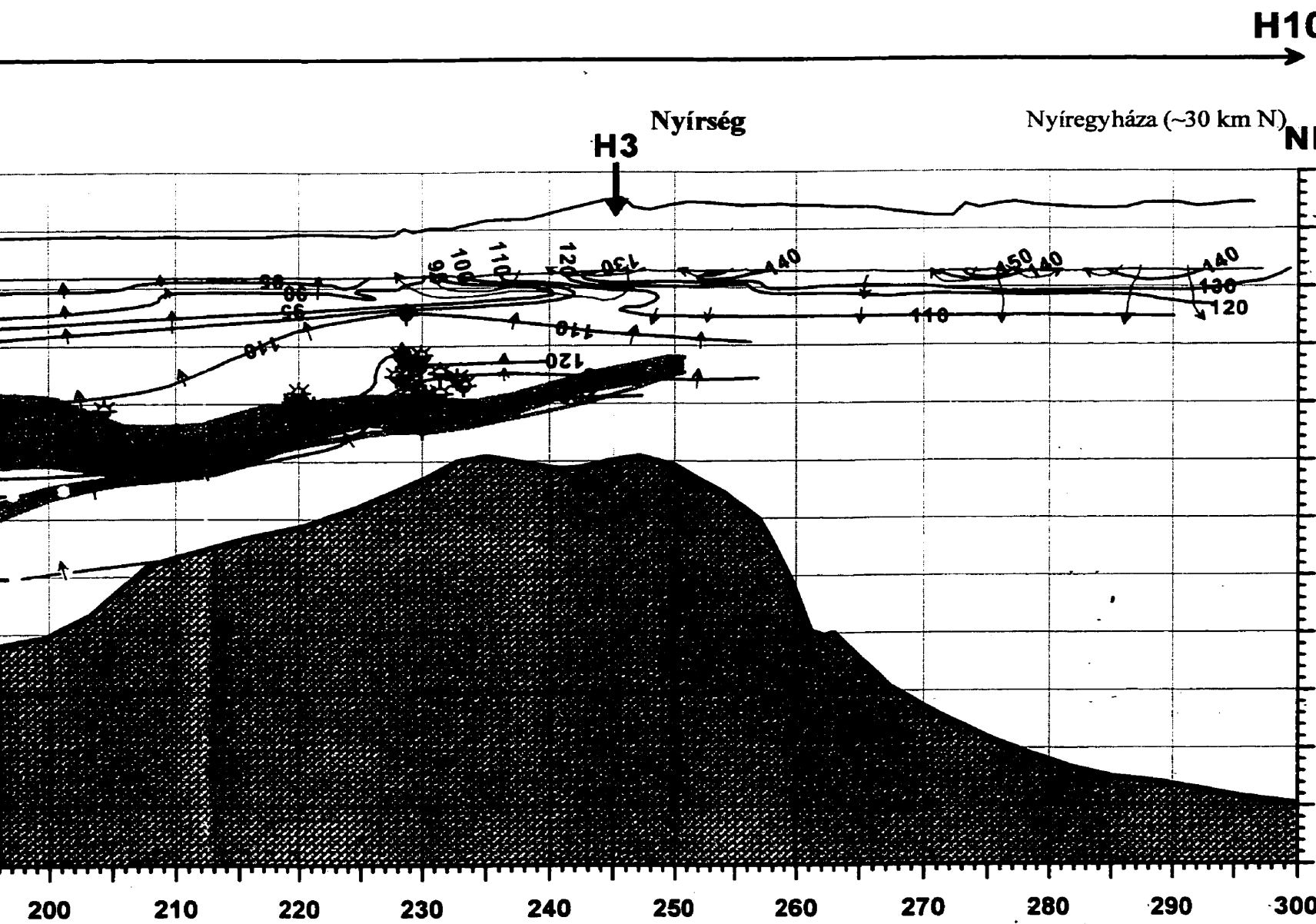




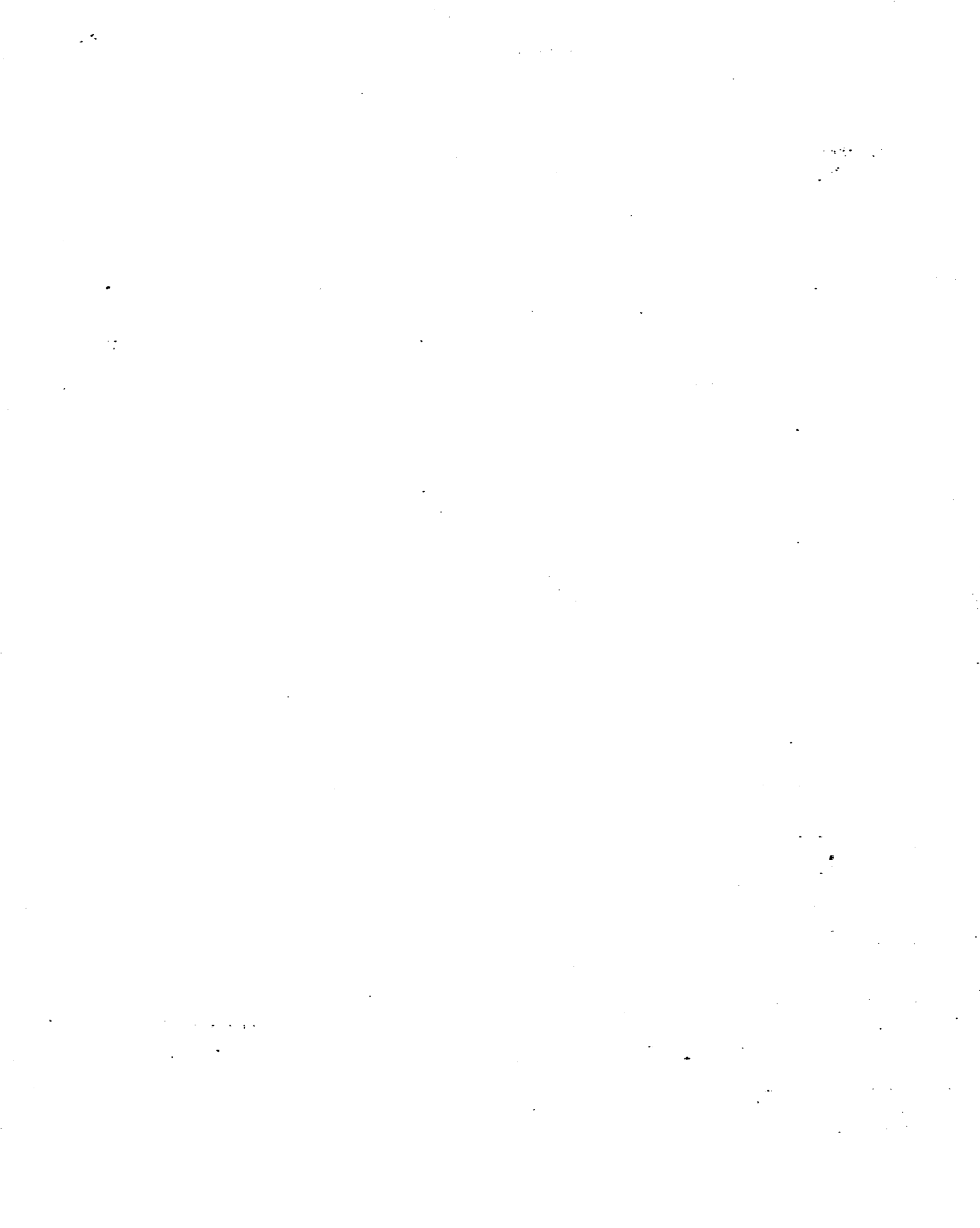
ons within 2 km distance from either side of the section (for location see Figure







e 4.4).



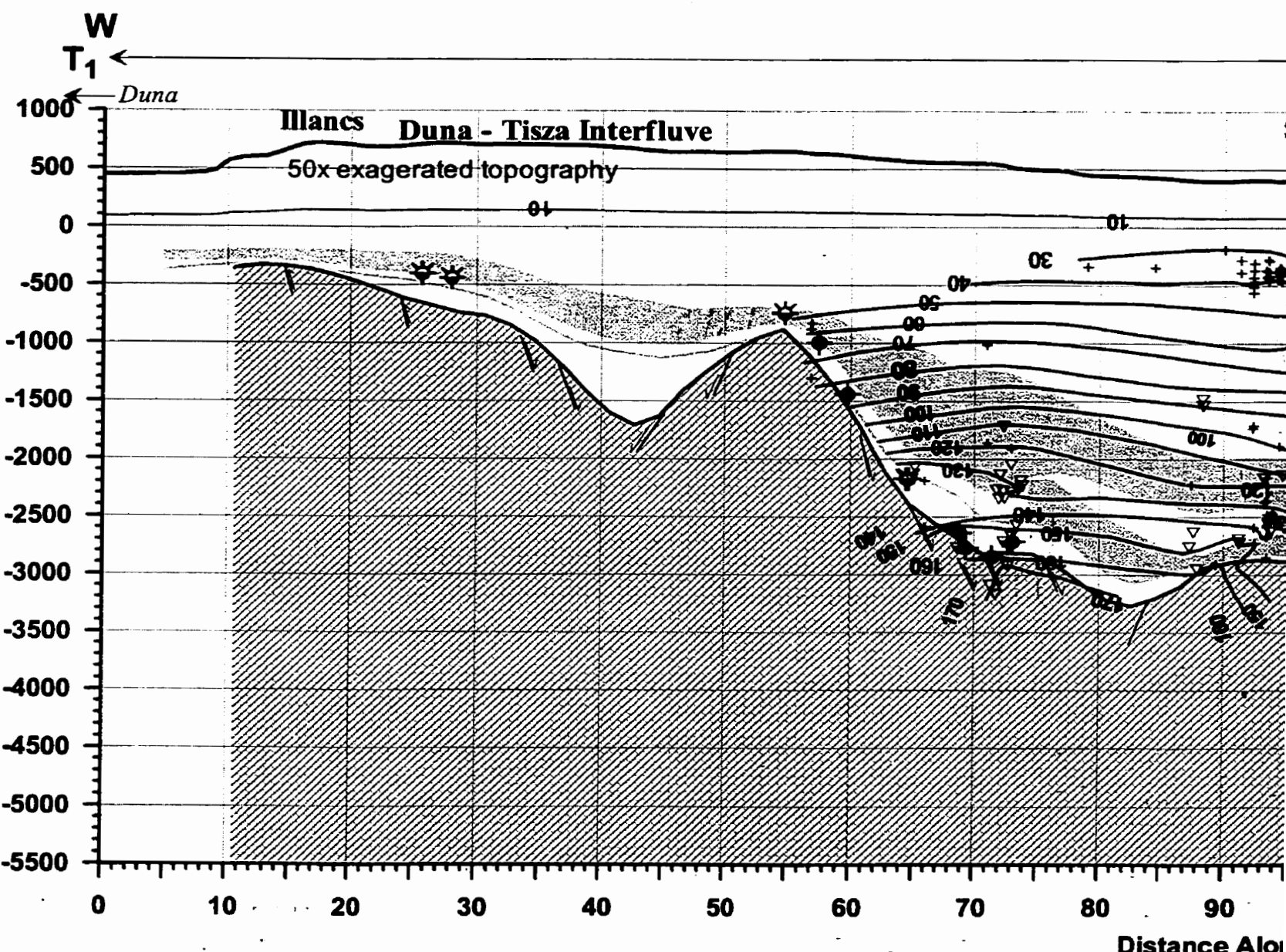
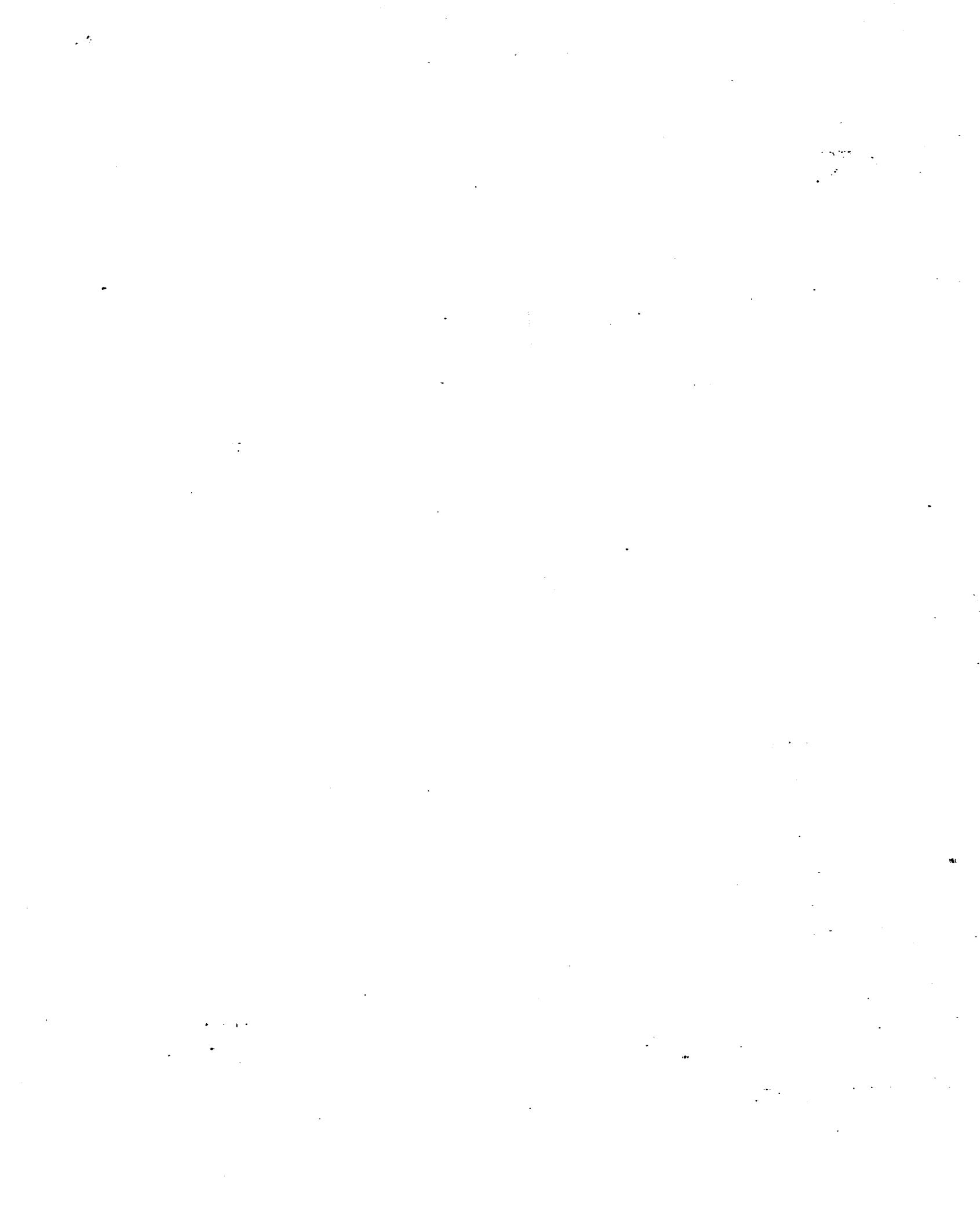
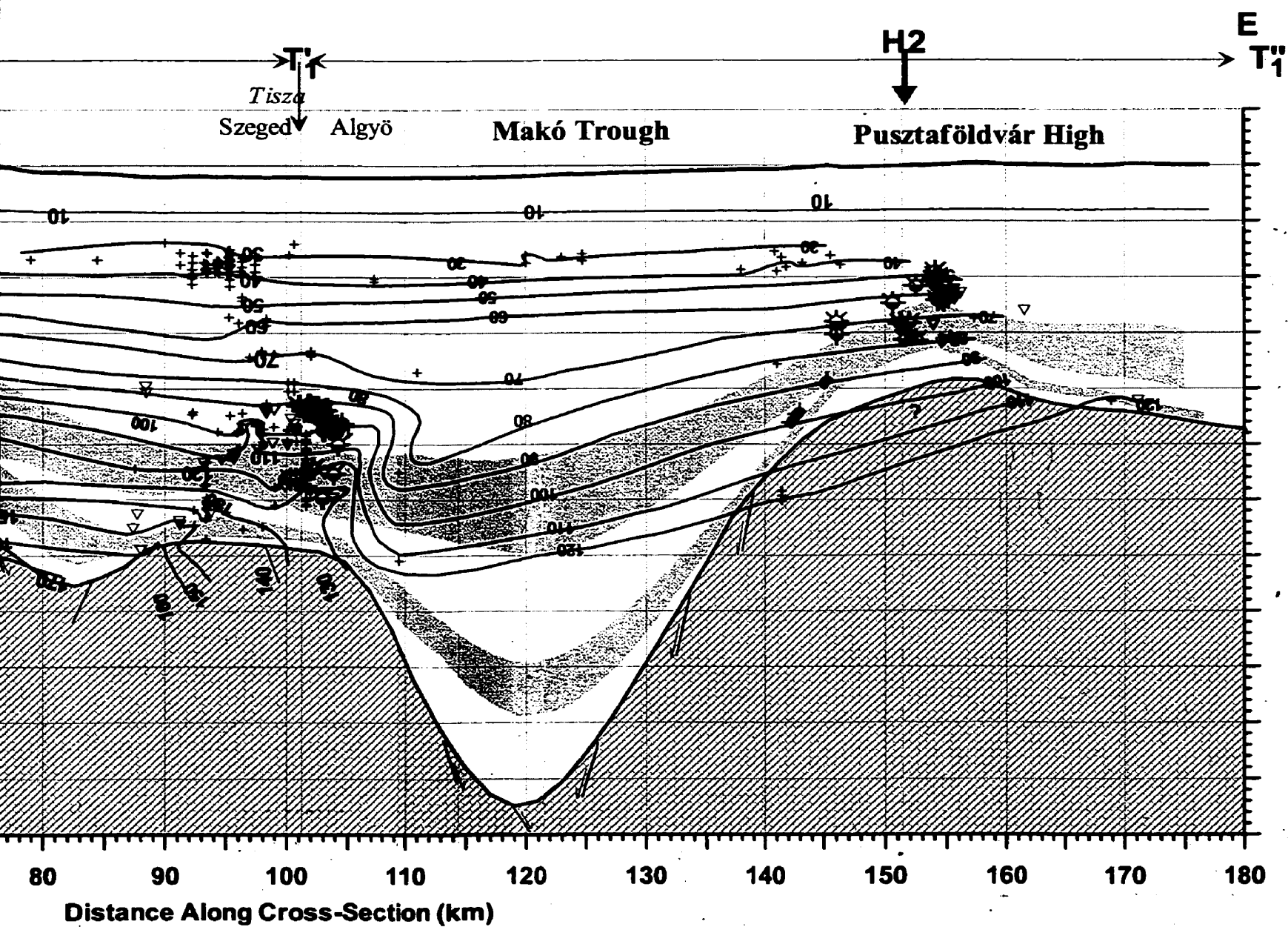
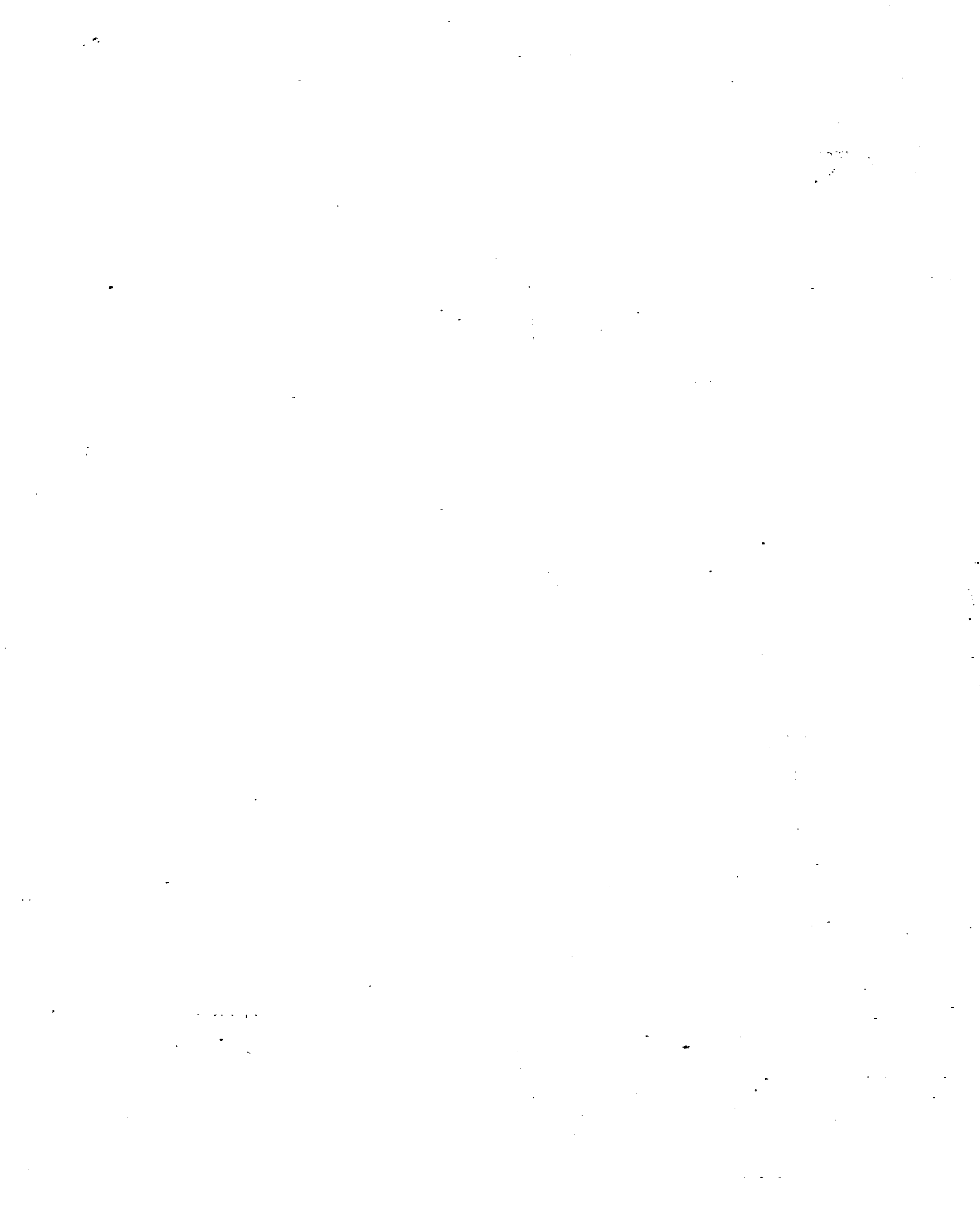


Figure 6.34: Geothermal cross section T1-T1'-T1'' and hydrocarbon accumulation (for location see Figure 6.8). Isotherm contours are in °C; symbols in kilometres of end-nodes and break-point: T1(640, 110), T1'(74





carbon accumulations within 2 km distance from either side of the section are in °C; symbols are explained in Figure 4.32, p. 119. EOv co-ordinates 640, 110), T1'(740, 104), and T1''(820, 120).



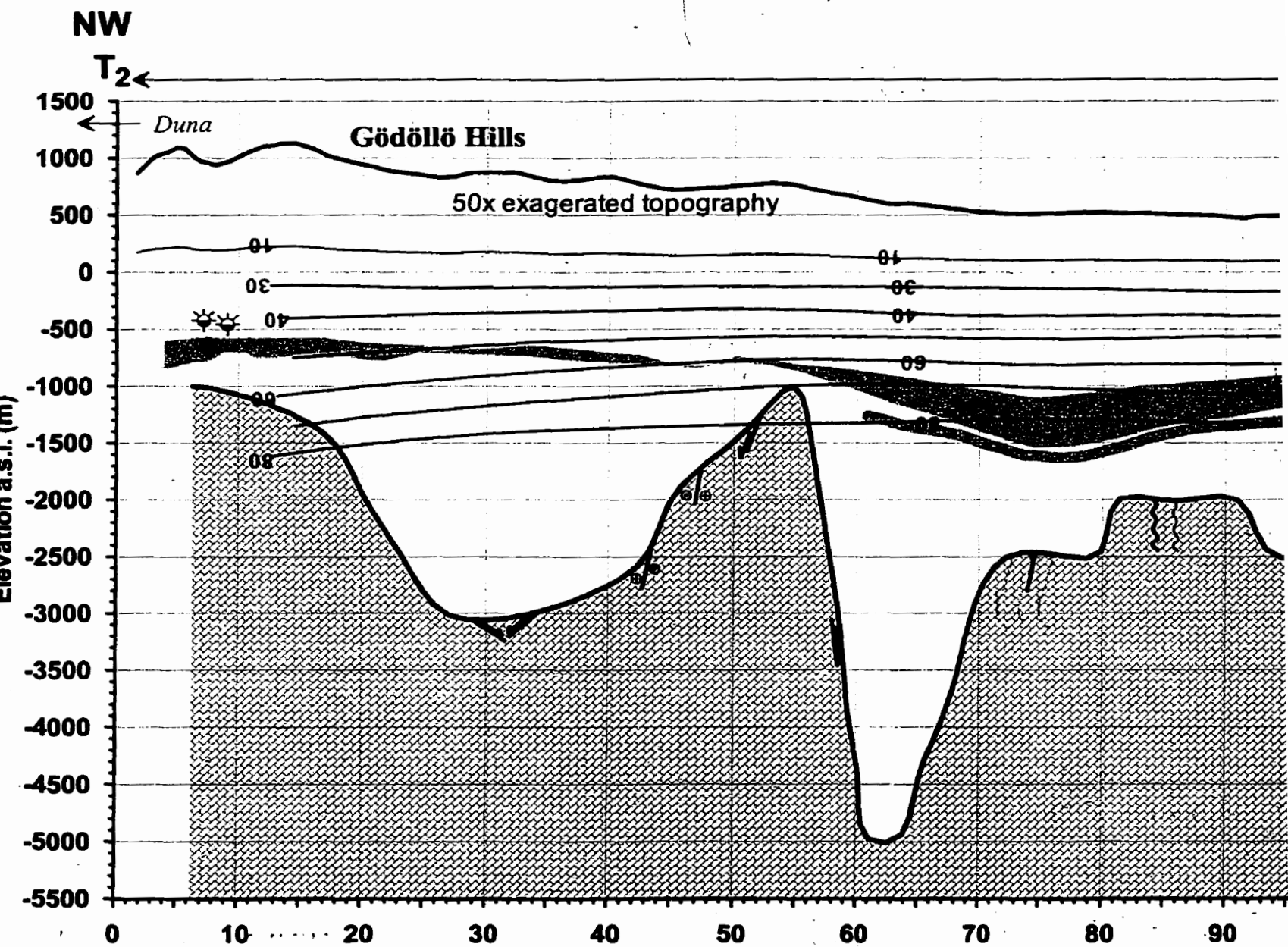
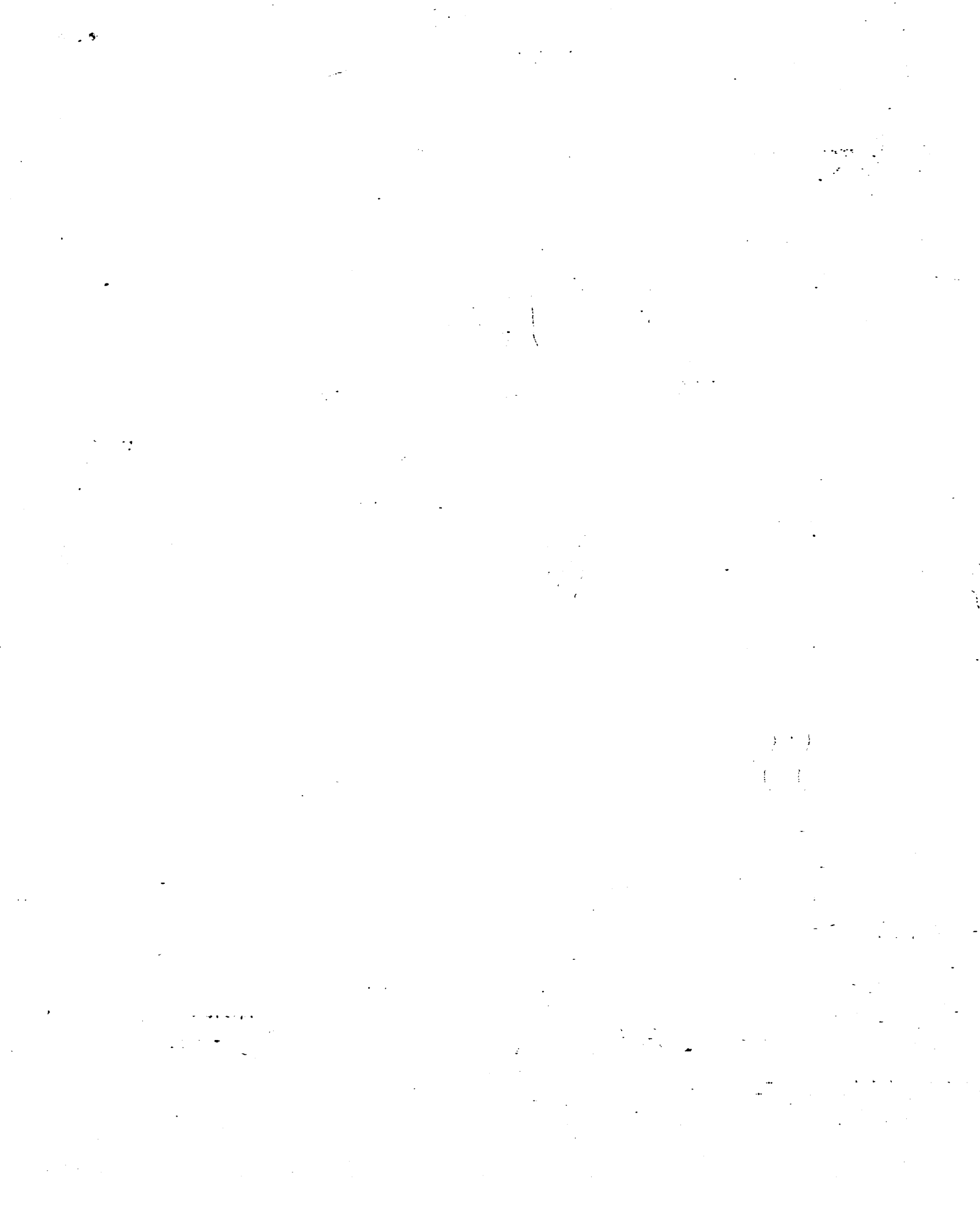
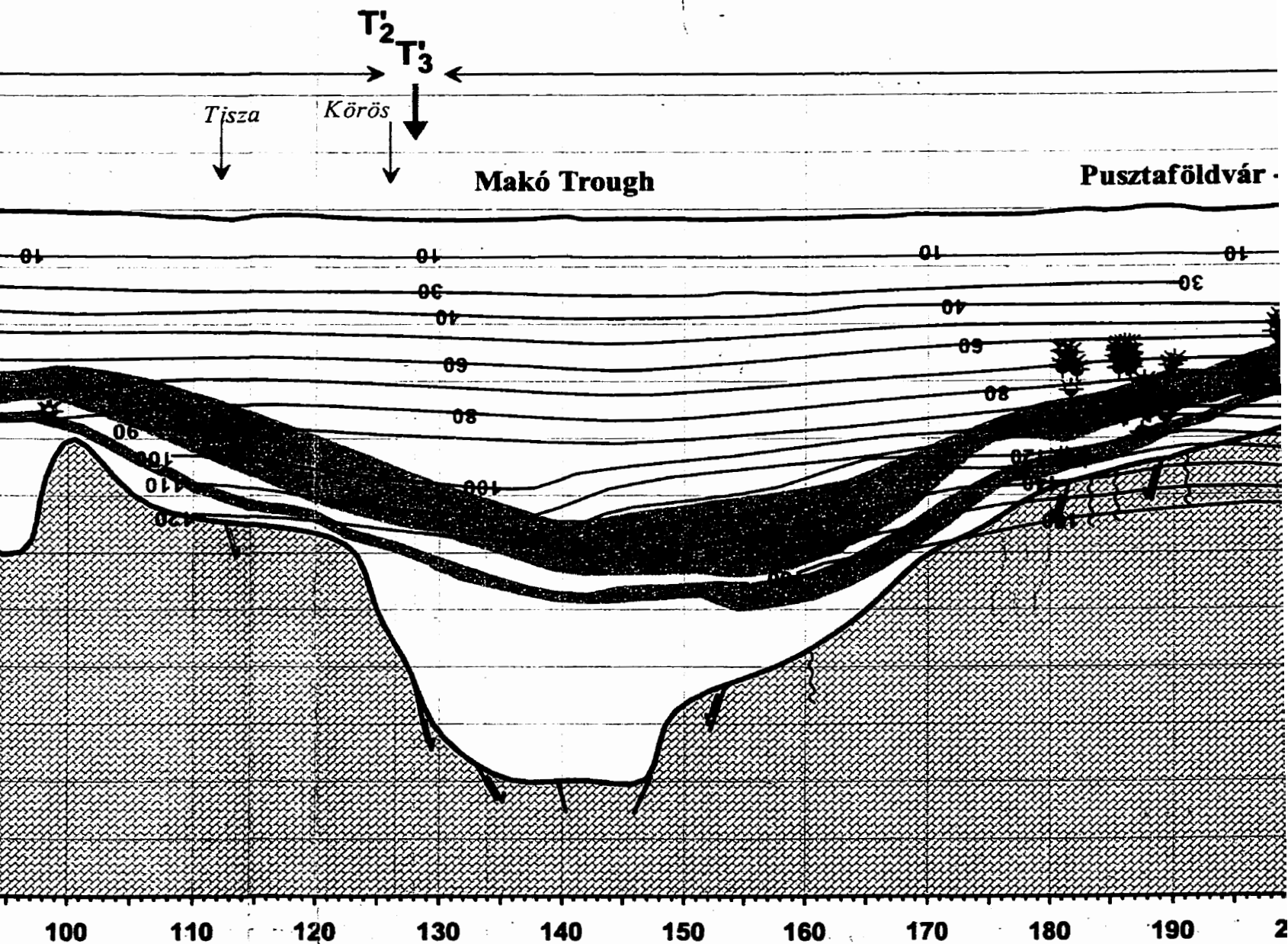


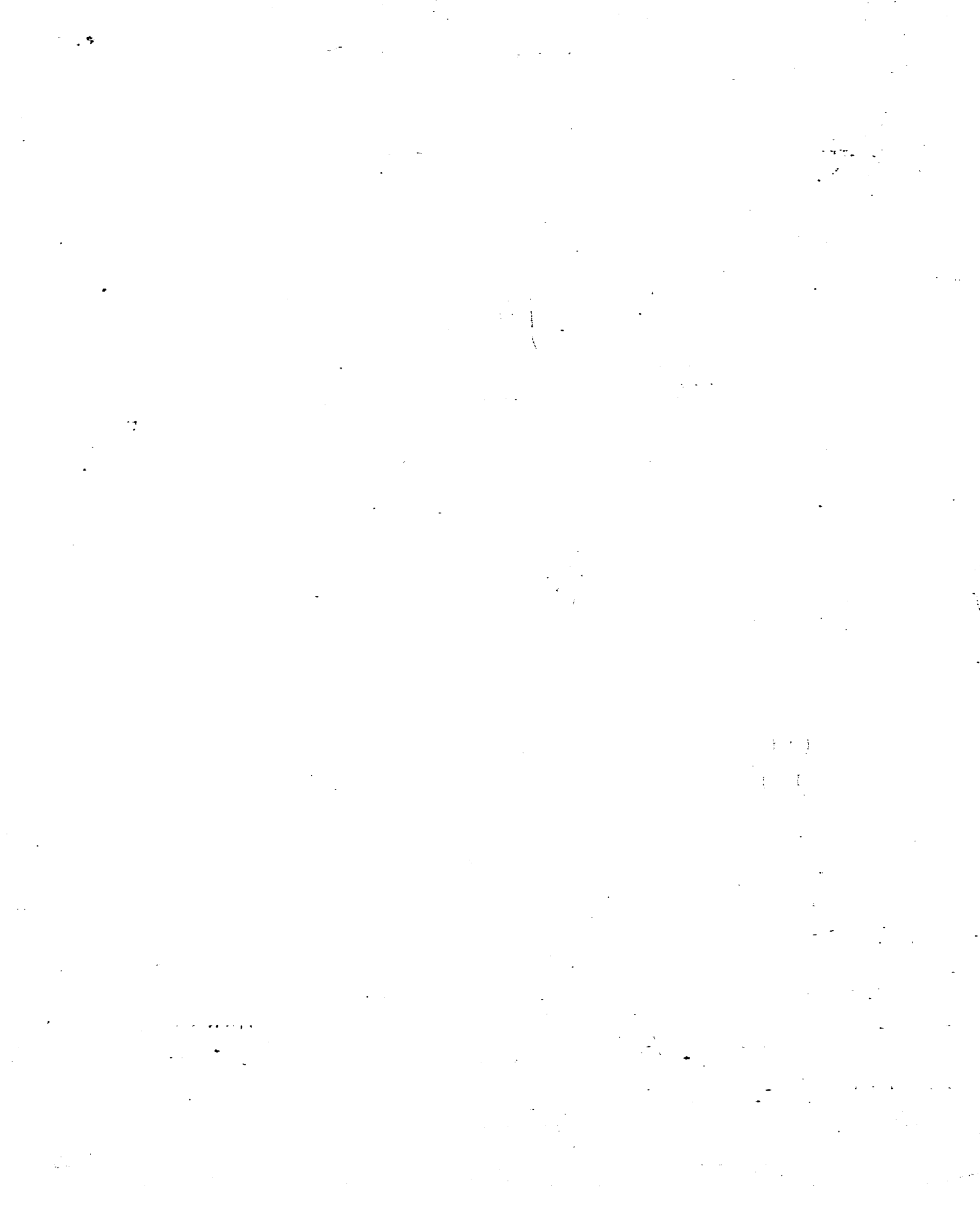
Figure 6.35: Geothermal cross section T2-T2'-T2'' and hydrocarbon accu
(for location see figure 6.8). Isotherm contours are in °C; syn
in kilometres of end-nodes and break-point: T1(660, 260), T2

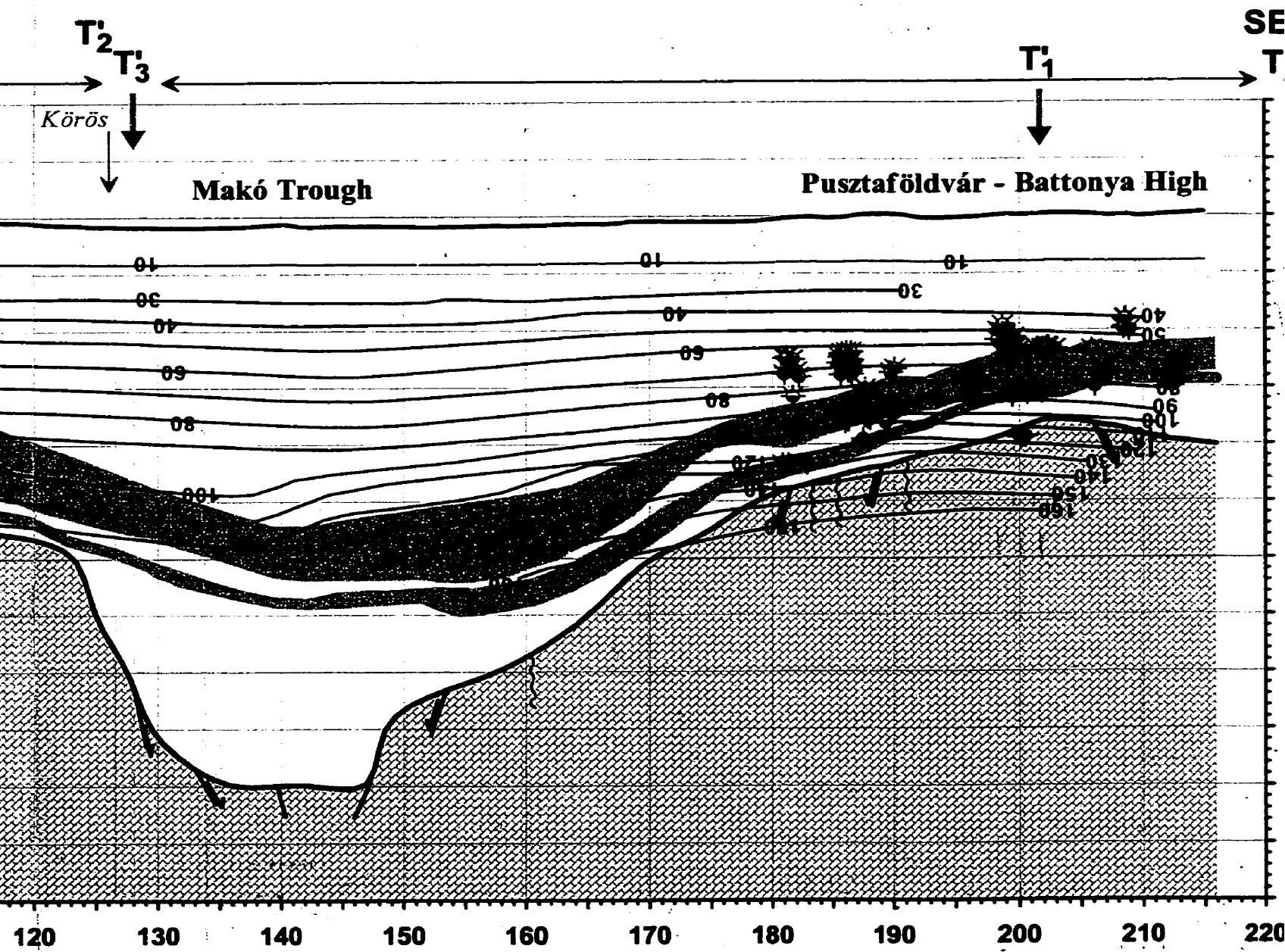




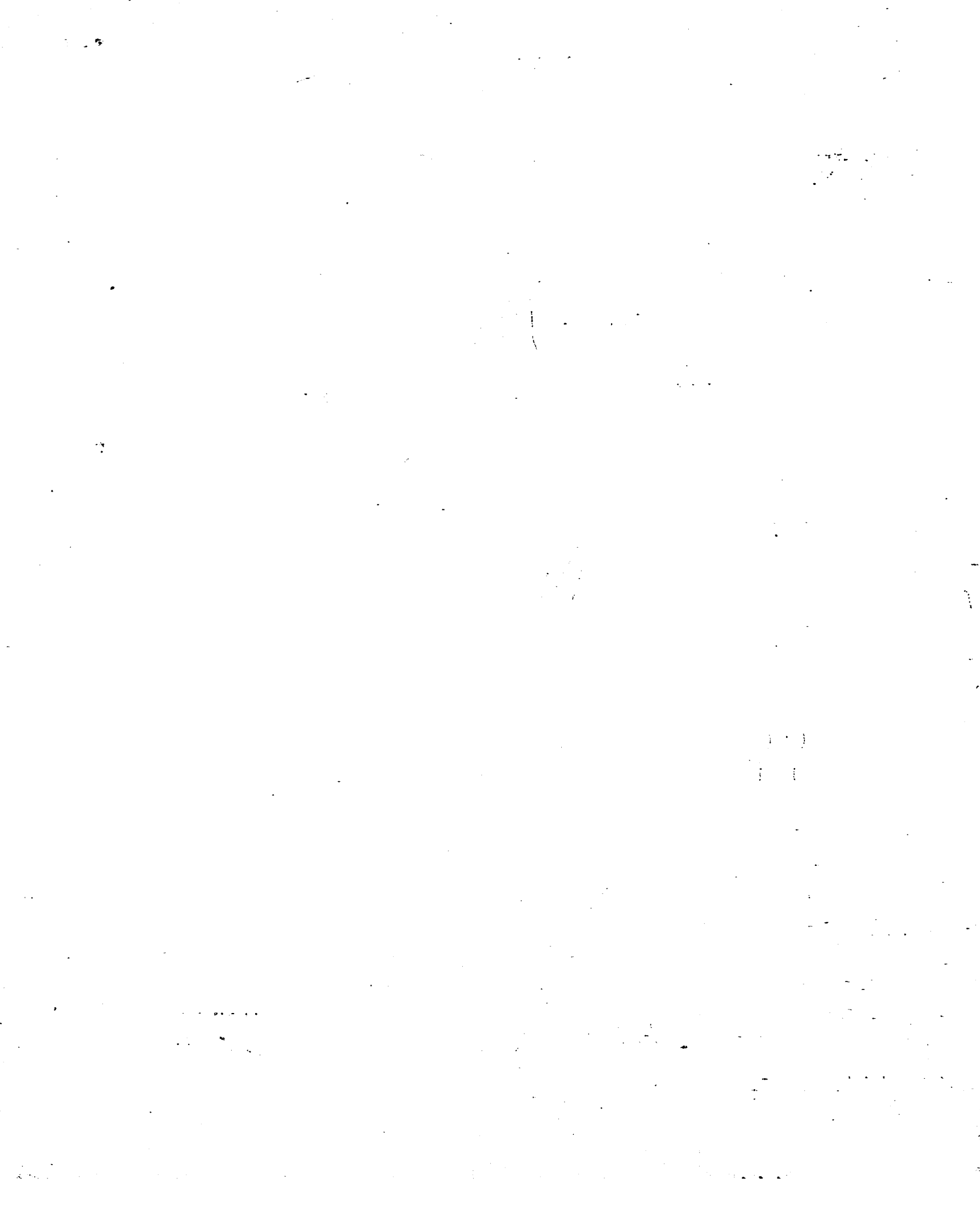
Distance along cross section (km)

Simulations within 2 km distance from either side of the section
 Symbols are explained in Figure 4.32, p. 119. EOVS co-ordinates
 T_2' (740, 160), and T_2'' (806, 102).





long cross section (km)
 in 2 km distance from either side of the section
 as defined in Figure 4.32, p. 119. EOV co-ordinates
 T₂'(806 102)



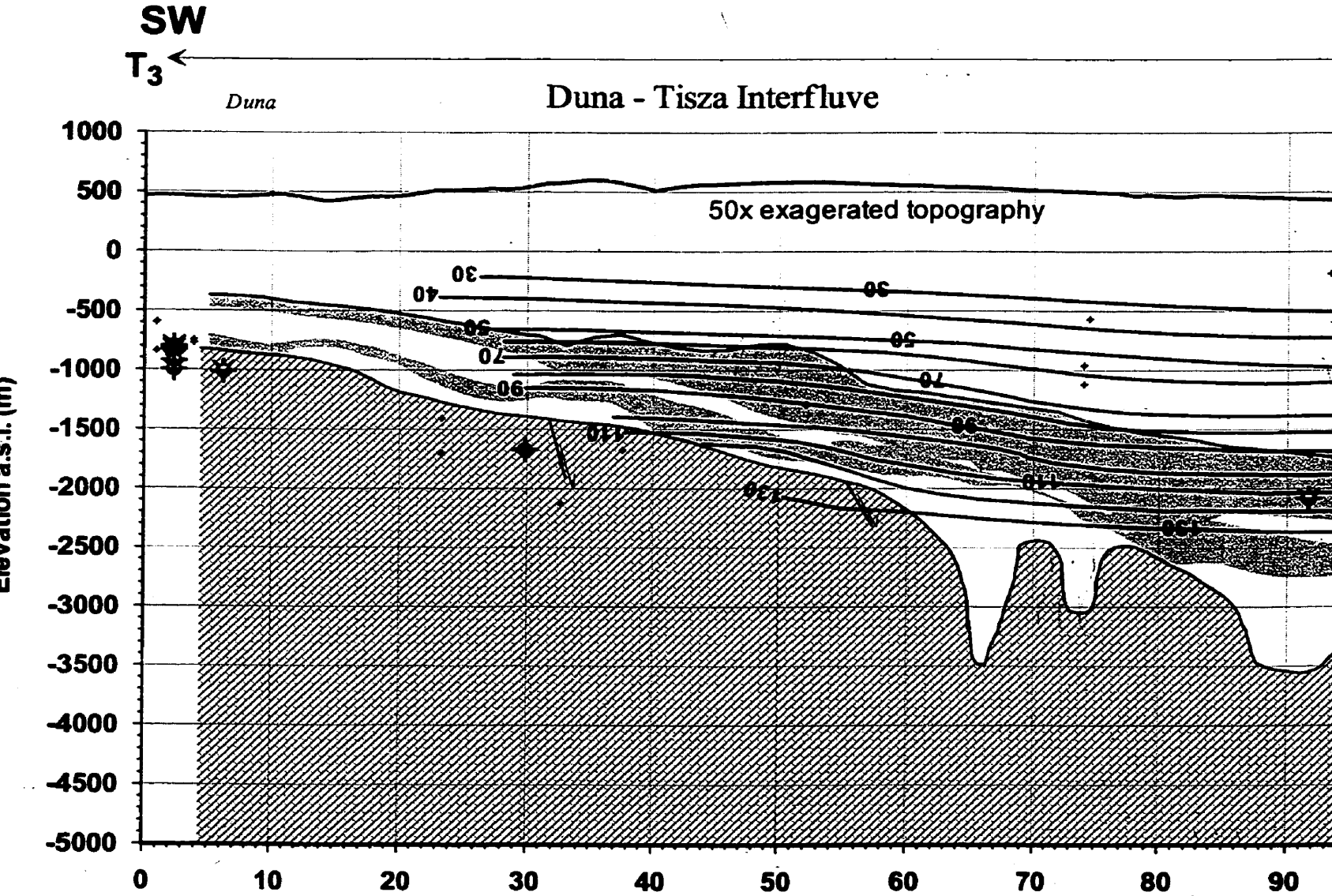
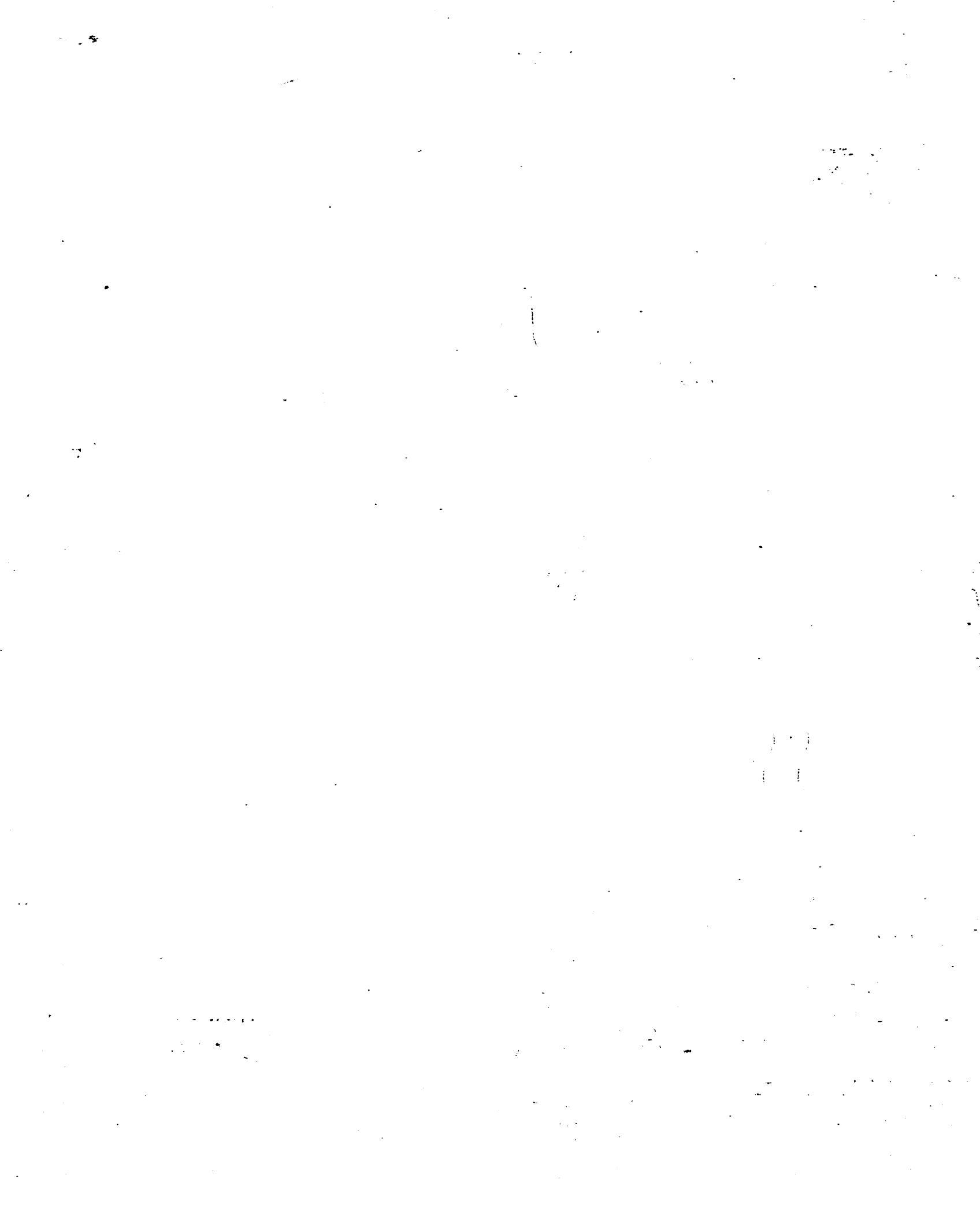
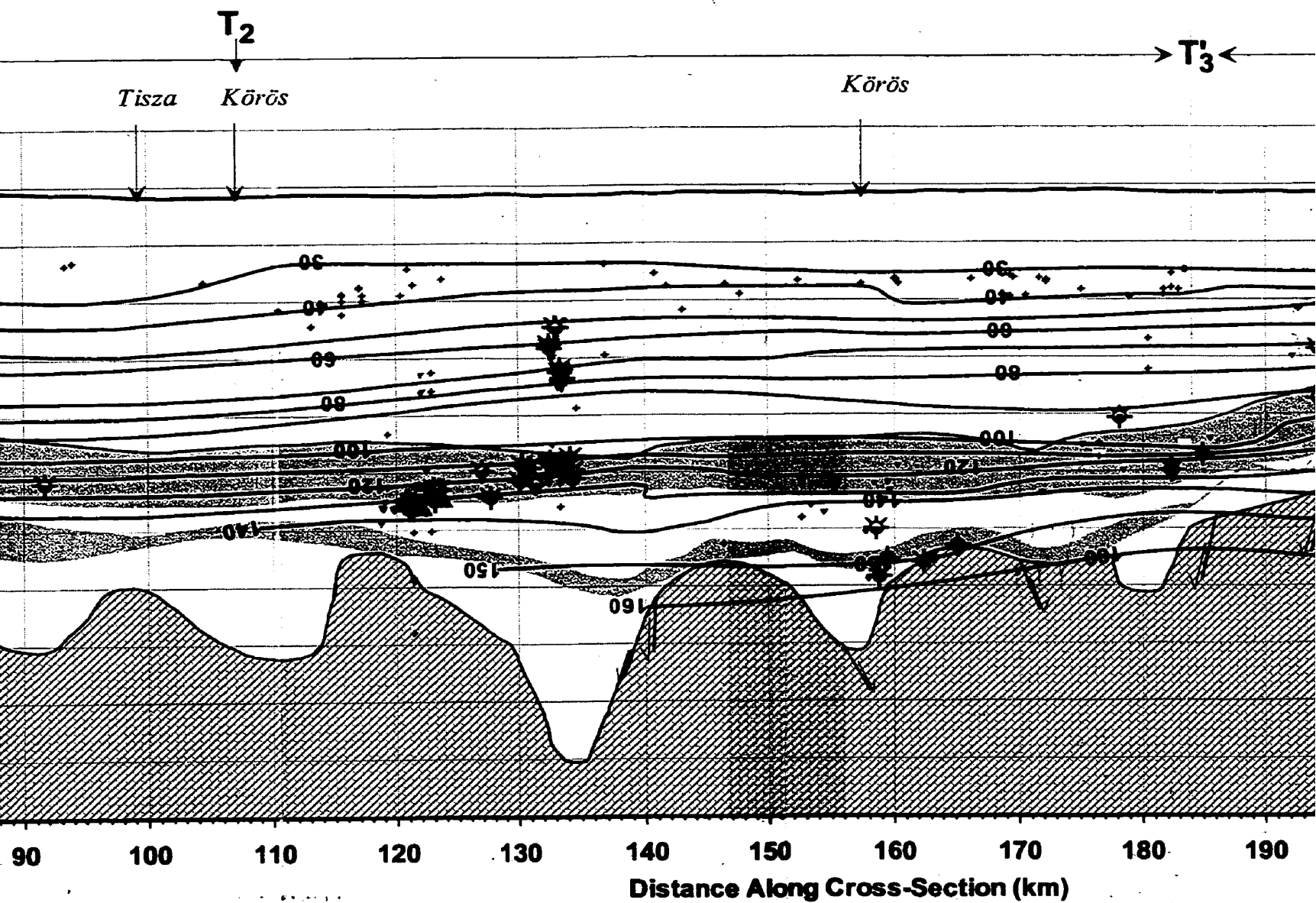
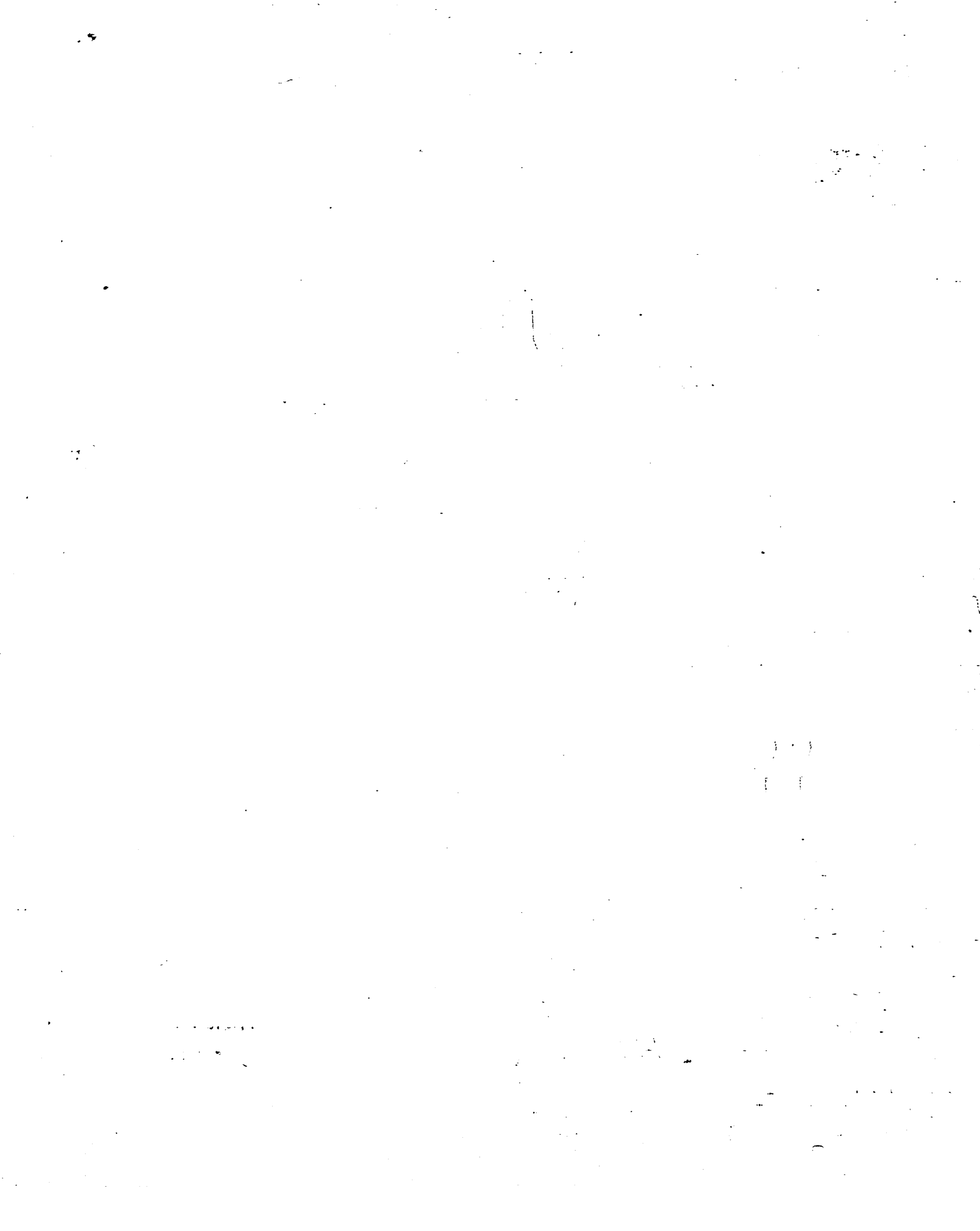


Figure 6.36: Geothermal Cross-Section T3 - T3' - T3'' and hydrocarbon accumulations (for location see figure 6.8). Isotherm contours are in °C; symbols indicate locations of wells in kilometres of end-nodes and break-point: T3(640, 120), T3'(810, 120), T3''(810, 120).





accumulations within 2 km distance from either side of the section
 symbols are explained in Figure 4.32, p. 119. EOv co-ordinates
 T3'(810, 190), T3"(850, 290).

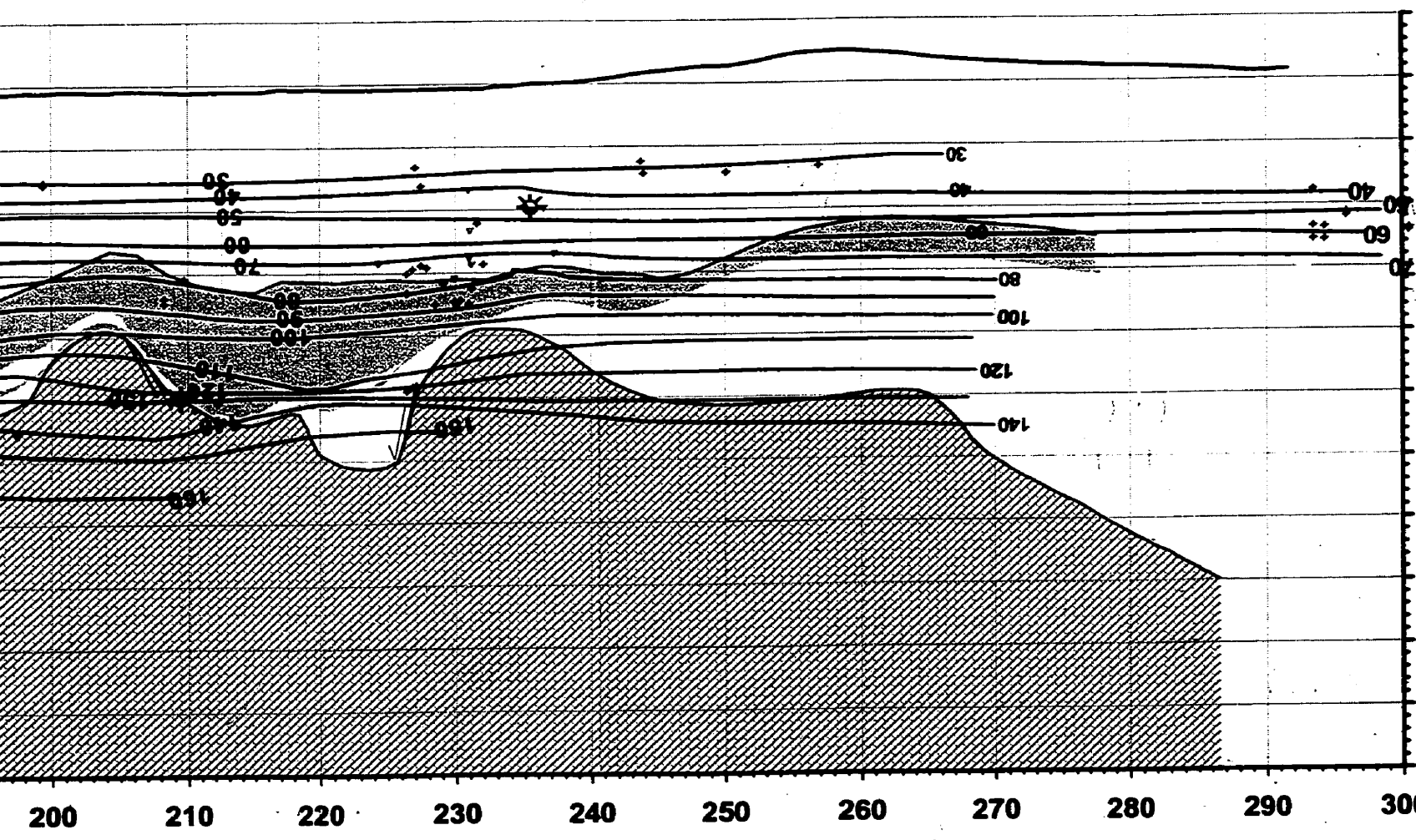


NE

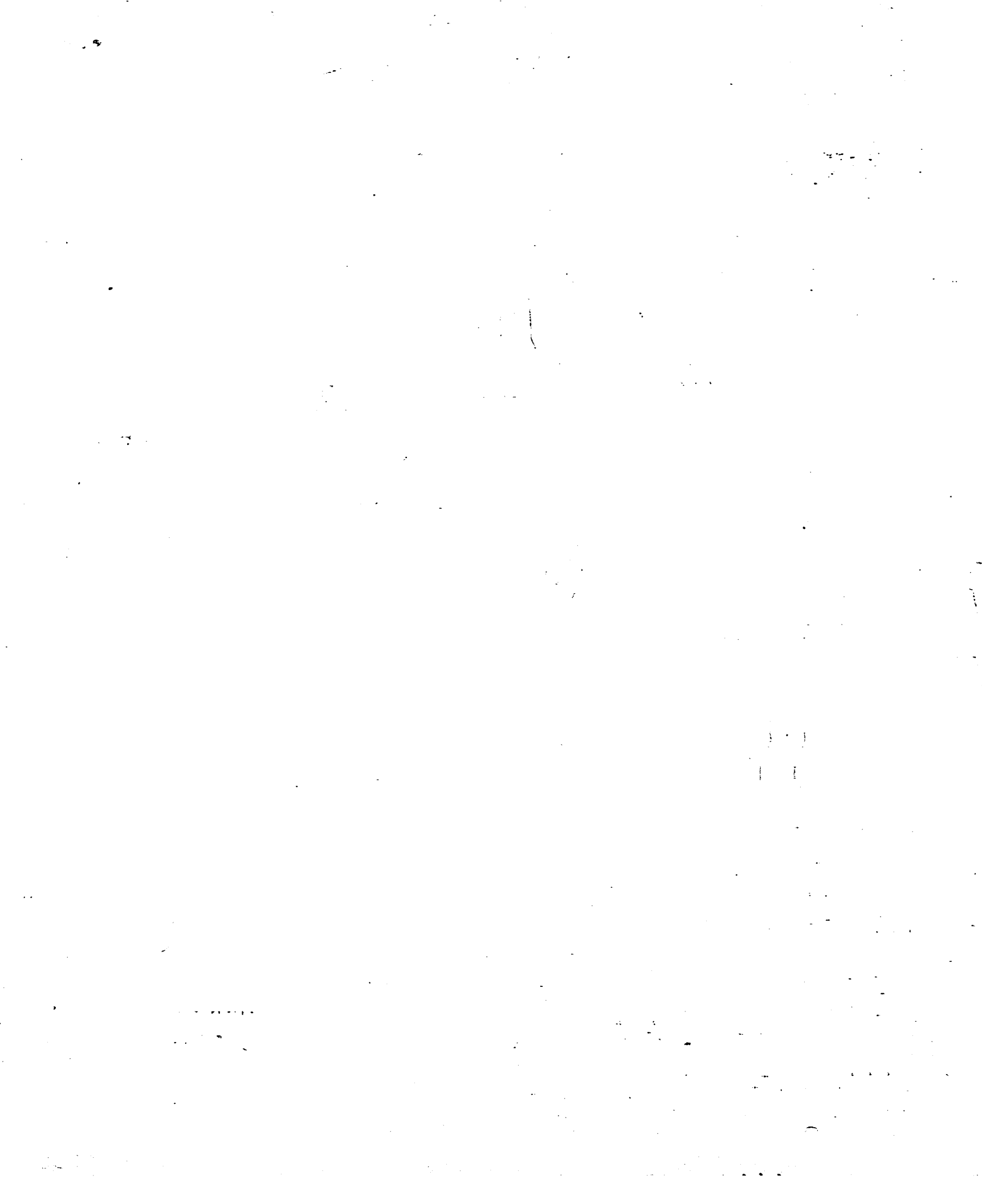
T₄

Nyírség

T



200 210 220 230 240 250 260 270 280 290 300



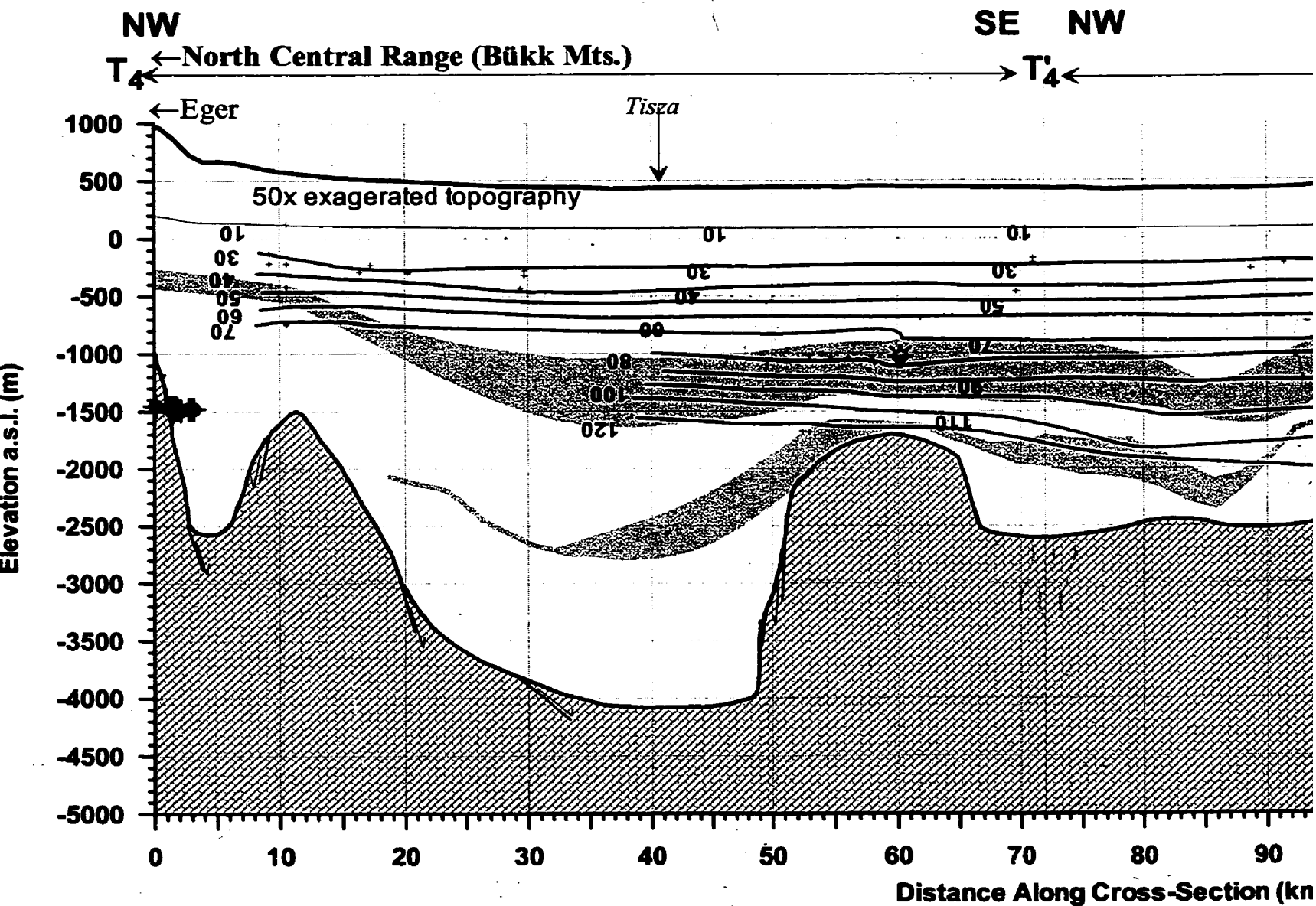
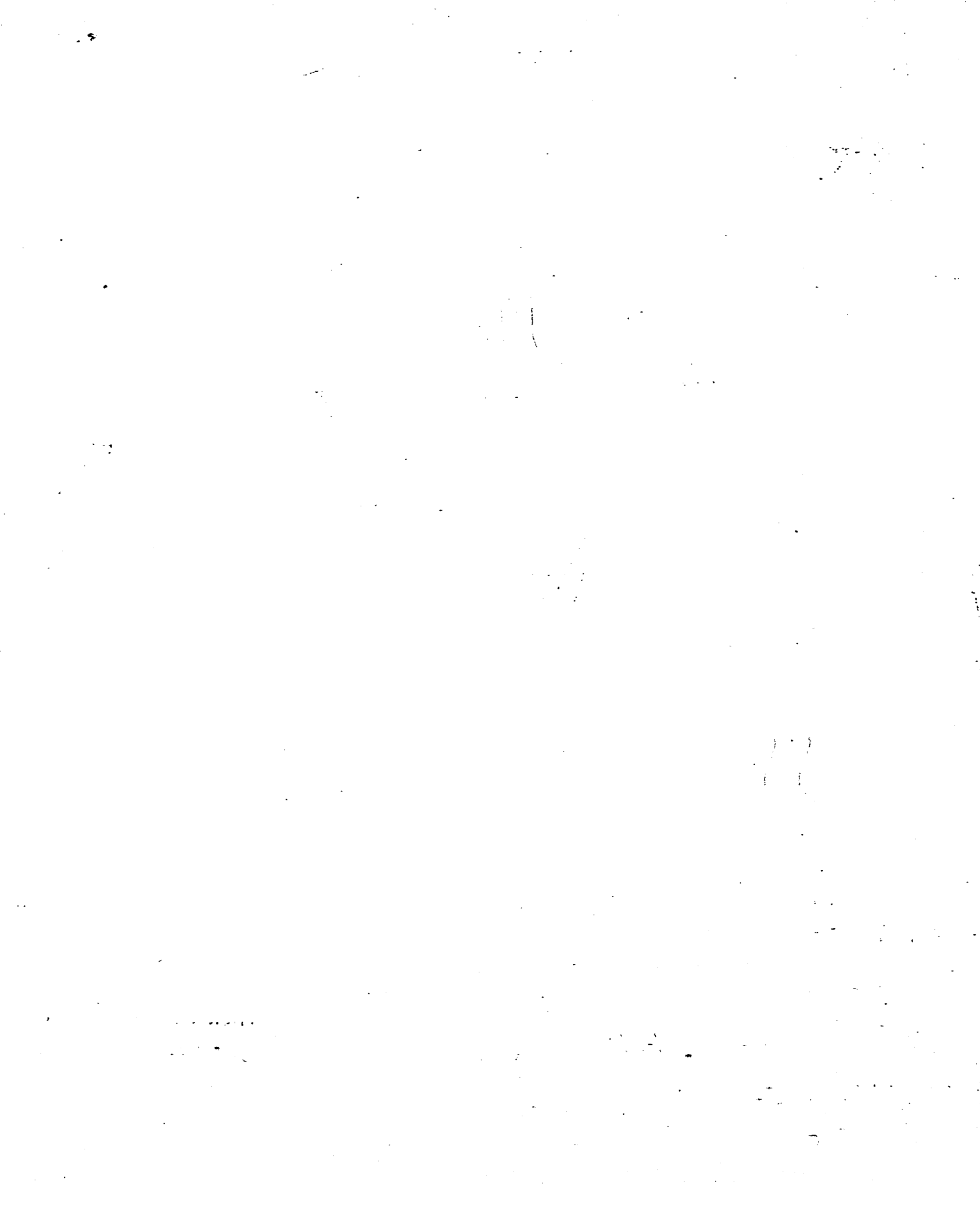
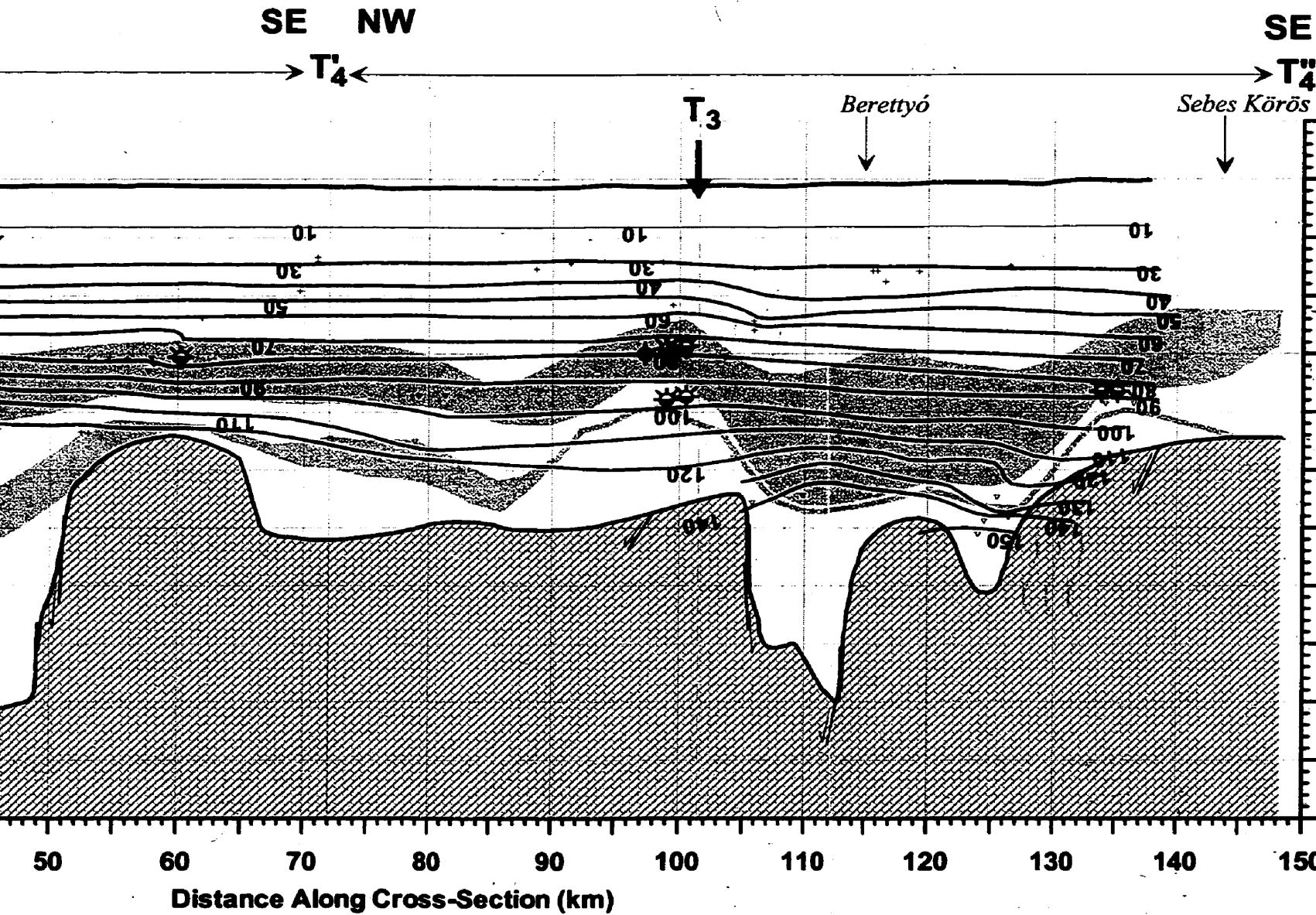


Figure 6.37: Geothermal cross section T₄-T₄'-T₄'' and hydrocarbon accumulations with isotherm contours (for location see figure 6.8). Isotherm contours are in °C; symbols are in kilometres of end-nodes and break-point: T₄(750, 280), T₄'(790, 220),





T4" and hydrocarbon accumulations within 2 km distance from either side of the section. Therm contours are in °C; symbols are explained in Figure 4.32, p. 119. EOv co-ordinates break-point: T4(750, 280), T4'(790, 220), and T4"(860, 190).

